

**THÈSE**

pour l'obtention du Diplôme de

**DOCTEUR DE L'UNIVERSITÉ PARIS VII**

**SPÉCIALITÉ : PHYSIQUE THÉORIQUE DES PARTICULES**

présentée et soutenue publiquement

par

Grégory MOREAU

le 27 Novembre 2000

*Titre :*

**Étude phénoménologique des interactions violant la  
symétrie de R-parité dans les théories  
supersymétriques**

---

*Directeur de thèse :*

Marc CHEMTOB

---

JURY

MM.	Pierre BINÉTRUY,	Rapporteur,
	Marc CHEMTOB,	Directeur de thèse,
	Herbert DREINER,	
	Jean-Pierre GAZEAU,	
	Stavros KATSANEVAS,	Rapporteur,
	Carlos SAVOY,	
	Yves SIROIS,	Président.







## *Remerciements*

**A**vant tout, je tiens à remercier P. Chiappetta, pour ses conseils avisés dans le choix de ma thèse, et mon directeur, M. Chemtob, d’avoir accepté de m’encadrer à l’occasion de ce doctorat. M. Chemtob a toujours su se montrer disponible tout en respectant ma liberté. Ma reconnaissance va aussi aux membres du jury de thèse, à savoir, P. Binétruy, H. Dreiner, J.-P. Gazeau, S. Katsanevas, C. Savoy et Y. Sirois.

Mes travaux ont souvent été le fruit d’un effort collectif. Aussi, je tiens à mentionner mes collaborateurs expérimentateurs et amis : M. Besançon, F. Déliot, G. Polesello, C. Royon et enfin E. Perez qui a répondu à mes nombreuses questions avec une constante attention. Je souhaite par ailleurs citer H.-U. Martyn et Y. Sirois qui m’ont fortement encouragé dans mon travail concernant la physique auprès des Collisionneurs Linéaires.

Par ailleurs, je tiens à exprimer ici toute ma reconnaissance et ma sympathie à R. Balian, F. Bernard, M. Boonekamp, F. Boudjema, A. Djouadi, E. Dudas, S. Gamblin, R. Grimm, J.-L. Kneur, C. Lachaud, J. Lamarcq, F. Ledroit, R. Lopez, P. Lutz, B. Marchet, P. Micout, G. Moulta, S. Munier, J.-M. Normand, R. Peschanski, V. Poireau, G. Sajot, C. Savoy, L. Schoeffel, G. Servant et X. Tata, qui m’ont accompagné et aidé durant ces trois années de thèse.

Ces trois années de thèse ont aussi été pour moi l’occasion d’inoubliables rencontres. Je pense aux longues, et parfois même tardives, discussions avec N. Ghodbane, qui ne concernaient pas seulement SUSYGEN. Je pense d’autre part au magicien à trois corps Y. Mambrini auprès duquel j’ai toujours éprouvé un grand plaisir à passer pour “Monsieur tout le monde” lors de ses impressionnants tours de magie. Je n’oublie pas la convivialité et la gentillesse de mes collègues de bureau, T. Duguet et N. Regnault, qui ont permis des conditions de travail plus qu’agréables durant ces trois années passées à l’Orme des Merisiers. N. Regnault a été un assistant scientifique et informatique de tout premier choix. Quant à T. Duguet, il a toujours eu à l’esprit un sujet original permettant d’initier un débat passionnant et de provoquer ainsi une pause bien méritée.

D'autre part, je dois en grande partie cette thèse à ma famille : R. Savoie m'a accompagné, supporté et soutenu, de par sa douce présence, pendant ce petit bout de vie. Mes parents, I. Jaglin, J.-M. Moreau, F. Jaglin et C. Moreau, ont su être à l'écoute de mes aspirations et respecter mes choix, rendant ainsi cette thèse envisageable. Mes frères, Anatole M., Arthur J., Clément J., Martin J. et Théophile M., et ma soeur, Valentine M., ainsi que S. Jendoubi et M. Villeger m'ont tous communiqué leur joie et leur bonheur. Enfin, J. Légasse, P. Bailhache, A. Aubanel et L. Savoie ont été d'un grand soutien.

Sans oublier mes ami(e)s, M. Boudet, M. Descottes, A. Devaux, E. Duque, F. Grand-jacques, A. Jeanmet, V. Knysak, T. Laval, A. Forgiel, A. Forgiel, T. Malbrancq, L. Meiers, C. Morel, A. Mouillaud, C. Vannini, E. de Tayrac, M. Tourdjman et M. Werner, qui m'ont apporté un certain recul par rapport à mon travail en m'apprenant le sens de la dérision, si nécessaire lors d'une thèse et à de nombreux autres moments de la vie.







# Table des matières

<b>1</b>	<b>Supersymétrie</b>	<b>9</b>
1.1	Origine des théories supersymétriques . . . . .	9
1.2	Algèbre de supersymétrie . . . . .	10
1.3	Motivations de la supersymétrie . . . . .	11
1.3.1	Le problème des hiérarchies d'échelles . . . . .	12
1.4	Formalisme des théories supersymétriques . . . . .	15
1.4.1	Exemple du spineur de Weyl . . . . .	15
1.4.2	Exemple du spineur de Majorana . . . . .	16
1.4.3	Champs auxiliaires . . . . .	16
1.4.4	Superspace . . . . .	17
1.4.5	Notation des spineurs à deux composantes . . . . .	18
1.4.6	Générateurs de supersymétrie dans le superspace . . . . .	20
1.4.7	Superchamps . . . . .	21
1.4.8	Lagrangiens supersymétriques . . . . .	23
1.4.9	Théories de jauge supersymétriques . . . . .	25
1.4.10	Théorème de non-renormalisation . . . . .	27
1.5	Brisure de la supersymétrie . . . . .	27
1.6	Modèle Standard Supersymétrique Minimal (MSSM) . . . . .	29
1.6.1	Le contenu en particules . . . . .	30
1.6.2	Le lagrangien . . . . .	30
1.6.3	Le spectre supersymétrique . . . . .	31
<b>2</b>	<b>Supergravité</b>	<b>37</b>
2.1	Motivations . . . . .	37
2.2	Lagrangiens de supergravité . . . . .	39
2.2.1	Procédure de Noether . . . . .	39
2.2.2	Lagrangien localement supersymétrique pour le multiplet de supergravité . . . . .	41
2.2.3	Lagrangien localement supersymétrique pour un supermultiplet chiral libre et non massif . . . . .	43
2.2.4	Lagrangien localement supersymétrique général . . . . .	45
2.3	Brisure spontanée en supergravité . . . . .	48
2.4	Brisure de la supersymétrie dans le secteur “caché” . . . . .	51
2.5	Effets de la brisure de supersymétrie locale dans le secteur “observable” . . . . .	53

<b>3</b>	<b>Origines et motivations théoriques de la symétrie de R-parité</b>	<b>58</b>
3.1	Généralité du superpotentiel du MSSM . . . . .	58
3.2	Désintégration du proton . . . . .	60
3.2.1	Opérateurs de dimension 5 . . . . .	61
3.3	Symétries du superpotentiel . . . . .	62
3.3.1	Les R-symétries . . . . .	62
3.3.2	Problèmes et intérêts des R-symétries . . . . .	65
3.3.3	Les R-symétries discrètes et la R-parité . . . . .	68
3.3.4	Les symétries discrètes . . . . .	69
3.4	Motivations théoriques de la parité de matière ou R-parité . . . . .	70
3.4.1	Point de vue des symétries discrètes de jauge . . . . .	71
3.4.2	Point de vue des théories de grande unification (GUT) . . . . .	74
3.4.3	Point de vue des théories de cordes . . . . .	76
3.4.4	Conclusion . . . . .	76
<b>4</b>	<b>Production simple des particules supersymétriques par les interactions violant la R-parité</b>	<b>79</b>
4.1	Motivations . . . . .	79
4.2	Collisionneurs hadroniques . . . . .	82
4.2.1	Signature trilepton . . . . .	85
4.2.2	Signature dilepton . . . . .	92
4.3	Collisionneurs leptoniques . . . . .	95
4.3.1	Production simple de chargino . . . . .	99
<b>5</b>	<b>Contributions des interactions <math>\mathcal{R}_p</math> aux taux de changement de saveur et aux asymétries liées à la violation de la symétrie CP</b>	<b>105</b>
5.1	Motivations . . . . .	105
5.2	Production de paires de fermions . . . . .	107
5.2.1	Taux de changement de saveur . . . . .	107
5.2.2	Asymétries liées à la violation de CP . . . . .	112
5.3	Production de paires de sfermions . . . . .	115
5.3.1	Taux de changement de saveur . . . . .	115
5.3.2	Asymétries liées à la violation de CP . . . . .	117

## Publications

	<b>Production of (s)particles at colliders through <math>\mathcal{R}_p</math> interactions</b>	<b>131</b>
1	Singly Produced Sparticles at $e^+e^-$ Colliders . . . . .	134
1.1	Resonant Production of Sneutrinos . . . . .	134
1.2	Single Gaugino Production . . . . .	135
1.3	Non Resonant Single Production . . . . .	140
1.4	Fermion Pair Production Via $\mathcal{R}_p$ . . . . .	140
1.5	Single Production in $e - \gamma$ Collisions . . . . .	144
1.6	$\mathcal{R}_p$ Contributions to Flavour Changing Neutral Currents . . . . .	145
1.7	$\mathcal{R}_p$ Contributions to CP Violation . . . . .	149

2	Singly Produced Sparticles at Hadronic Colliders . . . . .	153
2.1	Resonant Production of Sparticles . . . . .	153
2.2	Single Gaugino Production . . . . .	154
2.3	Non Resonant Single Production . . . . .	160
2.4	Fermion Pair Production Via $\mathcal{R}_p$ . . . . .	161
2.5	$\mathcal{R}_p$ Contributions to Flavour Changing Neutral Currents . . . . .	169
2.6	$\mathcal{R}_p$ Contributions to CP violation . . . . .	170

## **Resonant sneutrino production at Tevatron Run II 177**

### **Single superpartner production at Tevatron Run II 189**

1	Introduction . . . . .	192
2	Theoretical framework . . . . .	193
3	Single superpartner productions via $\lambda'_{ijk}$ at Tevatron Run II . . . . .	194
3.1	Resonant superpartner production . . . . .	194
3.2	Non-resonant superpartner production . . . . .	202
4	Three lepton signature analysis . . . . .	203
4.1	Signal . . . . .	203
4.2	Standard Model background of the 3 lepton signature at Tevatron . . . . .	203
4.3	Supersymmetric background of the 3 lepton signature at Tevatron . . . . .	204
4.4	Cuts . . . . .	205
4.5	Results . . . . .	209
5	Like sign dilepton signature analysis . . . . .	224
5.1	Signal . . . . .	224
5.2	Standard Model background of the like sign dilepton signature at Tevatron . . . . .	224
5.3	Supersymmetric background of the like sign dilepton signature at Tevatron . . . . .	225
5.4	Cuts . . . . .	225
5.5	Results . . . . .	228
6	Conclusion . . . . .	236
7	Acknowledgments . . . . .	237
1	Formulas for spin summed amplitudes . . . . .	238

### **Resonant sneutrino production in Supersymmetry with R-parity violation at the LHC 247**

1	Introduction . . . . .	250
2	The signal . . . . .	251
2.1	Theoretical framework . . . . .	251
2.2	Single chargino production cross-section . . . . .	253
2.3	Three leptons branching ratio . . . . .	254
3	Experimental analysis . . . . .	256
3.1	Mass reconstruction . . . . .	256
3.2	Standard Model Background . . . . .	262
3.3	Sensitivity on $\lambda'$ . . . . .	264
4	Analysis reach in various models . . . . .	265
4.1	Efficiency of the three-muon analysis . . . . .	267
4.2	Analysis reach in the MSSM . . . . .	267
4.3	Analysis reach in mSUGRA . . . . .	269

5	Conclusions . . . . .	274
6	Acknowledgements . . . . .	275
<b>Systematics of single superpartners production at leptonic colliders</b>		<b>279</b>
1	Introduction . . . . .	282
2	General Formalism . . . . .	283
2.1	Production Cross Sections . . . . .	283
2.2	Decays . . . . .	285
3	The model and its parameter space . . . . .	289
4	Results and discussion . . . . .	292
4.1	Total production rates . . . . .	292
4.2	Branching Ratios . . . . .	299
5	Dynamical distributions . . . . .	308
6	Conclusions . . . . .	310
7	Acknowledgments . . . . .	310
1	Formulas for spin summed amplitudes . . . . .	311
2	Formulas for partial decay widths . . . . .	313
<b>Single chargino production at linear colliders</b>		<b>319</b>
1	Introduction . . . . .	322
2	Theoretical framework . . . . .	324
3	Signal . . . . .	325
4	Background . . . . .	326
4.1	Non-physic background . . . . .	326
4.2	Standard Model background . . . . .	328
4.3	Supersymmetric background . . . . .	328
5	Analysis . . . . .	329
5.1	Polarization . . . . .	330
5.2	Cross sections and branching ratios . . . . .	330
5.3	Cuts . . . . .	334
5.4	Discovery potential . . . . .	340
5.5	SUSY mass spectrum . . . . .	342
5.6	Extension of the analysis to different center of mass energies . . . . .	344
5.7	Study based on the $3l + 2jets + \cancel{E}$ final state . . . . .	346
5.8	Study of the single chargino production through various $\mathcal{R}_p$ couplings . . . . .	347
5.9	Single neutralino production . . . . .	347
6	Conclusion . . . . .	348
7	Acknowledgments . . . . .	349
<b>Broken R parity contributions to flavor changing rates and CP asymmetries in fermion pair production at leptonic colliders</b>		<b>355</b>
1	Introduction . . . . .	359
2	Production of fermion pairs of different flavors . . . . .	361
2.1	Charged lepton-antilepton pairs . . . . .	362
2.2	Down-quark-antiquark pairs . . . . .	369
2.3	Up-quark-antiquark pairs . . . . .	370
3	Basic assumptions and results . . . . .	372

3.1	General context of flavor changing physics . . . . .	372
3.2	Choices of parameters and models . . . . .	374
3.3	Numerical results and discussion . . . . .	376
4	Conclusions . . . . .	379

**Polarized single top production at leptonic colliders from broken R parity interactions incorporating CP violation** **389**

1	Introduction . . . . .	392
2	Top-charm associated production . . . . .	393
2.1	Integrated rates . . . . .	393
2.2	Distributions for the semileptonic top decay events . . . . .	397
3	Top polarization observables and a test of CP violation . . . . .	400
3.1	Helicity basis amplitudes . . . . .	402
3.2	Charged lepton energy distribution . . . . .	404
3.3	Top polarization observables . . . . .	405
4	Conclusions . . . . .	409
1	Helicity amplitudes and one-loop $\mathcal{R}_p$ vector boson vertex functions . . . . .	411

**CP violation flavor asymmetries in slepton pair production at leptonic colliders from broken R-parity** **417**

1	Introduction . . . . .	420
2	Production of charged sleptons pairs . . . . .	421
2.1	General formalism . . . . .	421
2.2	Loop amplitudes . . . . .	423
3	Results and discussion . . . . .	425

## Annexes

**A Dimensions** **435**



*“Il n’y a pas de chemin vers le bonheur,  
le bonheur est le chemin.”*





# Chapitre 1

## Supersymétrie

### 1.1 Origine des théories supersymétriques

Deux grandes classes de symétries sont à distinguer en Physique : Les symétries d'espace-temps (réunies dans le groupe de Poincaré) et les symétries internes qui se classent en deux sous-catégories, à savoir les symétries globales (saveur, chirale) et les symétries de jauge (couleur, électrofaible). Les premières tentatives d'unification de ces deux genres de symétries furent non relativistes. Ces modèles concernaient les quarks et rassemblaient le groupe SU(2) de spin et SU(3) de saveur dans un groupe SU(6). En 1967, Coleman et Mandula furent à l'origine d'un théorème [1] qui est le plus précis et le plus puissant d'une série de "no-go theorems" traitant des symétries possibles de la matrice S, dans le cadre d'une théorie quantique des champs : D'après ce théorème, si G est un groupe de symétrie connexe de la matrice S qui contient le groupe de Poincaré, qui met un nombre fini de particules dans un supermultiplet et qui a des générateurs pouvant être représentés comme des opérateurs d'intégration dans l'espace des moments (avec des noyaux qui sont des distributions), si la matrice S n'est pas triviale et si les amplitudes de diffusion élastique sont des fonctions analytiques de  $s$  et  $t$  dans un voisinage de la région physique, alors G est localement isomorphe au produit direct du groupe de Poincaré et d'un groupe de symétrie interne. En 1971, Gol'fand et Likhtman montrèrent que l'algèbre d'une extension du groupe de Poincaré devait être graduée afin de ne pas violer la connection entre le spin et la statistique [2]. Une algèbre graduée comprend des générateurs  $B_i$ , appartenant à une algèbre de Lie, et des générateurs  $F_i$ , obéissant à des relations d'anti-commutation entre eux et à des relations de commutation avec les  $B_i$  :

$$[B_i, B_j] \sim B_k, [B_i, F_j] \sim F_k, \{F_i, F_j\} \sim B_k. \quad (1.1)$$

Si l'on considère une extension du groupe de Poincaré, les  $B_i$  représentent les générateurs du groupe de Poincaré ( $SO(1, 3) \times Translations$ ). La seconde relation permet à l'extension obtenue de ne pas être trivialement un produit direct entre le groupe de Poincaré et le groupe associé aux générateurs  $F_i$ . Ces générateurs  $F_i$ , ne commutant pas avec les transformations de Lorentz, changent le spin des particules. Les générateurs  $F_i$  possèdent donc un spin contrairement aux  $B_i$ , d'où la notation ( $B_i$  pour bosonique et  $F_i$  pour fermionique). De plus, le théorème de Coleman-Mandula supprime la possibilité de prendre les  $F_i$  de spin entier. Ce nouveau groupe échange donc les fermions et les bosons introduisant ainsi une nouvelle symétrie. Notons que cette symétrie Bose-Fermi a aussi été introduite

en 1971 par Neveu, Schwarz et Ramond, dans des modèles de cordes pour les fermions. Haag, Sohnius et Lopuszanski prouvèrent ensuite que l'algèbre de supersymétrie (ou superalgèbre) était la seule algèbre graduée généralisant le groupe de Poincaré, compatible avec une théorie quantique des champs [3, 4]. L'introduction de représentations linéaires de la supersymétrie dans le contexte de théories quantiques des champs fut donnée la première fois par Wess et Zumino en 1974 [5]. Peu après, Ferrara, Salam, Strathdee, Wess et Zumino inventèrent le formalisme des superspaces et superchamps [6, 7, 8, 9, 10]. Depuis le début des années 1980, des efforts importants ont été investis dans le développement de la supersymétrie tant sur le plan expérimental que théorique. Aucun partenaire supersymétrique d'une particule du Modèle Standard, c'est à dire aucune particule supersymétrique, n'a cependant été découvert à ce jour.

## 1.2 Algèbre de supersymétrie

Adoptons la notation suivante :  $C$  est l'opérateur conjugaison de charge,  $\eta^{\mu\rho}$  représente la métrique de Minkowski et enfin,  $\gamma^{\mu\nu} = \frac{1}{2}[\gamma^\mu, \gamma^\nu]$ , où les  $\gamma^\mu$  sont les matrices de Dirac. L'algèbre de la supersymétrie s'écrit alors :

$$\begin{aligned} [M^{\mu\nu}, M^{\rho\sigma}] &= -i(\eta^{\mu\rho} M^{\nu\sigma} + \eta^{\nu\sigma} M^{\mu\rho} - \eta^{\mu\sigma} M^{\nu\rho} - \eta^{\nu\rho} M^{\mu\sigma}), \\ [M^{\mu\nu}, P^\sigma] &= -i(\eta^{\mu\rho} P^\nu - \eta^{\nu\rho} P^\mu), \\ [P^\mu, P^\nu] &= 0, \\ [M^{\mu\nu}, Q_\alpha^i] &= \frac{i}{2}(\gamma^{\mu\nu} Q)_\alpha^i, \\ [P^\mu, Q_\alpha^i] &= 0, \\ \{Q_\alpha^i, Q_\beta^j\} &= -2(\gamma^\mu C)_{\alpha\beta} P_\mu \delta^{ij} + C_{\alpha\beta}(U^{ij} + \gamma_5 V^{ij}). \end{aligned} \quad (1.2)$$

Les  $P^\mu$  sont les générateurs des translations :  $P^\mu = -i\partial^\mu$ . L'indice  $\alpha$  des  $Q_\alpha^i$  est un indice spinoriel variant de 1 à 4 car les  $Q_\alpha^i$ , générateurs de la supersymétrie, sont des spineurs de Majorana. L'indice  $i$  des  $Q_\alpha^i$  distingue les différents générateurs. Dans le cas d'une supersymétrie à  $N$  générateurs, l'indice  $i$  varie de 1 à  $N$ . Les  $M^{\mu\nu}$  sont les générateurs du groupe de Poincaré :  $M^{\mu\nu} = i(x^\mu \partial^\nu - x^\nu \partial^\mu)$  pour une représentation de champ scalaire, et  $M^{\mu\nu} = \frac{i}{2}\gamma^{\mu\nu}$  pour une représentation de champ spinoriel. Enfin,  $U^{ij}$  et  $V^{ij}$  sont les charges centrales.

Les trois premières relations de Eq.1.2 ne sont rien d'autre que l'algèbre de Lie du groupe de Poincaré. Cherchons à expliquer la quatrième relation qui d'après Eq.1.1 est du type :

$$[M^{\mu\nu}, Q_\alpha^i] = (b^{\mu\nu})_\alpha^\beta Q_\beta^i. \quad (1.3)$$

En utilisant Eq.(1.3) et l'identité de Jacobi :  $[[B_1, B_2], F_3] + [[B_2, F_3], B_1] + [[F_3, B_1], B_2] = 0$ , avec  $B_1 = M^{\mu\nu}$ ,  $B_2 = M^{\rho\sigma}$  et  $F_3 = Q_\beta^i$ , on trouve :

$$[b^{\mu\nu}, b^{\rho\sigma}] = -i(\eta^{\mu\rho} M^{\nu\sigma} + \eta^{\nu\sigma} M^{\mu\rho} - \eta^{\nu\rho} M^{\mu\sigma} - \eta^{\mu\sigma} M^{\nu\rho}). \quad (1.4)$$

Ce commutateur est celui des générateurs  $M^{\mu\nu}$ . Ainsi, les  $b^{\mu\nu}$  forment une représentation de l'algèbre de Lorentz pour les spineurs. Leur expression est connue et vaut :  $b^{\mu\nu} = \frac{i}{2}\gamma^{\mu\nu}$ , d'où la quatrième relation. Par un raisonnement similaire, on obtient la cinquième relation, qui montre l'indépendance des transformations de supersymétrie vis à vis des translations.

Nous reviendrons plus tard sur la dernière relation. Étudions une conséquence importante de la cinquième relation : Soit un champ scalaire  $z$  et son partenaire supersymétrique un champ spinoriel  $\Psi$ . La cinquième relation entraîne :

$$\begin{aligned} [P^\mu P_\mu, Q_\alpha^i] = 0 &\Leftrightarrow P^2 Q_\alpha^i |z\rangle = Q_\alpha^i P^2 |z\rangle \Leftrightarrow \\ P^2 |\Psi\rangle = Q_\alpha^i (m^2 |z\rangle) &\Leftrightarrow m' |\Psi\rangle = m |\Psi\rangle \Leftrightarrow m = m'. \end{aligned} \quad (1.5)$$

Ainsi, les particules membres d'un même supermultiplet ont la même masse.

La transformation de supersymétrie infinitésimale d'un champ  $\phi$  s'écrit :

$$\delta\Phi = i\bar{\mathcal{E}}^\alpha Q_\alpha \Phi, \quad (1.6)$$

où  $\delta$  représente la transformation infinitésimale de supersymétrie et  $\mathcal{E}^\alpha$  ( $\alpha = 1, \dots, 4$ ), qui est un spineur anti-commutant (variable de Grassmann) satisfaisant à la condition de Majorana, est le paramètre de cette transformation. Des variables de Grassmann  $\mathcal{E}^\alpha$  ( $\alpha = 1, \dots, 4$ ) sont définies par les propriétés d'anti-commutation suivantes,

$$\{\mathcal{E}_1, \mathcal{E}_2\} = 0, \quad \{\mathcal{E}, Q\} = 0, \quad (1.7)$$

où  $\mathcal{E}_1$  et  $\mathcal{E}_2$  sont les paramètres associés à deux transformations infinitésimales de supersymétrie. Notons que le paramètre de transformation infinitésimale de supersymétrie  $\mathcal{E}^\alpha$  est indépendant de l'espace-temps dans le cas de la supersymétrie globale. Une transformation finie de supersymétrie sur un supermultiplet s'obtient par exponentiation de Eq.(1.6) :

$$\Phi' = \exp(i\bar{\mathcal{E}}^\alpha Q_\alpha) \Phi. \quad (1.8)$$

### 1.3 Motivations de la supersymétrie

Quelles sont aujourd'hui les motivations pour la supersymétrie ? Tout d'abord, la supersymétrie (SUSY) apporte un cadre particulièrement propice aux théories de grande unification dites théories GUT (Grand Unification Theory) [11, 12, 13, 14] ainsi qu'aux modèles d'unification des forces incluant la gravitation vers  $10^{19} GeV$  : Les théories de cordes (supercordes si elles incluent SUSY). Dans le modèle GUT supersymétrique basé sur le groupe de jauge  $SU(5)$ , si l'échelle effective de brisure de la supersymétrie est de l'ordre du  $TeV$ , les trois constantes de couplage du Modèle Standard s'unifient à l'échelle d'unification  $M_{GUT}$ , ce qui n'est pas le cas dans le modèle non supersymétrique GUT basé sur le groupe de jauge  $SU(5)$ . De plus, dans le modèle GUT  $SU(5)$  supersymétrique, l'échelle d'unification est repoussée de  $M_{GUT} \approx 10^{15} GeV$  (cas du modèle GUT  $SU(5)$  non supersymétrique) à  $M_{GUT} \approx 2 \cdot 10^{16} GeV$  ce qui augmente le temps de vie du proton. Notons cependant que dans les théories SUSY, la stabilité du proton est menacée par des opérateurs non renormalisables. Par ailleurs, SUSY offre un candidat naturel pour la masse cachée de l'Univers : La LSP (Lightest Supersymmetric Particle), qui est la particule supersymétrique la plus légère. En effet, la LSP est stable (excepté dans les scénarios dans lesquels la symétrie de R-parité est violée, comme nous le discuterons au début de la Section 4.1) et interagit faiblement avec la matière. Mais la principale motivation pour les théories SUSY reste la résolution du problème des hiérarchies d'échelles de masse comme nous le discuterons dans la prochaine Section.

### 1.3.1 Le problème des hiérarchies d'échelles

Le problème de hiérarchie est la grande différence entre l'échelle de brisure électrofaible qui est de l'ordre du  $TeV$  et l'échelle de la physique sous-jacente au Modèle Standard : l'échelle d'unification  $M_{GUT}$ , l'échelle des cordes  $M_{string}$ , l'échelle de Planck  $M_P, \dots$ . L'avantage des théories supersymétriques vis à vis de cette difficulté, comme nous allons le voir maintenant, est la possibilité de conserver au niveau des corrections radiatives une hiérarchie existant dans le potentiel effectif obtenu à l'ordre des arbres. Cette possibilité est liée à l'existence du théorème de non-renormalisation (voir Section 1.4.10) qui prédit notamment que les termes de masse des champs scalaires ne sont pas affectés par les corrections radiatives quadratiques dans les théories SUSY. Cette invariance provient de l'annulation de toutes les divergences quadratiques dans les théories SUSY qui est due elle à la compensation entre des graphes échangeant des particules du Modèle Standard et les graphes associés qui impliquent leur partenaire supersymétrique. Assurer la stabilité des hiérarchies de masse est certes important mais ne répond pas à l'autre question de nature 'dynamique' : Pourquoi existe-t-il des hiérarchies d'échelles d'énergie dans la nature et quelle est la dynamique responsable de leur apparition ? En effet, les théories SUSY n'apportent pas d'explication évidente à l'origine de ces deux échelles d'énergie si différentes qui apparaissent dans le potentiel à l'ordre des arbres. Dans certaines théories de supercordes, la valeur prédite de l'échelle de brisure de la symétrie GUT est proche de l'échelle des cordes, qui est elle-même reliée à l'échelle de Planck. Mais dans ce type de théories, l'origine de l'échelle de brisure électrofaible reste problématique. Une solution envisageable à ce problème est que l'échelle de brisure électrofaible soit déterminée par les corrections radiatives. Plus précisément, dans des modèles comportant des termes de brisure de la supersymétrie, la masse au carré du boson de Higgs du Modèle Standard est positive à l'échelle GUT mais l'évolution des constantes de couplages par le groupe de renormalisation rend la masse au carré du Higgs négative à l'échelle du  $TeV$ , provoquant ainsi la brisure électrofaible à l'échelle d'énergie souhaitée [15, 16]. Le problème de hiérarchie peut être expliqué de deux manières différentes que nous allons décrire maintenant.

La première explication du problème de hiérarchie s'appuie sur les valeurs moyennes dans le vide (VEV) du boson de Higgs et d'un boson associé à la brisure du groupe de jauge d'une théorie de grande unification. Dans les théories GUT, une première échelle d'énergie détermine l'échelle de brisure  $M_{GUT}$  de la symétrie GUT. Cette échelle est donnée par la VEV d'un champ  $\Phi$  et vaut typiquement,

$$\langle 0|\Phi|0 \rangle = V = O(10^{15} GeV). \quad (1.9)$$

La seconde échelle d'énergie de ces modèles est l'échelle de brisure électrofaible qui doit être,

$$\langle 0|\phi|0 \rangle = v \simeq 246 GeV. \quad (1.10)$$

Le problème de hiérarchie vient de la grande disparité entre ces deux échelles,

$$\frac{V}{v} = O(10^{13}), \quad (1.11)$$

ainsi que de la difficulté à rendre la coexistence de ces 2 échelles naturelle. Le potentiel effectif au niveau en arbres pour ces champs scalaires  $\Phi$  et  $\phi$  est,

$$V_0(\Phi, \phi) = -\frac{1}{2}A\Phi^2 + \frac{1}{4}B\Phi^4 - \frac{1}{2}a\phi^2 + \frac{1}{4}b\phi^4 + \frac{1}{2}\lambda\Phi^2\phi^2. \quad (1.12)$$

La brisure de la symétrie GUT (associée à l'échelle 1.9) est assurée par la condition,

$$V^2 = \frac{A}{B}, \quad (1.13)$$

qui fixe la masse du champ de Higgs lourd  $\Phi$ . Le problème vient en fait du terme  $\frac{1}{2}\lambda\Phi^2\phi^2$  qui est présent si  $A \neq 0$  et  $a \neq 0$  et qui communique l'échelle d'énergie  $V$  au secteur du champ de Higgs  $\phi$ . Le champ de Higgs lourd  $\Phi$  découple de telle sorte que la condition de brisure électrofaible devient,

$$v^2 = \frac{a - \lambda V^2}{b}. \quad (1.14)$$

D'après Eq.(1.14), afin d'obtenir l'échelle de brisure 1.10, il est nécessaire de faire un 'fine-tuning' du paramètre  $a/b$  qui doit être de l'ordre de  $(V/v)^2 \approx 10^{26} GeV$  (voir Eq.(1.11)). C'est précisément ce réglage fin qui n'est pas considéré comme étant naturel. Le problème de fine-tuning est accentué par le fait que les corrections radiatives produisent des corrections à l'ordre des boucles au potentiel effectif de telle sorte que le fine-tuning des paramètres,  $a, \lambda, V, b$ , du potentiel doit être refait à chaque ordre de la théorie des perturbations. C'est à ce stade que les théories SUSY sont intéressantes, car l'annulation des divergences quadratiques qui leur est propre assure que la masse du boson de Higgs  $\sqrt{a}$  (voir Eq.(1.12)) n'est pas modifiée par ces divergences quadratiques et donc que le fine-tuning ne doit être effectué qu'une seule fois. La situation n'est en fait pas aussi claire car la supersymétrie doit être brisée et les masses des particules du Modèle Standard doivent donc être différentes des masses de leur partenaire supersymétrique, comme nous le discuterons par la suite. Par conséquent, il ne doit pas y avoir d'annulation entre des graphes échangeant des particules du Modèle Standard et les graphes associés qui impliquent leur partenaire supersymétrique. Il doit donc exister des divergences quadratiques dans les théories SUSY et l'on doit obtenir des corrections radiatives non nulles à la masse du boson de Higgs de l'ordre de,

$$\delta\sqrt{a} \sim \frac{\lambda^2}{8\pi^2}\tilde{m}^2, \quad (1.15)$$

où  $\tilde{m}$  représente la différence de masse typique entre les particules du Modèle Standard et leur partenaire supersymétrique, et,  $\lambda$  est un couplage de Yukawa ou une constante de couplage associée à un groupe jauge. Le problème du fine-tuning à chaque ordre de la théorie des perturbations peut donc être résolu dans les théories SUSY mais uniquement pour un écart de masse dans le multiplet supersymétrique de l'ordre de l'échelle électrofaible donnée dans Eq.(1.10), ce qui s'écrit dans nos notations,

$$\tilde{m} \sim v. \quad (1.16)$$

En conclusion, les masses des particules supersymétriques ainsi que l'échelle de brisure électrofaible doivent être de l'ordre du TeV si l'on veut que le problème de hiérarchie soit "résolu" par la supersymétrie.

Certaines théories de supergravité (voir Chapitre 2) permettent d'engendrer des masses pour les particules supersymétriques de l'ordre du TeV. Ces modèles assument l'existence d'un secteur caché qui n'interagit avec les particules du secteur observable (quarks, leptons,...) que par les interactions gravitationnelles. Dans ces modèles, on peut obtenir des masses pour les particules SUSY de l'ordre de,

$$\tilde{m} \sim \frac{M_s^2}{M_P}, \quad (1.17)$$

où  $M_s$  est l'échelle de brisure de la supersymétrie et  $M_P$  est la masse de Planck. Donc, l'échelle du TeV requise pour l'écart de masse des supermultiplets est obtenue dans ces modèles si ,

$$M_s = O(10^{10} GeV). \quad (1.18)$$

De plus, dans les modèles de supergravité appelés 'no-scale' [17, 18, 19, 20, 21] cette échelle de brisure SUSY,  $M_s$ , est obtenue naturellement comme une suppression de l'échelle de Planck,  $M_P$ .

La seconde explication du problème de hiérarchie est basée uniquement sur l'étude du secteur scalaire du Modèle Standard, à savoir le secteur du boson de Higgs. Ce point de vue n'est donc pas restreint au seul cas des théories GUT mais est valable pour toute nouvelle physique au-delà du Modèle Standard. Dans le Modèle Standard, le potentiel du boson de Higgs  $H$  est  $V = -\mu^2 H H^\dagger + \frac{1}{2} \lambda (H H^\dagger)^2$  ce qui donne une valeur dans le vide à  $H H^\dagger$  de  $\frac{\mu^2}{\lambda}$ . Nous connaissons aujourd'hui les masses des bosons de jauge  $W^\pm$  et  $Z^0$  qui donnent à  $\langle H H^\dagger \rangle$  une valeur de l'ordre de  $10^4 GeV^2$ .  $\lambda$  ne pouvant pas être arbitrairement petit,  $\mu^2$  doit être du même ordre de grandeur que  $\langle H H^\dagger \rangle$ . Au niveau en arbre, nous pouvons donner à  $\mu^2$  sa valeur exacte (inconnue aujourd'hui). Cependant, les corrections quantiques ne préserveront pas ce choix. En effet, l'équation de renormalisation à une boucle est,

$$\mu_{RE}^2 = \mu^2 + C \alpha^2 M^2, \quad (1.19)$$

où  $\mu_{RE}$  est le paramètre  $\mu$  renormalisé et  $C$  un nombre de l'ordre de  $100 \pm 1$ .  $M$  est la coupure ultraviolette, identifiée à l'échelle de toute nouvelle physique sous-jacente au Modèle Standard pouvant exister à haute énergie. Par exemple,  $M = M_P = M_{PLANCK} \approx 10^{19} GeV$ ,  $M = M_{GUT} \approx 2 \cdot 10^{16} GeV$  ou toute autre échelle comprise entre  $M_P$  et l'échelle de Fermi :  $M_W = 80 GeV$ .  $\alpha$  est un paramètre relié aux constantes de couplage des interactions électrofaible et forte.  $\alpha$  ne pouvant être arbitrairement petit, il y a une différence d'ordre de grandeur entre  $\mu$  et  $\mu_{RE}$  d'à peu près  $10^{30} GeV^2$ . Il faut donc ajuster  $\mu^2$  très précisément de façon à ce que  $\mu_{RE}^2$  ait la bonne valeur, c'est à dire de l'ordre de  $10^4 GeV^2$  (fine-tuning). De plus, un nouvel ajustement doit être effectué à chaque ordre de la théorie des perturbations. Il est donc clair que l'existence de plusieurs échelles de masse n'est pas du tout naturelle. On retrouve le problème des hiérarchies d'échelles. Dans le cadre d'une théorie de SUSY, l'absence des divergences quadratiques assure que  $\mu^2$  est au plus logarithmiquement renormalisable et l'expression 1.19 de la masse renormalisée du boson de Higgs devient donc,

$$\mu_{RE}^2 = \mu^2 [1 + C \alpha^2 \ln(\frac{M^2}{\mu^2})]. \quad (1.20)$$

$\mu_{RE}^2$  et  $\mu^2$  sont maintenant du même ordre de grandeur et le problème de naturalité est résolu : Modifier très peu les paramètres fondamentaux (ici  $M$ ) n'affecte plus la physique à basse énergie.

Remarquons dans ce contexte une analogie entre le boson de Higgs et les autres particules du Modèle Standard. La masse des bosons de jauge est ‘protégée’ par les symétries de jauge et celle des fermions est ‘protégée’ par la nature chirale (par opposition à vectorielle) du groupe de jauge électrofaible. Quant à la masse des bosons de Higgs, sans être contrainte à prendre une valeur nulle, elle est ‘protégée’ des divergences quadratiques par la supersymétrie (voir 1.20).

## 1.4 Formalisme des théories supersymétriques

### 1.4.1 Exemple du spineur de Weyl

Établissons les transformations supersymétriques laissant invariant le lagrangien d'un spineur de Weyl libre. Le spineur de Weyl a un spin 1/2 et une hélicité donnée. Par conséquent, le spineur de Weyl ne possède que deux composantes non nulles et n'est pas massif. Les deux composantes non nulles d'un spineur de Weyl d'hélicité gauche (droite) décrivent l'hélicité gauche (droite) de la particule et l'hélicité droite (gauche) de l'antiparticule. Le spineur de Weyl est défini par :

$$L\Psi_L = \Psi_L \text{ ou } R\Psi_R = \Psi_R, \text{ avec } L = \frac{1 + \gamma_5}{2} \text{ et } R = \frac{1 - \gamma_5}{2}, \quad (1.21)$$

selon qu'il est d'hélicité gauche ( $\Psi_L$ ) ou droite ( $\Psi_R$ ). Considérons le lagrangien d'un spineur de Weyl d'hélicité gauche  $\Psi_L$  libre et de son partenaire scalaire supersymétrique  $\phi$  :

$$\mathcal{L} = (\partial_\mu \phi)^* (\partial^\mu \phi) + \bar{\Psi}_L (i\gamma_\mu \partial^\mu) \Psi_L, \quad (1.22)$$

avec selon nos notations,

$$\bar{\Psi}_L = \overline{(\Psi_L)} = \overline{(L\Psi)} = (L\Psi)^\dagger \gamma_0. \quad (1.23)$$

Les partenaires supersymétriques des champs fermioniques de spin 1/2 sont des champs scalaires et sont appelés sfermions (s pour scalaire) : squarks, sleptons,..., tandis que les partenaires des champs bosoniques sont des champs fermioniques de spin 1/2 et ont un nom prenant un suffixe ‘ino’ : wino, zino, photino, gluino, higgsino,... Les transformations de la supersymétrie  $N=1$  (voir Section 1.2) les plus générales laissant invariant le lagrangien 1.22 s'écrivent :

$$\begin{aligned} \delta\phi &= \sqrt{2}\bar{\mathcal{E}}_R \Psi_L, \\ \delta\phi^* &= \sqrt{2}\bar{\Psi}_L \mathcal{E}_R, \\ \delta\Psi_L &= -i\sqrt{2}\gamma^\mu \partial_\mu \phi \mathcal{E}_R, \\ \delta\bar{\Psi}_L &= -i\sqrt{2}\mathcal{E}_R \gamma^\mu \partial_\mu \phi^*. \end{aligned} \quad (1.24)$$

Nous avons adopté la notation :  $\mathcal{E}_R \Psi_L = \mathcal{E}_R^\alpha \Psi_{L\alpha}$  (voir Section 1.2). Les deux premières relations de Eq.1.24 sont des égalités entre scalaires et les deux dernières entre spineurs. Le

paramètre  $\mathcal{E}_R$  de cette transformation doit être un spineur de Weyl d'hélicité droite pour éviter  $\delta\phi = 0$  et afin d'avoir  $L\delta\Psi_L = \delta\Psi_L$ . Le facteur  $\sqrt{2}$  permet de simplifier les calculs. Remarquons finalement que le lagrangien 1.22 n'est invariant par les transformations 1.24 qu'à une dérivée près, mais les termes en dérivées du lagrangien ne modifient pas les équations du mouvement. En effet, l'action s'obtient en intégrant le lagrangien, or ces termes s'annulent après intégration car ils deviennent alors des valeurs de champs pris à l'infini.

### 1.4.2 Exemple du spineur de Majorana

Considérons maintenant un lagrangien décrivant un spineur de Majorana libre et son partenaire supersymétrique. Un spineur de Majorana est égal à son spineur conjugué de charge, ce qui s'écrit :

$$\Psi = \Psi^c = C\bar{\Psi}^T \quad (1.25)$$

où  $C$  est l'opérateur conjugaison de charge. D'après nos notations, nous écrivons,

$$\bar{\Psi}_H^c = \overline{[(\Psi^c)_H]} = \overline{[P_H(\Psi^c)]}, \quad H = L, R. \quad (1.26)$$

Le spineur de Majorana n'a que 2 composantes indépendantes du fait de la relation 1.25. Considérons le lagrangien décrivant un spineur de Majorana  $\Psi$  libre ainsi que son partenaire supersymétrique  $\phi$  :

$$\mathcal{L} = \frac{1}{2}(\partial_\mu B)(\partial^\mu B) + \frac{1}{2}(\partial_\mu A)(\partial^\mu A) - \frac{1}{2}m^2(A^2 + B^2) + \frac{1}{2}\bar{\Psi}(i\gamma_\mu\partial^\mu - m)\Psi \quad (1.27)$$

où  $A$  et  $B$  sont des champs scalaires réels tels que  $\phi = (A + iB)/\sqrt{2}$ . Il est plus transparent de travailler au niveau des champs  $A$  et  $B$  car les transformations de supersymétrie doivent respecter l'invariance sous la parité du lagrangien 1.25, c'est à dire que l'on doit avoir  $\delta A \rightarrow \delta A$  et  $\delta B \rightarrow -\delta B$  puisque les champs  $A$  et  $B$  se transforment sous l'action de l'opérateur parité par  $A \rightarrow A$  et  $B \rightarrow -B$ . Le spineur de Majorana se transforme sous l'action de l'opérateur parité selon :  $\Psi \rightarrow \gamma_0\Psi$ . Le lagrangien 1.27 est invariant sous les transformations de supersymétrie  $N = 1$  (voir Section 1.2) suivantes :

$$\begin{aligned} \delta A &= \bar{\mathcal{E}}\Psi, \\ \delta B &= i\bar{\mathcal{E}}\gamma_5\Psi, \\ \delta\Psi &= -[i\gamma^\mu\partial_\mu(A + iB\gamma_5) + m(A + iB\gamma_5)]\mathcal{E}, \end{aligned} \quad (1.28)$$

où le paramètre  $\mathcal{E}$  de transformation est un spineur de Majorana afin que sous l'action de l'opérateur parité on ait :  $\delta\Psi = \delta\Psi^c = C(\overline{\delta\Psi})^T$ . Nous remarquons d'après Eq.(1.27) que  $A$ ,  $B$  et  $\Psi$ , qui constituent le supermultiplet  $(A, B, \Psi)$ , ont la même masse. On retrouve une des propriétés de la supersymétrie : Les membres d'un même supermultiplet ont des masses identiques.

### 1.4.3 Champs auxiliaires

On dit que l'algèbre de supersymétrie ferme lorsque :

$$[\delta_1, \delta_2] = i\Delta_\mu P^\mu, \text{ avec } \Delta_\mu = -2i(\bar{\mathcal{E}}_2\gamma_\mu\mathcal{E}_1) \text{ et } P^\mu = -i\partial^\mu, \quad (1.29)$$



	BOSONS	Degrés de liberté	FERMIONS	Degrés de liberté
OFF SHELL	$A, B, F$ et $G$	$4 \times 1$	$\Psi$	$1 \times 4$
ON SHELL	$A$ et $B$	$2 \times 1$	$\Psi$	$1 \times 2$

TAB. 1.1: Degrés de liberté fermioniques et bosoniques dans un supermultiplet associé à un spineur de Majorana.

$\delta_1, \delta_2$  étant les variations infinitésimales associées à 2 transformations de supersymétrie, et  $\mathcal{E}_1, \mathcal{E}_2$  étant les paramètres de ces 2 transformations. Remarquons par ailleurs que,

$$[\delta_1, \delta_2] = -[\bar{\mathcal{E}}_1 Q, \bar{\mathcal{E}}_2 Q] = \bar{\mathcal{E}}_1 \bar{\mathcal{E}}_2 \{Q^\alpha, Q^\beta\}, \quad (1.30)$$

car les  $\mathcal{E}^\alpha$  sont des variables de Grassmann qui vérifient par définition les relations de Eq.(1.7). Les relations de Eq.(1.29) et Eq.(1.30) conduisent à la relation d’anti-commutation des générateurs  $Q$  de la supersymétrie (voir Eq.(1.2)). Donc, la condition de fermeture de l’algèbre de SUSY (Eq.(1.29)) permet de retrouver l’algèbre de SUSY (voir Eq.(1.2)).

La relation de Eq.(1.29) est satisfaite lorsque les particules sont sur la couche de masse (“on shell”), c’est à dire quand les champs vérifient les équations de mouvement du lagrangien correspondant. La relation de Eq.(1.29) est par exemple vérifiée dans les deux cas traités dans les Sections 1.4.1 et 1.4.2 si les particules sont on shell. Pour le spineur de Weyl du lagrangien 1.22, l’équation du mouvement est :  $\gamma_\mu \partial^\mu \Psi_L = 0$ , et pour le spineur de Majorana du lagrangien 1.27, l’équation du mouvement est  $(i\gamma_\mu \partial^\mu - m)\Psi = 0$ .

Afin que la relation de Eq.(1.29) soit aussi vérifiée dans le formalisme hors couche (“off shell”), on introduit des champs dits “auxiliaires”. Par exemple, dans le cas du spineur de Weyl (voir Section 1.4.1), on introduit le champ auxiliaire scalaire complexe  $f$  en ajoutant au lagrangien la partie  $\mathcal{L}_{AUX} = f f^\dagger$ , et en adjoignant la nouvelle loi de transformation pour  $f$  :  $\delta f = i\sqrt{2}\bar{\mathcal{E}}_R \gamma^\mu \partial_\mu \Psi_L$ . La relation de transformation du spineur de Weyl de Eq.(1.24) devient alors  $\delta \Psi_L = -\sqrt{2}(i\gamma^\mu \partial_\mu \phi + f)\mathcal{E}_R$ . L’équation de mouvement du champ  $f$  est  $f = 0$ . Dans le cas du spineur de Majorana (voir Section 1.4.2), on introduit les deux champs auxiliaires scalaires réels  $F$  et  $G$  en ajoutant au lagrangien le terme :  $\mathcal{L}_{AUX} = (F^2 + G^2)/2 - m(A F + B G)$ . Les lois de transformation de  $F$  et  $G$  sont :  $\delta F = i\bar{\mathcal{E}} \gamma^\mu \partial_\mu \Psi$  et  $\delta G = -\bar{\mathcal{E}} \gamma^\mu \partial_\mu \Psi$ . La relation de transformation du spineur de Majorana de Eq.(1.28) devient alors :  $\delta \Psi = -[i\gamma^\mu \partial_\mu (A + iB\gamma_5) + (F + iG\gamma_5)]\mathcal{E}$ . Les équations de mouvement des  $F$  et  $G$  sont  $F = mA$  et  $G = mB$ . Les champs auxiliaires ont aussi l’intérêt de rendre égaux les nombres de degrés de liberté fermioniques et bosoniques dans un supermultiplet chirale. Afin d’illustrer ce point, nous présentons dans la Table 1.1 les degrés de liberté dans un supermultiplet associé à un spineur de Majorana :

#### 1.4.4 Superespace

Commençons cette section par quelques rappels. Les transformations infinitésimales associées au groupe de Lorentz et aux translations s’écrivent,

$$Lorentz : \delta \Phi = i\frac{1}{2}\epsilon_{\mu\nu} M^{\mu\nu} \Phi, \quad (1.31)$$

$$Translations : \delta \Phi = i\Delta_\mu P^\mu \Phi, \quad (1.32)$$

où les paramètres de transformation associés au groupe de Lorentz  $\epsilon_{\mu\nu}$  et aux translations  $\Delta_\mu$  sont des nombres réels. Le facteur  $1/2$  apparaissant dans les transformations de

Lorentz permet d'éviter les doubles comptages liés au fait que l'on a  $M^{\mu\nu} = -M^{\nu\mu}$ . Les transformations totales associées au groupe de Lorentz et aux translations sont,

$$\text{Lorentz} : \Phi' = \exp\left(i\frac{1}{2}\epsilon_{\mu\nu}M^{\mu\nu}\right)\Phi, \quad (1.33)$$

$$\text{Translations} : \Phi' = \exp\left(i\Delta_\mu P^\mu\right)\Phi. \quad (1.34)$$

Dans le cas où  $\Phi$  est un champ scalaire, les générateurs du groupe de Lorentz et des translations sont,

$$M^{\mu\nu} = i(x^\mu\partial^\nu - x^\nu\partial^\mu), \quad P^\mu = -i\partial^\mu. \quad (1.35)$$

Si  $\Phi$  est un spineur, les générateurs du groupe de Lorentz et des translations s'écrivent alors,

$$M^{\mu\nu} = \frac{i}{4}[\gamma^\mu, \gamma^\nu], \quad P^\mu = -i\partial^\mu. \quad (1.36)$$

Enfin, une translation agit sur un champ  $\Phi$  comme :

$$\Phi'(x^\mu) = \Phi(x^\mu + \Delta_\mu). \quad (1.37)$$

Le produit anti-commutant des générateurs  $Q_\alpha$  de l'algèbre de supersymétrie est proportionnel au générateur  $P^\mu$  des translations. Il semble donc intéressant de tenter d'écrire les transformations de supersymétrie comme des translations généralisées. Pour cela l'espace-temps doit être généralisé en un espace comprenant des nouvelles coordonnées qui soient translatées par la supersymétrie : Le "superspace". Les champs contenus dans le superspace sont appelés "superchamps".

Le paramètre des transformations supersymétriques  $\mathcal{E}^\alpha$  (voir Eq.(1.6)) est un spineur anti-commutant (variable de Grassmann) qui satisfait à la condition de Majorana. Nous en déduisons d'après Eq.(1.37), par analogie entre le paramètre de transformation associé à l'algèbre de supersymétrie  $\mathcal{E}^\alpha$  (voir Eq.(1.6)) et celui associé aux translations  $\Delta_\mu$  (voir Eq.(1.32)), que les coordonnées du superspace sont,

$$(x^\mu, \theta, \bar{\theta}), \quad (1.38)$$

où  $\theta$  est aussi un spineur anti-commutant (variable de Grassmann) qui satisfait à la condition de Majorana. Un spineur de Majorana n'a que 2 composantes indépendantes (voir Section 1.4.2). Par conséquent, dans les sections suivantes, où nous allons développer le formalisme du superspace qui permet de construire de façon simple des théories supersymétriques, nous adopterons la notation à 2 composantes des spineurs. Dans la section suivante, nous rappelons donc le formalisme de la notation à 2 composantes pour les spineurs.

### 1.4.5 Notation des spineurs à deux composantes

Le champ de spin 1/2 à 2 composantes  $\psi_\alpha = \psi_L$  ( $\alpha = 1, 2$ ) appartient à la représentation (1/2,0) du groupe de Lorentz, c'est à dire qu'il se comporte comme un champ de spin

1/2 sous les transformations “gauches” et comme un champ scalaire sous les transformations “droites”, alors que le spineur à 2 composantes  $\bar{\psi}^{\dot{\alpha}} = \psi_R$  ( $\dot{\alpha} = 1, 2$ ) appartient à la représentation (0,1/2) du groupe de Lorentz.  $\psi_\alpha = \psi_L$  est donc un spineur de chiralité gauche et  $\bar{\psi}^{\dot{\alpha}} = \psi_R$  un spineur de chiralité droite. Par ailleurs, le tenseur antisymétrique à 2 indices  $\epsilon^{\alpha\beta}$  permet d’abaisser ou bien d’élever les indices des spineurs à 2 composantes :

$$\begin{aligned}\psi^\alpha &= \epsilon^{\alpha\beta}\psi_\beta, \\ \psi_\alpha &= \epsilon_{\alpha\beta}\psi^\beta.\end{aligned}\tag{1.39}$$

Les champs de spin 1/2 à 2 composantes se transforment sous le groupe de Lorentz  $SO(1, 3)$  par l’action des matrices  $M \in Sl(2, C)$  selon,

$$\begin{aligned}\psi'_\alpha &= M_\alpha^\beta \psi_\beta, & \psi'^\alpha &= (M^{-1})^\alpha_\beta \psi^\beta, \\ \bar{\psi}'_{\dot{\alpha}} &= (M^\star)_{\dot{\alpha}}^{\dot{\beta}} \bar{\psi}_{\dot{\beta}}, & \bar{\psi}'^{\dot{\alpha}} &= (M^{\star-1})^{\dot{\alpha}}_{\dot{\beta}} \bar{\psi}^{\dot{\beta}},\end{aligned}\tag{1.40}$$

l’étoile  $\star$  signifiant complexe conjugué. Les produits,

$$\psi_1 \psi_2 = \psi_1^\alpha \psi_{2\alpha}, \quad \bar{\psi}_1 \bar{\psi}_2 = \bar{\psi}_{1\dot{\alpha}} \bar{\psi}_2^{\dot{\alpha}}.\tag{1.41}$$

sont donc invariants de Lorentz. Enfin, le champ  $\Psi$  de spin 1/2 à 4 composantes et son conjugué de charge  $\Psi^c$  s’écrivent à partir des champs de spin 1/2 à 2 composantes  $\chi_\alpha$  et  $\eta_\alpha$ , comme suit,

$$\Psi = \begin{pmatrix} \chi_\alpha \\ \bar{\eta}^{\dot{\alpha}} \end{pmatrix}, \quad \bar{\Psi} = (\eta^\alpha, \bar{\chi}_{\dot{\alpha}}), \quad \Psi^c = \begin{pmatrix} \eta_\alpha \\ \bar{\chi}^{\dot{\alpha}} \end{pmatrix}, \quad \alpha = 1, 2, \quad \dot{\alpha} = 1, 2.\tag{1.42}$$

Le spineur de Majorana  $\Psi$  de spin 1/2 à 4 composantes s’écrit quant à lui,

$$\Psi = \begin{pmatrix} \chi_\alpha \\ \bar{\chi}^{\dot{\alpha}} \end{pmatrix}, \quad \alpha = 1, 2, \quad \dot{\alpha} = 1, 2.\tag{1.43}$$

Les produits  $\bar{\Psi}_1 P_{L,R} \Psi_2$  de spineurs à 4 composantes  $\Psi_1$  et  $\Psi_2$  s’écrivent à partir des spineurs à 2 composantes  $\chi_\alpha$  et  $\eta_\alpha$ , comme suit,

$$\bar{\Psi}_1 P_L \Psi_2 = \eta_1 \chi_2,\tag{1.44}$$

$$\bar{\Psi}_1 P_R \Psi_2 = \bar{\eta}_2 \bar{\chi}_1.\tag{1.45}$$

Par conséquent, un produit  $\bar{\Psi}_1 \Psi_2$  s’écrit,

$$\bar{\Psi}_1 \Psi_2 = \eta_1 \chi_2 + \bar{\eta}_2 \bar{\chi}_1.\tag{1.46}$$

Écrivant le générateur de supersymétrie  $Q$ , qui est un spineur de Majorana, dans la notation à deux composantes :

$$Q = \begin{pmatrix} Q_\alpha \\ \bar{Q}^{\dot{\alpha}} \end{pmatrix},\tag{1.47}$$

ainsi que le paramètre des transformations SUSY  $\mathcal{E}$  qui est aussi un spineur de Majorana :

$$\mathcal{E} = \begin{pmatrix} \mathcal{E}_\alpha \\ \bar{\mathcal{E}}^{\dot{\alpha}} \end{pmatrix},\tag{1.48}$$

la relation d'anti-commutation des générateurs  $Q$  de la supersymétrie (voir Eq.(1.2)) devient,

$$\begin{aligned}\{Q_\alpha, Q_\beta\} &= \{\bar{Q}_{\dot{\alpha}}, \bar{Q}_{\dot{\beta}}\} = 0, \\ \{Q_\alpha, \bar{Q}_{\dot{\beta}}\} &= -2P_\mu(\sigma^\mu)_{\alpha\dot{\beta}},\end{aligned}\tag{1.49}$$

et la transformation infinitésimale de SUSY (voir Eq.(1.6)) prend la forme,

$$\delta\Phi = i(\mathcal{E}^\alpha Q_\alpha + \bar{\mathcal{E}}_{\dot{\alpha}} \bar{Q}^{\dot{\alpha}})\Phi.\tag{1.50}$$

En utilisant Eq.(1.50) ainsi que les relations de définition de variables de Grassmann  $\mathcal{E}^\alpha$  dans la notation des spineurs à 2 composantes :

$$\begin{aligned}\{\mathcal{E}^\alpha, \mathcal{E}^\beta\} &= \{\mathcal{E}^\alpha, \bar{\mathcal{E}}^{\dot{\alpha}}\} = \{\bar{\mathcal{E}}^{\dot{\alpha}}, \bar{\mathcal{E}}^{\dot{\beta}}\} = 0, \\ \{\mathcal{E}^\alpha, Q^\alpha\} &= \{\mathcal{E}^\alpha, \bar{Q}^{\dot{\alpha}}\} = \{\bar{\mathcal{E}}^{\dot{\alpha}}, Q^\alpha\} = \{\bar{\mathcal{E}}^{\dot{\alpha}}, \bar{Q}^{\dot{\alpha}}\} = 0,\end{aligned}\tag{1.51}$$

nous obtenons l'équivalent de Eq.(1.29) dans la notation à 2 composantes, à savoir,

$$[\delta_1, \delta_2] = -2(\mathcal{E}_1\sigma^\mu\bar{\mathcal{E}}_2 - \mathcal{E}_2\sigma^\mu\bar{\mathcal{E}}_1)P_\mu, \text{ avec } \mathcal{E}\sigma^\mu\bar{\mathcal{E}} = \mathcal{E}^\alpha(\sigma^\mu)_{\alpha\dot{\alpha}}\bar{\mathcal{E}}^{\dot{\alpha}}.\tag{1.52}$$

À partir de maintenant et dans tout ce qui suit, nous adopterons la notation des spineurs à 2 composantes.

### 1.4.6 Générateurs de supersymétrie dans le superspace

Déterminons la forme générale dans le superspace du générateur  $Q_\alpha$  de l'algèbre de la supersymétrie  $N = 1$ . Ce générateur  $Q_\alpha$ , qui est associé à des translations dans le superspace  $(x^\mu, \theta, \bar{\theta})$  (voir Section 1.4.4), doit agir sur les superchamps par l'intermédiaire de dérivées par rapport à  $x^\mu$ ,  $\theta$  et  $\bar{\theta}$ , de même que le générateur  $P^\mu$  des translations dans l'espace-temps à 4 dimensions agit suivant des dérivées par rapport à  $x^\mu$  (voir Section 1.4.4). La forme générale du générateur  $Q_\alpha$  dans le superspace est donc,

$$\begin{aligned}Q_\alpha &= a_\alpha^\mu \partial_\mu + b \frac{\partial}{\partial \theta^\alpha} + c_{\alpha\dot{\alpha}} \frac{\partial}{\partial \bar{\theta}_{\dot{\alpha}}}, \\ \bar{Q}_{\dot{\alpha}} &= \bar{a}_{\dot{\alpha}}^\mu \partial_\mu + \bar{b} \frac{\partial}{\partial \bar{\theta}_{\dot{\alpha}}} + \bar{c}_{\dot{\alpha}}^\alpha \frac{\partial}{\partial \theta^\alpha}.\end{aligned}\tag{1.53}$$

où  $b$  et  $\bar{b}$  sont des nombres complexes indépendants.

Raisonnons par les dimensions. D'après Eq.(1.49),  $[Q_\alpha] = [\bar{Q}_{\dot{\alpha}}] = 1/2$  puisque  $P_\mu = -i\partial_\mu$  et  $[\partial_\mu] = 1$  (voir Appendice A). Par conséquent,  $[\mathcal{E}^\alpha] = [\bar{\mathcal{E}}_{\dot{\alpha}}] = -1/2$  selon Eq.(1.50). De plus, d'après Eq.(1.53),  $[a_\alpha^\mu] = [\bar{a}_{\dot{\alpha}}^\mu] = -1/2$  car  $[Q_\alpha] = [\bar{Q}_{\dot{\alpha}}] = 1/2$  et  $[\partial_\mu] = 1$ . Ayant  $[\theta^\alpha] = [\bar{\theta}_{\dot{\alpha}}] = [\mathcal{E}^\alpha] = [\bar{\mathcal{E}}_{\dot{\alpha}}] = -1/2$ , il est naturel de poser :

$$\begin{aligned}a_\alpha^\mu &= a(\sigma^\mu)_{\alpha\dot{\alpha}}\bar{\theta}^{\dot{\alpha}}, \\ \bar{a}_{\dot{\alpha}}^\mu &= \bar{a}\theta^\alpha(\sigma^\mu)_{\alpha\dot{\alpha}},\end{aligned}\tag{1.54}$$

où  $a$  et  $\bar{a}$  sont des nombres complexes indépendants tels que  $[a] = [\bar{a}] = 0$ . De plus,  $[c_{\alpha\dot{\alpha}}] = [\bar{c}_{\dot{\alpha}}^\alpha] = 0$  car  $[Q_\alpha] = [\bar{Q}_{\dot{\alpha}}] = 1/2$  et  $[\partial/\partial\theta^\alpha] = [\partial/\partial\bar{\theta}_{\dot{\alpha}}] = 1/2$ . Une inspection systématique montre que  $c_{\alpha\dot{\alpha}} = \bar{c}_{\dot{\alpha}}^\alpha = 0$ .

L'anti-commutateur  $\{Q_\alpha, \bar{Q}_\beta\}$  vaut,

$$\{Q_\alpha, \bar{Q}_\beta\} = (\bar{a}b + a\bar{b})(\sigma^\mu)_{\alpha\beta}\partial_\mu. \quad (1.55)$$

D'après Eq.(1.49) et sachant que  $P_\mu = -i\partial_\mu$ , on obtient  $\bar{a}b + a\bar{b} = -2i$ . L'algèbre de SUSY laisse donc un certain arbitraire dans le choix de  $a, \bar{a}, b$  et  $\bar{b}$ . On choisira ces nombres tels que :

$$\begin{aligned} Q_\alpha &= -i\left(\frac{\partial}{\partial\theta^\alpha} - i(\sigma^\mu)_{\alpha\dot{\alpha}}\bar{\theta}^{\dot{\alpha}}\partial_\mu\right), \\ \bar{Q}_{\dot{\alpha}} &= -i\left(-\frac{\partial}{\partial\bar{\theta}^{\dot{\alpha}}} + i\theta^\alpha(\sigma^\mu)_{\alpha\dot{\alpha}}\partial_\mu\right). \end{aligned} \quad (1.56)$$

### 1.4.7 Superchamps

Les superchamps  $S$  doivent être des fonctions des coordonnées du superspace à savoir  $x^\mu, \theta_\alpha$  et  $\bar{\theta}^{\dot{\alpha}}$ . Les puissances cubiques des variables de Grassmann s'annulent :  $\theta^\alpha\theta^\beta\theta^\gamma = 0$  ( $\alpha, \beta, \gamma = 1, 2$ ), car  $\theta^1\theta^1 = \theta^2\theta^2 = 0$  d'après Eq.(1.7). Par conséquent, la forme générale d'un superchamp  $S(x^\mu, \theta_\alpha, \bar{\theta}^{\dot{\alpha}})$  est :

$$\begin{aligned} S(x, \theta, \bar{\theta}) &= z(x) + \theta\psi(x) + \bar{\theta}\bar{\chi}(x) + \theta\theta f(x) + \bar{\theta}\bar{\theta}g(x) + \theta\sigma^\mu\bar{\theta}v_\mu(x) \\ &\quad + \theta\theta\bar{\theta}\bar{\lambda}(x) + \bar{\theta}\bar{\theta}\theta\eta(x) + \theta\theta\bar{\theta}\bar{\theta}D(x), \end{aligned} \quad (1.57)$$

où  $v_\mu(x)$  est un champ vectoriel complexe,  $z(x), f(x), g(x)$  et  $D(x)$  sont des champs scalaires complexes,  $\psi(x), \chi(x), \lambda(x)$ , et  $\eta(x)$  sont des champs de spin 1/2 à deux composantes, et où, d'après nos notations,  $\theta\theta = \theta^\alpha\theta_\alpha$ ,  $\bar{\theta}\bar{\theta} = \bar{\theta}_{\dot{\alpha}}\bar{\theta}^{\dot{\alpha}}$ ,  $\theta\psi = \theta^\alpha\psi_\alpha$  et  $\bar{\theta}\bar{\psi} = \bar{\theta}_{\dot{\alpha}}\bar{\psi}^{\dot{\alpha}}$  avec  $\alpha = 1, 2$  et  $\dot{\alpha} = 1, 2$ . L'expression générique 1.57 d'un superchamp  $S(x, \theta, \bar{\theta})$  indique que la dimension d'un superchamp est  $[S(x, \theta, \bar{\theta})] = [z(x)] = 1$  (voir Appendice A) et que le produit de superchamps est lui-même un superchamp. Eq.(1.57) montre aussi que le superchamp le plus général  $S(x, \theta, \bar{\theta})$  contient 16 degrés de liberté fermioniques ainsi que 16 degrés de liberté bosoniques, ce qui est trop pour décrire par exemple le supermultiplet  $(A, B, \Psi, F, G)$  contenant le spineur de Majorana (voir Section 1.4.3). Un moyen de réduire le nombre de degrés de liberté contenus dans un superchamp est l'imposition de contraintes.

### Superchamps chiraux

Une contrainte possible est l'annulation de certaines dérivées  $D_\alpha, \bar{D}_{\dot{\alpha}}$  du superchamp. Afin que cette contrainte soit consistante, les dérivées  $D_\alpha, \bar{D}_{\dot{\alpha}}$  doivent se transformer de façon covariante sous la supersymétrie :

$$D_\alpha(\delta S) = \delta(D_\alpha S), \quad \bar{D}_{\dot{\alpha}}(\delta S) = \delta(\bar{D}_{\dot{\alpha}} S) \quad (1.58)$$

D'après Eq.(1.50), cette condition s'écrit :

$$\{Q_\alpha, D_\beta\} = \{\bar{Q}_{\dot{\alpha}}, D_\beta\} = \{Q_\alpha, \bar{D}_{\dot{\beta}}\} = \{\bar{Q}_{\dot{\alpha}}, \bar{D}_{\dot{\beta}}\} = 0. \quad (1.59)$$

D'après Eq.(1.56), des expressions possibles pour  $D_\alpha$  et  $\bar{D}_{\dot{\alpha}}$  sont donc par exemple,

$$D_\alpha = \frac{\partial}{\partial\theta^\alpha} - i(\sigma^\mu)_{\alpha\dot{\alpha}}\bar{\theta}^{\dot{\alpha}}\partial_\mu,$$

$$\bar{D}_{\dot{\alpha}} = \frac{\partial}{\partial \bar{\theta}^{\dot{\alpha}}} - i\theta^{\alpha}(\sigma^{\mu})_{\alpha\dot{\alpha}}\partial_{\mu}. \quad (1.60)$$

Le superchamp chiral droit  $\bar{\Phi}$  est défini par :  $D_{\alpha}\bar{\Phi} = 0$  et le superchamp chiral gauche  $\Phi$  par  $\bar{D}_{\dot{\alpha}}\Phi = 0$ . La forme des superchamps chiraux s'obtient facilement en remarquant que :

$$\begin{aligned} D_{\alpha}\bar{\theta} &= 0, \text{ et } D_{\alpha}\bar{y}^{\mu} = 0 \text{ avec } \bar{y}^{\mu} = x^{\mu} + i\theta\sigma^{\mu}\bar{\theta}, \\ \bar{D}_{\dot{\alpha}}\theta &= 0, \text{ et } \bar{D}_{\dot{\alpha}}y^{\mu} = 0 \text{ avec } y^{\mu} = x^{\mu} - i\theta\sigma^{\mu}\bar{\theta}. \end{aligned} \quad (1.61)$$

Par exemple, d'après Eq.(1.61), un superchamp chiral gauche est une fonction de  $\theta$  et  $y^{\mu}$  exclusivement :

$$\Phi(y, \theta) = z(y) + \sqrt{2}\theta\psi(y) - \theta\theta f(y). \quad (1.62)$$

Développant  $z(y)$ ,  $\psi(y)$  et  $f(y)$  autour de  $x^{\mu}$ , l'expression 1.62 devient,

$$\begin{aligned} \Phi(x, \theta, \bar{\theta}) &= z(x) + \sqrt{2}\theta\psi(x) - \theta\theta f(x) - i(\theta\sigma^{\mu}\bar{\theta})\partial_{\mu}z(x) \\ &\quad + \frac{i}{\sqrt{2}}\theta\theta(\partial_{\mu}\psi(x)\sigma^{\mu}\bar{\theta}) - \frac{1}{4}\theta\theta\bar{\theta}\bar{\theta}\partial_{\mu}\partial^{\mu}z(x). \end{aligned} \quad (1.63)$$

De même, un superchamp chiral droit s'écrit :

$$\begin{aligned} \bar{\Phi}(x, \theta, \bar{\theta}) &= \bar{z}(x) + \sqrt{2}\bar{\theta}\bar{\psi}(x) - \bar{\theta}\bar{\theta}\bar{f}(x) + i(\theta\sigma^{\mu}\bar{\theta})\partial_{\mu}\bar{z}(x) \\ &\quad - \frac{i}{\sqrt{2}}\bar{\theta}\bar{\theta}(\theta\sigma^{\mu}\partial_{\mu}\bar{\psi}(x)) - \frac{1}{4}\theta\theta\bar{\theta}\bar{\theta}\partial_{\mu}\partial^{\mu}\bar{z}(x). \end{aligned} \quad (1.64)$$

Notons qu'un produit de superchamps chiraux est aussi un superchamp chiral car,

$$\begin{aligned} \bar{D}_{\dot{\alpha}}\Phi^n &= n\Phi^{n-1}\bar{D}_{\dot{\alpha}}\Phi = 0, \\ D_{\alpha}\bar{\Phi}^n &= n\bar{\Phi}^{n-1}D_{\alpha}\bar{\Phi} = 0. \end{aligned} \quad (1.65)$$

En calculant  $\delta\Phi = i(\mathcal{E}^{\alpha}Q_{\alpha} + \bar{\mathcal{E}}_{\dot{\alpha}}\bar{Q}^{\dot{\alpha}})\Phi$  au moyen des expressions 1.56 des générateurs de la supersymétrie, et en comparant le résultat à  $\delta\Phi(x, \theta, \bar{\theta}) = \delta z(x) + \sqrt{2}\theta\delta\psi(x) - \theta\theta\delta f(x)$ , on trouve les lois de transformations supersymétriques suivantes,

$$\begin{aligned} \delta z(x) &= \sqrt{2}\mathcal{E}\psi(x), \\ \delta\psi(x) &= -\sqrt{2}f(x)\mathcal{E} - i\sqrt{2}(\sigma^{\mu}\bar{\mathcal{E}})\partial_{\mu}z(x), \\ \delta f(x) &= -i\sqrt{2}\partial_{\mu}\psi(x)\sigma^{\mu}\bar{\mathcal{E}}. \end{aligned} \quad (1.66)$$

Les superchamps chiraux gauches  $\Phi$  (droits  $\bar{\Phi}$ ) contiennent donc les champs  $\psi_{\alpha} = \psi_L$  ( $\bar{\psi}^{\dot{\alpha}} = \psi_R$ ) de spin 1/2 et de chiralité gauche (droite) ainsi que leur partenaire supersymétrique  $z$  ( $\bar{z}$ ) qui sont des champs scalaires (voir Section 1.4.5). Par conséquent, les superchamps chiraux permettent de décrire les supermultiplets de matière, c'est à dire les supermultiplets contenant les leptons, les sleptons, les quarks, les squarks, les bosons de Higgs et les higgsinos.

## Superchamps vectoriels

Un autre choix de contrainte covariante consiste à imposer la condition de réalité à un superchamp. Un superchamp réel est dit “vectoriel”. Il est noté  $V$  et vérifie  $V = V^\dagger$ . Nous verrons que ce superchamp contient les bosons de jauge si l’on écrit la transformation de jauge comme,

$$V \rightarrow V + \Phi + \Phi^\dagger, \quad (1.67)$$

où  $\Phi$  est un superchamp chirale gauche. Dans la jauge dite de Wess-Zumino, le superchamp vectoriel ne contient que trois champs :

$$V(x^\mu, \theta, \bar{\theta}) = \theta\sigma^\mu\bar{\theta}v_\mu(x) + i\theta\theta\bar{\theta}\bar{\lambda} - i\bar{\theta}\bar{\theta}\theta\lambda + \frac{1}{2}\theta\theta\bar{\theta}\bar{\theta}D(x). \quad (1.68)$$

Notons qu’une combinaison linéaire à coefficients réels de superchamps réels est évidemment aussi un superchamp réel.

Par une méthode identique à celle utilisée dans la Section 1.4.7, on obtient les lois de transformations supersymétriques des champs contenus dans un superchamp vectoriel :

$$\begin{aligned} \delta v_\mu(x) &= i\mathcal{E}\sigma^\mu\bar{\lambda}(x) - i\lambda(x)\sigma^\mu\bar{\mathcal{E}}, \\ \delta\lambda(x) &= iD(x)\mathcal{E} - \frac{1}{2}(\sigma^\mu\bar{\sigma}^\nu\mathcal{E})(\partial_\mu v_\nu(x) - \partial_\nu v_\mu(x)), \\ \delta D(x) &= \mathcal{E}\sigma^\nu\partial_\nu\bar{\lambda}(x) + \partial_\nu\lambda(x)\sigma^\nu\bar{\mathcal{E}}. \end{aligned} \quad (1.69)$$

Les superchamps vectoriels contiennent donc des champs  $v_\mu(x)$  de spin 1 et leur partenaire supersymétrique : les champs  $\lambda(x)$  de spin 1/2. Par conséquent, les superchamps vectoriels permettent de décrire les supermultiplets de jauge, c’est à dire les supermultiplets contenant les bosons de jauges et les jauginos.

### 1.4.8 Lagrangiens supersymétriques

Remarquons que le champ auxiliaire  $f(x)$  du superchamp chirale gauche  $\Phi$ , c’est à dire la partie en  $\theta\theta$  du superchamp chirale gauche  $\Phi$  (voir Eq.(1.63)), se transforme en une dérivée sous la supersymétrie d’après Eq.(1.66). L’intégrale sur  $d^4x$  de la partie en  $\theta\theta$  d’un superchamp chirale gauche est donc invariante sous les transformations SUSY. Une puissance  $\Phi^n$  étant aussi un superchamp chirale (voir Eq.(1.65)), l’intégrale sur  $d^4x$  de sa partie en  $\theta\theta$ , notée  $[\Phi^n]_{\theta\theta}$ , est aussi invariante sous les transformations SUSY. Les intégrales sur  $d^4x$  des parties  $[\Phi^{n\dagger}]_{\theta\theta}$  et  $[\bar{\Phi}^n]_{\bar{\theta}\bar{\theta}}$  sont bien sûr aussi invariantes sous les transformations SUSY. De même, le champ auxiliaire  $D(x)$  du superchamp vectoriel  $V$ , c’est à dire la partie en  $\theta\theta\bar{\theta}\bar{\theta}$  du superchamp vectoriel  $V$  (voir Eq.(1.68)), se transforme en une dérivée sous la supersymétrie d’après Eq.(1.69). L’intégrale sur  $d^4x$  de la partie en  $\theta\theta\bar{\theta}\bar{\theta}$  d’un superchamp vectoriel est donc invariante sous les transformations SUSY. Le produit  $\Phi^\dagger\Phi$  étant un superchamp vectoriel, l’intégrale sur  $d^4x$  de sa partie en  $\theta\theta\bar{\theta}\bar{\theta}$ , notée  $[\Phi^\dagger\Phi]_{\theta\theta\bar{\theta}\bar{\theta}}$ , est aussi invariante sous les transformations SUSY. Nous pouvons donc écrire un premier lagrangien invariant sous les transformations supersymétriques :

$$\mathcal{L} = \Sigma_{i,j,k} \left( [\Phi_i^\dagger\Phi_i]_{\theta\theta\bar{\theta}\bar{\theta}} + [W(\Phi)]_{\theta\theta} + [\bar{W}(\Phi^\dagger)]_{\bar{\theta}\bar{\theta}} \right), \quad (1.70)$$

où  $W(\Phi)$  est un polynôme des superchamps chiraux gauches appelé superpotentiel et valant dans une théorie renormalisable,

$$\begin{aligned} W(\Phi) &= a_i \Phi_i + \frac{1}{2} m_{ij} \Phi_i \Phi_j + \frac{1}{3} \lambda_{ijk} \Phi_i \Phi_j \Phi_k, \\ \bar{W}(\Phi^\dagger) &= a_i^\dagger \Phi_i^\dagger + \frac{1}{2} m_{ij}^\dagger \Phi_i^\dagger \Phi_j^\dagger + \frac{1}{3} \lambda_{ijk}^\dagger \Phi_i^\dagger \Phi_j^\dagger \Phi_k^\dagger, \end{aligned} \quad (1.71)$$

$a_i$ ,  $m_{ij}$  et  $\lambda_{ijk}$  étant des constantes. Des puissances supérieures de superchamps dans le superpotentiel ne sont pas interdites mais mènent à des théories non renormalisables. Prendre la partie en  $\theta\theta$ ,  $\bar{\theta}\bar{\theta}$  ou  $\theta\theta\bar{\theta}\bar{\theta}$  revient à dériver un certain nombre de fois par rapport à  $\theta$  ou  $\bar{\theta}$ . La dérivation étant équivalente à l'intégration pour une variable de Grassmann, le lagrangien 1.70 peut aussi s'écrire,

$$\mathcal{L} = \Sigma_{i,j,k} \left( \int \Phi_i^\dagger \Phi_i d^2\theta d^2\bar{\theta} + \int W(\Phi) d^2\theta + \int \bar{W}(\Phi^\dagger) d^2\bar{\theta} \right). \quad (1.72)$$

Le lagrangien obtenu à partir du lagrangien 1.72 en remplaçant  $\Phi$  par  $\Phi(x, \theta) = z(x) + \sqrt{2}\theta\psi(x) - \theta\theta f(x)$  (voir Eq.(1.63)) est :

$$\begin{aligned} \mathcal{L} = & \Sigma_{i,j,k} \left( \frac{i}{2} (\psi_i \sigma^\mu \partial_\mu \bar{\psi}_i - \partial_\mu \psi_i \sigma^\mu \bar{\psi}_i) + (\partial^\mu z_i) (\partial_\mu z_i^\dagger) + f_i f_i^\dagger - a_i f_i - m_{ij} (z_i f_j + \frac{1}{2} \psi_i \psi_j) \right. \\ & \left. - \lambda_{ijk} (z_i z_j f_k + z_i \psi_j \psi_k) + c.c. \right), \end{aligned} \quad (1.73)$$

d'où l'on tire, en dérivant par rapport à  $f_i$ , l'équation du mouvement des champs auxiliaires  $f_i$  :

$$f_i^\dagger = a_i + m_{ij} z_j + \lambda_{ijk} z_j z_k = \frac{\partial W(z)}{\partial z_i}, \quad (1.74)$$

$W(z)$  étant défini comme en Eq.(1.71) en remplaçant les superchamps  $\Phi$  par leur composante scalaire  $z$ . Remplaçant  $f_i$  par son expression 1.74 dans l'expression 1.73 du lagrangien, on obtient :

$$\begin{aligned} \mathcal{L} = & \Sigma_{i,j} \left( \frac{i}{2} (\psi_i \sigma^\mu \partial_\mu \bar{\psi}_i - \partial_\mu \psi_i \sigma^\mu \bar{\psi}_i) + (\partial^\mu z_i) (\partial_\mu z_i^\dagger) \right. \\ & \left. - \left| \frac{\partial W(z)}{\partial z_i} \right|^2 - \frac{1}{2} \frac{\partial^2 W(z)}{\partial z_i \partial z_j} \psi_i \psi_j - \frac{1}{2} \frac{\partial^2 \bar{W}(z^*)}{\partial z_i^* \partial z_j^*} \bar{\psi}_i \bar{\psi}_j \right). \end{aligned} \quad (1.75)$$

En comparant Eq.(1.70) et Eq.(1.75), on voit que  $[\Phi_i^\dagger \Phi_i]_{\theta\theta\bar{\theta}\bar{\theta}}$  contient les termes cinétiques des spineurs à 2 composantes  $\psi_i$  (quarks et leptons) et de leur partenaire supersymétrique : les champs scalaires  $z_i$  (squarks et sleptons). On observe aussi que la partie du lagrangien associée au superpotentiel s'écrit,

$$\mathcal{L}_W = [W(\Phi)]_{\theta\theta} + [\bar{W}(\Phi^\dagger)]_{\bar{\theta}\bar{\theta}} = \int W(\Phi) d^2\theta + \int \bar{W}(\Phi^\dagger) d^2\bar{\theta} = \mathcal{L}_W^1 + \mathcal{L}_W^2, \quad (1.76)$$

$$\mathcal{L}_W^1 = \Sigma_i \left( - \left| \frac{\partial W(z)}{\partial z_i} \right|^2 \right), \quad (1.77)$$

$$\mathcal{L}_W^2 = \Sigma_{i,j} \left( - \frac{1}{2} \frac{\partial^2 W(z)}{\partial z_i \partial z_j} \psi_i \psi_j - \frac{1}{2} \frac{\partial^2 \bar{W}(z^*)}{\partial z_i^* \partial z_j^*} \bar{\psi}_i \bar{\psi}_j \right). \quad (1.78)$$

Nous voyons d'après cette expression que  $\mathcal{L}_W$  contient les couplages du potentiel et permet donc notamment de décrire les interactions de Yukawa qui couplent les bosons de Higgs  $z_i$  aux quarks et leptons  $\psi_i$ .



### 1.4.9 Théories de jauge supersymétriques

Le but de cette partie est de généraliser le formalisme des théories invariantes de jauge au cas supersymétrique. Nous nous appuyerons pour cela sur le lagrangien supersymétrique général obtenu dans Eq.(1.70).

Tout d'abord, nous remarquons qu'il manque au lagrangien de Eq.(1.70) les termes cinétiques des bosons de jauge  $v_{a\mu}$  et de leur partenaire supersymétrique de spin 1/2 : les jauginos  $\lambda_a$  (à 2 composantes). Ces termes cinétiques sont contenus dans,

$$\begin{aligned}\mathcal{L} &= \Sigma_a \left( \frac{1}{4} [W_a^\alpha W_{a\alpha}]_{\theta\theta} + \frac{1}{4} [\bar{W}_{a\dot{\alpha}} \bar{W}_a^{\dot{\alpha}}]_{\bar{\theta}\bar{\theta}} \right) \\ &= \Sigma_a \left( \frac{i}{2} (\lambda_a \sigma^\mu \partial_\mu \bar{\lambda}_a - \bar{\lambda}_a \sigma^\mu \partial_\mu \lambda_a) + \frac{1}{2} D_a^2 + F_{a\mu\nu} F_a^{\mu\nu} \right),\end{aligned}\quad (1.79)$$

où,

$$\begin{aligned}W_a^\alpha &= -\frac{1}{4} (\bar{D}\bar{D}) D_\alpha V_a, \\ \bar{W}_{a\dot{\alpha}} &= -\frac{1}{4} (D D) \bar{D}_{\dot{\alpha}} V_a,\end{aligned}\quad (1.80)$$

et,

$$F_{a\mu\nu} = \partial_\mu v_{a\nu} - \partial_\nu v_{a\mu}. \quad (1.81)$$

Le lagrangien 1.79 est invariant sous les transformations supersymétriques car  $W_a^\alpha$  et  $\bar{W}_{a\dot{\alpha}}$  sont respectivement des superchamps chiraux gauche et droit puisque  $\bar{D}_{\dot{\alpha}}(\bar{D}\bar{D}) = 0$  et  $D_\alpha(DD) = 0$ .

D'autre part, la transformation sous un groupe de jauge d'un superchamp chiral s'écrit,

$$\Phi' = \exp(i\Lambda)\Phi, \quad \Phi'^\dagger = \Phi^\dagger \exp(-i\Lambda^\dagger), \quad \Phi' = \exp(-i\Lambda)\Phi^c, \quad \text{avec } \Lambda = \Sigma_a \Lambda_a T_a, \quad (1.82)$$

où les  $\Lambda_a$  sont des paramètres réels (dépendants de l'espace-temps dans le cas d'un groupe de jauge agissant localement) et les  $T_a$  sont les générateurs du groupe de jauge. Les  $\Lambda_a$  peuvent être choisis comme étant des superchamps chiraux gauches de telle sorte que Eq.(1.82) soit une relation entre superchamps. L'équation Eq.(1.82) montre que les membres d'un même superchamp ont les mêmes nombres quantiques associés au groupe de jauge. Afin que le terme  $[\Phi_i^\dagger \Phi_i]_{\theta\theta\bar{\theta}\bar{\theta}}$  de Eq.(1.70) soit invariant de jauge, il doit être modifié en  $[\Phi_i^\dagger e^V \Phi_i]_{\theta\theta\bar{\theta}\bar{\theta}}$  où  $e^V$  se transforme sous l'action du groupe de jauge par,

$$\exp(V) \rightarrow \exp(i\Lambda^\dagger) \exp(V) \exp(-i\Lambda), \quad \text{avec } V = \Sigma_a V_a T_a, \quad (1.83)$$

$V_a$  représentant les superchamps vectoriels. Au premier ordre, le produit des exponentielles d'opérateurs  $A$  et  $B$  vaut,

$$\exp(A) \exp(B) = \exp\left(A + B + \frac{1}{2}[A, B]\right). \quad (1.84)$$

Cette relation nous permet de vérifier qu'au premier ordre le terme  $[\Phi_i^\dagger e^V \Phi_i]_{\theta\theta\bar{\theta}\bar{\theta}}$  est bien invariant sous l'action d'un groupe de jauge abélien puisque pour un tel groupe  $[T_a, T_b] = 0$ .

De plus, selon Eq.(1.84), pour un groupe de jauge abélien, Eq.(1.83) devient au premier ordre,

$$\exp(V) \rightarrow \exp(V + i\Lambda^\dagger - i\Lambda) \Leftrightarrow V \rightarrow V - i\Lambda + i\Lambda^\dagger. \quad (1.85)$$

On retrouve donc bien la transformation de Eq.(1.67) avec  $\Phi = -i\Lambda$ . Cette introduction de superchamps vectoriels, qui permet de rendre la théorie invariante de jauge, est analogue à l'introduction de champs de jauge dans les théories de jauge non supersymétriques. Par ailleurs, la transformation de Eq.(1.83) ne laisse pas invariant les termes  $[W_a^\alpha W_{a\alpha}]_{\theta\theta}$  et  $[\bar{W}_{a\dot{\alpha}} \bar{W}_a^{\dot{\alpha}}]_{\bar{\theta}\bar{\theta}}$  de Eq.(1.79). En revanche, si l'on redéfinit  $W_a^\alpha$  et  $\bar{W}_{a\dot{\alpha}}$  par,

$$\begin{aligned} W^\alpha &= -\frac{1}{4}(\bar{D}\bar{D})e^{-V}D_\alpha e^V, \\ \bar{W}_{\dot{\alpha}} &= -\frac{1}{4}(DD)e^{-V}\bar{D}_{\dot{\alpha}}e^V, \end{aligned} \quad (1.86)$$

ces superchamps chiraux subissent les transformations de jauge,

$$\begin{aligned} W^\alpha &\rightarrow \exp(i\Lambda)W^\alpha \exp(-i\Lambda), \\ \bar{W}_{\dot{\alpha}} &\rightarrow \exp(i\Lambda)\bar{W}_{\dot{\alpha}} \exp(-i\Lambda), \end{aligned} \quad (1.87)$$

de telle sorte que les termes  $Tr[W_a^\alpha W_{a\alpha}]_{\theta\theta}$  et  $Tr[\bar{W}_{a\dot{\alpha}} \bar{W}_a^{\dot{\alpha}}]_{\bar{\theta}\bar{\theta}}$ , la trace étant prise sur les indices de la représentation du groupe de jauge, sont invariants de jauge. Finalement, dans une théorie supersymétrique invariante de jauge, le superpotentiel doit avoir chacun de ces termes invariants de jauge.

Il faut aussi introduire les constantes de couplage  $g$  associées aux groupes de jauge. Pour cela, on redéfinit les champs des supermultiplets vectoriels par  $\lambda_a \rightarrow 2g\lambda_a$ ,  $v_{a\mu} \rightarrow 2gv_{a\mu}$  et  $D_a \rightarrow 2gD_a$ , ce qui équivaut à redéfinir le superchamp vectoriel lui-même par  $V \rightarrow 2gV$ .

Le lagrangien générique d'une théorie supersymétrique invariante sous un groupe de jauge a donc la forme suivante,

$$\begin{aligned} \mathcal{L} = & \Sigma_{i,j,k} \left( \left[ \Phi_i^\dagger (e^{2gV})_{ij} \Phi_j \right]_{\theta\theta\bar{\theta}\bar{\theta}} + \left[ W(\Phi) + \frac{1}{16g^2 n_R} Tr(W^\alpha W_\alpha) \right]_{\theta\theta} \right. \\ & \left. + \left[ \bar{W}(\Phi^\dagger) + \frac{1}{16g^2 n_R} Tr(\bar{W}_{\dot{\alpha}} \bar{W}^{\dot{\alpha}}) \right]_{\bar{\theta}\bar{\theta}} \right), \end{aligned} \quad (1.88)$$

où le nombre  $n_R$  est défini par  $[T_a, T_b] = n_R \delta_{ab}$ . Le facteur  $1/g^2$  dans Eq.(1.88) permet de ne pas générer de puissances de la constante  $g$  supérieures ou égales à 2. Après calcul, le lagrangien 1.88 devient,

$$\begin{aligned} \mathcal{L} = & \Sigma_{a,i,j,k} \left( \frac{i}{2} \psi_i \sigma^\mu (D_\mu \bar{\psi})_i - \frac{i}{2} (D_\mu \psi)_i \sigma^\mu \bar{\psi}_i + (D_\mu z)_i^\dagger (D^\mu z)_i - \frac{1}{4} F_{a\mu\nu} F_a^{\mu\nu} \right. \\ & + \frac{i}{2} \lambda_a \sigma^\mu (D_\mu \bar{\lambda})_a - \frac{i}{2} (D_\mu \lambda)_a \sigma^\mu \bar{\lambda}_a + i\sqrt{2}g(\bar{\psi}_i \bar{\lambda}_a) T_{aij} z_j - i\sqrt{2}g z_i^\dagger T_{aij} (\psi_j \lambda_a) \\ & \left. - \frac{1}{2} \frac{\partial^2 W(z)}{\partial z_i \partial z_j} \psi_i \psi_j - \frac{1}{2} \frac{\partial^2 \bar{W}(z^\dagger)}{\partial z_i^\dagger \partial z_j^\dagger} \bar{\psi}_i \bar{\psi}_j - V(z_i, z_j^\dagger) \right), \end{aligned} \quad (1.89)$$

où le superpotentiel  $W$  est donné dans Eq.(1.71), les dérivées covariantes sont définies par,

$$(D_\mu z)_i = \partial_\mu z_i + igv_{a\mu} T_{aij} z_j,$$

$$\begin{aligned}(D_\mu\psi)_i &= \partial_\mu\psi_i + igv_{a\mu}T_{aij}\psi_j, \\ (D_\mu\lambda)_a &= \partial_\mu\lambda_a - gf_{abc}v_{b\mu}\lambda_c,\end{aligned}\tag{1.90}$$

avec,

$$F_a^{\mu\nu} = \partial^\mu v_a^\nu - \partial^\nu v_a^\mu - gf_{abc}v_b^\mu v_c^\nu,\tag{1.91}$$

$$[T_a, T_b] = if_{abc}T^c,\tag{1.92}$$

et le potentiel vaut,

$$V(z_i, z_j^\dagger) = |f_i|^2 + \frac{1}{2}D_a^2,\tag{1.93}$$

avec,

$$f_i = \frac{\partial W(z)}{\partial z_i},\tag{1.94}$$

$$D_a = gz_i^\dagger T_{aij}z_j.\tag{1.95}$$

#### 1.4.10 Théorème de non-renormalisation

Introduisons tout d'abord un vocabulaire spécifique. On appelle respectivement terme F (F term) et terme D (D term) les termes  $[\dots]_{\theta\theta}$  (ou  $[\dots]_{\bar{\theta}\bar{\theta}}$ ) et  $[\dots]_{\theta\theta\bar{\theta}\bar{\theta}}$  du lagrangien (voir Eq.(1.88)). Cette appellation est due au fait que l'on dénote usuellement  $f(x)$  et  $D(x)$  les champs auxiliaires qui sont à l'origine de tels termes (voir Section 1.4.8).

Le théorème de non-renormalisation peut être énoncé comme suit : Dans les théories supersymétriques, les corrections à l'ordre des boucles sont toujours des termes D.

Une conséquence du théorème de non-renormalisation est que les paramètres du superpotentiel (voir Eq.(1.71) et Eq.(1.88)), et notamment les masses des champs scalaires comme les bosons de Higgs, ne reçoivent pas de corrections quantiques quadratiques tant que la supersymétrie est préservée. Cette conséquence est à l'origine de la résolution du problème de hiérarchie, comme nous l'avons discuté dans la Section 1.3.1.

Le théorème de non-renormalisation a pour origine l'absence de divergences quadratiques dans les théories supersymétriques. Cette absence de divergences quadratiques dans les théories supersymétriques provient de l'annulation de la somme de graphes échangeant des particules du Modèle Standard avec les graphes associés impliquant leur partenaire supersymétrique.

### 1.5 Brisure de la supersymétrie

Nous avons vu dans Eq.(1.5) que dans les théories supersymétriques les particules membres d'un même supermultiplet ont une masse identique (cette propriété a aussi été illustrée dans la Section 1.4.2). Or aucune particule supersymétrique de masse égale à une masse de particule du Modèle Standard n'a été découverte auprès des collisionneurs jusqu'à aujourd'hui. Nous en déduisons que si la nature est effectivement supersymétrique,

les masses des partenaires supersymétrique sont supérieures aux masses des particules du Modèle Standard et la supersymétrie est donc brisée.

Quels sont les critères de brisure spontanée de la supersymétrie ? La supersymétrie est brisée spontanément si le vide n'est pas invariant sous la supersymétrie, ce qui peut s'écrire,

$$\langle \delta\psi \rangle = \langle 0 | i(\mathcal{E}^\alpha Q_\alpha + \bar{\mathcal{E}}_{\dot{\alpha}} \bar{Q}^{\dot{\alpha}}) \psi | 0 \rangle \neq 0, \quad (1.96)$$

où  $Q$  est le générateur de la supersymétrie et  $\psi$  est un spineur. La valeur moyenne dans le vide des champs fermioniques est nulle à cause de l'invariance de Lorentz. On ne peut donc pas exprimer de condition de brisure spontanée de la supersymétrie sur  $\langle \delta\phi \rangle$ ,  $\phi$  étant un boson, qui doit toujours être nul. D'après les transformations supersymétriques des spineurs  $\psi(x)$  appartenant aux superchamps chiraux (Eq.(1.66)) et  $\lambda(x)$  appartenant aux superchamps vectoriels (Eq.(1.69)), la condition de brisure spontanée de SUSY de Eq.(1.96) est équivalente à,

$$\langle f_i \rangle \neq 0, \text{ ou } \langle D_a \rangle \neq 0, \quad (1.97)$$

$f_i$  et  $D_a$  étant respectivement les champs auxiliaires des supermultiplets chiraux et vectoriels (voir Eq.(1.94) et Eq.(1.95)). La condition de brisure spontanée de SUSY globale peut s'écrire différemment : En prenant la valeur moyenne dans le vide de la relation  $\{Q_\alpha, \bar{Q}_{\dot{\beta}}\} = -2P_\mu(\sigma^\mu)_{\alpha\dot{\beta}}$  (voir Eq.(1.49)), on obtient,

$$\langle 0 | Q_\alpha \bar{Q}_{\dot{\beta}} + \bar{Q}_{\dot{\beta}} Q_\alpha | 0 \rangle = 2 \langle 0 | H | 0 \rangle \delta_{\alpha\dot{\beta}}, \quad (1.98)$$

soit,

$$|Q_\alpha|0\rangle|^2 = \langle V \rangle, \quad (1.99)$$

où  $H$  est l'hamiltonien et  $\langle V \rangle$  la valeur moyenne du potentiel dans le vide. D'après Eq.(1.99), la condition de brisure spontanée de SUSY globale peut donc aussi s'écrire,

$$\langle V \rangle \neq 0. \quad (1.100)$$

Le potentiel étant positif ou nul d'après Eq.(1.93), la condition 1.100 est équivalente à,

$$\langle V \rangle > 0. \quad (1.101)$$

Nous vérifions de plus d'après Eq.(1.93) que les 2 conditions 1.97 et 1.101 de brisure spontanée de SUSY sont équivalentes.

En fait, une brisure spontanée de la supersymétrie dans le secteur observable engendre une hiérarchie entre les masses des particules qui n'est pas réaliste [22]. Plus précisément, après une brisure spontanée de la supersymétrie, les masses des particules fermioniques du Modèle Standard sont supérieures à certaines des masses de leur partenaire supersymétrique scalaire.

La supersymétrie si elle existe doit donc subir une brisure spontanée dans un secteur différent du secteur observable, appelé secteur "caché", et cette brisure de SUSY doit être médiée au secteur observable. Il existe aujourd'hui deux principaux types de modèles dans lesquels ce scénario de brisure de SUSY peut être réalisé : Les modèles de supergravité (voir

Chapitre 2) et les modèles dits GMSB (Gauge Mediated Supersymmetry Breaking) [23]. Dans les modèles de supergravité, le secteur caché n'interagit avec le secteur observable que par les interactions de type gravitationnel, et par conséquent la brisure de SUSY est médiée au secteur observable par les interactions de gravitationnelles. Dans les modèles GMSB, le secteur caché n'interagit avec le secteur observable que par les interactions de jauge, et par conséquent la brisure de SUSY est médiée au secteur observable par les interactions de jauge.

Les termes de brisure de la supersymétrie dans le secteur observable sont soumis à quelques contraintes. D'une part, les termes de brisure de la supersymétrie ne doivent pas introduire de divergences quadratiques qui engendreraient des corrections radiatives à la masse des bosons de Higgs et empêcheraient la résolution du problème de hiérarchie (voir Section 1.3.1). Les termes de brisure de la supersymétrie ne générant pas de divergences quadratiques sont appelés termes de brisure douce de la supersymétrie ou termes doux ('soft terms'). Les termes doux sont de manière générale,

$$\mathcal{L}_{doux} = \sum_{ijk} \left( f(z) + f^\dagger(z^\dagger) + m_0^{ij} z_i z_j^\dagger - \frac{1}{2} m_{1/2}^{ij} (\lambda_i \lambda_j + \bar{\lambda}_i \bar{\lambda}_j) \right),$$

$$\text{avec } f(z) = X^i z_i + \frac{1}{2} Y^{ij} z_i z_j + \frac{1}{3} A^{ijk} z_i z_j z_k, \quad (1.102)$$

où les  $z_i$  sont des champs scalaires et les  $\lambda_i$  des champs de spin 1/2 appartenant à un supermultiplet vectoriel. D'autre part, les masses des particules supersymétriques  $m_0$  et  $m_{1/2}$  provenant des termes de brisure de la supersymétrie (voir Eq.(1.102)) représentent typiquement la différence notée  $\tilde{m}$  (voir Section 1.3.1) entre les masses des particules du Modèle Standard et de leur partenaire supersymétrique. Or nous avons vu dans la Section 1.3.1 que  $\tilde{m}$  doit être typiquement inférieure au  $TeV$  afin que les corrections radiatives liées aux divergences quadratiques, et provenant de la non-annulation entre des graphes échangeant des particules du Modèle Standard et les graphes associés qui impliquent leur partenaire supersymétrique, n'engendrent pas des corrections à la masse des bosons de Higgs supérieures au  $TeV$  ce qui assure la conservation de la hiérarchie de masse existant au niveau des arbres.

Dans le cadre des modèles de supergravité aussi bien que des modèles GMSB, les termes de brisure de la supersymétrie dans le secteur observable peuvent être des termes de brisure douce de SUSY générant des masses de particules supersymétriques inférieures au  $TeV$ .

En conclusion, si la nature est réellement supersymétrique, la supersymétrie doit être brisée spontanément dans un secteur caché et les termes de brisure de SUSY dans le secteur observable doivent être des termes doux (c'est à dire de la forme de Eq.(1.102)) générant des masses  $\tilde{m}_z$  et  $\tilde{m}_\lambda$  de particules supersymétriques supérieures aux masses des particules du Modèle Standard et inférieures au  $TeV$ . Les modèles de supergravité ainsi que les modèles GMSB permettent de réaliser un tel scénario de brisure de la supersymétrie.

## 1.6 Modèle Standard Supersymétrique Minimal (MSSM)

Nous décrivons dans cette Section le Modèle Standard Supersymétrique Minimal (MSSM). Le MSSM est minimal en ce sens qu'il contient le nombre minimum de particules

nécessaire à l'extension supersymétrique du Modèle Standard. Le MSSM est parfaitement cohérent, il est bien défini théoriquement et peut être testé expérimentalement.

### 1.6.1 Le contenu en particules

Les superchamps chiraux du MSSM, qui décrivent les champs de matière, sont tous des superchamps chiraux gauches. Ces superchamps sont présentés dans Eq.(1.103) avec leurs nombres quantiques vis-à-vis du groupe de jauge du Modèle Standard  $SU(3)_c \times SU(2)_L \times U(1)_Y$ .

$$\begin{aligned} Q : (\mathbf{3}, \mathbf{2}, 1/6), \quad U^c : (\bar{\mathbf{3}}, \mathbf{1}, -2/3), \quad D^c : (\bar{\mathbf{3}}, \mathbf{1}, 1/3), \quad L : (\mathbf{1}, \mathbf{2}, -1/2), \\ E^c : (\mathbf{1}, \mathbf{1}, 1), \quad H_1 : (\mathbf{1}, \mathbf{2}, -1/2), \quad H_2 : (\mathbf{1}, \mathbf{2}, 1/2). \end{aligned} \quad (1.103)$$

Dans Eq.(1.103),  $L$  et  $Q$  sont respectivement les superchamps doublets de  $SU(2)_L$  de leptons et de quarks,  $E^c$ ,  $U^c$  et  $D^c$  sont les superchamps de leptons chargés, quarks up et down conjugués de charge et  $H_1$  et  $H_2$  sont les 2 superchamps de Higgs doublets de  $SU(2)_L$  s'écrivant,

$$H_1 = \begin{pmatrix} H_1^0 \\ H_1^- \end{pmatrix}, \quad H_2 = \begin{pmatrix} H_2^+ \\ H_2^0 \end{pmatrix}. \quad (1.104)$$

Dans le MSSM, il existe 2 superchamps de Higgs afin de pouvoir assurer l'annulation des anomalies du groupe  $U(1)_Y$  [13, 14, 24]. Pour que  $U(1)_Y$  n'ait pas d'anomalies, il faut que  $\sum_{fermions} Y^3 = 0$ . Or cette relation est vraie dans le Modèle Standard mais n'est à priori plus respectée dans une extension supersymétrique du Modèle Standard, celle-ci devant contenir le partenaire supersymétrique du boson de Higgs qui est un fermion d'hypercharge  $Y = -1/2$ . Afin de rétablir la relation  $\sum_{fermions} Y^3 = 0$ , un second superchamp chiral de Higgs d'hypercharge  $Y = 1/2$  peut être rajouté. C'est précisément ce qui est fait dans le MSSM (voir Eq.(1.103)).

Les superchamps vectoriels du MSSM contiennent les champs de jauge. Les superchamps vectoriels du MSSM associés aux groupes  $U(1)_Y$ ,  $SU(2)_L$  et  $SU(3)_c$  sont notés respectivement  $V_1$ ,  $V_2^a$  et  $V_3^b$ . Définissons pour la suite les superchamps vectoriels suivants,

$$V_2 = \sum_{a=1}^3 V_2^a \frac{\sigma^a}{2}, \quad V_3 = \sum_{b=1}^8 V_3^b \frac{\lambda^b}{2}, \quad (1.105)$$

où les  $\sigma^a$  sont les matrices de Pauli et les  $\lambda^b$  les matrices de Gell-Mann.

### 1.6.2 Le lagrangien

Le superpotentiel du MSSM, qui est une fonction des superchamps chiraux gauche, contient les couplages de Yukawa et le terme de masse du Higgs :

$$W_{MSSM} = h_{ij}^e H_1 L_i E_j^c + h_{ij}^d H_1 Q_i D_j^c + h_{ij}^u H_2 Q_i U_j^c + \mu H_1 H_2. \quad (1.106)$$

Dans Eq.(1.106),  $i$  et  $j$  sont des indices de saveur.

Le lagrangien du MSSM est défini par l'expression suivante,

$$\mathcal{L}_{MSSM} = \sum_{i,j} \left( \left[ Q_i^\dagger e^{\frac{1}{6} 2g_1 V_1} e^{2g_2 V_2} e^{2g_3 V_3} Q_i + U_i^{c\dagger} e^{-\frac{2}{3} 2g_1 V_1} e^{-2g_3 V_3} U_i^c + D_i^{c\dagger} e^{\frac{1}{3} 2g_1 V_1} e^{-2g_3 V_3} D_i^c \right. \right.$$

$$\begin{aligned}
& + \left[ L_i^\dagger e^{-\frac{1}{2}2g_1 V_1} e^{2g_2 V_2} L_i + E_i^{c\dagger} e^{2g_1 V_1} E_i^c + H_1^\dagger e^{-\frac{1}{2}2g_1 V_1} e^{2g_2 V_2} H_1^c + H_2^\dagger e^{\frac{1}{2}2g_1 V_1} e^{2g_2 V_2} H_2^c \right]_{\theta\theta\bar{\theta}\bar{\theta}} \\
& + \left[ W_{MSSM}(\Phi) + \frac{1}{16g_1^2} Tr(W_1^\alpha W_{1\alpha}) + \frac{1}{8g_2^2} Tr(W_2^\alpha W_{2\alpha}) + \frac{1}{8g_3^2} Tr(W_3^\alpha W_{3\alpha}) \right]_{\theta\theta} \\
& + \left[ \bar{W}_{MSSM}(\Phi^\dagger) + \frac{1}{16g_1^2} Tr(\bar{W}_1 \dot{\alpha} \bar{W}_1^{\dot{\alpha}}) + \frac{1}{8g_2^2} Tr(\bar{W}_2 \dot{\alpha} \bar{W}_2^{\dot{\alpha}}) + \frac{1}{8g_3^2} Tr(\bar{W}_3 \dot{\alpha} \bar{W}_3^{\dot{\alpha}}) \right]_{\bar{\theta}\bar{\theta}} \Bigg). \tag{1.107}
\end{aligned}$$

Pour être totalement complet, le lagrangien  $\mathcal{L}_{MSSM}$  du MSSM doit aussi contenir les termes de brisure douce de la supersymétrie qui sont donnés dans Eq.(1.102).

### 1.6.3 Le spectre supersymétrique

#### Masses des squarks et sleptons

Nous noterons  $\tilde{f}_L$  ( $\tilde{f}_R$ ) le partenaire supersymétrique de spin 0, noté  $z$  ( $\bar{z}$ ) dans la Section 1.4.7, d'un champ  $\psi_\alpha = \psi_L$  ( $\bar{\psi}^{\dot{\alpha}} = \psi_R$ ) de spin 1/2 et de chiralité gauche (droite).  $\tilde{f}_{L,R}$  désigne donc les sfermions c'est à dire les squarks  $\tilde{q}_{L,R} = \tilde{u}_{L,R}, \tilde{d}_{L,R}$  ainsi que les sleptons  $\tilde{l}_{L,R} = \tilde{e}_{L,R}, \tilde{\nu}_L$ .

Le lagrangien  $\mathcal{L}_{MSSM}$  du MSSM (voir Eq.(1.107) et Eq.(1.102)) engendre des termes de masse de sfermions qui s'écrivent comme suit,

$$\begin{aligned}
-\mathcal{L}_{mass}^{scal} &= (\tilde{u}_{iL}, \tilde{u}_{iR}^\dagger) \begin{pmatrix} (m_{LL}^u)^2 & (m_{LR}^u)^2 \\ (m_{LR}^u)^2 & (m_{RR}^u)^2 \end{pmatrix} \begin{pmatrix} \tilde{u}_{jL}^\dagger \\ \tilde{u}_{jR} \end{pmatrix} \\
&+ (\tilde{d}_{iL}, \tilde{d}_{iR}^\dagger) \begin{pmatrix} (m_{LL}^d)^2 & (m_{LR}^d)^2 \\ (m_{LR}^d)^2 & (m_{RR}^d)^2 \end{pmatrix} \begin{pmatrix} \tilde{d}_{jL}^\dagger \\ \tilde{d}_{jR} \end{pmatrix} \\
&+ (\tilde{e}_{iL}, \tilde{e}_{iR}^\dagger) \begin{pmatrix} (m_{LL}^e)^2 & (m_{LR}^e)^2 \\ (m_{LR}^e)^2 & (m_{RR}^e)^2 \end{pmatrix} \begin{pmatrix} \tilde{e}_{jL}^\dagger \\ \tilde{e}_{jR} \end{pmatrix} + (m_{LL}^\nu)^2 \tilde{\nu}_{iL} \tilde{\nu}_{jL}^\dagger, \tag{1.108}
\end{aligned}$$

où  $i$  et  $j$  sont des indices de saveur et où,

$$\begin{aligned}
(m_{LL}^u)^2 &= m_{ij}^2(\tilde{u}_L) + (m_u m_u^\dagger)_{ij} + \cos 2\beta m_Z^2 \left(-\frac{1}{2} + \frac{2}{3} \sin^2 \theta_W\right) \delta_{ij}, \\
(m_{LL}^d)^2 &= m_{ij}^2(\tilde{d}_L) + (m_d m_d^\dagger)_{ij} + \cos 2\beta m_Z^2 \left(\frac{1}{2} - \frac{2}{3} \sin^2 \theta_W\right) \delta_{ij}, \\
(m_{RR}^u)^2 &= m_{ij}^2(\tilde{u}_R) + (m_u m_u^\dagger)_{ij} - \cos 2\beta m_Z^2 \frac{2}{3} \sin^2 \theta_W \delta_{ij}, \\
(m_{RR}^d)^2 &= m_{ij}^2(\tilde{d}_R) + (m_d m_d^\dagger)_{ij} + \cos 2\beta m_Z^2 \frac{1}{3} \sin^2 \theta_W \delta_{ij}, \\
(m_{LL}^e)^2 &= m_{ij}^2(\tilde{e}_L) + (m_e m_e^\dagger)_{ij} + \cos 2\beta m_Z^2 \left(\frac{1}{2} - \sin^2 \theta_W\right) \delta_{ij}, \\
(m_{LL}^\nu)^2 &= m_{ij}^2(\tilde{\nu}_L) + (m_\nu m_\nu^\dagger)_{ij} - \cos 2\beta m_Z^2 \frac{1}{2} \delta_{ij}, \\
(m_{RR}^e)^2 &= m_{ij}^2(\tilde{e}_R) + (m_e m_e^\dagger)_{ij} + \cos 2\beta m_Z^2 \sin^2 \theta_W \delta_{ij}, \\
(m_{LR}^u)^2 &= \left(A_u^{ij} + \frac{\mu}{\tan \beta}\right) (m_u)_{ij}, \\
(m_{LR}^d)^2 &= \left(A_d^{ij} + \mu \tan \beta\right) (m_d)_{ij}, \\
(m_{LR}^e)^2 &= \left(A_e^{ij} + \mu \tan \beta\right) (m_e)_{ij}, \tag{1.109}
\end{aligned}$$

A étant défini dans Eq.(1.102). Dans Eq.(1.109),  $\sin \theta_W$  est le sinus de l'angle électrofaible et  $\tan \beta = \langle h_2^0 \rangle / \langle h_1^0 \rangle$ ,  $h_1^0$  et  $h_2^0$  étant les composantes scalaires des superchamps  $H_1^0$  et  $H_2^0$  de Eq.(1.104). Par exemple, les termes  $(m_u m_u^\dagger)_{ij}$  de Eq.(1.109) viennent de  $|\frac{\partial W_{MSSM}(\tilde{f})}{\partial \tilde{u}_{i(L,R)}}|^2$  (voir Eq.(1.93) et Eq.(1.94)) où  $W_{MSSM}$  est donné dans Eq.(1.106). Le terme  $\frac{\mu}{\tan \beta} (m_u)_{ij}$  de Eq.(1.109) vient lui de  $|\frac{\partial W_{MSSM}(\tilde{f})}{\partial h_2^0}|^2$  (voir Eq.(1.93) et Eq.(1.94)). Prenons un dernier exemple : Le terme  $\cos 2\beta m_Z^2 (-\frac{1}{2} + \frac{2}{3} \sin^2 \theta_W) \delta_{ij}$  provient des termes de Eq.(1.95) (voir aussi Eq.(1.93)) qui sont des termes D puisqu'ils sont engendrés par des termes du type  $[\Phi^\dagger(e^{2gV})\Phi]_{\theta\theta\bar{\theta}\bar{\theta}}$  (voir Eq.(1.88)).

Les masses des sfermions notées  $m_{ij}^2(\tilde{f}_{L,R})$  dans Eq.(1.109) sont des masses douces, c'est à dire des masses du type  $m_0$  provenant des termes de brisure douce de la supersymétrie (voir Eq.(1.102)). Dans les modèles basés sur la supergravité, un lagrangien effectif supersymétrique accompagné de termes de brisure douce de SUSY est engendré à l'échelle de Planck  $M_P \sim 10^{19} GeV$  qui est supérieure à l'échelle d'unification  $M_{GUT} \sim 2 \cdot 10^{16} GeV$  (voir Chapitre 2). Ces termes de brisure douce peuvent donner une masse universelle  $m_0$  à tous les champs scalaires ainsi qu'une masse universelle  $m_{1/2}$  à tous les jauginos. Les masses douces des champs scalaires et des jauginos à des énergies inférieures à  $M_{SUGRA}$  sont obtenues à partir des masses  $m_0$  et  $m_{1/2}$  par les solutions des équations du groupe de renormalisation. Si les masses douces des différents champs scalaires sont égales entre elles à l'échelle de Planck, elles le restent aux énergies supérieures à l'échelle d'unification  $M_{GUT}$  puisque les champs scalaires appartiennent aux mêmes représentations du groupe de jauge de grande unification et ont donc des couplages identiques. En revanche, à des énergies inférieures à  $M_{GUT}$ , les masses douces des différents champs scalaires deviennent différentes car chaque champ scalaire est chargé différemment vis-à-vis du groupe de jauge  $SU(3)_c \times SU(2)_L \times U(1)_Y$  et a donc ses propres couplages. Il en est de même pour les masses douces des jauginos. Admettant que les champs scalaires (jauginos) aient une masse commune  $m_0$  ( $m_{1/2}$ ) à l'échelle  $M_{GUT}$  qui soit identique pour les 3 saveurs et négligeant les couplages de Yukawa, l'intégration des équations du groupe de renormalisation donne les expressions suivantes pour les masses douces des champs scalaires à une échelle  $Q$  inférieure à  $M_{GUT}$  [25],

$$\begin{aligned}
m^2(\tilde{u}_L) &= m_0^2 + 2m_{1/2}^2 \left( \frac{1}{36} \tilde{\alpha}_1 f_1 + \frac{3}{4} \tilde{\alpha}_2 f_2 + \frac{4}{3} \tilde{\alpha}_3 f_3 \right), \\
m^2(\tilde{d}_L) &= m_0^2 + 2m_{1/2}^2 \left( \frac{1}{36} \tilde{\alpha}_1 f_1 + \frac{3}{4} \tilde{\alpha}_2 f_2 + \frac{4}{3} \tilde{\alpha}_3 f_3 \right), \\
m^2(\tilde{u}_R) &= m_0^2 + 2m_{1/2}^2 \left( \frac{4}{9} \tilde{\alpha}_1 f_1 + \frac{4}{3} \tilde{\alpha}_3 f_3 \right), \\
m^2(\tilde{d}_R) &= m_0^2 + 2m_{1/2}^2 \left( \frac{1}{9} \tilde{\alpha}_1 f_1 + \frac{4}{3} \tilde{\alpha}_3 f_3 \right), \\
m^2(\tilde{e}_L) &= m_0^2 + 2m_{1/2}^2 \left( \frac{1}{4} \tilde{\alpha}_1 f_1 + \frac{3}{4} \tilde{\alpha}_2 f_2 \right), \\
m^2(\tilde{\nu}_L) &= m_0^2 + 2m_{1/2}^2 \left( \frac{1}{4} \tilde{\alpha}_1 f_1 + \frac{3}{4} \tilde{\alpha}_2 f_2 \right), \\
m^2(\tilde{e}_R) &= m_0^2 + 2m_{1/2}^2 \tilde{\alpha}_1 f_1,
\end{aligned} \tag{1.110}$$

avec,

$$\tilde{\alpha}_i = \frac{\alpha_i(M_{GUT})}{4\pi}, \quad f_i = \frac{(2 + b_i \tilde{\alpha}_i t)}{(1 + b_i \tilde{\alpha}_i t)^2} t, \tag{1.111}$$



$t$  valant  $t = 2 \log(M_{GUT}/Q)$ , les  $\alpha_i$  ( $i = 1, 2, 3$ ) étant les 3 constantes de couplage du groupe de jauge  $SU(3)_c \times SU(2)_L \times U(1)_Y$  du Modèle Standard et les  $b_i = (-3, 1, 11)$  étant les coefficients des fonctions  $\beta$  à une boucle associées aux interactions  $SU(3)_c$ ,  $SU(2)_L$  et  $U(1)_Y$ , respectivement.

## Masses des jauginos et higgsinos

- **Charginos** Définissons avant tout les vecteurs,

$$\psi^+ = \begin{pmatrix} -i\lambda^+ \\ \psi_{H^+} \end{pmatrix}, \quad \psi^- = \begin{pmatrix} -i\lambda^- \\ \psi_{H^-} \end{pmatrix}, \quad (1.112)$$

où  $\lambda^\pm$  est le wino c'est à dire le partenaire supersymétrique de spin 1/2 (à 2 composantes) du boson  $W^\pm$ , et où  $\psi_{H^+}$  et  $\psi_{H^-}$  sont les higgsinos chargés c'est à dire les partenaires supersymétriques de spin 1/2 (à 2 composantes) des bosons de Higgs chargés. Plus précisément,  $\psi_{H^+}$  et  $\psi_{H^-}$  sont respectivement les composantes spinorielles des superchamps  $H^+$  et  $H^-$  définis dans Eq.(1.104).

Le lagrangien  $\mathcal{L}_{MSSM}$  du MSSM (voir Eq.(1.107) et Eq.(1.102)) engendre des termes de masse pour le wino et les higgsinos chargés qui s'écrivent comme suit,

$$-\mathcal{L}_{mass}^{charg} = \frac{1}{2}((\psi^+)^T, (\psi^-)^T) \begin{pmatrix} 0 & X^T \\ X & 0 \end{pmatrix} \begin{pmatrix} \psi^+ \\ \psi^- \end{pmatrix} + h.c., \quad (1.113)$$

avec,

$$X = \begin{pmatrix} M_2 & M_W \sqrt{2} \sin \beta \\ M_W \sqrt{2} \cos \beta & \mu \end{pmatrix}. \quad (1.114)$$

Dans Eq.(1.114),  $M_2$  est la masse douce du wino à l'échelle  $Q$  considérée, c'est à dire une masse du type  $m_{1/2}$  provenant des termes de brisure douce de la supersymétrie (voir Eq.(1.102)). Par exemple, dans un modèle basé sur la supergravité,  $M_2$  peut être obtenue par le biais des solutions des équations du groupe de renormalisation à partir des masses universelles  $m_0$  et  $m_{1/2}$  à l'échelle  $M_{GUT}$ . Notons aussi que dans Eq.(1.114)  $M_W$  est la masse du boson  $W^\pm$  qui s'exprime dans le MSSM,

$$M_W^2 = \frac{1}{4} g_2^2 (< h_1^0 >^2 + < h_2^0 >^2). \quad (1.115)$$

Le terme de masse en  $\mu$  de Eq.(1.114) provient du terme  $-\frac{1}{2} \frac{\partial^2 W_{MSSM}(\tilde{f})}{\partial h^+ \partial h^-} \psi_{H^+} \psi_{H^-}$  de Eq.(1.89),  $h^+$  et  $h^-$  étant respectivement les composantes scalaires des superchamps  $H^+$  et  $H^-$  définis dans Eq.(1.104). Les termes de masse en  $M_W \sqrt{2} \sin \beta$  et  $M_W \sqrt{2} \cos \beta$  de Eq.(1.114) proviennent des termes  $[H_1^\dagger e^{-\frac{1}{2} 2g_1 V_1} e^{2g_2 V_2} H_1^c + H_2^\dagger e^{\frac{1}{2} 2g_1 V_1} e^{2g_2 V_2} H_2^c]_{\theta\theta\bar{\theta}\bar{\theta}}$  de Eq.(1.107), qui engendrent des termes du type  $i\sqrt{2}g(\bar{\psi}_{H_{1,2}} \bar{\lambda}_a) T_a h_{1,2} - i\sqrt{2}gh_{1,2}^\dagger T_a (\psi_{H_{1,2}} \lambda_a)$  (voir Eq.(1.89)), les  $T_a$  étant les générateurs du groupe  $SU(2)_L$  et les  $h_{1,2}$  ( $\psi_{H_{1,2}}$ ) les composantes scalaires (spinorielles) des superchamps  $H_{1,2}$  de Eq.(1.104) qui sont des doublets de  $SU(2)_L$ .

Les termes de masse de Eq.(1.113) peuvent s'écrire après diagonalisation de la matrice  $X$  [26],

$$-\mathcal{L}_{mass}^{charg} = (\chi_1^-, \chi_2^-) \begin{pmatrix} \tilde{m}_1 & 0 \\ 0 & \tilde{m}_2 \end{pmatrix} \begin{pmatrix} \chi_1^+ \\ \chi_2^+ \end{pmatrix} + h.c., \quad (1.116)$$

où,

$$\begin{pmatrix} \chi_1^+ \\ \chi_2^+ \end{pmatrix} = V\psi^+, \quad \begin{pmatrix} \chi_1^- \\ \chi_2^- \end{pmatrix} = U\psi^-, \quad U^* X V^{-1} = \begin{pmatrix} \tilde{m}_1 & 0 \\ 0 & \tilde{m}_2 \end{pmatrix}, \quad (1.117)$$

$U$  et  $V$  étant des matrices unitaires  $2 \times 2$ . Les spineurs à 2 composantes  $\chi_{1,2}^\pm$  sont donc les états propres de masse de la matrice  $X$  c'est à dire des mélanges entre wino  $\lambda^\pm$  et higgsinos  $\psi_{H^\pm}$ . En utilisant Eq.(1.46), on peut exprimer le lagrangien 1.116 en terme de spineurs à 4 composantes comme suit,

$$-\mathcal{L}_{mass}^{charg} = (\tilde{\chi}_1, \tilde{\chi}_2) \begin{pmatrix} \tilde{m}_1 & 0 \\ 0 & \tilde{m}_2 \end{pmatrix} \begin{pmatrix} \tilde{\chi}_1 \\ \tilde{\chi}_2 \end{pmatrix}, \quad (1.118)$$

$\tilde{\chi}_1$  et  $\tilde{\chi}_2$  étant les spineurs à 4 composantes appelés charginos et définis par,

$$\tilde{\chi}_1 = \begin{pmatrix} \chi_1^+ \\ \tilde{\chi}_1^- \end{pmatrix}, \quad \tilde{\chi}_2 = \begin{pmatrix} \chi_2^+ \\ \tilde{\chi}_2^- \end{pmatrix}. \quad (1.119)$$

• **Neutralinos** Définissons avant tout le vecteur,

$$(\psi^0)^T = (-i\lambda', -i\lambda^3, \psi_{H_1^0}, \psi_{H_2^0}), \quad (1.120)$$

où  $\lambda'$  ( $\lambda^3$ ) est le bino (wino) c'est à dire le partenaire supersymétrique de spin 1/2 (à 2 composantes) du boson  $B$  ( $W^3$ ), et où  $\psi_{H_1^0}$  et  $\psi_{H_2^0}$  sont les higgsinos neutres c'est à dire les partenaires supersymétriques de spin 1/2 (à 2 composantes) des bosons de Higgs neutres. Plus précisément,  $\psi_{H_1^0}$  et  $\psi_{H_2^0}$  sont respectivement les composantes spinorielles des superchamps  $H_1^0$  et  $H_2^0$  définis dans Eq.(1.104).

Le lagrangien  $\mathcal{L}_{MSSM}$  du MSSM (voir Eq.(1.107) et Eq.(1.102)) engendre des termes de masse pour le bino, le wino et les higgsinos neutres qui s'écrivent comme suit,

$$-\mathcal{L}_{mass}^{neut} = \frac{1}{2}(\psi^0)^T Y \psi^0 + h.c., \quad (1.121)$$

avec,

$$Y = \begin{pmatrix} M_1 & 0 & -M_Z \cos \beta \sin \theta_W & M_Z \sin \beta \sin \theta_W \\ 0 & M_2 & M_Z \cos \beta \cos \theta_W & -M_Z \sin \beta \cos \theta_W \\ -M_Z \cos \beta \sin \theta_W & M_Z \cos \beta \cos \theta_W & 0 & -\mu \\ M_Z \sin \beta \sin \theta_W & -M_Z \sin \beta \cos \theta_W & -\mu & 0 \end{pmatrix}. \quad (1.122)$$

Dans Eq.(1.122),  $M_1$  ( $M_2$ ) est la masse douce du bino (wino) à l'échelle  $Q$  considérée, c'est à dire une masse du type  $m_{1/2}$  provenant des termes de brisure douce de la supersymétrie (voir Eq.(1.102)). Les termes de masse en  $-\mu$  de Eq.(1.122) proviennent du terme  $-\frac{1}{2} \frac{\partial^2 W_{MSSM}(\tilde{f})}{\partial h_1^0 \partial h_2^0} \psi_{H_1^0} \psi_{H_2^0}$  de Eq.(1.89),  $h_1^0$  et  $h_2^0$  étant respectivement les composantes scalaires des superchamps  $H_1^0$  et  $H_2^0$  définis dans Eq.(1.104). Les termes de masse en  $M_Z f(\beta, \theta_W)$  de Eq.(1.122) proviennent des termes  $[H_1^\dagger e^{-\frac{1}{2} 2g_1 V_1} e^{2g_2 V_2} H_1^c + H_2^\dagger e^{\frac{1}{2} 2g_1 V_1} e^{2g_2 V_2} H_2^c]_{\theta\theta\bar{\theta}\bar{\theta}}$  de Eq.(1.107), qui engendrent des termes du type  $i\sqrt{2}g(\bar{\psi}_{H_{1,2}} \bar{\lambda}_a) T_a h_{1,2} - i\sqrt{2}g h_{1,2}^\dagger T_a (\psi_{H_{1,2}} \lambda_a)$  (voir Eq.(1.89)), les  $T_a$  étant les générateurs du groupe  $SU(2)_L$  et les  $h_{1,2}$  ( $\psi_{H_{1,2}}$ ) les composantes scalaires (spinorielles) des superchamps  $H_{1,2}$  de Eq.(1.104) qui sont des doublets de  $SU(2)_L$ .

Les termes de masse de Eq.(1.121) peuvent s'écrire après diagonalisation de la matrice  $Y$  [26],

$$-\mathcal{L}_{mass}^{neut} = \frac{1}{2}(\chi_1^0, \chi_2^0, \chi_3^0, \chi_4^0) \begin{pmatrix} \tilde{m}_1^0 & 0 & 0 & 0 \\ 0 & \tilde{m}_2^0 & 0 & 0 \\ 0 & 0 & \tilde{m}_3^0 & 0 \\ 0 & 0 & 0 & \tilde{m}_4^0 \end{pmatrix} \begin{pmatrix} \chi_1^0 \\ \chi_2^0 \\ \chi_3^0 \\ \chi_4^0 \end{pmatrix} + h.c., \quad (1.123)$$

où,

$$\begin{pmatrix} \chi_1^0 \\ \chi_2^0 \\ \chi_3^0 \\ \chi_4^0 \end{pmatrix} = N\psi^0, \quad N^* Y N^{-1} = \begin{pmatrix} \tilde{m}_1^0 & 0 & 0 & 0 \\ 0 & \tilde{m}_2^0 & 0 & 0 \\ 0 & 0 & \tilde{m}_3^0 & 0 \\ 0 & 0 & 0 & \tilde{m}_4^0 \end{pmatrix}, \quad (1.124)$$

$N$  étant une matrice unitaires  $4 \times 4$ . Les spineurs à 2 composantes  $\chi_{1,2,3,4}^0$  sont donc les états propres de masse de la matrice  $Y$  c'est à dire des mélanges entre bino  $\lambda'$ , wino  $\lambda^3$  et higgsinos  $\psi_{H_{1,2}^0}$ . En utilisant Eq.(1.46), on peut exprimer le lagrangien 1.123 en terme de spineurs à 4 composantes comme suit,

$$-\mathcal{L}_{mass}^{neut} = \frac{1}{2}(\tilde{\chi}_1^0, \tilde{\chi}_2^0, \tilde{\chi}_3^0, \tilde{\chi}_4^0) \begin{pmatrix} \tilde{m}_1^0 & 0 & 0 & 0 \\ 0 & \tilde{m}_2^0 & 0 & 0 \\ 0 & 0 & \tilde{m}_3^0 & 0 \\ 0 & 0 & 0 & \tilde{m}_4^0 \end{pmatrix} \begin{pmatrix} \tilde{\chi}_1^0 \\ \tilde{\chi}_2^0 \\ \tilde{\chi}_3^0 \\ \tilde{\chi}_4^0 \end{pmatrix}, \quad (1.125)$$

$\tilde{\chi}_1^0, \tilde{\chi}_2^0, \tilde{\chi}_3^0$  et  $\tilde{\chi}_4^0$  étant les spineurs à 4 composantes appelés neutralinos et définis par,

$$\tilde{\chi}_1^0 = \begin{pmatrix} \chi_1^0 \\ \tilde{\chi}_1^0 \end{pmatrix}, \quad \tilde{\chi}_2^0 = \begin{pmatrix} \chi_2^0 \\ \tilde{\chi}_2^0 \end{pmatrix}, \quad \tilde{\chi}_3^0 = \begin{pmatrix} \chi_3^0 \\ \tilde{\chi}_3^0 \end{pmatrix}, \quad \tilde{\chi}_4^0 = \begin{pmatrix} \chi_4^0 \\ \tilde{\chi}_4^0 \end{pmatrix}. \quad (1.126)$$



# Chapitre 2

## Supergravité

### 2.1 Motivations

Les symétries fondamentales en physique des particules (comme par exemple les symétries de jauge) sont réalisées localement plutôt que globalement. Cela nous suggère que si la supersymétrie est réellement une symétrie de la nature, elle doit aussi être effective de façon locale. L'algèbre de supersymétrie (voir Section 1.2) contient le générateur des translations  $P_\mu$ . Par conséquent, dans une théorie de supersymétrie locale, nous devons considérer les translations qui varient d'un point à l'autre de l'espace-temps. Cela signifie qu'une théorie localement supersymétrique doit être une théorie de transformations générales des coordonnées de l'espace-temps. En d'autres termes, une théorie de supersymétrie locale doit contenir la théorie de la gravitation. Cela ne nous étonne que peu puisque les générateurs de la supersymétrie ne commutent pas avec les générateurs du groupe de Poincaré. C'est donc pour cette raison que les théories de supersymétrie locale sont aussi appelées théories de supergravité. En effet, comme nous allons le voir dans ce chapitre, la gravitation joue naturellement un rôle majeur lorsque nous tentons de rendre la supersymétrie locale. Plus précisément, le partenaire supersymétrique du graviton, le gravitino, va permettre à la supersymétrie d'agir localement, de même que les bosons de jauge permettent aux symétries de jauge d'agir localement. En ce sens, il existe une forte analogie entre la supersymétrie locale (et le gravitino) et les symétries de jauge (et les bosons de jauge). Le rôle naturel de la gravitation dans les théories de supersymétrie locale est une motivation supplémentaire pour la construction de telles théories.

Outre leurs motivations théoriques, les théories de supergravité ont de nombreux traits phénoménologiques (que nous avons déjà mentionné dans la Section 1.5). Effectivement, comme nous allons l'expliquer en détail dans ce chapitre, dans certaines théories de supergravité la supersymétrie locale est brisée spontanément dans un secteur caché et un lagrangien effectif supersymétrique accompagné de termes de brisure douce de SUSY (voir Section 1.5) peut ainsi être engendré dans le secteur observable. De plus, les masses générées pour les partenaires supersymétriques par ces termes de brisure douce peuvent être supérieures aux masses des particules du Modèle Standard à l'échelle électrofaible. Enfin, les masses des partenaires supersymétriques, bien que définies à l'échelle de Planck (gravitation), peuvent être inférieures au  $TeV$ , à l'échelle électrofaible, ce qui est nécessaire pour résoudre le problème de hiérarchie (voir Section 1.3.1).

Nous avons vu dans la Section 1.5 que les modèles dits GMSB (Gauge Mediated Su-

persymmetry Breaking) [23] peuvent aussi générer, suite à une brisure spontanée de la supersymétrie dans un secteur caché, des termes de brisure douce de SUSY engendrant des masses pour les partenaires supersymétriques supérieures aux masses des particules du Modèle Standard et inférieures au  $TeV$ , à l'échelle électrofaible. Comparons les intérêts phénoménologiques des modèles GMSB et des modèles basés sur la supergravité.

D'un point de vue phénoménologique, la principale différence entre les modèles GMSB et les modèles de supergravité est liée au problème de la saveur : Le lagrangien du Modèle Standard sans les couplages de Yukawa est invariant sous la symétrie globale  $U(3)^5$ , chaque groupe  $U(3)$  agissant dans l'espace des saveurs des 5 représentations irréductibles de fermions du groupe de jauge :  $(q_L, u_R^c, d_R^c, l_L, e_R^c)_i$  ( $i = 1, 2, 3$ ). Or, nous ignorons la dynamique responsable de la brisure de la symétrie de saveur, dont la seule trace à basse énergie est visible dans la structure des couplages de Yukawa. Supposons que cette dynamique de brisure a lieu au-delà d'une échelle  $\Lambda_F$ .

Dans les modèles de supergravité, les termes doux de brisure sont définis à l'échelle de Planck, c'est à dire à une échelle nécessairement supérieure à  $\Lambda_F$ . Il n'y a donc pas de raison évidente pour que les termes doux de brisure soient indépendants de la saveur. Cette violation de la saveur dans les termes doux, qui sont entre autres des termes de masse pour les squarks et les sleptons, est très dangereuse car elle engendre des contributions supersymétriques à des processus comme le mélange  $K^0 - \bar{K}^0$  ou encore la désintégration  $\mu \rightarrow e\gamma$  sur lesquels les bornes expérimentales sont fortes. C'est le problème de changement de saveur en supersymétrie qui est lié au fait que les matrices de masse pour les fermions et leurs partenaires supersymétriques ne sont pas a priori diagonales dans la même base. Bien sûr, cela ne signifie pas que les scénarios de supergravité ne sont pas réalistes. Il se peut qu'au niveau de la gravité quantique les termes doux soient indépendants de la saveur, ou bien que certaines symétries de saveur [27, 28] ou certains mécanismes dynamiques [29] soient responsables d'un alignement approximatif entre les matrices de masse des fermions et des sfermions.

En ce qui concerne les modèles GMSB, les termes doux sont définis à une échelle  $M$ , qui représente la masse des messagers. Cette échelle n'est a priori pas reliée à  $\Lambda_F$  et peut donc être choisie telle que  $M < \Lambda_F$ . Pour un tel choix de l'échelle  $M$ , les termes doux, qui sont générés par des graphes à l'ordre des boucles mettant en jeu les interactions de jauge, ne ressentiraient pas les effets de violation de saveur présents dans ce cas uniquement dans les couplages de Yukawa. Le mécanisme de GIM peut alors être généralisé au mécanisme de superGIM incluant les particules et leur partenaire supersymétrique. Le problème de changement de saveur est donc naturellement découplé dans les modèles GMSB, en contraste avec les théories de supergravité.

Par ailleurs, les modèles GMSB posent le "problème du terme  $\mu$ " (qui sera exposé dans la Section 3.3.2) ce qui n'est pas le cas des théories de supergravité.

Enfin, les versions *minimales* des modèles GMSB et des modèles de supergravité sont toutes deux assez prédictives vis à vis du spectre de masse des particules supersymétriques, ce qui leur permettra d'être testées auprès des futurs collisionneurs de particules. De plus, dans les modèles GMSB, la LSP est le gravitino ( $\equiv$  partenaire supersymétrique du graviton) ce qui engendre des signaux phénoménologiques spécifiques.

## 2.2 Lagrangiens de supergravité

### 2.2.1 Procédure de Noether

Afin de dériver les lagrangiens localement supersymétriques, nous allons utiliser la procédure de Noether. La procédure de Noether est une méthode systématique pour obtenir une action ayant une symétrie locale à partir de l'action ayant une symétrie globale. Dans cette partie, nous illustrons cette procédure en prenant l'exemple d'une symétrie de jauge.

Considérons donc l'action d'un champ de Dirac libre et non massif,

$$S_0 = i \int d^4x \bar{\psi} \gamma^\mu \partial_\mu \psi. \quad (2.1)$$

Cette action est invariante sous la transformation,

$$\psi \rightarrow e^{-i\xi} \psi, \quad (2.2)$$

où  $\xi$  est une phase constante.  $S_0$  a donc une symétrie globale abélienne. Pour que cette symétrie soit locale, la phase  $\xi$  doit être une fonction des coordonnées d'espace-temps. La transformation de Eq.(2.2) s'écrit alors,

$$\psi \rightarrow e^{-i\xi(x)} \psi. \quad (2.3)$$

L'action  $S_0$  de Eq.(2.1) n'est plus invariante sous cette symétrie de jauge. La variation de l'action  $S_0$  par la transformation locale de Eq.(2.2l) est,

$$\delta S_0 = \int d^4x \bar{\psi} \gamma^\mu \psi \partial_\mu \xi = \int d^4x j^\mu \partial_\mu \xi, \quad (2.4)$$

où,

$$j^\mu = \bar{\psi} \gamma^\mu \psi, \quad (2.5)$$

est le courant de Noether associé à la symétrie (2.2) de  $S_0$ . Afin de restaurer l'invariance, un champ de jauge  $A_\mu$  est introduit. Ce dernier doit se transformer sous la symétrie 2.3 par,

$$A_\mu \rightarrow A_\mu + \partial_\mu \xi, \quad (2.6)$$

et un terme de couplage entre ce champ de jauge et le courant de Noether doit être ajouté à l'action  $S_0$  :

$$S = S_0 - \int d^4x j^\mu A_\mu = \int d^4x i \bar{\psi} \gamma^\mu (\partial_\mu + i A_\mu) \psi = \int d^4x i \bar{\psi} \gamma^\mu D_\mu \psi, \quad (2.7)$$

où  $D_\mu = \partial_\mu + i A_\mu$  est une dérivée covariante. La variation de ce terme sous la symétrie locale 2.3 va exactement compenser la variation de  $S_0$  de Eq.(2.7). L'action  $S$  est alors invariante sous les transformations de jauge 2.3 et 2.6.

Plus généralement, pour une symétrie globale initiale non abélienne, cette méthode n'est applicable qu'au premier ordre d'un paramètre donné et doit donc être itérée. A chaque étape, un terme supplémentaire doit être ajouté à l'action (Eq.(2.7)) afin de

compenser les variations à l'ordre correspondant de cette même action. En général, un terme supplémentaire doit aussi être ajouté à la loi de transformation du champ de jauge (Eq.(2.6)). Après un nombre fini d'itérations (avec de la chance!) une action est obtenue, qui est exactement invariante sous la symétrie locale considérée (Eq.(2.3) + forme finale de Eq.(2.6)).

Afin d'illustrer ces propos, nous allons maintenant appliquer la procédure de Noether sur une théorie ayant une symétrie non-abélienne. De plus, nous allons considérer une action de champs de jauge, ce qui nous sera utile par la suite. L'action considérée est la suivante,

$$S_0 = -\frac{1}{4} \int d^4x G_a^{\mu\nu} G_{\mu\nu}^a, \quad (2.8)$$

où,

$$G_a^{\mu\nu} = \partial^\mu A_\nu^a - \partial^\nu A_\mu^a, \quad (2.9)$$

et les  $A_\mu^a$ ,  $a = 1, \dots, r$ , sont des champs vectoriels appartenant à la représentation adjointe de dimension  $r$  d'un groupe de Lie donné. Les générateurs,  $T_a$ , et les constantes de structure,  $f_{abc}$ , de ce groupe de Lie vérifient,

$$[T_a, T_b] = if_{abc} T_c. \quad (2.10)$$

L'action de Eq.(2.8) est invariante sous la transformation *infinitésimale* de paramètre  $\xi_a$  à l'ordre  $g$ ,

$$A_\mu^a \rightarrow A_\mu^a + gf_{abc} \xi_b A_\mu^c. \quad (2.11)$$

En revanche, si le paramètre  $\xi_a$  de Eq.(2.11) dépend de l'espace-temps, l'action  $S_0$  de Eq.(2.8) n'est plus invariante et sa variation vaut,

$$\delta S_0 = \int d^4x j_a^\mu \partial_\mu \xi_a, \quad (2.12)$$

où,

$$j_a^\mu = gf_{abc} G_b^{\mu\nu} A_\nu^c, \quad (2.13)$$

est le courant de Noether associé à la symétrie correspondant aux générateurs  $T_a$ . Nous remarquons l'analogie entre les équations Eq.(2.4) et Eq.(2.12). L'invariance est restaurée à l'ordre  $g$  si on ajoute à l'action de Eq.(2.8) le terme,

$$S_1 = S_0 - \frac{1}{2} \int d^4x j_a^\mu A_\mu^a, \quad (2.14)$$

et si la loi de transformation (2.11) est modifiée en,

$$A_\mu^a \rightarrow A_\mu^a + gf_{abc} \xi_b A_\mu^c + \partial^\mu \xi_a. \quad (2.15)$$

Remarquons à nouveau l'analogie entre les équations Eq.(2.7), Eq.(2.3) et Eq.(2.14), Eq.(2.15). Notons aussi que l'action de Eq.(2.8) est invariante sous la transformation locale,

$$A_\mu^a \rightarrow A_\mu^a + \partial^\mu \xi_a, \quad (2.16)$$



qui correspond à une symétrie abélienne. Lorsque la transformation du groupe de Lie est considérée au second ordre en  $g$ , la variation de l'action  $S_1$  sous (2.15) (au second ordre) est,

$$\delta S_1 = \int d^4x j_\mu^d \partial^\mu \xi_d. \quad (2.17)$$

avec,

$$j_\mu^d = -g^2 f_{abc} f_{bde} A_\mu^a A_\nu^c A_e^\nu. \quad (2.18)$$

Comme précédemment, l'invariance est restaurée en ajoutant à l'action un terme :

$$S = S_1 - \frac{1}{4} \int d^4x j_\mu^d A_d^\mu. \quad (2.19)$$

Il n'est pas nécessaire ici de modifier la loi de transformation (2.15) définie au second ordre. En fait, un effort supplémentaire nous montrerait même que l'action  $S$  de Eq.(2.19) est invariante à tout ordre en  $g$ . Cette action  $S$  peut aussi s'écrire,

$$S = -\frac{1}{4} \int d^4x F_{\mu\nu}^a F_a^{\mu\nu}, \quad (2.20)$$

avec,

$$F_a^{\mu\nu} = G_a^{\mu\nu} - g f_{abc} A_b^\mu A_c^\nu = \partial^\mu A_a^\nu - \partial^\nu A_a^\mu - g f_{abc} A_b^\mu A_c^\nu. \quad (2.21)$$

Et nous reconnaissons ici l'action d'une théorie de jauge non-abélienne pure.

## 2.2.2 Lagrangien localement supersymétrique pour le multiplet de supergravité

L'action globalement supersymétrique pour le multiplet de supergravité est la suivante,

$$S = -\frac{1}{2} \int d^4x \epsilon^{\mu\nu\rho\sigma} \bar{\Psi}_\mu \gamma_5 \gamma_\nu \partial_\rho \Psi_\sigma - \frac{1}{2} \int d^4x (R_{\mu\nu}^L - \frac{1}{2} \eta_{\mu\nu} R^L) h^{\mu\nu}, \quad (2.22)$$

où  $\epsilon^{\mu\nu\rho\sigma}$  désigne le tenseur antisymétrique de Levi-Civita défini tel que  $\epsilon^{0123} = 1$ ,  $R_{\mu\nu}^L$  dénote le tenseur de Ricci donné par,

$$R_{\mu\nu}^L = \frac{1}{2} \left( -\frac{\partial^2 h_{\mu\nu}}{\partial x^\lambda \partial x_\lambda} + \frac{\partial^2 h_\nu^\lambda}{\partial x^\mu \partial x^\lambda} + \frac{\partial^2 h_\mu^\lambda}{\partial x^\nu \partial x^\lambda} - \frac{\partial^2 h_\lambda^\lambda}{\partial x^\mu \partial x^\nu} \right), \quad (2.23)$$

et  $R^L$  est la courbure scalaire donnée par  $R^L = \eta^{\mu\nu} R_{\mu\nu}^L$ .

Le premier terme de Eq.(2.22) est l'action de Rarita-Schwinger qui fournit un terme cinétique au partenaire supersymétrique  $\Psi_\mu$  du graviton. Le champ  $\Psi_\mu$ , qui est appelé le gravitino, a un spin 3/2. Le partenaire du graviton aurait pu être choisi comme étant un champ de spin 5/2, mais les théories contenant des particules de spin plus grand que 2 ont des particularités indésirables. Nous vérifierons par la suite que ce choix est correct puisque le gravitino de spin 3/2 apparaîtra comme le "champ de jauge" associé à la supersymétrie locale. Le second terme de Eq.(2.22) est l'action d'Einstein linéarisée, c'est

à dire l'action d'Einstein écrite au premier ordre en  $\kappa$  et exprimée en fonction du champ du graviton  $h_{\mu\nu}$  défini par,

$$g_{\mu\nu} = \eta_{\mu\nu} + \kappa h_{\mu\nu}, \quad (2.24)$$

où  $g_{\mu\nu}$  est la métrique d'espace-temps,  $\eta_{\mu\nu}$  est la métrique de Minkowski et  $\kappa$  est donné par,

$$8\pi G_N M_P^2 = \kappa^2 M_P^2 = 1, \quad (2.25)$$

$G_N$  étant la constante gravitationnelle de Newton et  $M_P$  la masse de Planck (il sera parfois utile de choisir l'unité  $\kappa^2 = 1$ ). Le facteur  $\kappa$  est introduit dans Eq.(2.24) afin que  $h_{\mu\nu}$  ait une dimension 1, comme cela est approprié pour un champ bosonique décrivant le graviton. Nous utilisons ici l'action d'Einstein linéarisée (Eq.(2.22)) pour deux raisons. La première est que cette forme de l'action d'Einstein fait apparaître des termes cinétiques pour le graviton  $h_{\mu\nu}$  qui sont quadratiques (Eq.(2.23)). La seconde est que nous allons déterminer dans la suite l'action de supergravité pure (Eq.(2.22)) invariante sous la supersymétrie locale au premier ordre en  $\kappa$ .

L'action du multiplet de supergravité (Eq.(2.22)) est invariante sous les transformations de supersymétrie globale de paramètre  $\mathcal{E}$  constant,

$$h_{\mu\nu} \rightarrow h_{\mu\nu} + \delta_{\mathcal{E}} h_{\mu\nu} = h_{\mu\nu} - \frac{i}{2} \bar{\mathcal{E}} (\gamma_{\mu} \Psi_{\nu} + \gamma_{\nu} \Psi_{\mu}), \quad (2.26)$$

$$\Psi_{\mu} \rightarrow \Psi_{\mu} + \delta_{\mathcal{E}} \Psi_{\mu} = \Psi_{\mu} - i \sigma^{\rho\tau} \partial_{\rho} h_{\tau\mu} \mathcal{E}. \quad (2.27)$$

Nous renvoyons le lecteur à la référence [21] pour ce qui est de la détermination du lagrangien de supergravité pure (Eq.(2.22)) ainsi que des transformations de supersymétrie globale associées (Eq.(2.26) et Eq.(2.27)).

Tentons à présent de rendre l'action de supergravité pure (Eq.(2.22)) invariante au premier ordre en  $\kappa$  sous la supersymétrie locale, c'est à dire sous l'action de  $e^{i\mathcal{E}(x)Q}$ , où  $Q$  est un générateur de SUSY et  $\mathcal{E}(x)$  est un spineur de Majorana dépendant des coordonnées d'espace et de temps. La variation de l'action de supergravité pure (Eq.(2.22)) sous la supersymétrie locale à l'ordre  $\kappa$  est,

$$\delta S = \int d^4 x \bar{j}^{\mu} \partial_{\mu} \mathcal{E}, \quad (2.28)$$

où le spineur de Majorana vectoriel  $j^{\mu}$  est le courant de Noether donné par,

$$\bar{j}^{\mu} = \frac{i}{2} \epsilon^{\mu\nu\rho\sigma} \bar{\Psi}_{\rho} \gamma_5 \gamma_{\nu} \sigma^{\lambda\tau} \partial_{\lambda} h_{\tau\sigma}. \quad (2.29)$$

L'invariance sous la supersymétrie locale peut être obtenue à l'ordre  $\kappa$ , en modifiant la loi de transformation du gravitino de Eq.(2.27) en,

$$\Psi_{\mu} \rightarrow \Psi_{\mu} + \delta_{\mathcal{E}} \Psi_{\mu} = \Psi_{\mu} - i \sigma^{\rho\tau} \partial_{\rho} h_{\tau\mu} \mathcal{E} + a \kappa^{-1} \partial_{\mu} \mathcal{E}, \quad (2.30)$$

où  $a$  est une constante, et en ajoutant un terme à l'action (2.22) du type,

$$S_1 = S - \frac{\kappa}{2a} \int d^4 x \bar{j}^{\mu} \Psi_{\mu}. \quad (2.31)$$

Aucune modification de la loi de transformation (2.27) n'est requise à ce stade. Nous remarquons l'analogie entre les équations Eq.(2.15), Eq.(2.14) et Eq.(2.30), Eq.(2.31).

En itérant ce processus, nous obtenons comme dans la Section 2.2.1, les transformations finales de supersymétrie locale qui sont,

$$e_\mu^m \rightarrow e_\mu^m + \delta_\mathcal{E} e_\mu^m = e_\mu^m - i\kappa \bar{\mathcal{E}} \gamma^m \Psi_\mu, \quad (2.32)$$

où  $e_\mu^m$  est le vierbein ( $\mu$  étant l'index d'univers et  $m$  l'index local de Lorentz) satisfaisant à,  $h_{\mu\nu} = e_\mu^m e_\nu^n \eta_{mn}$ , et,

$$\Psi_\mu \rightarrow \Psi_\mu + \delta_\mathcal{E} \Psi_\mu = \Psi_\mu + 2\kappa^{-1} D_\mu \mathcal{E}, \quad (2.33)$$

où  $D_\mu$  est la dérivée covariante,

$$D_\mu = \partial_\mu - i\tilde{w}_{\mu mn} \frac{\sigma^{mn}}{4} \quad (2.34)$$

avec,

$$\tilde{w}_{\mu mn} = w_{\mu mn} + \frac{i\kappa^2}{4} (\bar{\Psi}_\mu \gamma_m \Psi_n + \bar{\Psi}_m \gamma_\mu \Psi_n - \bar{\Psi}_\mu \gamma_n \Psi_m) \quad (2.35)$$

et,

$$w_{\mu mn} = \frac{1}{2} e_m^\nu (\partial_\mu e_{n\nu} - \partial_\nu e_{n\mu}) + \frac{1}{2} e_m^\rho e_n^\sigma \partial_\sigma e_{\rho\mu} - (m \rightarrow n), \quad (2.36)$$

qui est la connection de spin standard. Et l'action finale localement supersymétrique que l'on obtient est :

$$S = -\frac{1}{2\kappa^2} \int d^4x |det e| R - \frac{1}{2} \int d^4x \epsilon^{\mu\nu\rho\sigma} \bar{\Psi}_\mu \gamma_5 \gamma_\nu D_\rho \Psi_\sigma. \quad (2.37)$$

Le premier terme est l'action d'Einstein sous sa forme générale (non linéarisée) car l'action de Eq.(2.37) est exactement invariante sous la supersymétrie locale (non pas seulement au premier ordre en  $\kappa$ , comme l'est l'action de Eq.(2.31)). Le second terme est l'action de Rarita-Schwinger avec une dérivée covariante. Cette dérivée covariante implique le champ du gravitino (voir Eq.(2.34)) de même que les dérivées covariantes des théories de jauge impliquent les bosons de jauge (voir Eq.(2.7)).

En conclusion, la supersymétrie locale est réalisée grâce au fait que le gravitino se comporte comme le “boson de jauge” de la supersymétrie (voir Eq.(2.30), Eq.(2.31) et Eq.(2.34)). Le gravitino joue donc un rôle aussi naturel que majeur dans les théories de supersymétrie locale.

### 2.2.3 Lagrangien localement supersymétrique pour un supermultiplet chiral libre et non massif

Considérons le lagrangien du supermultiplet chiral libre et non massif du modèle de Wess Zumino :

$$\mathcal{L}_0 = \partial_\mu \phi^* \partial^\mu \phi + \frac{i}{2} \bar{\Psi} \gamma^\mu \partial_\mu \Psi \quad (2.38)$$

où  $\Psi$  est un spineur de Majorana. Le lagrangien de Eq.(2.38) est invariant sous les transformations de supersymétrie globale suivantes (voir Section 1.4.2) :

$$\delta A = \bar{\mathcal{E}}\Psi, \quad (2.39)$$

$$\delta B = i\bar{\mathcal{E}}\gamma_5\Psi, \quad (2.40)$$

$$\delta\Psi = -i\gamma^\mu\partial_\mu(A + i\gamma_5 B)\mathcal{E}, \quad (2.41)$$

où  $A$  et  $B$  sont les champs réels définis à partir du champ  $\phi$  par,

$$\phi = \frac{1}{\sqrt{2}}(A + iB), \quad (2.42)$$

et  $\mathcal{E}$  est le paramètre spineur de Majorana donné par,

$$\mathcal{E} = \begin{pmatrix} \mathcal{E}_W \\ \bar{\mathcal{E}}_W \end{pmatrix}. \quad (2.43)$$

Lorsque la supersymétrie devient locale, c'est à dire lorsque le paramètre  $\mathcal{E}$  des transformations (2.39)-(2.41) dépend de l'espace-temps, la variation du lagrangien (2.38) est (à une dérivée près),

$$\delta\mathcal{L}_0 = \partial_\mu\bar{\mathcal{E}}j^\mu, \quad (2.44)$$

où  $j^\mu$  est le spineur vectoriel suivant,

$$j^\mu = \not{D} (A - i\gamma_5 B)\gamma^\mu\Psi. \quad (2.45)$$

Remarquons l'analogie entre les équations Eq.(2.44) et Eq.(2.28). Afin de rendre le lagrangien  $\mathcal{L}_0$  localement supersymétrique, et par analogie avec l'équation Eq.(2.31), nous ajoutons au lagrangien le terme,

$$\mathcal{L} = \mathcal{L}_0 + a\bar{\Psi}_\mu j^\mu, \quad (2.46)$$

où  $\Psi_\mu$  doit être un spineur vectoriel de même que  $j^\mu$ . Nous associons ce spineur vectoriel au champ du gravitino. Si le gravitino se transforme sous la supersymétrie locale selon,

$$\Psi_\mu \rightarrow \Psi_\mu + 2\kappa^{-1}\partial_\mu\mathcal{E}, \quad (2.47)$$

alors le lagrangien  $\mathcal{L}$  de Eq.(2.46) est invariant sous la supersymétrie locale au premier ordre en  $\kappa$  pour,

$$a = -\frac{\kappa}{2}. \quad (2.48)$$

Le lagrangien localement supersymétrique final, obtenu en itérant cette méthode plusieurs fois, vaut,

$$\mathcal{L}_f = -\frac{1}{2\kappa^2}|det\,e|R - \frac{1}{2}\epsilon^{\mu\nu\rho\sigma}\bar{\Psi}_\mu\gamma_5\gamma_\nu\tilde{D}_\rho\Psi_\sigma + |det\,e|\partial_\mu\phi^*\partial^\mu\phi$$

$$\begin{aligned}
& -\frac{\kappa}{2} |det e| \bar{\Psi}_\mu \phi (A - i\gamma_5 B) \gamma^\mu \Psi - \frac{i\kappa^2}{4} \epsilon^{\mu\tau\rho\sigma} \bar{\Psi}_\mu \gamma_\tau \Psi_\rho A \overleftrightarrow{D}_\sigma B \\
& -\frac{\kappa^2}{4} |det e| \bar{\Psi} \gamma_5 \gamma^\mu \Psi A \overleftrightarrow{D}_\mu B + \text{Termes}(4 \text{ fermions}),
\end{aligned} \tag{2.49}$$

où les dérivées  $D_\mu$  sont des dérivées covariantes vis-à-vis de la gravitation. Les lois de supersymétrie locale obtenues sont,

$$\delta A = \bar{\mathcal{E}} \Psi, \tag{2.50}$$

$$\delta B = i\bar{\mathcal{E}} \gamma_5 \Psi, \tag{2.51}$$

$$\delta e_\mu^m = -i\kappa \bar{\mathcal{E}} \gamma^m \Psi_\mu \tag{2.52}$$

$$\delta \Psi_\mu = 2\kappa^{-1} D_\mu \mathcal{E} + i\kappa \mathcal{E} A \overleftrightarrow{D}_\mu B + \text{Termes}(2 \text{ fermions}), \tag{2.53}$$

$$\delta \Psi = -i\gamma^\mu D_\mu (A + i\gamma_5 B) \mathcal{E} + \text{Termes}(2 \text{ fermions}). \tag{2.54}$$

Les deux premiers termes du lagrangien  $\mathcal{L}_f$  de Eq.(2.49) sont les deux termes du lagrangien de supergravité pure (voir Eq.(2.37)). Par ailleurs, la transformation du gravitino 2.53 contient la transformation du gravitino 2.33 d'une théorie de supergravité pure. Nous en concluons que le choix du gravitino comme boson de jauge de la supersymétrie locale est cohérent. Une fois encore donc, le gravitino acquiert naturellement un rôle crucial lorsque la supersymétrie locale est requise.

Notons finalement qu'une approche similaire permet de dériver les couplages du supermultiplet vectoriel à la supergravité.

## 2.2.4 Lagrangien localement supersymétrique général

Le lagrangien localement supersymétrique général peut s'obtenir à partir du lagrangien globalement supersymétrique, en utilisant, comme dans les sections précédentes, la procédure de Noether. Cependant, en pratique, ce résultat compliqué a été déduit de la méthode de calcul tensoriel local [30, 31, 32]. Nous présentons ici ce lagrangien général de supergravité. Le lagrangien globalement supersymétrique le plus général s'écrit,

$$\mathcal{L}_{GLOBAL} = -3 \int d^4\theta e^{-\frac{1}{3}K(\Phi^\dagger e^{2gV}, \Phi)} + \int d^2\theta (W(\Phi) + h.c.) + \int d^2\theta (f_{ab}(\Phi) W_a^\alpha W_{\alpha b} + h.c.), \tag{2.55}$$

où  $W_a^\alpha$  représente le superchamp de jauge,  $\alpha$  étant l'indice spinoriel et  $a$  l'indice du groupe de jauge.  $K$  est une fonction générale de  $\Phi_i$  et  $\Phi_i^\dagger e^{2gV}$  appelée potentiel de Kähler qui autorise des termes cinétiques non renormalisables et  $f_{ab}$  est une fonction arbitraire de  $\Phi_i$  se réduisant à  $\delta_{ab}$  dans le cas renormalisable. De même, le superpotentiel  $W$  peut contenir des puissances arbitraires des superchamps  $\Phi_i$ . Il apparaît en fait que le lagrangien de

supergravité ne dépend que d'une fonction simple des champs scalaires,  $\phi_i$  et  $\phi_i^*$ , appelée potentiel de Kähler généralisé et définie par,

$$G(\phi, \phi^*) = K(\phi, \phi^*) + \ln|W|^2. \quad (2.56)$$

Les mêmes lagrangiens de supergravité peuvent être obtenus pour différents choix de  $K$  et  $W$ , car  $G$  est invariant sous les transformations suivantes :

$$\begin{aligned} K &\rightarrow K + h(\phi) + h^*(\phi^*) \\ W &\rightarrow e^{-h}W \end{aligned} \quad (2.57)$$

pour une fonction  $h$  arbitraire.

Le lagrangien de supergravité général  $\mathcal{L}_{SUGRA}$  peut se décomposer en,

$$\mathcal{L}_{SUGRA} = \mathcal{L}_B + \mathcal{L}_{FK} + \mathcal{L}_F + \tilde{\mathcal{L}}_B + \tilde{\mathcal{L}}_{FK} + \tilde{\mathcal{L}}_F, \quad (2.58)$$

où  $\mathcal{L}_B$  contient les champs scalaires,  $\mathcal{L}_{FK}$  contient les champs fermioniques ainsi que des dérivées covariantes (en particulier les termes cinétiques pour les fermions) et  $\mathcal{L}_F$  contient les champs fermioniques (en particulier les couplages de Yukawa) mais pas de dérivées covariantes. Les lagrangiens  $\tilde{\mathcal{L}}_B$ ,  $\tilde{\mathcal{L}}_{FK}$  et  $\tilde{\mathcal{L}}_F$  contiennent les champs de jauge. Si  $R$  est la courbure scalaire et  $|det e|$  le déterminant du vierbein  $e_\mu^m$ , alors la partie bosonique du lagrangien est donnée par (en unités telles que  $\kappa^2 = 1$ ),

$$|det e|^{-1}\mathcal{L}_B = -\frac{1}{2}R + G_j^i D_\mu \phi_i D^\mu \phi^{j*} + e^G (3 - G_i (G^{-1})^i_j G^j), \quad (2.59)$$

où les dérivées  $D_\mu$  sont covariantes vis à vis des groupes de jauge mais aussi de la gravité. Les dérivées du potentiel de Kähler généralisé par rapport aux champs scalaires  $\phi_i$  et  $\phi^{i*}$  sont notées,

$$G_i = \frac{\partial G}{\partial \phi^{i*}}, \quad G^i = \frac{\partial G}{\partial \phi_i}, \quad G_j^i = \frac{\partial^2 G}{\partial \phi_i \partial \phi^{j*}}. \quad (2.60)$$

De plus, l'inverse  $(G^{-1})_j^i$  est défini par,

$$(G^{-1})_j^i G_k^j = \delta_k^i. \quad (2.61)$$

Les termes cinétiques fermioniques sont donnés par le lagrangien suivant,

$$\begin{aligned} |det e|^{-1}\mathcal{L}_{FK} = & -\frac{1}{2}|det e|^{-1}\epsilon^{\mu\nu\rho\sigma}\bar{\Psi}_\mu\gamma_5\gamma_\nu D_\rho\Psi_\sigma + \frac{1}{4}|det e|^{-1}\epsilon^{\mu\nu\rho\sigma}\bar{\Psi}_\mu\gamma_\nu\Psi_\rho(G^i D_\sigma\phi_i - G_i D_\sigma\phi^{i*}) \\ & + \left( \frac{i}{2}G_j^i\bar{\Psi}_{iL}\gamma^\mu D_\mu\Psi_L^j + \frac{i}{2}\bar{\Psi}_{iL}\not{D}\phi_j\Psi_{kL}(-G_k^{ij} + \frac{1}{2}G_k^i G^j) \right. \\ & \left. + \frac{1}{\sqrt{2}}G_j^i\bar{\Psi}_{\mu L}\not{D}\phi^{i*}\gamma^\mu\Psi_{jR} + h.c. \right), \end{aligned} \quad (2.62)$$

et les interactions de Yukawa viennent de (voir la littérature originelle [33] et la revue sur la supersymétrie [34] pour le lagrangien complet),

$$|det e|^{-1}\mathcal{L}_F = \frac{i}{2}e^{G/2}\bar{\Psi}_\mu\sigma^{\mu\nu}\Psi_\nu$$

$$\begin{aligned}
& + \left( \frac{1}{2} e^{G/2} (-G^{ij} - G^i G^j + G_k^{ij} (G^{-1})^k_l G^l) \bar{\Psi}_{iL} \Psi_{jR} \frac{i}{\sqrt{2}} e^{G/2} G^i \bar{\Psi}_{\mu L} \gamma^\mu \Psi_{iL} + h.c. \right) \\
& + \text{Termes}(4 \text{ fermions}).
\end{aligned} \tag{2.63}$$

$\tilde{\mathcal{L}}_B$  est donné par,

$$\begin{aligned}
|\det e|^{-1} \tilde{\mathcal{L}}_B &= -\frac{1}{4} \text{Re}(f_{ab})(F_a)_{\mu\nu} F_b^{\mu\nu} - \frac{i}{4} \text{Im}(f_{ab})(F_a)_{\mu\nu} \tilde{F}_b^{\mu\nu} \\
&\quad - \frac{g^2}{2} \text{Re}(f_{ab}^{-1}) G^i (T_a)_{ij} \phi_j G^k (T_b)_{kl} \phi_l,
\end{aligned} \tag{2.64}$$

où les  $(T_a)_{ij}$  sont les générateurs du groupe de jauge, les champs de jauge sont définis par,

$$(F_a)_{\mu\nu} = \partial_\mu V_{\nu a} - \partial_\nu V_{\mu a} - g f_{abc} V_{\mu b} V_{\nu c}, \tag{2.65}$$

et leur dual par,

$$(\tilde{F}_a)_{\mu\nu} = \epsilon_{\mu\nu\rho\sigma} (F_a)^{\rho\sigma}. \tag{2.66}$$

$\tilde{\mathcal{L}}_{FK}$  s'écrit,

$$\begin{aligned}
|\det e|^{-1} \tilde{\mathcal{L}}_{FK} &= \frac{1}{2} \text{Re}(f_{ab}(\phi)) \left( \frac{1}{2} \bar{\lambda}_a \not{D} \lambda_b + \frac{1}{2} \bar{\lambda}_a \gamma^\mu \sigma^{\nu\rho} \Psi_\mu (F_b)_{\nu\rho} + \frac{1}{2} G^i D^\mu \phi_i \bar{\lambda}_{aL} \gamma_\mu \lambda_{bL} \right) \\
&\quad - \frac{i}{8} \text{Im}(f_{ab}(\phi)) D_\mu (|\det e| \bar{\lambda}_a \gamma_5 \gamma^\mu \lambda_b) - \frac{1}{2} \frac{\partial f_{ab}(\phi)}{\partial \phi_i} \bar{\Psi}_{iR} \sigma^{\mu\nu} (F_a)_{\mu\nu} \lambda_{bL} + h.c.,
\end{aligned} \tag{2.67}$$

où  $\lambda_a$  est le jaugino. Finalement,  $\tilde{\mathcal{L}}_F$  vaut,

$$\begin{aligned}
|\det e|^{-1} \tilde{\mathcal{L}}_F &= \frac{1}{4} e^{G/2} \frac{\partial f_{ab}^*}{\partial \phi^{j*}} (G^{-1})^j_k G^k \lambda_a \lambda_b - \frac{i}{2} g G^i (T_a)_{ij} \phi_j \bar{\Psi}_{\mu L} \gamma^\mu \lambda_{aL} + 2ig G_j^i (T_a)_{ik} \phi_k \bar{\lambda}_{aR} \Psi_{iL} \\
&\quad - \frac{i}{2} g \text{Re}(f_{ab}^{-1}) \frac{\partial f_{bc}}{\partial \phi_k} G^i (T_a)_{ij} \phi_j \bar{\Psi}_{kR} + \lambda_{cL} + h.c. + \text{Termes}(4 \text{ fermions}).
\end{aligned} \tag{2.68}$$

Notons que le lagrangien de Eq.(2.68) peut donner des termes de masse pour les jauginos si les champs scalaires  $\phi_i$  développent des valeurs moyennes dans le vide.

Les transformations de supersymétrie locale associées au lagrangien  $\mathcal{L}_{SUGRA}$  (Eq.(2.58)) sont définies par les variations infinitésimales suivantes (voir la littérature originelle [33] pour les expressions complètes),

$$\delta \phi_i = \sqrt{2} \bar{\mathcal{E}} \Psi_i = \sqrt{2} \bar{\mathcal{E}}_R \Psi_{iL}, \tag{2.69}$$

$$\delta e_\mu^m = -i \kappa \bar{\mathcal{E}} \gamma^m \Psi_\mu, \tag{2.70}$$

$$\delta \Psi_\mu = 2\kappa^{-1} D_\mu \mathcal{E} + \kappa \mathcal{E} (G^i D_\mu \phi_i - G_i D_\mu \phi^{i*}) + ie^{G/2} \gamma_\mu \mathcal{E} + \text{Termes}(2 \text{ fermions}), \tag{2.71}$$

$$\delta \Psi_i = -i \not{D} (A_i + i\gamma_5 B_i) \mathcal{E} - \sqrt{2} e^{G/2} (G^{-1})^j_i G_j \mathcal{E} + \text{Termes}(2 \text{ fermions}), \tag{2.72}$$

$$\delta V_a^\mu = -\bar{\mathcal{E}}_L \gamma^\mu \lambda_{aL} + h.c., \quad (2.73)$$

$$\delta \lambda_{aL} = \sigma^{\mu\nu} (F_a)_{\mu\nu} \mathcal{E}_L + \frac{i}{2} g \text{Re}(f_{ab}^{-1}) G^i (T_b)_{ij} \phi_j \mathcal{E}_L + \text{Termes}(2 \text{ fermions}), \quad (2.74)$$

où  $\phi_i$  se décompose en deux champs scalaires réels  $A_i$  et  $B_i$  comme,

$$\phi_i = \frac{1}{\sqrt{2}} (A_i + iB_i). \quad (2.75)$$

Remarquons que le lagrangien invariant par supergravité n'incluant pas de champs de jauge (supermultiplets vectoriels),  $\mathcal{L} = \mathcal{L}_B + \mathcal{L}_{FK} + \mathcal{L}_F$ , génère le lagrangien invariant sous la supersymétrie globale (accompagné de termes non renormalisables), pour un superpotentiel de la forme,

$$W(\Phi) = \lambda_{ijk} \Phi_i \Phi_j \Phi_k, \quad (2.76)$$

et pour un potentiel de Kähler valant,

$$K(\Phi^\dagger, \Phi) = -3 \ln(1 - \frac{1}{3} \Phi_i^\dagger \Phi_i). \quad (2.77)$$

Bien que la constante n'aie pas de signification dans une théorie globalement supersymétrique, celle-ci est importante dans une théorie de supersymétrie locale qui est couplée à la gravité.

Par ailleurs, une théorie incluant la gravité n'a pas de raison d'être renormalisable. En particulier, le potentiel de Kähler n'est pas obligatoirement celui qui correspond uniquement à des termes cinétiques renormalisables dans la théorie supersymétrique globale. Il est en revanche utile pour les calculs de définir la forme du potentiel de Kähler qui donne les termes cinétiques minimaux dans le lagrangien de supergravité. Cette forme du potentiel de Kähler est,

$$K(\Phi^\dagger, \Phi) = \Phi_i \Phi_i^\dagger, \quad (2.78)$$

soit,

$$G = \phi_i \phi_i^{i*} + \ln|W|^2, \quad (2.79)$$

d'où,

$$G_j^i = \delta_j^i. \quad (2.80)$$

D'après l'Eq.(2.80), les termes cinétiques sont simplement,  $\partial_\mu \phi_i \partial^\mu \phi_i^\star$ , pour les champs scalaires (voir  $\mathcal{L}_B$ ) et,  $\frac{i}{2} \bar{\Psi}_{iL} \gamma^\mu \partial_\mu \Psi_{iL} + h.c.$ , pour les champs fermioniques (voir  $\mathcal{L}_{FK}$ ).

## 2.3 Brisure spontanée en supergravité

Pour avoir une brisure spontanée en supergravité, au moins un des champs doit avoir une VEV qui n'est pas invariante sous l'action de la supersymétrie locale. Les seules transformations supersymétriques parmi les Eq.(2.69)-Eq.(2.74) pouvant avoir un membre



de droite ayant une VEV non nulle sans briser l'invariance de Lorentz, sont les lois des Eq.(2.72) et (2.74). Si nous supposons qu'il n'y a pas de VEV pour les termes impliquant des champs fermioniques, les valeurs moyennes dans le vide des Eq.(2.72) et (2.74) s'écrivent,

$$\langle 0|\delta\Psi_i|0\rangle = -e^{G/2}(G^{-1})^j_i G_j \mathcal{E}, \quad (2.81)$$

$$\langle 0|\delta\lambda_a|0\rangle = \frac{i}{2}g\text{Re}f_{ab}^{-1}G^i(T_b)_{ij}\phi_j \mathcal{E}, \quad (2.82)$$

où les champs scalaires ont été utilisés afin de dénoter les VEV.

Considérons tout d'abord le cas simple d'un superchamp chiral singlet de jauge avec les termes cinétiques minimaux, c'est à dire le cas :

$$G = \phi\phi^* + \ln|W|^2. \quad (2.83)$$

Les Eq.(2.81) et (2.82) deviennent alors,

$$\langle 0|\delta\Psi|0\rangle = -\frac{\exp(\frac{1}{2}(\phi^*\phi + \ln|W|^2))}{W^*} \left( \frac{\partial W^*}{\partial \phi^*} + \phi W^* \right) \mathcal{E}, \quad (2.84)$$

$$\langle 0|\delta\lambda_a|0\rangle = 0. \quad (2.85)$$

Le critère de brisure spontanée est donc,

$$\frac{\partial W}{\partial \phi} + \phi^* W \neq 0. \quad (2.86)$$

Ceci est la généralisation de la brisure de supersymétrie globale par un terme F.

Qu'en est-il du potentiel ? D'après l'équation Eq.(2.83) et le lagrangien  $\mathcal{L}_B$ , le potentiel vaut,

$$V = e^{\phi^*\phi} \left( \left| \frac{\partial W}{\partial \phi} + \phi^* W \right|^2 - 3|W|^2 \right), \quad (2.87)$$

à comparer avec,  $V = |W|^2$ , dans le cas d'une supersymétrie globale. D'après Eq.(2.87), l'énergie du vide a maintenant la possibilité d'être négative. Nous remarquons même d'après Eq.(2.86) que l'énergie du vide supersymétrique est négative puisque le potentiel correspondant vaut,

$$V = -3e^{\phi^*\phi}|W|^2. \quad (2.88)$$

D'après Eq.(2.86), lorsque la supersymétrie est brisée, une annulation dans le potentiel (Eq.(2.87)) peut donner un vide d'énergie nulle. Dans les théories de supergravité, il existe donc une possibilité d'obtenir un état du vide ayant une constante cosmologique nulle, si la supersymétrie est brisée.

Étudions à présent le cas d'un superchamp chiral appartenant à une représentation non triviale du groupe de jauge avec les termes cinétiques minimaux (voir Eq.(2.79)). Choisissons aussi les termes cinétiques minimums pour les champs de jauge, c'est à dire,

$$f_{ab}(\phi) = \delta_{ab}. \quad (2.89)$$

Les Eq.(2.81) et (2.82) deviennent alors,

$$\langle 0|\delta\Psi_i|0\rangle = -\frac{\exp(\frac{1}{2}(\phi^{j*}\phi_j + \ln|W|^2))}{W^*} \left( \frac{\partial W^*}{\partial \phi_i^*} + \phi^i W^* \right) \mathcal{E}, \quad (2.90)$$

$$\langle 0|\delta\lambda_a|0\rangle = \frac{i}{2} g G^i(T_a)_{ij} \phi_j \mathcal{E}. \quad (2.91)$$

Il y a dans ce cas deux critères possibles de brisure spontanée :

$$\frac{\partial W}{\partial \phi_i} + \phi_i^* W \neq 0, \text{ pour certaines valeurs de } i, \quad (2.92)$$

$$G^i(T_a)_{ij} \phi_j \neq 0, \text{ pour certaines valeurs de } a, \quad (2.93)$$

qui sont les généralisations de la brisure de supersymétrie globale par un terme F ou par un terme D, respectivement.

D'après l'équation Eq.(2.79) et les lagrangiens  $\mathcal{L}_B$  et  $\tilde{\mathcal{L}}_B$ , le potentiel vaut,

$$V = e^{\phi^{j*}\phi_j} \left( \left| \frac{\partial W}{\partial \phi_i} + \phi^{i*} W \right|^2 - 3|W|^2 \right) + \frac{g^2}{2} G^i(T_a)_{ij} \phi_j G^k(T_a)_{kl} \phi_l, \quad (2.94)$$

où,

$$G^i = \phi^{i*} + \frac{1}{W} \frac{\partial W}{\partial \phi_i} \quad (2.95)$$

à comparer avec le potentiel semi-défini positif d'une théorie globalement supersymétrique,

$$V = \left| \frac{\partial W}{\partial \phi_i} \right|^2 + \frac{g^2}{2} \phi^{i*}(T_a)_{ij} \phi_j \phi^{k*}(T_a)_{kl} \phi_l. \quad (2.96)$$

Nous remarquons d'après Eq.(2.95) que la condition de brisure de Eq.(2.92) est équivalente à  $G^i \neq 0$ . Et le champ  $G^i \Psi_i$  n'est en fait rien d'autre que le fermion de Goldstone associé à la brisure de supersymétrie. Il y a un mélange entre ce fermion de Goldstone et le gravitino  $\Psi_\mu$ , comme nous le voyons dans le lagrangien  $\mathcal{L}_F$ . Le fermion de Goldstone (de spin  $\frac{1}{2}$ ) est en fait "mangé" par le gravitino (de spin  $\frac{3}{2}$ ) qui devient alors massif. C'est ce que l'on nomme le mécanisme de super-Higgs. Le terme de masse du gravitino est le premier terme du lagrangien  $\mathcal{L}_F$ . La masse du gravitino,  $m_{3/2}$ , est une fonction de la valeur dans le vide de la fonction  $G$ , notée  $G_0$ , ainsi que de la masse de Planck,  $M_P$  :

$$m_{3/2} \approx e^{G_0/2} M_P, \quad (2.97)$$

puisque nous avons choisi de travailler en unités de  $\kappa^2$  qui est défini dans Eq.(2.25).

Remarquons que le gravitino se comporte une fois encore comme un 'boson de jauge' pour la supersymétrie locale dans la mesure où il acquiert une masse lors de la brisure spontanée de la supersymétrie locale.

## 2.4 Brisure de la supersymétrie dans le secteur “caché”

Comme nous allons le voir dans la prochaine section, la brisure de supersymétrie locale opère de manière satisfaisante lorsqu’elle est transmise au secteur ”observable” à partir d’un secteur “caché”. Par brisure satisfaisante de la supersymétrie locale nous entendons une brisure engendrant, par le biais de termes de brisure douce (voir Section 1.5), des masses pour les particules supersymétriques supérieures aux masses des particules du Modèle Standard et inférieures au TeV (voir Section 1.3.1). Par ailleurs, le secteur caché est un ensemble de particules interagissant avec les particules du MSSM uniquement via les forces gravitationnelles.

Considérons donc le modèle le plus simple de brisure de la supersymétrie locale dans un secteur caché : Le modèle de Polonyi. Dans ce modèle, le secteur caché comprend un unique superchamp chiral  $\Phi$  et le superpotentiel associé est le suivant,

$$W(\Phi) = m^2(\Phi + \beta), \quad (2.98)$$

$m$  et  $\beta$  étant des paramètres réels ayant des dimensions de masse. Pour des raisons de simplicité nous adoptons aussi le choix de scénario dans lequel les termes cinétiques sont minimaux (voir Eq.(2.83)). Pour le superpotentiel de Eq.(2.98), le potentiel s’écrit donc, d’après Eq.(2.87),

$$V = m^4 e^{\phi^* \phi} (|1 + \phi^*(\phi + \beta)|^2 - 3|\phi + \beta|^2). \quad (2.99)$$

Nous pouvons montrer que pour la valeur,  $\beta = 2 - \sqrt{3}$ , le potentiel  $V$  a un minimum absolu en,  $\phi = \phi_0 = \sqrt{3} - 1$ , pour lequel,  $V = 0$  (constante cosmologique nulle). De plus, pour ce minimum, la supersymétrie est brisée par l’équivalent d’un terme F car on a,  $\frac{\partial W}{\partial \phi} + \phi^* W = \sqrt{3}m^2 \neq 0$  (voir Eq.(2.86)). D’après Eq.(2.97), le gravitino acquiert la masse suivante,

$$m_{3/2} = \exp\left[\frac{1}{2}(\sqrt{3} - 1)^2\right] \frac{m^2}{M_P^2} M_P, \quad (2.100)$$

après restauration de la constante  $M_P$ . Nous voyons ici que la masse du gravitino peut être très inférieure à la masse de Planck si,  $\frac{m^2}{M_P^2} \ll 1$ .

D’après Eq.(2.81) qui est, rappelons-le, la généralisation de la brisure de SUSY par un terme F, l’échelle de brisure de la supersymétrie est,

$$M_S^2 = e^{G/2} (G^{-1})_i^j G_j. \quad (2.101)$$

Dans le cas présent,

$$M_S^2 = e^{G/2} \left( \phi^* + \frac{1}{W} \frac{\partial W}{\partial \phi} \right) = \sqrt{3} m_{3/2} M_P. \quad (2.102)$$

Ce résultat est général pour les théories dans lesquelles le vide brisant la supersymétrie est en  $V = 0$ . L’équation Eq.(2.102) donne pour la masse du gravitino,

$$m_{3/2} = \frac{M_S^2}{\sqrt{3} M_P}. \quad (2.103)$$

La masse du gravitino est donc petite par rapport à l'échelle de brisure de SUSY, si celle-ci est petite comparativement à la masse de Planck.

D'après  $\mathcal{L}_B$ , les champs scalaires, du seul supermultiplet chirale du secteur caché, acquièrent les masses suivantes,

$$\mathcal{L}_B^m = -2m_{3/2}^2 \phi'^* \phi' - 2(\sqrt{3} - 1)m_{3/2}^2 (\phi' \phi' + \phi'^* \phi'^*), \quad (2.104)$$

où nous avons pris,  $\phi = \phi_0 + \phi'$ ,  $\phi_0$  étant la VEV décrite plus haut. Définissant les champs  $A$  et  $B$  par,  $\phi' = \frac{1}{\sqrt{2}}(A + iB)$ , nous obtenons les masses,  $m_A^2 = 2\sqrt{3}m_{3/2}^2$  et  $m_B^2 = 2(2 - \sqrt{3})m_{3/2}^2$ . Nous remarquons donc que les particules scalaires  $A$  et  $B$  ont bien des masses supérieures à celles de leur partenaires supersymétriques fermioniques (qui sont ici nulles). Dans le cas où l'on a un multiplet de supergravité et  $N$  supermultiplets chiraux, ceci reste vrai comme le montre la supertrace qui est toujours positive :

$$STr(M^2) = 2(N - 1)m_{3/2}^2. \quad (2.105)$$

### Condensation de jauginos

Dans une théorie de jauge non abélienne de type  $SU(N)$ , la brisure spontanée de la supersymétrie dans le secteur caché peut aussi être assurée par une condensation de jauginos, autrement dit un produit de deux champs fermioniques de jauginos développant une VEV, issue d'un mécanisme non perturbatif. En effet, la variation infinitésimale par supersymétrie du champ fermionique  $\Psi_i$  (Eq.(2.74)) contient un terme proportionnel à un produit de jauginos :

$$\begin{aligned} \delta\lambda_{aL} &= \sigma^{\mu\nu}(F_a)_{\mu\nu}\mathcal{E}_L + \frac{i}{2}gRe(f_{ab}^{-1})G^i(T_b)_{ij}\phi_j\mathcal{E}_L - \frac{1}{8}f_{abj}(G^{-1})_i^j\lambda_a\lambda_b \\ &+ other \text{ Termes}(2 \text{ fermions}), \end{aligned} \quad (2.106)$$

avec,

$$f_{abj} = \frac{\partial f_{ab}}{\partial \phi^{j*}}, \quad (2.107)$$

$f_{ab}$  étant défini dans Eq.(2.55). Une VEV pour  $\lambda_a\lambda_b$  peut donc briser la supersymétrie en rendant la valeur dans le vide de  $\Psi_i$  non invariante sous les transformations supersymétriques. Pour qu'un tel scénario de brisure soit réalisable, il est nécessaire que certaines composantes de  $f_{abj}$  ne soient pas nulle, c'est à dire que les termes cinétiques pour les champs de jauge ne soient pas minimaux. Par ailleurs, il est possible que la condensation de jauginos ait lieu dans un secteur caché de la théorie si le groupe de jauge est un produit direct. Par exemple, dans les théories de cordes hétérotiques, le groupe de jauge peut être  $E_8 \times E_8$ , le premier groupe exceptionnel contenant le groupe de jauge du Modèle Standard et le second contenant le groupe de jauge du secteur caché.

Comme dans le cas de la brisure par une VEV de champ scalaire, le boson de Goldstone, qui est ici  $\eta = f_{ab}^i < \lambda_a\lambda_b > \Psi_i$ , se mélange au gravitino. Ce mélange est explicite dans le terme de couplage à 4 fermions du lagrangien 2.68 :

$$|det e|^{-1}\mathcal{L}_{MIX} = \frac{1}{2}f_{ab}^i\bar{\Psi}_{iL}\sigma^{\mu\nu}\lambda_{aL}\bar{\Psi}_{\nu L}\gamma_\mu\lambda_{bR} + h.c. \quad (2.108)$$

La masse du gravitino est aussi donnée dans le cas de la condensation de jauginos par le premier terme du lagrangien  $\mathcal{L}_F$  et vaut donc toujours  $m_{3/2} \approx e^{G_0/2} M_P$  (voir Eq.(2.97)). Cette masse peut aussi s'exprimer comme précédemment en fonction de l'échelle de brisure de supersymétrie,  $M_s$ , à savoir,  $m_{3/2} = M_s^2/M_P$  (voir Eq.(2.103)). En revanche, l'échelle de brisure de supersymétrie est différente. Dans un scénario de brisure dynamique, le condensât de jauginos développe la VEV,

$$\langle \lambda^a \lambda^b \rangle = c\mu^3, \quad (2.109)$$

où  $c$  est de l'ordre de 1 et où  $\mu$  est l'échelle dynamique (analogue à  $\Lambda_{QCD}$ ), c'est à dire l'échelle d'énergie à laquelle la constante de couplage du groupe de jauge associé devient forte. Or dans la limite de basse énergie  $M_P \rightarrow \infty$ , nous savons que la supersymétrie n'est pas brisée et que l'échelle de brisure doit donc tendre vers zéro. Nous pouvons donc estimer l'échelle de brisure de supersymétrie  $M_s$  comme étant au maximum,

$$M_s^2 \approx \frac{\mu^3}{M_P}, \quad (2.110)$$

avec éventuellement une puissance plus grande de  $1/M_P$ . Notons finalement que pour une telle échelle de brisure, la masse du gravitino est d'après Eq.(2.103),

$$m_{3/2} \approx \frac{\mu^3}{M_P^2}. \quad (2.111)$$

Même pour une grande valeur de l'échelle d'énergie  $\mu$ , une petite masse peut être obtenue pour le gravitino dans la mesure où  $\mu$  est petit devant l'échelle de Planck.

## 2.5 Effets de la brisure de supersymétrie locale dans le secteur “observable”

Maintenant que nous avons discuté un mécanisme de brisure de la supersymétrie locale dans le secteur caché, nous devons étudier la manière dont cette brisure est transmise au secteur observable.

Nous désignerons les superchamps (champs scalaires) du secteur caché par,  $Z_i$  ( $z_i$ ), et les superchamps (champs scalaires) du secteur observable par,  $Y_r$  ( $y_r$ ). Le superpotentiel de la théorie contient les superchamps du secteur caché et du secteur observable de manière additive afin qu'il n'y ait pas d'interactions entre eux :

$$W(Z_i, Y_r) = \bar{W}(Z_i) + \tilde{W}(Y_r). \quad (2.112)$$

Supposons une fois de plus que les termes cinétiques sont minimaux :

$$G = M_P^{-2}(z^{i*}z_i + y^{r*}y_r) + \ln\left(\frac{|W|^2}{M_P^6}\right), \quad (2.113)$$

où les dimensions sont maintenant explicites. D'après Eq.(2.94), le potentiel sans les termes D s'écrit ici,

$$V = \exp\left(\frac{z^{i*}z_i + y^{r*}y_r}{M_P^2}\right) \left( \left| \frac{\partial \bar{W}}{\partial z_i} + \frac{z^{i*}}{M_P^2}(\bar{W} + \tilde{W}) \right|^2 \right)$$

$$+ \left| \frac{\partial \tilde{W}}{\partial y_r} + \frac{y^{r\star}}{M_P^2} (\bar{W} + \tilde{W}) \right|^2 - 3|W|^2 \Big). \quad (2.114)$$

Nous vérifions bien d'après ce potentiel que si l'on prend la limite,  $M_P \rightarrow \infty$ , c'est à dire si l'on néglige les interactions gravitationnelles, il n'y a plus d'interactions entre les particules des secteurs cachés et observables. En effet, Dans cette limite, le potentiel de Eq.(2.114) s'écrit,  $V = |\frac{\partial \tilde{W}}{\partial z_i}|^2 + |\frac{\partial \tilde{W}}{\partial y_r}|^2$ . Autrement dit les seules interactions entre les champs des deux secteurs sont proportionnelles à une puissance négative de la masse de Planck, c'est à dire qu'il s'agit des interactions gravitationnelles. Afin d'obtenir une forme effective du potentiel (de Eq.(2.114)) appropriée aux basses énergies, nous allons remplacer le champ scalaire  $z_i$  par sa VEV et prendre la limite de basse énergie :  $M_P \rightarrow \infty$ . En général, les VEV correspondant à une brisure de la supersymétrie dans le secteur caché sont du type,

$$\langle z_i \rangle = a_i M_P, \quad (2.115)$$

$$\langle \bar{W} \rangle = \mu M_P^2, \quad (2.116)$$

$$\langle \frac{\partial \bar{W}}{\partial z_i} \rangle = c_i \mu M_P, \quad (2.117)$$

où  $a_i$  et  $c_i$  sont des quantités sans dimensions et  $\mu$  est une échelle caractéristique du superpotentiel du secteur caché (comme par exemple  $m$  dans le superpotentiel de Polonyi). D'après Eq.(2.97), la masse du gravitino est donnée par,

$$m_{3/2} \approx e^{|a_i|^2/2} \mu. \quad (2.118)$$

La limite à basse énergie revient à faire tendre  $M_P$  vers l'infini tout en gardant la masse du gravitino  $m_{3/2}$  fixe. D'après Eq.(2.118), cela est équivalent à travailler au premier ordre en  $\mu/M_P$ . Notons que les éventuelles VEV des champs scalaires du secteur observable sont de l'ordre de l'échelle électrofaible et sont donc bien inférieures à l'échelle de Planck :  $\langle y_r \rangle \ll M_P$ . Le potentiel de Eq.(2.114) s'écrit donc à basse énergie,

$$V = e^{|a_i|^2} \left[ \left| \frac{\partial \tilde{W}}{\partial y_r} \right|^2 + \mu^2 |y_r|^2 + \mu \left( y_r \frac{\partial \tilde{W}}{\partial y_r} + (A - 3)\tilde{W} + C.C. \right) \right], \quad (2.119)$$

où  $A = (c_i^* + a_i)a_i^*$ . En utilisant Eq.(2.118) et en redéfinissant le superpotentiel par,  $e^{|a_i|^2/2} \tilde{W} \rightarrow W'$ , le potentiel de Eq.(2.119) peut encore s'écrire,

$$V = \left| \frac{\partial W'}{\partial y_r} \right|^2 + m_{3/2}^2 |y_r|^2 + m_{3/2} \left( y_r \frac{\partial W'}{\partial y_r} + (A - 3)W' + C.C. \right). \quad (2.120)$$

Le premier terme est le potentiel d'une théorie de supersymétrie globale avec un superpotentiel  $W'$ . Les termes suivants sont des termes de brisure explicite de la supersymétrie globale. En particulier, le terme de masse pour le champ scalaire  $y_r$  vient du terme,

$$e^{\left( \frac{\langle z_i^* \rangle \langle z_i \rangle}{M_P^2} \right)} \left| \frac{\langle \bar{W} \rangle}{M_P^2} y^{r\star} \right|^2, \quad (2.121)$$

du potentiel de Eq.(2.114). Ce terme de masse pour le champ scalaire du secteur observable vient donc bien d'une interaction gravitationnelle : Nous voyons clairement ici que la brisure de la supersymétrie est transmise par la gravitation.

Si nous reprenons l'exemple du modèle de Polonyi, les VEV du champ scalaire appartenant au secteur caché et du superpotentiel étaient,  $\langle z_i \rangle = (\sqrt{3} - 1)M_P$ , et,  $\langle \bar{W} \rangle = m^2 M_P$ , respectivement. D'après Eq.(2.121), la masse du champ scalaire  $y_r$  est par conséquent,  $\exp((\sqrt{3} - 1)^2) \frac{m^4}{M_P^2} = m_{3/2}^2$  (voir Eq.(2.100)). Nous retrouvons donc bien le fait que la masse des scalaires  $y_r$  est égale à celle du gravitino  $m_{3/2}$ . Par ailleurs, il est facile de montrer que dans le modèle de Polonyi, la constante  $A$  définie ultérieurement vaut,  $A = 3 - \sqrt{3}$ . Il est intéressant de noter qu'à l'échelle de Planck, il y a universalité des masses des champs scalaires. C'est à dire que les champs scalaires acquièrent tous la même masse. Effectivement, le potentiel de Eq.(2.120) montre que la masse du champ scalaire est égale à la masse du gravitino, pour chaque multiplet chirale. Il est possible d'obtenir des potentiels effectifs dans lesquels l'universalité est absente, en ne choisissant pas les termes cinétiques minimaux pour les superchamps chiraux. Cependant l'universalité est intéressante puisque c'est une solution naturelle au problème phénoménologique des courants neutres changeant la saveur. Notons que l'universalité est ici présente à l'échelle de Planck, ce qui n'implique pas nécessairement l'universalité à des échelles d'énergie inférieures.

Le cas où le superpotentiel du secteur observable  $W'$  est trilineaire dans les superchamps chiraux est particulièrement intéressant car cela évite les petits ( $\approx 100 GeV$ ) ajustements de paramètres de masse. Dans ce cas, le potentiel se simplifie en,

$$V = \left| \frac{\partial W'}{\partial y_r} \right|^2 + m_{3/2}^2 |y_r|^2 + A m_{3/2} (W' + W'^*). \quad (2.122)$$

Une autre source de brisure de la supersymétrie globale dans le secteur observable apparaît dans le premier terme du lagrangien  $\tilde{\mathcal{L}}_F$ . Il s'agit d'un terme de masse pour les jauginos :

$$\frac{1}{4} e^{G/2} (G^{-1})_k^j G^k \frac{\partial f_{ab}^*}{\partial \phi^{j*}} \lambda_a \lambda_b. \quad (2.123)$$

Afin que ce terme ne soit pas nul, la fonction  $f_{ab}(\phi_j)$  ne doit pas être une fonction triviale. C'est à dire que les termes cinétiques de jauge ne doivent pas être minimaux. La seconde condition est que l'expression,  $e^{G/2} (G^{-1})_k^j G^k$ , ait une VEV non nulle. Ceci est assuré par la condition de brisure de la supersymétrie locale par l'équivalent d'un terme F (voir Eq.(2.81)) dans le secteur caché. Notons en effet qu'ici les indices j et k désignent des champs du secteur caché. La VEV des champs scalaires du secteur caché étant proportionnelle à la masse de Planck,  $\langle \phi^{j*} \rangle \approx M_P$ , le terme de Eq.(2.123) est un terme proportionnel à une puissance négative de la masse de Planck. C'est donc un terme d'interaction gravitationnelle. La transmission de la brisure de SUSY est donc effectuée une fois encore par les interactions gravitationnelles. Étant dans le cas d'une brisure par l'équivalent d'un terme F, l'échelle de brisure de SUSY est donnée par Eq.(2.101). Par conséquent, d'après Eq.(2.123) et Eq.(2.103), la masse des jauginos vaut,

$$m_{jaug} \approx \frac{M_S^2}{M_P} \approx m_{3/2}. \quad (2.124)$$

La masse des jauginos est donc, comme la masse des champs scalaires, de l'ordre de la masse du gravitino.

Enfin, de manière générale, le potentiel effectif de basse énergie peut aussi contenir des termes D. D'après Eq.(2.113), le lagrangien  $\tilde{\mathcal{L}}_B$  donne un potentiel du type,

$$V = \left| \frac{\partial W'}{\partial y_r} \right|^2 + m_{3/2}^2 |y_r|^2 + m_{3/2} \left( y_r \frac{\partial W'}{\partial y_r} + (A - 3)W' + C.C. \right) + \frac{g^2}{2} \text{Re}(f_{ab}^{-1}) y^{r*} (T_a)_{rs} y_s y^{k*} (T_b)_{kl} y_l. \quad (2.125)$$

Les termes D du potentiel de Eq.(2.125) sont des termes D du secteur observable. Leur présence impliquerait une brisure de la supersymétrie locale dans le secteur observable si  $f_{ab}(\phi) = \delta_{ab}$  (voir Eq.(2.93)). Notons que nous n'avons pas non plus traité les termes D du secteur caché puisque nous avons étudié une brisure de la supersymétrie locale dans le secteur caché par (une généralisation) des termes F. Et la transmission de cette brisure de SUSY au secteur observable s'effectue aussi via les termes F du potentiel (voir Eq.(2.114)). Rappelons cependant qu'une brisure de SUSY dans le secteur caché par des termes D est possible ( $\neq$  transmission au secteur observable). La masse du gravitino est aussi donnée dans ce cas par l'équation Eq.(2.97). En revanche, l'échelle de brisure est alors donnée par Eq.(2.82).

En conclusion, dans les théories de supergravité la brisure spontanée de la supersymétrie locale dans un secteur caché permet d'obtenir, à l'échelle de Planck  $M_P$ , un secteur observable régit par un lagrangien globalement supersymétrique accompagné de termes de brisure douce (voir Section 1.5). Ces termes de brisure peuvent donner une masse universelle  $m_0$  aux champs scalaires et une masse universelle  $m_{1/2}$  aux jauginos du secteur observable à l'échelle de Planck. Les masses des champs scalaires  $m_0$  et des jauginos  $m_{1/2}$  sont de l'ordre de la masse du gravitino  $m_{3/2}$  à l'échelle de Planck. Typiquement, la formule de Eq.(2.103) nous montre que pour une échelle de brisure de la supersymétrie de l'ordre de,  $M_S \approx 10^{10} GeV$ , la masse du gravitino est de l'ordre de,  $m_{3/2} \approx 100 GeV$  à l'échelle de Planck. Par conséquent, à l'échelle électrofaible, les masses des particules supersymétriques peuvent être inférieures au TeV et le problème de hiérarchie (voir Section 1.3.1) peut ainsi être résolu. De plus, à l'échelle électrofaible, les masses des particules supersymétriques peuvent être supérieures à celles de leur partenaire supersymétrique du Modèle Standard.





# Chapitre 3

## Origines et motivations théoriques de la symétrie de R-parité

### 3.1 Généralité du superpotentiel du MSSM

Le superpotentiel de Eq.(1.106) contient tous les termes nécessaires à l'extension supersymétrique minimale du Modèle Standard : le MSSM. Cependant, ce superpotentiel n'est pas le plus général dans le sens où il existe d'autres couplages invariants de jauge qui n'ont pas été pris en compte. Pour être totalement général le superpotentiel de Eq.(1.106) doit contenir en plus les termes suivants :

$$W_{\mathcal{R}_p} = \sum_{i,j,k} \left\{ \frac{1}{2} \lambda_{ijk} L_i L_j E_k^c + \lambda'_{ijk} L_i Q_j D_k^c + \frac{1}{2} \lambda''_{ijk} U_i^c D_j^c D_k^c + \mu_i H_2 L_i \right\}, \quad (3.1)$$

où les indices  $i, j, k$  désignent les 3 générations. Le symbole  $\mathcal{R}_p$  ainsi que les facteurs  $\frac{1}{2}$  seront explicités par la suite. Quant aux  $\lambda_{ijk}$ ,  $\lambda'_{ijk}$  et  $\lambda''_{ijk}$ , ce sont des nouvelles constantes de couplage s'ajoutant aux paramètres du MSSM. Remarquons que les deux premiers termes trilineaires ainsi que le terme bilinéaire de Eq.(3.1) peuvent être obtenus en remplaçant le superchamp de Higgs  $H_1$  par le superchamp leptonique  $L_i$  dans le superpotentiel du MSSM (voir Eq.(1.106)) qui contient notamment les couplages de Yukawa. En effet, les superchamps  $H_1$  et  $L_i$  ont les mêmes nombres quantiques.

Combien de paramètres supplémentaires sont effectivement introduits par le superpotentiel de Eq.(3.1) ? Le “tenseur”  $\lambda_{ijk}$  des constantes de couplage est antisymétrique par rapport aux indices de famille  $i$  et  $j$  à cause de du tenseur antisymétrique  $\epsilon_{ab}$  de  $SU(2)$  :

$$\begin{aligned} \lambda_{ijk} L_i L_j E_k^c &= \lambda_{ijk} L_i^a L_j^b E_k^c \epsilon_{ab} = \lambda_{jik} L_j^a L_i^b E_k^c \epsilon_{ab} = -\lambda_{jik} L_j^a L_i^b E_k^c \epsilon_{ba} \\ &= -\lambda_{jik} L_i^b L_j^a E_k^c \epsilon_{ba} = -\lambda_{jik} L_i L_j E_k^c. \end{aligned} \quad (3.2)$$

De même,  $\lambda''_{ijk}$  est antisymétrique par rapport aux indices  $j$  et  $k$  à cause de l'antisymétrie du tenseur  $\epsilon_{mnp}$  de  $SU(3)$ . En effet, le terme trilineaire en  $\lambda''_{ijk}$  est un couplage invariant de  $SU(3)$  du type **333** contracté par le tenseur antisymétrique  $\epsilon_{mnp}$  de  $SU(3)$  :  $\lambda''_{ijk} U_i^c D_j^c D_k^c = \lambda''_{ijk} U_i^c {}^m D_j^c {}^n D_k^c {}^p \epsilon_{mnp}$ .

Par conséquent, il n'existe que 9 constantes  $\lambda_{ijk}$  et 9 constantes  $\lambda''_{ijk}$  alors qu'il y a 27 constantes du type  $\lambda'_{ijk}$ . Le superpotentiel de Eq.(3.1) introduit donc dans le MSSM 45 paramètres réels supplémentaires. En effet, le terme bilinéaire de Eq.(3.1) peut être

éliminé par une redéfinition des superchamps : Si l'on définit  $L_\alpha = (H_1, L_1, L_2, L_3)$  et  $\mu_\alpha = (\mu, \mu_1, \mu_2, \mu_3)$ , les termes bilinéaires de Eq.(1.106) et Eq.(3.1) s'écrivent  $\mu_\alpha H_2 L_\alpha$ . Or, en effectuant la transformation  $L_\alpha \rightarrow U_{\alpha\beta} L^\beta$  où  $U_{\alpha\beta}$  est donné en première approximation par,

$$U_{\alpha\beta} \approx \begin{pmatrix} 1 & -\frac{\mu_m}{\mu} \\ \frac{\mu_m}{\mu} & I_3 \end{pmatrix}, \quad (3.3)$$

$I_3$  étant la matrice identité  $3 \times 3$  et  $m$  valant  $m = 1, 2, 3$ , le terme  $\mu_\alpha H_2 L_\alpha$  se réduit au terme bilinéaire de Eq.(1.106) :  $\mu H_1 H_2$ . Cependant, notons que la redéfinition des champs de Eq.(3.3) n'élimine pas les termes bilinéaires présents parmi les termes de brisure douce de SUSY, si ces termes bilinéaires ont une structure générique.

Quelle est la dimension des constantes  $\lambda$ ,  $\lambda'$  et  $\lambda''$ ? La dimension des variables de Grassmann est  $[\theta^\alpha] = -1/2$  comme nous l'avons mentionné dans la Section 1.4.6. La dimension de la dérivée par rapport à une variable de Grassmann vaut donc  $[\partial/\partial\theta^\alpha] = 1/2$ . D'après Eq.(1.76), le superpotentiel doit avoir une dimension  $[W] = 3$  puisque l'intégration est équivalente à la dérivation pour une variable de Grassmann et que la dimension du lagrangien est  $[\mathcal{L}] = 4$  (voir Appendice A). La dimension d'un superchamp  $S$  étant égale à  $[S] = 1$  (voir Section 1.4.7), l'expression du superpotentiel de Eq.(3.1) indique que les constantes  $\lambda_{ijk}$ ,  $\lambda'_{ijk}$  et  $\lambda''_{ijk}$  sont sans dimension :  $[\lambda_{ijk}] = [\lambda'_{ijk}] = [\lambda''_{ijk}] = 0$ .

Nous allons maintenant déterminer le lagrangien associé aux termes trilineaires du superpotentiel de Eq.(3.1). La contribution de ces termes au potentiel scalaire, qui se déduit de Eq.(1.77), donne des opérateurs quadruples dans les champs de sleptons et de squarks. Ces interactions entre particules supersymétriques de spin 0 n'ont pas de conséquences phénoménologiques à basse énergie pour des particules supersymétriques lourdes. L'autre contribution des termes trilineaires du superpotentiel de Eq.(3.1) au lagrangien est donnée par Eq.(1.78). Nous effectuerons explicitement le calcul de cette contribution uniquement pour le terme en  $\lambda_{ijk}$  de Eq.(3.1), la méthode étant tout à fait similaire pour les termes en  $\lambda'_{ijk}$  et  $\lambda''_{ijk}$ . Explicitons tout d'abord le produit sous  $SU(2)$  de ces termes en  $\lambda_{ijk}$  :

$$\frac{1}{2}\lambda_{ijk}L_iL_jE_k^c = \frac{1}{2}\lambda_{ijk}L_i^aL_j^bE_k^c\epsilon_{ab} = \frac{1}{2}\lambda_{ijk}\left(N_iE_j - E_iN_j\right)E_k^c, \quad (3.4)$$

où  $N_i$  et  $E_i$  sont les superchamps de chiralité gauche associés au neutrino et au lepton chargé respectivement. Dans Eq.(3.4), la somme sur les indices  $i, j, k$  est implicite. De même, dans tout ce calcul nous n'écrirons plus le symbole  $\sum_{i,j,k}$  afin d'alléger les équations. Le lagrangien associé aux termes de Eq.(3.4) et donné par Eq.(1.78) s'écrit,

$$\begin{aligned} \mathcal{L}_\lambda = & - \frac{1}{2} \sum_{a,b} \frac{\partial^2 \left[ \frac{1}{2} \lambda_{ijk} \left( \tilde{\nu}_{iL} \tilde{e}_{jL} - \tilde{e}_{iL} \tilde{\nu}_{jL} \right) \tilde{e}_{kR}^c \right]}{\partial z_a \partial z_b} \psi_a \psi_b \\ & - \frac{1}{2} \sum_{a,b} \frac{\partial^2 \left[ \frac{1}{2} \lambda_{ijk}^* \left( \tilde{\nu}_{iL}^* \tilde{e}_{jL}^* - \tilde{e}_{iL}^* \tilde{\nu}_{jL}^* \right) \tilde{e}_{kR}^{c*} \right]}{\partial z_a^* \partial z_b^*} \bar{\psi}_a \bar{\psi}_b, \end{aligned} \quad (3.5)$$

où l'exposant  $\star$  signifie complexe conjugué. Remarquons que nous avons écrit le partenaire scalaire du spineur de chiralité gauche à quatre composantes du positron  $e_{kL}^c$  :  $scal[e_{kL}^c] = scal[(e_{kR})^c] = \tilde{e}_{kR}^c = \tilde{e}_{kR}^{c*}$ . Le lagrangien de Eq.(3.5) s'écrit,

$$\mathcal{L}_\lambda = - \frac{1}{2} \lambda_{ijk} \left( \chi_{\nu_i} \chi_{e_j} \tilde{e}_{kR}^c + \chi_{\nu_i} \eta_{e_k} \tilde{e}_{jL} + \chi_{e_j} \eta_{e_k} \tilde{\nu}_{iL} - (i \leftrightarrow j) \right)$$

$$- \frac{1}{2} \lambda_{ijk}^* \left( \bar{\chi}_{\nu_i} \bar{\chi}_{e_j} \tilde{e}_{kR}^{c*} + \bar{\chi}_{\nu_i} \bar{\eta}_{e_k} \tilde{e}_{jL}^* + \bar{\chi}_{e_j} \bar{\eta}_{e_k} \tilde{\nu}_{iL}^* - (i \leftrightarrow j) \right), \quad (3.6)$$

où les spineurs à deux composantes de l'électron et du neutrino sont définis à partir des spineurs à quatre composantes correspondants, notés  $e$ ,  $\nu$  et  $e^c$ ,  $\nu^c$  (conjugués de charge), par,

$$e = \begin{pmatrix} \chi_e \\ \bar{\eta}_e \end{pmatrix}, \quad e^c = \begin{pmatrix} \eta_e \\ \bar{\chi}_e \end{pmatrix}, \quad \nu = \begin{pmatrix} \chi_\nu \\ \bar{\eta}_\nu \end{pmatrix}, \quad \nu^c = \begin{pmatrix} \eta_\nu \\ \bar{\chi}_\nu \end{pmatrix}. \quad (3.7)$$

En passant de Eq.(3.5) à Eq.(3.6), le facteur  $1/2$  venant de Eq.(1.78) s'est éliminé. L'explication est que la somme sur  $a$  et  $b$  effectuée dans Eq.(3.5) et provenant aussi de Eq.(1.78) fait apparaître deux fois le même couplage. En effet, la dérivée seconde de Eq.(3.5) donne par exemple un couplage identique pour  $z_a = \tilde{\nu}_{iL}$ ,  $z_b = \tilde{e}_{jL}$  et  $z_a = \tilde{e}_{jL}$ ,  $z_b = \tilde{\nu}_{iL}$ . Notons que la dérivée seconde  $d^2/dz_a dz_b$  prise dans Eq.(3.5) est nulle pour  $a = b$ . En revanche, ce facteur  $1/2$  venant de Eq.(1.78) apparaît dans le terme de masse du lagrangien pour un spineur de Majorana qui s'écrit,  $\mathcal{L} = \frac{1}{2} m \bar{\psi} \psi$ , car la somme sur  $a$  et  $b$  de Eq.(1.78) n'est alors prise que sur un seul champ puisque le superpotentiel générant cette masse est  $W = m \Phi^2$ ,  $\Phi$  étant le superchamp associé au spineur de Majorana.

En utilisant les formules de Eq.(1.44) et Eq.(1.45) reliant les spineurs à deux composantes  $\chi$ ,  $\eta$  aux spineurs à quatre composantes  $\Psi$ ,  $\Psi^c$ , on peut exprimer le lagrangien de Eq.(3.6) en fonction des spineurs à quatre composantes :

$$\begin{aligned} \mathcal{L}_\lambda = & - \frac{1}{2} \lambda_{ijk} \left( \bar{\nu}_i^c P_L e_j \tilde{e}_{kR}^* + \bar{e}_k P_L \nu_i \tilde{e}_{jL} + \bar{e}_k P_L e_j \tilde{\nu}_{iL} - (i \leftrightarrow j) \right) \\ & - \frac{1}{2} \lambda_{ijk}^* \left( \bar{e}_j P_R \nu_i^c \tilde{e}_{kR} + \bar{\nu}_i P_R e_k \tilde{e}_{jL}^* + \bar{e}_j P_R e_k \tilde{\nu}_{iL}^* - (i \leftrightarrow j) \right). \end{aligned} \quad (3.8)$$

Afin d'exprimer le premier terme du lagrangien de Eq.(3.6) en fonction de spineurs à quatre composantes, nous avons considéré  $\chi_\nu$  comme étant le spineur conjugué de charge du neutrino appartenant à la représentation  $(0, 1/2)$  du groupe de Lorentz (voir Eq.(3.7)). Les facteurs  $1/2$  dans Eq.(3.8) s'éliminent lorsque la somme sur  $i, j, k$  est effectuée, car des couples de couplages identiques apparaissent alors, à cause de l'antisymétrie de  $\lambda_{ijk}$ . En répétant le même exercice pour les interactions en  $\lambda'_{ijk}$  et  $\lambda''_{ijk}$ , nous trouvons l'ensemble de la contribution au lagrangien décrite dans Eq.(1.78) des termes trilineaires du superpotentiel de Eq.(3.1) :

$$\begin{aligned} \mathcal{L}_{\mathcal{R}_p} = & \sum_{ijk} \left\{ \lambda_{ijk} \frac{1}{2} \left( \tilde{\nu}_{iL} \bar{e}_{kR} e_{jL} + \tilde{e}_{jL} \bar{e}_{kR} \nu_{iL} + \tilde{e}_{kR}^* \bar{\nu}_{iR}^c e_{jL} - (i \leftrightarrow j) \right) \right. \\ & + \lambda'_{ijk} \left( \tilde{\nu}_{iL} \bar{d}_{kR} d_{jL} + \tilde{d}_{jL} \bar{d}_{kR} \nu_{iL} + \tilde{d}_{kR}^* \bar{\nu}_{iR}^c d_{jL} \right. \\ & \quad \left. - \tilde{e}_{iL} \bar{d}_{kR} u_{jL} - \tilde{u}_{jL} \bar{d}_{kR} e_{iL} - \tilde{d}_{kR}^* \bar{e}_{iR}^c u_{jL} \right) \\ & + \lambda''_{ijk} \frac{1}{2} \left( \tilde{u}_{iR}^* \bar{d}_{jR} d_{kL}^c + \tilde{d}_{jR}^* \bar{u}_{iR} d_{kL}^c \right. \\ & \quad \left. + \tilde{d}_{kR}^* \bar{u}_{iR} d_{jL}^c - (j \leftrightarrow k) \right) \left. \right\} + h.c. \end{aligned} \quad (3.9)$$

## 3.2 Désintégration du proton

Les termes du lagrangien 3.9 sont des opérateurs dangereux dans le sens où ils peuvent donner lieu à une désintégration rapide du proton [35, 36, 37, 38, 39]. En effet, les interac-

tions en  $\lambda_{ijk}$ ,  $\lambda'_{ijk}$  violent le nombre leptonique et les interactions en  $\lambda''_{ijk}$  violent le nombre baryonique. Cette désintégration du proton est en fait liée à la présence simultanée des couplages  $\lambda'_{ijk}$  et  $\lambda''_{ijk}$ . Les bornes expérimentales sur le temps de vie du proton peuvent donc être utilisées pour contraindre les produits de constantes de couplage du type  $\lambda'\lambda''$ .

Par exemple, le proton peut se désintégrer en un pion et un positron, comme  $P \rightarrow \pi^0 e^+$ , via le processus  $ud \rightarrow \tilde{d}_k^* \rightarrow e^+ \bar{u}$  qui implique les couplages  $\lambda''_{11k} \tilde{d}_{kR}^* \bar{u}_R d_L^c$  et  $\lambda'_{11k} \tilde{d}_{kR}^* \bar{e}_R^c u_L$ . La largeur de cette désintégration peut être estimée par,

$$\Gamma(P \rightarrow \pi^0 e^+) \approx \alpha(\lambda'_{11k})\alpha(\lambda''_{11k}) \frac{M_{proton}^5}{m_{\tilde{d}_k}^4}, \quad (3.10)$$

où  $\alpha(\lambda) = \lambda^2/4\pi$ . L'équation Eq.(3.10) et la contrainte expérimentale sur le temps de vie du proton relative à la désintégration du proton en pion,  $\tau(P \rightarrow \pi^0 e^+) > 10^{32} ans$  [40], permettent de borner le produit  $\lambda'_{11k}\lambda''_{11k}$  par,

$$\lambda'_{11k}\lambda''_{11k} \lesssim 2.10^{-27} \left(\frac{m_{\tilde{d}_k}}{100 GeV}\right)^2. \quad (3.11)$$

Il a même été montré dans [41] que l'étude de la désintégration du proton poussée à l'ordre d'une boucle pouvait contraindre chaque produit  $\lambda'\lambda''$  de façon conservative par,

$$\lambda'\lambda'' < 10^{-9}. \quad (3.12)$$

### 3.2.1 Opérateurs de dimension 5

Les nombres leptonique L et baryonique B peuvent aussi être violés par des opérateurs non renormalisables. Les opérateurs de dimension 5 violant les nombres leptonique et baryonique sont en  $1/M$  où  $M$  est l'échelle de la physique au-delà du Modèle Standard (supersymétrique minimal) générant une violation de L et B. L'échelle  $M$  typique est l'échelle des théories de grande unification  $M_{GUT}$ , et l'échelle  $M$  la plus grande est bien sûr celle de Planck  $M_P$ . Les opérateurs de dimension 5 du superpotentiel (termes F) invariants sous le groupe de jauge du MSSM et violant les nombres leptonique et baryonique sont, en termes des superchamps,

$$\begin{aligned} \mathcal{O}_1 &= QQQ L & \mathcal{O}_4 &= Q U^c E^c H_1 \\ \mathcal{O}_2 &= U^c U^c D^c E^c & \mathcal{O}_5 &= L L H_2 H_2 \\ \mathcal{O}_3 &= Q Q Q H_1 & \mathcal{O}_6 &= L H_1 H_2 H_2 \end{aligned} \quad (3.13)$$

De tels opérateurs existent aussi parmi les termes en  $\int d^2\theta d^2\bar{\theta}$  (termes D) et s'écrivent en termes des superchamps,

$$\begin{aligned} \mathcal{O}_7 &= H_2 H_2 E^{c\dagger} & \mathcal{O}_9 &= Q U^c L^\dagger \\ \mathcal{O}_8 &= H_2^{c\dagger} H_1 E^c & \mathcal{O}_{10} &= U^c D^{c\dagger} E^c \end{aligned} \quad (3.14)$$

D'après Eq.(1.72), les opérateurs de Eq.(3.13) et Eq.(3.14) sont bien de dimension 5, puisque  $[\partial/\partial\theta^\alpha] = 1/2$  et que la dimension d'un superchamp est égale à 1.

Les bornes expérimentales sur les temps de vie des nucléons contraignent la plupart de ces opérateurs de dimension 5 de manière significative, même si la violation de L et B apparaît à une échelle  $M = M_P$ . Les processus impliquant deux fois un opérateur  $\mathcal{O}_i$

sont supprimés par un facteur  $(m/M_P)^2$ , où  $m = m_{SUSY}, m_{weak}$ , et donnent donc une limite peu significative sur les coefficients  $\eta_i$  de ces opérateurs. L'opérateur  $\mathcal{O}_1$  couple des particules supersymétriques et peut donc contribuer à la désintégration du nucléon en un méson et un lepton par un graphe à une boucle impliquant des winos. L'amplitude du processus correspondant est réduit d'un facteur de boucle et d'un facteur  $m_{SUSY}/M_P$ . Les données expérimentales sur les désintégrations nucléoniques impliquent la borne  $\eta_1 < 10^{-7}$  [42] sur le coefficient de  $\mathcal{O}_1$  pour  $m_{\tilde{W}} \approx m_W$ . L'opérateur  $\mathcal{O}_2$ , couplant des particules supersymétriques n'interagissant pas avec les winos, ne peut contribuer à la désintégration du nucléon par un graphe à une boucle impliquant des winos. Le coefficient  $\eta_2$  n'est donc pas contraint de façon significative. L'opérateur  $\mathcal{O}_3$  ne peut pas non plus contribuer à la désintégration du nucléon par un graphe à une boucle impliquant des winos. En revanche, les opérateurs  $\mathcal{O}_3$ , considéré avec la vev  $v$  associée au superchamp  $H_1$ , et  $LQD^c$  permettent la désintégration du nucléon via un processus du type  $qq \rightarrow \tilde{q} \rightarrow ql$  qui est supprimé par un facteur  $v/M_P$ . La limite qui en découle est  $\lambda'\eta_3 < 10^{-10}$  pour  $v \approx 100 GeV$ . Les combinaisons entre opérateurs  $\mathcal{O}_i$  et opérateurs en  $\lambda, \lambda', \lambda''$  donnent aussi des limites significatives sur les coefficients  $\eta_i$  des  $\mathcal{O}_i$  ( $i = 4, \dots, 10$ ). Les contraintes relatives aux opérateurs  $\mathcal{O}_i$  mentionnées ci-dessus sont les seules qui soient significatives.

### 3.3 Symétries du superpotentiel

Les fortes contraintes sur les produits de constantes de couplage  $\lambda'\lambda''$  déduites des bornes expérimentales sur le temps de vie du proton (voir Section 3.2) ainsi que les violations des nombres leptonique et baryonique engendrées par les interactions en  $\lambda, \lambda'$  et  $\lambda''$ , respectivement, suggèrent que les couplages du lagrangien 3.9 soient interdits par une certaine symétrie. Cependant, le problème de la désintégration rapide du proton peut aussi être résolu par l'imposition d'une symétrie permettant uniquement les couplages en  $\lambda'$  ou en  $\lambda''$  du lagrangien 3.9. Les symétries discrètes interdisant les couplages en  $\lambda, \lambda', \lambda''$  sont appelées parités de matière, en  $\lambda, \lambda'$  (couplages violant le nombre leptonique) parités leptoniques et en  $\lambda''$  (couplages violant le nombre baryonique) parités baryoniques. Dans ce chapitre, nous discutons les diverses symétries du superpotentiel, pouvant protéger le proton de sa désintégration, et leurs caractéristiques.

La suppression par des symétries des opérateurs dangereux de dimension 5, vus dans la Section 3.2.1, est moins motivée. En effet, la violation de L et B dans une théorie au-delà du MSSM peut éventuellement être supprimée par un autre type de mécanisme propre à cette nouvelle théorie.

#### 3.3.1 Les R-symétries

Les R-symétries furent proposées par A. Salam et J. Strathdee dans [43] et par P. Fayet dans [44] pour interdire la violation des nombres leptonique ou baryonique. Les R-symétries apparaissent naturellement dans les théories les plus simples.

La R-symétrie est une symétrie  $U(1)$  continue agissant sur les superchamps vectoriels  $V$  et chiraux  $\Phi$  et  $\bar{\Phi}$  par les transformations,

$$V_k(x, \theta, \bar{\theta}) \rightarrow V_k(x, \theta e^{-i\alpha}, \bar{\theta} e^{i\alpha}), \quad (3.15)$$

$$\Phi_l(x, \theta) \rightarrow e^{iR_l\alpha} \Phi_l(x, \theta e^{-i\alpha}), \quad (3.16)$$

$$\bar{\Phi}_l(x, \bar{\theta}) \rightarrow e^{-iR_l\alpha} \bar{\Phi}_l(x, \bar{\theta}e^{i\alpha}), \quad (3.17)$$

où les charges  $R_l$  sont des nouveaux nombres quantiques additifs. Le choix de ces charges est arbitraire et caractérise la R-symétrie. En remplaçant dans Eq.(3.15) et Eq.(3.16) les superchamps par leur expression littérale (voir Eq.(1.63), Eq.(1.64) et Eq.(1.68)), nous obtenons,

$$\begin{aligned} \theta\sigma^\mu\bar{\theta}v_{k\mu}(x) + i\theta\theta\bar{\theta}\bar{\lambda}_k(x) - i\bar{\theta}\bar{\theta}\theta\lambda_k(x) + \frac{1}{2}\theta\theta\bar{\theta}\bar{\theta}D_k(x) \rightarrow \\ \theta\sigma^\mu\bar{\theta}v_{k\mu}(x) + i\theta\theta\bar{\theta}e^{-i\alpha}\bar{\lambda}_k(x) - i\bar{\theta}\bar{\theta}\theta e^{i\alpha}\lambda_k(x) + \frac{1}{2}\theta\theta\bar{\theta}\bar{\theta}D_k(x), \end{aligned} \quad (3.18)$$

$$\begin{aligned} z_l(x) + \sqrt{2}\theta\psi_l(x) - \theta\theta f_l(x) \rightarrow \\ e^{iR_l\alpha} \left( z_l(x) + \sqrt{2}\theta e^{-i\alpha}\psi_l(x) - \theta\theta e^{-2i\alpha}f_l(x) \right), \end{aligned} \quad (3.19)$$

$$\begin{aligned} \bar{z}_l(x) + \sqrt{2}\bar{\theta}\bar{\psi}_l(x) - \bar{\theta}\bar{\theta}\bar{f}_l(x) \rightarrow \\ e^{-iR_l\alpha} \left( \bar{z}_l(x) + \sqrt{2}\bar{\theta}e^{i\alpha}\bar{\psi}_l(x) - \bar{\theta}\bar{\theta}e^{2i\alpha}\bar{f}_l(x) \right). \end{aligned} \quad (3.20)$$

Les formules 3.18, 3.19 et 3.20 montrent que les transformations de R-symétrie 3.15, 3.16 et 3.17 définies sur les superchamps et les variables de Grassmann peuvent de manière équivalente être définies sur les champs eux-mêmes par,

$$\begin{aligned} z_l(x) &\rightarrow e^{iR_l\alpha} z_l(x), \\ \bar{z}_l(x) &\rightarrow e^{-iR_l\alpha} \bar{z}_l(x), \\ v_{k\mu}(x) &\rightarrow v_{k\mu}(x), \\ \bar{\lambda}_k(x) &\rightarrow e^{-i\alpha} \bar{\lambda}_k(x), \quad \psi_l(x) \rightarrow e^{i(R_l-1)\alpha} \psi_l(x), \\ \lambda_k(x) &\rightarrow e^{i\alpha} \lambda_k(x), \quad \bar{\psi}_l(x) \rightarrow e^{-i(R_l-1)\alpha} \bar{\psi}_l(x), \\ D_k(x) &\rightarrow D_k(x), \quad f_l(x) \rightarrow e^{i(R_l-2)\alpha} f_l(x), \\ &\quad \bar{f}_l(x) \rightarrow e^{-i(R_l-2)\alpha} \bar{f}_l(x). \end{aligned} \quad (3.21)$$

Travaillons dans la représentation chirale des matrices  $\gamma$ . La matrice  $\gamma_5$  et les projecteurs de chiralité gauche et droite s'écrivent alors,

$$\gamma_5 = \begin{pmatrix} I_2 & 0 \\ 0 & -I_2 \end{pmatrix}, P_L = \frac{I_4 + \gamma_5}{2} = \begin{pmatrix} I_2 & 0 \\ 0 & 0 \end{pmatrix}, P_R = \frac{I_4 - \gamma_5}{2} = \begin{pmatrix} 0 & 0 \\ 0 & I_2 \end{pmatrix}, \quad (3.22)$$

où  $I_2$  et  $I_4$  sont les matrices identité  $2 \times 2$  et  $4 \times 4$ , respectivement. Les spineurs à quatre composantes de chiralité gauche et droite sont donc donnés par,

$$\Psi_L = P_L \Psi = P_L \begin{pmatrix} \chi \\ \bar{\eta} \end{pmatrix} = \begin{pmatrix} \chi \\ 0 \end{pmatrix}, \quad \Psi_R = P_R \Psi = P_R \begin{pmatrix} \chi \\ \bar{\eta} \end{pmatrix} = \begin{pmatrix} 0 \\ \bar{\eta} \end{pmatrix}, \quad (3.23)$$

Par conséquent, le spineur à 2 composantes  $\psi$  ( $\bar{\psi}$ ) a la même charge  $R$  que le spineur à 4 composantes  $\Psi_L$  ( $\Psi_R$ ). Nous pouvons donc réécrire les transformations en terme de spineurs à 4 composantes comme :

$$\begin{aligned} \tilde{f}_{lL}(x) &\rightarrow e^{iR_l\alpha} \tilde{f}_{lL}(x), \\ v_{k\mu}(x) &\rightarrow v_{k\mu}(x), \quad \tilde{f}_{lR}(x) \rightarrow e^{-iR_l\alpha} \tilde{f}_{lR}(x), \\ \Lambda_k(x) &\rightarrow e^{i\gamma_5\alpha} \Lambda_k(x), \quad \Psi_l(x) \rightarrow e^{i\gamma_5(R_l-1)\alpha} \Psi_l(x), \\ D_k(x) &\rightarrow D_k(x), \quad f_l(x) \rightarrow e^{i(R_l-2)\alpha} f_l(x), \\ &\quad \bar{f}_l(x) \rightarrow e^{-i(R_l-2)\alpha} \bar{f}_l(x). \end{aligned} \quad (3.24)$$

Dans Eq.(3.24), nous avons noté les spineurs à 4 composantes  $\Lambda(x)$  pour les jauginos et  $\Psi(x)$  pour les quarks et les leptons. Par ailleurs, les notations pour les champs scalaires gauche et droit ont été changé par rapport à Eq.(3.21) selon  $z \rightarrow \tilde{f}_L$  et  $\bar{z} \rightarrow \tilde{f}_R$ , respectivement.

Les transformations 3.24 permettent de déterminer quels sont les termes du lagrangien invariants sous la R-symétrie (R-invariants). Nous constatons d'après Eq.(3.24) que les termes cinétiques pour les champs de spin 0,  $(\partial_\mu \tilde{f}_{L,R})^*(\partial^\mu \tilde{f}_{L,R})$ , de spin 1/2,  $i\bar{\Psi}\gamma^\mu\partial_\mu\Psi$ , et de spin 1,  $-(1/4)F_{\mu\nu}F^{\mu\nu}$  où  $F_{\mu\nu} = \partial_\mu v_\nu - \partial_\nu v_\mu$ , sont tous invariants sous les R-symétries. L'invariance sous les R-symétries pour les termes du lagrangien dérivés du superpotentiel peut aussi être testée au niveau du superpotentiel lui-même. En effet, le lagrangien  $\mathcal{L}$  associé au superpotentiel  $W$  dépendant des superchamps chiraux  $\Phi_l(x, \theta)$  est obtenu par (voir Eq.(1.76)),

$$\mathcal{L} = \int d^2\theta W(\Phi_l(x, \theta)). \quad (3.25)$$

Ce lagrangien  $\mathcal{L}$  se transforme sous la R-symétrie considérée par,

$$\int d^2\theta W(\Phi_l(x, \theta)) \rightarrow \int d^2\theta e^{iR_W\alpha} W(\Phi_l(x, \theta e^{-i\alpha})), \quad (3.26)$$

où  $R_W$  est la charge associée au superpotentiel dépendant des charges  $R_l$  des superchamps  $\Phi_l(x, \theta)$ . Afin de pouvoir mieux comparer les membres de gauche et de droite de la transformation 3.26, effectuons pour le membre de droite le changement de variable suivant,

$$\theta \rightarrow \theta' e^{i\alpha}, d\theta \rightarrow d\theta' e^{-i\alpha}, d^2\theta \rightarrow d^2\theta' e^{-2i\alpha}. \quad (3.27)$$

La différence de signe dans les transformations de changement de variable pour  $\theta$  et  $d\theta$  vient du fait que pour une variable de Grassmann l'intégration est équivalente à la dérivation. La transformation de R-symétrie 3.26 s'écrit maintenant,

$$\int d^2\theta W(\Phi_l(x, \theta)) \rightarrow \int d^2\theta' e^{-2i\alpha} e^{iR_W\alpha} W(\Phi_l(x, \theta')). \quad (3.28)$$

Finalement, nous voyons clairement dans la transformation 3.28 que le lagrangien  $\mathcal{L}$  associé au superpotentiel  $W$  (Eq.(3.25)) est invariant sous les R-symétries donnant une charge  $R_W = 2$  à  $W$ .

Les R-symétries permettent d'interdire certains des couplages en  $\lambda$ ,  $\lambda'$  et  $\lambda''$  du superpotentiel 3.1 ou bien l'ensemble de ces couplages. Étudions un exemple de R-symétrie interdisant tous les couplages du superpotentiel 3.1 (comme le fait une parité de matière). Considérons la R-symétrie,

$$V(x, \theta, \bar{\theta}) \rightarrow V(x, \theta e^{-i\alpha}, \bar{\theta} e^{i\alpha}), \quad (3.29)$$

$$H_{1,2}(x, \theta) \rightarrow H_{1,2}(x, \theta e^{-i\alpha}), \quad (3.30)$$

$$\Phi(x, \theta) \rightarrow e^{i\alpha} \Phi(x, \theta e^{-i\alpha}), \quad \Phi = Q, U^c, D^c, L, E^c. \quad (3.31)$$

Dans Eq.(3.29),  $V$  désigne chaque superchamp vectoriel du groupe de jauge  $SU(3) \times SU(2) \times U(1)$  du MSSM. Les transformations 3.30 et 3.31 des superchamps chiraux sont



associées aux charges suivantes :  $R = 0$  pour  $H_1, H_2$  et  $R = 1$  pour  $Q, U^c, D^c, L, E^c$ . Par conséquent, les transformations de cette R-symétrie sur les champs s'écrivent,

$$\begin{aligned}
v_\mu(x) &\rightarrow v_\mu(x), & h_{1,2}(x) &\rightarrow h_{1,2}(x), & \tilde{f}_L(x) &\rightarrow e^{i\alpha} \tilde{f}_L(x), \\
\Lambda(x) &\rightarrow e^{i\gamma_5\alpha} \Lambda(x), & \tilde{h}_{1,2}(x) &\rightarrow e^{-i\gamma_5\alpha} \tilde{h}_{1,2}(x), & \tilde{f}_R(x) &\rightarrow e^{-i\alpha} \tilde{f}_R(x), \\
D(x) &\rightarrow D(x), & f_h(x) &\rightarrow e^{-2i\alpha} f_h(x), & \Psi(x) &\rightarrow \Psi(x), \\
&& \bar{f}_h(x) &\rightarrow e^{2i\alpha} \bar{f}_h(x), & f(x) &\rightarrow e^{-i\alpha} f(x), \\
&& && \bar{f}(x) &\rightarrow e^{i\alpha} \bar{f}(x),
\end{aligned} \tag{3.32}$$

où  $v_\mu(x)$  désigne les bosons de jauge,  $\Lambda(x)$  les jauginos,  $h_{1,2}(x)$  les bosons de Higgs,  $\tilde{h}_{1,2}(x)$  les higgsinos,  $\tilde{f}$  les squarks et les sleptons et  $\Psi(x)$  les quarks et les leptons.

Les interactions en  $\lambda$ ,  $\lambda'$  et  $\lambda''$  du lagrangien 3.9 sont interdites par cette R-symétrie, qui agit donc comme une parité de matière. En effet, les transformations 3.32 montrent que les couplages du lagrangien 3.9 qui sont du type  $\bar{\Psi}\Psi\tilde{f}_{L,R}$  sont interdits par cette R-symétrie. Nous pouvons aussi raisonner au niveau du superpotentiel : Les termes trilineaires du superpotentiel 3.1 sont interdits car ils ont une charge  $R_W = 3$  puisque les superchamps  $Q, U^c, D^c, L$  et  $E^c$  ont chacun une charge  $R = 1$ . Notons que le terme bilinéaire du superpotentiel 3.1 a une charge  $R_W = 1$  et n'est donc pas non plus invariant. En revanche, les couplages de Yukawa qui sont du type  $h_{1,2}\bar{\Psi}\Psi$  sont autorisés par cette R-symétrie, d'après Eq.(3.32). Cette R-invariance des couplages de Yukawa nous est confirmée par le fait que les termes trilineaires correspondant à ces couplages dans le superpotentiel (voir Eq.(1.106)) ont une charge  $R_W = 2$ , d'après Eq.(3.30) et Eq.(3.31).

### 3.3.2 Problèmes et intérêts des R-symétries

Les R-symétries souffrent de deux principaux problèmes. Nous expliquons ici la première difficulté qui est essentiellement théorique [45].

Comme nous l'avons vu dans la Section 2.1, le caractère local des symétries de jauge suggère que si la supersymétrie est une symétrie fondamentale de la nature elle doit être réalisée de façon locale. Une théorie dans laquelle la supersymétrie est une symétrie locale, doit contenir la théorie de la gravitation et est par conséquent appelée une théorie de supergravité. Les théories de supersymétrie locale sont donc aussi motivées par le rôle naturel que joue la gravitation dans ces théories. Outre ces motivations théoriques, les théories de supergravité permettent une brisure spontanée réaliste de la supersymétrie (voir Section 2.1). Dans ce contexte des théories de supergravité, le gravitino, qui est la particule de jauge de la supersymétrie locale, acquiert une masse  $m_{3/2}$  lors de la brisure spontanée de la supersymétrie, de même que les bosons de jauge du Modèle Standard acquièrent une masse lors de la brisure spontanée du groupe de jauge  $SU(2)_L \times U(1)_Y$ . Or, les R-symétries n'autorisent pas les termes de masse pour le gravitino. En effet, généralisant les transformations 3.24 nous obtenons les transformations sous une R-symétrie du vierbein  $e_\mu^m$  et du champ de spin 3/2 du gravitino  $\Psi_\mu$ ,

$$\begin{aligned}
e_\mu^m(x) &\rightarrow e_\mu^m(x), \\
\Psi_\mu(x) &\rightarrow e^{i\gamma_5\alpha} \Psi_\mu(x),
\end{aligned} \tag{3.33}$$

qui sont incompatibles avec l'existence du terme de masse pour le gravitino,  $m_{3/2}\bar{\Psi}_\mu[\gamma^\mu, \gamma^\nu]\Psi_\nu$ , qui implique des champs  $\Psi_\mu$  et  $\Psi_\nu$  de chiralité opposées. En conclusion, la coexistence

d'une R-symétrie avec les théories de supergravité, qui présentent en outre de nombreux attrait, paraît difficile.

La seconde difficulté est davantage phénoménologique. D'après Eq.(3.24), les R-symétries interdisent les termes de brisure douce de supersymétrie donnant directement une masse aux jauginos :

$$-\frac{i}{2}M_1\tilde{B}\tilde{B} - \frac{i}{2}M_2\tilde{W}_3\tilde{W}_3 - M_2\tilde{W}\tilde{W} - \frac{i}{2}M_3\tilde{g}\tilde{g}, \quad (3.34)$$

où nous avons dénoté les jauginos  $\Lambda = \tilde{B}$  (bino),  $\tilde{W}_3$  (wino neutre),  $\tilde{W}$  (wino chargé),  $\tilde{g}$  (gluino).  $\tilde{B}$ ,  $\tilde{W}_3$  et  $\tilde{g}$  sont des spineurs de Majorana. La raison est qu'un terme de masse pour un spineur à 4 composantes est du type,  $\tilde{\Psi}_H\Psi_{H'}$  où  $H, H' = L, R$  avec  $H \neq H'$ , et que les transformations 3.24 distinguent les spineurs de chiralité gauche et droite lorsqu'il s'agit de jauginos. Cependant, certaines R-symétries, comme la R-symétrie définie dans Eq.(3.32), autorisent les termes de mélange entre jauginos et higgsinos qui sont du type  $\tilde{\Lambda}\tilde{h}_{1,2}$  et génèrent aussi des masses pour les jauginos. Dans le MSSM, de tels termes de mélange existent pour les winos et le bino qui peuvent donc acquérir une masse. Par exemple, les matrices de masse des charginos et neutralinos dans le MSSM (voir Section 1.6.3) munie de la R-symétrie définie dans Eq.(3.32) sont respectivement,

$$\begin{pmatrix} (M_2 = 0) & M_W\sqrt{2}\sin\beta \\ M_W\sqrt{2}\cos\beta & (\mu = 0) \end{pmatrix}, \quad (3.35)$$

et,

$$\begin{pmatrix} (M_1 = 0) & 0 & -M_Z\sqrt{2}\cos\beta\sin\theta_W & M_Z\sqrt{2}\sin\beta\sin\theta_W \\ 0 & (M_2 = 0) & M_Z\sqrt{2}\cos\beta\cos\theta_W & -M_Z\sqrt{2}\sin\beta\cos\theta_W \\ -M_Z\sqrt{2}\cos\beta\sin\theta_W & M_Z\sqrt{2}\cos\beta\cos\theta_W & 0 & (-\mu = 0) \\ M_Z\sqrt{2}\sin\beta\sin\theta_W & -M_Z\sqrt{2}\sin\beta\cos\theta_W & (-\mu = 0) & 0 \end{pmatrix}. \quad (3.36)$$

Notons qu'il existe d'autres R-symétries que celle définie dans Eq.(3.32) pouvant simultanément interdire les couplages violant les nombres leptonique et baryonique du lagrangien 3.9, autoriser certains termes de mélange entre jauginos et higgsinos et autoriser le terme  $\mu H_1 H_2$ , qui est nécessaire à la brisure électrofaible et donne une masse aux higgsinos. En revanche, le MSSM ne contient pas de termes mélangeant higgsinos et gluinos. Dans le cadre du MSSM, les R-symétries sont donc incompatibles avec l'existence d'un terme de masse au niveau des arbres pour les gluinos. Les R-symétries semblent donc être en contradiction avec les données expérimentales qui donnent une limite inférieure sur la masse du gluino :  $m_{\tilde{g}} > 173\text{GeV}$  pour  $\mu = -200\text{GeV}$ ,  $\tan\beta = 2$  [46].

Quelles solutions s'offrent au problème de la masse du gluino dans les théories munies de R-symétries ? Tout d'abord, la masse du gluino ne peut être générée spontanément. En effet, les couplages du gluino  $\tilde{q}\tilde{q}\tilde{g}$  impliquent les champs de squarks qui ne peuvent acquérir une valeur moyenne dans le vide (vev), le groupe de jauge  $SU(3)_c$  du Modèle Standard ne devant pas être brisé. Cela nous amène aux alternatives intéressantes d'une masse de gluino générée radiativement ou par un mécanisme dynamique, pour lesquelles la masse du gluino est prédite [47, 48, 49]. Cependant, de tels modèles donnent des gluinos trop légers et sont exclus [50]. Un superchamp chiral octet de  $SU(3)_c$  peut aussi être ajouté pour donner une masse au gluino, mais ces scénarios ne sont pas naturels et brisent en

général  $SU(3)_c$  [47]. Enfin, le gluino peut acquérir une masse lors d’une brisure spontanée de R-symétrie [49]. Mais cette masse est petite et la brisure spontanée d’une R-symétrie pose le problème de l’existence d’un indésirable pseudo boson de Goldstone léger appelé R-axion [51]. En conclusion, le problème de la masse du gluino n’a pas de solution évidente.

Malgré les deux problèmes de l’existence d’une masse pour le gravitino et le gluino, les R-symétries ont suscité un grand intérêt dans la littérature. Voici les intérêts majeurs des R-symétries, outre la possibilité de garantir la conservation des nombres leptonique et baryonique. Tout d’abord, de même que la symétrie de Peccei-Quinn [51], la R-invariance a été proposée comme une solution originale au problème de la violation forte de CP [52], ainsi qu’au problème du moment dipolaire électrique du neutron [52, 53]. De plus, il a été montré dans [54] que l’existence d’une R-symétrie est une condition nécessaire à la brisure dynamique de la supersymétrie. Les auteurs de [54] ont aussi montré que la présence d’une R-symétrie brisée spontanément est une condition suffisante pour la brisure dynamique de la supersymétrie, dans le cas où le lagrangien effectif est un lagrangien générique consistant avec les symétries de la théorie (pas de fine-tuning) et où la théorie de basse énergie peut être décrite par un lagrangien effectif supersymétrique de Wess-Zumino sans champs de jauge. Tous les modèles connus aujourd’hui de brisure dynamique de la supersymétrie possèdent une telle R-symétrie brisée spontanément et contiennent donc un axion pouvant être problématique. Cependant, les auteurs de [54] ont montré que la R-symétrie peut dans beaucoup de cas être brisée explicitement sans restaurer la supersymétrie de telle sorte que l’axion puisse acquérir une masse suffisamment grande. Enfin, certaines R-symétries interdisent le terme de mélange des superchamps de Higgs dans le superpotentiel :

$$W = \mu H_1 H_2, \quad (3.37)$$

comme par exemple la R-symétrie définie dans Eq.(3.29,3.30,3.31) qui assigne une charge  $R = 0$  à  $H_1$  et  $H_2$ . Or la brisure spontanée de telles R-symétries permet de contrôler naturellement la valeur du paramètre  $\mu$  qui doit être de l’ordre de l’échelle électrofaible afin de permettre une brisure électrofaible réaliste, c’est à dire donnant une masse permise par les bornes expérimentales au boson de Higgs léger et donnant les masses attendues aux particules du Modèle Standard. (“problème du terme  $\mu$ ”). Le terme de Eq.(3.37) peut effectivement être généré par un terme du type,

$$W = \alpha \frac{1}{M_P^{n-1}} \left[ \prod_{i=1}^n S_i \right] H_1 H_2, \quad (3.38)$$

où les  $S_i$  sont des nouveaux superchamps chiraux singlets de jauge dont les charges de R-symétrie vérifient  $\sum_{i=1}^n R_i = 2$ . (dans le cas de la R-symétrie de Eq.(3.29,3.30,3.31)) et dont les champs scalaires acquièrent une vev. Le terme  $\mu$  de Eq.(3.37) sera alors donné par,

$$\mu = \alpha \frac{\langle S_1 S_2 \dots S_n \rangle}{M_P^{n-1}}, \quad (3.39)$$

$M_P$  étant l’échelle de Planck, et peut être de l’ordre de l’échelle électrofaible pour  $\langle S_i \rangle \ll M_P$ . Les R-symétries offrent donc un cadre propice à la résolution du problème du  $\mu$  [55, 56, 57, 58]. Rappelons toutefois que la brisure spontanée d’une R-symétrie pose le problème de l’existence du R-axion. Notons aussi que cette solution au problème du  $\mu$  via l’imposition d’une R-symétrie est très analogue à la solution caractérisée par l’existence d’une symétrie de Peccei-Quinn [58, 59].

### 3.3.3 Les R-symétries discrètes et la R-parité

Les R-symétries discrètes permettent d'éviter les problèmes de l'existence d'une masse pour le gravitino et le gluino. Considérons par exemple la R-symétrie discrète obtenue à partir de la R-symétrie définie dans Eq.(3.29,3.30,3.31) et Eq.(3.32) en prenant  $\alpha = \pi$ . Les transformations associées à la R-symétrie discrète ainsi obtenue s'écrivent sur les superchamps,

$$V(x, \theta, \bar{\theta}) \rightarrow V(x, -\theta, -\bar{\theta}), \quad (3.40)$$

$$H_{1,2}(x, \theta) \rightarrow H_{1,2}(x, -\theta), \quad (3.41)$$

$$\Phi(x, \theta) \rightarrow -\Phi(x, -\theta), \quad \Phi = Q, U^c, D^c, L, E^c, \quad (3.42)$$

et donc sur les champs,

$$\begin{array}{llll} v_\mu(x) \rightarrow v_\mu(x), & h_{1,2}(x) \rightarrow h_{1,2}(x), & \tilde{f}_L(x) \rightarrow -\tilde{f}_L(x), \\ \Lambda(x) \rightarrow -\Lambda(x), & \tilde{h}_{1,2}(x) \rightarrow -\tilde{h}_{1,2}(x), & \tilde{f}_R(x) \rightarrow -\tilde{f}_R(x), \\ D(x) \rightarrow D(x), & f_h(x) \rightarrow f_h(x), & \Psi(x) \rightarrow \Psi(x), \\ & \bar{f}_h(x) \rightarrow \bar{f}_h(x), & f(x) \rightarrow -f(x), \\ & & \bar{f}(x) \rightarrow -\bar{f}(x). \end{array} \quad (3.43)$$

La R-symétrie discrète de Eq.(3.43) autorise le terme de masse du gravitino ainsi que les termes de masse des jauginos exprimés dans Eq.(3.34). En effet, les transformations 3.43 sont identiques pour les champs de jauginos de chiralité gauche et droite, à l'inverse des transformations générales de R-symétrie données dans Eq.(3.24).

Les R-symétries discrètes peuvent être aussi bien des parités de matière que des parités leptoniques ou des parités baryoniques. Une étude des différentes R-symétries discrètes possibles a été traitée dans [60].

Nous observons que la R-symétrie discrète de Eq.(3.43) est une parité de matière, puisqu'elle interdit les couplages en  $\lambda$ ,  $\lambda'$  et  $\lambda''$  de Eq.(3.9), ce qui est cohérent car la R-symétrie originelle, définie dans Eq.(3.32), agit aussi comme une parité de matière. En fait, la R-symétrie discrète de Eq.(3.43) est la symétrie dite de *R-parité*. La symétrie de R-parité a été considérée les premières fois dans [35, 66, 61, 62, 63, 64, 65]. Bien que la R-parité ne soit pas la seule parité de matière, on associe souvent aujourd'hui, pour des raisons historiques, la symétrie interdisant les couplages en  $\lambda$ ,  $\lambda'$  et  $\lambda''$  à la R-parité plutôt qu'à la parité de matière. D'après Eq.(3.43), la R-parité transforme les champs des particules du Modèle Standard avec un facteur  $+1$  et les champs des particules supersymétriques avec un facteur  $-1$ . La R-parité peut donc être définie de façon équivalente à Eq.(3.43) par l'action de l'opérateur [66],

$$R_p = (-1)^{3B+L+2S}, \quad (3.44)$$

où  $B$  est le nombre baryonique,  $L$  le nombre leptonique et  $S$  le spin de la particule. Nous remarquons que la R-parité autorise les couplages de Yukawa, de même que la R-symétrie originelle définie par Eq.(3.32).

	$Q$	$U^c$	$D^c$	$L$	$E^c$	$H_1$	$H_2$
PM1	0	-1	1	0	1	-1	1
PM2	0	-1	0	-1	1	0	1
PL1	0	0	0	-1	1	0	0
PL2	0	0	-1	-2	1	1	0
PB1	0	-1	1	-1	2	-1	1
PB2	0	-1	0	-2	2	0	1

TAB. 3.1: *Charges des superchamps associées aux symétries PM1, PM2 (parités de matière), PL1, PL2 (parités leptoniques), PB1 et PB2 (parités baryoniques) qui représentent les symétries  $Z_2$  indépendantes autorisant les couplages de Yukawa.*

### 3.3.4 Les symétries discrètes

De simples symétries discrètes peuvent aussi être utilisées pour supprimer les différents couplages du lagrangien 3.9 et assurer ainsi un temps de vie suffisamment long au proton [67]. Par exemple, la symétrie,

$$(Q, U^c, D^c, L, E^c) \rightarrow -(Q, U^c, D^c, L, E^c), (H_1, H_2) \rightarrow (H_1, H_2), \quad (3.45)$$

est une parité de matière, la symétrie,

$$(L, E^c) \rightarrow -(L, E^c), (Q, U^c, D^c, H_1, H_2) \rightarrow (Q, U^c, D^c, H_1, H_2), \quad (3.46)$$

est une parité leptonique et la symétrie,

$$(Q, U^c, D^c) \rightarrow -(Q, U^c, D^c), (L, E^c, H_1, H_2) \rightarrow (L, E^c, H_1, H_2), \quad (3.47)$$

est une parité baryonique. Ces trois symétries discrètes sont définies sur les superchamps chiraux et laissent les superchamps vectoriels invariants. Notons que les composantes de spin 0, 1/2 et 1 des superchamps se transforment sous des symétries discrètes comme les superchamps eux-mêmes. Les couplages de Yukawa sont conservés sous les symétries 3.45, 3.46 et 3.47. Souvent, on appelle ces symétries 3.45, 3.46 et 3.47 parités de matière, parités leptoniques et parités baryoniques, respectivement, et on nomme les symétries interdisant les couplages en  $\lambda, \lambda', \lambda''$  parités de matière généralisées, en  $\lambda, \lambda'$  parités leptoniques généralisées et en  $\lambda''$  parités baryoniques généralisées.

Dans [60], la forme générale d'une symétrie  $Z_N$  définie par,

$$\Phi_l \rightarrow e^{iq_l \frac{2\pi}{N}} \Phi_l, \quad \Phi_l = Q, U^c, D^c, L, E^c, H_1, H_2, \quad (3.48)$$

et autorisant les couplages de Yukawa a été donnée. Cette forme générale a permis aux auteurs de [60] de déterminer la liste complète des symétries  $Z_2$  et  $Z_3$  indépendantes qui autorisent les couplages de Yukawa. Des symétries  $Z_N$  avec de grandes valeurs de  $N$  sont peu naturelles d'un point de vue esthétique ainsi que du point de vue des théories de cordes. Nous présentons dans la Table 3.1 les charges associées à toutes les symétries  $Z_2$  indépendantes autorisant les couplages de Yukawa. La Table 3.1 montre que le nombre de ces symétries  $Z_2$  est étonnement petit étant donné le peu de contraintes imposées. Le nombre des symétries  $Z_2$  indépendantes et compatibles avec l'existence des couplages

de Yukawa peut même être réduit davantage si l'on requiert l'existence un terme  $\mu$  du type de Eq.(3.37) ainsi que l'absence de toute contribution significative par des opérateurs de dimension 5 (voir Eq.(3.13) et Eq.(3.14)) à la désintégration des nucléons. En effet, les seules symétries satisfaisant à ces deux conditions supplémentaires sont les symétries PL1 et PB1 (voir Table 3.1). La symétrie PL1 autorise l'opérateur  $\mathcal{O}_3$  de Eq.(3.13) mais interdit les couplages en  $\lambda'$  de sorte que  $\mathcal{O}_3$  ne peuvent contribuer dangereusement à la désintégration des nucléons (voir Section 3.2.1). De même, la symétrie PB1 permet l'existence des  $\mathcal{O}_4, \dots, \mathcal{O}_{10}$  de Eq.(3.13) et Eq.(3.14) mais interdit les couplages en  $\lambda''$  et donc les  $\mathcal{O}_4, \dots, \mathcal{O}_{10}$  ne peuvent contribuer à la désintégration des nucléons de façon significative. En effet, les seules contraintes relevantes sur les coefficients  $\eta_4, \dots, \eta_{10}$  viennent de combinaisons entre les opérateurs  $\mathcal{O}_4, \dots, \mathcal{O}_{10}$  et  $U^c D^c D^c$ . Les deux conditions supplémentaires décrites plus haut ne sont cependant pas obligatoires. D'une part, un terme  $\mu$  (nécessaire à une brisure électrofaible correcte) interdit par une certaine symétrie discrète peut tout de même être généré par la brisure spontanée de cette symétrie. Ce mécanisme permet en outre de prédire la valeur de  $\mu$  comme nous l'avons expliqué dans la Section 3.3.2 pour le cas de la brisure spontanée d'une R-symétrie. D'autre part, la suppression de toute contribution significative par des opérateurs de dimension 5 à la désintégration des nucléons n'est pas nécessairement assurée par des symétries, et son origine peut être liée à une nouvelle physique, comme mentionné au début de la Section 3.3.

### 3.4 Motivations théoriques de la parité de matière ou R-parité

Si le proton n'est pas protégé de sa désintégration par une parité de matière, mais seulement par une parité leptonique ou baryonique ou bien par une symétrie interdisant uniquement les couplages  $\lambda'$  ou  $\lambda + \lambda''$ , certains couplages  $\lambda, \lambda'$  ou  $\lambda''$  du lagrangien 3.9 peuvent être présents. Un tel scénario implique des effets importants sur la phénoménologie de la supersymétrie auprès des collisionneurs de particules. D'un point de vue phénoménologique, l'impact majeur d'une violation de la parité de matière, ou violation de la R-parité ( $\mathcal{R}_p$ ), est lié à la stabilité de la particule supersymétrique la plus légère (LSP) : En présence des couplages  $\mathcal{R}_p \lambda, \lambda'$  ou  $\lambda''$ , la LSP n'est plus stable car elle peut se désintégrer en particules du Modèle Standard plus légères qu'elle. Les signaux caractéristiques des réactions supersymétrique ne sont alors plus des états finals avec une grande énergie manquante mais des signatures multileptoniques ou multi-jets, suivant le couplage  $\mathcal{R}_p$  dominant. En présence de couplages  $\mathcal{R}_p$ , une particule supersymétrique peut aussi être produite à la résonance et donner ainsi lieu à une découverte spectaculaire de la supersymétrie auprès d'un collisionneur de particules. Par conséquent, étant donné les effets importants des couplages  $\mathcal{R}_p$  sur la phénoménologie de la supersymétrie, il est crucial de savoir si le proton est protégé par une parité de matière, ou en d'autres termes, si la symétrie de R-parité est conservée. Dans cette partie, nous nous demanderons si les théories actuelles majeurs favorisent davantage les modèles avec ou sans parité de matière. Nous constaterons qu'aujourd'hui aucun argument théorique ne permet de trancher clairement entre un scénario  $\mathcal{R}_p$  et  $\mathcal{R}_p$ .

### 3.4.1 Point de vue des symétries discrètes de jauge

Un résultat théorique fort intéressant a été obtenu dans [68] : Toute symétrie non jaugée est fortement violée par des effets de gravité quantique. Les symétries globales ainsi violées ne peuvent pas garantir la stabilité du proton [69]. Les auteurs de [70] ont cependant montré que les symétries discrètes obtenues par brisure spontanée de symétries de jauge (symétries discrètes de jauge) échappent à ces effets de gravité quantique et peuvent donc être conservées. Cela suggère que la symétrie discrète assurant la stabilité du proton soit une symétrie discrète de jauge. Or les symétries discrètes de jauge sont soumises à certaines contraintes provenant des conditions d'annulation des anomalies des symétries de jauge originelles. Ces contraintes sont intéressantes dans la mesure où elles constituent des arguments théoriques en faveur de l'élimination de certaines symétries discrètes jusqu'alors possibles.

Par exemple, considérons une théorie effective de basse énergie comprenant les superchamps non massifs  $\Phi_i$  de charges  $q_i \in \mathbf{Z}$  sous une symétrie  $Z_N$  donnée. Supposons que cette symétrie  $Z_N$  descende d'une symétrie de jauge  $U(1)$ . La condition d'annulation de l'anomalie  $U(1) - U(1) - U(1)$  de la symétrie de jauge  $U(1)$  originelle s'écrit,

$$\sum_{\alpha} Q_{\alpha}^3 = 0, \quad (3.49)$$

où les  $Q_{\alpha}$  sont les charges associées à la symétrie  $U(1)$  de tous les fermions non massifs de la théorie. Ces charges sont nécessairement du type,

$$Q(\Phi_i) = q_i + m_i N, \quad Q(H) = m_H N, \quad m_i, m_H \in \mathbf{Z}, \quad (3.50)$$

pour les superchamps  $\Phi_i$  et le superchamp  $H$  dont la composante scalaire acquiert une vev brisant la symétrie de jauge  $U(1)$ . En effet, l'invariance sous  $U(1)$  du terme du superpotentiel responsable de la brisure spontanée de  $U(1)$ ,

$$W = \Phi_1 \Phi_2 \dots \Phi_n H^h, \quad h \in \mathbf{Z}, \quad (3.51)$$

implique d'après Eq.(3.50),

$$\sum_{i=1}^n Q(\Phi_i) + h Q(H) = \sum_{i=1}^n (q_i + m_i N) + h m_H N = 0. \quad (3.52)$$

Par conséquent, après que la symétrie  $U(1)$  est brisée par la vev de  $H$ , il apparaît bien que le terme 3.51 qui devient alors,

$$W = \Phi_1 \Phi_2 \dots \Phi_n \langle H \rangle^h, \quad h \in \mathbf{Z}, \quad (3.53)$$

est invariant sous la symétrie  $Z_N$  puisque l'on a d'après Eq.(3.52),

$$\sum_{i=1}^n q_i = - \sum_{i=1}^n m_i N - h m_H N = k N, \quad k \in \mathbf{Z}. \quad (3.54)$$

La théorie dans sa totalité contient les superchamps  $\Phi_i$  de la théorie effective mais aussi les superchamps qui acquièrent une masse lors de la brisure du groupe  $U(1)$ . Or les charges  $U(1)$  de ces derniers doivent aussi être prises en compte dans Eq.(3.49). Les charges  $U(1)$

des superchamps  $\Phi_j$  acquérant une masse lors de la brisure de  $U(1)$  sont du même type que les charges  $U(1)$  des superchamps effectifs  $\Phi_i$  (voir Eq.(3.50)), c'est à dire du type  $Q(\Phi_j) = q_j + m_j N$ , où  $q_j$  est la charge de  $\Phi_j$  sous la symétrie  $Z_N$  et  $m_j \in \mathbf{Z}$ . Les charges  $Z_N$  des superchamps  $\Phi_j$  sont contraintes, par l'invariance sous  $Z_N$  des termes de masse  $W = m\Phi_j^c\Phi_j$ , à être du type,

$$q_j^c + q_j = l_j N, \quad l_j \in \mathbf{Z}. \quad (3.55)$$

Cette équation est équivalente à l'équation,

$$q_j^c + m_j^c N + q_j + m_j N = (l_j + m_j^c + m_j) N, \quad l_j, m_j^c, m_j \in \mathbf{Z}, \quad (3.56)$$

qui donne une relation sur les charges  $U(1)$  des superchamps  $\Phi_j$  :

$$Q(\Phi_j^c) + Q(\Phi_j) = p_j N, \quad p_j \in \mathbf{Z}, \quad (3.57)$$

qui peut aussi s'écrire,

$$Q^3(\Phi_j^c) + Q^3(\Phi_j) = p_j N \left( 3Q^2(\Phi_j) - 3p_j N Q(\Phi_j) + p_j^2 N^2 \right), \quad p_j \in \mathbf{Z}. \quad (3.58)$$

Les charges  $Z_N$  des superchamps de Majorana  $S_j$ , acquérant eux une masse par des termes du type  $W = mS_j^2$  lors de la brisure de  $U(1)$ , sont contraintes par,

$$q_j^s = \frac{k_j N}{2}, \quad k_j \in \mathbf{Z}. \quad (3.59)$$

où  $k_j$  est pair si  $N$  est impair, soit encore,

$$q_j^s + m_j^s N = \frac{(k_j + 2m_j^s) N}{2}, \quad p'_j \in \mathbf{Z}, \quad (3.60)$$

avec  $k_j$  pair si  $N$  est impair. L'équation Eq.(3.60) donne une relation sur les charges  $U(1)$  des superchamps  $S_j$  :

$$Q(S_j) = \frac{p'_j N}{2}, \quad p'_j \in \mathbf{Z}. \quad (3.61)$$

où  $p'_j$  est pair si  $N$  est impair. Finalement, en remplaçant Eq.(3.50), Eq.(3.58) et Eq.(3.61) dans Eq.(3.49), on obtient une contrainte, sur les charges  $q_i$  d'une symétrie  $Z_N$  descendant d'une symétrie de jauge  $U(1)$ , qui peut s'écrire [71],

$$\sum_i q_i^3 = mN + \eta n \frac{N^3}{8}, \quad m, n \in \mathbf{Z}, \quad (3.62)$$

avec  $\eta = 1, 0$  pour  $N \equiv \text{pair}, \text{impair}$  et,

$$\begin{aligned} m &= -\sum_i \left( 3q_i^2 m_i + 3q_i m_i^2 N + m_i^3 N^3 \right) \\ &\quad - \sum_j \left( p_j N (3Q^2(\Phi_j) - 3p_j N Q(\Phi_j) + p_j^2 N^2) \right), \\ n &= -\sum_j p_j'^3, \end{aligned} \quad (3.63)$$

la somme sur  $i$  étant prise sur les superchamps de la théorie effective et la somme sur  $j$  sur les superchamps acquérant une masse lors de la brisure de  $U(1)$ . De même, les conditions



d'annulation des anomalies  $U(1) - \text{Gravitation} - \text{Gravitation}$ ,  $U(1) - SU(M) - SU(M)$  donnent respectivement les contraintes,

$$\sum_i q_i = pN + \eta q \frac{N}{2}, \quad p, q \in \mathbf{Z}, \quad (3.64)$$

$$\sum_i T_i q_i = \frac{1}{2} r N, \quad r \in \mathbf{Z}, \quad (3.65)$$

où les  $T_i$  sont les Casimirs quadratiques de  $SU(M)$  correspondant à chaque représentation, avec une normalisation telle que le Casimir est égal à  $1/2$  pour un M-plet. Dans Eq.(3.64) et Eq.(3.65) les nombres  $p, q$  et  $r$  obéissent à des égalités du type de Eq.(3.63) [71]. Il est important de réaliser que les égalités 3.62, 3.64 et 3.65 représentent des conditions nécessaires mais pas suffisantes pour que la symétrie  $Z_N$  considérée puisse découler d'une symétrie de jauge  $U(1)$ . En effet, pour une symétrie  $Z_N$  donnée il n'existe pas nécessairement un modèle acceptable comprenant une symétrie de jauge originelle  $U(1)$  satisfaisant entre autre à Eq.(3.63). Certains modèles réalistes contenant des symétries de jauge  $U(1)$  engendrant des symétries discrètes  $Z_N$  à basse énergie ont été construits explicitement dans [71, 60].

Dans [60], il a été montré, à partir de la forme générale d'une symétrie  $Z_N$  autorisant les couplages de Yukawa, que les seules symétries  $Z_N$  respectant les contraintes 3.62, 3.64 et 3.65, c'est à dire les seules symétries  $Z_N$  pouvant découler d'une symétrie de jauge  $U(1)$ , sont la symétrie PM1 (voir Section 3.3.4) et la symétrie  $Z_3$  définie par les charges suivantes,

$$q(Q) = 0, \quad q(U^c) = -1, \quad q(D^c) = 1, \quad q(L) = -1, \quad q(E^c) = 2, \quad q(H_1) = -1, \quad q(H_2) = 1. \quad (3.66)$$

Ces deux symétries autorisent un terme  $\mu$  (voir Eq.(3.37)). La symétrie de Eq.(3.66) supprime toute contribution dangereuse par des opérateurs de dimension 5 (voir Eq.(3.13) et Eq.(3.14)) à la désintégration des nucléons, pour les mêmes raisons que la symétrie PB1 (voir Section 3.3.4). En revanche, la symétrie PM1 autorise l'existence de l'opérateur  $\mathcal{O}_1$  qui engendre une désintégration rapide du proton (voir Section 3.2.1). En conclusion, si la symétrie protégeant le proton est une symétrie discrète de jauge  $Z_N$  provenant d'une symétrie de jauge  $U(1)$ , elle peut être aussi bien une parité de matière (PM1) ou une parité baryonique (symétrie  $Z_3$  définie dans Eq.(3.66)), avec une préférence pour la parité baryonique qui interdit toute contribution dangereuse par des opérateurs de dimension 5 à la désintégration des nucléons. Les auteurs de [72] ont même montré que les résultats de [60] dépendent du modèle considéré, autorisant ainsi un plus grand nombre de symétries discrètes de jauge.

Mentionnons aussi que dans certains modèles [73] les couplages en  $\lambda, \lambda'$  et  $\lambda''$  sont supprimés par un facteur  $M_X/M_P$  dans lequel  $M_X$  est l'échelle de brisure d'une symétrie de jauge supplémentaire  $U(1)$ .

Les R-symétries discrètes de jauge proviennent de R-symétries jaugées, or les R-symétries continues posent de sérieux problèmes liés aux masses du gravitino et des gluinos comme nous l'avons vu dans la Section 3.3.2. De plus, les R-symétries ne peuvent être jaugées que dans un contexte de supersymétrie locale [74]. En effet, d'après Eq.(3.15, 3.16, 3.17) les transformations associées à une R-symétrie de jauge s'écrivent,

$$V_k(x, \theta, \bar{\theta}) \rightarrow V_k(x, \theta e^{-i\alpha(x)}, \bar{\theta} e^{i\alpha(x)}), \quad (3.67)$$

$$\Phi_l(x, \theta) \rightarrow e^{iR_l\alpha(x)} \Phi_l(x, \theta e^{-i\alpha(x)}), \quad (3.68)$$

$$\bar{\Phi}_l(x, \bar{\theta}) \rightarrow e^{-iR_l\alpha(x)} \bar{\Phi}_l(x, \bar{\theta} e^{i\alpha(x)}), \quad (3.69)$$

et sont des formes spéciales de transformations locales dans le superspace qui peuvent être vues comme des transformations locales sur les champs. Le fait que les R-symétries de jauge n'existent que dans les théories de supersymétrie locale peut aussi être vu de la manière suivante. Il est clair que les transformations de R-symétries (voir Eq.(3.15), Eq.(3.16) et Eq.(3.17)) ne commutent pas avec les transformations de supersymétrie. La relation d'anti-commutation entre les générateurs  $R$  de R-symétries et les générateurs  $Q_\alpha$  de la supersymétrie s'écrit  $[Q_\alpha, R] = i(\gamma_5)_\alpha^\beta Q_\beta$  [31]. Or, cette relation d'anti-commutation reste vraie quand le générateur  $R$  dépend des coordonnées d'espace-temps, seulement si les générateurs  $Q_\alpha$  deviennent eux aussi les générateurs d'une supersymétrie locale. Malgré les difficultés engendrées par les R-symétries de jauge et la nécessité de considérer de telles symétries en supersymétrie locale, certains modèles basés sur des R-symétries jaugées ont été construits [74, 75, 76]. De tels modèles peuvent préserver la stabilité du proton soit en engendrant des R-symétries discrètes de jauge soit en générant des couplages en  $\lambda, \lambda', \lambda''$  supprimés par un facteur  $M/M_P$ ,  $M$  étant une échelle d'énergie. Certains des modèles avec R-symétrie de jauge construits [74] peuvent protéger le proton de sa désintégration tout en autorisant certains couplages  $\mathcal{R}_p$ .

### 3.4.2 Point de vue des théories de grande unification (GUT)

Nous considérons dans un premier temps le cas du modèle de grande unification basé sur le groupe de jauge  $SU(5)$  [77] qui est le groupe le plus petit pouvant contenir le groupe de jauge du Modèle Standard sans rajouter de nouveaux fermions. Puis nous discuterons les théories de grande unification en général.

Rappelons que dans le modèle de grande unification  $SU(5)$ , les superchamps  $L$  et  $D^c$  sont contenus dans une représentation  $\bar{\mathbf{5}}$  de  $SU(5)$ , alors que  $Q$ ,  $U^c$  et  $E^c$  appartiennent à une représentation  $\mathbf{10}$  de  $SU(5)$  :

$$\bar{\mathbf{5}} = \begin{pmatrix} D^c \\ i\sigma_2 L \end{pmatrix}, \quad \mathbf{10} = \begin{pmatrix} U^c & -Q \\ Q & -E^c i\sigma_2 \end{pmatrix}, \quad (3.70)$$

où  $\sigma_2$  est une des matrices de Pauli. Quant aux superchamps de Higgs  $H_1$  et  $H_2$ , ils sont dans des représentations  $\bar{\mathbf{5}}_H$  et  $\mathbf{5}_H$ , respectivement. Ces deux représentations contiennent aussi des superchamps de Higgs additionnels triplets de  $SU(3)_c$ . La théorie GUT basée sur le groupe de jauge  $SU(5)$  contient le superchamp  $\Sigma$  appartenant à la représentation  $\mathbf{24}$  (adjointe de  $SU(5)$ ) qui brise spontanément  $SU(5)$ , donnant ainsi aux bosons de jauge de  $SU(5)$  ainsi qu'aux superchamps de Higgs triplets de  $SU(3)_c$  des masses de l'ordre de  $\langle \Sigma \rangle \sim M_{GUT}$ ,  $M_{GUT}$  étant l'échelle de la théorie GUT. Dans le modèle  $SU(5)$ , les interactions de Yukawa s'écrivent,

$$W = h_{ij} \mathbf{10}^i \mathbf{10}^j \mathbf{5}_H + \bar{h}_{ij} \mathbf{10}^i \bar{\mathbf{5}}^j \bar{\mathbf{5}}_H, \quad (3.71)$$

où les  $h_{ij}$  et  $\bar{h}_{ij}$  sont les constantes de couplages de Yukawa. Quant aux interactions  $\mathcal{R}_p$ , elles découlent toutes d'un seul et même opérateur :

$$\mathbf{10}^i \bar{\mathbf{5}}^j \bar{\mathbf{5}}^k \mapsto \lambda_{ijk} L_j L_k E_i^c, \lambda'_{ijk} L_k Q_i D_j^c, \lambda''_{ijk} U_i^c D_j^c D_k^c. \quad (3.72)$$

Par conséquent il ne semble pas à priori possible d'interdire uniquement certains termes  $\mathcal{R}_p$ , comme par exemple les couplages en  $\lambda'$ , en imposant une symétrie. La seule symétrie protégeant le proton paraît donc être une parité de matière, dans le modèle  $SU(5)$ . En réalité, cette première conclusion est fausse car certains couplages  $\mathcal{R}_p$  sont engendrés par des opérateurs distincts non renormalisables de dimension 5 et 6 qui deviennent renormalisables après brisure de  $SU(5)$  :

$$(\mathbf{10}^i \Sigma)_{\mathbf{10}} (\bar{\mathbf{5}}^j \bar{\mathbf{5}}^k)_{\bar{\mathbf{10}}} \mapsto \lambda_{ijk} L_j L_k E_i^c, \lambda'_{ijk} L_k Q_i D_j^c, \lambda''_{ijk} U_i^c D_j^c D_k^c \quad (3.73)$$

$$(\mathbf{10}^i \Sigma)_{\mathbf{15}} (\bar{\mathbf{5}}^j \bar{\mathbf{5}}^k)_{\bar{\mathbf{15}}} \mapsto \lambda'_{ijk} L_k Q_i D_j^c \quad (3.74)$$

$$(\mathbf{10}^i \Sigma)_{\mathbf{15}} ([\bar{\mathbf{5}}^j \bar{\mathbf{5}}^k]_{\bar{\mathbf{10}}} \Sigma)_{\bar{\mathbf{15}}} \mapsto \lambda'_{ijk} L_k Q_i D_j^c. \quad (3.75)$$

Dans l'opérateur de Eq.(3.74) c'est la représentation symétrique ( $\bar{\mathbf{15}}$ ) du produit  $\bar{\mathbf{5}}^j \bar{\mathbf{5}}^k$  qui est sélectionnée. Par conséquent cet opérateur engendre des couplages  $\Lambda_{ijk}$  symétriques dans les indices de saveur  $j$  et  $k$ , puisque l'on a,

$$\Lambda_{ijk}(\bar{\mathbf{5}}_a^j \bar{\mathbf{5}}_b^k)_{\bar{\mathbf{15}}} = \Lambda_{ijk}(\bar{\mathbf{5}}_b^j \bar{\mathbf{5}}_a^k)_{\bar{\mathbf{15}}} = \Lambda_{ikj}(\bar{\mathbf{5}}_b^k \bar{\mathbf{5}}_a^j)_{\bar{\mathbf{15}}} = \Lambda_{ikj}(\bar{\mathbf{5}}_a^j \bar{\mathbf{5}}_b^k)_{\bar{\mathbf{15}}}, \quad (3.76)$$

où  $a, b = 1, \dots, 5$  sont des indices du groupe  $SU(5)$ . C'est pour cette raison que l'opérateur de Eq.(3.74) n'engendre pas les couplages  $\lambda_{ijk}$  et  $\lambda''_{ijk}$  qui sont antisymétriques dans les indices de saveur  $j$  et  $k$  (voir Eq.(3.2) avec la notation des couplages  $\mathcal{R}_p$  de Eq.(3.72)). L'opérateur de Eq.(3.73) engendre les couplages  $\lambda_{ijk}, \lambda'_{ijk}$  et  $\lambda''_{ijk}$  car c'est la représentation antisymétrique ( $\bar{\mathbf{10}}$ ) du produit  $\bar{\mathbf{5}}^j \bar{\mathbf{5}}^k$  qui est sélectionnée. L'opérateur de Eq.(3.75) ne génère pas  $\lambda_{ijk}$  et  $\lambda''_{ijk}$  car  $(\mathbf{10}^i \Sigma)_{\mathbf{15}}$  ne se projette que sur le superchamp  $Q$  de la représentation  $\mathbf{10}$  de Eq.(3.70) après brisure de  $SU(5)$ . Des opérateurs comprenant des puissances  $n > 2$  de  $\langle \Sigma \rangle^n$  se réduisent à des combinaisons des opérateurs de Eq.(3.73), Eq.(3.74) et Eq.(3.75) car  $\langle \Sigma \rangle^n$  est une combinaison linéaire de  $\langle \Sigma \rangle$  et de l'identité pour tout  $n$ . Il est donc possible d'imposer une symétrie supprimant les opérateurs de Eq.(3.72), Eq.(3.73) et Eq.(3.74) et autorisant l'opérateur de Eq.(3.75), protégeant ainsi le proton en permettant uniquement l'existence de couplages  $\lambda'_{ijk}$ . Ce scénario est aussi possible si seul l'opérateur de Eq.(3.74) existe. Illustrons cette alternative par un "toy model". Considérons un modèle contenant, en plus des superchamps du modèle  $SU(5)$ , deux superchamps  $S$  et  $\bar{S}$  appartenant respectivement à des représentations  $\mathbf{15}$  et  $\bar{\mathbf{15}}$  de  $SU(5)$  ainsi qu'un superchamp  $\Phi$  singlet de jauge. La présence simultanée du superchamp  $S$  et de son conjugué de charge  $\bar{S}$  préserve l'annulation des anomalies de  $SU(5)$ . Imposons la symétrie discrète  $Z_N$  caractérisée par les charges,

$$q(\mathbf{10}) = -1, q(\bar{\mathbf{5}}) = 3, q(\mathbf{5}_H) = 2, q(\bar{\mathbf{5}}_H) = -2, q(\Sigma) = 0, q(S) = -6, q(\bar{S}) = 1, q(\Phi) = 5. \quad (3.77)$$

Cette symétrie autorise les couplages de Yukawa de Eq.(3.71), les couplages responsables de la brisure de  $SU(5)$  et  $SU(3)_c \times SU(2)_L \times U(1)_Y$  et enfin les termes suivants,

$$W = \bar{S}(\mathbf{10}^i \Sigma)_{\mathbf{15}} + S(\bar{\mathbf{5}}^j \bar{\mathbf{5}}^k)_{\bar{\mathbf{15}}} + \bar{S} S \Phi. \quad (3.78)$$

Si  $\Phi$  acquiert une vev  $\langle \Phi \rangle \sim M_X$  à l'échelle  $M_X > M_{GUT}$ , la théorie effective à  $M_{GUT}$ , obtenue en intégrant  $S$  et  $\bar{S}$  dans Eq.(3.78), contient l'opérateur de Eq.(3.74). Dans un tel modèle, les couplages  $\lambda'$  générés sont en  $\lambda' \sim M_{GUT}/M_X$ .

Il est aussi possible dans le modèle  $SU(5)$  de protéger le proton par une parité leptonique ou baryonique [77]. En effet, supposons une symétrie interdisant les opérateurs de

Eq.(3.72) et de Eq.(3.73), Eq.(3.74) et Eq.(3.75) mais autorisant les termes bilinéaires de Eq.(3.1) (représentant des couplages  $\mathcal{R}_p$ ) qui s'écrivent dans le modèle  $SU(5)$ ,

$$W = \mu_k \bar{\mathbf{5}}^k \mathbf{5}_H. \quad (3.79)$$

Ce terme couple le superchamp de Higgs triplet de  $SU(3)_c$  contenu dans la représentation  $\mathbf{5}_H$  avec le superchamp  $D^c$  de la représentation  $\bar{\mathbf{5}}$  de Eq.(3.70). Or, ce superchamp de Higgs triplet de  $SU(3)_c$  acquiert une masse de l'ordre de  $\langle \Sigma \rangle \sim M_{GUT}$ . Donc, en intégrant ce superchamp dans les superpotentiels 3.71 et 3.79, on obtient dans la théorie effective à une échelle juste inférieure à  $M_{GUT}$  uniquement des couplages  $\lambda''$  et qui sont de l'ordre,

$$\lambda''_{ijk} \sim \bar{h}_{ij} \frac{\mu_k}{M_{GUT}}. \quad (3.80)$$

De même, l'intégration du superchamp de Higgs du MSSM dans les superpotentiels 3.71 et 3.79 permet de ne générer que des couplages  $\lambda_{ijk}$  et  $\lambda'_{ijk}$ , qui seraient alors de l'ordre de  $\bar{h}_{ij}\mu_k/\mu$ ,  $\mu$  étant le paramètre de Eq.(3.37).

De manière général, dans les théories GUT, les superchamps de quarks et de leptons sont compris dans les mêmes supermultiplets et ont par conséquent les mêmes charges associées aux symétries discrètes. Il ne semble donc pas possible à priori d'imposer dans les théories GUT une symétrie n'interdisant que certains couplages parmi  $\lambda, \lambda'$  et  $\lambda''$ , qui distingue typiquement les quarks des leptons, et le seul type de symétrie paraissant pouvoir protéger le proton est une parité de matière. Cependant, plusieurs modèles GUT protégeant le proton par des symétries différentes de la R-parité ont été élaborés dans la littérature [67, 77, 78, 79, 80]. En général, ces modèles engendrent certains des couplages  $\lambda, \lambda', \lambda''$  à partir d'opérateurs non renormalisables qui deviennent renormalisables après brisure du groupe de jauge de grande unification. De tels modèles GUT ont par exemple été construits pour les groupes de jauge  $SU(5)$  [67, 77],  $SO(10)$  [77] et  $SU(5) \times U(1)$  [77, 78, 79]. En conclusion, le choix entre une parité de matière et une autre symétrie pour protéger le proton reste de manière général tout à fait arbitraire dans les théories GUT.

### 3.4.3 Point de vue des théories de cordes

Dans les théories de cordes, l'unification des interactions du Modèle Standard peut être réalisée sans un groupe simple, par contraste avec les modèles de grande unification mentionnés dans la Section 3.4.2. Les superchamps de quarks et de leptons peuvent donc sans difficulté appartenir à des multiplets différents et avoir ainsi des charges distinctes sous une symétrie discrète, de telle sorte que cette symétrie puisse protéger le proton de sa désintégration en interdisant seulement certains couplages  $\mathcal{R}_p$  parmi  $\lambda, \lambda'$  et  $\lambda''$ . Des théories de cordes avec conservation ou violation de la R-parité ont toutes deux été construites dans la littérature [81, 82]. Il ne semble pas par ailleurs y avoir d'arguments théoriques en faveur d'une parité de matière ou d'une autre symétrie empêchant la désintégration rapide du proton, du point de vue des théories de cordes à l'heure actuelle.

### 3.4.4 Conclusion

En conclusion, le cadre théorique actuel ne motive pas davantage un scénario avec violation ou conservation de la symétrie de R-parité. Par conséquent, les deux types de

modèles  $R_p$  et  $\mathcal{R}_p$  doivent être considérés au même titre du point de vue de la phénoménologie de la supersymétrie auprès des prochains collisionneurs.



# Chapitre 4

## Production simple des particules supersymétriques par les interactions violant la R-parité

### 4.1 Motivations

D’après la conclusion du Chapitre 3, d’un point de vue théorique, les modèles avec violation de la R-parité sont à considérer au même titre que les modèles dans lesquels la R-parité est conservée. Par conséquent, les modèles avec violation de la R-parité doivent être étudiés dans la phénoménologie de la supersymétrie auprès des collisionneurs de particules actuels et futurs. D’un point de vue phénoménologique, il apparaît aussi tout à fait important d’étudier les scénarios de violation de la R-parité dans la mesure où les signaux de la supersymétrie dans les collisionneurs sont fondamentalement différents dans les scénarios de violation et de conservation de la R-parité. En effet, la production de particules supersymétriques dans les collisionneurs donnerait lieu typiquement à des cascades de désintégrations se terminant par la production de la particule supersymétrique la plus légère appelée LSP (Lightest Supersymmetric Particle). Or la LSP ne peut se désintégrer ni par des interactions de jauge ni par des interactions de Yukawa, qui couplent toutes un nombre pair de particules supersymétriques (voir Chapitre 1). En revanche, la LSP a la possibilité de se désintégrer uniquement en particules du Modèle Standard par des interactions violant la R-parité (voir Chapitre 3). Les états finals caractéristiques de la production de particules supersymétriques dans les collisionneurs sont donc des états contenant une grande énergie manquante dans les scénarios  $R_p$  et des états multileptoniques ou multijets dans les scénarios  $\mathcal{R}_p$  (si le temps de vie de la LSP est suffisamment court pour que celle-ci se désintègre dans le détecteur).

Dans l’hypothèse où certains couplages  $\mathcal{R}_p$  ne seraient pas nuls, il serait naturel de tenter de déterminer expérimentalement l’intensité de ces couplages. Le premier problème phénoménologique sur lequel nous nous sommes penchés a donc été le calcul de la sensibilité qui peut être obtenue sur la valeur absolue des différentes constantes de couplage  $\mathcal{R}_p$ .

Tout d’abord, la valeur des constantes de couplage  $\mathcal{R}_p$  peut être déduite de la longueur de “vol” de la LSP, c’est à dire de la distance entre le vertex de production de la LSP et le vertex de désintégration de la LSP par des interactions  $\mathcal{R}_p$ . Notons que cette méthode n’est

envisageable que si les positions des vertex de production et de désintégration la LSP sont identifiables, c'est à dire si ces vertex connectent au moins 2 particules détectables par les calorimètres hadroniques et leptoniques, à savoir des jets ou des leptons chargés mais pas des neutrinos. De plus, cette méthode est particulièrement délicate dans les collisionneurs hadroniques qui génèrent de nombreuses traces de particules dans les détecteurs. Cherchons maintenant les valeurs maximums de constantes de couplage  $\mathcal{R}_p$  auxquelles seraient sensibles une telle étude de vertex déplacé de la LSP. Ces valeurs maximums dépendant de la nature de la LSP ainsi que de la géométrie et des performances du détecteur considéré. Nous considérerons le détecteur d'un futur collisionneur linéaire [83, 127] afin de travailler dans un contexte de collisions leptoniques et dans des conditions de performance optimale. Par ailleurs, nous supposons que la LSP est le plus léger des neutralinos (noté  $\tilde{\chi}_1^0$ ), comme c'est le cas typiquement dans les modèles de supergravité. Partons de la longueur de vol du  $\tilde{\chi}_1^0$  dans le référentiel du laboratoire qui est donnée en mètres par [84],

$$c\gamma\tau_{LSP} \sim 3\gamma \cdot 10^{-3}m \left(\frac{\tilde{M}}{100GeV}\right)^4 \left(\frac{1GeV}{M_{LSP}}\right)^5 \left(\frac{1}{\Lambda}\right)^2, \quad (4.1)$$

où  $\Lambda = \lambda, \lambda' \text{ ou } \lambda''$ ,  $c$  est la vitesse de la lumière,  $\gamma$  le facteur du boost de Lorentz,  $\tau_{LSP}$  le temps de vie du  $\tilde{\chi}_1^0$ ,  $M_{LSP}$  la masse du  $\tilde{\chi}_1^0$  et  $\tilde{M}$  la masse de la particule supersymétrique échangée dans la désintégration du  $\tilde{\chi}_1^0$  impliquant le couplage  $\Lambda$  considéré : La désintégration du  $\tilde{\chi}_1^0$  par des interactions  $\mathcal{R}_p$  est du type  $\tilde{\chi}_1^0 \rightarrow \tilde{f}_i^* f_i$ ,  $\tilde{f}_i^* \rightarrow f_j f_k$  où  $\tilde{f}_i^*$  est une particule scalaire supersymétrique virtuelle et  $f_i, f_j$  et  $f_k$  sont des fermions du Modèle Standard. Aux collisionneurs linéaires, la précision sur les paramètres d'impact devrait être nettement améliorée par rapport aux performances de LEP II : Alors que la précision sur la position de vertex secondaires est typiquement de  $5 \cdot 10^{-5}m$  au LEP, la précision espérée aux collisionneurs linéaires atteint  $5 \cdot 10^{-6}m$ . Par conséquent, si l'on prend la convention de demander quatre écarts standards ( $4\sigma$ ) et si l'on suppose que l'erreur sur la distance séparant les vertex primaire et secondaire est principalement contrôlée par l'incertitude sur la position du vertex secondaire, alors la distance minimum entre deux vertex nécessaire pour distinguer expérimentalement ces deux vertex, et donc la plus petite longueur de vol mesurable, est de l'ordre de  $2 \cdot 10^{-5}m$  aux collisionneurs linéaires. D'après Eq.(4.1), les valeurs de constantes de couplage  $\mathcal{R}_p$  pouvant être testées par la méthode d'analyse de vertex déplacé sont donc typiquement majorées par,

$$\Lambda < 1.2 \cdot 10^{-4} \gamma^{1/2} \left(\frac{\tilde{M}}{100GeV}\right)^2 \left(\frac{100GeV}{M_{LSP}}\right)^{5/2}. \quad (4.2)$$

Or les limites expérimentales indirectes sur les constantes de couplage  $\mathcal{R}_p$  obtenues à basse énergie sont de l'ordre de  $\Lambda < 10^{-1} - 10^{-2}$  pour des masses des particules supersymétriques de  $100GeV$  [85, 86, 87]. La méthode d'analyse de vertex déplacé de la LSP ne permet donc pas de tester tout l'intervalle des valeurs de constantes de couplage  $\mathcal{R}_p$  possibles.

La seconde méthode permettant de déterminer la valeur des constantes de couplage  $\mathcal{R}_p$  est l'étude de la production de particules du Modèle Standard (MS) ou de particules supersymétriques par des interactions  $\mathcal{R}_p$ . En effet, les sections efficaces de telles productions sont proportionnelles à des puissances des constantes de couplage  $\mathcal{R}_p$  et l'on peut donc déduire de leur valeur l'intensité des couplages  $\mathcal{R}_p$  en fonction d'autres paramètres supersymétriques. L'étude de la production de particules du MS ou de particules supersymétriques par des interactions  $\mathcal{R}_p$  permet de tester plus facilement de grandes valeurs



des constantes de couplage  $\mathcal{R}_p$ , celles-ci favorisant les sections efficaces des productions étudiées par rapport aux sections efficaces des bruits de fond associés. Les études de productions de particules du MS via des interactions  $\mathcal{R}_p$  dans les collisionneurs hadroniques [88]-[94] et leptoniques [95]-[109] ont montrées que les constantes de couplage  $\mathcal{R}_p$  pouvaient être testées jusqu'à des valeurs inférieures aux limites de basse énergie [85, 86, 87]. Les productions de particules du MS via des interactions  $\mathcal{R}_p$ , qui sont en fait des contributions  $\mathcal{R}_p$  à des réactions du MS, impliquent 2 vertex  $\mathcal{R}_p$  et ont donc des sections efficaces proportionnelles à  $\Lambda^4$  ( $\Lambda = \lambda, \lambda'$  ou  $\lambda''$ ). Les productions de particules impliquant un seul vertex  $\mathcal{R}_p$  ont des sections efficaces proportionnelles à  $\Lambda^2$  qui sont donc moins réduites étant donné les bornes existant sur les couplages  $\mathcal{R}_p$  [85, 86, 87]. Les productions de particules impliquant un seul vertex  $\mathcal{R}_p$  sont des productions d'une seule particule supersymétrique appelées productions simples de particule supersymétrique. L'étude des productions simples de particule supersymétrique permet, tout comme l'étude des contributions  $\mathcal{R}_p$  à des réactions du MS, de tester des valeurs des constantes de couplage  $\mathcal{R}_p$ . Les études de contributions  $\mathcal{R}_p$  à des réactions du MS permettent d'établir des limites sur certaines constantes de couplage  $\mathcal{R}_p$  qui ne sont pas testables via les productions simples, comme par exemple la constante de couplage  $\lambda_{133}$  [110]. De plus, les études de contributions  $\mathcal{R}_p$  à des réactions du MS permettent d'étudier des produits de différents couplages  $\mathcal{R}_p$  ce qui est impossible via les productions simples. En revanche, les productions simples ayant des sections efficaces proportionnelles à  $\Lambda^2$  uniquement, leur étude permet d'obtenir de fortes sensibilités sur certains couplages  $\mathcal{R}_p$  comparativement aux limites de basse énergie mais aussi par rapport aux sensibilités obtenues via les contributions  $\mathcal{R}_p$  à des réactions du MS, comme nous le montrerons dans les Sections 4.2 et 4.3. De plus, l'étude des productions simples permet de tester des valeurs des constantes de couplage  $\mathcal{R}_p$  pouvant atteindre  $\sim 10^{-4}$ , comme nous allons aussi le montrer dans les Sections 4.2 et 4.3, mettant ainsi en évidence une grande complémentarité entre les 2 méthodes de détermination des valeurs des constantes de couplage  $\mathcal{R}_p$  (analyse de vertex déplacé de la LSP et étude de la production de particules supersymétriques par des interactions  $\mathcal{R}_p$ ).

Du point de vue de la découverte de la supersymétrie, la production simple présente aussi certains intérêts. En effet, dans un contexte de violation de la R-parité, l'analyse de la production simple de particule supersymétrique permet, tout comme l'analyse de la production de paire de particules supersymétriques, d'étudier les paramètres SUSY et de reconstruire les masses des particules SUSY d'une manière indépendante du modèle théorique. Dans un scénario  $\mathcal{R}_p$  où les valeurs des constantes de couplage  $\mathcal{R}_p$  sont faibles, la production simple de particule SUSY a une section efficace inférieure à celle de la production de paire de particules SUSY qui n'implique pas de vertex  $\mathcal{R}_p$ . Dans un tel scénario, la production de paire de particules SUSY est la réaction favorisée pour l'étude des paramètres SUSY et de la reconstruction des masses des particules SUSY auprès des futurs collisionneurs leptoniques (collisionneurs linéaires) [111] et hadroniques, à savoir le Tevatron (Run II) [112, 113, 114, 115] et le LHC [116]. En revanche, dans un scénario  $\mathcal{R}_p$  où les valeurs des constantes de couplage  $\mathcal{R}_p$  sont proches de leur borne indirecte actuelle [85, 86, 87], l'analyse de la production simple de particule SUSY permet d'obtenir une meilleure sensibilité sur certains paramètres SUSY que celle obtenue par la production de paire de particules SUSY, comme nous allons le voir dans les Sections 4.2 et 4.3. La raison est que l'espace de phase de la production simple est moins réduit que celui de la production de paire. De plus, dans un tel scénario, la production simple de parti-

culé SUSY permet de reconstruire les masses des particules SUSY avec un bruit de fond combinatoire plus faible que celui de la production de paire de particules SUSY, comme nous le montrerons aussi dans les Sections 4.2 et 4.3. Ceci est dû au fait que la production simple de particule SUSY ne génère qu’une seule cascade de désintégration de particules SUSY alors que la production de paire en génère deux ce qui complique l’identification de l’origine des particules de l’état final.

Nous nous sommes donc intéressés à l’étude de la production simple de particule supersymétrique. Dans les deux sections suivantes, nous présentons les résultats de cette étude dans le cadre des collisionneurs hadroniques (Section 4.2) et leptoniques (Section 4.3), en se concentrant sur la sensibilité qui peut être obtenue par une telle étude sur les constantes de couplage  $\mathcal{R}_p$ .

## 4.2 Collisionneurs hadroniques

Nous présentons dans cette section des études de production simple de particule SUSY aux collisionneurs hadroniques. Précisons que dans ces études, pour des raisons de simplification, nous avons toujours supposé qu’une seule constante de couplage  $\mathcal{R}_p$  était dominante par rapport aux autres. Cette hypothèse peut être justifiée par l’analogie entre les structures des interactions de Yukawa et des interactions  $\mathcal{R}_p$  et la forte hiérarchie existant parmi les couplages de Yukawa.

La production simple de particule SUSY aux collisionneurs hadroniques implique des interactions  $\lambda'$  ou  $\lambda''$ . Dans le cas d’une constante de couplage  $\lambda''$  dominante, la particule SUSY créée dans la production simple donnerait lieu à une cascade de désintégration se terminant par la désintégration de la LSP en 3 jets via le couplage  $\lambda''$  dominant. La production simple conduirait donc typiquement à des états finals multijets, or les états finals multijets ont un grand bruit de fond QCD [88, 89]. Il est donc plus prometteur dans un premier temps de se concentrer sur les productions simples de particule SUSY aux collisionneurs hadroniques impliquant des interactions  $\lambda'$ .

Par ailleurs, il est plus intéressant de considérer les productions simples de particule SUSY du type  $2 \rightarrow 2 - \text{corps}$  afin d’optimiser l’espace de phase. Toutes les productions simples de particule SUSY aux collisionneurs hadroniques du type  $2 \rightarrow 2 - \text{corps}$  et impliquant des interactions  $\lambda'$  sont présentées dans la Figure 4.1 et dans la liste suivante,

- la production de gluino  $\bar{u}_j d_k \rightarrow \tilde{g} l_i$  via l’échange d’un squark  $\tilde{u}_{jL}$  ( $\tilde{d}_{kR}$ ) dans la voie  $t$  ( $u$ ),
- la production de squark  $\bar{d}_j g \rightarrow \tilde{d}_{kR}^* \nu_i$  via l’échange d’un squark  $\tilde{d}_{kR}$  (quark  $d_j$ ) dans la voie  $t$  ( $s$ ),
- la production de squark  $\bar{u}_j g \rightarrow \tilde{d}_{kR}^* l_i$  via l’échange d’un squark  $\tilde{d}_{kR}$  (quark  $u_j$ ) dans la voie  $t$  ( $s$ ),
- la production de squark  $d_k g \rightarrow \tilde{d}_{jL} \nu_i$  via l’échange d’un squark  $\tilde{d}_{jL}$  (quark  $d_k$ ) dans la voie  $t$  ( $s$ ),
- la production de squark  $d_k g \rightarrow \tilde{u}_{jL} l_i$  via l’échange d’un squark  $\tilde{u}_{jL}$  (quark  $d_k$ ) dans la voie  $t$  ( $s$ ),
- la production de sneutrino  $\bar{d}_j d_k \rightarrow Z \tilde{\nu}_{iL}$  via l’échange d’un quark  $d_k$  ou  $d_j$  (sneutrino  $\tilde{\nu}_{iL}$ ) dans la voie  $t$  ( $s$ ),

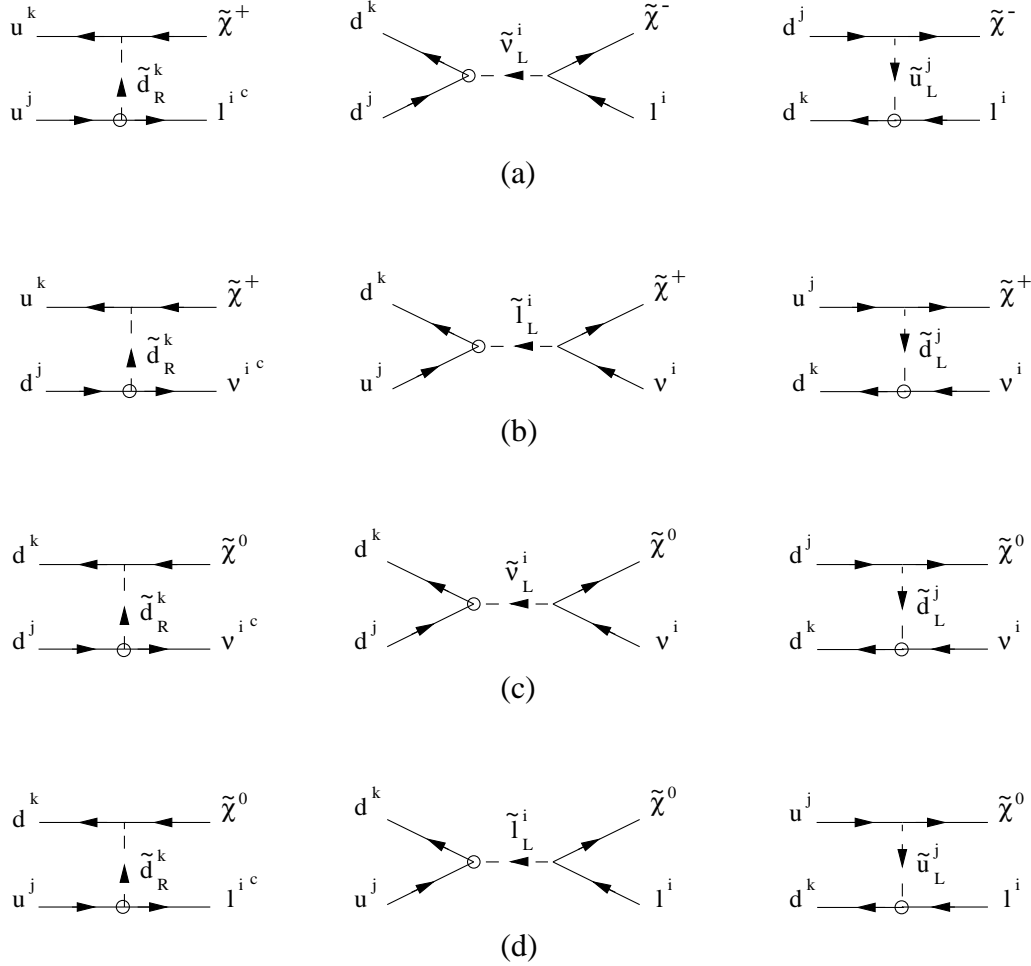


FIG. 4.1: Diagrammes de Feynman des 4 processus de production simple de particule SUSY via  $\lambda'_{ijk}$  aux collisionneurs hadroniques qui sont du type  $2 \rightarrow 2$  - corps et qui reçoivent une contribution de la production résonante d'un partenaire supersymétrique. Les couplages  $\lambda'_{ijk}$  sont symbolisés par des cercles et les flèches représentent les moments des particules.

- la production de slepton chargé  $\bar{u}_j d_k \rightarrow Z \tilde{l}_{iL}$  via l'échange d'un quark  $d_k$  ou  $u_j$  (slepton  $\tilde{l}_{iL}$ ) dans la voie  $t$  ( $s$ ),
- la production de sneutrino  $\bar{u}_j d_k \rightarrow W^- \tilde{\nu}_{iL}$  via l'échange d'un quark  $d_j$  (slepton  $\tilde{l}_{iL}$ ) dans la voie  $t$  ( $s$ ),
- la production de slepton chargé  $\bar{d}_j d_k \rightarrow W^+ \tilde{l}_{iL}$  via l'échange d'un quark  $u_j$  (sneutrino  $\tilde{\nu}_{iL}$ ) dans la voie  $t$  ( $s$ ).

Les productions simples représentées dans la Figure reçoivent une contribution de la production résonante d'une particule supersymétrique, à l'inverse des productions simples listées ci-dessus. Effectivement, les seules productions simples parmi la liste ci-dessus pouvant éventuellement recevoir une contribution de production résonante de particule SUSY sont les réactions  $\bar{u}_j d_k \rightarrow \tilde{l}_{iL} \rightarrow W^- \tilde{\nu}_{iL}$  et  $\bar{d}_j d_k \rightarrow \tilde{\nu}_{iL} \rightarrow W^+ \tilde{l}_{iL}$ . Or, dans la plupart des modèles SUSY, comme par exemple les modèles de supergravité ou les modèles GMSB, la différence de masse entre le slepton chargé Left et le sneutrino Left est due aux termes D de telle sorte qu'elle est fixée par la relation  $m_{\tilde{l}_L^\pm}^2 - m_{\tilde{\nu}_L}^2 = \cos 2\beta M_W^2$  [25] et n'excède

donc pas la masse du boson  $W^\pm$ . Notons cependant que dans les scénarios à grand  $\tan\beta$ , les masses Left-Right  $(m_{LR})_{ij}$  peuvent atteindre des valeurs non négligeables pour les particules appartenant à la troisième famille (voir Eq.(1.109)), générant ainsi un mélange entre les particules scalaires Left et Right de la troisième famille. Les particules scalaires de troisième génération peuvent donc avoir un état propre de masse inférieure aux masses des particules scalaires Left et Right de première et seconde génération et l'autre état propre de masse supérieure aux masses des particules scalaires Left et Right de première et seconde génération. Dans un scénario à grand  $\tan\beta$ , on peut par exemple avoir la hiérarchie suivante parmi les sleptons chargés :  $m_{\tilde{\tau}_2^\pm} > m_{\tilde{e}_L^\pm}, m_{\tilde{e}_R^\pm}, m_{\tilde{\mu}_L^\pm}, m_{\tilde{\mu}_R^\pm} > m_{\tilde{\tau}_1^\pm}, \tilde{\tau}_1^\pm$  et  $\tilde{\tau}_2^\pm$  étant les états propres de masse de stau. En particulier, dans un scénario à grand  $\tan\beta$ , la différence de masse entre le sneutrino  $\tilde{\nu}_\tau$  et l'état propre de masse  $\tilde{\tau}_1^\pm$  peut être supérieure à la masse du  $W^\pm$ , de telle sorte que la production simple de stau  $\bar{d}_j d_k \rightarrow \tilde{\nu}_\tau \rightarrow W^\pm \tilde{\tau}_1^\mp$  reçoive la contribution de la production résonante de sneutrino.

Discutons maintenant les sections efficaces des productions simples de particule SUSY aux collisionneurs hadroniques du type  $2 \rightarrow 2 - \text{corps}$  et impliquant des interactions  $\lambda'$ . Les sections efficaces des productions simples “non résonantes” listées ci-dessus ne peuvent atteindre de grandes valeurs : La section efficace de la production simple de gluino est limitée par les bornes expérimentales sur les masses de squarks et de gluinos qui sont de l'ordre de  $m_{\tilde{q}}, m_{\tilde{g}} \gtrsim 200 \text{ GeV}$  [46]. En effet, la production simple de gluino a lieu par l'échange de squark dans les voies  $t$  et  $u$ , comme nous l'avons vu plus haut, et donc sa section efficace décroît si les masses de squarks et de gluinos augmentent. Pour la valeur  $m_{\tilde{q}} = m_{\tilde{g}} = 250 \text{ GeV}$  qui est proche de la limite expérimentale, nous trouvons la section efficace de production simple de gluino suivante,  $\sigma(p\bar{p} \rightarrow \tilde{g}\mu) \approx 10^{-2} \text{ pb}$ . Les sections efficaces données dans ce paragraphe ont été calculées grâce à la version 33.18 du programme COMPHEP [117] pour une énergie dans le centre de masse de  $\sqrt{s} = 2 \text{ TeV}$  (Run II du Tevatron) avec la fonction de structure CTEQ4m [118] et pour une valeur de la constante de couplage  $\mathcal{R}_p$  de  $\lambda'_{211} = 0.09$ . De même, le taux de production simple de squark ne peut être grand. Pour  $m_{\tilde{q}} = 250 \text{ GeV}$ , la section efficace  $\sigma(p\bar{p} \rightarrow \tilde{u}_L \mu)$  est de l'ordre de  $\sim 10^{-3} \text{ pb}$ . De plus, la production d'un slepton accompagné d'un boson de jauge massif a un petit espace de phase et n'implique pas d'interactions fortes. Le taux de ce type de production est donc faible. Pour  $m_{\tilde{l}} = 100 \text{ GeV}$ , nous obtenons  $\sigma(p\bar{p} \rightarrow Z \tilde{\mu}_L) \approx 10^{-2} \text{ pb}$ . Par ailleurs, nous avons calculé toutes les amplitudes des productions simples “résonantes” présentées dans la Figure 4.1. Dans [158] (voir Publication III : “*Single superpartner production at Tevatron Run II*”), nous donnons les résultats analytiques du calcul de ces amplitudes et nous présentons une analyse numérique de l'évolution des valeurs des sections efficaces correspondantes dans l'espace des paramètres supersymétriques. D'après cette étude, les sections efficaces des productions simples résonantes atteignent des valeurs de l'ordre de la dizaine de picobarns.

Bien que les productions simples non résonantes soient intéressantes du fait que certaines d'entre elles dépendent de peu de paramètres SUSY, à savoir une constante de couplage  $\mathcal{R}_p$  et une masse de particule scalaire supersymétrique, l'étude des productions simples résonantes est plus attrayante car les sections efficaces de ces dernières sont plus importantes.

### 4.2.1 Signature trilepton

La production d'un chargino et d'un lepton chargé aux collisionneurs hadroniques (voir Figure 4.1(a)) donne lieu à un état final contenant 3 leptons chargés si la cascade de désintégration initiée par le chargino produit est  $\tilde{\chi}^\pm \rightarrow \tilde{\chi}_1^0 l^\pm \nu$ ,  $\tilde{\chi}_1^0 \rightarrow l_i^\pm u_j d_k$ , les indices  $i, j, k$  correspondant aux indices de la constante  $\lambda'_{ijk}$ . L'état final à 3 leptons chargés est particulièrement intéressant comme candidat de signal de la supersymétrie car le bruit de fond provenant du Modèle Standard est faible. Dans [157] (voir Publication II : “*Resonant sneutrino production at Tevatron Run II*”), [158], [159] et [160] (voir Publication IV : “*The three-leptons signature from resonant sneutrino production at the LHC*”), nous avons étudié le signal à 3 leptons chargés engendré par la production simple de chargino (voir Figure 4.1(a)) et le bruit de fond associé. Le processus de production simple de chargino a été implémenté dans une version du générateur d'événements SUSYGEN [119] incluant la simulation des collisions hadroniques. Ceci a permis de générer le signal avec SUSYGEN et les bruits de fond provenant du Modèle Standard et des réactions supersymétriques avec les générateurs d'événements PYTHIA [120] (ainsi que ONETOP [121] pour certains processus) et SHERWIG [122], respectivement. SUSYGEN, PYTHIA et SHERWIG ont été interfacés avec le simulateur de détecteur SHW [123] pour l'étude dans le cadre de la physique au Run II du Tevatron et avec le simulateur de détecteur ATLFast [124] pour l'étude dans le cadre de la physique au LHC. Lors de la génération du signal et du bruit de fond, des coupures basées sur des distributions de variables cinématiques (angles d'émission des particules, quadri-impulsions,...) ont été appliquées afin d'augmenter le signal par rapport au bruit de fond.

### Potentiel de découverte

Nous présentons dans la Figure 4.2 la sensibilité dans le plan  $\lambda'_{211}$  versus le paramètre  $m_0$  qui pourrait être obtenue à partir de l'analyse de l'état final à 3 leptons chargés (trilepton) au Run II du Tevatron, dans le cadre d'un modèle de supergravité (SUGRA) et pour des valeurs fixées des autres paramètres supersymétriques du modèle. Cette figure a été obtenue après avoir appliqué les coupures mentionnées plus haut et en supposant que la production simple de chargino avait lieu par l'intermédiaire d'un couplage du type  $\lambda'_{211}$ , ce qui correspond au cas où le lepton produit avec le chargino est un muon (voir Figure 4.1(a)). Les régions de la Figure 4.2 se situant au-dessus des courbes seraient exclues par l'analyse expérimentale de la signature trilepton. En particulier, le contour de découverte à  $5\sigma$  définit la région de l'espace des paramètres pour lesquels  $S/\sqrt{B} > 5$  où  $S = \sigma_S \times \mathcal{L} \times \mathcal{E}_S$  et  $B = \sigma_B \times \mathcal{L} \times \mathcal{E}_B$ ,  $\sigma_S$  ( $\sigma_B$ ) étant la section efficace du signal (bruit de fond),  $\mathcal{L}$  la luminosité et  $\mathcal{E}_S$  ( $\mathcal{E}_B$ ) l'efficacité du signal (bruit de fond) après les coupures. L'évolution de la sensibilité avec les paramètres du modèle SUGRA observée dans la Figure 4.2 s'explique par les variations de la section efficace du signal (voir [158]).

D'après la Figure 4.2, la sensibilité obtenue sur  $\lambda'_{211}$  dans certaines régions de l'espace des paramètres SUGRA par l'étude de la signature trilepton au Run II du Tevatron permettrait d'améliorer la limite actuelle sur cette constante de couplage  $\mathcal{R}_p$  qui vaut :  $\lambda'_{211} < 0.09(m_{\tilde{d}_R}/100\text{GeV})$  à  $1\sigma$  ( $\pi$  decay) [86]. L'étude de la signature trilepton permet aussi d'améliorer les limites indirectes de nombreuses autres constantes de couplage  $\mathcal{R}_p$  si l'on suppose que la production simple de chargino a lieu de façon dominante par l'intermédiaire d'une autre constante de couplage  $\mathcal{R}_p$ . Dans la Table 4.1, nous donnons

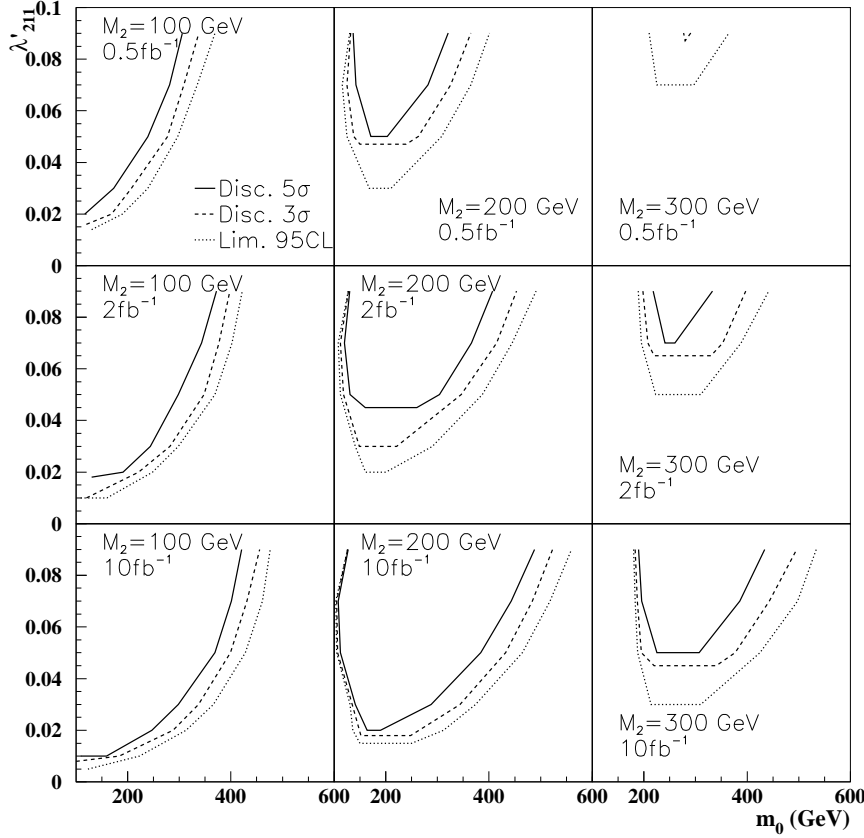


FIG. 4.2: Contours de découverte à  $5\sigma$  (ligne),  $3\sigma$  (tirés) et limites à 95%  $C.L.$  (pointillés) associés à l'étude du canal trilepton au Run II du Tevatron ( $\sqrt{s} = 2TeV$ ) et présentés dans le plan  $\lambda'_{211}$  versus le paramètre  $m_0$  pour  $sign(\mu) < 0$ ,  $\tan\beta = 1.5$  et différentes valeurs du paramètre  $M_2$  et de la luminosité.

les prévisions des sensibilités sur toutes les constantes de couplage  $\mathcal{R}_p$  de type  $\lambda'_{ijk}$  obtenues au Run II du Tevatron par l'étude de la signature trilepton pour un point de l'espace des paramètres SUGRA. Les sensibilités sur les constantes de couplage  $\lambda'_{2jk}$  et  $\lambda'_{3jk}$  présentées dans la Table 4.1 représentent toutes une amélioration par rapport aux limites de basse énergie sur ces mêmes constantes de couplage, que nous rappelons ici [86] :  $\lambda'_{21k} < 0.09(m_{\tilde{d}_{kR}}/100GeV)$  à  $1\sigma$  (désintégration du  $\pi$ ),  $\lambda'_{22k} < 0.18(m_{\tilde{d}_{kR}}/100GeV)$  à  $1\sigma$  (désintégration du  $D$ ),  $\lambda'_{231} < 0.22(m_{\tilde{b}_L}/100GeV)$  à  $2\sigma$  (diffusion profondément inélastique du  $\nu_\mu$ ),  $\lambda'_{232} < 0.36(m_{\tilde{q}}/100GeV)$  à  $1\sigma$  ( $R_\mu$ ),  $\lambda'_{233} < 0.36(m_{\tilde{q}}/100GeV)$  à  $1\sigma$  ( $R_\mu$ ),  $\lambda'_{31k} < 0.10(m_{\tilde{d}_{kR}}/100GeV)$  à  $1\sigma$  ( $\tau^- \rightarrow \pi^- \nu_\tau$ ),  $\lambda'_{32k} < 0.20$  (pour  $m_{\tilde{l}} = m_{\tilde{q}} = 100GeV$ ) à  $1\sigma$  (mixing  $D^0 - \bar{D}^0$ ),  $\lambda'_{33k} < 0.48(m_{\tilde{q}}/100GeV)$  à  $1\sigma$  ( $R_\tau$ ). Les bornes indirectes sur les constantes de type  $\lambda'_{1jk}$  sont typiquement plus fortes que les bornes sur les constantes  $\lambda'_{2jk}$  et  $\lambda'_{3jk}$  [86]. De ce fait, l'étude de la signature trilepton permet de

$\lambda'_{111}$	$\lambda'_{112}$	$\lambda'_{113}$	$\lambda'_{121}$	$\lambda'_{122}$	$\lambda'_{123}$	$\lambda'_{131}$	$\lambda'_{132}$	$\lambda'_{133}$
0.02	0.04	0.07	0.05	0.12	0.21	0.10	0.36	0.63
$\lambda'_{211}$	$\lambda'_{212}$	$\lambda'_{213}$	$\lambda'_{221}$	$\lambda'_{222}$	$\lambda'_{223}$	$\lambda'_{231}$	$\lambda'_{232}$	$\lambda'_{233}$
0.02	0.04	0.07	0.05	0.12	0.21	0.10	0.36	0.63
$\lambda'_{311}$	$\lambda'_{312}$	$\lambda'_{313}$	$\lambda'_{321}$	$\lambda'_{322}$	$\lambda'_{323}$	$\lambda'_{331}$	$\lambda'_{332}$	$\lambda'_{333}$
0.06	0.13	0.23	0.18	0.41	0.70	0.33	1.17	2.05

TAB. 4.1: *Sensibilités à 95%CL sur toutes les constantes de couplage de type  $\lambda'_{ijk}$  dans le cadre de la physique au Run II du Tevatron pour une luminosité de  $\mathcal{L} = 2fb^{-1}$  et pour les paramètres SUGRA suivants,  $m_0 = 180GeV$ ,  $M_2 = 200GeV$ ,  $\tan\beta = 1.5$  et  $\mu = -200GeV$  ( $m_{\tilde{u}_L} = 601GeV$ ,  $m_{\tilde{d}_L} = 603GeV$ ,  $m_{\tilde{u}_R} = 582GeV$ ,  $m_{\tilde{d}_R} = 580GeV$ ,  $m_{\tilde{l}_L} = 253GeV$ ,  $m_{\tilde{l}_R} = 205GeV$ ,  $m_{\tilde{\nu}_L} = 248GeV$ ,  $m_{\tilde{\chi}_1^\pm} = 199GeV$ ,  $m_{\tilde{\chi}_1^0} = 105GeV$ ).*

tester un moins grand nombre de constantes  $\lambda'_{1jk}$  que de constantes  $\lambda'_{2jk}$  ou  $\lambda'_{3jk}$ . Par exemple, pour le point SUGRA considéré dans la Table 4.1, seules les sensibilités sur les constantes de couplage  $\lambda'_{112}$ ,  $\lambda'_{113}$ ,  $\lambda'_{121}$ ,  $\lambda'_{131}$  et  $\lambda'_{132}$  représentent une amélioration vis à vis de leur borne indirecte :  $\lambda'_{11k} < 0.02(m_{\tilde{d}_{kR}}/100GeV)$  à  $2\sigma$  (universalité du courant chargé),  $\lambda'_{1j1} < 0.035(m_{\tilde{q}_{jL}}/100GeV)$  à  $2\sigma$  (violation de la parité atomique),  $\lambda'_{132} < 0.34$  à  $1\sigma$  pour  $m_{\tilde{q}} = 100GeV$  ( $R_e$ ).

Nous présentons dans la Figure 4.3 (4.4) la sensibilité dans le plan  $m_0$  versus  $m_{1/2}$  qui pourrait être obtenue à partir de l'analyse de l'état final trilepton au Run II du Tevatron (LHC) dans le cadre d'un modèle SUGRA et pour des valeurs fixées des autres paramètres supersymétriques du modèle.

En comparant les Figures 4.3 et 4.4, nous observons que le LHC permettra d'obtenir une meilleure sensibilité que le Tevatron sur la constante de couplage  $\lambda'_{211}$ . Cette amélioration est due aux grandes énergies et luminosités qui devraient être atteintes par le LHC.

Nous avons montré dans [158] ([160]) que l'étude du canal trilepton de la production de paires de particules supersymétriques dans le cadre de la physique au Run II du Tevatron (au LHC) permettait de tester dans le modèle SUGRA considéré dans la Figure 4.3 (4.4) des valeurs du paramètre  $m_{1/2}$  allant jusqu'à  $\sim 200GeV$ , et ceci quelque soit la valeur de la constante de couplage  $\mathcal{R}_p$  considérée (pourvu que cette constante soit suffisamment grande pour que la LSP se désintègre dans le détecteur). Par conséquent, dans la région  $m_{1/2} \gtrsim 200GeV$  des Figures 4.3 et 4.4, la sensibilité obtenue sur les constantes de couplage  $\mathcal{R}_p$  par la production simple de chargino n'est pas affectée par la production de paires de superpartenaires. En revanche, dans la région  $m_{1/2} \lesssim 200GeV$ , la production de paires de superpartenaires représente un bruit de fond pour la production simple de chargino car elle n'implique pas les interactions  $\mathcal{R}_p$  qui sont l'objet de cette étude. Le bruit de fond engendré par la production de paires peut être réduit par des coupures cinématiques basées sur la reconstruction de masse des particules supersymétriques (voir Section 4.2.1).

Plaçons nous maintenant du point de vue du test des paramètres de brisure douce de la supersymétrie (masses des superpartenaires), et non plus du point de vue du test des constantes de couplage  $\mathcal{R}_p$ . Les limites actuelles sur les masses des particules supersymétriques déduites des données expérimentales du collisionneur LEP II, dans le contexte d'un modèle  $\mathcal{R}_p$  contenant des couplages de type  $\lambda'$  non nuls, sont :  $m_{\tilde{\chi}_1^0} > 26GeV$  (pour

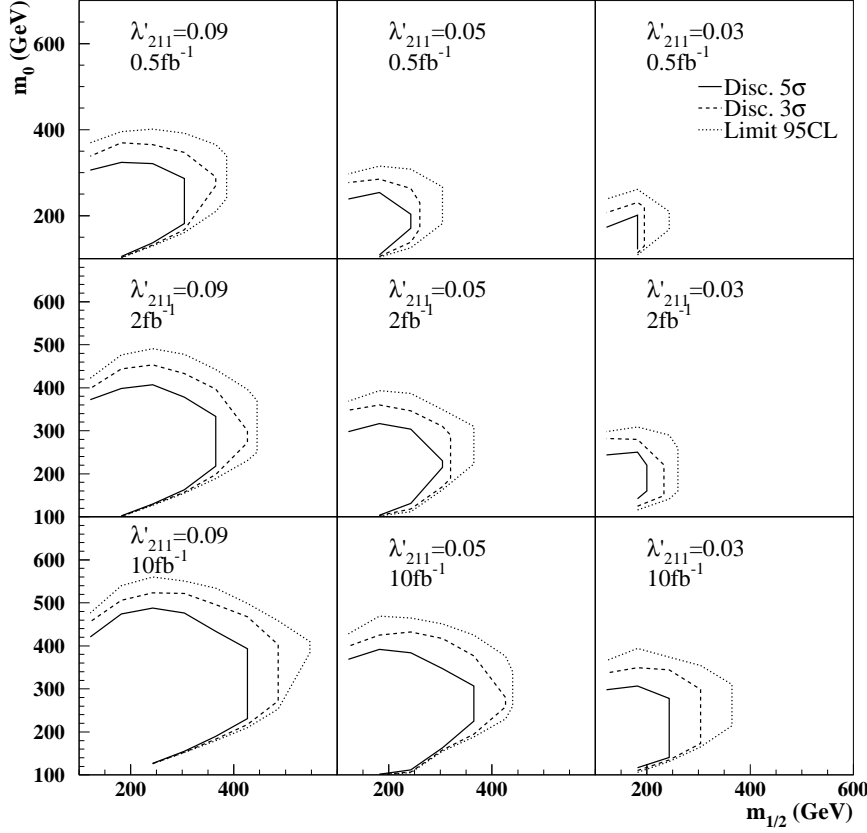


FIG. 4.3: Contours de découverte à  $5\sigma$  (ligne),  $3\sigma$  (tirés) et limites à 95%  $C.L.$  (pointillés) associés à l'étude du canal trilepton au Run II du Tevatron ( $\sqrt{s} = 2TeV$ ) et présentés dans le plan  $m_0$  versus  $m_{1/2}$  pour  $sign(\mu) < 0$ ,  $\tan\beta = 1.5$  et différentes valeurs de  $\lambda'_{211}$  et de la luminosité.

$m_0 = 200GeV$  et  $\tan\beta = \sqrt{2}$  [125]),  $m_{\tilde{\chi}_1^\pm} > 100GeV$ ,  $m_{\tilde{l}} > 93GeV$ ,  $m_{\tilde{\nu}} > 86GeV$  [126]. Or les valeurs minimums des paramètres  $m_0$  et  $m_{1/2}$  de l'espace des paramètres des Figures 4.2 et 4.3 correspondent aux valeurs  $m_0 = 100GeV$  et  $M_2 = 100GeV$  pour lesquelles le spectre de masse supersymétrique est le suivant :  $m_{\tilde{\chi}_1^\pm} = 113GeV$ ,  $m_{\tilde{\chi}_1^0} = 54GeV$ ,  $m_{\tilde{\nu}_L} = 127GeV$ ,  $m_{\tilde{l}_L} = 137GeV$ ,  $m_{\tilde{l}_R} = 114GeV$ . Puisque ces masses ne sont pas exclues par les données de LEP II [125, 126] et que les masses des particules supersymétriques augmentent avec  $m_0$  et  $m_{1/2}$ , l'espace des paramètres des Figures 4.2 et 4.3 n'est pas exclu par les données de LEP II [125, 126]. Par conséquent, le potentiel de découverte pour le Run II du Tevatron (Figure 4.3) représente une amélioration importante par rapport aux limites actuelles sur les paramètres  $m_0$  et  $m_{1/2}$  du modèle SUGRA considéré.

De plus, la Figure 4.3 montre que la sensibilité obtenue au Run II du Tevatron, dans le plan des paramètres  $m_0$  et  $m_{1/2}$  du modèle SUGRA considéré, par l'étude du canal



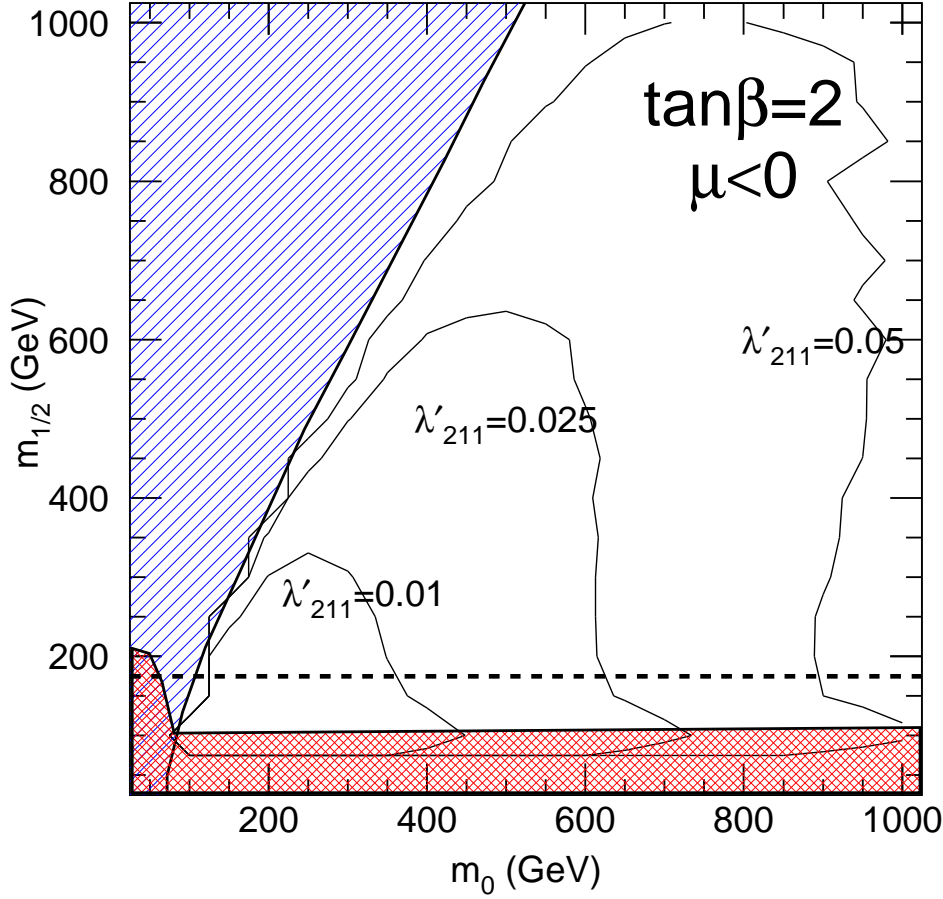


FIG. 4.4: Limites à 95% *C.L.* associées à l'étude du canal trilepton au LHC ( $\sqrt{s} = 14\text{TeV}$ ,  $\mathcal{L} = 30\text{fb}^{-1}$ ) et présentées dans le plan  $m_{1/2}$  versus  $m_0$  pour  $\text{sign}(\mu) < 0$ ,  $\tan\beta = 2$  et différentes valeurs de  $\lambda'_{211}$ . La région hachurée en haut à gauche de la figure correspond au cas où  $m_{\tilde{\chi}_1^\pm} > m_{\tilde{\nu}}$ . La région hachurée en bas de la figure donne la limite cinématique de la production de paires de  $\tilde{\chi}_1^\pm$  et de  $\tilde{l}$  à LEP II pour une énergie de  $\sqrt{s} = 200\text{GeV}$ . Dans la région se situant en-dessous des pointillés, le  $\tilde{\chi}_1^\pm$  ne peut pas se désintégrer en un boson  $W^\pm$  réel.

trilepton de la production simple de chargino permettrait d'étendre la sensibilité obtenue par l'étude du canal trilepton de la production de paires de superpartenaires. En effet, comme nous l'avons déjà mentionné, l'étude du canal trilepton de la production de paires de superpartenaires au Run II du Tevatron permettrait de tester dans le modèle SUGRA considéré dans la Figure 4.3 des valeurs du paramètre  $m_{1/2}$  allant jusqu'à  $\sim 200\text{GeV}$  [158]. De plus, la sensibilité obtenue via la production de paires est indépendante du couplage  $\mathcal{R}_p$  considéré [158]. En revanche, d'après la Figure 4.3, la sensibilité dans le plan  $m_0$  versus  $m_{1/2}$  obtenue via la production simple de chargino est d'autant plus forte que la constante de couplage  $\mathcal{R}_p$ , et donc la section efficace de cette production, est grande. Or, de plus

grandes valeurs de la constante de couplage  $\mathcal{R}_p$  auraient pu être considérées dans la Figure 4.3, car la limite indirecte sur cette constante est  $\lambda'_{211} < 0.09(m_{\tilde{d}_R}/100\text{GeV})$  [86] et, dans le modèle SUGRA considéré dans la Figure 4.3, la masse du  $\tilde{d}_R$  vaut  $m_{\tilde{d}_R} = 304\text{GeV}$  pour  $m_0 = 100.0\text{GeV}$  et  $m_{1/2} = 121.6\text{GeV}$ . Par conséquent, des sensibilités encore plus fortes que celles présentées dans la Figure 4.3 peuvent être obtenues dans le plan  $m_0$  versus  $m_{1/2}$  via la production simple de chargino.

En ce qui concerne la physique au LHC, nous voyons sur la Figure 4.4 que les sensibilités prédites, dans le plan des paramètres  $m_{1/2}$  et  $m_0$  du modèle SUGRA considéré, s'étendent aussi bien au-delà du domaine exclu par les limites actuelles de LEP II. De plus, la Figure 4.4 montre que la sensibilité obtenue au LHC, dans le plan des paramètres  $m_{1/2}$  et  $m_0$  du modèle SUGRA considéré, par l'étude du canal trilepton de la production simple de chargino permettrait d'étendre la sensibilité obtenue par l'étude du canal trilepton de la production de paires de superpartenaires. En effet, comme nous l'avons déjà mentionné, l'étude du canal trilepton de la production de paires de superpartenaires au LHC permettrait de tester dans le modèle SUGRA considéré dans la Figure 4.4 des valeurs du paramètre  $m_{1/2}$  allant jusqu'à  $\sim 200\text{GeV}$  [160]. Enfin, de même que dans le contexte de la physique au Tevatron, pour de plus grandes valeurs de la constante de couplage  $\mathcal{R}_p$  que celles considérées dans la Figure 4.4, des sensibilités encore plus fortes que celles présentées dans la Figure 4.4 peuvent être obtenues dans le plan  $m_{1/2}$  versus  $m_0$  via la production simple de chargino.

Les constantes de couplage de type  $\lambda'_{ijk}$  peuvent aussi être testées par l'étude de la contribution des interactions  $\mathcal{R}_p$  à la production d'un état final dijet dans un collisionneur hadronique :  $p\bar{p}(\text{ou } pp) \rightarrow q\bar{q}'$  [94]. Cette contribution implique l'échange d'un slepton dans les voies  $s$ ,  $t$  et  $u$ . Il a été montré dans [94] que les valeurs des sensibilités obtenues sur les constantes de couplage  $\lambda'_{ijk}$  par l'étude de cette contribution dans le cadre de la physique au Run II du Tevatron sont supérieures à  $\sim 10^{-1}$  pour une luminosité de  $\mathcal{L} = 2\text{fb}^{-1}$ . Ces sensibilités sont donc inférieures à la plupart des sensibilités obtenues sur les mêmes constantes de couplage  $\lambda'_{ijk}$  par l'étude de la production simple de chargino au Run II du Tevatron (voir Table 4.1 et Figure 4.2). En revanche, si le seul superpartenaire pouvant être produit à la résonance via un couplage  $\lambda'_{ijk}$  dans les collisions hadroniques est la LSP, celui-ci ne peut se désintégrer une fois produit à la résonance que via le même couplage  $\lambda'_{ijk}$  en deux jets. Dans ce cas, la contribution des interactions  $\mathcal{R}_p$  à la production de l'état final dijet aux collisionneurs hadroniques peut avoir lieu via la production résonante d'un superpartenaire, à l'inverse des productions simples de la Figure 4.1, et elle est donc plus sensible aux constantes de couplage  $\lambda'_{ijk}$  que les productions simples de la Figure 4.1. D'autre part, les constantes de couplage de type  $\lambda'_{ijk}$  pourraient être testées par l'étude de la contribution des interactions  $\mathcal{R}_p$  au processus de Drell-Yan  $p\bar{p}(\text{ou } pp) \rightarrow l\nu, l\bar{l}$  [94]. Cependant, Cette contribution, qui implique l'échange d'un squark dans les voies  $t$  et  $u$ , est en fait peu significative pour des valeurs des constantes de couplage  $\lambda'_{ijk}$  respectant leur limite actuelle [94].

Finalement, les constantes de couplage de type  $\lambda'_{ijk}$  peuvent être testées par l'étude de la contribution des interactions  $\mathcal{R}_p$  au processus  $l^+l^- \rightarrow q\bar{q}$  [110, 109]. Cette contribution implique l'échange d'un squark dans la voie  $t$ . Les sensibilités obtenues par l'étude de cette contribution sur les constantes de couplage  $\lambda'_{ijk}$  dans le cadre de la physique aux collisionneurs leptoniques sont de l'ordre de  $10^{-1}$  pour des masses de squarks inférieures au  $\text{TeV}$  [110, 109]. Ces sensibilités sont donc inférieures à la plupart des sensibilités obtenues

sur les mêmes constantes de couplage  $\lambda'_{ijk}$  par l'étude de la production simple de chargino au Run II du Tevatron (voir Table 4.1 et Figure 4.2).

Remarquons par ailleurs que la production simple de chargino et de neutralino peut avoir lieu au collisionneur HERA par l'intermédiaire des constantes de couplage de type  $\lambda'_{ijk} : ep \rightarrow q\tilde{\chi}^{\pm,0}$  [128]. L'étude de cette réaction permet d'obtenir une sensibilité sur les constantes de couplage  $\lambda'_{1j1}$  de l'ordre de  $10^{-2}$  pour une masse de squark de  $m_{\tilde{q}} \approx 200 GeV$ , une énergie dans le centre de masse de  $\sqrt{s} \approx 300 GeV$  et une luminosité de  $\mathcal{L} = 500 pb^{-1}$  [128]. Ces sensibilités sont comparables, voir inférieures, à celles obtenues sur les mêmes constantes de couplage  $\lambda'_{1j1}$  par l'étude de la production simple de chargino au Run II du Tevatron (voir Table 4.1 et Figure 4.2).

## Reconstruction de masse

La contribution dominante à la production simple de chargino est la production résonante de sneutrino (voir Figure 4.1(a)). Or la cascade de désintégration initiée par la désintégration du sneutrino et produisant la signature triplepton,  $\tilde{\nu}_i \rightarrow \tilde{\chi}_1^{\pm} l_i^{\mp}$ ,  $\tilde{\chi}_1^{\pm} \rightarrow \tilde{\chi}_1^0 l^{\pm} \nu$ ,  $\tilde{\chi}_1^0 \rightarrow l_i^{\pm} u_j d_k$ , peut être intégralement reconstruite. Par conséquent, l'étude du canal triplepton généré par la production simple de chargino permet de reconstruire les masses des  $\tilde{\chi}_1^0$ ,  $\tilde{\chi}_1^{\pm}$  et  $\tilde{\nu}$ , et ce de manière indépendante du cadre théorique. Nous avons étudié ces reconstructions de masse dans le cadre de la physique au Run II du Tevatron [157, 158] et au LHC [159, 160].

Tout d'abord, la masse du  $\tilde{\chi}_1^0$  peut être reconstruite en calculant la masse invariante des deux jets et du lepton chargé produits dans la désintégration  $\tilde{\chi}_1^0 \rightarrow l_i^{\pm} u_j d_k$ . Les deux jets sont identifiés comme étant les deux jets les plus énergétiques de l'état final. La raison est que ces deux jets sont les seuls jets produits dans le processus supersymétrique considéré et que les jets provenant des radiations QCD des états initial et final ont typiquement des énergies inférieures à celles des jets issus de réactions supersymétriques. Quant à l'identification du lepton chargé, elle est basée sur la saveur ainsi que la charge électrique de celui-ci. En fait, la masse du  $\tilde{\chi}_1^0$  est déterminée à partir du pic apparaissant dans la distribution de la masse invariante des deux jets et du lepton chargé. Ce pic n'est pas un pic de Dirac à cause du bruit de fond combinatoire qui est du dans ce cas au fait que les deux jets de l'état final peuvent être confondus avec les jets irradiés par l'état initial. La masse du  $\tilde{\chi}_1^0$  peut être reconstruite au LHC avec une erreur statistique de  $\sim 100 MeV$  [160].

La masse du  $\tilde{\chi}_1^{\pm}$ , qui se désintègre via  $\tilde{\chi}_1^{\pm} \rightarrow \tilde{\chi}_1^0 l^{\pm} \nu$ , peut alors être déterminée à partir de la reconstruction du  $\tilde{\chi}_1^0$ . Cette détermination est cependant plus précise lorsque la désintégration  $\tilde{\chi}_1^{\pm} \rightarrow \tilde{\chi}_1^0 l^{\pm} \nu$  a lieu via un boson  $W^{\pm}$  réel (voir Figure 4.4) selon la cascade  $\tilde{\chi}_1^{\pm} \rightarrow \tilde{\chi}_1^0 W^{\pm}$ ,  $W^{\pm} \rightarrow l^{\pm} \nu$ . En effet, dans ce cas la quadri-impulsion du neutrino peut être calculée exactement en exprimant la condition d'égalité entre la masse du boson  $W^{\pm}$  et la masse invariante des deux leptons provenant de la désintégration  $W^{\pm} \rightarrow l^{\pm} \nu$ . Le lepton chargé produit dans la désintégration  $W^{\pm} \rightarrow l^{\pm} \nu$  est une fois de plus identifié grâce à sa saveur et son signe. Nous avons trouvé une valeur de  $\sim 6 GeV$  pour la largeur du pic associé à la masse reconstruite du  $\tilde{\chi}_1^{\pm}$ , dans le cadre de la physique au LHC [160].

Enfin, la masse du  $\tilde{\nu}$ , qui se désintègre via  $\tilde{\nu}_i \rightarrow \tilde{\chi}_1^{\pm} l_i^{\mp}$ , peut être déterminée à partir de la reconstruction du  $\tilde{\chi}_1^{\pm}$ . Le lepton chargé issu de la désintégration du sneutrino est identifié grâce à sa saveur et son signe. Nous avons trouvé une valeur de  $\sim 10 GeV$  pour la largeur du pic associé à la masse reconstruite du  $\tilde{\nu}$ , dans le cadre de la physique au

LHC [160].

En conclusion, aux collisionneurs hadroniques, si le  $\tilde{\chi}_1^0$  était la LSP (comme c'est le cas dans la plupart des modèles supersymétriques), sa masse devrait être facilement reconstruite [116, 127] car il serait alors produit en grand nombre dans les productions de paires de gluinos et de squarks qui ont d'importantes sections efficaces [160]. Par conséquent, pour de faibles valeurs des couplages  $\mathcal{R}_p$ , et donc de la section efficace de la production simple de chargino, la reconstruction du  $\tilde{\chi}_1^0$  la plus précise est à priori obtenue par l'étude des productions de paires de gluinos et de squarks. Pour des valeurs des couplages  $\mathcal{R}_p$  proches de leur limite actuelle, les précisions sur la reconstruction de la masse du  $\tilde{\chi}_1^0$  obtenues par l'étude des productions de paires de gluinos/squarks [116] et par l'étude de la production simple de chargino [159, 160] sont comparables. En revanche, la production simple de chargino permet d'obtenir facilement une grande précision sur la reconstruction des masses des  $\tilde{\chi}_1^\pm$  et  $\tilde{\nu}$  [159, 160] ce qui n'est pas le cas de la production de paires de particules supersymétriques [116, 127]. Ceci est dû au fait que la production simple de particule SUSY ne génère qu'une seule cascade de désintégration de particules SUSY alors que la production de paire en génère deux ce qui complique l'identification de l'origine des particules de l'état final et augmente ainsi le bruit de fond combinatoire. Par ailleurs, même si le pic associé à la reconstruction de la masse du  $\tilde{\chi}_1^0$  via la production simple de chargino était rendu invisible par la production de paires de superpartenaires, la reconstruction des masses des  $\tilde{\chi}_1^\pm$  et  $\tilde{\nu}$  via la production simple de chargino resterait possible connaissant la valeur de la masse du  $\tilde{\chi}_1^0$  déterminée via la production de paires de superpartenaires [116, 127].

## 4.2.2 Signature dilepton

L'état final contenant deux leptons chargés de même signe et de même saveur a un faible bruit de fond provenant du Modèle Standard. Cette signature dilepton peut être générée par les réactions suivantes (voir Figure 4.1) :  $p\bar{p} \rightarrow \tilde{\chi}_1^0 l_i^\pm$  ;  $p\bar{p} \rightarrow \tilde{\chi}_2^0 l_i^\pm$ ,  $\tilde{\chi}_2^0 \rightarrow \tilde{\chi}_1^0 + X$  ( $X \neq l^\pm$ ) ;  $p\bar{p} \rightarrow \tilde{\chi}_1^\pm l_i^\mp$ ,  $\tilde{\chi}_1^\pm \rightarrow \tilde{\chi}_1^0 q\bar{q}'$  et  $p\bar{p} \rightarrow \tilde{\chi}_1^\pm \nu_i$ ,  $\tilde{\chi}_1^\pm \rightarrow \tilde{\chi}_1^0 l^\pm \nu$ ,  $i$  correspondant à l'indice de saveur de la constante de couplage  $\lambda'_{ijk}$ . En effet, le  $\tilde{\chi}_1^0$  étant une particule de Majorana, il se désintègre via  $\lambda'_{ijk}$  en un lepton selon  $\tilde{\chi}_1^0 \rightarrow l_i u_j \bar{d}_k$  et en un anti-lepton selon  $\tilde{\chi}_1^0 \rightarrow \bar{l}_i \bar{u}_j d_k$  avec la même probabilité. Les réactions  $p\bar{p} \rightarrow \tilde{\chi}_{3,4}^0 l_i^\pm$ ,  $p\bar{p} \rightarrow \tilde{\chi}_2^\pm l_i^\mp$  et  $p\bar{p} \rightarrow \tilde{\chi}_2^\pm \nu_i$  ne représentent pas des contributions significatives à la signature dilepton du fait de leur relativement faibles sections efficaces [158]. Dans [158] nous avons étudié dans le cadre de la physique au Run II du Tevatron le signal dilepton engendré par les productions simples de superpartenaires ainsi que le bruit de fond associé. Les quatre processus de production simple de la Figure 4.1 ont été implémentés dans une version du générateur d'événements SUSYGEN [119] incluant la simulation des collisions hadroniques. Ceci a permis de générer le signal avec SUSYGEN et les bruits de fond provenant du Modèle Standard et des réactions supersymétriques avec les générateurs d'événements PYTHIA [120] et SHERWIG [122], respectivement. SUSYGEN, PYTHIA et SHERWIG ont été interfacés avec le simulateur SHW [123] des détecteurs D0 et CDF du Tevatron (Run II). Lors de la génération du signal et du bruit de fond, des coupures basées sur des distributions de variables cinématiques (angles démission des particules, quadri-impulsions,...) ont été appliquées afin d'augmenter le signal par rapport au bruit de fond.

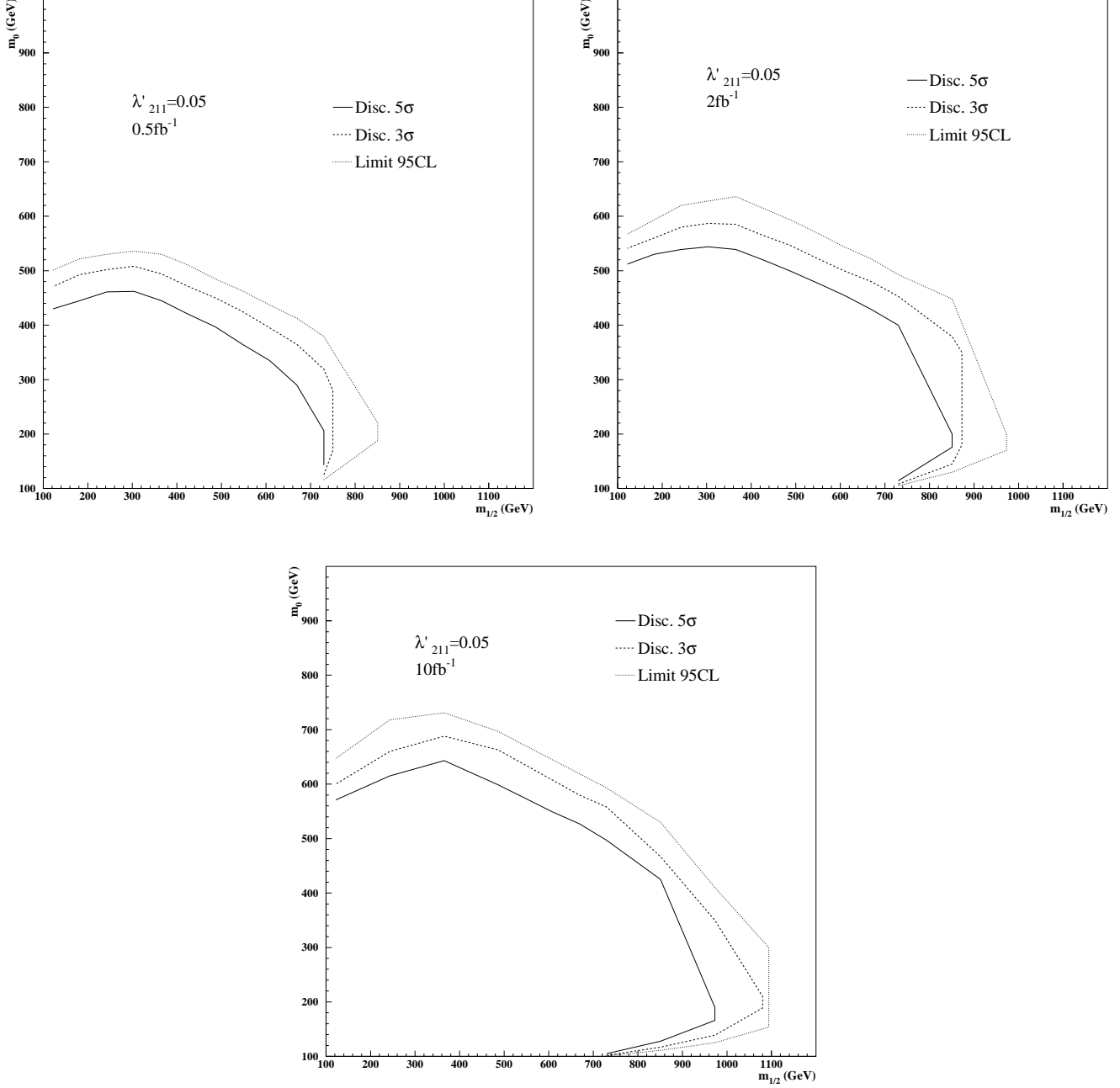


FIG. 4.5: Contours de découverte à  $5\sigma$  (ligne),  $3\sigma$  (tirés) et limites à 95%  $C.L.$  (pointillés) associés à l'étude du canal dilepton au Run II du Tevatron ( $\sqrt{s} = 2\text{TeV}$ ) et présentés dans le plan  $m_0$  versus  $m_{1/2}$  pour  $\text{sign}(\mu) < 0$ ,  $\tan\beta = 1.5$ ,  $\lambda'_{211} = 0.05$  et différentes valeurs de la luminosité.

### Potentiel de découverte

Nous présentons dans la Figure 4.5 la sensibilité dans le plan des paramètres  $m_0$  et  $m_{1/2}$  qui pourrait être obtenue à partir de l'analyse de l'état final dilepton au Run II du Tevatron, dans le cadre d'un modèle SUGRA et pour des valeurs fixées des autres

paramètres supersymétriques du modèle. Cette figure a été obtenue après avoir appliqué les coupures mentionnées plus haut et en supposant que la production simple avait lieu par l'intermédiaire d'un couplage du type  $\lambda'_{211}$ , ce qui correspond au cas où le lepton produit avec le neutralino ou le chargino est un  $\mu^\pm$  ou un  $\nu_\mu$  (voir Figure 4.1).

D'après la Figure 4.5, la sensibilité obtenue sur  $\lambda'_{211}$  dans certaines régions de l'espace des paramètres SUGRA par l'étude de la signature dilepton au Run II du Tevatron permettrait d'améliorer la limite actuelle sur cette constante de couplage  $\mathcal{R}_p$  qui vaut :  $\lambda'_{211} < 0.09(m_{\tilde{d}_R}/100\text{GeV})$  [86]. L'étude de la signature dilepton devrait aussi permettre d'améliorer les limites indirectes de nombreuses autres constantes de couplage  $\mathcal{R}_p$ .

Nous avons montré dans [158] que l'étude du canal dilepton de la production de paires de particules supersymétriques dans le cadre de la physique au Run II du Tevatron permettrait de tester dans le modèle SUGRA considéré dans la Figure 4.5 des valeurs du paramètre  $m_{1/2}$  allant jusqu'à  $\sim 200\text{GeV}$ , et ceci quelque soit la valeur de la constante de couplage  $\mathcal{R}_p$  considérée. Par conséquent, dans la région  $m_{1/2} \gtrsim 200\text{GeV}$  de la Figure 4.5, la sensibilité obtenue sur les constantes de couplage  $\mathcal{R}_p$  par la production simple n'est pas affectée par la production de paires de superpartenaires. En revanche, dans la région  $m_{1/2} \lesssim 200\text{GeV}$ , la production de paires de superpartenaires représente un bruit de fond pour la production simple car elle n'implique pas les interactions  $\mathcal{R}_p$  qui sont l'objet de cette étude. Le bruit de fond engendré par la production de paires peut être réduit par des coupures cinématiques basées sur la reconstruction de masse des particules supersymétriques (voir Section 4.2.2).

Plaçons nous maintenant du point de vue de la recherche de la supersymétrie auprès des collisionneurs. De même que pour les Figures 4.2 et 4.3, l'espace des paramètres de la Figure 4.5 n'est pas exclu par les données de LEP II [125, 126]. Par conséquent, le potentiel de découverte pour le Run II du Tevatron (Figure 4.5) représente une amélioration importante par rapport aux limites actuelles sur les paramètres supersymétriques du modèle SUGRA considéré.

De plus, la Figure 4.5 montre que la sensibilité obtenue au Run II du Tevatron, dans le plan des paramètres  $m_0$  et  $m_{1/2}$  du modèle SUGRA considéré, par l'étude du canal dilepton de la production simple permettrait d'étendre la sensibilité obtenue par l'étude du canal dilepton de la production de paires de superpartenaires. En effet, comme nous l'avons déjà mentionné, l'étude du canal dilepton de la production de paires de superpartenaires au Run II du Tevatron permettrait de tester dans le modèle SUGRA considéré dans la Figure 4.5 des valeurs du paramètre  $m_{1/2}$  allant jusqu'à  $\sim 200\text{GeV}$  [158].

De plus, la sensibilité obtenue via la production de paires est indépendante du couplage  $\mathcal{R}_p$  considéré [158]. En revanche, la sensibilité dans le plan  $m_0$  versus  $m_{1/2}$  obtenue via la production simple est d'autant plus forte que la constante de couplage  $\mathcal{R}_p$ , et donc la section efficace de production simple, est grande. Or, de plus grandes valeurs de la constante de couplage  $\mathcal{R}_p$  auraient pu être considérées dans la Figure 4.5, car la limite indirecte sur cette constante est  $\lambda'_{211} < 0.09(m_{\tilde{d}_R}/100\text{GeV})$  [86] et, dans le modèle SUGRA considéré dans la Figure 4.5, la masse du  $\tilde{d}_R$  vaut  $m_{\tilde{d}_R} = 304\text{GeV}$  pour  $m_0 = 100.0\text{GeV}$  et  $m_{1/2} = 121.6\text{GeV}$ . Par conséquent, des sensibilités encore plus fortes que celles présentées dans la Figure 4.5 peuvent être obtenues dans le plan  $m_0$  versus  $m_{1/2}$  via la production simple.

Remarquons finalement que l'étude du canal dilepton (voir Figure 4.5) permet d'obtenir une plus grande sensibilité sur la constante de couplage  $\lambda'_{211}$  que l'étude du canal

trilepton (voir Figure 4.3) [158].

## Reconstruction de masse

La contribution dominante du signal  $\mathcal{R}_p$  au canal dilepton est la réaction  $p\bar{p} \rightarrow \tilde{l}_i^\pm \rightarrow \tilde{\chi}_1^0 \tilde{l}_i^\pm, \tilde{\chi}_1^0 \rightarrow \tilde{l}_i^\pm u_j d_k$  car celle-ci a la plus grande section efficace [158]. Or les masses des  $\tilde{\chi}_1^0$  et  $\tilde{l}_i^\pm$  peuvent être reconstruites grâce à cette réaction, et ce de manière indépendante du cadre théorique. Nous avons étudié ces reconstructions de masse dans le cadre de la physique au Run II du Tevatron [157, 158].

Tout d’abord, la masse du  $\tilde{\chi}_1^0$  peut être reconstruite en calculant la masse invariante des deux jets et du lepton chargé produits dans la désintégration  $\tilde{\chi}_1^0 \rightarrow \tilde{l}_i^\pm u_j d_k$ . Les deux jets sont simples à identifier puisque ce sont les seuls jets ‘durs’ de l’état final considéré. Quant à l’identification du lepton chargé, elle ne peut être basée ni sur la saveur ni sur le signe de celui-ci car l’état final considéré contient deux leptons chargés de même signe et de même saveur. Le lepton produit dans la désintégration du neutralino peut en revanche être identifié par son énergie [158]. Le lepton produit dans la désintégration du neutralino peut aussi être identifié comme étant le lepton le plus proche dans l’espace  $(\eta, \phi)$  des deux jets de l’état final [129]. La masse du  $\tilde{\chi}_1^0$  peut être reconstruite au Tevatron (Run II) avec une précision de  $\pm 11 \text{ GeV}$  [158].

La masse du  $\tilde{l}^\pm$ , qui se désintègre via  $\tilde{l}_i^\pm \rightarrow \tilde{\chi}_1^0 \tilde{l}_i^\pm$ , peut alors être déterminée à partir de la reconstruction du  $\tilde{\chi}_1^0$ . Le lepton chargé issu de la désintégration du slepton peut être identifié par son énergie [158]. Nous avons trouvé une précision de  $\pm 20 \text{ GeV}$  pour la masse reconstruite du  $\tilde{l}^\pm$ , dans le cadre de la physique au Run II du Tevatron PubliB.

En conclusion, aux collisionneurs hadroniques, si le  $\tilde{\chi}_1^0$  était la LSP (comme c’est le cas dans la plupart des modèles supersymétriques), sa masse devrait être facilement reconstruite car il serait alors produit en grand nombre dans les productions de paires de gluinos et de squarks qui ont d’importantes sections efficaces [158]. En revanche, la production simple permet d’obtenir facilement une grande précision sur la reconstruction de masse du  $\tilde{l}^\pm$  [158] à l’inverse de la production de paires de particules supersymétriques. Ceci est dû au fait que la production simple de particule SUSY ne génère qu’une seule cascade de désintégration de superpartenaires alors que la production de paire en génère deux ce qui complique l’identification de l’origine des particules de l’état final et augmente ainsi le bruit de fond combinatoire. Par ailleurs, même si le pic associé à la reconstruction de la masse du  $\tilde{\chi}_1^0$  via la production simple était rendu invisible par la production de paires de superpartenaires, la reconstruction de masse du  $\tilde{l}^\pm$  via la production simple resterait possible connaissant la valeur de la masse du  $\tilde{\chi}_1^0$  déterminée via la production de paires de superpartenaires.

## 4.3 Collisionneurs leptoniques

Nous présentons dans cette section des études de production simple de particule SUSY aux collisionneurs leptoniques. Précisons que dans ces études, comme précédemment, nous avons toujours supposé qu’une seule constante de couplage  $\mathcal{R}_p$  était dominante par rapport aux autres.

La production simple de particule SUSY aux collisionneurs leptoniques implique uniquement des interactions  $\lambda$ . Toutes les productions simples de particule SUSY aux colli-

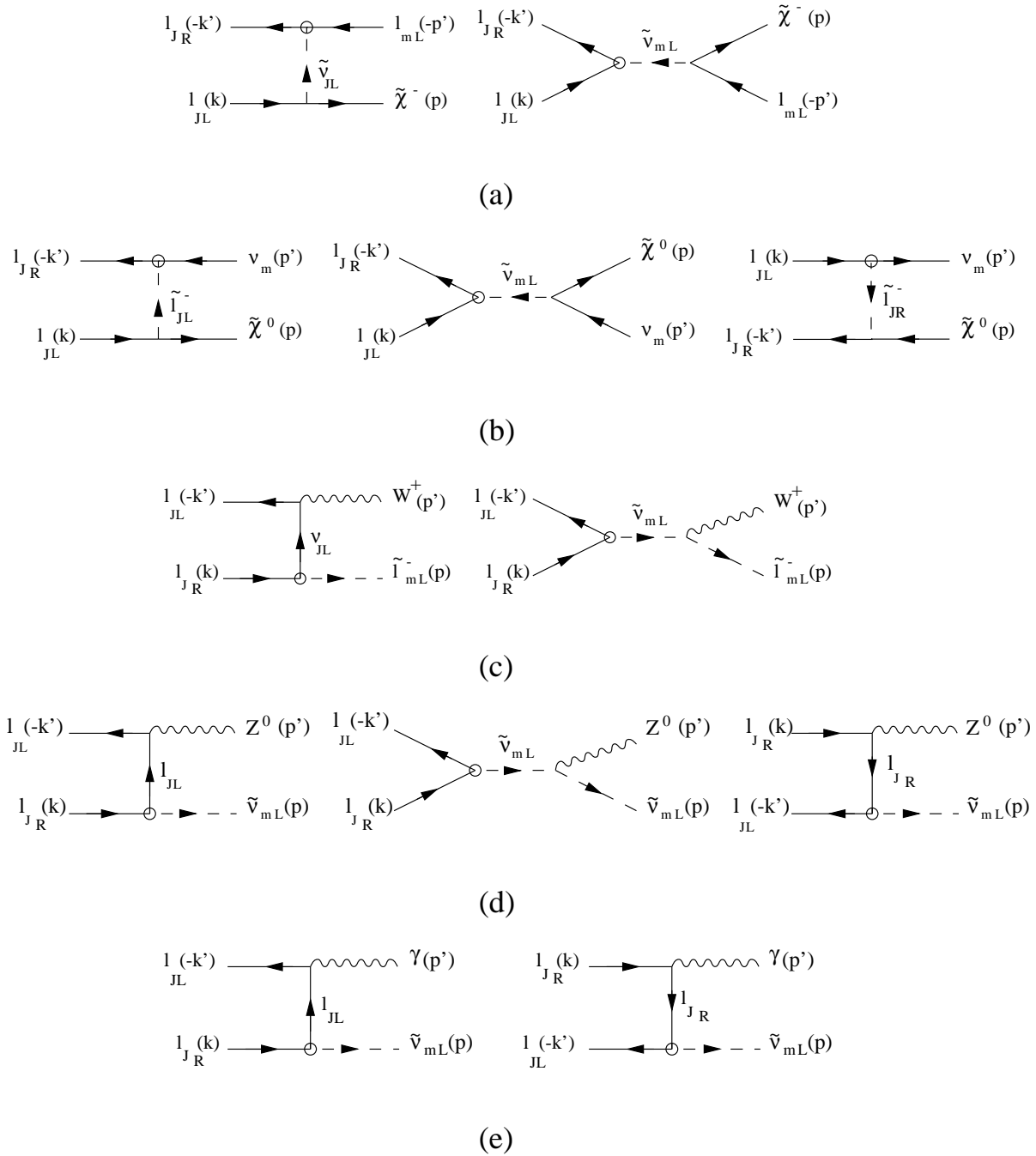


FIG. 4.6: Diagrammes de Feynman des 5 processus de production simple de particule SUSY via  $\lambda_{mJJ}$  aux collisionneurs leptoniques qui sont du type  $2 \rightarrow 2$  – corps. Les couplages  $\lambda_{mJJ}$  impliqués sont symbolisés par des cercles et les flèches représentent les moments des particules.

sionneurs leptoniques du type  $2 \rightarrow 2$  – corps sont présentées dans la Figure 4.6. Toutes les amplitudes des productions simples de la Figure 4.6 ont été calculées analytiquement et les résultats sont donnés dans [161] (voir Publication V : “*Systematics of single superpartners production at leptonic colliders*”). Basés sur ces calculs d’amplitudes, nous avons étudié le comportement des sections efficaces des productions simples dans l’espace des paramètres SUGRA [161] [163] (voir Publication VI : “*Single chargino production at linear*



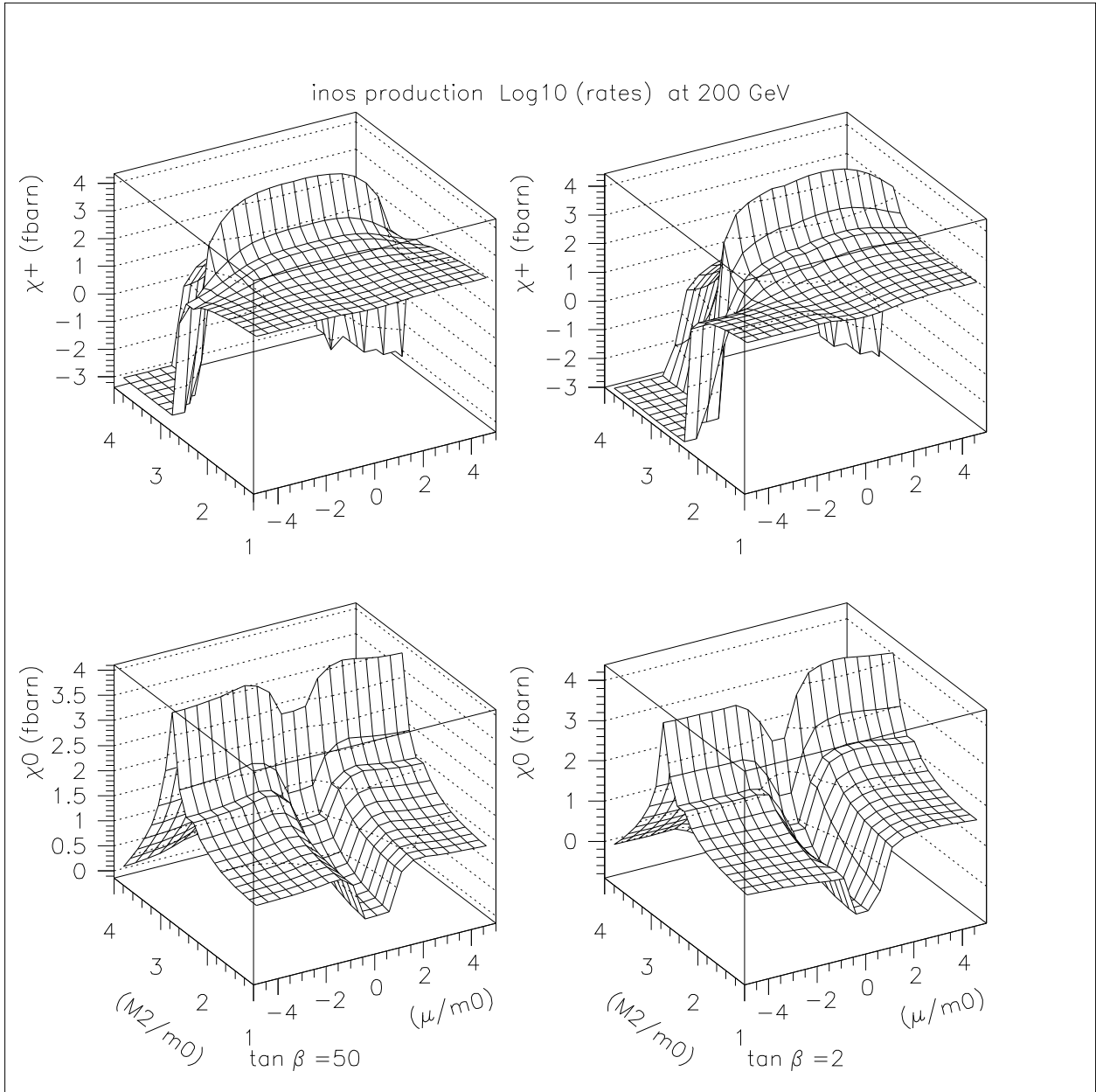


FIG. 4.7: Sections efficaces (en fbarns) de production simple de  $\tilde{\chi}_1^\pm$  et de  $\tilde{\chi}_1^0$  (voir Figure 4.6) en fonction des paramètres  $M_2/m_0$ ,  $\mu/m_0$  (avec  $m_0 = 100\text{GeV}$ ) et  $\tan\beta$  du modèle de supergravité décrit dans [161], pour une énergie dans le centre de masse de  $\sqrt{s} = 200\text{GeV}$  et une constante de couplage  $R_p$  égale à  $\lambda_{121} = 0.05$  (limite actuelle pour  $m_{\tilde{e}_R} = 100\text{GeV}$  [86]).

colliders”). Dans les Figures 4.7 et 4.8, nous présentons des courbes complémentaires de celles montrées dans [161, 163] : les sections efficaces de production simple de  $\tilde{\chi}_1^\pm$  et de  $\tilde{\chi}_1^0$  (voir Figure 4.6) en fonction des paramètres  $M_2/m_0$ ,  $\mu/m_0$  et  $\tan\beta$  du modèle de supergravité décrit dans [161], pour des énergies dans le centre de masse de  $\sqrt{s} = 200\text{GeV}$  et  $\sqrt{s} = 1000\text{GeV}$ . Par ailleurs, dans [161] nous avons calculé les largeurs des canaux de désintégration des particules supersymétriques produites et nous avons étudié leur évolution dans l’espace des paramètres SUGRA. Il ressort de cette étude que, mis à part

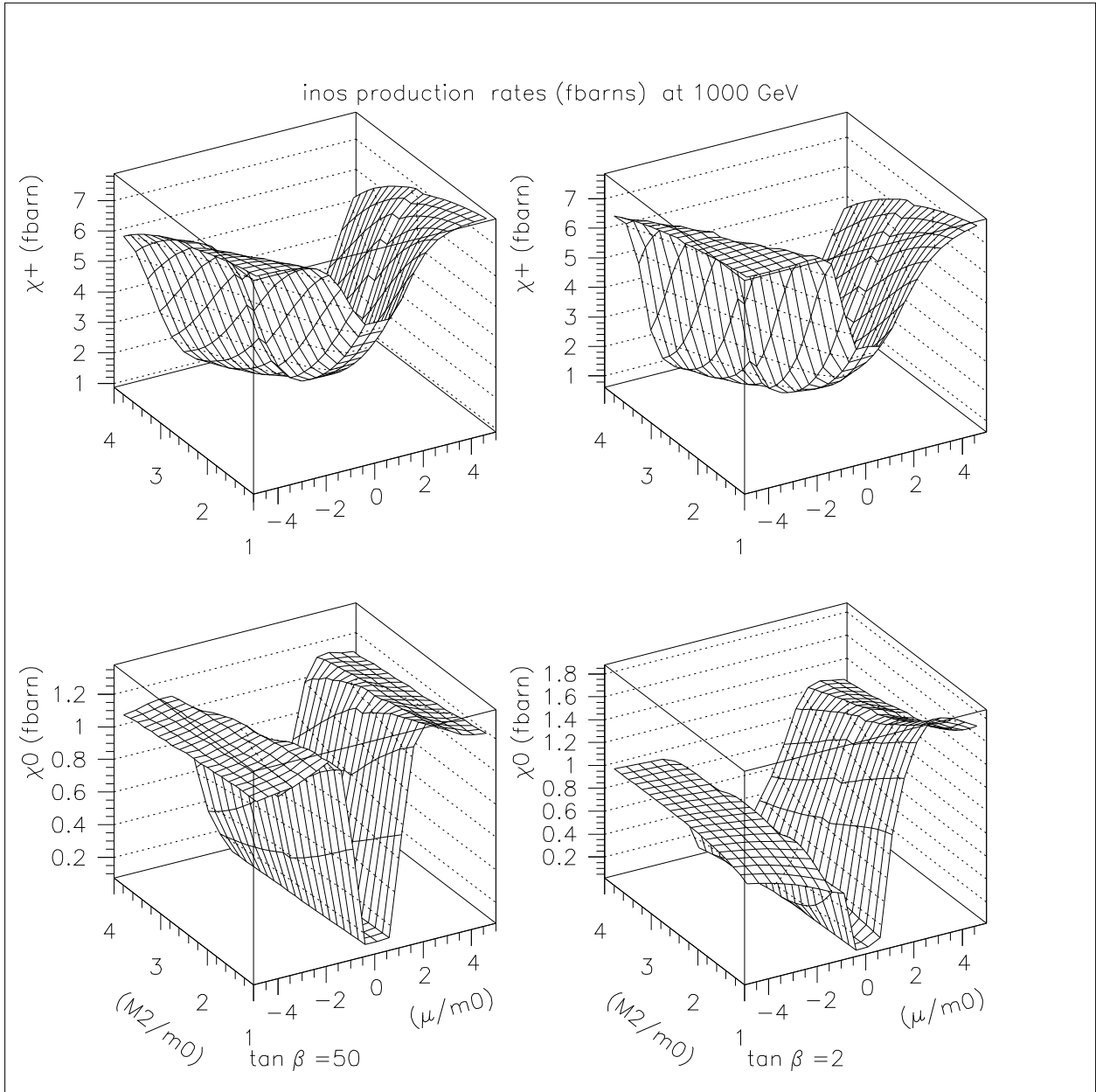


FIG. 4.8: Sections efficaces (en fbarns) de production simple de  $\tilde{\chi}_1^\pm$  et de  $\tilde{\chi}_1^0$  (voir Figure 4.6) en fonction des paramètres  $M_2/m_0$ ,  $\mu/m_0$  (avec  $m_0 = 100\text{GeV}$ ) et  $\tan\beta$  du modèle de supergravité décrit dans [161], pour une énergie dans le centre de masse de  $\sqrt{s} = 1000\text{GeV}$  et une constante de couplage  $R_p$  égale à  $\lambda_{121} = 0.05$  (limite actuelle pour  $m_{\tilde{e}_R} = 100\text{GeV}$  [86]).

la production simple de neutralino (voir Figure 4.6(b)), dans la plupart des régions de l'espace des paramètres SUGRA les productions simples représentées dans la Figure 4.6 engendrent des cascades de désintégration impliquant des interactions de jauge. Ces cascades de désintégration donnent lieu à de multiples signatures riches en leptons chargés et en jets et ayant un faible bruit de fond provenant du Modèle Standard. Il s'agit d'états finals tels que :

$$4l + \cancel{E}, 6l, 6l + \cancel{E}, 3l + 2j + \cancel{E}, \dots$$

### 4.3.1 Production simple de chargino

Dans [162, 163], nous nous sommes concentrés sur la production simple  $e^+e^- \rightarrow \tilde{\chi}_1^\pm l_m^\mp$  via  $\lambda_{1m1}$  qui a typiquement la plus importante section efficace parmi les productions simples représentées dans la Figure 4.6 [161, 163]. La production simple de  $\tilde{\chi}_1^\pm$  a aussi l'intérêt de pouvoir engendrer de claires signatures multi-jets et multi-leptoniques [161, 162, 163]. En particulier, nous avons considéré la réaction  $e^+e^- \rightarrow \tilde{\chi}_1^\pm \mu^\mp$  qui implique la constante de couplage  $\lambda_{121}$ .

La production simple  $e^+e^- \rightarrow \tilde{\chi}_1^\pm \mu^\mp$  a une voie  $t$  et peut aussi recevoir la contribution de la production résonante d'un sneutrino (voir Figure 4.6(a)). À  $\sqrt{s} = 200\text{GeV}$  la section efficace de production simple du chargino hors du pôle du sneutrino est de l'ordre de  $100\text{fbarns}$  [161] pour une constante de couplage  $\mathcal{R}_p$  égale à sa limite actuelle qui est  $\lambda_{121} = 0.05$  pour  $m_{\tilde{e}_R} = 100\text{GeV}$  [86]. La section efficace hors du pôle du sneutrino est donc à la limite d'observabilité à LEP II pour une luminosité de  $\mathcal{L} \approx 200\text{pb}^{-1}$ . Au pôle du sneutrino, la production simple de chargino atteint de grandes valeurs de la section efficace. Par exemple pour  $\lambda_{121} = 0.05$ , la section efficace de production simple du chargino peut atteindre  $2 \cdot 10^{-1}\text{pb}$  à la résonance du sneutrino [130]. C'est la raison pour laquelle les analyses expérimentales de la production simple de chargino au LEP [103, 104, 105, 131, 132] permettent de tester des valeurs des constantes de couplage  $\mathcal{R}_p$  inférieures aux limites actuelles seulement à la résonance  $\sqrt{s} = m_{\tilde{\nu}_L}$ , et, grâce aux radiations de l'état initial (ISR), dans un intervalle de  $\sim 50\text{GeV}$  autour du pôle du sneutrino. Au pôle même du sneutrino, les sensibilités sur la constante de couplage  $\lambda_{121}$  obtenues à LEP II atteignent des valeurs de l'ordre de  $10^{-3}$  [103, 104, 105, 131, 132].

Les collisionneurs linéaires constitueront un cadre propice à l'étude de la production simple de chargino de par les grandes énergies ( $\sqrt{s} \approx 1\text{TeV}$ ) et luminosités ( $\mathcal{L} \approx 500\text{fb}^{-1}$ ) atteintes [83, 127]. En particulier, les luminosités attendues aux collisionneurs linéaires permettront d'être sensible à la section efficace de production simple du chargino hors du pôle du sneutrino qui est de l'ordre de  $10\text{fbarns}$  [161] pour  $1000\text{GeV} > \sqrt{s} > 500\text{GeV}$  et une constante de couplage  $\mathcal{R}_p$  égale à  $\lambda_{121} = 0.05$ . Cependant, aux collisionneurs linéaires, la production simple de chargino risque de souffrir d'un grand bruit de fond provenant de la production de paires de particules supersymétriques. En effet, aux grandes énergies espérées dans ces collisionneurs, la production de paire de superpartenaires peut atteindre de grandes sections efficaces.

### Potentiel de découverte

Dans [163], nous avons montré que malgré le bruit de fond provenant de la production de paire de superpartenaires, l'étude de la production simple de chargino aux collisionneurs linéaires offrira la possibilité d'obtenir une plus forte sensibilité sur la constante de couplage  $\lambda_{121}$  que celle obtenue à LEP [103, 104, 105, 131, 132]. Pour cela, nous avons étudié l'état final composé de quatre leptons chargés et d'énergie manquante qui possède un faible bruit de fond provenant du Modèle Standard [111] et qui est généré par la production simple de chargino lorsque celui-ci se désintègre selon  $\tilde{\chi}_1^\pm \rightarrow \tilde{\chi}_1^0 l\nu$ ,  $\tilde{\chi}_1^0 \rightarrow \bar{e}e\nu_\mu$ ,  $\bar{e}e\nu_\mu$ ,  $\mu\bar{e}\nu_e$  ou  $\bar{\mu}\nu_e$  via  $\lambda_{121}$ . Nous avons montré que la contribution de la production de paire de superpartenaires au signal  $4l + \cancel{E}$  pouvait être réduite par rapport à la contribution de la production simple de chargino. Cette réduction est basée sur deux points. Tout d'abord, la polarisation des faisceaux d'électrons et de positrons incidents aux collision-

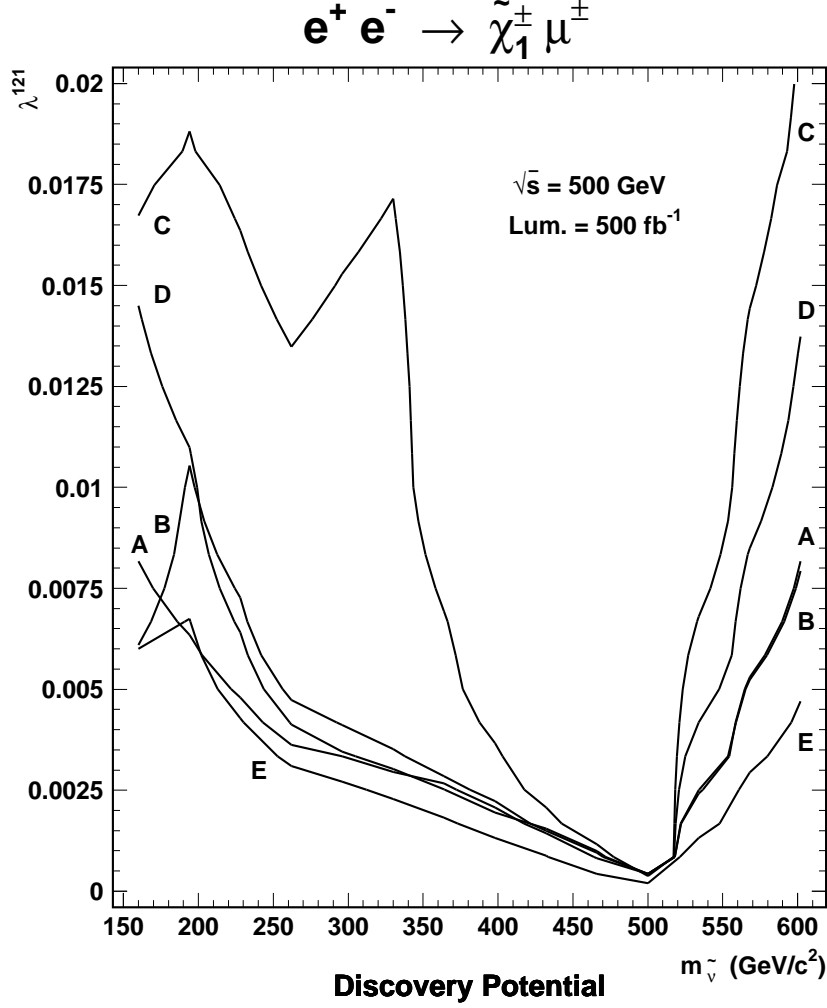


FIG. 4.9: Potentiel de découverte à  $5\sigma$  dans le plan  $\lambda_{121}$  versus  $m_{\tilde{\nu}}$  (in  $\text{GeV/c}^2$ ) pour une luminosité de  $\mathcal{L} = 500 \text{ fb}^{-1}$  et une énergie dans le centre de masse de  $\sqrt{s} = 500 \text{ GeV}$ . Les points A, B, C, D et E correspondent aux points de l'espace des paramètres du Modèle Standard Supersymétrique Minimal (MSSM) définis par, A :  $M_1 = 200 \text{ GeV}$ ,  $M_2 = 250 \text{ GeV}$ ,  $\mu = 150 \text{ GeV}$ ,  $\tan \beta = 3$ ,  $m_{\tilde{l}^\pm} = 300 \text{ GeV}$ ,  $m_{\tilde{q}} = 600 \text{ GeV}$  ( $m_{\tilde{\chi}_1^\pm} = 115.7 \text{ GeV}$ ,  $m_{\tilde{\chi}_1^0} = 101.9 \text{ GeV}$ ,  $m_{\tilde{\chi}_2^0} = 154.5 \text{ GeV}$ ); B :  $M_1 = 100 \text{ GeV}$ ,  $M_2 = 200 \text{ GeV}$ ,  $\mu = 600 \text{ GeV}$ ,  $\tan \beta = 3$ ,  $m_{\tilde{l}^\pm} = 300 \text{ GeV}$ ,  $m_{\tilde{q}} = 600 \text{ GeV}$  ( $m_{\tilde{\chi}_1^\pm} = 189.1 \text{ GeV}$ ,  $m_{\tilde{\chi}_1^0} = 97.3 \text{ GeV}$ ,  $m_{\tilde{\chi}_2^0} = 189.5 \text{ GeV}$ ); C :  $M_1 = 100 \text{ GeV}$ ,  $M_2 = 400 \text{ GeV}$ ,  $\mu = 400 \text{ GeV}$ ,  $\tan \beta = 3$ ,  $m_{\tilde{l}^\pm} = 300 \text{ GeV}$ ,  $m_{\tilde{q}} = 600 \text{ GeV}$  ( $m_{\tilde{\chi}_1^\pm} = 329.9 \text{ GeV}$ ,  $m_{\tilde{\chi}_1^0} = 95.5 \text{ GeV}$ ,  $m_{\tilde{\chi}_2^0} = 332.3 \text{ GeV}$ ); D :  $M_1 = 150 \text{ GeV}$ ,  $M_2 = 300 \text{ GeV}$ ,  $\mu = 200 \text{ GeV}$ ,  $\tan \beta = 3$ ,  $m_{\tilde{l}^\pm} = 300 \text{ GeV}$ ,  $m_{\tilde{q}} = 600 \text{ GeV}$  ( $m_{\tilde{\chi}_1^\pm} = 165.1 \text{ GeV}$ ,  $m_{\tilde{\chi}_1^0} = 121.6 \text{ GeV}$ ,  $m_{\tilde{\chi}_2^0} = 190.8 \text{ GeV}$ ); E :  $M_1 = 100 \text{ GeV}$ ,  $M_2 = 200 \text{ GeV}$ ,  $\mu = 600 \text{ GeV}$ ,  $\tan \beta = 3$ ,  $m_{\tilde{l}^\pm} = 150 \text{ GeV}$ ,  $m_{\tilde{q}} = 600 \text{ GeV}$  ( $m_{\tilde{\chi}_1^\pm} = 189.1 \text{ GeV}$ ,  $m_{\tilde{\chi}_1^0} = 97.3 \text{ GeV}$ ,  $m_{\tilde{\chi}_2^0} = 189.5 \text{ GeV}$ ).

neurs linéaires peut être utilisée pour réduire la source de bruit de fond que représente la production de paire de superpartenaires. De plus, la cinématique spécifique de type  $2 \rightarrow 2 - \text{corps}$  de la production simple de chargino permet d'imposer des coupures sur les distributions des moments transverses des leptons chargés de l'état final favorisant la production simple de chargino par rapport à la production de paire de superpartenaires.

Nous présentons dans la Figure 4.9 la sensibilité obtenue dans le plan  $\lambda_{121}$  versus  $m_{\tilde{\nu}}$  grâce à l'étude de la production simple de  $\tilde{\chi}_1^\pm$  basée sur la signature  $4l + \cancel{E}$  aux collisionneurs linéaires [163]. Afin d'obtenir les résultats présentés dans la Figure 4.9 la production simple de chargino ainsi que le bruit de fond provenant de la production de paire de superpartenaires ont été simulés avec la nouvelle version [133] du générateur d'événements SUSYGEN [119] incluant les effets de polarisation des faisceaux incidents. Lors de la génération des événements, les coupures et polarisations mentionnées ci-dessus ont été appliquées. Les sensibilités dans le plan  $\lambda_{121}$  versus  $m_{\tilde{\nu}}$  présentées dans la Figure 4.9 ont été obtenues pour des points caractéristiques de l'espace des paramètres du Modèle Standard Supersymétrique Minimal (MSSM). Ces points ont été choisis tels que la masse du  $\tilde{\chi}_1^0$  soit proche de la limite actuelle ( $m_{\tilde{\chi}_1^0} > 52 GeV$  pour  $\tan \beta = 20$  dans le cadre d'un modèle ayant une constante de couplage  $\lambda_{ijk}$  non nulle [105]) afin de maximiser la section efficace de la production de paires de neutralinos qui représente la principale source de bruit de fond issue de la production de paires de superpartenaires.

Les sensibilités sur la constante de couplage  $\lambda_{121}$  présentées dans la Figure 4.9 représentent une amélioration par rapport à la borne indirecte,  $\lambda_{121} < 0.05(m_{\tilde{e}_R}/100 GeV)$  [86], dans un intervalle de  $\sim 500 GeV$  autour de la résonance du sneutrino, et atteignent des valeurs de l'ordre de  $10^{-4}$  au pôle du sneutrino. La sensibilité sur la constante de couplage  $\lambda_{121}$  qui pourra être obtenue auprès des futurs collisionneurs linéaires améliorera donc nettement les résultats de LEP II [103, 104, 105, 131, 132] (voir ci-dessus).

Par ailleurs, les sensibilités obtenues via la production simple de chargino aux collisionneurs linéaires et présentées dans la Figure 4.9 représentent notamment une amélioration par rapport à la limite expérimentale actuelle sur la masse du sneutrino,  $m_{\tilde{\nu}} > 78 GeV$  (dans le cadre d'un modèle ayant une constante de couplage  $\lambda_{ijk}$  non nulle) [105]. De plus, dans le domaine  $m_{\tilde{\nu}} > \sqrt{s}/2$ , le sneutrino peut être produit comme une résonance aux collisionneurs linéaires alors qu'il ne peut être produit par paires. Cela signifie que dans ce domaine cinématique, la production simple de chargino aux collisionneurs linéaires, qui reçoit sa principale contribution de la production résonante de sneutrino, permet de tester la masse du sneutrino, comme l'illustre la Figure 4.9 pour  $\sqrt{s} = 500 GeV$ , à l'inverse de la production de paires de particules supersymétriques.

Enfin, notons que la constante de couplage  $\lambda_{121}$  peut aussi être testée par l'étude de la contribution des interactions  $\mathcal{R}_p$  à la diffusion Bhabha  $e^+e^- \rightarrow e^+e^-$  [110]. Cette contribution implique l'échange dans les voies  $s$  et  $t$  d'un sneutrino. Les sensibilités obtenues sur la constante de couplage  $\lambda_{121}$  par l'étude de cette contribution dans le cadre de la physique au LEP sont de l'ordre de  $10^{-2}$  à la résonance du sneutrino [110]. Or ces sensibilités sont inférieures à celles obtenues sur la même constante de couplage  $\lambda_{121}$  par l'étude de la production simple de chargino au LEP [103, 104, 105, 131, 132] (voir ci-dessus).

## Reconstruction de masse

L'énergie du muon  $E(\mu)$  produit dans la réaction de type  $2 \rightarrow 2-corps$ ,  $e^+e^- \rightarrow \tilde{\chi}_1^\pm \mu^\mp$ , est une fonction de l'énergie dans le centre de masse  $\sqrt{s}$  et de la masse du muon  $m_\mu$  et du chargino  $m_{\tilde{\chi}_1^\pm}$  :

$$E(\mu) = \frac{s + m_\mu^2 - m_{\tilde{\chi}_1^\pm}^2}{2\sqrt{s}}. \quad (4.3)$$

Par conséquent, la masse du  $\tilde{\chi}_1^\pm$  devrait pouvoir être déduite, via Eq.(4.3), de l'énergie du muon produit avec le chargino dans les collisionneurs linéaires. En fait, à cause de l'ISR, un photon est irradié par l'état initial de telle sorte que la production simple de chargino doit être étudiée comme la réaction de type  $2 \rightarrow 3$  corps,  $e^+e^- \rightarrow \tilde{\chi}_1^\pm \mu^\mp \gamma$ . La relation 4.3 n'est donc pas vérifiée. Cependant, la masse du  $\tilde{\chi}_1^\pm$  peut être déduite de l'énergie du muon dans le centre de masse du sneutrino  $E^*(\mu)$  et de la masse du sneutrino  $m_{\tilde{\nu}}$  et du muon  $m_\mu$  par la relation [163],

$$E^*(\mu) = \frac{m_{\tilde{\nu}}^2 + m_\mu^2 - m_{\tilde{\chi}_1^\pm}^2}{2m_{\tilde{\nu}}}. \quad (4.4)$$

En effet, la masse du sneutrino peut être déduite de l'étude du signal  $4l + \cancel{E}$  aux collisionneurs linéaires en effectuant un scan sur l'énergie dans le centre de masse afin de déterminer la valeur de  $\sqrt{s}$  correspondant au maximum de la section efficace de production simple du chargino associé à la résonance du sneutrino [163]. De plus, l'énergie du muon dans le centre de masse du sneutrino  $E^*(\mu)$  peut être déterminée grâce à la distribution du moment transverse du muon produit avec le chargino [163]. La masse du sneutrino pouvant être déterminée avec une erreur de  $\pm 3.5 GeV$  par un scan sur l'énergie dans le centre de masse aux collisionneurs linéaires, l'erreur sur la masse du  $\tilde{\chi}_1^\pm$  reconstruite par la méthode décrite ci-dessus peut atteindre  $\pm 5.9 GeV$  [163]. La masse du  $\tilde{\chi}_2^\pm$  peut aussi être reconstruite par la méthode décrite ci-dessus [163].

En conclusion, aux collisionneurs linéaires, la production simple de chargino permet d'obtenir facilement une grande précision sur la reconstruction de masse du  $\tilde{\nu}$  et du  $\tilde{\chi}_1^\pm$  [163] à l'inverse de la production de paires de particules supersymétriques [111]. Ceci est dû au fait que la production simple de particule SUSY ne génère qu'une seule cascade de désintégration de superpartenaires alors que la production de paire en génère deux ce qui complique l'identification de l'origine des particules de l'état final et augmente ainsi le bruit de fond combinatoire. De plus, dans le cadre d'un modèle ayant une constante de couplage  $\lambda$  non nulle, si le  $\tilde{\chi}_1^0$  est la LSP (comme c'est le cas dans la plupart des modèles supersymétriques) les deux cascades de désintégration issues de la production de paires de superpartenaires se terminent par la désintégration  $\tilde{\chi}_1^0 \rightarrow l\bar{l}\nu$ . Or les neutrinos ainsi produits génèrent de l'énergie manquante dans l'état final, ce qui rend délicat la reconstruction de masse du  $\tilde{\chi}_1^0$  et donc des autres particules supersymétriques. Notons par ailleurs que les reconstructions des masses du  $\tilde{\nu}$  et du  $\tilde{\chi}_1^\pm$  basées sur la production simple de chargino restent possibles tant que la distribution du moment transverse du muon produit avec le chargino n'est pas noyée par le bruit de fond issu de la production de paires de particules supersymétriques (voir Figure 4.9) [163].

### Extension à différentes constantes de couplage $\mathcal{R}_p$

La production simple de chargino dans les collisions  $e^+e^-$  peut uniquement avoir lieu par les interactions  $\lambda_{121}$  et  $\lambda_{131}$ , à cause de l'antisymétrie de la constante de couplage  $\lambda_{ijk}$  (voir Chapitre 3.1). La production simple de chargino via  $\lambda_{131}$  correspond à la production d'un lepton tau :  $e^+e^- \rightarrow \tilde{\chi}^\pm \tau^\mp$  (voir Figure 4.6(a)). Du fait de la nature instable du lepton tau, la sensibilité sur la constante de couplage  $\lambda_{131}$  obtenue via la production simple de chargino devrait être moins forte que celle sur  $\lambda_{121}$  (voir Figure 4.9) car les coupures mentionnées dans la Section 4.3.1 sont moins efficaces dans le cas de l'étude

de la constante  $\lambda_{131}$  [163]. D'autre part, les désintégrations du lepton tau rendent les reconstructions de masse du  $\tilde{\nu}$  et du  $\tilde{\chi}_1^\pm$  difficiles [163].

La production simple de chargino pourrait aussi avoir lieu dans les futurs collisionneurs muoniques [134, 135] via la constante de couplage  $\lambda_{2J2}$  ( $J = 1, 3$ ) :  $\mu^+\mu^- \rightarrow \tilde{\chi}^\pm l_J^\mp$  (voir Figure 4.6(a)). L'étude des constantes de couplage  $\lambda_{212}$  et  $\lambda_{232}$  basée sur la production simple de chargino aux collisionneurs muoniques est identique, à quelques détails près (voir [163]), à l'étude des constantes  $\lambda_{121}$  et  $\lambda_{131}$  via la production simple de chargino aux collisionneurs linéaires. Par conséquent, les sensibilités sur les constantes de couplage  $\lambda_{212}$  et  $\lambda_{232}$  obtenues aux collisionneurs muoniques devraient être du même ordre de grandeur que celles attendues sur les constantes  $\lambda_{121}$  et  $\lambda_{131}$  aux collisionneurs linéaires. De même, les résultats sur les reconstructions de masse basées sur la production simple de chargino devraient être comparables aux collisionneurs linéaires et aux collisionneurs muoniques [163].

Par ailleurs, notons que les productions simples de sleptons  $\gamma e^\pm \rightarrow e^\pm \tilde{\nu}$  et  $\gamma e^\pm \rightarrow \tilde{e}^\pm \nu$  aux collisionneurs linéaires permettront de tester les constantes de couplage  $\lambda_{121}$ ,  $\lambda_{131}$ ,  $\lambda_{122}$ ,  $\lambda_{123}$ ,  $\lambda_{132}$ ,  $\lambda_{133}$ ,  $\lambda_{231}$ ,  $\lambda_{232}$  et  $\lambda_{233}$  [136, 137]. Cependant, la production résonante de sneutrino dans les collisions  $e^+e^-$  est davantage sensible aux constantes de couplage  $\lambda_{121}$  et  $\lambda_{131}$  que ces productions simples de sleptons [136].





# Chapitre 5

## Contributions des interactions $\mathcal{R}_p$ aux taux de changement de saveur et aux asymétries liées à la violation de la symétrie CP

### 5.1 Motivations

Comme nous l'avons discuté dans le Chapitre 3 et la Section 4.1, d'un point de vue théorique aussi bien que phénoménologique, les modèles avec violation et conservation de la symétrie de R-parité doivent être traités avec la même attention vis-à-vis de la phénoménologie de la supersymétrie.

Dans l'hypothèse où certains couplages  $\mathcal{R}_p$  ne seraient pas nuls, ces couplages pourraient avoir des phases complexes et constituer ainsi de nouvelles sources indépendantes de violation de la symétrie CP. Notons que même si les couplages  $\mathcal{R}_p$  existant avaient des phases complexes nulles, ils pourraient conduire en combinaison avec d'autres sources de violation de CP du MSSM à de nouveaux tests de violation de CP [138, 139, 140, 141].

Dans un second travail, nous avons développé des études [165] (voir Publication VII : *“Broken R-parity contributions to flavor changing rates and CP asymmetries in fermion pair production at leptonic colliders”*) [166] (voir Publication VIII : *“Polarized single top production at leptonic colliders from broken R-parity interactions incorporating CP violation”*) [167] (voir Publication IX : *“CP violation flavor asymmetries in slepton pair production at leptonic colliders from broken R-parity”*) [168] permettant de mettre en évidence la partie imaginaire des constantes de couplage  $\mathcal{R}_p$  par des effets de violation de la symétrie CP dans le cadre de la physique des collisionneurs de haute énergie. L'idée de contributions des interactions  $\mathcal{R}_p$  à des effets de violation de CP a déjà motivé de nombreuses études dans le cadre de la physique de basse énergie [138, 139, 140, 142].

Les effets de violation de la symétrie CP offrent un cadre propice à l'étude des interactions  $\mathcal{R}_p$  et plus généralement de toute autre physique au-delà du Modèle Standard Supersymétrique Minimal (MSSM). La raison est que les contributions des interactions du Modèle Standard aux effets de violation de CP sont faibles car elles impliquent des diagrammes à l'ordre des boucles et sont réduites par la quasi dégénérescence existant entre les masses des quarks et des leptons. (voir par exemple l'étude des asymétries de violation

de CP liées à la désintégration des bosons de jauge  $W^\pm$  et  $Z^0$  [143, 144]). De plus, les contributions des interactions du MSSM aux effets de violation de CP (voir par exemple l'étude des asymétries de violation de CP liées à la production de paires de sleptons [145]) sont contraintes par des données expérimentales sur la physique de basse énergie [148]. Dans la plupart des modèles de physique sous-jacente au MSSM, des effets importants de violation de CP sont prédits [146, 147]). Cependant, dans les différentes études effectuées, nous avons supposé que les contributions aux effets de violation de CP des interactions  $\mathcal{R}_p$  étaient dominantes.

Nous avons étudié les réactions de production de paires de fermions [165, 166] et de sfermions [167] de saveurs différentes dans les collisionneurs leptoniques :

$$l^+l^- \rightarrow f_J \bar{f}_{J'} \quad [J \neq J'], \quad (5.1)$$

$$l^+l^- \rightarrow \tilde{f}_J \tilde{f}_{J'}^* \quad [J \neq J']. \quad (5.2)$$

Ces réactions simples et très étudiées ainsi que l'environnement 'propre' des collisionneurs leptoniques offrent un cadre propice aux tests de violation de CP.

Dans [165, 166], nous avons calculé les asymétries de violation de CP,

$$\mathcal{A}_{JJ'} = \frac{|M^{JJ'}|^2 - |\bar{M}^{JJ'}|^2}{|M^{JJ'}|^2 + |\bar{M}^{JJ'}|^2}, \quad (5.3)$$

associées aux contributions des interactions  $\mathcal{R}_p$  à la réaction de Eq.(5.1). Dans Eq.(5.3),  $M^{JJ'}$  ( $\bar{M}^{JJ'}$ ) désigne l'amplitude de la réaction  $l^+l^- \rightarrow f_J \bar{f}_{J'}$  ( $l^+l^- \rightarrow f_{J'} \bar{f}_J$ ) [ $J \neq J'$ ].  $M^{JJ'}$  et  $\bar{M}^{JJ'}$  sont donc les amplitudes de processus CP conjugués. Notons que certaines asymétries de violation de CP associées à des réactions impliquant des couplages  $\mathcal{R}_p$  peuvent être fonction du spin des particules de l'état final [149, 150].

Nous avons donc été amené à étudier dans [165, 166] les contributions des interactions  $\mathcal{R}_p$  à la réaction changeant la saveur  $l^+l^- \rightarrow f_J \bar{f}_{J'}$  [ $J \neq J'$ ] [165, 166]. Or l'étude de ces contributions a aussi permis de développer un test de l'intensité des couplages  $\mathcal{R}_p$ . En effet, les contributions des interactions du Modèle Standard aux effets de changement de saveur sont faibles. En particulier, les contributions des interactions du Modèle Standard aux courants neutres changeant la saveur sont peu significatives puisqu'elles impliquent des diagrammes à l'ordre des boucles [143, 144]. Les contributions des interactions du Modèle Standard à la désintégration du boson de jauge  $Z^0$  en une paire de quarks de différentes générations sont particulièrement faibles. La raison est que dans le lagrangien effectif du Modèle Standard, le couplage  $Z^0 \bar{q}_J q_{J'}$  entre le boson de jauge  $Z^0$  et une paire de quarks de différentes générations a une structure du type  $\sum_i V_{iJ}^* V_{iJ'} f(m_i^2/m_{Z^0}^2)$ , où les  $V_{ij}$  sont les éléments de la matrice Cabibbo-Kobayashi-Maskawa et  $f(m_i^2/m_{Z^0}^2)$  est une fonction issue d'un calcul de boucle et dépendant des masses du boson de jauge  $Z^0$  et des quarks propagés dans la boucle. Le couplage  $Z^0 \bar{q}_J q_{J'}$  est donc fortement supprimé à cause de la dégénérescence des masses des quarks relativement à la masse du boson de jauge  $Z^0$  (valide pour tous les quarks à l'exception du quark top) et de la propriété d'unitarité de la matrice Cabibbo-Kobayashi-Maskawa. De plus, les contributions des interactions du MSSM aux effets de changement de saveur sont contraintes par des données expérimentales sur la physique de basse énergie [148]. Plus précisément, ces contributions sont contraintes par une dégénérescence des masses des particules scalaires supersymétriques (qui sont

issues des termes de brisure douce de SUSY) ou par un alignement entre les matrices de transformation de la base de courant à la base de masse des fermions du Modèle Standard et de leur partenaire scalaire. Les effets de changement de saveur offrent donc un cadre propice à l'étude des interactions  $\mathcal{R}_p$  mais aussi de toute autre physique au-delà du MSSM. La majorité des théories au-delà du MSSM prévoit des effets de changement de saveur significatifs [143, 144, 151]. Nous avons néanmoins travaillé dans l'hypothèse selon laquelle les principales contributions aux effets de changement de saveur sont dûes aux couplages  $\mathcal{R}_p$ .

Dans [167], nous avons calculé les asymétries de violation de CP,

$$\tilde{\mathcal{A}}_{JJ'} = \frac{|\tilde{M}^{JJ'}|^2 - |\tilde{M}^{JJ'}|^2}{|\tilde{M}^{JJ'}|^2 + |\tilde{M}^{JJ'}|^2}, \quad (5.4)$$

associées aux contributions des interactions  $\mathcal{R}_p$  à la réaction du type de Eq.(5.2). Dans Eq.(5.4),  $\tilde{M}^{JJ'}$  ( $\tilde{M}^{JJ'}$ ) désigne l'amplitude de la réaction  $l^+l^- \rightarrow \tilde{e}_{HJ}\tilde{e}_{HJ'}^*$  ( $l^+l^- \rightarrow \tilde{e}_{HJ'}\tilde{e}_{HJ}^*$ ) [ $H = L, R; J \neq J'$ ].  $\tilde{M}^{JJ'}$  et  $\tilde{M}^{JJ'}$  sont donc les amplitudes de processus CP conjugués.

Nous avons donc été amené à étudier dans [167] les contributions des interactions  $\mathcal{R}_p$  à la réaction changeant la saveur  $l^+l^- \rightarrow \tilde{e}_{HJ}\tilde{e}_{HJ'}^*$  [ $H = L, R; J \neq J'$ ] [165, 166]. Or l'étude de ces contributions a aussi permis de développer un test de l'intensité des couplages  $\mathcal{R}_p$ . En effet, les contributions des interactions du MSSM aux effets de changement de saveur sont contraintes par des données expérimentales sur la physique de basse énergie [148]. Plus précisément, ces contributions sont contraintes par une dégénérescence des masses des particules scalaires supersymétriques (qui sont issues des termes de brisure douce de SUSY) ou par un alignement entre les matrices de transformation de la base de courant à la base de masse des fermions du Modèle Standard et de leur partenaire scalaire. Les interactions  $\mathcal{R}_p$  pourraient donc apporter une contribution à la réaction changeant la saveur  $l^+l^- \rightarrow \tilde{e}_{HJ}\tilde{e}_{HJ'}^*$  [ $H = L, R; J \neq J'$ ] qui soit significative relativement aux contributions des interactions du MSSM [152].

## 5.2 Production de paires de fermions

### 5.2.1 Taux de changement de saveur

Les graphes de Feynman des contributions des interactions  $\mathcal{R}_p$  à la réaction de Eq.(5.1) sont présentés dans les Figures 5.1 et 5.2. Nous avons considéré les contributions des interactions  $\mathcal{R}_p$  à l'ordre d'une boucle pour des raisons qui apparaîtront claires dans la Section 5.2.2.

Les contributions des interactions  $\mathcal{R}_p$  à la production de paires de leptons chargés appartenant à des familles différentes  $l^+l^- \rightarrow l_J^+l_{J'}^-$  [ $J \neq J'$ ] impliquent les produits de constantes de couplage  $\lambda_{i11}\lambda_{iJJ'}^*$  (voie  $s$ ),  $\lambda_{iJ1}\lambda_{iJ'1}^*$  (voie  $t$ ) ou  $\lambda_{i1J}\lambda_{i1J'}^*$  (voie  $t$ ) au niveau en arbre (l'indice  $i$  correspond à la saveur du sneutrino échangé) et  $\lambda_{iJ'k}\lambda_{iJk}^*$ ,  $\lambda_{ijJ}\lambda_{ijJ'}^*$  ou  $\lambda_{J'jk}'\lambda_{Jjk}'^*$  à l'ordre d'une boucle (les indices  $i, j$  et  $k$  correspondent aux saveurs des fermions et sfermions échangés dans la boucle).

Les contributions des interactions  $\mathcal{R}_p$  à la production de paires de quarks down appartenant à des familles différentes  $l^+l^- \rightarrow d_J\bar{d}_{J'}$  [ $J \neq J'$ ] impliquent les produits de constantes

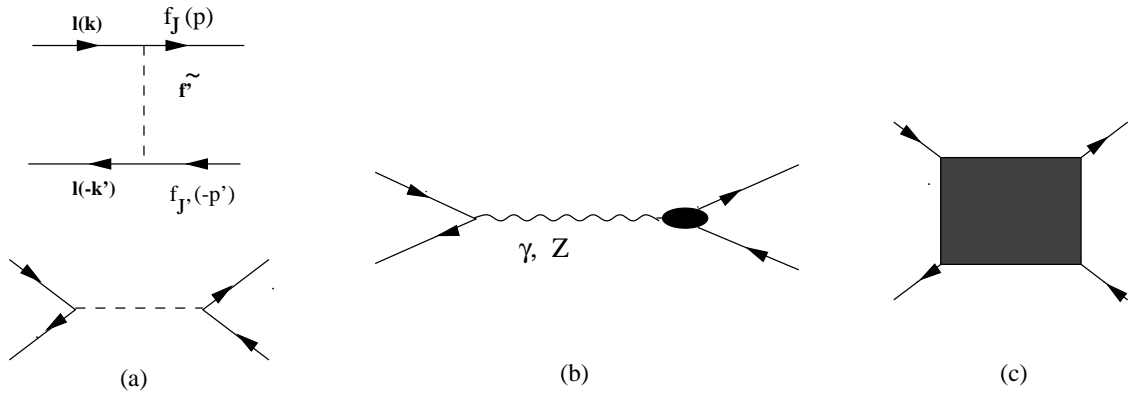


FIG. 5.1: Diagrammes de Feynman des contributions des interactions  $\mathcal{R}_p$  à la réaction  $l^+l^- \rightarrow f_J \bar{f}_{J'}$  [ $J \neq J'$ ].  $f$  dénote un fermion et  $\tilde{f}$  un sfermion. Les diagrammes de Feynman des contributions à l'ordre d'une boucle au vertex  $Z^0 f_J \bar{f}_{J'}$  [ $J \neq J'$ ] sont présentés dans la Figure 5.2.

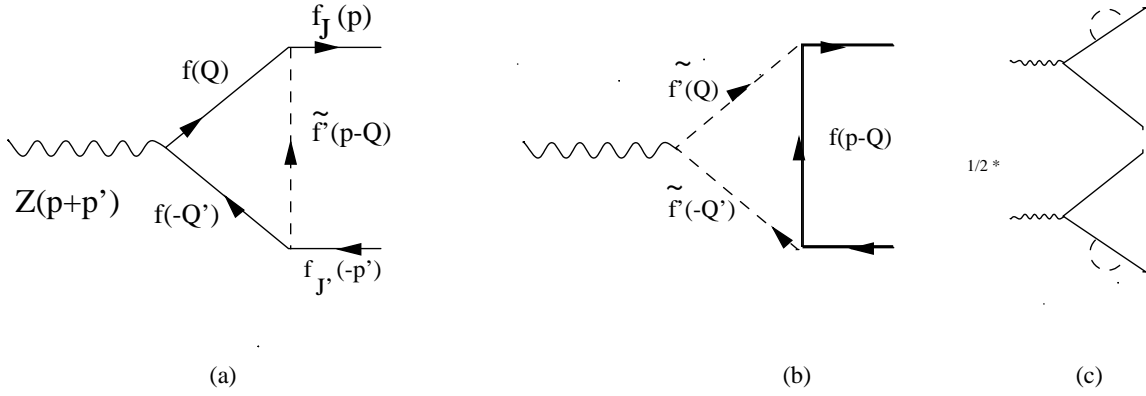


FIG. 5.2: Diagrammes de Feynman des contributions des interactions  $\mathcal{R}_p$  à l'ordre d'une boucle au vertex  $Z^0 f_J \bar{f}_{J'}$  [ $J \neq J'$ ].  $f$  dénote un fermion et  $\tilde{f}$  un sfermion.

de couplage  $\lambda_{i11} \lambda_{iJJ'}^*$  (voie  $s$ ) ou  $\lambda'_{1jJ} \lambda_{1jJ'}^*$  (voie  $t$ ) au niveau en arbre (les indices  $i$  et  $j$  correspondent à la saveur du squark up échangé) et  $\lambda'_{iJ'k} \lambda_{iJk}^*$  ou  $\lambda'_{ijJ} \lambda_{ijJ'}^*$  à l'ordre d'une boucle (les indices  $i$ ,  $j$  et  $k$  correspondent aux saveurs des fermions et sfermions échangés dans la boucle).

Les contributions des interactions  $\mathcal{R}_p$  à la production de paires de quarks up appartenant à des familles différentes  $l^+l^- \rightarrow u_J \bar{u}_{J'}$  [ $J \neq J'$ ] impliquent les produits de constantes de couplage  $\lambda'_{1J'k} \lambda_{1Jk}^*$  (voie  $t$ ) au niveau en arbre (l'indice  $k$  correspond à la saveur du squark down échangé) et  $\lambda'_{iJ'k} \lambda_{iJk}^*$  à l'ordre d'une boucle (les indices  $i$  et  $k$  correspondent aux saveurs des fermions et sfermions échangés dans la boucle).

Nous notons les amplitudes des contributions des interactions  $\mathcal{R}_p$  à la réaction de Eq.(5.1),

$$M^{JJ'} = a_0^{JJ'} + \sum_{\alpha} a_{\alpha}^{JJ'} F_{\alpha}^{JJ'}(s + i\epsilon), \quad (5.5)$$

$$\bar{M}^{JJ'} = a_0^{JJ'*} + \sum_{\alpha} a_{\alpha}^{JJ'*} F_{\alpha}^{JJ'}(s + i\epsilon), \quad (5.6)$$

où  $a_0^{JJ'}$  représente l'amplitude des contributions des interactions  $\mathcal{R}_p$  au niveau en arbre

et  $\sum_{\alpha} a_{\alpha}^{JJ'} F_{\alpha}^{JJ'}(s + i\epsilon)$  l'amplitude des contributions des interactions  $\mathcal{R}_p$  à l'ordre d'une boucle.  $a_0^{JJ'}$  est proportionnel au produit de constantes de couplage  $\mathcal{R}_p$  impliqué par le processus au niveau en arbre et que l'on note  $t_i^{JJ'}$ ,  $i$  correspondant à la saveur du sfermion échangé au niveau en arbre. L'expression de  $a_0^{JJ'}$  fait intervenir une sommation sur l'indice  $i$  dont dépend aussi la masse du sfermion échangé. De même,  $a_{\alpha}^{JJ'}$  est proportionnel au produit de constantes de couplage  $\mathcal{R}_p$  impliqué dans la boucle et que l'on note  $l_{\alpha}^{JJ'}$ ,  $\alpha$  correspondant aux deux indices de saveur des fermions et sfermions échangés dans la boucle. Enfin,  $F_{\alpha}^{JJ'}(s + i\epsilon)$  est une fonction issue d'un calcul de boucle ayant une partie imaginaire (voir [165]) et dépendant notamment des masses des fermions et sfermions échangés dans la boucle et donc de  $\alpha$ .

À des énergies dans le centre de masse supérieures à la masse du boson  $Z^0$ , les contributions dominantes des interactions  $\mathcal{R}_p$  à la réaction de Eq.(5.1) proviennent de processus à l'ordre des arbres (voir Figure 5.1). Les sections efficaces  $\sigma_{JJ'}$  de ces contributions sont de l'ordre de [165],

$$\sigma_{JJ'} \approx \left(\frac{\Lambda}{0.1}\right)^4 \left(\frac{100\text{GeV}}{\tilde{m}}\right)^2 \sim (0.1 - 10) \text{ fbarns}, \quad (5.7)$$

si l'on suppose que toutes les masses des sfermions (toutes les valeurs absolues des constantes de couplage  $\mathcal{R}_p$  de type  $\lambda$ ,  $\lambda'$  ou  $\lambda''$ ) sont égales à une même valeur notée  $\tilde{m}$  ( $\Lambda$ ). À la résonance du sneutrino, les sections efficaces des contributions des interactions  $\mathcal{R}_p$  à la réaction  $l^+ l^- \rightarrow l_J^+ l_{J'}^-$  [ $J \neq J'$ ] peuvent atteindre  $(\Lambda/0.1)^4 10^4 \text{ fbarns}$ .

Au pôle du boson de jauge  $Z^0$ , les canaux de désintégration  $Z \rightarrow f_J + \bar{f}_{J'}$  [ $J \neq J'$ ] impliquent des diagrammes à l'ordre des boucles (voir Figure 5.2). Les rapports de branchement  $B_{JJ'}$  de ces canaux de désintégration s'écrivent,

$$B_{JJ'} = \frac{\Gamma(Z \rightarrow f_J + \bar{f}_{J'}) + \Gamma(Z \rightarrow f_{J'} + \bar{f}_J)}{\Gamma(Z \rightarrow \text{all})}, \quad (5.8)$$

et sont de l'ordre de [165],

$$B_{JJ'} \approx \left(\frac{\Lambda}{0.1}\right)^4 \left(\frac{100\text{GeV}}{\tilde{m}}\right)^{2.5} 10^{-9}, \quad (5.9)$$

si l'on suppose que toutes les masses des sfermions (toutes les valeurs absolues des constantes de couplage  $\mathcal{R}_p$  de type  $\lambda$ ,  $\lambda'$  ou  $\lambda''$ ) sont égales à une même valeur notée  $\tilde{m}$  ( $\Lambda$ ).

Les limites actuelles sur les constantes de couplage  $\mathcal{R}_p$  sont typiquement de l'ordre de  $10^{-1}(\tilde{m}/100\text{GeV})$ ,  $\tilde{m}$  étant la masse des sfermions [86]. Par conséquent, les sections efficaces de Eq.(5.7) peuvent être supérieures à  $\sim 10 \text{ fbarns}$  et les rapports de branchement de Eq.(5.9) supérieurs à  $\sim 10^{-9}$ .

Étant donné les sections efficaces  $\sigma_{JJ'}$  de Eq.(5.7), les contributions des interactions  $\mathcal{R}_p$  à la réaction de Eq.(5.1) hors du pôle du boson de jauge  $Z^0$  sont potentiellement observables à LEP II ainsi qu'aux futurs collisionneurs linéaires pour lesquels les luminosités attendues sont de l'ordre de  $500 \text{ fb}^{-1}$  [83, 127].

D'après les rapports de branchement  $B_{JJ'}$  de Eq.(5.9), les limites expérimentales actuelles sur les rapports de branchement du boson de jauge  $Z^0$ ,  $B(Z \rightarrow \bar{e}\mu + \bar{\mu}e) < 1.7 \cdot 10^{-6}$ ,  $B(Z \rightarrow \bar{e}\tau + \bar{\tau}e) < 9.8 \cdot 10^{-6}$  et  $B(Z \rightarrow \bar{\mu}\tau + \bar{\tau}\mu) < 1.7 \cdot 10^{-5}$  [153], imposent les bornes

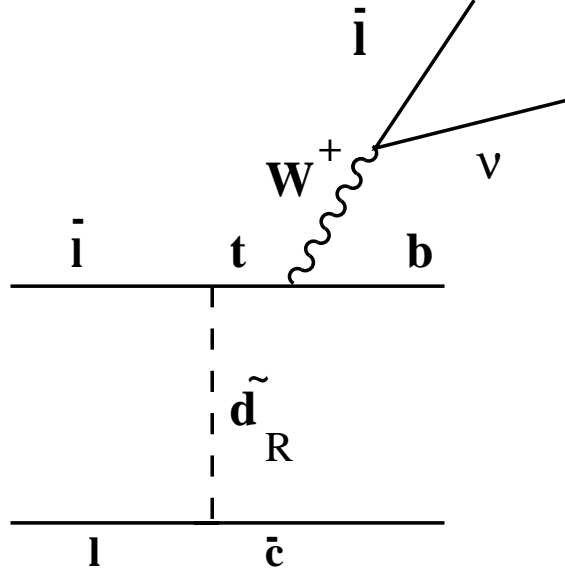


FIG. 5.3: Diagramme de Feynman de l'amplitude au niveau en arbre de la contribution des interactions  $\mathcal{R}_p$  au processus  $l^+l^- \rightarrow \bar{c}t \rightarrow \bar{c}b\bar{l}\nu$ .  $\tilde{d}_R$  désigne un squark down droit.

suivantes sur les produits de constantes de couplage  $\mathcal{R}_p$  [165],

$$\lambda_{ijJ}\lambda_{ijJ'}^* < [0.46, 1.1, 1.4] \text{ pour } [JJ' = 12, 23, 13], \quad (5.10)$$

$$\lambda'_{J'jk}\lambda_{Jjk}^* < [0.38, 0.91, 1.2] \times 10^{-1} \text{ pour } [JJ' = 12, 23, 13], \quad (5.11)$$

dans l'hypothèse d'un produit de constantes de couplage  $\mathcal{R}_p$  dominant et pour une masse des sfermions de  $\tilde{m} = 100\text{GeV}$ . Les bornes de Eq.(5.10,5.11) seront améliorées dans le cadre de la physique aux collisionneurs linéaires et pourraient même devenir plus fortes que les limites indirectes actuelles [86].

Les rapports de branchement de Eq.(5.9) sont du même ordre de grandeur que les rapports de branchement des désintégrations hadroniques du boson de jauge  $Z^0$  calculées dans le cadre du Modèle Standard qui valent,  $B(Z \rightarrow \bar{b}s + \bar{s}b) = 10^{-7}$ ,  $B(Z \rightarrow \bar{b}d + \bar{d}b) = 10^{-9}$  et  $B(Z \rightarrow \bar{s}d + \bar{d}s) = 10^{-11}$  [143, 144].

### PRODUCTION SIMPLE DE QUARK TOP :

Dans le secteur des quarks, les effets de changement de saveur liés à la réaction  $l^+l^- \rightarrow q_J\bar{q}_{J'}$  [ $J \neq J'$ ] sont difficilement détectables à cause de la mauvaise identification expérimentale de la saveur des quarks. Dans ce contexte, la production simple de quark top  $l^+l^- \rightarrow t\bar{c} / \bar{t}c$  paraît intéressante car le quark top donne lieu à une signature caractéristique. En effet, de par sa grande masse, le quark top possède un temps de vie  $\tau_{top} = [1.56 \text{ GeV}(\frac{m_{top}}{180 \text{ GeV}})^3]^{-1}$  qui est plus court que le temps typique d'hadronisation  $1/\Lambda_{QCD}$ . Par conséquent, le quark top, une fois produit, se désintègre, et son principal canal de désintégration est  $t \rightarrow bW^\pm$ . Le quark top donne donc lieu à une signature claire de type  $bl\nu$  lorsque le boson de jauge  $W^\pm$  se désintègre en leptons.

Dans [166], nous avons étudié l'état final  $cb\nu$ , [ $l = e, \mu$ ] issu de la contribution des interactions  $\lambda'_{12k}$  et  $\lambda_{13k}^*$  ( $k$  correspondant à l'indice de génération du squark down droit

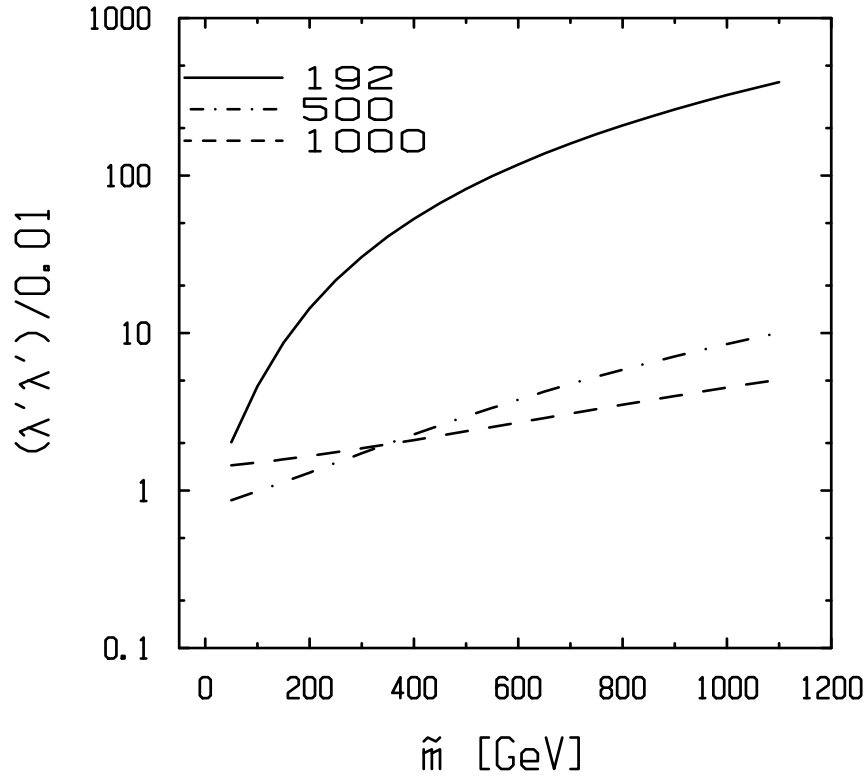


FIG. 5.4: Sensibilité sur le produit de constantes de couplage  $\mathcal{R}_p \lambda'_{12k} \lambda'^*_{13k}/0.01$  en fonction de la masse du squark down droit  $\tilde{m}$  obtenue par l'étude de la signature  $cbl\nu$ ,  $[l = e, \mu]$  à des énergies dans le centre de masse  $s^{\frac{1}{2}} = [192., 500, 1000]$  GeV et pour les luminosités associées  $\mathcal{L} = [2., 100., 100.] fb^{-1}$ . Les régions se situant au-dessus des courbes correspondent à une exclusion à 95% C.L., c'est à dire que ces domaines sont tels que  $S/\sqrt{S+B} > 3$  où  $S$  représente le nombre d'évènements du signal  $\mathcal{R}_p$  et  $B$  le nombre d'évènements du bruit de fond issu du Modèle Standard.

$\tilde{d}_{kR}$  échangé dans la voie  $t$ ) à la réaction  $l^+l^- \rightarrow ct \rightarrow cbl\nu$ ,  $[l = e, \mu]$  (voir Figure 5.3). Nous avons calculé des distributions de variables cinématiques permettant d'appliquer des coupures réduisant le bruit de fond issu du Modèle Standard et associé à la signature  $cbl\nu$ ,  $[l = e, \mu]$ . Ce bruit de fond provient principalement de la réaction  $l^+l^- \rightarrow W^\pm W^\mp \rightarrow cbl\nu$ ,  $[l = e, \mu]$ . Nous avons obtenu une efficacité pour les coupures cinématiques mentionnées ci-dessus de 0.8 pour le signal  $\mathcal{R}_p$  et de  $3 \cdot 10^{-3}$  pour le bruit de fond issu du Modèle Standard. Ces efficacités dépendent faiblement de l'énergie dans le centre de masse et de la masse du  $\tilde{d}_{kR}$ . Basés sur ces efficacités, nous avons calculé le potentiel de découverte associé à l'analyse de la signature  $cbl\nu$ ,  $[l = e, \mu]$ . Dans la Figure 5.4, nous présentons ce potentiel de découverte dans le plan  $\lambda'_{12k} \lambda'^*_{13k}/0.01$  versus la masse du  $\tilde{d}_{kR}$ . La Figure 5.4 montre que l'étude de la réaction  $l^+l^- \rightarrow ct \rightarrow cbl\nu$ ,  $[l = e, \mu]$  auprès des futurs collisionneurs linéaires, dont les luminosités devraient être de l'ordre de  $10^2 fb^{-1}$  [83, 127], permettra d'améliorer les limites sur (ou bien de détecter) les produits de constantes de couplage  $\lambda'_{121} \lambda'^*_{131}$  et  $\lambda'_{122} \lambda'^*_{132}$ . Effectivement, la borne indirecte actuelle sur le produit  $\lambda'_{121} \lambda'^*_{131}$  ( $\lambda'_{122} \lambda'^*_{132}$ ) est  $\lambda'_{121} \lambda'^*_{131} < 1.225 \cdot 10^{-3} (m_{\tilde{s}_L}/100 GeV)(m_{\tilde{b}_L}/100 GeV)$  ( $\lambda'_{122} \lambda'^*_{132} < 6.8 \cdot 10^{-3} (m_{\tilde{s}}/100 GeV)^{3/2}$ ) et vaut donc  $\lambda'_{121} \lambda'_{131}/0.01 < 1.225 \cdot 10^{-1}$  ( $\lambda'_{122} \lambda'_{132}/0.01 < 6.8 \cdot 10^{-1}$ ) pour  $m_{\tilde{d}_k} = 100 GeV$  et  $\lambda'_{121} \lambda'_{131}/0.01 < 12.25$  ( $\lambda'_{122} \lambda'_{132}/0.01 < 21.50$ ) pour  $m_{\tilde{d}_k} = 1 TeV$  [86]. En revanche, l'étude de la production simple de quark top ne permet-

tra pas d'améliorer la limite sur le produit  $\lambda'_{123}\lambda'^*_{133}$  dont la borne indirecte actuelle est très forte :  $\lambda'_{123}\lambda'_{133} < 1.4 \cdot 10^{-4}$  pour  $m_{\tilde{q}} = 100 \text{ GeV}$  [86]. L'étude des contributions des interactions  $\mathcal{R}_p$  à la réaction  $l^+l^- \rightarrow ct \rightarrow cbl\nu$ , [ $l = e, \mu$ ] est la seule étude permettant de tester efficacement le produit de constantes de couplage  $\lambda'_{12k}\lambda'^*_{13k}$  ( $k = 1, 2$ ) dans les collisions de haute énergie [166]. Remarquons finalement qu'une étude dans le même contexte de la réaction  $l^+l^- \rightarrow ut \rightarrow ubl\nu$ , [ $l = e, \mu$ ] donnerait des résultats semblables sur le produit dominant de constantes de couplage  $\mathcal{R}_p \lambda'_{11k}\lambda'^*_{13k}$  car l'état final que nous avons effectivement considéré est  $2 \text{ jets} + l + \nu$ .

### 5.2.2 Asymétries liées à la violation de CP

En remplaçant dans Eq.(5.3) les amplitudes par leur expression explicite (voir Eq.(5.5,5.6)), nous trouvons après calcul les expressions suivantes pour les asymétries liées à la violation de CP et associées aux contributions des interactions  $\mathcal{R}_p$  à la réaction de Eq.(5.1) [165],

$$\begin{aligned} \mathcal{A}_{JJ'} &= \frac{2}{|a_0^{JJ'}|^2} \left[ \sum_{\alpha} \text{Im}(a_0^{JJ'} a_{\alpha}^{JJ'\star}) \text{Im}(F_{\alpha}^{JJ'}(s + i\epsilon)) \right. \\ &\quad \left. - \sum_{\alpha < \alpha'} \text{Im}(a_{\alpha}^{JJ'} a_{\alpha'}^{JJ'\star}) \text{Im}(F_{\alpha}^{JJ'}(s + i\epsilon) F_{\alpha'}^{JJ'\star}(s + i\epsilon)) \right]. \end{aligned} \quad (5.12)$$

Le premier terme de Eq.(5.12) correspond à une interférence entre les amplitudes au niveau en arbre et à l'ordre d'une boucle. Quant au second terme, il provient d'une interférence entre des contributions à l'ordre d'une boucle impliquant différentes générations de (s)fermions. Nous remarquons que les deux termes de Eq.(5.12) ne sont pas nuls uniquement si les constantes de couplage  $\mathcal{R}_p$  ont une phase complexe et si l'on considère les parties imaginaires issues des calculs de boucle. Hors du pôle du boson de jauge  $Z^0$ , la contribution majeur à l'asymétrie de violation de CP définie dans Eq.(5.12) provient du premier terme de Eq.(5.12).

Au pôle du boson de jauge  $Z^0$ , l'observable liée à la violation de CP correspondant à l'asymétrie de Eq.(5.3) est définie par,

$$\begin{aligned} \mathcal{A}_{JJ'} &= \frac{\Gamma(Z \rightarrow f_J + \bar{f}_{J'}) - \Gamma(Z \rightarrow f_{J'} + \bar{f}_J)}{\Gamma(Z \rightarrow f_J + \bar{f}_{J'}) + \Gamma(Z \rightarrow f_{J'} + \bar{f}_J)} \\ &= -2 \frac{\sum_{H=L,R} \sum_{\alpha < \alpha'} \text{Im}(l_{\alpha}^{JJ'} l_{\alpha'}^{JJ'\star}) \text{Im}(I_{H\alpha}^{JJ'}(s + i\epsilon) I_{H\alpha'}^{JJ'\star}(s + i\epsilon))}{\sum_{H=L,R} |\sum_{\alpha} l_{\alpha}^{JJ'} I_{H\alpha}^{JJ'}(s + i\epsilon)|^2}, \end{aligned} \quad (5.13)$$

où  $I_{H\alpha}^{JJ'}(s + i\epsilon)$  est une fonction issue d'un calcul de boucle ayant une partie imaginaire (voir [165]) et dépendant notamment des masses des fermions et sfermions échangés dans la boucle et donc de  $\alpha$  qui, rappelons-le, correspond aux deux indices de saveur des fermions et sfermions échangés dans la boucle. L'observable définie dans Eq.(5.13) est basée sur une interférence entre des contributions à l'ordre d'une boucle impliquant différentes générations de (s)fermions. Remarquons qu'au pôle du boson de jauge  $Z^0$ , les asymétries de violation de CP (voir Eq.(5.13)), tout comme les contributions aux taux de changement de saveur (voir Eq.(5.8)), impliquent des processus à l'ordre des boucles.

À des énergies dans le centre de masse supérieures à la masse du boson  $Z^0$ , les asymétries liées à la violation de CP de Eq.(5.12) sont de l'ordre de [165],

$$\mathcal{A}_{JJ'} \approx (10^{-2} - 10^{-3}) \sin \psi, \quad (5.14)$$



si l'on suppose que toutes les masses des sfermions (toutes les valeurs absolues des constantes de couplage  $\mathcal{R}_p$  de type  $\lambda$ ,  $\lambda'$  ou  $\lambda''$ ) sont égales à une même valeur notée  $\tilde{m}$  ( $\Lambda$ ). Le résultat de Eq.(5.14) a été obtenu en supposant que seuls les produits de constantes de couplage  $\mathcal{R}_p$  impliquées dans les processus à l'ordre d'une boucle ont une phase complexe et que cette phase complexe  $\psi$  est identique pour tous ces produits de constantes de couplage  $\mathcal{R}_p$ , c'est à dire dans nos notations  $\arg(t_i^{JJ'}) = 0$  et  $\arg(l_\alpha^{JJ'}) = \psi$  pour tout  $i$ ,  $\alpha$ ,  $J$  et  $J'$ .

Au pôle du boson de jauge  $Z^0$ , les asymétries liées à la violation de CP de Eq.(5.13) sont de l'ordre de [165],

$$\mathcal{A}_{JJ'} \approx (10^{-1} - 10^{-3}) \sin \psi, \quad (5.15)$$

si l'on suppose que toutes les masses des sfermions (toutes les valeurs absolues des constantes de couplage  $\mathcal{R}_p$  de type  $\lambda$ ,  $\lambda'$  ou  $\lambda''$ ) sont égales à une même valeur notée  $\tilde{m}$  ( $\Lambda$ ). Le résultat de Eq.(5.15) a été obtenu en supposant que seuls les produits de constantes de couplage  $\mathcal{R}_p$  impliquées dans les boucles dans lesquelles sont échangés des (s)fermions appartenant à la troisième famille ont une phase complexe et que cette phase complexe  $\psi$  est identique pour tous ces produits de constantes de couplage  $\mathcal{R}_p$ , ce qui s'écrit dans nos notations  $\arg(t_i^{JJ'}) = 0$  et  $\arg(l_\alpha^{JJ'}) = \psi$  pour tout  $i$ ,  $J$ ,  $J'$  et si aucun (au moins un) des deux indices de  $\alpha$  n'est (est) égal à 3.

Les asymétries définies dans Eq.(5.12) et Eq.(5.13) ont une dépendance dans les constantes de couplage  $\mathcal{R}_p$  du type,

$$\frac{\sum_i \sum_\alpha \text{Im}(t_i^{JJ'} l_\alpha^{JJ'\star})}{|\sum_i t_i^{JJ'}|^2}, \quad (5.16)$$

et,

$$\frac{\sum_{\alpha < \alpha'} \text{Im}(l_\alpha^{JJ'} l_{\alpha'}^{JJ'\star})}{|\sum_\alpha l_\alpha^{JJ'}|^2}, \quad (5.17)$$

respectivement, qui pourraient conduire à d'importants facteurs de réduction ou d'augmentation si les constantes de couplage  $\mathcal{R}_p$  exhibaient une grande hiérarchie dans l'espace des saveurs.

Nous avons vu dans [166] que les erreurs statistiques sur les asymétries définies dans Eq.(5.12) sont du même ordre de grandeur que les asymétries elles-mêmes pour une luminosité de  $\mathcal{L} = 100 fb^{-1}$  et une valeur du produit de constantes de couplage  $\mathcal{R}_p$  impliqué dans le processus au niveau en arbre de  $\Lambda\Lambda = 0.1$ . Cependant, si la structure des constantes de couplage  $\mathcal{R}_p$  exhibait une forte hiérarchie dans l'espace des saveurs, les valeurs des asymétries seraient augmentées devenant ainsi supérieures aux incertitudes statistiques. Par ailleurs, un calcul des incertitudes statistiques plus précis que celui effectué dans [166] donnerait des résultats plus optimistes.

Pour des énergies comprises dans l'intervalle  $10^2 GeV - 10^3 GeV$ , la quantité  $2\sigma_{JJ'} \times \mathcal{A}_{JJ'} \times 500 fb^{-1}$  ( $\mathcal{A}_{JJ'}$  étant défini dans Eq.(5.12)) est de l'ordre de  $(1 - 10) (\Lambda/0.1)^4 (100 GeV/\tilde{m})^2 - 3 \sin \psi$ . Par conséquent, si les constantes de couplage  $\mathcal{R}_p$  ne sont pas effectivement proches de leur limite actuelle [86] et si la structure des constantes de couplage  $\mathcal{R}_p$  n'exhibe pas de forte hiérarchie dans l'espace des saveurs, les asymétries de violation de CP dûes aux interactions  $\mathcal{R}_p$  seront difficilement observables auprès des futurs collisionneurs linéaires [83, 127].

Les asymétries de Eq.(5.15) sont du même ordre de grandeur que les asymétries de violation de CP associées aux désintégrations hadroniques du boson de jauge  $Z^0$  calculées dans le cadre du Modèle Standard qui valent,  $\mathcal{A}_{bs} = 10^{-5} \sin \delta_{CKM}$ ,  $\mathcal{A}_{bd} = 10^{-3} \sin \delta_{CKM}$  et  $\mathcal{A}_{sd} = 10^{-1} \sin \delta_{CKM}$  [143, 144].

### PRODUCTION SIMPLE DE QUARK TOP :

La réaction  $l^+l^- \rightarrow c\bar{t} / \bar{c}t$ ,  $\bar{t} \rightarrow \bar{b}l\nu / t \rightarrow b\bar{l}\nu$  [ $l = e, \mu$ ] permet de tester les effets de changement de saveur (voir Section 5.2.1) et donc les effets de violation de CP, dans le secteur des quarks. Pour cette réaction, la quantité  $2\sigma_{23} \times \mathcal{A}_{23} \times 500 fb^{-1}$  ( $\mathcal{A}_{JJ'}$  étant défini dans Eq.(5.12)) est diminuée d'un facteur  $B(W \rightarrow l\nu) = 21.1\%$  [ $l = e, \mu$ ] par rapport aux réactions du type  $l^+l^- \rightarrow f_J\bar{f}_{J'}$ ,  $\bar{f}_J f_{J'}$ , mais elle reste du même ordre de grandeur. Les conclusions sur les incertitudes statistiques et sur l'observabilité des asymétries de violation de CP définies dans Eq.(5.12) sont donc similaires pour les processus  $l^+l^- \rightarrow c\bar{t} / \bar{c}t$ ,  $\bar{t} \rightarrow \bar{b}l\nu / t \rightarrow b\bar{l}\nu$  [ $l = e, \mu$ ] et  $l^+l^- \rightarrow f_J\bar{f}_{J'}$ ,  $\bar{f}_J f_{J'}$ .

Dans [166], nous nous sommes intéressés à une autre asymétrie que celle définie dans Eq.(5.12) en vue d'obtenir une meilleure sensibilité sur les effets de violation de CP liés au processus  $l^+l^- \rightarrow c\bar{t} / \bar{c}t$ ,  $\bar{t} \rightarrow \bar{b}l\nu / t \rightarrow b\bar{l}\nu$  [ $l = e, \mu$ ]. L'asymétrie de violation de CP que nous avons calculé dépend du spin du quark top produit et est définie par,

$$\mathcal{A}^{pol} = \frac{\frac{d\sigma^+}{dE_l} - \frac{d\sigma^-}{dE_l}}{\frac{d\sigma^+}{dE_l} + \frac{d\sigma^-}{dE_l}}, \quad (5.18)$$

où  $\sigma^+$  et  $\sigma^-$  sont respectivement les sections efficaces des processus  $l^+l^- \rightarrow t\bar{c}$  et  $l^+l^- \rightarrow \bar{t}c$  et  $E_l$  est l'énergie du lepton chargé produit dans la désintégration du quark top  $t \rightarrow bl\nu$ . La quantité  $d\sigma^+/dE_l$  est fonction de la polarisation du quark top  $t$  alors que la quantité  $d\sigma^-/dE_l$  est fonction de la polarisation de l'anti-quark top  $\bar{t}$  [166].

À des énergies dans le centre de masse comprises dans l'intervalle  $10^2 GeV - 10^3 GeV$ , les asymétries liées à la violation de CP de Eq.(5.18) sont de l'ordre de [166],

$$\mathcal{A}^{pol} \approx (10^{-2} - 10^{-3}) \sin \psi, \quad (5.19)$$

si l'on suppose que toutes les masses des sfermions (toutes les valeurs absolues des constantes de couplage  $\mathcal{R}_p$  de type  $\lambda'$ ) sont égales à une même valeur  $\tilde{m} = 100 GeV$  ( $\Lambda$ ). Le résultat de Eq.(5.19) a été obtenu en supposant que seuls les produits de constantes de couplage  $\mathcal{R}_p$  impliquées dans les processus à l'ordre d'une boucle ont une phase complexe et que cette phase complexe  $\psi$  est identique pour tous ces produits de constantes de couplage  $\mathcal{R}_p$ , c'est à dire dans nos notations  $arg(t_i^{23}) = 0$  et  $arg(l_\alpha^{23}) = \psi$  pour tout  $i$  et  $\alpha$ .

Les asymétries définies dans Eq.(5.18) ont une dépendance dans les constantes de couplage  $\mathcal{R}_p$  du type,

$$\frac{\sum_i \sum_\alpha Im(t_i^{23} l_\alpha^{23*})}{|\sum_i t_i^{23}|^2}, \quad (5.20)$$

qui pourrait conduire à un important facteur de réduction ou d'augmentation si une grande hiérarchie existait parmi les constantes de couplage  $\mathcal{R}_p$  dans l'espace des saveurs.

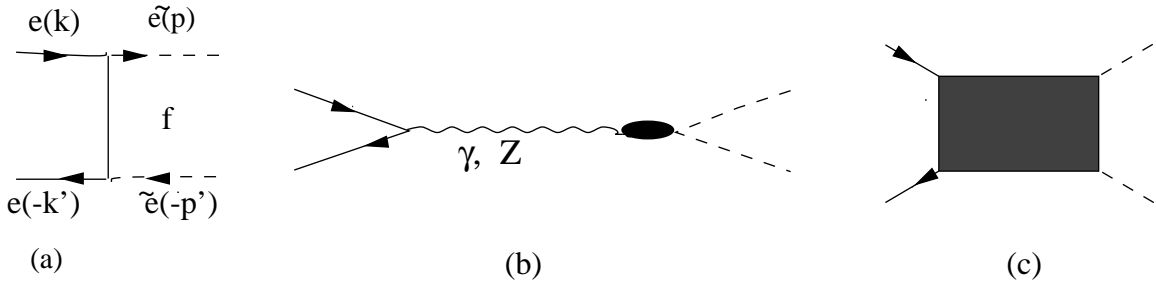


FIG. 5.5: Diagrammes de Feynman des contributions des interactions  $\mathcal{R}_p$  à la réaction  $l^+l^- \rightarrow \tilde{e}_{HJ}\tilde{e}_{HJ}^*$  [ $H = L, R$ ;  $J \neq J'$ ].  $f$  dénote un fermion et  $\tilde{e}$  un slepton chargé. Les diagrammes de Feynman des contributions à l'ordre d'une boucle au vertex  $Z^0\tilde{e}_{HJ}\tilde{e}_{HJ}^*$  [ $H = L, R$ ;  $J \neq J'$ ] sont présentés dans la Figure 5.6.

Nous avons vu dans [166] que les erreurs statistiques sur les asymétries définies dans Eq.(5.18) sont du même ordre de grandeur que les asymétries elles-mêmes pour une luminosité de  $\mathcal{L} = 100fb^{-1}$  et une valeur du produit de constantes de couplage  $\mathcal{R}_p$  impliqué dans le processus au niveau en arbre de  $\lambda'_{12k}\lambda_{13k}^* = 0.1$ . Cependant, si la structure des constantes de couplage  $\mathcal{R}_p$  exhibait une forte hiérarchie dans l'espace des saveurs, les valeurs des asymétries seraient augmentées devenant ainsi supérieures aux incertitudes statistiques. Par ailleurs, un calcul des incertitudes statistiques plus précis que celui effectué dans [166] donnerait des résultats plus optimistes.

Pour des énergies comprises dans l'intervalle  $10^2GeV - 10^3GeV$ , la quantité  $2\sigma_{JJ'} \times \mathcal{A}^{pol} \times 500fb^{-1}$  ( $\mathcal{A}^{pol}$  étant défini dans Eq.(5.18)) est de l'ordre de  $(1 - 10)(\Lambda/0.1)^4 (100GeV/\tilde{m})^2 - 3 \sin \psi$ . Par conséquent, pour le processus  $l^+l^- \rightarrow c\bar{t} / \bar{c}t$ ,  $\bar{t} \rightarrow b\bar{l}\nu / t \rightarrow b\bar{l}\nu$  [ $l = e, \mu$ ], la conclusion concernant les asymétries de type  $\mathcal{A}^{pol}$  est identique à celle concernant les asymétries de violation de CP définies dans Eq.(5.12) : si les constantes de couplage  $\mathcal{R}_p$  ne sont pas effectivement proches de leur limite actuelle [86] et si la structure des constantes de couplage  $\mathcal{R}_p$  n'exhibe pas de forte hiérarchie dans l'espace des saveurs, les contributions des interactions  $\mathcal{R}_p$  aux asymétries de violation de CP seront difficilement observables auprès des futurs collisionneurs linéaires [83, 127].

Remarquons finalement qu'une étude dans le même contexte de la réaction  $l^+l^- \rightarrow ut \rightarrow ubl\nu$ , [ $l = e, \mu$ ] donnerait des résultats semblables sur les phases complexes du produit dominant de constantes de couplage  $\lambda'_{11k}\lambda_{13k}^*$  car l'état final que nous avons effectivement considéré est  $2 jets + l + \nu$ .

## 5.3 Production de paires de sfermions

### 5.3.1 Taux de changement de saveur

Les graphes de Feynman des contributions des interactions  $\mathcal{R}_p$  à la réaction du type de Eq.(5.2),  $l^+l^- \rightarrow \tilde{e}_{HJ}\tilde{e}_{HJ}^*$  [ $H = L, R$ ;  $J \neq J'$ ], sont présentés dans les Figures 5.5 et 5.6. Nous avons considéré les contributions des interactions  $\mathcal{R}_p$  à l'ordre d'une boucle pour des raisons qui apparaîtront claires dans la Section 5.3.2.

Les contributions des interactions  $\mathcal{R}_p$  à la production de paires de sleptons chargés gauches appartenant à des familles différentes  $l^+l^- \rightarrow \tilde{e}_{LJ}\tilde{e}_{LJ}^*$  [ $J \neq J'$ ] impliquent les

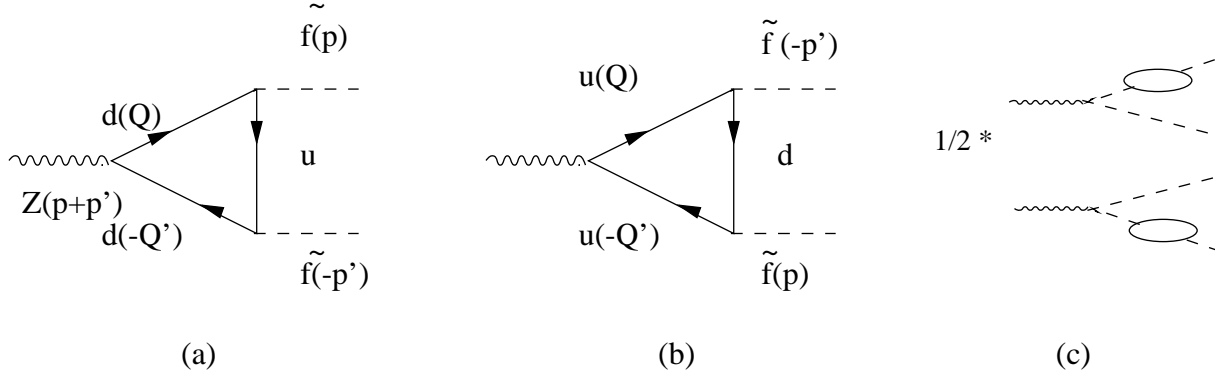


FIG. 5.6: Diagrammes de Feynman des contributions des interactions  $\mathcal{R}_p$  à l'ordre d'une boucle au vertex  $Z^0 \tilde{e}_{HJ} \tilde{e}_{HJ'}^*$  [ $H = L, R$ ;  $J \neq J'$ ].  $u$  et  $d$  dénotent des fermions et  $\tilde{f}$  un slepton chargé.

produits de constantes de couplage  $\lambda_{iJ'1} \lambda_{iJ1}^*$  (voie  $t$ ) au niveau en arbre (l'indice  $i$  correspond à la saveur du neutrino échangé) et  $\lambda_{J'jk} \lambda_{Jjk}^*$  ou  $\lambda'_{J'jk} \lambda_{Jjk}^*$  à l'ordre d'une boucle (les indices  $j$  et  $k$  correspondent aux saveurs des fermions échangés dans la boucle).

Les contributions des interactions  $\mathcal{R}_p$  à la production de paires de sleptons chargés droits appartenant à des familles différentes  $l^+ l^- \rightarrow \tilde{e}_{RJ} \tilde{e}_{RJ'}^*$  [ $J \neq J'$ ] impliquent les produits de constantes de couplage  $\lambda_{i1J} \lambda_{i1J'}^*$  (voie  $t$ ) au niveau en arbre (l'indice  $i$  correspond à la saveur du neutrino échangé) et  $\lambda_{ijJ} \lambda_{ijJ'}^*$  à l'ordre d'une boucle (les indices  $i$  et  $j$  correspondent aux saveurs des leptons échangés dans la boucle).

La production de paires de sleptons chargés gauche et droit appartenant à des familles différentes  $l^+ l^- \rightarrow \tilde{e}_{LJ} \tilde{e}_{RJ'}^*$  [ $J \neq J'$ ] ne reçoit pas de contributions des interactions  $\mathcal{R}_p$  au niveau en arbre pour des neutrinos de masses nulles et n'a donc pas été considérée.

Nous notons les amplitudes des contributions des interactions  $\mathcal{R}_p$  à la réaction  $l^+ l^- \rightarrow \tilde{e}_{HJ} \tilde{e}_{HJ'}^*$  [ $H = L, R$ ;  $J \neq J'$ ],

$$\tilde{M}^{JJ'} = a_0^{JJ'} + \sum_{\alpha} a_{\alpha}^{JJ'} F_{\alpha}^{JJ'}(s + i\epsilon), \quad (5.21)$$

$$\tilde{\bar{M}}^{JJ'} = a_0^{JJ'\star} + \sum_{\alpha} a_{\alpha}^{JJ'\star} F_{\alpha}^{JJ'}(s + i\epsilon), \quad (5.22)$$

où  $a_0^{JJ'}$  représente l'amplitude des contributions des interactions  $\mathcal{R}_p$  au niveau en arbre et  $\sum_{\alpha} a_{\alpha}^{JJ'} F_{\alpha}^{JJ'}(s + i\epsilon)$  l'amplitude des contributions des interactions  $\mathcal{R}_p$  à l'ordre d'une boucle.  $a_0^{JJ'}$  est proportionnel au produit de constantes de couplage  $\mathcal{R}_p$  impliqué par le processus au niveau en arbre et que l'on note  $t_i^{JJ'}$ ,  $i$  correspondant à la saveur du neutrino échangé au niveau en arbre. L'expression de  $a_0^{JJ'}$  fait intervenir une sommation sur l'indice  $i$  dont dépend aussi la masse du neutrino échangé. De même,  $a_{\alpha}^{JJ'}$  est proportionnel au produit de constantes de couplage  $\mathcal{R}_p$  impliqué dans la boucle et que l'on note  $l_{\alpha}^{JJ'}$ ,  $\alpha$  correspondant aux deux indices de saveur des fermions échangés dans la boucle. Enfin,  $F_{\alpha}^{JJ'}(s + i\epsilon)$  est une fonction issue d'un calcul de boucle ayant une partie imaginaire (voir [167]) et dépendant notamment des masses des fermions échangés dans la boucle et donc de  $\alpha$ .

Les contributions dominantes des interactions  $\mathcal{R}_p$  à la réaction du type de Eq.(5.2),  $l^+ l^- \rightarrow \tilde{e}_{HJ} \tilde{e}_{HJ'}^*$  [ $H = L, R$ ;  $J \neq J'$ ], proviennent de processus à l'ordre des arbres (voir Figure 5.5). Pour des énergies dans le centre de masse comprises dans l'intervalle

$10^2 GeV < \sqrt{s} < 10^3 GeV$ , les sections efficaces  $\tilde{\sigma}_{JJ'}$  de ces contributions sont de l'ordre de [167],

$$\tilde{\sigma}_{JJ'} \approx \left(\frac{\Lambda}{0.1}\right)^4 (2 - 20) fbarns, \quad (5.23)$$

si l'on suppose que toutes les masses des sfermions (toutes les valeurs absolues des constantes de couplage  $\mathcal{R}_p$  de type  $\lambda$ ,  $\lambda'$  ou  $\lambda''$ ) sont égales à une même valeur  $\tilde{m} < 400 GeV$  ( $\Lambda$ ).

Les limites actuelles sur les constantes de couplage  $\mathcal{R}_p$  sont typiquement de l'ordre de  $10^{-1}(\tilde{m}/100 GeV)$ ,  $\tilde{m}$  étant la masse des sfermions [86]. Par conséquent, les sections efficaces de Eq.(5.23) peuvent être supérieures à  $\sim 20 fbarns$ .

Étant donné les sections efficaces  $\tilde{\sigma}_{JJ'}$  de Eq.(5.23), les contributions des interactions  $\mathcal{R}_p$  à la réaction  $l^+ l^- \rightarrow \tilde{e}_{HJ} \tilde{e}_{HJ'}^*$  [ $H = L, R$ ;  $J \neq J'$ ] seront potentiellement observables aux futurs collisionneurs linéaires pour lesquels les luminosités attendues sont de l'ordre de  $500 fb^{-1}$  [83, 127].

Les sections efficaces de Eq.(5.23) sont du même ordre de grandeur que les sections efficaces des contributions des interactions du MSSM à la réaction  $l^+ l^- \rightarrow \tilde{e}_{HJ} \tilde{e}_{HJ'}^*$  [ $H = L, R$ ;  $J \neq J'$ ] qui sont comprises entre 0.1 (0.01) et 250 (100)  $fbarns$ , pour  $\sqrt{s} = 190 GeV$  ( $\sqrt{s} = 500 GeV$ ) [152].

### 5.3.2 Asymétries liées à la violation de CP

En remplaçant dans Eq.(5.4) les amplitudes par leur expression explicite (voir Eq.(5.22)), nous trouvons après calcul les expressions suivantes pour les asymétries liées à la violation de CP et associées aux contributions des interactions  $\mathcal{R}_p$  à la réaction  $l^+ l^- \rightarrow \tilde{e}_{HJ} \tilde{e}_{HJ'}^*$  [ $H = L, R$ ;  $J \neq J'$ ] [167],

$$\tilde{\mathcal{A}}_{JJ'} \approx \frac{2}{|a_0^{JJ'}|^2} \left[ \sum_{\alpha} Im(a_0^{JJ'} a_{\alpha}^{JJ'*}) Im(F_{\alpha}^{JJ'}(s + i\epsilon)) \right]. \quad (5.24)$$

L'observable définie dans Eq.(5.24) correspond à une interférence entre les amplitudes au niveau en arbre et à l'ordre d'une boucle. Nous remarquons que l'asymétrie de Eq.(5.24) n'est pas nulle uniquement si les constantes de couplage  $\mathcal{R}_p$  ont une phase complexe et si l'on considère les parties imaginaires issues des calculs de boucle.

À des énergies dans le centre de masse comprises dans l'intervalle  $10^2 GeV < \sqrt{s} < 10^3 GeV$ , les asymétries liées à la violation de CP de Eq.(5.24) sont de l'ordre de [167],

$$\tilde{\mathcal{A}}_{JJ'} \approx (10^{-2} - 10^{-3}) \sin \psi, \quad (5.25)$$

si l'on suppose que toutes les masses des sfermions (toutes les valeurs absolues des constantes de couplage  $\mathcal{R}_p$  de type  $\lambda$ ,  $\lambda'$  ou  $\lambda''$ ) sont égales à une même valeur notée  $\tilde{m}$  ( $\Lambda$ ). Le résultat de Eq.(5.25) a été obtenu en supposant que seuls les produits de constantes de couplage  $\mathcal{R}_p$  impliquées dans les processus à l'ordre d'une boucle ont une phase complexe et que cette phase complexe  $\psi$  est identique pour tous ces produits de constantes de couplage  $\mathcal{R}_p$ , c'est à dire dans nos notations  $arg(t_i^{JJ'}) = 0$  et  $arg(l_{\alpha}^{JJ'}) = \psi$  pour tout  $i$ ,  $\alpha$ ,  $J$  et  $J'$ .

Les asymétries définies dans Eq.(5.24) ont une dépendance dans les constantes de couplage  $\mathcal{R}_p$  du type,

$$\frac{\sum_i \sum_\alpha \text{Im}(t_i^{JJ'} l_\alpha^{JJ'\star})}{|\sum_i t_i^{JJ'}|^2}, \quad (5.26)$$

qui pourrait conduire à un important facteur de réduction ou d'augmentation si une grande hiérarchie existait parmi les constantes de couplage  $\mathcal{R}_p$  dans l'espace des saveurs. À titre d'exemple, supposons que les constantes de couplage  $\mathcal{R}_p$  soient égales à leur limite indirecte actuelle provenant des contraintes de la physique de basse énergie [86]. Dans ce cas, un facteur  $\frac{\text{Im}(\lambda_{331}\lambda_{321}^*\lambda_{233}\lambda_{333}^*)}{|\lambda_{131}\lambda_{121}^*|^2} \approx 90 \sin \psi$ , correspondant à  $J = 3$  et  $J' = 2$ , apparaîtrait dans les asymétries issues des contributions des interactions  $\lambda$  (au niveau en arbre) et  $\lambda'$  (à l'ordre d'une boucle) à la réaction  $l^+ l^- \rightarrow \tilde{e}_{LJ} \tilde{e}_{LJ'}^*$  [ $J \neq J'$ ].

Pour des énergies dans le centre de masse supérieures à  $500 \text{ GeV}$  et une masse universelle des sfermions  $\tilde{m} < 400 \text{ GeV}$ , la quantité  $2\tilde{\sigma}_{JJ'} \times \tilde{\mathcal{A}}_{JJ'}$  est de l'ordre de  $(\Lambda/0.1)^4 10^{-1} \sin \psi \text{ fbarns}$ . Par conséquent, Les asymétries liées à la violation de CP et associées aux contributions des interactions  $\mathcal{R}_p$  à la réaction  $l^+ l^- \rightarrow \tilde{e}_{HJ} \tilde{e}_{HJ'}^*$  [ $H = L, R; J \neq J'$ ] seront potentiellement détectables auprès des futurs collisionneurs linéaires dont les luminosités devraient atteindre  $500 \text{ fb}^{-1}$  pour  $\sqrt{s} > 500 \text{ GeV}$  [83, 127].

Pour une masse universelle des sfermions  $\tilde{m} < 400 \text{ GeV}$ , la quantité  $2\tilde{\sigma}_{JJ'} \times \tilde{\mathcal{A}}_{JJ'}$  ( $\tilde{\mathcal{A}}_{JJ'}$  étant défini dans Eq.(5.4)) est de l'ordre de  $(\Lambda/0.1)^4 (10^{-1} - 10^0) \sin \psi \text{ fbarns}$ . Cette valeur typique est inférieure à la valeur de la quantité  $\tilde{\sigma}_{JJ'} - \tilde{\sigma}_{J'J} \approx (3 - 16) \text{ fbarns}$  issue des contributions à la réaction  $l^+ l^- \rightarrow \tilde{e}_{HJ} \tilde{e}_{HJ'}^*$  [ $H = L, R; J \neq J'$ ] provenant des oscillations des sleptons dans le cadre du MSSM [145]. Mentionnons cependant que les contributions provenant de l'oscillation des sleptons peuvent dépendre davantage du modèle considéré que les contributions calculées ci-dessus et que les prédictions de [145] ont été obtenues dans le cadre d'hypothèses tendant à maximiser les effets de violation de CP.



# Bibliographie

- [1] S. Coleman and J. Mandula, Phys. Rev. **159** (1967) 1251.
- [2] Yu. A. Gol’fand and E. P. Likhtman, JETP Lett. **13** (1971) 323.
- [3] R. Haag, J. Lopuszanski and M. Sohnius, Nucl. Phys. **B 88** (1975) 257.
- [4] J. Wess and J. Bagger, “Supersymmetry and Supergravity”, Princeton Series in Physics, ed. P. W. Anderson and A. S. Wightman.
- [5] J. Wess and B. Zumino, Nucl. Phys. **B 70** (1974) 39.
- [6] A. Salam and J. Strathdee, Nucl. Phys. **B 76** (1974) 477.
- [7] A. Salam and J. Strathdee, Nucl. Phys. **B 80** (1974) 499.
- [8] S. Ferrara, B. Zumino and J. Wess, Phys. Lett. **B 51** (1974) 239.
- [9] D. F. Brewer, “Supersymmetry, Superfields and Supergravity : an introduction”, Graduate Student Series in Physics.
- [10] S. Ferrara, “Supersymmetry”, North Holland/World Scientific.
- [11] J. C. Pati and A. Salam, Phys. Rev. **D 10** (1974) 275.
- [12] H. Georgi and S. L. Glashow, Phys. Rev. Lett. **32** (1974) 438.
- [13] R. N. Mohapatra, “Unification and Supersymmetry”, Second Edition, Graduate Texts in Contemporary Physics, Springer-Verlag.
- [14] G. G. Ross, “Grand Unified Theories”, Frontiers in Physics, The Benjamin/Cummings Publishing Company, Inc.
- [15] L. E. Ibañez and G. G. Ross, Phys. Lett. **B 105** (1981) 439.
- [16] L. E. Ibañez and G. G. Ross, Phys. Lett. **B 110** (1982) 215.
- [17] E. Cremmer, S. Ferrara, C. Kounnas and D. V. Nanopoulos, Phys. Lett. **B 133** (1983) 61.
- [18] J. Ellis, A. B. Lahanas, D. V. Nanopoulos and K. Tamvakis, Phys. Lett. **B 134** (1984) 429.
- [19] J. Ellis, C. Kounnas and D. V. Nanopoulos, Nucl. Phys. **B 247** (1984) 373.
- [20] R. Barbieri, E. Cremmer and S. Ferrara, Phys. Lett. **B 163** (1985) 143.
- [21] D. Bailin and A. Love, “Supersymmetric gauge field theory and string theory”, Graduate student series in physics, Institute of physics publishing, ed. by Prof. Douglas F. Brewer.
- [22] J.-P. Derendinger, Lectures Notes on “Globally Supersymmetric Theories in Four and Two Dimensions”, ETH-TH / 90-21 (Juillet 1990).



- [23] G. F. Giudice and R. Rattazzi, Phys. Rep. **322** (1999) 419 ; **322** (1999) 50.
- [24] M. E. Peskin and D. V. Schroeder, “An Introduction to Quantum Field Theory”, Addison-Wesley Publishing Company, 1995.
- [25] L. E. Ibañez and G. G. Ross, CERN-TH.6412/92, in *Perspectives in Higgs Physics*, ed. by G. L. Kane, World Scientific, Singapore, 1993.
- [26] H. E. Haber and G. L. Kane, Phys. Rep. **117** (1985) 175.
- [27] M. Dine, R. Leigh and A. Kagan, Phys. Rev. **D 48** (1993) 2214.
- [28] Y. Nir and N. Seiberg, Phys. Lett. **B 309** (1993) 337.
- [29] S. Dimopoulos, G. F. Giudice and N. Tetradis, Nucl. Phys. **B 454** (1995) 59.
- [30] E. Cremmer, S. Ferrara, L. Girardello and A. van Proeyen, Nucl. Phys. **B 212** (1983) 413.
- [31] P. West, “Introduction to Supersymmetry and Supergravity”, World Scientific, Singapore, 1986.
- [32] J. Wess and J. Bagger, “Supersymmetry and Supergravity”, Princeton Univ. Press, 1983.
- [33] E. Cremmer, B. Julia, J. Sherk, S. Ferrara, L. Girardelli and P. van Nieuwenhuizen, Nucl. Phys. **B 147** (1979) 105.
- [34] H. P. Nilles, Phys. Rep. **110** (1984) 1.
- [35] S. Weinberg, Phys. Rev. **D 26** (1982) 287.
- [36] N. Sakai and T. Yanagida, Phys. Lett. **B 197** (1982) 533.
- [37] I. Hinchliffe and T. Kaeding, Phys. Rev. **D 47** (1993) 279.
- [38] J. L. Goity and M. Sher, Phys. Lett. **B 346** (1995) 69, Erratum-ibid. **B 385** (1996) 500.
- [39] C. E. Carlson, P. Roy and M. Sher, Phys. Lett. **B 357** (1995) 99.
- [40] Particle Data Group, Phys. Rev. **D 54** (1996) 1.
- [41] A. Y. Smirnov and F. Vissani, Phys. Lett. **B 380** (1996) 317.
- [42] J. Ellis, J. Hagelin, D. Nanopoulos and K. Tamvakis, Phys. Lett. **B 124** (1983) 484.
- [43] A. Salam and J. Strathdee, Nucl. Phys. **B 87** (1975) 85.
- [44] P. Fayet, Nucl. Phys. **B 90** (1975) 104.
- [45] P. Fayet, Phys. Lett. **B 70** (1977) 461.
- [46] Particle Data Group, Eur. Phys. Jour. **C 3** (1998) 1.
- [47] L. Hall and L. Randall, Nucl. Phys. **B 352** (1991) 289.
- [48] R. Barbieri, L. Girardello and A. Masiero, Phys. Lett. **B 127** (1983) 429 ; R. Barbieri and L. Maiani, Nucl. Phys. **B 243** (1984) 429.
- [49] G. Farrar and A. Masiero, Rutgers Preprint RU-94-38, hep-ph/9410401.
- [50] A. M. Cooper et al., Phys. Lett. **B 160** (1985) 212 ; H. E. Haber in *Supersymmetry and Unification of Fundamental Interactions*, World Scientific, Singapore, 1993, hep-ph/9308235 ; M. Barnett, talk given at SUSY’95, Paris, France, May 1995.
- [51] R. D. Peccei, in *CP Violation*, ed. C. Jarlskog, World Scientific, Singapore, 1989.

- [52] W. Buchmüller, D. Wyler, Phys. Lett. **B 121** (1983) 321.
- [53] I. Affleck and M. Dine, Phys. Lett. **B 154** (1985) 368.
- [54] A. E. Nelson and N. Seiberg, Nucl. Phys. **B 416** (1994) 46.
- [55] L. Hall and L. Randall, Nucl. Phys. **B 352** (1991) 289.
- [56] M. Dine and D. A. MacIntire, Phys. Rev. **D 46** (1992) 2594.
- [57] E. J. Chun, J.E. Kim and H.P. Nilles, Nucl. Phys. **B 370** (1992) 105.
- [58] J. E. Kim and H. P. Nilles, Mod. Phys. Lett. **A 9** (1994) 3575.
- [59] J. E. Kim and H. P. Nilles, Phys. Lett. **B 138** (1984) 150.
- [60] L. E. Ibañez and G. G. Ross, Nucl. Phys. **B 368** (1992) 3.
- [61] S. Dimopoulos and H. Georgi, Nucl. Phys. **B 193** (1981) 150.
- [62] N. Sakai, Z. Phys. **C 11** (1981) 153.
- [63] H. P. Nilles and S. Raby, Nucl. Phys. **B 198** (1982) 102.
- [64] N. Sakai and T. Yanagida, Nucl. Phys. **B 197** (1982) 533.
- [65] S. Dimopoulos, S. Raby and F. Wilczek, Phys. Lett. **B 112** (1982) 133.
- [66] G. Farrar and P. Fayet, Phys. Lett. **B 76** (1978) 575.
- [67] L. Hall and M. Suzuki, Nucl. Phys. **B 231** (1984) 419.
- [68] For a review and references see : T. Banks, Santa Cruz preprint SCIPP 89/17 (1989).
- [69] G. Gilbert, Nucl. Phys. **B 328** (1989) 159 and references therein.
- [70] T. Banks, Nucl. Phys. **B 323** (1989) 90 ; L. Krauss, Gen. Rel. Grav. **22** (1990) 50 ; M. Alford et al., Nucl. Phys. **B 337** (1990) 695 ; J. Preskill and L. Krauss, Nucl. Phys. **B 341** (1990) 50 ; M. Alford et al., preprint HUTP-90/A040 (1990).
- [71] L. E. Ibañez and G. G. Ross, Phys. Lett. **B 260** (1991) 291.
- [72] T. Banks and M. Dine, Phys. Rev. **D 45** (1992) 1424.
- [73] A. H. Chamseddine and H. Dreiner, Nucl. Phys. **B 447** (1995) 195.
- [74] A. H. Chamseddine and H. Dreiner, Nucl. Phys. **B 458** (1996) 65.
- [75] T. Banks, Y. Grossman, E. Nardi and Y. Nir, Phys. Rev. **D 52** (1995) 5319.
- [76] D. J. Castaño, D. Z. Freedman and C. Manuel, Nucl. Phys. **B 461** (1996) 50.
- [77] G. F. Giudice and R. Rattazzi, Phys. Lett. **B 406** (1997) 321.
- [78] D. Brahm and L. Hall, Phys. Rev. **D 40** (1989) 2449.
- [79] K. Tamvakis, Phys. Lett. **B 382** (1996) 251.
- [80] A. Y. Smirnov and F. Vissani, Nucl. Phys. **B 460** (1996) 37 ; R. Hempfling, Nucl. Phys. **B 478** (1996) 3 ; K. Tamvakis, Phys. Lett. **B 383** (1996) 307 ; R. Barbieri, Z. Berezhiani and A. Strumia, Phys. Lett. **B 407** (1997) 250 ;
- [81] M. Bento, L. Hall and G. G. Ross, Nucl. Phys. **B 292** (1987) 400.
- [82] N. Ganoulis, G. Lazarides and Q. Shafi, Nucl. Phys. **B 323** (1989) 374.
- [83] ‘Conceptual Design Report of a 500GeV  $e^+e^-$  Linear Collider with Integrated X-ray Laser Facility’, DESY 1997-048, ECFA 1997-182, ed. R. Brinkmann, G. Materlik, J. Rossbach and A. Wagner, [www.desy.de/~schreibr/cdr/cdr.html](http://www.desy.de/~schreibr/cdr/cdr.html).  
See also [wwwhephy.oeaw.ac.at/susy/lcws/tdr.html](http://wwwhephy.oeaw.ac.at/susy/lcws/tdr.html).

- [84] H. Dreiner and G. G. Ross, Nucl. Phys. **B 365** (1991) 597.
- [85] H. Dreiner, published in *Perspectives on Supersymmetry*, ed. G. L. Kane, World Scientific (1998), hep-ph/9707435.
- [86] G. Bhattacharyya, Invited talk presented at ‘Beyond the Desert’, Castle Ringberg, Tegernsee, Germany, 8-14 June 1997; Susy ’96, Nucl. Phys. B Proc. Suppl. **A 52** (1997) 83.
- [87] R. Barbier et al., Report of the French Group on the R-parity Violation, hep-ph/9810232.
- [88] S. Dimopoulos, R. Esmailzadeh, L. J. Hall, J. Merlo and G.D. Starkman, Phys. Rev. **D 41** (1990) 2099.
- [89] P. Binétruy et al., ECFA Large Hadron Collider (LHC) Workshop, Aachen, 1990, Vol. II.
- [90] D. K. Ghosh, S. Raychaudhuri and K. Sridhar, Phys. Lett. **B 396** (1997) 177.
- [91] A. Datta, J. M. Yang, B.-L. Young and X. Zhang, Phys. Rev. **D 56** (1997) 3107.
- [92] R. J. Oakes, K. Whisnant, J. M. Yang, B.-L. Young and X. Zhang, Phys. Rev. **D 57** (1998) 534.
- [93] S. Bar-Shalom, G. Eilam and A. Soni, Phys. Rev. **D 59** (1999) 055012.
- [94] J. L. Hewett and T. G. Rizzo, “*Proceedings of the XXIX International Conference on High Energy Physics*”, Vancouver, CA, 23-29 July 1998, hep-ph/9809525.
- [95] S. Dimopoulos and L. J. Hall, Phys. Lett. **B 207** (1988) 210.
- [96] V. Barger, G. F. Giudice and T. Han, Phys. Rev. **D 40** (1989) 2987.
- [97] J. Kalinowski, R. Rückl, H. Spiesberger and P. M. Zerwas, Z. Phys. **C 74** (1997) 595.
- [98] J. Kalinowski, R. Rückl, H. Spiesberger and P. M. Zerwas, Phys. Lett. **B 406** (1997) 314.
- [99] J. Kalinowski, Talk presented at the 5th International Workshop on “*Deep Inelastic Scattering and QCD*” (DIS’97), Chicago, Illinois, USA, April 14-18, 1997, hep-ph/9706203.
- [100] J. Kalinowski, R. Rückl, H. Spiesberger and P. M. Zerwas, Phys. Lett. **B 414** (1997) 297.
- [101] J. Kalinowski, Proceedings of “*Beyond the Desert 97 – Accelerator and Non-Accelerator Approaches*”, Ringberg Castle, Germany, June 1997, hep-ph/9708490.
- [102] J. Kalinowski, Acta Phys. Polon. **B 28** (1997) 2423.
- [103] ALEPH Collaboration, submitted to ICHEP’98 (Abstract Number 949), ALEPH 98-070, CONF 039 (1998).
- [104] Y. Arnoud et al., DELPHI Collaboration, submitted to HEP’97 (Abstract Number 589), DELPHI 97-119, CONF 101 (1997).
- [105] N. Benekos et al., DELPHI Collaboration, submitted to HEP’99 (Abstract Number 7.209), DELPHI 99-79, CONF 266 (1999).
- [106] J. Erler, J. L. Feng and N. Polonsky, Phys. Rev. Lett. **78** (1997) 3063.

- [107] J. L. Feng, J. F. Gunion and T. Han, Phys. Rev. **D 58** (1998) 071701 ; J. L. Feng, Proceedings of the Workshop on Physics at the First Muon Collider and at the Front End of a Muon Collider, Fermi National Accelerator Laboratory, 6-9 november 1997, hep-ph/9801248.
- [108] S. Bar-Shalom, G. Eilam and A. Soni, Phys. Rev. Lett. **80** (1998) 4629.
- [109] D. Choudhury and S. Raychaudhuri, hep-ph/9807373.
- [110] D. Choudhury, Phys. Lett. **B 376** (1996) 201.
- [111] D. K. Ghosh, R. M. Godbole, S. Raychaudhuri, hep-ph/9904233.
- [112] V. Barger et al., Phys. Rev. **D 50** (1994) 4299.
- [113] H. Baer, C. Kao and X. Tata, Phys. Rev. **D 51** (1995) 2180.
- [114] H. Baer, C.-H. Chen and X. Tata, Phys. Rev. **D 55** (1997) 1466.
- [115] B. Allanach et al., ‘Searching for R-Parity Violation at Run-II of the Tevatron’, hep-ph/9906224.
- [116] ATLAS Coll., ‘ATLAS Detector and Physics Performance Technical Design Report’, Vol. II, ATLAS TDR 15, 25 May 1999, CERN/LHCC 99-15, atlasinfo.cern.ch/Atlas-/GROUPS/PHYSICS/TDR/access.html.
- [117] A. Pukhov, E. Boos, M. Dubinin, V. Edneral, V. Ilyin, D. Kovalenko, A. Kryukov, V. Savrin, S. Shichanin, and A. Semenov, ”CompHEP - a package for evaluation of Feynman diagrams and integration over multi-particle phase space. User’s manual for version 33.”, Preprint INP MSU 98-41/542, hep-ph/9908288.
- [118] CTEQ Coll., Phys. Rev. **D 55** (1997) 1280.
- [119] SUSYGEN 3.0/06, ‘A Monte Carlo Event generator for MSSM sparticle production for  $e^+e^-$ ,  $\mu^+\mu^-$  and  $ep$  colliders’, N. Ghodbane, S. Katsanevas, P. Morawitz and E. Perez, lyoinfo.in2p3.fr/susygen/susygen3.html.
- [120] T. Sjöstrand, Comp. Phys. Comm. **82** (1994) 74 ; S. Mrenna, Comp. Phys. Comm. **101** (1997) 232.
- [121] D. O. Carlson, S. Mrenna, C. P. Yuan, private communication ; D. O. Carlson and C. P. Yuan, Phys. Lett. **B 306** (1993) 386.
- [122] HERWIG 6.1 Release Note, hep-ph/9912396 ; G. Marchesini, B. R. Webber, G. Abbiendi, I. G. Knowles, M. H. Seymour and L. Stanco, Comp. Phys. Comm. **67** (1992) 465.
- [123] J. Conway, talk given at the SUSY/Higgs Workshop Meeting, Fermilab, May 14-16, 1998.  
See also [www.physics.rutgers.edu/jconway/soft/shw/shw.html](http://www.physics.rutgers.edu/jconway/soft/shw/shw.html).
- [124] E. Richter-Was, D. Froidevaux, L. Poggioli, “*ATLFAST 2.0 : a fast simulation package for ATLAS*”, ATLAS Internal Note ATL-PHYS-98-131 (1998).
- [125] ALEPH Collaboration, ALEPH 98-017, CONF 007 (1998).
- [126] ALEPH Collaboration, ALEPH 2000-013, CONF 010 (2000).
- [127] J. A. Bagger, Nucl. Phys. (Proc. Suppl.) **B 62** (1998) 23.
- [128] E. Perez, Y. Sirois and H. Dreiner, Published in the Proceedings of the Workshop “*Future Physics at HERA*”, ed. by G. Ingelman, A. De Roeck and R. Klanner, hep-ph/9703444.

- [129] H. Dreiner, P. Richardson and M. H. Seymour, hep-ph/0007228.
- [130] H. Dreiner and S. Lola, published in “Munich-Annecy-Hamburg 1991/93, Proceedings,  $e^+e^-$  Collisions at 500 GeV : The Physics Potential”, DESY 92-123A+B, 93-123C; “Annecy-Gran Sasso-Hamburg 1995, Proceedings,  $e^+e^-$  Collisions at TeV Energies : The Physics Potential”, DESY 96-123D, ed. P. M. Zerwas; “Searches for New Physics”, contribution to the LEP II Workshop, 1996, hep-ph/9602207; “Physics with  $e^+e^-$  Linear Colliders”, DESY-97-100, hep-ph/9705442.
- [131] F. Ledroit-Guillon and R. López-Fernández, DELPHI Collaboration, DELPHI 98-165 PHYS 805.
- [132] F. Ledroit-Guillon and R. López-Fernández, DELPHI Collaboration, DELPHI 99-30, CONF 229 (1999).
- [133] N. Ghodbane, hep-ph/9909499.
- [134] V. Barger, “*Physics at Muon Colliders*”, Talk present at FCP97, Workshop on Fundamental Particles and Interactions, Vanderbilt University, May 1997, hep-ph/9801441.
- [135] J. F. Gunion, “*Muon Colliders : The Machine and The Physics*”, Proceedings of “*Beyond the Standard Model V*”, Balholm, Norway, May, 1997, hep-ph/9707379.
- [136] B. C. Allanach, H. Dreiner, P. Morawitz and M. D. Williams, hep-ph/9708495.
- [137] ALEPH Collaboration, ALEPH contribution to the 2000 Winter Conferences, ALEPH 2000-027, CONF 022 (2000).
- [138] D. E. Kaplan, “*Violating R parity at the B factory*”, hep-ph/9703347.
- [139] D. Guetta, Phys. Rev. **D 58** (1998) 116008.
- [140] J.-H. Jang and J. S. Lee, KAIST-TH 98/12, hep-ph/9808406.
- [141] M. Frank and H. Hamidian, J. Phys. *G* **24** (1998) 2203.
- [142] C. H. Chen, C. Q. Geng and C. C. Lih, Phys. Rev. **D 56** (1997) 6856.
- [143] J. Bernabéu, A. Santamaria and M.B. Gavela, Phys. Rev. Lett. **57** (1986) 1514.
- [144] W.-S. Hou, N.G. Deshpande, G. Eilam and A. Soni, Phys. Rev. Lett. **57** (1986) 1406.
- [145] N. Arkani-Hamed, J. L. Feng and L. J. Hall, Nucl. Phys. **B 505** (1997) 3.
- [146] J. Bernabéu and M. B. Gavela, in “*CP violation*”, ed. C. Jarlskog (World Scientific, Singapore, 1988); D. Chang, Workshop on physics at current accelerators and supercolliders, (June 2-5, 1993, Argonne Nat. Lab.); A. Soni, Nucl. Phys. B (Proc. Suppl.) **A 51** (1996) 32.
- [147] D. Atwood, S. Bar-Shalom, G. Eilam and A. Soni, Phys. Rev. **D 54** (1996) 5412.
- [148] E. Gabrielli, A. Masiero and L. Silvestrini, Proceedings of “*Susy 95*”, International Workshop on Supersymmetry and Unification of Fundamental Interactions, ed. by I. Antoniadis and H. Videau.
- [149] S. Bar-Shalom, G. Eilam and A. Soni, Phys. Rev. Lett. **80** (1998) 4629.
- [150] S. Bar-Shalom, G. Eilam and A. Soni, Phys. Rev. **D 59** (1999) 055012.
- [151] D. Atwood, L. Reina and A. Soni, Phys. Rev. **D 53** (1996) 1199; **D 55** (1997) 3157.

- [152] N. Arkani-Hamed, H. C. Cheng, J. L. Feng and L. J. Hall, Phys. Rev. Lett. **77** (1996) 1937.
- [153] Particle Data Group, L. Wolfenstein and T. G. Trippe, Eur. Phys. Jour. **C 3** (1998) 62.

### Bibliographie de l'auteur :

- [154] R. Barbier et al., Report of the GDR working group on the R-parity violation, hep-ph/9810232.
- [155] R. Barbier, C. Bérat, M. Besançon, M. Chemtob, A. Deandrea, E. Dudas, P. Fayet, S. Lavignac, F. Ledroit-Guillon, G. Moreau and Y. Sirois, Review on R-parity violating supersymmetry, to be submitted to Phys. Rep.
- [156] G. Moreau, “*Etudes phénoménologiques de la violation de R parité*”, Proceedings of the ‘Rencontres Jeunes Chercheurs 1998’, ed. by the ‘Société Française de Physique’.
- [157] F. Déliot, G. Moreau, C. Royon, E. Perez and M. Chemtob, “*Resonant sneutrino production at Tevatron Run II*”, Phys. Lett. **B 475** (2000) 184, hep-ph/9910341.
- [158] F. Déliot, G. Moreau and C. Royon, “*Single superpartner production at Tevatron Run II*”, to appear in Eur. Phys. Jour. **C**, hep-ph/0007288.
- [159] G. Moreau, E. Perez and G. Polesello, “*The three-leptons signature from resonant sneutrino production at the LHC*”, Proceedings of the Workshop “*Physics at TeV Colliders*”, 8-18 June, 1999, Les Houches, France, hep-ph/0002130, hep-ph/0005142.
- [160] G. Moreau, E. Perez and G. Polesello, “*The three-leptons signature from resonant sneutrino production at the LHC*”, to appear in Nucl. Phys. **B**, hep-ph/0003012.
- [161] M. Chemtob and G. Moreau, “*Systematics of single superpartners production at leptonic colliders*”, Phys. Rev. **D 59** (1999) 055003, hep-ph/9807509.
- [162] M. Besançon and G. Moreau, “*Experimental aspects of supersymmetry with R-parity violating couplings at the  $e^+e^-$  Linear Collider*”, Contribution to the Proceedings of the International Workshop on Linear Colliders, April 28-May 5, 1999, Sitges, Spain, hep-ph/9909441.
- [163] G. Moreau, “*Single chargino production at linear colliders*”, Linear Collider note LC-TH-2000-040, hep-ph/0009140.
- [164] Participation to the TESLA Technical Design Report (T.D.R.) to be published in March 2001, Physics Editorial Board : R.-D. Heuer, D. Miller, F. Richard and P. Zerwas ; Detector Editorial Board : T. Behnke, S. Bertolucci, R.-D. Heuer and R. Settles, see  
<http://www.desy.de/~lcnotes/tdr/>
- [165] M. Chemtob and G. Moreau, “*Broken R-parity contributions to flavor changing rates and CP asymmetries in fermion pair production at leptonic colliders*”, Phys. Rev. **D 59** (1999) 116012, hep-ph/9806494.
- [166] M. Chemtob and G. Moreau, “*Polarized single top production at leptonic colliders from broken R-parity interactions incorporating CP violation*”, Phys. Rev. **D 61** (2000) 116004, hep-ph/9910543.
- [167] M. Chemtob and G. Moreau, “*CP violation flavor asymmetries in slepton pair production at leptonic colliders from broken R-parity*”, Phys. Lett. **B 448** (1999) 57, hep-ph/9808428.
- [168] M. Chemtob and G. Moreau, “*R-parity violating contributions to flavor changing and CP violation effects in fermion and sfermion pair production*”, Contribution to the Proceedings of the International Workshop on Linear Colliders, April 28-May 5, 1999, Sitges, Spain, hep-ph/9909370.





## *PUBLICATIONS*



# Publication I



# Production of (s)particles at colliders through $\bar{R}_p$ interactions

G. Moreau

*Service de Physique Théorique  
CE-Saclay F-91191 Gif-sur-Yvette, Cedex France*

Part of the review on R-parity violating supersymmetry to be submitted to Phys. Rep.  
and written by R. Barbier, C. Bérat, M. Besançon, M. Chemtob, A. Deandrea,  
E. Dudas, P. Fayet, S. Lavignac, F. Ledroit-Guillon, G. Moreau and Y. Sirois

# 1 Singly Produced Sparticles at $e^+e^-$ Colliders

The measure of the  $\mathcal{R}_p$  coupling constants could be performed via the detection of the displaced vertex associated to the  $\mathcal{R}_p$  decay of the LSP. The sensitivities on the  $\mathcal{R}_p$  couplings obtained through this method depend on the detector geometry and performances. Let us estimate the largest values of the  $\mathcal{R}_p$  coupling constants that can be measured via the displaced vertex analysis. We suppose that the LSP is the lightest neutralino ( $\tilde{\chi}_1^0$ ). The flight length of the LSP in the laboratory frame is then given in meters by [13],

$$c\gamma\tau \sim 3\gamma \, 10^{-3}m\left(\frac{\tilde{m}}{100GeV}\right)^4\left(\frac{1GeV}{m_{LSP}}\right)^5\left(\frac{1}{\Lambda}\right)^2, \quad (1.1)$$

where  $\Lambda = \lambda, \lambda'$  or  $\lambda''$ ,  $c$  is the light speed,  $\gamma$  the Lorentz boost factor,  $\tau$  the LSP life time,  $m_{LSP}$  the LSP mass and  $\tilde{m}$  the mass of the supersymmetric scalar particle involved in the three-body  $\mathcal{R}_p$  decay of the LSP. Since the displaced vertex analysis is an experimental challenge at hadronic colliders, we consider here the futur linear colliders. Assuming that the minimum distance between two vertex necessary to distinguish them experimentally is of order  $2 \, 10^{-5}m$  at linear colliders, we see from Eq.(1.1) that the  $\mathcal{R}_p$  couplings could be measured up to the values,

$$\Lambda < 1.2 \, 10^{-4}\gamma^{1/2}\left(\frac{\tilde{m}}{100GeV}\right)^2\left(\frac{100GeV}{m_{LSP}}\right)^{5/2}. \quad (1.2)$$

There is a gap between these values and the low-energy experimental constraints on the  $\mathcal{R}_p$  couplings which range typically in the interval  $\Lambda < 10^{-1} - 10^{-2}$  for superpartners masses of  $100GeV$ . However, the domain lying between these low-energy bounds and the values of Eq.(1.2) can be tested through another way : The study of the single production of supersymmetric particles. Indeed, the cross sections of such reactions are directly proportional to a power of the relevant  $\mathcal{R}_p$  coupling constant(s), which allows to determine the values of the  $\mathcal{R}_p$  couplings. Therefore, there exists a complementarity between the displaced vertex analysis and the study of singly produced sparticles, since these two methods allow to investigate different ranges of values of the  $\mathcal{R}_p$  coupling constants.

Another interest of the single superpartner production is the possibility to produce supersymmetric particles at lower center of mass energies than through the superpartner pair production, which is the favored reaction in R-parity conserved models.

## 1.1 Resonant Production of Sneutrinos

At leptonic colliders, the sneutrinos  $\tilde{\nu}_\mu$  and  $\tilde{\nu}_\tau$  can be produced at the resonance through the couplings  $\lambda_{211}$  and  $\lambda_{311}$ , respectively. The sneutrino may then decay either via an  $\mathcal{R}_p$  interaction, for example through  $\lambda_{ijk}$  as,  $\tilde{\nu}^i \rightarrow \bar{l}_j l_k$ , or via gauge interaction as,  $\tilde{\nu}_L^i \rightarrow \tilde{\chi}_a^+ l^i$ , or,  $\tilde{\nu}_L^i \rightarrow \tilde{\chi}_a^0 \nu_L^i$  [14]. The sneutrino partial widths associated to the leptonic and gauge decay channel are given in the following equations [15],

$$\Gamma(\tilde{\nu}_L^i \rightarrow \bar{l}_j l_k) = \frac{\lambda_{ijk}^2}{16\pi} m_{\tilde{\nu}_L^i}, \quad (1.3)$$

$$\Gamma(\tilde{\nu}_L^i \rightarrow \tilde{\chi}_a^+ l^i, \tilde{\chi}_a^0 \nu_L^i) = \frac{C g^2}{16\pi} m_{\tilde{\nu}_L^i} \left(1 - \frac{m_{\tilde{\chi}_a^+}^2}{m_{\tilde{\nu}_L^i}^2}\right)^2, \quad (1.4)$$

where  $C = |V_{a1}|^2$  for the decay into chargino and  $C = |N_{a2}|^2$ , for the neutralino case, with  $V_{a1}$  and  $N_{a2}$  the mixing matrix elements written in the notations of [16]. For reasonable values of  $\lambda_{ijk}$  ( $\leq 0.1$ ) and most of the region of the supersymmetric parameter space, the decay modes of Eq.(1.4) are dominant, if kinematically accessible [17, 15]. In a SUGRA parameter space, if  $m_{\tilde{\nu}_L^i} > 80$  GeV, with  $M_2 = 80$  GeV,  $\mu = 150$  GeV and  $\tan\beta = 2$ , the total sneutrino width is higher than 100 MeV which is comparable to or greater than the typical expected experimental resolutions. The cross section formula, for the sneutrino production in the  $s$ -channel, is the following [15],

$$\sigma(e^+e^- \rightarrow \tilde{\nu}_L^i \rightarrow X) = \frac{4\pi s}{m_{\tilde{\nu}_L^i}^2} \frac{\Gamma(\tilde{\nu}_L^i \rightarrow e^+e^-)\Gamma(\tilde{\nu}_L^i \rightarrow X)}{(s - m_{\tilde{\nu}_L^i}^2)^2 + m_{\tilde{\nu}_L^i}^2 \Gamma_{\tilde{\nu}_L^i}^2}, \quad (1.5)$$

where  $\Gamma(X)$  generally denotes the partial width for the sneutrino decay into the final state  $X$ . At sneutrino resonance, Eq.(1.5) takes the form,

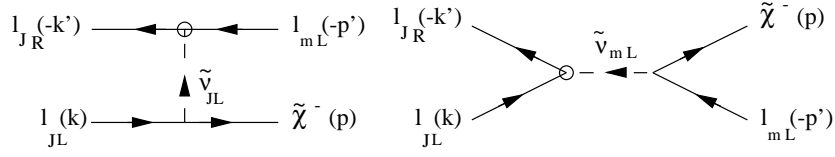
$$\sigma(e^+e^- \rightarrow \tilde{\nu}_L^i \rightarrow X) = \frac{4\pi}{m_{\tilde{\nu}_L^i}^2} B(\tilde{\nu}_L^i \rightarrow e^+e^-) B(\tilde{\nu}_L^i \rightarrow X), \quad (1.6)$$

where  $B(\tilde{\nu}_L^i \rightarrow X)$  generally denotes the partial width for sneutrino decay into a final state  $X$ .

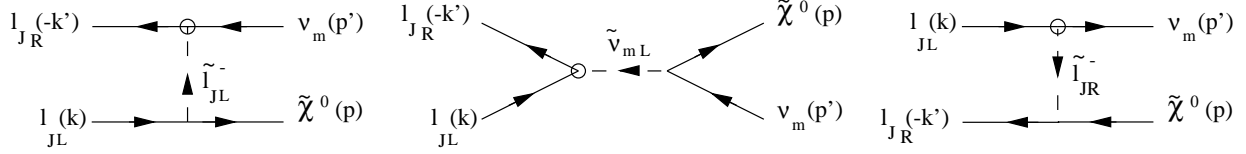
## 1.2 Single Gaugino Production

Two single superpartner productions receive the contribution from the resonant sneutrino production at  $e^+e^-$  colliders : The single chargino and neutralino productions (see Fig.1(a)(b)). The single production of chargino,  $e^+e^- \rightarrow \tilde{\chi}_a^\pm l_j^\mp$  (via  $\lambda_{1j1}$ ), receives a contribution from the  $s$ -channel exchange of a  $\tilde{\nu}_{jL}$  sneutrino and another one from the exchange of a  $\tilde{\nu}_{eL}$  sneutrino in the  $t$ -channel (see Fig.1(a)). The single neutralino production,  $e^+e^- \rightarrow \tilde{\chi}_a^0 \nu_j$  (via  $\lambda_{1j1}$ ), occurs through the  $s$ -channel  $\tilde{\nu}_{jL}$  sneutrino exchange and also via the exchange of a  $\tilde{e}_L$  slepton in the  $t$ -channel or a  $\tilde{e}_R$  slepton in the  $u$ -channel (see Fig.1(b)).

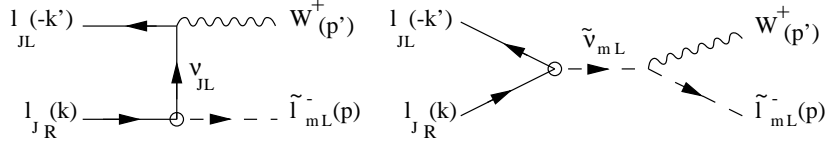
For  $\lambda_{1j1} = 0.05$ ,  $50 \text{ GeV} < m_0 < 150 \text{ GeV}$  and  $50 \text{ GeV} < M_2 < 200 \text{ GeV}$  in a SUGRA parameter space, the off pole values of the cross sections are typically of order 100 fb (10 fb) for the single chargino production and 10 fb (1 fb) for the single neutralino production at  $\sqrt{s} = 200 \text{ GeV}$  (500 GeV) [18] (see Fig.2 and Fig.3). At the sneutrino resonance, the cross sections of the single gaugino productions reach high values : using Eq.(1.6), the rate for the neutralino production in association with a neutrino is of order  $3 \cdot 10^3$  in units of the QED point cross section,  $R = \sigma_{pt} = 4\pi\alpha^2/3s$ , for  $M_2 = 200 \text{ GeV}$ ,  $\mu = 80 \text{ GeV}$ ,  $\tan\beta = 2$  and  $\lambda_{1j1} = 0.1$  at  $\sqrt{s} = m_{\tilde{\nu}_L^j} = 120 \text{ GeV}$  [15]. The cross section for the single chargino production reaches  $2 \cdot 10^{-1} \text{ pb}$  at  $\sqrt{s} = m_{\tilde{\nu}_L^j} = 500 \text{ GeV}$ , for  $\lambda_{1j1} = 0.01$  and  $m_{\tilde{\chi}^\pm} = 490 \text{ GeV}$  [26]. The Initial State Radiation (ISR) lowers the single gaugino production cross section at the  $\tilde{\nu}$  pole but increases greatly the single gaugino production rate in the domain  $m_{gaugino} < m_{\tilde{\nu}} < \sqrt{s}$ . This ISR effect can be observed in Fig.4 which shows the single charginos and neutralinos productions cross sections as a



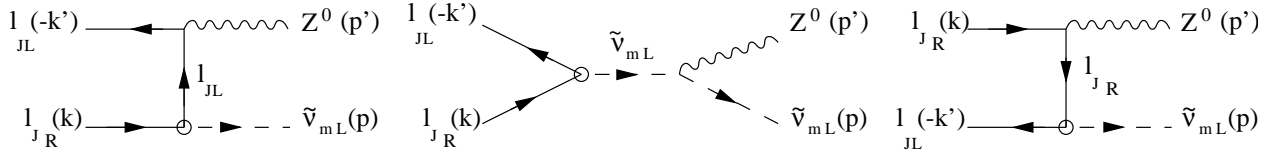
(a)



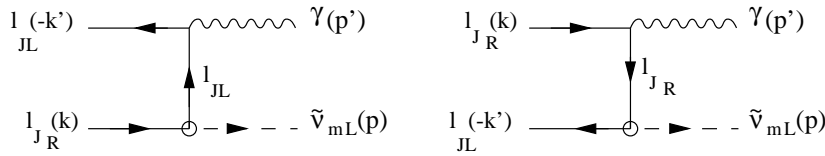
(b)



(c)



(d)



(e)

FIG. 1: Feynman diagrams for the single production processes at leptonic colliders, namely,  $l_J^+ l_J^- \rightarrow \tilde{\chi}^- l_m^+$  (a),  $l_J^+ l_J^- \rightarrow \tilde{\chi}^0 \tilde{\nu}_m$  (b),  $l_J^+ l_J^- \rightarrow \tilde{l}_{mL}^- W^+$  (c),  $l_J^+ l_J^- \rightarrow \tilde{\nu}_{mL} Z^0$  (d) and  $l_J^+ l_J^- \rightarrow \tilde{\nu}_{mL} \gamma$  (e). The circled vertex correspond to the  $\tilde{R}_p$  interaction, with the coupling constant  $\lambda_{mJJ}$ , and the arrows denote flow of momentum.



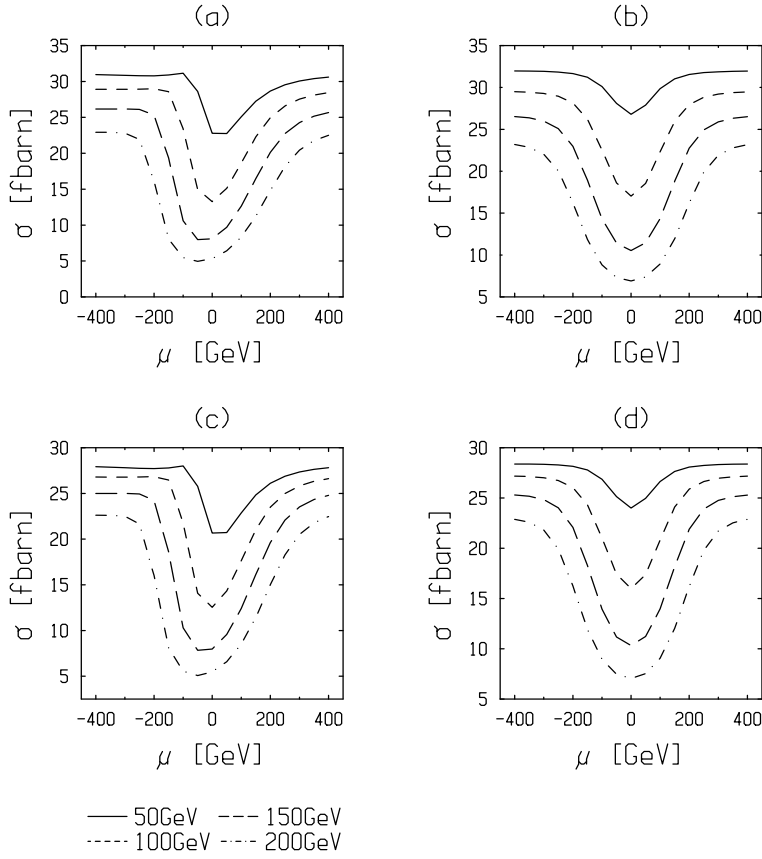


FIG. 2: The integrated cross-sections [18] for the process  $e^+e^- \rightarrow \tilde{\chi}_1^- l_j^+$ , at a center of mass energy of 500 GeV, are shown as a function of  $\mu$  for discrete choices of the remaining parameters : (a)  $\tan \beta = 2$ ,  $m_0 = 50$  GeV, (b)  $\tan \beta = 50$ ,  $m_0 = 50$  GeV, (c)  $\tan \beta = 2$ ,  $m_0 = 150$  GeV, and (d)  $\tan \beta = 50$ ,  $m_0 = 50$  GeV, with  $\lambda_{1j1} = 0.05$ . The windows conventions are such that  $\tan \beta = 2, 50$  horizontally and  $m_0 = 50, 150$  GeV vertically. The different curves refer to the value of  $M_2$  of 50 GeV (continuous line), 100 GeV (dot-dashed line), 150 GeV (dotted line), as indicated at the bottom of the figure.

function of the center of mass energy for a given MSSM point [17].

The single  $\tilde{\chi}_1^\pm$  ( $\tilde{\chi}_1^0$ ) production rate is reduced in the higgsino dominated region  $|\mu| \ll M_1, M_2$  where the  $\tilde{\chi}_1^\pm$  ( $\tilde{\chi}_1^0$ ) is dominated by its higgsino component, compared to the wino dominated domain  $|\mu| \gg M_1, M_2$  in which the  $\tilde{\chi}_1^\pm$  ( $\tilde{\chi}_1^0$ ) is mainly composed by the higgsino [18]. Besides, the single  $\tilde{\chi}_1^\pm$  ( $\tilde{\chi}_1^0$ ) production cross section depends weakly on the sign of the  $\mu$  parameter at large values of  $\tan \beta$ . However, as  $\tan \beta$  decreases the rates increase (decrease) for  $\text{sign}(\mu) > 0$  ( $< 0$ ). This evolution of the rates with the  $\tan \beta$  and  $\text{sign}(\mu)$  parameters is explained by the evolution of the  $\tilde{\chi}_1^\pm$  and  $\tilde{\chi}_1^0$  masses in the supersymmetric parameter space [18].

The experimental searches of the single chargino and neutralino productions have been performed at the LEP collider at various center of mass energies [8, 19, 20, 21, 22]. The single  $\tilde{\chi}_1^\pm$  production has mainly been studied through the  $4l^\pm + \cancel{E}$  final state and the single  $\tilde{\chi}_1^0$  production via the  $2l^\pm + \cancel{E}$  signature. The motivations were that if the lightest neutralino is the LSP it decays as  $\tilde{\chi}_1^0 \rightarrow l\bar{l}\nu$  via the  $\lambda$  coupling and the lightest chargino

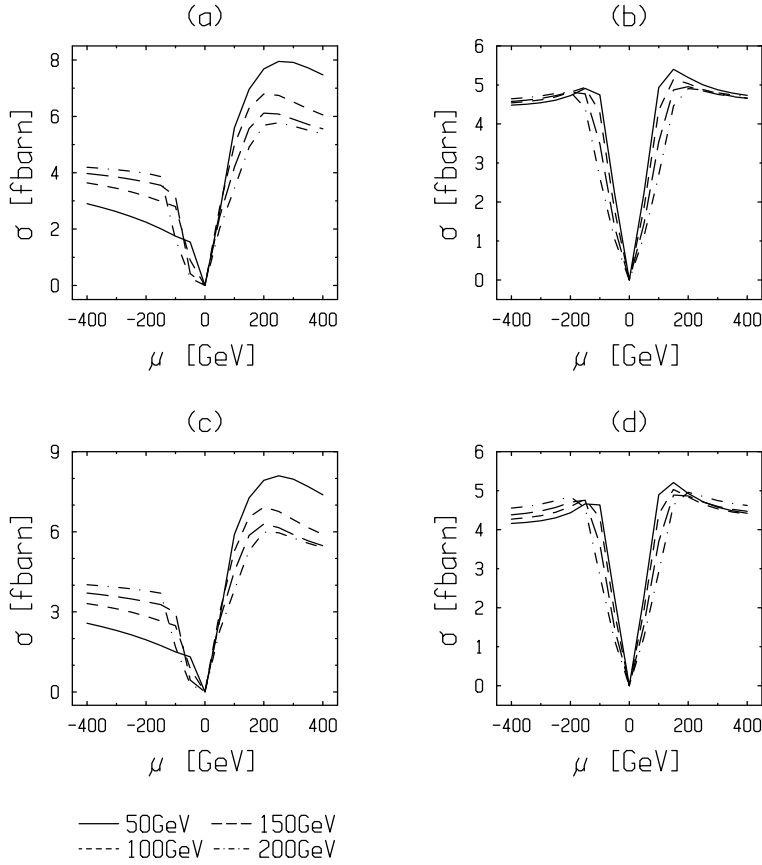


FIG. 3: The integrated cross-sections [18] for the process  $e^+e^- \rightarrow \tilde{\chi}_1^0 \tilde{\nu}_j$ , at a center of mass energy of 500 GeV, are shown as a function of  $\mu$  for discrete choices of the remaining parameters : (a)  $\tan \beta = 2$ ,  $m_0 = 50$  GeV, (b)  $\tan \beta = 50$ ,  $m_0 = 50$  GeV, (c)  $\tan \beta = 2$ ,  $m_0 = 150$  GeV, and (d)  $\tan \beta = 50$ ,  $m_0 = 50$  GeV, with  $\lambda_{1j1} = 0.05$ . The windows conventions are such that  $\tan \beta = 2, 50$  horizontally and  $m_0 = 50, 150$  GeV vertically. The different curves refer to the value of  $M_2$  of 50 GeV (continuous line), 100 GeV (dot-dashed line), 150 GeV (dotted line), as indicated at the bottom of the figure.

can decay as  $\tilde{\chi}_1^\pm \rightarrow \tilde{\chi}_1^0 l^\pm \nu$ . The off pole effects of the single gaugino productions rates (see above) are at the limit of observability at the LEP collider even with the integrated luminosity of LEP II :  $\mathcal{L} \approx 200 pb^{-1}$ . Therefore, the experimental analyses of the single gaugino productions have excluded values of the  $\lambda_{1j1}$  couplings smaller than the low-energy bounds only at the sneutrino resonance point  $\sqrt{s} = m_{\tilde{\nu}}$  and, due to the ISR effect, in a range of typically  $\Delta m_{\tilde{\nu}} \approx \sim 50 GeV$  around the  $\tilde{\nu}$  pole. Nevertheless, recall that these analyses have been performed at several center of mass energies  $\sqrt{s}$ , which has allowed to cover a wide range of the  $\tilde{\nu}$  mass. We finally note that at the various sneutrino resonances, the sensitivities on the  $\lambda_{1j1}$  couplings which have been derived from the LEP data reach values of order  $10^{-3}$ .

The experimental analyses of the single chargino and neutralino productions (via both the sneutrino resonance study and the off pole effects) at linear colliders should be interesting due to the high luminosities and energies expected at these futur colliders [23, 24]. However, the single gaugino productions might suffer a large supersymmetric background

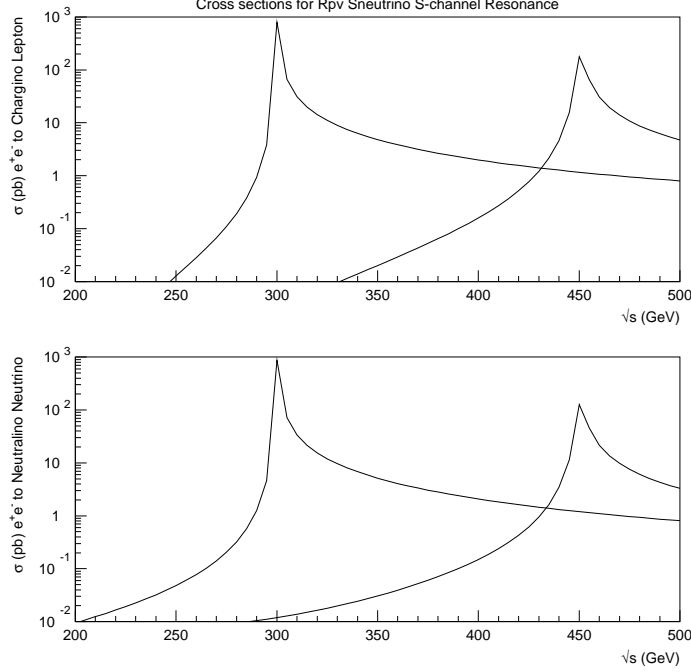


FIG. 4: Cross sections of the single charginos and neutralinos productions as a function of the center of mass energy for the two values  $m_{\tilde{\nu}} = 300\text{GeV}, 450\text{GeV}$  with  $m_{\tilde{e}} = 1\text{TeV}$ ,  $M_2 = 250\text{GeV}$ ,  $\mu = -200\text{GeV}$ ,  $\tan\beta = 2$  and  $\lambda_{1j1} = 0.1$ . The rates values are calculated by including the ISR effect and by summing over the productions of the different  $\tilde{\chi}_i^\pm$  and  $\tilde{\chi}_j^0$  eigenstates which can all be produced for this MSSM point.

at linear colliders. Indeed, due to the high energies reached at these colliders, the pair productions of supersymmetric particles may have large cross sections. In [25], it was shown that the SUSY background of the  $4l^\pm + \cancel{E}$  signature generated by the  $\tilde{\chi}_1^\pm \mu^\mp$  production via  $\lambda_{121}$  could be greatly reduced with respect to the signal : First, this SUSY background can be suppressed by making use of the beam polarization capability of the linear colliders. Secondly, the specific kinematics of the single chargino production reaction allows to put some efficient cuts on the transverse momentum of the lepton produced together with the chargino. By consequence of this SUSY background reduction, the sensitivity on the  $\lambda_{121}$  coupling obtained from the  $\tilde{\chi}_1^\pm \mu^\mp$  production study at linear colliders for  $\sqrt{s} = 500\text{GeV}$  and  $\mathcal{L} = 500\text{fb}^{-1}$  [23] would be of order  $10^{-4}$  at the sneutrino resonance and would improve the low-energy constraint over a range of  $\Delta m_{\tilde{\nu}} \approx 500\text{GeV}$  around the  $\tilde{\nu}$  pole, assuming the largest SUSY background allowed by the experimental limits on the SUSY masses [25]. We mention that due to the high luminosities reached at linear colliders, the off resonance contributions to the cross section play an important role in the single  $\tilde{\chi}_1^\pm$  production analysis.

Besides, the two-body kinematics of the reactions  $e^+e^- \rightarrow \tilde{\chi}_{1,2}^\pm l^\mp$  should allow to determine the  $\tilde{\chi}_1^\pm$  and  $\tilde{\chi}_2^\pm$  masses [25]. As a matter of fact, the energy of the lepton produced together with the chargino  $E(l^\mp)$  is completely fixed by the center of mass

energy  $\sqrt{s}$ , the lepton mass  $m_{l^\mp}$  and the chargino mass  $m_{\tilde{\chi}_{1,2}^\pm}$  via the relation,

$$E(l^\mp) = \frac{s + m_{l^\mp}^2 - m_{\tilde{\chi}_{1,2}^\pm}^2}{2\sqrt{s}}. \quad (1.7)$$

The lepton momentum  $P(l^\mp)$ , which is related to the lepton energy by  $P(l^\mp) = (E(l^\mp)^2 - m_{l^\mp}^2 c^4)^{1/2}/c$ , is thus also fixed. Therefore, the experimental momentum value of the produced lepton should allow to determine the  $\tilde{\chi}_1^\pm$  and  $\tilde{\chi}_2^\pm$  masses through Eq.(1.7). In fact, a photon is radiated from the initial state due to the ISR so that the single chargino production must be treated as the three-body reaction  $e^+e^- \rightarrow \tilde{\chi}_{1,2}^\pm l^\mp \gamma$ . However, it was shown in [25] that the  $\tilde{\chi}_{1,2}^\pm$  masses determinations would remain possible in the case of a large ISR effect and that the accuracy on  $m_{\tilde{\chi}_1^\pm}$  could reach  $\sim 6\text{GeV}$  at linear colliders in such a case.

### 1.3 Non Resonant Single Production

The slepton and the sneutrino can also be singly produced via the coupling  $\lambda_{1j1}$  in the (non-resonant) reactions  $e^+e^- \rightarrow \tilde{l}_L^\mp W^\pm$ ,  $e^+e^- \rightarrow \tilde{\nu}_L^j Z^0$  and  $e^+e^- \rightarrow \tilde{\nu}_L^j \gamma$ . Those reactions receive contributions from the exchange of a charged or neutral lepton of the first generation in the  $t$ - or  $u$ -channel (see Fig.1). The single productions of a sneutrino accompanied by a  $Z^0$  or a  $W^\pm$  boson also occur through the exchange in the  $s$ -channel of a  $\tilde{\nu}_L^j$  sneutrino which can not be produced on-shell (see Section 2.3). When kinematically allowed, these processes have some rates of order 100 fb at  $\sqrt{s} = 200$  GeV and 10 fb at  $\sqrt{s} = 500$  GeV, for  $\lambda_{1j1} = 0.05$  and various masses of the scalar supersymmetric particles [18].

### 1.4 Fermion Pair Production Via $\mathcal{R}_p$

The single production involves only one  $\mathcal{R}_p$  coupling so that the corresponding rate is proportional to the Yukawa coupling squared. This is in contrast to  $\mathcal{R}_p$  contributions (via additional sparticle exchange) to Standard Model processes which are suppressed in proportion to the square of the Yukawa coupling squared.

• **One dominant  $\mathcal{R}_p$  coupling constant** One may first consider the usual case of one dominant  $\mathcal{R}_p$  coupling constant. This hypothesis, which is often made for simplifications reasons, has two main justifications. First, the low energy indirect bounds are more stringent on the products of the  $\mathcal{R}_p$  couplings  $\lambda$ ,  $\lambda'$  or  $\lambda''$  than on the coupling constants separately. For instance, the bounds imposed on the products  $\lambda'\lambda''$  by the experimental limits on proton decay are severe, and moreover, apply on all the different flavor combinations of this product. Second, from a theoretical point of view, by analogy with the Higgs Yukawa couplings structure, a strong hierarchy can be assumed on the flavor indices of the  $\mathcal{R}_p$  coupling constants.

**Dilepton production** The resonant sneutrino  $\tilde{\nu}_\mu$  or  $\tilde{\nu}_\tau$  production via  $\lambda_{121}$  or  $\lambda_{131}$  respectively followed by a decay through the same coupling constant (i.e.  $\tilde{\nu}^i \rightarrow \bar{l}_j l_k$  via  $\lambda_{ijk}$ ) would lead to a spectacular signature, namely, an excess of events in the Bhabha scattering [14]. For  $\Gamma_{\tilde{\nu}(\mu,\tau)} = 1$  GeV and  $\lambda_{1(2,3)1} = 0.1$ , the cross section of the Bhabha scattering, including the  $\tilde{\nu}_{(\mu,\tau)}$  sneutrino  $s$ -channel exchange and the interference terms,

reaches 3 pb at  $\sqrt{s} = m_{\tilde{\nu}_{(\mu,\tau)}} = 200$  GeV [1, 2, 3]. Due to these great cross sections, the values  $\lambda_{(2,3)11} > 0.05$  can be ruled out at 95% CL for  $\sqrt{s} = m_{\tilde{\nu}_{(\mu,\tau)}} = 192$  GeV with  $\mathcal{L} = 500 \text{ pb}^{-1}$  [4].

In a scenario where none of the supersymmetric particles can be produced with a significant cross section, due to very heavy supersymmetric particles or too weak couplings for the lighter ones with the Standard Model particles, the supersymmetric effects could only be virtual. In particular, different  $\mathcal{R}_p$  interactions could manifest themselves as contact terms in many contributions to Standard Model processes. By calculating the deviations of the cross sections values with respect to the Standard Model, bounds can be set on the relevant  $\mathcal{R}_p$  coupling constants values.

In [1] the analysis of different contributions to Standard Model processes was based on the R-parity violation interpretation of the high  $x$ , high  $Q^2$  anomalous HERA events. Interpreting the HERA events as top squark production ( $\lambda'_{131} > 0.05$ , see Eq.(1.9)), then the constraints on the  $\mathcal{R}_p$  coupling constants products,  $\lambda_{121}\lambda'_{131} < 1.8 \cdot 10^{-4}$ ,  $\lambda_{131}\lambda'_{131} < 2.0 \cdot 10^{-3}$  and  $\lambda_{123}\lambda'_{131} < 2.4 \cdot 10^{-3}$ , as imposed by the rare  $B$  decays, put strong bounds on some of the  $\lambda$  couplings which are relevant for leptonic processes :  $\lambda_{121} < 0.0036$ ,  $\lambda_{131} < 0.04$  and  $\lambda_{123} < 0.048$ . However, if the HERA data are due to the charm squark production ( $\lambda'_{121} > 0.05$ , see Eq.(1.9)), the rare  $K$  decays do not constrain the  $\lambda_{131}$  and  $\lambda_{123}$  couplings. In the situation where the  $\mathcal{R}_p$  coupling constant  $\lambda_{131}$  dominates, the Bhabha scattering receives a contribution from the exchange of a  $\tilde{\nu}_\tau$  sneutrino in the  $s$ - and  $t$ -channels, while the  $\tau^+\tau^-$  production can occur via the exchange of a  $\tilde{\nu}_e$  sneutrino in the  $t$ -channel only. For this reason, the impact of the  $\mathcal{R}_p$  diagram on the Bhabha scattering is higher than on the  $\tau$  pair production : At  $\sqrt{s} = 192$  GeV, for  $m_{\tilde{\nu}} = 300$  GeV and  $\lambda_{131} = 0.1$ , the effects on the cross sections are,  $\frac{\sigma(SM+RPV)}{\sigma(SM)} - 1 = 4 \cdot 10^{-3}$  and  $2 \cdot 10^{-2}$  for the  $\tau^+\tau^-$  and  $e^+e^-$  productions, respectively [1, 2, 3]. From the study of the  $\mathcal{R}_p$  contribution to the Bhabha scattering, the coupling  $\lambda_{131}$  could be probed at 95% CL at  $\sqrt{s} = 192$  GeV with  $\mathcal{L} = 500 \text{ pb}^{-1}$  down to 0.28, 0.57, 0.84 for  $m_{\tilde{\nu}_\tau} = 400$  GeV, 700 GeV, 1 TeV, respectively [4]. The limit on  $\lambda_{131}$  from the fits to the cross section and forward-backward asymmetry, using data collected by the DELPHI detector during the run of LEP in 1995 (1996) at  $\sqrt{s} = 130$  and 136 GeV ( $\sqrt{s} = 161$  and 172 GeV) corresponding to a luminosity of order 6  $\text{pb}^{-1}$  (20  $\text{pb}^{-1}$ ), is  $\lambda_{131} < 0.74$  for  $m_{\tilde{\nu}_e} = 200$  GeV at 95% CL [5] (similar analyses on the  $\mathcal{R}_p$  contributions to the  $e^+e^- \rightarrow l^+l^-$  reaction have been performed by the L3 [6] and OPAL [7] Collaborations). In case of a dominant coupling  $\lambda_{123}$ , the  $t$ -channel  $\tilde{\nu}_\tau$  exchange would contribute to  $\tau^+\tau^-$  pair production. Through this contribution, the coupling  $\lambda_{123}$  could be probed with a 95% CL at  $\sqrt{s} = 192$  GeV with  $\mathcal{L} = 500 \text{ pb}^{-1}$  down to 0.3, 0.5, 0.7 for  $m_{\tilde{\nu}_\tau} = 400$  GeV, 700 GeV, 1 TeV, respectively [4].

The other  $\mathcal{R}_p$  coupling constants  $\lambda$  relevant for virtual effects in the Standard Model processes,  $e^+e^- \rightarrow l\bar{l}$ , namely,  $\lambda_{121}, \lambda_{231}, \lambda_{122}, \lambda_{132}$  and  $\lambda_{133}$ , were studied in [4]. Since the  $\mathcal{R}_p$  interactions have a spin structure different from the Standard Model ones, the angular distribution for the lepton pair production is a sensitive probe for the existence of the former. Hence, it was proposed to divide the experimental angular width into bins, and to compare the observed number of events in each bin with the Standard Model prediction. The more optimistic results hold for the couplings,  $\lambda_{122}, \lambda_{132}$  and  $\lambda_{133}$ , which can be probed with a 95% CL at  $\sqrt{s} = 192$  GeV with  $\mathcal{L} = 500 \text{ pb}^{-1}$  down to 0.3, 0.5, 0.7 for  $m_{\tilde{\nu}} = 400$  GeV, 700 GeV, 1 TeV, respectively. Besides, the limit on  $\lambda_{121}$  from the fits to the cross section and forward-backward asymmetry for the reaction,  $e^+e^- \rightarrow \mu^+\mu^-$ , using

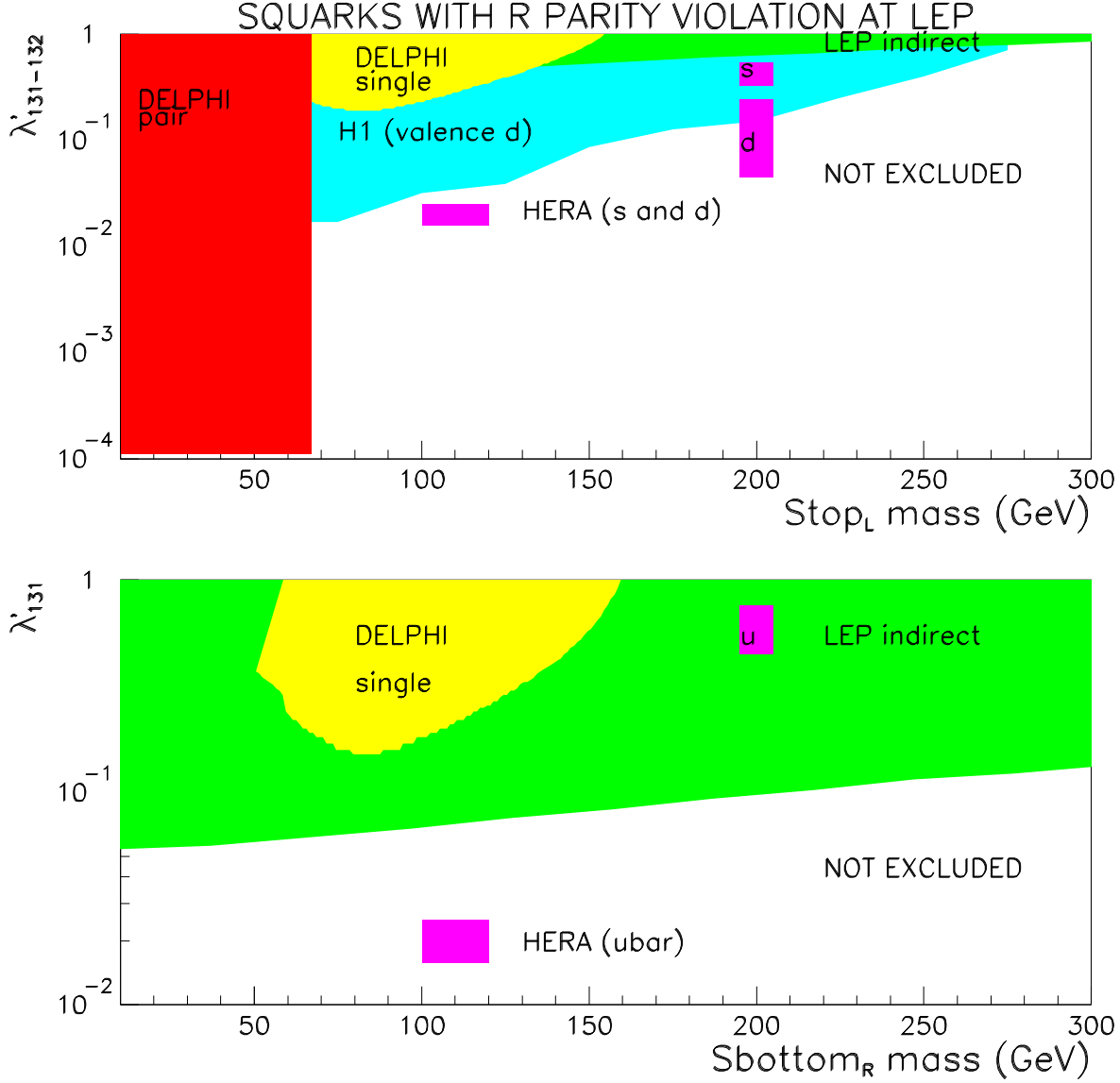


FIG. 5: Exclusion domain in the  $\lambda'$  versus  $m_{\tilde{q}}$  plane.

data collected by the DELPHI detector, is  $\lambda_{121} < 0.55$  ( $\lambda_{121} < 0.68$ ) for  $m_{\tilde{\nu}_e} = 100$  GeV (200 GeV) at a 95% confidence level [5].

**b) Dijet production** One may also think of a single dominant  $\lambda'_{ijk}$  coupling. This hypothesis allows  $\mathcal{R}_p$  contributions to quark pair production through the exchange of a squark in the  $t$ -channel. For experimental reasons of quark tagging, the  $\mathcal{R}_p$  contributions to,  $e^+e^- \rightarrow b\bar{b}, c\bar{c}$ , via,  $\lambda'_{1k3}, \lambda'_{12k}$ , respectively, are the most easier to analyse at LEP energies. Among these couplings  $\lambda'_{1k3}$  and  $\lambda'_{12k}$ , the most stringent constraint, predicted from the study of the quark pair production [4], arises for the constant  $\lambda'_{123}$  which is subject to bounds of order, 0.4, 0.67, 0.92, for  $m_{\tilde{q}} = 400$  GeV, 700 GeV, 1 TeV at  $\sqrt{s} = 192$  GeV

with a 95% confidence level and a luminosity,  $\mathcal{L} = 500 \text{ pb}^{-1}$ . The effects of R-parity violation in quark pair production have also been investigated experimentally [8], using the 1997 LEP data and the results of [9]. Assuming that the  $\mathcal{R}_p$  contribution through the exchange of a given squark to a given flavour channel is the only source of deviation from the Standard Model processes, the limits of Fig.5 (indicated by “LEP indirect”) have been derived. The LEP indirect limit represented in the upper plot of Fig.5 derives from the analysis of the process  $e^+e^- \rightarrow d\bar{d}$  ( $e^+e^- \rightarrow s\bar{s}$ ) occuring through the  $\lambda'_{131}$  ( $\lambda'_{132}$ ) coupling constant via the exchange of a top-squark in the  $t$ -channel. The LEP indirect limit in the lower plot of Fig.5 is deduced from the analysis of the process  $e^+e^- \rightarrow u\bar{u}$  involving  $\lambda'_{113}$  and occuring through the exchange of a bottom-squark in the  $t$ -channel. The negative interference term between the squark exchange and the Standard Model amplitudes is maximal for a down type squark [10]. The sensitivity of the measurement is therefore reduced for the up squark exchange, as can be observed in Fig.5. Note that using bottom, charm or light quarks (u,d,s) tagging, the effects on separate quark flavours could also be studied [10]. Besides, if with more data, a rate effect is seen at LEP II in  $s\bar{s}$  or  $b\bar{b}$  production, the charge asymmetry will help in confirming the squark exchange hypothesis. On Fig.5, the relevant exclusion domain from the H1 Collaboration is also shown (indicated by “H1 (valence d)”), as well as the bands indicated by u,d,s which would have been relevant for the so called HERA anomaly found in 1997. These u,d,s bands are respectively associated with the three interpretations of the HERA anomalous events,

$$e^+\bar{u} \rightarrow \tilde{s}_R, \tilde{b}_R(\lambda'_{112}, \lambda'_{113}), \quad (1.8)$$

$$e^+d \rightarrow \tilde{c}_L, \tilde{t}_L(\lambda'_{121}, \lambda'_{131}), \quad (1.9)$$

$$e^+s \rightarrow \tilde{c}_L, \tilde{t}_L(\lambda'_{122}, \lambda'_{132}). \quad (1.10)$$

In particular, we observe on Fig.5 that the experimental results on the search for the indirect effects of R-parity violation in quark pair production at LEP completely exclude the HERA interpretation of Eq.(1.8) via  $\lambda'_{113}$ .

• **One dominant product of  $\mathcal{R}_p$  coupling constants**

**a) Dilepton production** Another interesting hypothesis consist in considering that two lepton number violating  $\lambda_{ijk}$  Yukawa couplings are much larger than all the others, where both  $\mathcal{R}_p$  couplings violate one and the same lepton flavour. In this scenario, low energy experiments are not restrictive and typically allow for couplings,  $\lambda < 0.1(\tilde{m}/200 \text{ GeV})$  [1]. In case where the couplings  $\lambda_{131}$  and  $\lambda_{232}$  are simultaneously different of zero, the process  $e^+e^- \rightarrow \mu^+\mu^-$  receives an additional contribution from  $s$ -channel  $\tilde{\nu}_\tau$  exchange. At  $\sqrt{s} = 192 \text{ GeV}$ , for  $m_{\tilde{\nu}_\tau} = 300 \text{ GeV}$  and  $\lambda_{131} = \lambda_{232} = 0.1$ , the effects on the cross sections and on the forward-backward asymmetries are,  $\frac{\sigma(SM+RPV)}{\sigma(SM)} - 1 = 1.5 \cdot 10^{-3}$ , and,  $A_{FB}(SM+RPV) - A_{FB}(SM) = 9 \cdot 10^{-4}$  [1, 2, 3]. The 95% CL limit on  $\lambda = \lambda_{131} = \lambda_{232}$  resulting from the fits on cross section and forward-backward asymmetry based on the 1995 ( $\sqrt{s} = 130$  and  $136 \text{ GeV}$ ) and 1996 ( $\sqrt{s} = 161$  and  $172 \text{ GeV}$ ) LEP data, has been obtained in [5]. The best limits on  $\lambda$  are obtained for,  $m_{\tilde{\nu}_\tau} \approx \sqrt{s}$ , but the radiative return process gives a significant sensitivity between those points. For,  $m_{\tilde{\nu}_\tau} = 130, 136, 161, 172 \text{ GeV}$ , one get limits, respectively, of order,  $\lambda < 0.035, 0.03, 0.03, 0.02$ , assuming a tau-sneutrino width of

1 GeV. Now, if the couplings  $\lambda_{121}$  and  $\lambda_{323}$  do not vanish, the  $s$ -channel exchange of a  $\tilde{\nu}_\mu$  sneutrino contributes to the  $\tau^+\tau^-$  pair production. The 95% CL limit on  $\lambda = \lambda_{121} = \lambda_{323}$  [5] resulting from the fits of the  $\sigma(e^+e^- \rightarrow \tilde{\nu} \rightarrow \tau^+\tau^-)$  cross section based on the 1995 and 1996 LEP data are of the same order of the limits on  $\lambda = \lambda_{131} = \lambda_{232}$ .

**b) Dijet production** Finally, we can concentrate on the case where one of the dominant  $\mathcal{R}_p$  coupling constants is a  $\lambda_{ijk}$  while the other is a  $\lambda'_{ijk}$ . In such a scenario, a  $\tilde{\nu}_i$  sneutrino which is produced at the resonance, could decay via  $\lambda'_{ijk}$  into two down squarks,  $\tilde{q}_j \tilde{q}_k^*$ . Since the  $\lambda'_{3jk}$  are the less constrained constants, the resonant  $\tilde{\nu}_\tau$  production (via  $\lambda_{131}$ ) is the most promising. The  $\tilde{\nu}_\tau$  sneutrino can decay via  $\lambda'_{333}$  into  $b$  quarks, which can be tagged experimentally with a rather good efficiency. The effective luminosity required to discover an excess of  $b\bar{b}$  events at  $5\sigma$  confidence level at LEP II, assuming a tagging efficiency of 40%, is  $1.1 \text{ pb}^{-1}/\text{GeV}$ ,  $0.43 \text{ pb}^{-1}/\text{GeV}$  for  $m_{\tilde{\nu}_\tau} = 110 \text{ GeV}$ ,  $145 \text{ GeV}$ ,  $\lambda_{131} = 0.01, 0.005$  and  $\lambda'_{333} = 1.0, 0.1$ , respectively [11]. Assuming that the  $\tilde{\nu}_\tau$  sneutrino decays into  $b\bar{b}$ , the limit on  $\lambda_{131}$  at 95% CL can be derived from the experimental measurement of the  $b$  quark pair production, using the LEP data at  $\sqrt{s} = 161 \text{ GeV}$  and  $\sqrt{s} = 172 \text{ GeV}$  [8]. A most interesting window for the sneutrino resonance exists near the  $Z$  boson pole. The sneutrino resonance could still be observable since then it would increase the branching ratio  $R_b(Z^0 \rightarrow b\bar{b})$  and reduce the  $b$  quark forward-backward asymmetry  $A_{FB}(b)$ . The resonant  $\tilde{\nu}_\tau$  sneutrino could also decay into a pair of down quarks,  $d\bar{d}$ , through the coupling  $\lambda'_{311}$ . Since the angular distribution of the  $d$  and  $\bar{d}$  jets is nearly isotropic on the sneutrino resonance, the strong forward-backward asymmetry in the Standard Model continuum,  $A_{FB}(b) \approx 0.65$  at  $\sqrt{s} = 200 \text{ GeV}$ , is reduced to  $\approx 0.03$  on top of the sneutrino resonance [12]. If the total cross section  $\sigma(e^+e^- \rightarrow \text{hadrons})$  can be measured with an accuracy of about 1% at  $\sqrt{s} = 184(192) \text{ GeV}$ , the Yukawa couplings can be bounded to  $(\lambda_{131}\lambda'_{311})^{1/2} < 0.072(0.045)$  for a 200 GeV tau-sneutrino mass [12]. This limit is estimated for energies much below the resonance,  $|\sqrt{s} - m_{\tilde{\nu}_\tau}| \ll \Gamma_{\tilde{\nu}_\tau}$ , and is thus independent of the sneutrino width.

As a conclusion, the analysis at leptonic colliders of the  $\mathcal{R}_p$  contributions to Standard Model processes lead to bounds on the lepton number violating coupling constants which are not as stringent as the low energy limits.

## 1.5 Single Production in $e - \gamma$ Collisions

The charged and neutral sleptons can also be singly produced at leptonic colliders in the lepton-photon collisions,  $e^\pm\gamma \rightarrow l^\pm\tilde{\nu}, \tilde{l}^\pm\nu$ , where the photon is an on shell photon radiated by one of the colliding leptons. Those productions, which were considered in [27], allow to study the  $\mathcal{R}_p$  couplings,  $\lambda_{122}, \lambda_{123}, \lambda_{132}, \lambda_{133}, \lambda_{231}$ , which are not involved in the single productions from  $e^+e^-$  reactions. The slepton or sneutrino production occurs via the exchange of a charged lepton in the  $s$ -channel, and a charged slepton or lepton, respectively, in the  $t$ -channel. Therefore, since the  $t$ -channel is dominant and  $m_{\tilde{l}} \gg m_l$ , the slepton production is about two order of magnitude less than the sneutrino production, which is,  $\sigma(e^+e^- \rightarrow \tilde{\nu}_j e \tau) = 30 \text{ fb}$  (300 fb) at  $\sqrt{s} = 192 \text{ GeV}$  (500 GeV), for  $m_{\tilde{\nu}_j} = 150 \text{ GeV}$  and  $\lambda_{j13} = 0.05$ . The produced sneutrino can either decay directly via  $\lambda$  into 2 leptons, or indirectly via lighter neutralinos and charginos (e.g.  $\tilde{\nu} \rightarrow \nu\tilde{\chi}^0$ ) leading respectively to either  $4l$  or  $4l + \cancel{E}$  final states. Those various signatures were simulated together with the associated Standard Model backgrounds in order to apply some kinematic cuts. The



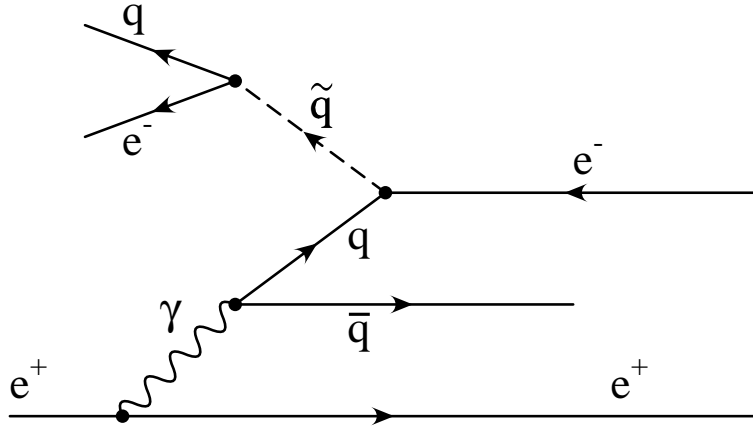


FIG. 6: *Single squark production in electron-photon collisions.*

indirect decay of the sneutrino via  $\lambda_{122}$  leads to the signal with the higher sensitivity, allowing to probe the coupling constant  $\lambda_{122}$  down to the values 0.025, 0.04, 0.065 at a  $5\sigma$  discovery level with an energy  $\sqrt{s} = 192$  GeV and a luminosity  $\mathcal{L} = 100 \text{ pb}^{-1}$  for  $m_{\tilde{\nu}} = 100$  GeV, 125 GeV, 150 GeV, respectively.

The single production of a squark is also possible in the  $e\gamma$  interactions, as shown in Fig.6, through  $\lambda'$  couplings. Assuming a squark LSP, the produced squark will have a direct decay via  $\lambda'$  into a lepton plus a quark, so that the final state topologies will be energetic mono-jet with one well isolated energetic electron and eventually a low energy jet in the forward region of the detector, in case where the initial electron which scatters the quasi real photon escapes the detection. These events have been searched experimentally [8], using the 1997 LEP data at  $\sqrt{s} = 161$  GeV and  $\sqrt{s} = 172$  GeV, and since no evidence have been found for the single squark production, an exclusion domain has been deduced in the plane  $\lambda'$  vs.  $m_{\tilde{q}}$  as shown in Fig.5 (indicated by “DELPHI single”). The difference between the two exclusion plots is explained by the fact that the only possible  $\tilde{R}_p$  stop decay via  $\lambda'$  is,  $\tilde{t} \rightarrow ed$ , while for the sbottom, the charged lepton channel branching ratio is,  $B(\tilde{b} \rightarrow eu) \approx 50\%$ .

## 1.6 $\tilde{R}_p$ Contributions to Flavour Changing Neutral Currents

In the Standard Model, the flavor changing effects are exceedingly small [28, 29, 30]. In particular, it is useful to recall that the flavor changing neutral current effects arise through loop diagrams only. For instance, the typical structure of the one loop diagram for the  $Z$  boson and quarks pair vertex  $Zq_J\bar{q}_{J'}$ , is,  $\sum_i V_{iJ}^* V_{iJ'} f(m_i^2/m_Z^2)$ , where  $V_{ij}$  are the elements of the CKM matrix and  $m_i$  are the masses of the quarks involved in the loop. This schematic formula shows explicitly how the CKM matrix unitarity, along with the quarks masses degeneracies relative to the  $Z^0$  boson mass scale (valid for all quarks with the exception of the top quark) strongly suppress the flavor changing neutral current effects. Although flavor changing effects are expected to attain observable levels in several extensions of the Standard Model, the contributions from the MSSM are bounded by postulating either a degeneracy of the soft Supersymmetry breaking scalars masses or an alignment of the fermion and scalar superpartners mass matrices. Those constraints are

imposed by some low-energy experimental bounds. Early calculations of the  $Z^0$  boson flavor changing decay rates,  $Z \rightarrow q_J \bar{q}_{J'}$ , through triangle diagrams involving squarks and gluinos, found small results compared to that of the Standard Model [31, 32]. Therefore, the flavor changing effects offer the opportunity to probe physics beyond the MSSM. The  $\mathcal{R}_p$  interaction, because of its non trivial flavour structure, opens up the possibility of observable flavor changing effects at the tree level.

• **Fermion pair production** The fermion pair production is a relatively simple and well known reaction and hence offers the opportunity of testing new physics. Besides, the leptonic colliders provide a clean environment to study flavor changing physics. These considerations have motivated the study of the  $\mathcal{R}_p$  contributions to the flavor changing neutral current reactions,  $l^+ l^- \rightarrow f_J \bar{f}_{J'}$ , with  $J \neq J'$  [36]. These  $\mathcal{R}_p$  processes occur at the tree level through the exchange of a supersymmetric scalar particle in the  $s$ - or  $t$ -channel, and at one loop level at the  $Z^0$  boson pole. Both fermion and scalar particles are running in the triangle loop diagram. Considering simple assumptions on the scalars masses and for the flavour structures of the  $\mathcal{R}_p$  coupling constants, the lepton number violating interactions contributions to the  $Z$ -boson flavour off-diagonal decays branching ratios,  $B_{JJ'} = B(Z \rightarrow l_J^- l_{J'}^+)$ , scale approximately as  $B_{JJ'} \approx (\frac{\lambda}{0.1})^4 (\frac{100 \text{ GeV}}{\tilde{m}})^{2.5} 10^{-9}$ , where  $\tilde{m}$  represents a supersymmetric particle mass. At energies well above the  $Z$ -boson pole, the flavor changing rates,  $\sigma_{JJ'} = \sigma(l^+ l^- \rightarrow l_J^- l_{J'}^+)$ , are of order,  $\sigma_{JJ'} \approx (\frac{\lambda}{0.1})^4 (\frac{100 \text{ GeV}}{\tilde{m}})^{2-3} (1 - 10) \text{ fb}$ , and slowly decrease with the c.m. energy. Note that the corresponding results for quarks pair production have an extra color factor,  $N_c = 3$ . Besides, the rates are evidently greatly enhanced at the resonance of the sneutrino, which is exchanged in the  $s$ -channel. As a conclusion, due to the strong sensitivity on the  $\mathcal{R}_p$  couplings and on the supersymmetric particles masses, the flavor changing rates are comparable to the flavor changing rates calculated in the framework of the Standard Model. Indeed, for the down-quark-antiquark case, for instance, the  $Z^0$  decays branching fractions were estimated at the values,  $10^{-7}$  for  $(\bar{b}s + \bar{s}b)$ ,  $10^{-9}$  for  $(\bar{b}d + \bar{d}b)$  and  $10^{-11}$  for  $(\bar{d}s + \bar{s}d)$ . Nevertheless, at energies well above the  $Z^0$  mass, the flavor changing rates are high enough to be observable with the luminosities expected at the Next Linear Colliders [24]. Finally, the current experimental limits on the flavour non-diagonal leptonic branching ratios [39],  $B_{JJ'} < [1.7, 9.8, 17.] 10^{-6}$ , for the family couples  $JJ' = [12, 23, 13]$ , constrain the  $\mathcal{R}_p$  coupling constants products to be  $\lambda_{ijJ} \lambda_{ijJ'}^* < [0.46, 1.1, 1.4]$  and  $\lambda'_{Jjk} \lambda'_{J'jk} < [0.38, 0.91, 1.2] 10^{-1}$ , for the same flavour configurations  $JJ' = [12, 23, 13]$ , under the hypothesis of a pair of dominant coupling constants and if  $\tilde{m} = 100 \text{ GeV}$ . These bounds, which are not competitive with the low energy limits, should be improved in the context of the physics at linear colliders.

• **Single top quark production** Of special interest is the case of single top quark production,  $l^+ l^- \rightarrow t \bar{c}$ ,  $\bar{t} c$  [33, 34, 35, 36, 37]. The contribution from the Standard Model to the single top quark production [28, 29, 30] proceeds at one loop level through the exchange in the  $s$ -channel of either an off shell  $Z$ -boson or photon. It is particularly reduced since, unlike  $b\bar{s}$  production for example, it does not get a large contribution from heavy fermion in the loop. Since the MSSM contribution has been shown to be small compared to the Standard Model one [31, 32], an excess of events in the single top quark production would probe the existence of new physics beyond the minimal supersymmetric standard model. Furthermore, the single top production offers the opportunity to learn about flavor changing neutral current effects in the up-type quarks sector, since as we will see in Section 2.4, the top quark offers some extremely clean signatures, with a rather

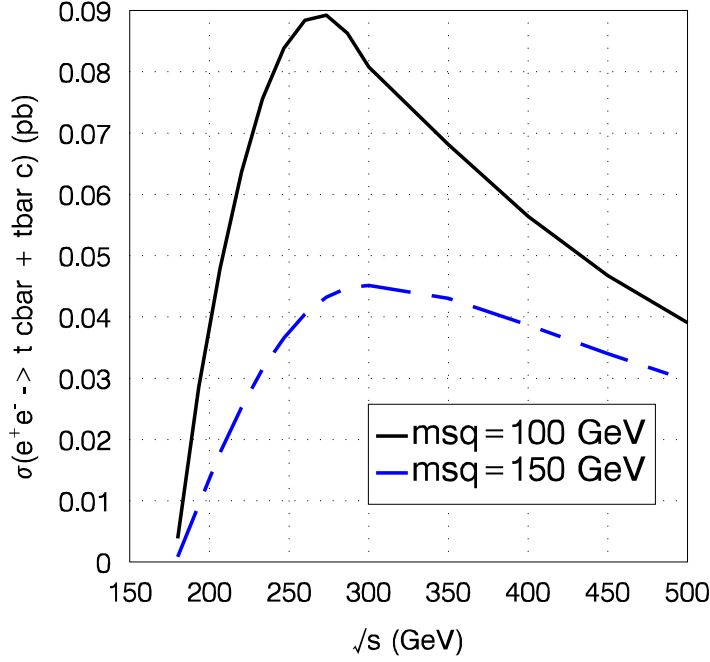


FIG. 7: Cross section of the reaction  $e^+e^- \rightarrow t\bar{c} + \bar{t}c$  as a function of the center of mass energy for  $\lambda'_{12k}\lambda'_{13k} = 0.01$ . The solid line corresponds to  $m_{\tilde{d}_{kR}} = 100\text{GeV}$  and the dashed line to  $m_{\tilde{d}_{kR}} = 150\text{GeV}$ .

energetic lepton, some missing energy and a b jet which can be tagged with a good efficiency.

The reaction  $e^+e^- \rightarrow t\bar{c} + \bar{t}c$  occurs via the exchange of a  $\tilde{d}_{kR}$  squark in the  $t$ -channel through the  $\mathcal{R}_p$  couplings  $\lambda'_{12k}$  and  $\lambda'_{13k}$ . In Fig.7 [34] the cross section of this process is shown as a function of the center of mass energy for a value of  $\lambda'_{12k}\lambda'_{13k}$  equal to 0.01 which is the order of magnitude of the low-energy constraint on this product of  $\mathcal{R}_p$  couplings for  $m_{\tilde{f}} = 100\text{GeV}$ .

Since the top quark mainly decays as  $t \rightarrow bW$ , the reaction  $e^+e^- \rightarrow tc$  leads to the interesting final state  $bcl\nu$  if the  $W$ -boson decays leptonically. This signature has the Standard Model background  $e^+e^- \rightarrow W^+W^- \rightarrow bcl\nu$ . Nevertheless, this background can be suppressed by some kinematical cuts [35]. For instance, an effective cut can be based on the fact that the  $c$  quark produced in the reaction  $e^+e^- \rightarrow tc$  has a fixed energy which is given by  $E(c) = (s + m_t^2 - m_c^2)/2\sqrt{s}$ . Hence, the study of the final state  $bcl\nu$  would allow to probe values of the product  $\lambda'_{12k}\lambda'_{13k}$  down to  $\sim 0.1$  for  $m_{\tilde{d}_{kR}} = 1\text{TeV}$  at linear colliders with a center of mass energy of  $\sqrt{s} = 500\text{GeV}$  and a luminosity of  $\mathcal{L} = 100\text{fb}^{-1}$  [35].

The reaction  $e^+e^- \rightarrow t\bar{c} + \bar{t}c$  receives also contributions at one loop level from the  $\lambda''$  interactions [36, 34]. These contributions exchange a  $\tilde{d}_R$  squark in the loop and involve the  $\lambda''_{2jk}$  and  $\lambda''_{3jk}$  coupling constants. In Fig.8 [34] the rate of the sum of these contributions is shown as a function of the center of mass energy for a value of the involved product of  $\mathcal{R}_p$  couplings  $\lambda''_{223}\lambda''_{323}$  equal to its low-energy limit for  $m_{\tilde{f}} = 100\text{GeV}$  namely 0.625. The

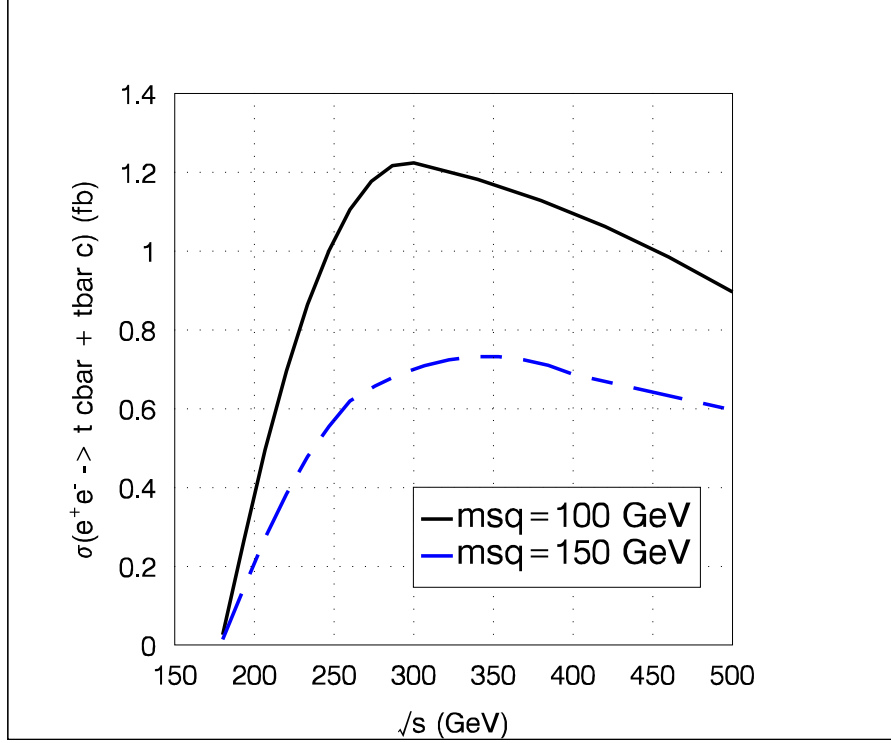


FIG. 8: Cross section of the reaction  $e^+e^- \rightarrow t\bar{c} + \bar{t}c$  as a function of the center of mass energy for  $\lambda''_{223}\lambda''_{323} = 0.625$ . The solid line corresponds to  $m_{\tilde{d}_R} = 100\text{GeV}$  and the dashed line to  $m_{\tilde{d}_R} = 150\text{GeV}$ .

motivation for considering the product  $\lambda''_{223}\lambda''_{323}$  is that it has the less stringent low-energy constraint among the  $\lambda''_{2jk}\lambda''_{3jk}$  products.

The  $t\bar{c}/\bar{t}c$  production at leptonic colliders can also occur at one loop level via photon-photon reactions as  $e^+e^- \rightarrow \gamma\gamma \rightarrow t\bar{c} + \bar{t}c$ . These reactions involve the products of  $\mathcal{R}_p$  couplings  $\lambda'_{i2k}\lambda'_{i3k}$  when  $\tilde{l}_{iL}$  sleptons or  $\tilde{d}_{kR}$  squarks are exchanged in the loop and the products  $\lambda''_{2jk}\lambda''_{3jk}$  when  $\tilde{d}_R$  squarks run in the loop. In Fig.9 (Fig.10) [37] the rate of the reaction  $e^+e^- \rightarrow \gamma\gamma \rightarrow t\bar{c} + \bar{t}c$  is shown as a function of the center of mass energy for a value of the involved product of  $\mathcal{R}_p$  couplings  $\lambda'_{323}\lambda'_{333}$  ( $\lambda''_{223}\lambda''_{323}$ ) equal to its low-energy bound for  $m_{\tilde{f}} = 100\text{GeV}$  namely 0.096 (0.625). The motivation for choosing the product  $\lambda'_{323}\lambda'_{333}$  ( $\lambda''_{223}\lambda''_{323}$ ) is that it has the less stringent low-energy constraint among the  $\lambda'_{i2k}\lambda'_{i3k}$  ( $\lambda''_{2jk}\lambda''_{3jk}$ ) products.

By comparing Fig.7 and Fig.9, we observe that the cross section of the reaction  $e^+e^- \rightarrow t\bar{c} + \bar{t}c$  via  $\lambda'$  interactions is typically one order of magnitude larger than the rate of the process  $e^+e^- \rightarrow \gamma\gamma \rightarrow t\bar{c} + \bar{t}c$  via the same interactions. This is due to the fact that in the case of the  $\lambda'$  interactions, the reaction  $e^+e^- \rightarrow t\bar{c} + \bar{t}c$  occurs at tree level while the process  $e^+e^- \rightarrow \gamma\gamma \rightarrow t\bar{c} + \bar{t}c$  occurs only at one loop level. In contrast, it turns out by comparing Fig.8 and Fig.10 that the  $\lambda''$  couplings give similar effects in the reactions  $e^+e^- \rightarrow t\bar{c} + \bar{t}c$  and  $e^+e^- \rightarrow \gamma\gamma \rightarrow t\bar{c} + \bar{t}c$ . Therefore, a combination of the results from the  $e^+e^-$  and  $\gamma\gamma$  collisions would allow to distinguish between the  $\lambda'$  and  $\lambda''$  effects on the  $t\bar{c}/\bar{t}c$  production.

Finally, the reaction  $\mu^+\mu^- \rightarrow t\bar{c}/\bar{t}c$  occurs via the exchange of a  $\tilde{d}_{kR}$  squark in the

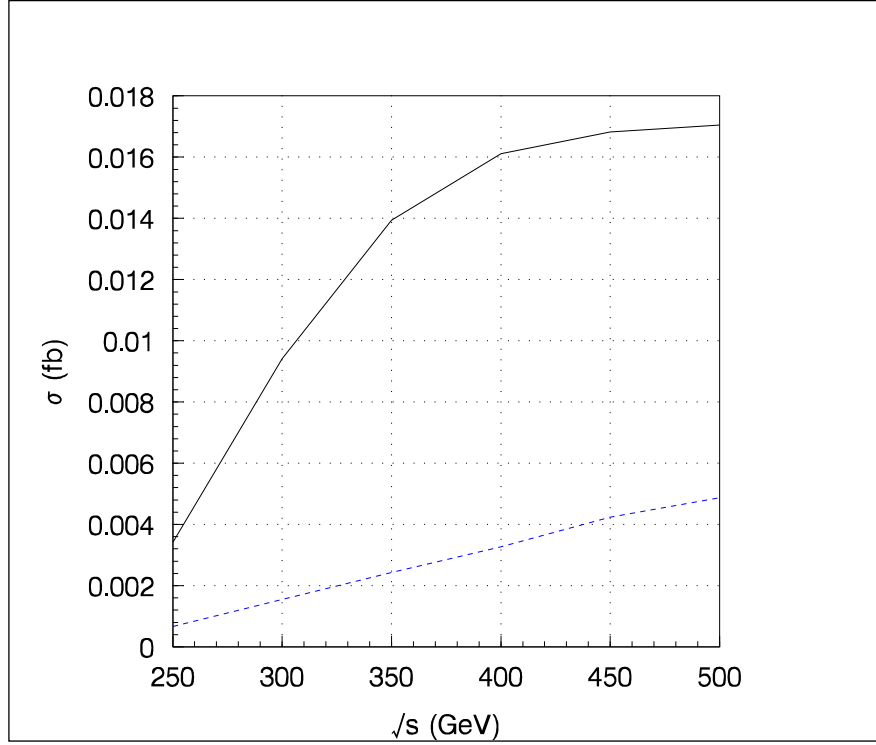


FIG. 9: Cross section of the reaction  $e^+e^- \rightarrow \gamma\gamma \rightarrow t\bar{c} + \bar{t}c$  as a function of the center of mass energy for  $\lambda'_{323}\lambda'_{333} = 0.096$ . The solid line corresponds to  $m_{\tilde{l}_{iL}} = m_{\tilde{d}_{kR}} = 100\text{GeV}$  and the dashed line to  $m_{\tilde{l}_{iL}} = m_{\tilde{d}_{kR}} = 150\text{GeV}$ .

$t$ -channel through the  $\mathcal{R}_p$  couplings  $\lambda'_{22k}$  and  $\lambda'_{23k}$ . In Fig.11 [34] the rate of this process is shown as a function of the center of mass energy for a value of the involved product of  $\mathcal{R}_p$  couplings  $\lambda'_{223}\lambda'_{233}$  equal to its low-energy limit for  $m_{\tilde{f}} = 100\text{GeV}$  namely 0.065. The motivation for considering the product  $\lambda'_{223}\lambda'_{233}$  is that it has the less stringent low-energy constraint among the  $\lambda'_{22k}\lambda'_{23k}$  products.

• **Sfermion pair production** In a version of the MSSM without degeneracies in the sleptons mass spectra, flavor changing effects can be induced in the supersymmetric particle pair production, which should be investigated with high precision measurement in the Next Linear Colliders [24]. The  $\mathcal{R}_p$  interactions could also generate such effects, through the exchange of a neutrino in the  $t$ -channel, in one of the much studied reaction : the slepton pair production,  $e^+e^- \rightarrow \tilde{l}_J\tilde{l}_{J'}^*$  ( $J \neq J'$ ). The flavour non-diagonal rates vary in the range,  $\sigma_{JJ'} \approx (\frac{\Lambda}{0.1})^4(2 - 20)$  fb [38], with  $\Lambda = \lambda, \lambda'$ , for sleptons masses,  $m_{\tilde{l}} < 400$  GeV, as one spans the interval of c.m. energies from the  $Z$  boson pole up to the TeV. Due to the strong dependence on the  $\mathcal{R}_p$  couplings, the flavour non-diagonal rates reach smaller values than the rates obtained in the flavours oscillation approach [40], which range between 250(100) and 0.1(0.01) fb for  $\sqrt{s} = 190(500)$  GeV.

## 1.7 $\mathcal{R}_p$ Contributions to CP Violation

The CP violation effects provide also some effective tests for new physics, since the contributions to the CP asymmetries in the Standard Model are small. It is the case,

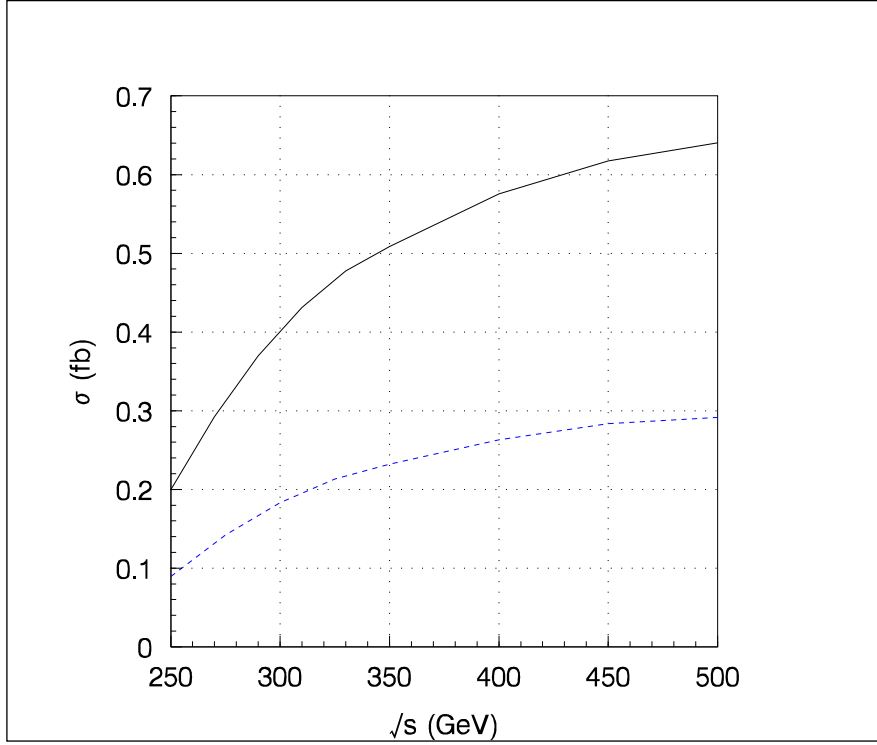


FIG. 10: Cross section of the reaction  $e^+e^- \rightarrow \gamma\gamma \rightarrow t\bar{c} + \bar{t}c$  as a function of the center of mass energy for  $\lambda''_{223}\lambda''_{323} = 0.625$ . The solid line corresponds to  $m_{\tilde{d}_R} = 100\text{GeV}$  and the dashed line to  $m_{\tilde{d}_R} = 150\text{GeV}$ .

for example, of the vector bosons ( $Z$  and/or  $W$  boson) decay rates CP-odd asymmetries [41, 42, 43]. On the other hand, in most proposals of physics beyond the Standard Model, the prospects for observing flavor changing effects in CP rate asymmetries are on the optimistic side. The MSSM contributions to CP violation are constrained from experimental bounds on low energy physics.

The R-parity odd coupling constants could have a complex phase and hence be by themselves an independent source of CP violation. This idea has motivated many studies on low energy  $\mathcal{R}_p$  physics. Furthermore, even if one assumes that the R-parity odd interactions are CP conserving, these could still lead, in combination with the other possible source of complex phase in the MSSM to new tests of CP Violation. For instance, the  $\mathcal{R}_p$  couplings could bring a dependence on the CKM matrix elements due to the fermion mass matrix transformation from current basis to mass basis.

The effects of  $\mathcal{R}_p$  interactions on the CP asymmetries in the processes,  $l^+l^- \rightarrow f_J\bar{f}_{J'}$ , with  $J \neq J'$ , were calculated in [36]. The  $\mathcal{R}_p$  contributions to these CP asymmetries, are controlled by interference terms between tree and loop level amplitudes. The consideration of loop amplitudes was restricted to the photon and  $Z$ -boson vertex corrections. The flavour off-diagonal CP asymmetries defined, at the  $Z$ -boson pole, as

$$A_{JJ'} = \frac{B_{JJ'} - B_{J'J}}{B_{JJ'} + B_{J'J}}, \quad (1.11)$$

lie approximately at,  $A_{JJ'} \approx (10^{-1} - 10^{-3})\sin\psi$ , where  $\psi$  is the CP odd phase. The off

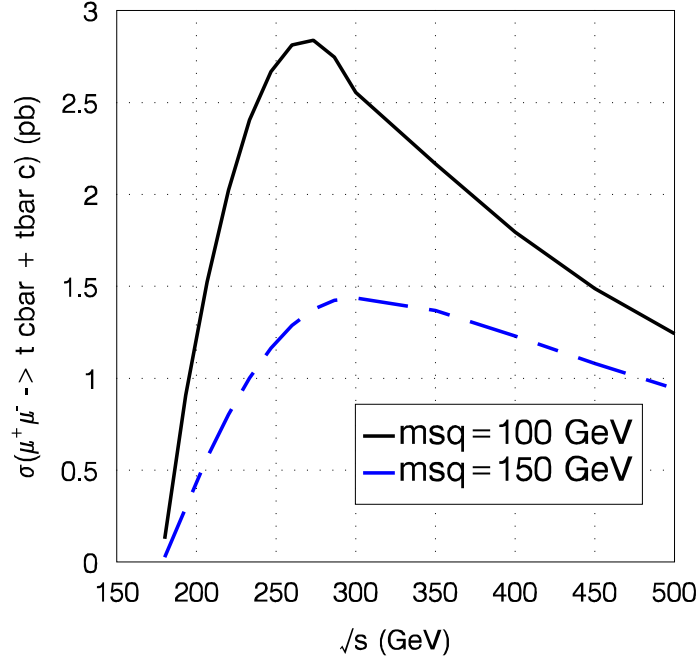


FIG. 11: Cross section of the reaction  $\mu^+\mu^- \rightarrow t\bar{c} + \bar{t}c$  as a function of the center of mass energy for  $\lambda'_{223}\lambda'_{233} = 0.065$ . The solid line corresponds to  $m_{\tilde{d}_{kR}} = 100\text{GeV}$  and the dashed line to  $m_{\tilde{d}_{kR}} = 150\text{GeV}$ .

Z-boson pole asymmetries given by,

$$A_{JJ'} = \frac{\sigma_{JJ'} - \sigma_{J'J}}{\sigma_{JJ'} + \sigma_{J'J}}, \quad (1.12)$$

lie at,  $A_{JJ'} \approx (10^{-2} - 10^{-3})\sin\psi$ , for leptons and quarks, irrespective of whether one deals with light or heavy flavours. The CP asymmetries depend on a ratio of different  $\mathcal{R}_p$  coupling constants, and are therefore less sensitive to these couplings than the flavour changing rates, which involve higher power of the  $\mathcal{R}_p$  constants. This is the reason why the results are optimistic with respect to the CP asymmetries for the  $Z$  decays in the Standard Model, which are,  $A_{JJ'} = [10^{-5}, 10^{-3}, 10^{-1}]\sin\delta_{CKM}$ ,  $\delta_{CKM}$  being the CP odd phase from the CKM matrix, for the production of  $(\bar{b}s + \bar{s}b)$ ,  $(\bar{b}d + \bar{d}b)$  and  $(\bar{d}s + \bar{s}d)$ , respectively [41, 42]. The particular rational dependence of the CP asymmetries on the couplings is of the form,  $\text{Im}(\lambda\lambda^*\lambda\lambda^*)/\lambda^4$ , and may thus lead to strong enhancement or suppression factors, depending on the largely unknown flavour hierarchical structure of the involved Yukawa couplings.

The study of the reaction  $l^+l^- \rightarrow t\bar{c}$  allows to learn about CP violation in the quark sector, due to the clear signature of the top quark :  $t \rightarrow bW \rightarrow bl\nu$ . In this reaction, the CP violation can be probed through the quantity defined in Eq.(1.12) or via the following

flavour off-diagonal CP asymmetry [35],

$$A = \frac{\frac{d\sigma^+}{dE_l} - \frac{d\sigma^-}{dE_l}}{\frac{d\sigma^+}{dE_l} + \frac{d\sigma^-}{dE_l}}, \quad (1.13)$$

where  $\sigma^+ = \sigma(l^+l^- \rightarrow t\bar{c} \rightarrow b\bar{c}l\nu)$ ,  $\sigma^- = \sigma(l^+l^- \rightarrow \bar{t}c \rightarrow \bar{b}cl\bar{\nu})$  and  $E_l$  is the energy of the produced charged lepton. The values of the CP asymmetries defined in Eq.(1.13) range typically in the interval  $A \approx (10^{-2} - 10^{-3}) \sin \psi$  for  $0\text{GeV} < E_l < 300\text{GeV}$  [35]. These CP asymmetries, as those defined in Eq.(1.12), could be enhanced up to  $\sim 10^{-1} \sin \psi$  should the  $\mathcal{R}_p$  coupling constants exhibit large hierarchies with respect to the generations.

If both non-degeneracies and mixing angles between all slepton flavours, as well as the CP odd phase, do not vanish, CP violation asymmetries could also be observable in supersymmetric particles pair production. The R-parity odd interactions could provide an alternative mechanism for explaining CP violation asymmetries in such productions, through possible  $\psi$  CP odd phase incorporated in the relevant dimensionless coupling constant. As for the fermion pair production, the  $\mathcal{R}_p$  contributions to the CP asymmetries in scalar particles pair production are controlled by interference terms between tree and loop level amplitudes. The flavour non-diagonal CP asymmetries for the slepton pair production,  $e^+e^- \rightarrow \tilde{l}_J \tilde{l}_{J'}^*$  ( $J \neq J'$ ), which are defined as in Eq.(1.12), are predicted to be of order,  $A_{JJ'} \approx (10^{-2} - 10^{-3}) \sin \psi$  [38].

Finally, the  $\mathcal{R}_p$  interactions could give rise to CP violation effects at tree level in the reaction  $e^+e^- \rightarrow \tau^+\tau^-$  via the observation of the double spin correlations for the produced tau-leptons pair. This possibility, which was studied in [44], stands out as an extremely interesting issue by itself, since previous studies of CP violating effects in,  $e^+e^- \rightarrow \tau^+\tau^-$ , that can emanate from multi-Higgs doublet model, leptoquark, Majorana  $\tilde{\nu}$  and supersymmetry, all occur at one loop level. Here, the CP asymmetries are generated from the exchange of a resonant  $\tilde{\nu}_\mu$  sneutrino in the  $s$ -channel, via the real coupling  $\lambda_{121}$  and a complex constant  $\lambda_{323}$ , if there is a  $\tilde{\nu}_\mu - \tilde{\bar{\nu}}_\mu$  mixing. This sneutrino mixing could generate both CP-even and CP-odd spin asymmetries which are forbidden in the Standard Model and that could be measured for  $\tau$  leptons at leptonic colliders. The observation of such asymmetries would provide explicit information about three different aspects of new physics :  $\tilde{\nu}_\mu - \tilde{\bar{\nu}}_\mu$  mixing, CP violation and R-parity violation. The sneutrino-antisneutrino mixing phenomena, which have been gaining some interest recently [45, 46, 47], is interesting since it is closely related to the generation of neutrino masses [45, 46]. At a centre of mass energy,  $\sqrt{s} = 192 \text{ GeV}$ , it is remarkable that the maximum value of these spin asymmetries can reach 75% for  $\Delta m_{\tilde{\nu}\mu} = \Gamma_{\tilde{\nu}\mu}$  and 10% for  $\Delta m_{\tilde{\nu}\mu} = \Gamma_{\tilde{\nu}\mu}/10$ , where  $\Delta m_{\tilde{\nu}\mu}$  is the mass splitting between the CP even  $\tilde{\nu}_+^\mu$  and CP odd  $\tilde{\nu}_-^\mu$  muon-sneutrino mass eigenstates and  $\Gamma_{\tilde{\nu}\mu}$  is the sneutrino width. Note that the condition  $\Delta m_{\tilde{\nu}\mu} \leq \Gamma_{\tilde{\nu}\mu}$  is necessary since then, if  $\Gamma_{\tilde{\nu}\mu} = 10^{-2} m_{\tilde{\nu}_\pm^\mu}$ , which is a viable estimation that has been assumed in the present study, the constraint,  $\Delta m_{\tilde{\nu}\mu}/m_{\tilde{\nu}_\pm^\mu} \ll 1$ , imposed by bounds on neutrino masses [46], is well respected. Furthermore, in the case,  $\Delta m_{\tilde{\nu}\mu} \leq \Gamma_{\tilde{\nu}\mu}$ , the two  $\tilde{\nu}_+^\mu$  and  $\tilde{\nu}_-^\mu$  resonances will overlap and distinguishing between them becomes a non trivial experimental task. Thus, the polarization asymmetries provide a feasible alternative for establishing the mass splitting,  $m_{\tilde{\nu}_+^\mu} \neq m_{\tilde{\nu}_-^\mu}$ . Assuming  $\mathcal{L} = 0.5 \text{ fb}^{-1}$  as the total integrated luminosity for LEP II at  $\sqrt{s} = 192 \text{ GeV}$  and setting,  $\lambda_{121} = 0.05$ ,  $|\lambda_{323}| = 0.06$ , the CP even and CP odd asymmetries may be detectable, under the best circumstances,



around the resonance region  $189.5 \text{ GeV} < m_{\tilde{\nu}^\mu} < 194 \text{ GeV}$  with a sensitivity of  $3\sigma$  for  $\Delta m_{\tilde{\nu}^\mu} = \Gamma_{\tilde{\nu}^\mu}/4$ . The polarization asymmetries depend on the relative values of the real part,  $a$ , and the imaginary part,  $b$ , of the complex coupling constant  $\lambda_{323}$ . With the simultaneous measurement of the CP conserving and CP violating asymmetries, the whole range,  $0 \leq \frac{b}{a+b} \leq 1$ , can be covered to at least  $3\sigma$  for  $\Delta m_{\tilde{\nu}^\mu} = \Gamma_{\tilde{\nu}^\mu}/4$  and  $m_{\tilde{\nu}^\mu} = \sqrt{s} = 192 \text{ GeV}$ . At the Next Linear Colliders, with an energy of  $\sqrt{s} = 500 \text{ GeV}$ , the CP asymmetries could be probed to at least  $3\sigma$  (best effects are at the  $20\sigma$  level) for the range  $490 \text{ GeV} < m_{\tilde{\nu}^\mu} < 510 \text{ GeV}$  and for  $\Delta m_{\tilde{\nu}^\mu} = \Gamma_{\tilde{\nu}^\mu}/5$ . Also, with  $\Delta m_{\tilde{\nu}^\mu} = 1 \text{ GeV}$ , the NLC will have a sensitivity above  $3\sigma$  over almost the entire range,  $0 \leq \frac{b}{a+b} \leq 1$ .

## 2 Singly Produced Sparticles at Hadronic Colliders

### 2.1 Resonant Production of Sparticles

The SUSY particles can be produced as resonances at hadronic colliders through the  $\mathcal{R}_p$  interactions. This is particularly attractive as hadronic colliders allow to probe for resonances over a wide mass range given the continuous energy distribution of the colliding partons. If a single  $\mathcal{R}_p$ -violating coupling is dominant, the resonant SUSY particle may decay through the same coupling involved in its production, giving a two quarks final state at the partonic level. However, it is also possible that the decay of the resonant SUSY particle is mainly due to gauge interactions, giving rise to a cascade decay.

• **Resonant production via  $\lambda'$**  First, a resonant sneutrino can be produced in  $d\bar{d}$  annihilations through the constant  $\lambda'_{ijk}$ . The associated formula can be written as follows [64] :

$$\sigma(d_k \bar{d}_j \rightarrow \tilde{\nu}^i \rightarrow X_1 X_2) = \frac{4}{9} \frac{\pi \Gamma_{d_k \bar{d}_j} \Gamma_f}{(\hat{s} - m_{\tilde{\nu}^i}^2)^2 + m_{\tilde{\nu}^i}^2 \Gamma_{\tilde{\nu}^i}^2}, \quad (2.1)$$

where  $\Gamma_{d_k \bar{d}_j}$ , and  $\Gamma_f$  are the partial width of the channels,  $\tilde{\nu}^i \rightarrow d_k \bar{d}_j$ , and,  $\tilde{\nu}^i \rightarrow X_1 X_2$ , respectively,  $\Gamma_{\tilde{\nu}^i}$  is the total width of the sneutrino,  $m_{\tilde{\nu}^i}$  is the sneutrino mass and  $\hat{s}$  is the square of the parton center of mass energy. The factor  $1/3$  in front is from matching the initial colors, and  $\Gamma_{d_k \bar{d}_j}$  is given by,

$$\Gamma_{d_k \bar{d}_j} = \frac{3}{4} \alpha_{\lambda'_{ijk}} m_{\tilde{\nu}^i}, \quad (2.2)$$

where  $\alpha_{\lambda'_{ijk}} = \lambda'^2_{ijk}/4\pi$ . To compute the rate at a  $p\bar{p}$  collider, the usual formalism of the parton model of hadrons can be used [65] :

$$\sigma(p\bar{p} \rightarrow \tilde{\nu}^i \rightarrow X_1 X_2) = \sum_{j,k} \int_{\tau_0}^1 \frac{d\tau}{\tau} \left( \frac{1}{s} \frac{dL_{jk}}{d\tau} \right) \hat{s} \sigma(d_k \bar{d}_j \rightarrow \tilde{\nu}^i \rightarrow X_1 X_2), \quad (2.3)$$

where  $s$  is the center of mass energy squared,  $\tau_0$  is given by  $\tau_0 = (M_{X_1} + M_{X_2})^2/s$  and  $\tau$  is defined by  $\tau = \hat{s}/s = x_1 x_2$ ,  $x_1, x_2$  denoting the longitudinal momentum fractions of the initial partons  $j$  and  $k$ , respectively. The quantity  $dL_{jk}/d\tau$  is the parton luminosity defined by,

$$\frac{dL_{jk}}{d\tau} = \int_{\tau}^1 \frac{dx_1}{x_1} [f_j^{\bar{p}}(x_1) f_k^p(\tau/x_1) + f_j^p(x_1) f_k^{\bar{p}}(\tau/x_1)], \quad (2.4)$$

where the parton distribution  $f_j^h(x_1)$  denotes the probability of finding a parton  $j$  with momentum fraction  $x_1$  inside a hadron  $h$ , and generally depends on the Bjorken variable,  $Q^2$ , the square of the characteristic energy scale of the process under consideration. The parton distributions are measured experimentally at a given scale, and are evolved to the very large momentum scales of interest, via the Altarelli-Parisi equations. In order to see the effects of the parton distributions on the resonant sneutrino production, some values of the rates are given in the following [49] : For instance, with an initial state,  $d\bar{d}$ , for the hard process, the cross section value is,  $\sigma(p\bar{p} \rightarrow \tilde{\nu}^i) = 8.5$  nanobarns, for a sneutrino mass of 100 GeV and a coupling,  $\lambda'_{i11} = 1$ , at  $\sqrt{s} = 2$  TeV. For identical values of the parameters and of the c.m. energy, the cross section is  $\sigma(p\bar{p} \rightarrow \tilde{\nu}^i) = 4$  nanobarns with an initial state,  $d\bar{s}$ , and  $\sigma(p\bar{p} \rightarrow \tilde{\nu}^i) = 0.8$  nanobarns with an initial state,  $d\bar{b}$ .

The charged slepton can also be produced as a resonance at hadronic colliders from an initial state  $u_j\bar{d}_k$  and via the constant  $\lambda'_{ijk}$ . The cross section value is,  $\sigma(p\bar{p} \rightarrow \tilde{l}_L^i) = 2$  nanobarns, for  $m_{\tilde{l}_L} = 100$  GeV,  $\sqrt{s} = 2$  TeV and  $\lambda'_{i11} = 1$  ([49, 12]).

• **Resonant production via  $\lambda''$**  The baryon number violating couplings  $\lambda''_{ijk}$  allows for resonant production of squarks at hadronic colliders. Either a squark  $\tilde{u}_i$  or  $\tilde{d}_k$  can be produced at the resonance from an initial state,  $\bar{d}_j\bar{d}_k$  or  $\bar{u}_i\bar{d}_j$ , respectively. For  $m_{\tilde{d}_R^k} = 100$  GeV,  $\sqrt{s} = 2$  TeV and  $\lambda''_{11k} = 1$ , the rate of the down squark production at the Tevatron is  $\sigma(p\bar{p} \rightarrow \tilde{d}_R^k) = 25$  nanobarns [49]. For  $m_{\tilde{t}_1} = 600$  GeV,  $\sqrt{s} = 2$  TeV and  $\lambda''_{323} = 0.1$ , the rate of the resonant stop production is  $\sigma(p\bar{p} \rightarrow \tilde{t}_1) = 10^{-3}$  picobarns [69]. Note that this rate is higher than the stop pair production rate at the same c.m. energy and for the same stop mass, which is of order  $\sigma(p\bar{p} \rightarrow \tilde{t}_1\tilde{t}_1) = 10^{-6}$  picobarns.

## 2.2 Single Gaugino Production

• **Single production via  $\lambda''$**  The single superpartner production could also occur as a  $2 \rightarrow 2$ -body process, through an  $\mathcal{R}_p$  coupling  $\lambda''$  and an ordinary gauge interaction vertex. In baryon number violating models, any gaugino (including gluino) can be produced in association with a quark, in quark-quark scattering, by the exchange of a squark in the  $s$ -,  $t$ - or  $u$ -channel.

For example, let us consider the photino and gluino production [49] : The rate values in the  $t$ - and  $u$ -channel are,  $\sigma(p\bar{p} \rightarrow \tilde{\gamma}q) = 2 \cdot 10^{-2}$  nb , and,  $\sigma(p\bar{p} \rightarrow \tilde{g}q) = 3 \cdot 10^{-1}$  nb , for,  $m_{\tilde{q}} = m_{\tilde{g}} = m_{\tilde{\gamma}} = 100$  GeV,  $\sqrt{s} = 2$  TeV and  $\lambda''_{111} = 1$ . The photino or gluino which is produced will then decay into three jets via the  $\lambda''$  coupling, resulting in a four jets final state. The corresponding QCD background is strong : It is estimated to be about 10 nb for  $\sqrt{s} = 2$  TeV [68]. Of course, the ratio signal over background can be enhanced considerably by looking at the mass distribution of the jets : the QCD 4 jets are produced relatively uncorrelated, while the trijet mass distribution of the signal should peak around the gaugino mass. However, frequently one of the three jets will be too soft to be measured and at other times jet coalescence would occur, especially for small values of the gaugino mass. The study of this example bring us to the conclusion that, due to high QCD background, the analysis of the single production via  $\lambda''$  remains a challenge.

Nevertheless, there is one case of interest, were the final state could be particularly clear [69, 92] : A  $\tilde{\chi}_1^+$  chargino can be produced through the resonant production of a top squark,  $\bar{d}_j\bar{d}_k \rightarrow \tilde{t}_1 \rightarrow b\tilde{\chi}_1^+$  (via  $\lambda''_{3jk}$ ), and then decay into the lightest neutralino plus leptons as  $\tilde{\chi}_1^+ \rightarrow \bar{l}_i\nu_i\tilde{\chi}_1^0$ . Due to the stop resonance, this reaction could reach high

rate values. The cascade decay demands the mass hierarchy,  $m_{\tilde{t}_1} > m_{\chi_1^+} > m_{\chi_1^0}$ , to be respected, and by consequence is not allowed in all regions of the Supergravity parameter space. If we made the hypothesis that  $\tilde{\chi}_1^0$  is the LSP and undergo an  $\mathcal{R}_p$  decay outside of the detector, the neutralino should then be treated as a stable particle. Then, the signal for our process would be very clear since it would consist of a tagged b quark jet, a lepton and missing transverse energy. The Standard Model background for such a signature comes from the the single top quark production, via  $W g$  fusion, and the production of a  $W$  gauge boson in association with  $b\bar{b}$ ,  $c\bar{c}$  or a jet that is mistaken for a b quark. Applying some cuts in order to simulate the acceptance of the detector and to reduce the background, it has been found that values of  $\lambda'' > 0.03 - 0.2$  and  $\lambda'' > 0.01 - 0.03$  can be excluded at the 95% confidence level for,  $180 \text{ GeV} < m_{\tilde{t}_1} < 285 \text{ GeV}$ , at the Run I of the Tevatron ( $\sqrt{s} = 1.8 \text{ TeV}$  and  $\int \mathcal{L} dt = 110 \text{ pb}^{-1}$ ) and for,  $180 < m_{\tilde{t}_1} < 325 \text{ GeV}$ , at the Run II of the Tevatron ( $\sqrt{s} = 2 \text{ TeV}$  and  $\int \mathcal{L} dt = 2 \text{ fb}^{-1}$ ), respectively. This result is based on the leading-order CTEQ-4L parton distribution functions [70] and holds for the normalization,  $\lambda'' = \lambda''_{312} = \lambda''_{313} = \lambda''_{323}$ , and for the point of a minimal Supergravity model,  $m_{1/2} = 150 \text{ GeV}$ ,  $A_0 = -300 \text{ GeV}$  and  $\tan \beta = 4$ . The constraints obtained on  $\lambda''$  are stronger than the present low energy bounds.

• **Single production via  $\lambda'$**  The single production of SUSY particles via  $\lambda'$  occuring through  $2 \rightarrow 2$ -body processes, offers the opportunity to study the parameter space of the  $\mathcal{R}_p$  models with a quite high sensitivity at hadronic colliders.

In Fig.12, we present all the single superpartner productions which occur via  $\lambda'_{ijk}$  through  $2 \rightarrow 2$ -body processes at hadronic colliders and receive a contribution from a resonant SUSY particle production [74]. The spin summed amplitudes of those reactions including the higgsino contributions have been calculated in [74]. In a SUGRA model, the rates of the reactions presented in Fig.12 depend mainly on the  $m_0$  and  $M_2$  parameters.

In Fig.13, we show the variations of the  $\sigma(p\bar{p} \rightarrow \tilde{\chi}_{1,2}^+ \mu^-)$  cross sections with  $m_0$  for fixed values of  $M_2$ ,  $\mu$  and  $\tan \beta$  and various  $\mathcal{R}_p$  couplings of the type  $\lambda'_{2jk}$  at Tevatron Run II in a SUGRA model [74]. The  $\mathcal{R}_p$  couplings giving the highest cross sections have been considered. The  $\sigma(p\bar{p} \rightarrow \tilde{\chi}_{1,2}^+ \mu^-)$  rates decrease when  $m_0$  increases since then the sneutrino becomes heavier and more energetic initial partons are required in order to produce the resonant sneutrino. A decrease of the cross sections also occurs at small values of  $m_0$ , the reason being that when  $m_0$  approaches  $M_2$  the  $\tilde{\nu}$  mass is getting closer to the  $\tilde{\chi}^\pm$  masses so that the phase space factors associated to the decays  $\tilde{\nu}_\mu \rightarrow \chi_{1,2}^\pm \mu^\mp$  decrease. The differences between the  $\tilde{\chi}_1^+ \mu^-$  production rates occuring via the various  $\lambda'_{2jk}$  couplings are explained by the different partonic luminosities. Indeed, as shown in Fig.12 the hard process associated to the  $\tilde{\chi}_1^+ \mu^-$  production occuring through the  $\lambda'_{2jk}$  coupling constant has a partonic initial state  $\bar{q}_j q_k$ . The  $\tilde{\chi}_1^+ \mu^-$  production via the  $\lambda'_{211}$  coupling has first generation quarks in the initial state which provide the maximum partonic luminosity.

In Fig.14, we show the variations of the rates of the reactions  $p\bar{p} \rightarrow \tilde{\chi}_1^- \nu$ ,  $p\bar{p} \rightarrow \tilde{\chi}_{1,2}^0 \mu^-$  and  $p\bar{p} \rightarrow \tilde{\chi}_1^0 \nu$  with the  $m_0$  parameter in a SUGRA model [74]. We see in this figure that the single neutralino productions do not decrease at small  $m_0$  values in contrast with the single chargino productions (see also Fig.13). This is due to the fact that in SUGRA scenarios the  $\tilde{\chi}_1^0$  and  $\tilde{l}_L$  ( $\tilde{l}_L = \tilde{l}_L^\pm, \tilde{\nu}_L$ ) masses are never close enough to induce a significant decrease of the phase space factor associated to the decay  $\tilde{l}_L \rightarrow \tilde{\chi}_1^0 l$  ( $l = l^\pm, \nu$ ). By analysing Fig.13 and Fig.14, we also remark that the  $\tilde{\chi}^- \nu$  ( $\tilde{\chi}^0 \mu^-$ ) production rate is larger than the  $\tilde{\chi}^+ \mu^-$  ( $\tilde{\chi}^0 \nu$ ) production rate. The explanation is that in  $p\bar{p}$  collisions the

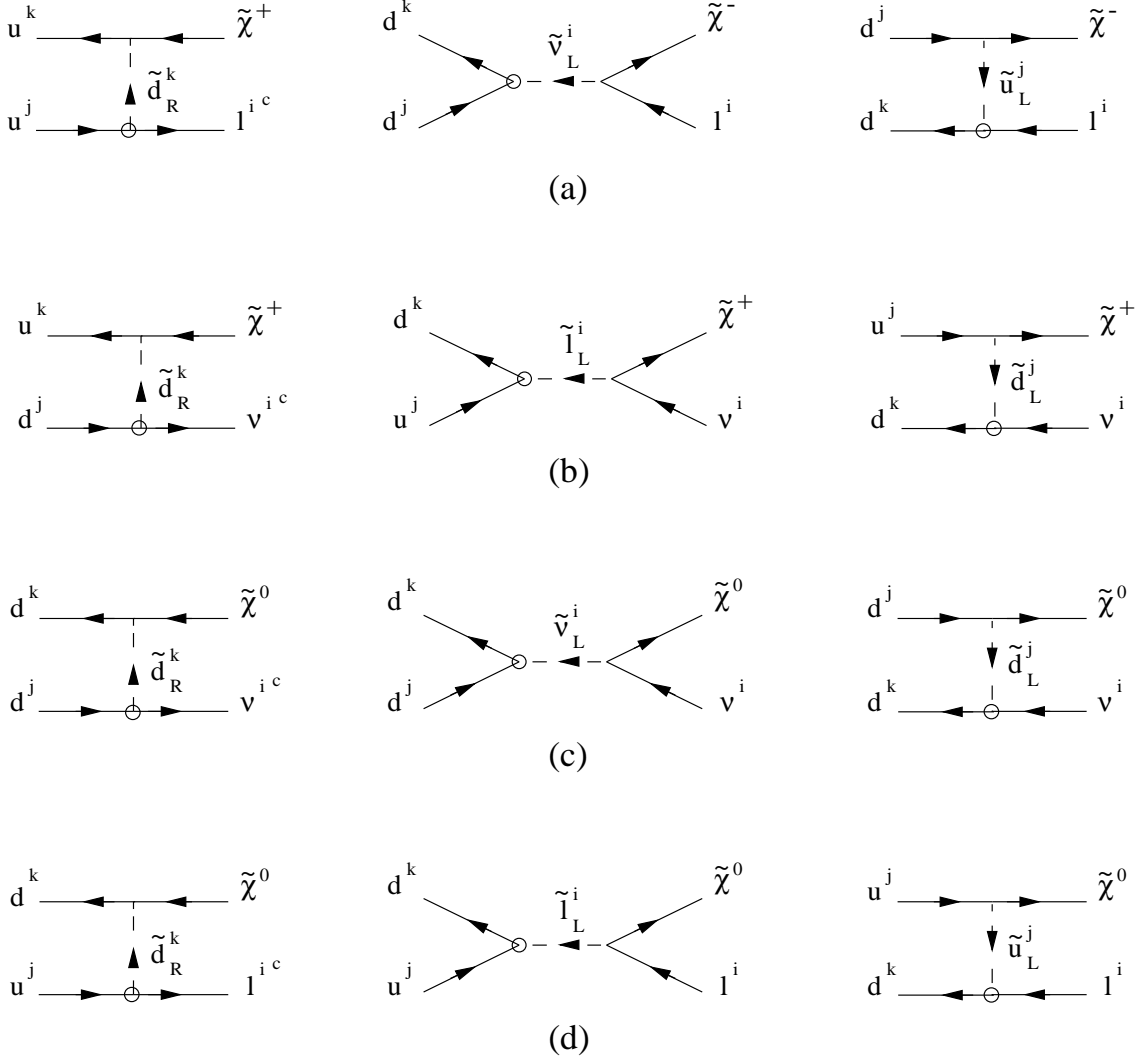


FIG. 12: Feynman diagrams for the four single superpartner production reactions involving  $\lambda'_{ijk}$  at hadronic colliders which receive a contribution from a resonant supersymmetric particle production. The  $\lambda'_{ijk}$  coupling constant is symbolised by a small circle and the arrows denote the flow of the particle momentum.

initial states of the resonant charged slepton production  $u_j \bar{d}_k, \bar{u}_j d_k$  have higher partonic luminosities than the initial states of the resonant sneutrino production  $d_j \bar{d}_k, \bar{d}_j d_k$ .

The neutralino production in association with a charged lepton via  $\lambda'$  (see Fig.12(d)) is an interesting case at Tevatron [49]. The topology of the events consists of an isolated lepton in one hemisphere balanced by a lepton plus two jets in the other hemisphere, coming from the neutralino decay via  $\lambda'$ . The Standard Model background arising from the production of two jets plus a  $Z^0$ , decaying into two leptons, has a cross section of order  $10^{-3}$  nb [65], and can be greatly reduced by excluding lepton pairs with an invariant mass equal to the  $Z^0$  mass. The other source of Standard Model background, which is the Drell-Yan mechanism into 2 leptons accompanied by 2 jets, is suppressed by a factor,  $10^{-6}/\alpha_\lambda$ . Moreover, the signal can be enhanced by looking at the invariant mass of the 2 jets and

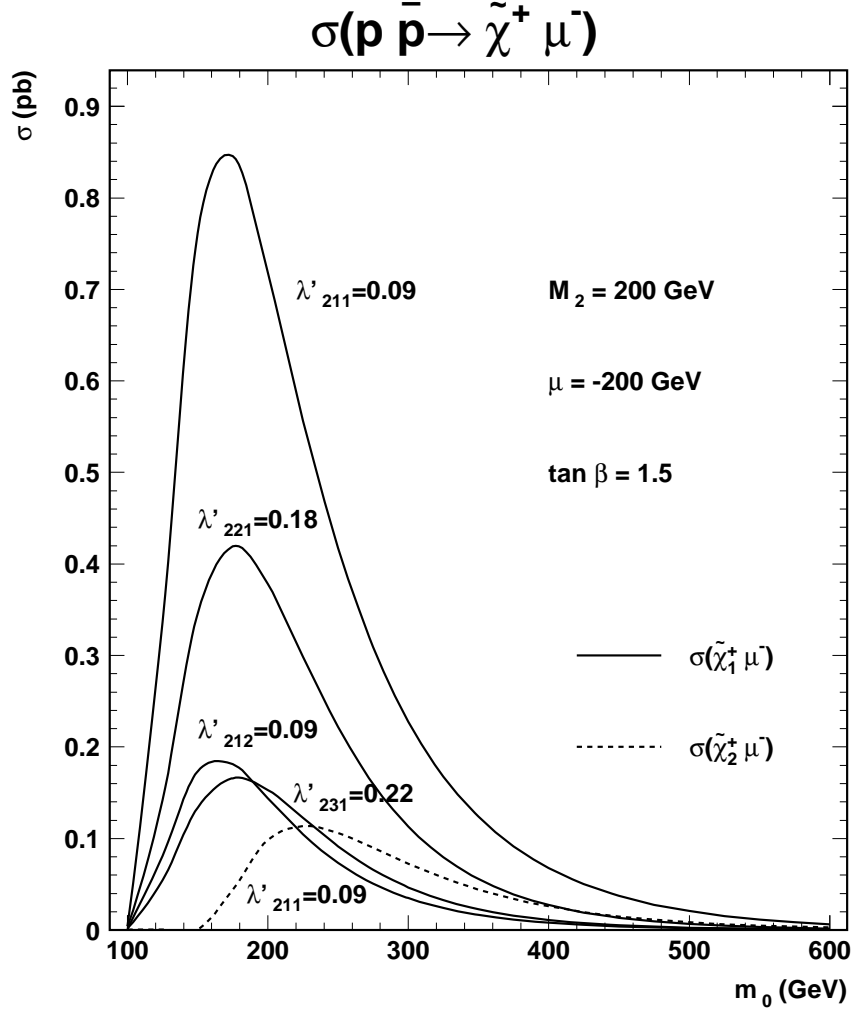


FIG. 13: Cross sections (in  $pb$ ) of the single chargino productions  $p\bar{p} \rightarrow \tilde{\chi}_{1,2}^+ \mu^-$  as a function of the  $m_0$  parameter (in  $GeV$ ). The center of mass energy is taken at  $\sqrt{s} = 2TeV$  and the considered set of parameters is :  $\lambda'_{211} = 0.09$ ,  $M_2 = 200GeV$ ,  $\tan \beta = 1.5$  and  $\mu = -200GeV$ . The rates for the  $\tilde{\chi}_1^+$  production via the  $\mathcal{R}_p$  couplings  $\lambda'_{212} = 0.09$ ,  $\lambda'_{221} = 0.18$  and  $\lambda'_{231} = 0.22$  are also given. The chosen values of the  $\mathcal{R}_p$  couplings correspond to the low-energy limits for a squark mass of  $100GeV$  [75].

the lepton in the same hemisphere, which should peak around the neutralino mass.

The single production via  $\lambda'$  of the neutralino together with a charged lepton can also generate clean signatures free from large Standard Model background at the Tevatron Run II, containing two like-sign charged leptons [13, 71, 92, 72, 73, 74]. As a matter of fact, the neutralino has a decay channel into a lepton and two jets through the coupling  $\lambda'_{ijk}$  and due to its Majorana nature, the neutralino decays to the charge conjugate final states with equal probability :  $\Gamma(\tilde{\chi}^0 \rightarrow l_i u_j \bar{d}_k) = \Gamma(\tilde{\chi}^0 \rightarrow \bar{l}_i \bar{u}_j d_k)$ . Therefore, the lepton coming from the production can have the same sign than the one coming from the neutralino decay. Since  $\lambda'_{111}$  has a strong indirect bound, it is interesting to consider the coupling

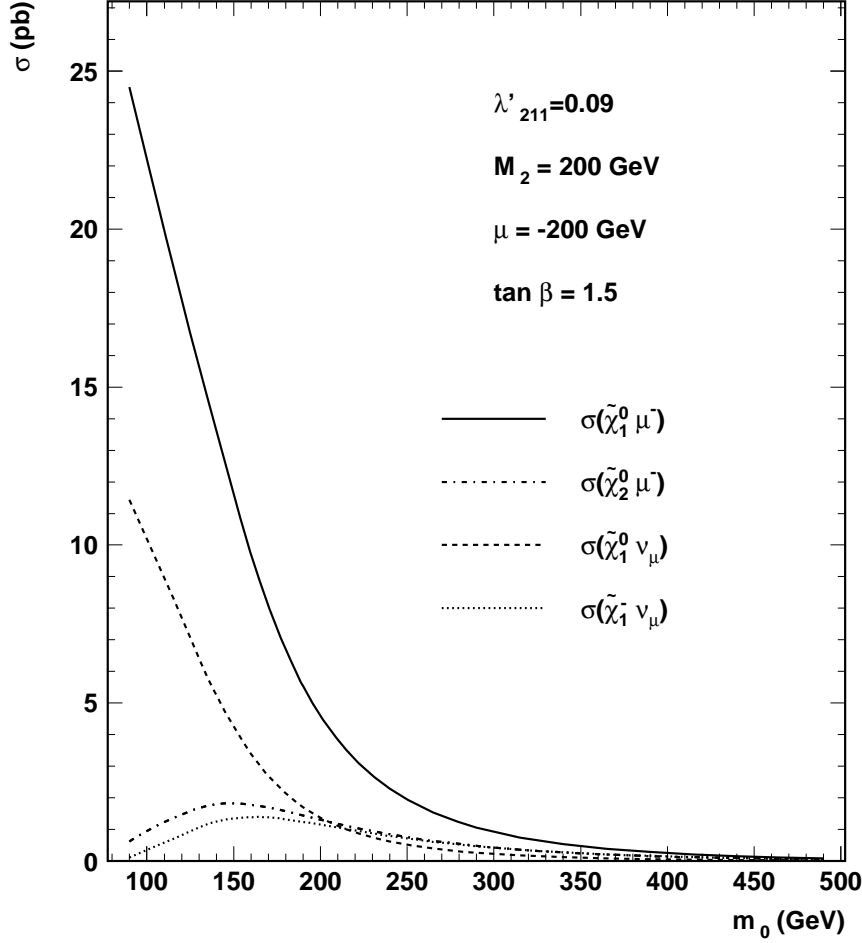


FIG. 14: Cross sections (in  $pb$ ) of the  $\tilde{\chi}_1^- \nu$ ,  $\tilde{\chi}_{1,2}^0 \mu^-$  and  $\tilde{\chi}_1^0 \nu$  productions at Tevatron Run II as a function of the  $m_0$  parameter (in  $GeV$ ). The center of mass energy is taken at  $\sqrt{s} = 2TeV$  and the considered set of parameters is :  $\lambda'_{211} = 0.09$ ,  $M_2 = 200GeV$ ,  $\tan \beta = 1.5$  and  $\mu = -200GeV$ .

constant  $\lambda'_{211}$ , which corresponds to the dimuons production with an initial state  $u\bar{d}$  or  $\bar{u}d$  (see Fig.12(d)) composed of first generation quarks. The analysis of the like sign ditau signature generated by the  $\tilde{\chi}^0 \tau^\pm$  production through the  $\lambda'_{311}$  coupling (see Fig.12(d)) suffers a reduction of the cuts efficiency due to the tau-lepton decay. Besides, the study of the  $\tilde{\chi}_1^0 \mu^\pm$  production via  $\lambda'_{211}$  in a scenario where the  $\tilde{\chi}_1^0$  is the LSP is particularly attractive since then the  $\tilde{\chi}_1^0$  can only undergo  $\tilde{R}_p$  decays. It was found that in a SUGRA model, such a study could probe values of the  $\lambda'_{211}$  coupling at the  $5\sigma$  discovery level down to  $2 \cdot 10^{-3}$  ( $10^{-2}$ ) for a muon-slepton mass of  $m_{\tilde{\mu}_L} = 100GeV$  ( $m_{\tilde{\mu}_L} = 300GeV$ ) with  $M_2 = 100GeV$ ,  $2 < \tan \beta < 10$  and  $|\mu| < 10^3GeV$  at Tevatron Run II assuming a luminosity of  $\mathcal{L} = 2fb^{-1}$  [71, 92], and down to  $2 \cdot 10^{-3}$  ( $10^{-2}$ ) for  $m_{\tilde{\mu}_L} = 223GeV$  ( $m_{\tilde{\mu}_L} = 540GeV$ ) with  $m_{1/2} = 300GeV$ ,  $A = 300GeV$ ,  $\tan \beta = 2$  and  $sign(\mu) > 0$  at the

$\lambda'_{211}$	$\lambda'_{212}$	$\lambda'_{213}$	$\lambda'_{221}$	$\lambda'_{222}$	$\lambda'_{223}$	$\lambda'_{231}$	$\lambda'_{232}$	$\lambda'_{233}$
0.01	0.02	0.02	0.02	0.03	0.05	0.03	0.06	0.09

TAB. 1: Sensitivities on the  $\lambda'_{2jk}$  coupling constants for  $\tan\beta=1.5$ ,  $M_1 = 100$  GeV,  $M_2 = 200$  GeV,  $\mu = -500$  GeV,  $m_{\tilde{q}} = m_{\tilde{l}} = 300$  GeV and  $m_{\tilde{\nu}} = 400$  GeV, assuming an integrated luminosity of  $\mathcal{L} = 30fb^{-1}$ .

LHC assuming a luminosity of  $\mathcal{L} = 10fb^{-1}$  [72, 73]. It was also shown in [74], by using a detector response simulation, that the study of the single LSP production at Tevatron Run II  $p\bar{p} \rightarrow \tilde{\chi}_1^0 \mu^\pm$  would allow to probe  $m_{1/2}$  values up to  $\sim 850GeV$  and  $m_0$  values up to  $\sim 550GeV$  at the  $5\sigma$  discovery level, in a SUGRA scenario where  $sign(\mu) < 0$ ,  $A = 0$ ,  $\tan\beta = 1.5$  and  $\lambda'_{211} = 0.05$  and assuming a luminosity of  $\mathcal{L} = 2fb^{-1}$ .

Besides, the like sign dilepton signature analysis based on the  $\tilde{\chi}_1^0 \mu^\pm$  production (see Fig.12(d)) allows the  $\tilde{\chi}_1^0$  and  $\tilde{\mu}_L^\pm$  mass reconstructions since the decay chain  $\tilde{\mu}_L^\pm \rightarrow \tilde{\chi}_1^0 \mu^\pm$ ,  $\tilde{\chi}_1^0 \rightarrow \mu^\pm u d$  can be fully reconstructed [74]. Based on the like sign dilepton signature analysis, the  $\tilde{\chi}_1^0$  ( $\tilde{\mu}_L^\pm$ ) mass could be measured with a statistical error of  $\sim 11GeV$  ( $\sim 20GeV$ ) at the Tevatron Run II [74].

The single  $\tilde{\chi}_1^\pm$  production in association with a charged lepton (see Fig.12(a)) is another interesting reaction at hadronic colliders. In a scenario where  $\tilde{\chi}_1^0$  is the LSP and  $m_{\tilde{\nu}}, m_{\tilde{l}}, m_{\tilde{q}} > m_{\tilde{\chi}_1^\pm}$ , this single production receives a contribution from the resonant sneutrino production and the singly produced chargino decays into quarks and leptons with branching ratios respectively of  $B(\tilde{\chi}_1^\pm \rightarrow \tilde{\chi}_1^0 d_p u_{p'}) \approx 70\%$  ( $p = 1, 2, 3; p' = 1, 2$ ) and  $B(\tilde{\chi}_1^\pm \rightarrow \tilde{\chi}_1^0 l_p^\pm \nu_p) \approx 30\%$  due to the color factor. The neutralino decays via  $\lambda'_{ijk}$  either into a lepton as,  $\tilde{\chi}_1^0 \rightarrow l_i u_j \bar{d}_k, \bar{l}_i \bar{u}_j d_k$ , or into a neutrino as,  $\tilde{\chi}_1^0 \rightarrow \nu_i d_j \bar{d}_k, \bar{\nu}_i \bar{d}_j d_k$ . Hence, if both the  $\tilde{\chi}_1^\pm$  and  $\tilde{\chi}_1^0$  decay into charged leptons, the  $\tilde{\chi}_1^\pm l_i^\mp$  production can lead to the three charged leptons signature which has a small Standard Model background at hadronic colliders [76, 77, 73, 78, 74]. The study of the three leptons signature generated by the  $\tilde{\chi}_1^\pm \mu^\mp$  production via the  $\lambda'_{211}$  coupling constant is particularly interesting for the same reasons as above. The sensitivity on the  $\lambda'_{211}$  coupling obtained from this study at Tevatron Run II would reach a maximum value of  $\sim 0.04$  for  $m_0 \approx 200GeV$  in a SUGRA model with  $M_2 = 200GeV$ ,  $sign(\mu) < 0$ ,  $A = 0$  and  $\tan\beta = 1.5$ , assuming a luminosity of  $\mathcal{L} = 2fb^{-1}$  [74]. In Table 1 we show the sensitivities on the  $\lambda'_{2jk}$  couplings that could be obtained from the trilepton analysis based on the  $\tilde{\chi}_1^\pm \mu^\mp$  production at the LHC for a given set of MSSM parameters [78]. For each of the  $\lambda'_{2jk}$  couplings the sensitivity has been obtained assuming that the considered coupling was the single dominant one. The difference between the various results presented in this table is due to the fact that each  $\lambda'_{2jk}$  coupling involves a specific initial state (see Fig.12(a)) with its own parton density. Besides, all the sensitivities shown in Table 1 improve greatly the present low-energy constraints. The trilepton analysis based on the  $\tilde{\chi}_1^\pm e^\mp$  ( $\tilde{\chi}_1^\pm \tau^\mp$ ) production would allow to test the  $\lambda'_{1jk}$  ( $\lambda'_{3jk}$ ) couplings constants. While the sensitivities obtained on the  $\lambda'_{1jk}$  couplings are expected to be of the same order of those presented in Table 1, the sensitivities on the  $\lambda'_{3jk}$  couplings should be weaker due to the tau-lepton decay. The results presented in Table 1 illustrate the fact that even if some studies on the single superpartner production via  $\lambda'$  at hadronic colliders (see Fig.12) only concern the  $\lambda'_{211}$  coupling constant, the analysis of a given single superpartner production at Tevatron or LHC allows to probe many  $\lambda'_{ijk}$  coupling constants down to values smaller than the associated low-energy limits.

Besides, the three leptons final state study based on the  $\tilde{\chi}_1^\pm \mu^\mp$  production (see Fig.12(a)) allows to reconstruct the  $\tilde{\chi}_1^0$ ,  $\tilde{\chi}_1^\pm$  and  $\tilde{\nu}$  masses [76, 77, 73, 78, 74]. Indeed, the decay chain  $\tilde{\nu}_i \rightarrow \tilde{\chi}_1^\pm l_i^\mp$ ,  $\tilde{\chi}_1^\pm \rightarrow \tilde{\chi}_1^{0\pm} \nu_p$ ,  $\tilde{\chi}_1^0 \rightarrow l_i^\pm u_j d_k$  can be fully reconstructed since the produced charged leptons can be identified thanks to their flavours and signs. Based on the tripleton signature analysis, the  $\tilde{\chi}_1^0$  mass could be measured with a statistical error of  $\sim 9\text{GeV}$  at the Tevatron Run II [76, 74] and of  $\sim 100\text{MeV}$  at the LHC [77, 73, 78]. Furthermore, the width of the gaussian shape of the invariant mass distribution associated to the  $\tilde{\chi}_1^\pm$  ( $\tilde{\nu}$ ) mass is of  $\sim 6\text{GeV}$  ( $\sim 10\text{GeV}$ ) at the LHC for the MSSM point defined by  $M_1 = 75\text{GeV}$ ,  $M_2 = 150\text{GeV}$ ,  $\mu = -200\text{GeV}$ ,  $m_{\tilde{f}} = 300\text{GeV}$  and  $A = 0$  [77, 73, 78]. Let us make a general remark concerning the superpartner mass reconstructions based on the single superpartner production studies at hadronic colliders : The combinatorial background associated to these mass reconstructions is smaller than in the mass reconstructions analyses based on the supersymmetric particle pair production since in the single superpartner production studies only one cascade decay must be reconstructed.

## 2.3 Non Resonant Single Production

At hadronic colliders, some supersymmetric particles can also be singly produced through  $2 \rightarrow 2$ -body processes which generally do not receive contribution from resonant superpartner production [74] : Some single productions of squark (slepton) in association with a gauge boson can occur through the exchange of a quark in the  $t$ -channel or a squark (slepton) in the  $s$ -channel via  $\lambda''$  ( $\lambda'$ ). From an initial state  $g$   $q$ , a squark (slepton) can also be singly produced together with a quark (lepton) with a coupling constant  $\lambda''$  ( $\lambda'$ ) via the exchange of a quark or a squark in the  $t$ -channel, and of a quark in the  $s$ -channel. Finally, a gluino can be produced in association with a lepton (quark) through a coupling constant  $\lambda'$  ( $\lambda''$ ) via the exchange of a squark in the  $t$ -channel (and in the  $s$ -channel).

Let us enumerate the single scalar particle and gluino productions occuring via the  $2 \rightarrow 2$ -body processes which involve the  $\lambda'_{ijk}$  coupling constants [74] (one must also add the charge conjugate processes) :

- The gluino production  $\bar{u}_j d_k \rightarrow \tilde{g} l_i$  via the exchange of a  $\tilde{u}_{jL}$  ( $\tilde{d}_{kR}$ ) squark in the  $t$  ( $u$ ) channel.
- The squark production  $\bar{d}_j g \rightarrow \tilde{d}_{kR}^* \nu_i$  via the exchange of a  $\tilde{d}_{kR}$  squark ( $d_j$  quark) in the  $t$  ( $s$ ) channel.
- The squark production  $\bar{u}_j g \rightarrow \tilde{d}_{kR}^* l_i$  via the exchange of a  $\tilde{d}_{kR}$  squark ( $u_j$  quark) in the  $t$  ( $s$ ) channel.
- The squark production  $d_k g \rightarrow \tilde{d}_{jL} \nu_i$  via the exchange of a  $\tilde{d}_{jL}$  squark ( $d_k$  quark) in the  $t$  ( $s$ ) channel.
- The squark production  $d_k g \rightarrow \tilde{u}_{jL} l_i$  via the exchange of a  $\tilde{u}_{jL}$  squark ( $d_k$  quark) in the  $t$  ( $s$ ) channel.
- The sneutrino production  $\bar{d}_j d_k \rightarrow Z \tilde{\nu}_{iL}$  via the exchange of a  $d_k$  or  $d_j$  quark ( $\tilde{\nu}_{iL}$  sneutrino) in the  $t$  ( $s$ ) channel.
- The charged slepton production  $\bar{u}_j d_k \rightarrow Z \tilde{l}_{iL}$  via the exchange of a  $d_k$  or  $u_j$  quark ( $\tilde{l}_{iL}$  slepton) in the  $t$  ( $s$ ) channel.
- The sneutrino production  $\bar{u}_j d_k \rightarrow W^- \tilde{\nu}_{iL}$  via the exchange of a  $d_j$  quark ( $\tilde{l}_{iL}$  sneutrino) in the  $t$  ( $s$ ) channel.



- The charged slepton production  $\bar{d}_j d_k \rightarrow W^+ \tilde{l}_{iL}$  via the exchange of a  $u_j$  quark ( $\tilde{\nu}_{iL}$  sneutrino) in the  $t$  ( $s$ ) channel.

Among these single productions only the  $\bar{u}_j d_k \rightarrow W^- \tilde{\nu}_{iL}$  and  $\bar{d}_j d_k \rightarrow W^+ \tilde{l}_{iL}$  reactions could receive a contribution from a resonant sparticle production. However, in most of the SUSY models, as for example the supergravity or the gauge mediated models, the mass difference between the Left charged slepton and the Left sneutrino is due to the D-terms so that it is fixed by the relation  $m_{\tilde{l}_L^\pm}^2 - m_{\tilde{\nu}_L}^2 = \cos 2\beta M_W^2$  [48] and thus it does not exceed the  $W^\pm$ -boson mass. We note that in the scenarios of large  $\tan \beta$  values, a scalar particle of the third generation produced as a resonance can generally decay into the  $W^\pm$ -boson due to the large mixing in the third family sfermions sector. For instance, in the SUGRA model with a large  $\tan \beta$  a tau-sneutrino produced as a resonance in  $d_k \bar{d}_j \rightarrow \tilde{\nu}_\tau$  through  $\lambda'_{3jk}$  can decay as  $\tilde{\nu}_\tau \rightarrow W^\pm \tilde{\tau}_1^\mp$ ,  $\tilde{\tau}_1^\mp$  being the lightest stau.

Similarly, the single scalar particle and gluino productions occuring via the  $2 \rightarrow 2$ -body processes which involve the  $\lambda''_{ijk}$  coupling constants cannot receive a contribution from a resonant scalar particle production for low  $\tan \beta$ . Indeed, the only reactions among these  $2 \rightarrow 2$ -body processes which could receive such a contribution are of the type  $qq \rightarrow \tilde{q} \rightarrow \tilde{q}W$ . In this type of reaction, the squark produced in the  $s$  channel, is produced via  $\lambda''_{ijk}$  and is thus either a Right squark  $\tilde{q}_R$ , which does not couple to the  $W^\pm$ -boson, or the squarks  $\tilde{t}_{1,2}$ ,  $\tilde{b}_{1,2}$ .

Therefore, the single scalar particle and gluino productions occuring via the  $2 \rightarrow 2$ -body processes are generally non resonant single superpartner productions, as we have already mentioned at the begining of this section. These non resonant single superpartner productions have typically smaller cross sections than the reactions receiving a contribution from a resonant superpartner production. For instance, with  $m_{\tilde{q}} = 250 \text{ GeV}$ , the cross section  $\sigma(p\bar{p} \rightarrow \tilde{u}_L \mu)$  is of order  $\sim 10^{-3} \text{ pb}$  at a center of mass energy of  $\sqrt{s} = 2 \text{ TeV}$ , assuming an  $\mathcal{R}_p$  coupling of  $\lambda'_{211} = 0.09$  [74]. However, the non resonant single productions could lead to interesting signatures. For instance, the production,  $q\bar{q} \rightarrow \tilde{f}W$  leads to the final state  $2l + 2j + W$  for a non vanishing  $\mathcal{R}_p$  coupling constant  $\lambda'$  and to the signature  $4j + W$  for a  $\lambda''$  [13]. Furthermore, the non resonant single productions are interesting as their cross section involves few SUSY parameters, namely only one or two scalar superpartner(s) mass(es) and one  $\mathcal{R}_p$  coupling constant.

## 2.4 Fermion Pair Production Via $\mathcal{R}_p$

- **Dijet production** R-parity violating reactions at hadronic colliders can induce some contributions to Standard Model processes. First, the jets pair production receives contributions from reactions involving either  $\lambda'$  or  $\lambda''$  coupling constants. As a matter of fact, a pair of quarks can be produced through the  $\lambda''$  couplings with an initial state  $ud$  or  $\bar{u}\bar{d}$  ( $dd$  or  $\bar{d}\bar{d}$ ) by the exchange of a  $\tilde{d}$  ( $\tilde{u}$ ) squark in the  $s$ -channel, and also with an initial state  $u\bar{u}$  or  $d\bar{d}$  ( $u\bar{d}$  or  $\bar{u}d$ ) by the exchange of a  $\tilde{u}$  or  $\tilde{d}$  ( $\tilde{d}$ ) squark in the  $t$  channel. In case where the  $s$ -channel exchanged particle is produced on shell, the resonant diagram is of course dominant with respect to the  $t$ -channel diagram. The dijet channel can also be generated via the  $\lambda'$  couplings from an initial state  $u\bar{d}$ ,  $\bar{u}d$  or  $d\bar{d}$  through the exchange of a  $\tilde{l}$  or  $\tilde{\nu}$  slepton, respectively, in the  $s$ -channel.

If the dominant mechanism for either the slepton or the squark decay was into two jets, the resonant production of such a scalar particle would result in a bump in the two-jet

invariant mass plot [14, 49], which would be a very clean signature.

However the dijet production through  $\mathcal{R}_p$  coupling constants will be hard to study at LHC where QCD backgrounds are expected to be severe for searches for narrow resonances which are not strongly produced [13, 50]. Similarly, at the Tevatron, for both the D0 and CDF detectors, the resonant production of the stau  $\tilde{\tau}$ , for example, would lead to observable peak in the dijet invariant mass distribution only for relatively high values of the  $\mathcal{R}_p$  couplings, namely,  $0,001 < \lambda'_{311}\lambda'_{3jk}B_{2j} < 0,01$  and  $300 \text{ GeV} < m_{\tilde{\tau}} < 1200 \text{ GeV}$ , with an integrated luminosity of  $30 \text{ fb}^{-1}$  during the Run II [51]. In these notations,  $B_{2j}$  is the dijet branching ratio and  $m_{\tilde{\tau}}$  the stau mass. The study of  $\lambda'_{311}$  is particularly interesting here since this coupling involves an initial state, for the hard subprocess, composed by first generation quarks which are valence quarks. Besides, the low energy constraint is less stringent for  $\lambda'_{311}$  than for  $\lambda'_{111}$  and  $\lambda'_{211}$ . In conclusion, due to strong QCD background, the dijet production is not the best framework to test the  $\lambda'$  and  $\lambda''$  coupling constants at hadronic colliders.

• **Dilepton production** Similarly, some reactions involving both  $\lambda'$  and  $\lambda$  coupling constants can mimic the Drell-Yan signatures. In the Standard Model the charged lepton pair production occurs through the neutral current channel. In  $\mathcal{R}_p$  models, it can occur through the exchange of  $\tilde{d}$  squark in the  $t$ -channel with an initial state  $u\bar{u}$ , and also via the exchange of  $\tilde{u}$  squark in the  $t$  channel or a  $\tilde{\nu}$  sneutrino in the  $s$ -channel with an initial state  $d\bar{d}$ . The charged current channel receives also an  $\mathcal{R}_p$  contribution : there are two Feynman graphs with a lepton plus a neutrino in the final state and an initial state  $u\bar{d}$  or  $\bar{u}d$  : One exchanges a  $\tilde{d}$  squark in the  $t$ -channel while the other exchanges a  $\tilde{l}$  charged slepton in the  $s$ -channel. The influence on cross sections of the  $t$ -channels on the resonant ones is quite small if the indirect bounds are satisfied.

The resonant production of a sneutrino could lead to a spectacular signature : A bump in the dilepton invariant mass can be observed for an important branching ratio of the decay,  $\tilde{\nu} \rightarrow l\bar{l}$  [49].

Motivated by the weak low-energy constraints on the  $\mathcal{R}_p$  coupling constants containing flavor index from the third generation, the search reach in the resonant  $\tilde{\nu}_\tau$  tau-sneutrino (neutral current) and  $\tilde{\tau}$  stau (charged current) production channels have been obtained in [51], for both the Tevatron and LHC colliders, in the plane  $M$  versus  $X$ , where  $M$  is the scalar mass and  $X = \lambda'_{311}\lambda_{3jk}B_l$ ,  $B_l$  being the leptonic branching ratio. Not only is it important to notice the very large slepton mass reach (of order 800 GeV at the Run II Tevatron and 4 TeV at the LHC) for sizeable values of  $X$  ( $\approx 10^{-3}$ ), but also the small  $X$  ( $X = 10^{-(5-8)}$ ) reach for relatively small slepton masses (of order the hundred of GeV). The search reach is greater in the charged current channel due to the higher parton luminosities. This analysis is easily extended to the first and second generation of slepton as well.

Since the charged lepton pair production provides a very clear signature, its  $\mathcal{R}_p$  contributions, from the resonant production of a sneutrino, have been treated in more details in the literature. One may first consider the contribution to  $e^+e^-$  production. The couplings product  $\lambda'_{311}\lambda_{311}$  is of particular interest here. This choice of couplings is motivated by an initial state with high parton luminosity,  $d\bar{d}$ , and by the fact that among the couplings  $\lambda'_{i11}$  and  $\lambda_{i11}$ ,  $\lambda'_{311}$  and  $\lambda_{311}$  have the lowest low-energy bounds. In this framework, existing Tevatron data [52] from the CDF detector on the  $e^+e^-$  production have been exploited in [12] to derive bounds on the product  $\lambda'_{311}\lambda_{311}$ . In this study, the cross sections for the

$\mathcal{R}_p$  diagrams, in the  $s$ - and  $t$ -channel, contributing to  $e^+e^-$  production are computed, but only the resonant sneutrino production is taken into account. The CTEQ-3L parameterization [53] is used together with the multiplicative K factor calculated for the higher QCD corrections to Drell-Yan pair production [52]. Since the corresponding K factor for slepton production has not been determined yet, the couplings  $\lambda'\lambda$  are theoretically uncertain at a level of about 10%, which is tolerable at a first stage of the analysis. Assuming the sneutrino contribution to be smaller than the experimental error of the data points in the  $e^+e^-$  invariant mass distribution, the Yukawa couplings can be estimated to be,

$$(\lambda'_{311}\lambda_{311})^{1/2} < 0.08 \Gamma_{\tilde{\nu}_\tau}^{1/4}, \quad (2.5)$$

for sneutrino masses in the range 120 – 250 GeV, where  $\Gamma_{\tilde{\nu}_\tau}$  denotes the sneutrino width in units of GeV.

For the  $\mathcal{R}_p$  contributions via resonant sneutrino production to the two last families lepton pair production, a different approach, based on the total cross section study, has been adopted in [54]. The motivation, which holds mainly for the  $\tau^+\tau^-$  production, is the following : It is experimentally easier to determine the production rate above some values of the dilepton invariant mass than to reconstruct the dilepton invariant mass itself. In [54], the  $\mu^+\mu^-$  production case was studied in details. By combining the low energy limits on individuals  $\mathcal{R}_p$  couplings with the limits which exist on products  $\lambda\lambda'$ , we are left with only two relevant  $\mathcal{R}_p$  coupling constants products, namely,  $\lambda_{232}\lambda'_{311}$  and  $\lambda_{232}\lambda'_{322}$ , if we neglect the contributions from the annihilation of the sea quarks,  $b\bar{b}$ . The  $1\sigma$ -limit contours plot in the plane,  $\lambda_{232}\lambda'_{311}$  versus  $\lambda_{232}\lambda'_{322}$ , has been obtained for the reaction,  $p\bar{p} \rightarrow \mu^+\mu^- + X$ . For example, the attainable  $1\sigma$ -limits are  $-0.003 < \lambda_{232}\lambda'_{311} < 0.003$  and  $-0.011 < \lambda_{232}\lambda'_{322} < 0.011$ , for a  $\tau$  sneutrino mass of 200 GeV, at energy  $\sqrt{s} = 2$  TeV with a total integrated luminosity  $\mathcal{L} = 2 \text{ fb}^{-1}$  appropriate for the Tevatron Run II. We observe that due to larger valence d quark probability functions, a significant improvement over the present limits may be obtained for the  $\mathcal{R}_p$  product  $\lambda_{232}\lambda'_{311}$ . Note also that the cross sections were calculated applying an upper cut on the  $\mu^+\mu^-$  system invariant mass of  $M_{\mu^+\mu^-}^+ = 500$  GeV and a lower cut of  $M_{\mu^+\mu^-}^- = 150$  GeV. This lower cut practically removes the  $s$ -channel  $Z$  resonance contribution.

In conclusion, dilepton production clearly offers a unique way to explore the R-parity violating parameter space :  $\lambda\lambda'$  versus the slepton mass.

Finally, if such a resonance were observed, how could we distinguish between a scalar or a new gauge boson resonance? This point is treated in [51] : In the case of neutral current, one immediate difference would be the observation of the very unusual  $e\nu$  final states, which would be a truly remarkable signature for R-parity violation. A universality violation, namely, a substantially different rate for the  $e^+e^-$  and the  $\mu^+\mu^-$  final states, would also eliminate the possibility of a resonant  $Z'$  boson. If such differences would have not been observed, the measurement of the forward-backward asymmetry ( $A_{FB}$ ) could discriminate between a scalar resonance, which produces a null asymmetry, and a boson resonance, which lead to  $A_{FB} \neq 0$  due to parity violating fermionic couplings. A more complex situation arises when  $Z'$  naturally has  $A_{FB} = 0$ . In such a case, the complete angular distribution analysis would be conclusive as to the identity of the resonance. Of course, the required statistics for these measurements results in a significant loss in the mass reach : For example, for a fixed value of  $X$  (same notation as above), if the Tevatron were able to discover a sneutrino with a mass of 700 GeV, the value of  $A_{FB}$  could only be

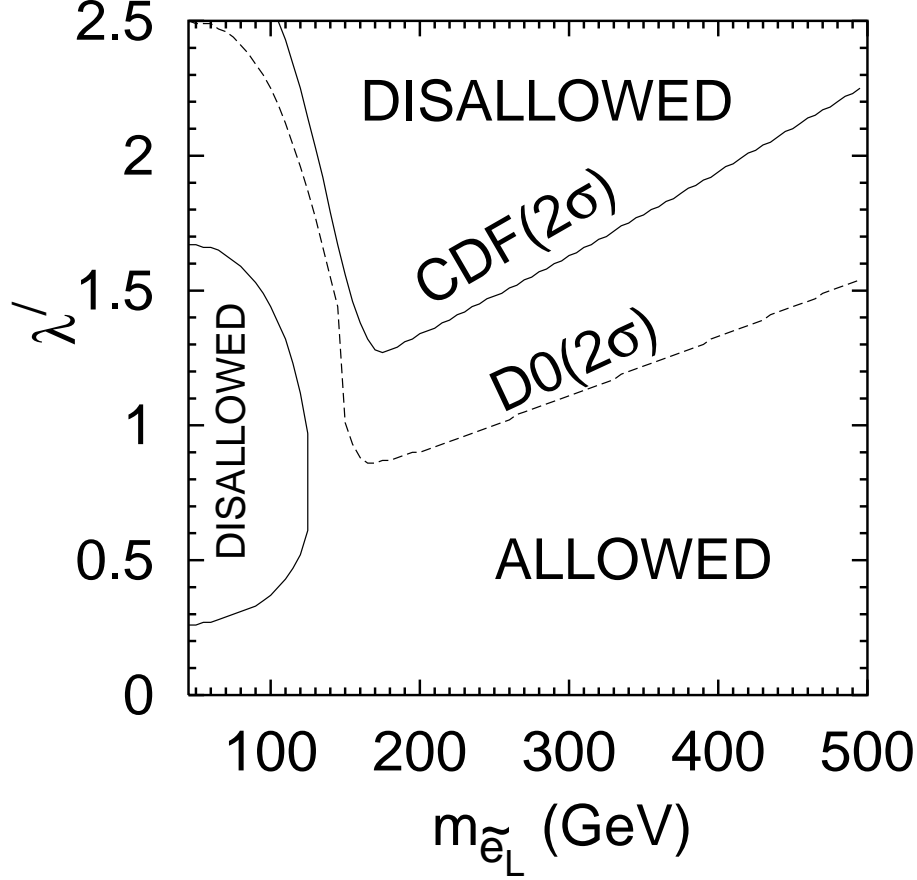


FIG. 15: Allowed regions in the plane of  $\lambda'_{i3k}$  and the mass of the left slepton in a lepton number-violating scenario. Solid (dashed) lines correspond to the  $2\text{-}\sigma$  bounds from the CDF (D0) collaborations.

extracted for  $m_{\tilde{\nu}} = 500$  GeV, and the angular distribution for  $m_{\tilde{\nu}} = 400$  GeV. In the case of charge current, one interesting possibility is to examine the leptonic charge asymmetry for the electrons and muons in the final state, which is defined as :

$$A(\eta) = \frac{dN_+/d\eta - dN_-/d\eta}{dN_+/d\eta + dN_-/d\eta}, \quad (2.6)$$

where  $N_{\pm}$  are the number of positively/negatively charged leptons of a given rapidity,  $\eta$ . The presence of the slepton tends to drive the asymmetry to smaller absolute values as might be expected in the Standard Model, while the deviation due to either type of  $W'$  substantially increases the magnitude of the asymmetry. The minimum value of the product  $\lambda\lambda'$  for which the asymmetry differs significantly from the Standard Model expectation at the Tevatron ( $\sqrt{s} = 2$  TeV) is 0.1, for a luminosity of  $2 \text{ fb}^{-1}$ , assuming  $m_{\tilde{l}} = 750$  GeV and  $\Gamma_{\tilde{l}}/m_{\tilde{l}} = 0,004$ .

• **Top quark physics** The large mass of the top quark,  $m_{top}$ , entails a top lifetime,  $\tau_{top} = [1.56 \text{ GeV} m_{top}/180 \text{ GeV}]^3$ , sufficiently shorter than the typical QCD hadronization time so that decay occurs before fragmentation. The top decays mainly into a bottom quark in association with a  $W$  gauge boson, which can have a leptonic decay channel,  $W \rightarrow l\nu$ , with a branching ratio of  $2/9$ . Therefore, the top quark production

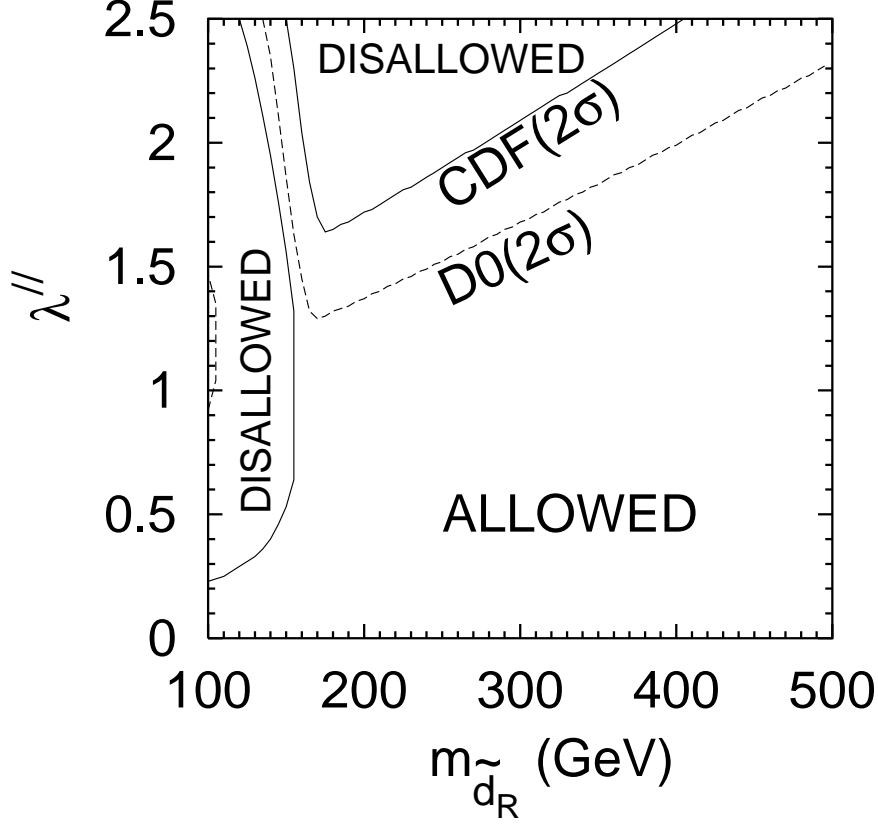


FIG. 16: Allowed regions in the plane of  $\lambda''_{3ki}$  and the mass of the right  $d$ -squark in a baryon number-violating scenario. Solid (dashed) lines correspond to the  $2\text{-}\sigma$  bounds from the CDF (D0) collaborations.

offers some very clean signatures, with a rather energetic lepton, some missing energy and a  $b$  jet which can be tagged with a good efficiency. This particular behavior of the top quark, together with the fact that the low energy constraints on  $\lambda'$  and  $\lambda''$  couplings involving third-generation fields are not very stringent, has motivated numerous studies on the top physics.

**a) Top quark pair production** The top quark pair production could receive a contribution from diagrams with an initial state,  $d_k \bar{d}_k$ , and exchanging either a  $\tilde{l}_L^i$  slepton (via  $\lambda'_{i3k}$ ) or a  $\tilde{d}_R^i$  squark (via  $\lambda''_{3ki}$ ) in the  $t$ -channel (see Fig.17). Those amplitudes have been calculated in [55], with the CTEQ-3M parton distributions [53] and folding by the  $K$  factor which is extracted from the resummed QCD cross sections [56] in the  $q\bar{q}$  annihilation channel. The region of the supersymmetric parameter space allowed at a 95% confidence level by the D0 and CDF data [57] on  $t\bar{t}$  production cross section have also been obtained in [55], and are shown in Fig.15 in the plane,  $\lambda'_{i31}/m_{\tilde{l}_L^i}$ , and in Fig.16 in the plane,  $\lambda''_{31i}/m_{\tilde{d}_R^i}$ . For squark masses smaller than the top mass, the bounds on the  $\lambda''_{31i}$  are weakened considerably because the decay channel,  $t \rightarrow d\tilde{d}_R$ , opens up, and this tends to dilute the signal from the Standard Model decay mode. Simultaneously, the opening up of the decay channel,  $t \rightarrow d\tilde{l}_L$ , does not affect the bounds on the  $\lambda'_{i31}$  quite as much, because the relevant branching ratio is suppressed by a smaller colour factor. The colour factors

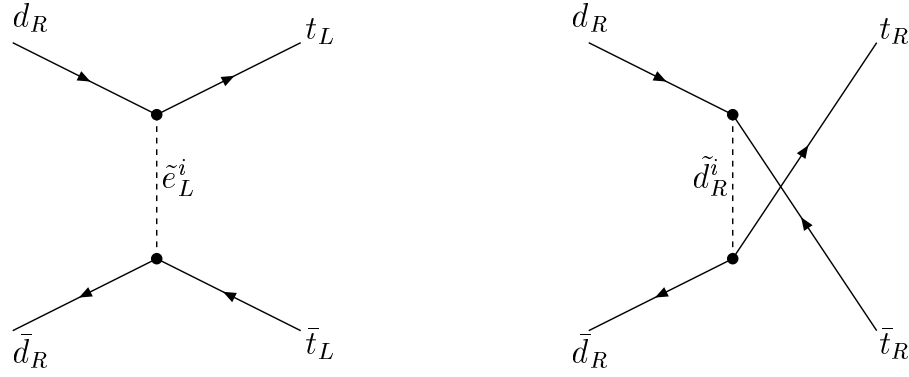


FIG. 17: Feynman diagrams for the  $L$ -violating process  $d\bar{d} \rightarrow t_L\bar{t}_L$  via the  $\lambda'$  coupling and for the  $B$ -violating process  $d\bar{d} \rightarrow t_R\bar{t}_R$  due to the coupling  $\lambda''$ .

that appear in the  $\mathcal{R}_p$   $t\bar{t}$  productions also explain why the  $\lambda'_{i31}$  are more constrained than the  $\lambda''_{31i}$ . Nevertheless, the bounds obtained on  $\lambda''_{31i}$  are comparable to the indirect limits, for  $m_{\tilde{q}} = 100$  GeV. Note that since these interactions are chiral, they induce polarization of the final state. Polarization can be a useful observable for probing the  $\mathcal{R}_p$  couplings [58]. At the LHC energy, while the gluon initiated contribution is much larger, the usual annihilation process in QCD is further suppressed because it is an  $s$ -channel process. The  $t$ -channel  $\mathcal{R}_p$  subprocess does not suffer this suppression and those effects, while smaller than the corresponding effects at the TeVatron, are still sizeable.

**b) Single top quark production** Single top quark production is of special importance in the context of fermion pair production. In contrast to the QCD process of  $t\bar{t}$  production, the single top quark production,  $u\bar{d} \rightarrow t\bar{b}$ , involves only the electroweak interactions and can therefore be used to probe the electroweak theory and to study models of new physics. The single top quark production can also come from the  $W$ -gluon fusion. Since the structure functions are better known for the quarks than for the gluons, the cross section accuracy is higher for the single top quark production through the exchange of a  $W$  gauge boson than for the  $W$ -gluon fusion. Hence the process,  $u\bar{d} \rightarrow t\bar{b}$ , is a better test for new physics than the  $W$ -gluon fusion. The feasibility of single top quark production via squark and slepton exchanges to probe several combinations of  $R$  parity violating couplings at hadron colliders has been studied in [59, 60, 61, 62]. According to those studies, the LHC is better at probing the  $B$  violating couplings  $\lambda''$  whereas the Tevatron and the LHC have a similar sensitivity to  $\lambda'$  couplings. The number of signal events depends on the mass and width of the exchanged sparticle, and on the value of the Yukawa couplings. The width of the exchanged sparticle is a sum of the widths due to  $R$ -parity conserving and  $R$ -parity violating decays :

$$\Gamma_{tot} = \Gamma_{R_p} + \Gamma_{\mathcal{R}_p} \quad (2.7)$$

where  $\Gamma_{\mathcal{R}_p}$  is given by

$$\Gamma_{\mathcal{R}_p}(\tilde{d}_R^{*k} \longrightarrow u^i d^j) = \frac{(\lambda''_{ijk})^2 (M_{\tilde{d}_R^k}^2 - M_{u^i}^2 - M_{d^j}^2)^2}{2\pi M_{\tilde{d}_R^k}^3} \quad (2.8)$$

for the squarks, and by

$$\Gamma_{\mathcal{R}_p}(\tilde{l}_L^i \longrightarrow \bar{u}^j d^k) = \frac{3(\lambda'_{ijk})^2 (M_{\tilde{l}_L^i}^2 - M_{u^j}^2 - M_{d^k}^2)^2}{16\pi M_{\tilde{l}_L^i}^3} \quad (2.9)$$

for the sleptons.

We consider at first a quark-antiquark initial parton state which is of relevance at the Tevatron as in this case both particles can be valence quarks in the initial state and may have therefore a considerably higher cross section in  $p\bar{p}$  collisions. Quark-quark initial parton states are examined later on in connection with LHC studies. It has been shown [59] that the signal for  $u\bar{d} \rightarrow t\bar{b}$  is potentially observable at the Tevatron with  $2 - 3 \text{ fb}^{-1}$  integrated luminosity, although at the LHC it will be relatively suppressed by the sea structure functions and overwhelmed by the large background from  $t\bar{t}$  production plus  $W$ -gluon fusion.

The single top quark production,  $u_j \bar{d}_k \rightarrow t\bar{b}$ , can occur through the exchange of a  $\tilde{l}_L^i$  slepton in the  $s$ -channel via the couplings product,  $\lambda'_{ijk} \lambda'_{i33}$ . Using a CTEQ-3L [53] parton distribution, summing over the flavor index  $i$  (the sleptons  $\tilde{l}_L^i$  are supposed degenerate in mass) and taking for the values of the  $\mathcal{R}_p$  coupling constants the values of the indirect bounds, the ratio of the resonant slepton contribution cross section over the Standard Model cross section was found [60] to exceed 20% at the upgraded Tevatron when slepton mass lies in the narrow range,  $200 \text{ GeV} - 270 \text{ GeV}$ , and  $M_2 = -\mu > 200 \text{ GeV}$ . This large slepton mass suppression of the ratio can be understood as follows : When the slepton mass is large, the parton cross section contribution coming from the slepton resonant production requires large momenta from the initial partons, which is suppressed by their structure functions. An additional suppression is caused by the increase of the slepton width when the slepton mass increases. Note also that the ratio increases with the increase of the supersymmetric parameters  $M_2$  and  $\mu$ , since then the neutralino and chargino masses increase and thus the width of the slepton decreases. The dominant process,  $u\bar{d} \rightarrow \tilde{l}_L^i \rightarrow t\bar{b}$ , which involves the sum of couplings,  $\lambda'_{111} \lambda'_{133} + \lambda'_{211} \lambda'_{233} + \lambda'_{311} \lambda'_{333}$ , was considered in [61]. An interesting signature for this process is an energetic charged lepton, missing  $E_T$  and double b-quark jets. Using a series of kinematic cuts in order to reduce the Standard Model background and to consider the detector acceptance, the values of the slepton mass versus the couplings to be observable at 95% confidence level were calculated. The result shows that for values of the couplings below the low energy bounds, the slepton mass can only be probed in the range,  $200 \text{ GeV} < m_{\tilde{l}_L} < 340 \text{ GeV}$ , for the upgraded Tevatron and in the interval,  $200 \text{ GeV} < m_{\tilde{l}_L} < 400 \text{ GeV}$ , for the LHC. Although larger parton momenta are favored at the LHC, the result is not really improved at LHC because of the relative suppression of the  $\bar{d}$  quark structure function compared to the  $d$  quark one. The difference between the results based on the two sets of structure functions, MRSA' [63] and CTEQ-3M [53], has been found to be small.

The single top quark production,  $u_i \bar{d}_j \rightarrow t\bar{b}$ , receives also a contribution from the exchange of a  $\tilde{d}_R^k$  squark in the  $t$ -channel, through the product of couplings  $\lambda''_{i3k} \lambda''_{3jk}$ . Since

the non-observation of proton decay imposes very stringent conditions on the simultaneous presence of  $\lambda'$  and  $\lambda''$ , only their separate effects in single top quark production are interesting to study. Choosing the initial state of the reaction,  $u_i \bar{d}_j \rightarrow t \bar{b}$ , fix the flavor indices of the coupling constants product  $\lambda''_{i3k} \lambda''_{3jk}$  because of the antisymmetry of the constants  $\lambda''$ . Due to either too strong low energy constraints on the couplings or too low parton luminosities, the only product of interest is  $\lambda''_{132} \lambda''_{312}$ . If we assume an observable level of,  $\Delta\sigma/\sigma_0 > 20\%$ , where  $\Delta\sigma$  is the  $\mathcal{R}_p$  cross section and  $\sigma_0$  is the Standard Model cross section, the coupling  $\lambda''_{132} \lambda''_{312}$  can be probed at the upgraded Tevatron down to 0.01, 0.02, 0.03, 0.04, 0.06, 0.08, 0.1 and 0.13 for  $M_{\tilde{s}_R} = 100, 200, 300, 400, 500, 600, 700$  and 800 GeV, respectively [60].

Another interesting single top quark production is the reaction,  $u_i d_j \rightarrow t b$ , which can occur through the exchange of a  $\tilde{d}_R^k$  squark in the s channel via the couplings product  $\lambda''_{ijk} \lambda''_{33k}$ . Although the corresponding events can have the unique signal of an energetic charged lepton, missing transverse energy and two same sign  $b$  quarks, since the tagging can not distinguish a  $b$  quark from a  $\bar{b}$  quark, the background is quite as important as that of the reaction,  $u_i \bar{d}_j \rightarrow t \bar{b}$ . Quark-quark initial parton states may be valence contributions from the structure functions at a  $pp$  collider as the LHC. Note however that the strong indirect bound on  $\lambda''_{112}$  makes very small the valence-valence  $ud$  contribution to the cross section. An example of cross sections that are obtained from different initial parton states at the LHC is given in table 2. Using some effective kinematical cuts, the sensibility

Initial partons	$cd$	$cs$	$ub$	$cb$	
Exchanged particle	$\tilde{s}$	$d$	$\tilde{s}$	$\tilde{d}$	$\tilde{s}$
Couplings	$\lambda''_{212} \lambda''_{332}$	$\lambda''_{212} \lambda''_{331}$	$\lambda''_{132} \lambda''_{332}$	$\lambda''_{231} \lambda''_{331}$	$\lambda''_{232} \lambda''_{332}$
Cross section in pb	3.98	1.45	5.01	0.659	

TAB. 2: Cross section in pb of the reaction  $u_i d_j \rightarrow \tilde{d}_R^k \rightarrow t b$  at LHC for a squark of mass of 600 GeV assuming  $\Gamma_{R_p} = 0.5$  GeV and  $\lambda''_{ijk} = 0.1$ .

plot at 95% confidence level has been obtained in the plane  $\lambda''_{212} \lambda''_{332}$  versus  $m_{\tilde{s}_R}$  in [61] : The coupling product  $\lambda''_{212} \lambda''_{332}$  can be probed up to 0.5, 0.1 and 1.5 for  $m_{\tilde{s}_R} = 700, 800$  and  $1000 \text{ GeV}$  at the upgraded Tevatron, and for  $m_{\tilde{s}_R} = 2100, 2700$  and  $3100 \text{ GeV}$  at the LHC, respectively. The sensitivity on the squark mass is quite higher at the LHC than at the Tevatron. Note that the process,  $cs \rightarrow \tilde{d}_R \rightarrow t b$ , cannot be probed as efficiently as,  $cd \rightarrow \tilde{s}_R \rightarrow t b$ , because of the relative suppression of the strange quark structure function compared to the valence down quark. As illustrated in Fig.18, the study of [62] on the reaction  $u_i d_j \rightarrow t b$  at LHC, which was performed at an higher degree of precision in the simulation process than in [61], has lead to weaker sensitivities on the  $\lambda''_{ijk} \lambda''_{33k}$  product of coupling constants than the analysis of [61].

The reaction  $u_j d_k \rightarrow t b$  receives also a contribution from the exchange of a  $\tilde{l}_{iL}^\pm$  slepton in the u channel, via the  $\lambda'_{ij3}$  and  $\lambda'_{i3k}$  couplings [62].

The single top quark production at hadronic colliders via  $\mathcal{R}_p$  couplings offers the opportunity to reconstruct supersymmetric particle masses. For instance, the invariant mass distribution associated to the the two  $b$  quarks, the charged lepton and the reconstructed neutrino produced in the reaction  $ub \rightarrow \tilde{s} \rightarrow t b \rightarrow W b b \rightarrow l \nu b b$ , occuring via the couplings  $\lambda''_{132}$  and  $\lambda''_{332}$ , allows to reconstruct the  $\tilde{s}$  mass. The error on this mass reconstruction per-



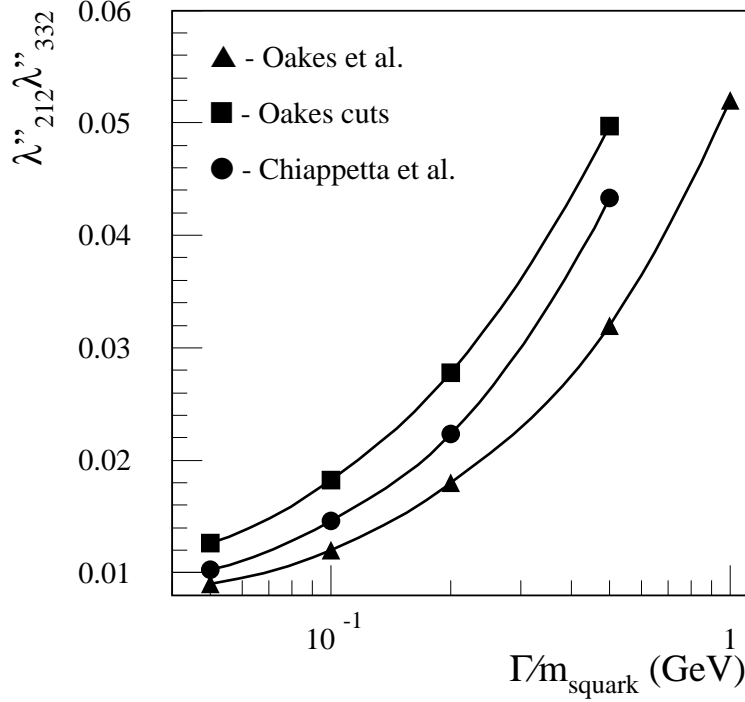


FIG. 18: Sensitivity limits on the  $\lambda''_{212}\lambda''_{332}$  Yukawa couplings obtained from the analysis of the reaction  $cd \rightarrow \tilde{s}^* \rightarrow tb$  at the LHC after 1 year with low luminosity for  $m_{\tilde{s}} = 300 \text{ GeV}$ , found in [62] (circles) and in [61] (triangles). The squares indicate the results obtained in [62] by applying the simplified cuts used in [61].

formed from the events observed in the ATLAS detector at LHC would be dominated by the 1% systematic uncertainty on the jet energy scale in ATLAS, for  $m_{\tilde{s}} = 600 \text{ GeV}$ ,  $\lambda''_{132}\lambda''_{332} = 10^{-2}$  and assuming a luminosity of  $\mathcal{L} = 30 \text{ fb}^{-1}$  [62].

To conclude, the top quark physics is more favorable to the tests on the  $\lambda''$  than on the  $\lambda'$  couplings. Furthermore, it is the only framework in which the constraints on  $\lambda''$  from physics at colliders are comparable or better than the low energy bounds on the  $\lambda''$  coupling constants.

## 2.5 $\mathcal{R}_p$ Contributions to Flavour Changing Neutral Currents

As for the leptonic colliders physics, the  $\mathcal{R}_p$  interactions could induce flavor changing neutral current effects at hadronic colliders in reactions as simple as the lepton pair production,  $q\bar{q} \rightarrow \bar{l}_J l_{J'}$  ( $J \neq J'$ ). Nevertheless, the environment is not as clean as for the leptonic colliders and these flavor changing neutral current effects are less easily observable. Those flavor changing lepton productions occur from an initial state  $d_j \bar{d}_k$  ( $d_k \bar{d}_k$ ) through the exchange of a  $\tilde{\nu}_L^i$  sneutrino ( $\tilde{u}_L^j$  squark) in the  $s$ -channel ( $t$ -channel) via the couplings product  $\lambda'_{ijk}\lambda'_{iJJ'}$  ( $\lambda'_{Jjk}\lambda'_{J'jk}$ ), or, from an initial state  $u_j \bar{u}_j$  through the exchange of a  $\tilde{d}_R^k$  squark in the  $t$ -channel via the couplings product  $\lambda'_{Jjk}\lambda'_{J'jk}$ .

## 2.6 $\mathcal{R}_p$ Contributions to CP violation

The resonant production of a sneutrino gives rise to the possibility of having CP violation effects at tree level, which are therefore quite important. This was treated in [54] for hadronic colliders in analogy with the case of leptonic colliders [44], which was exposed above (Section 1.6). If the  $\tau$  spins could be measured, the future Tevatron runs will be capable of detecting CP violation effects in the polarization asymmetries of the hard process,  $d_j \bar{d}_k \rightarrow \tilde{\nu}^\mu \rightarrow \tau^+ \tau^-$ . The  $\mathcal{R}_p$  coupling constant  $\lambda'_{2jk}$  which enters this subprocess is chosen real, while  $\lambda_{233}$  is taken complex in order to generate CP asymmetries. The spin asymmetries study at hadronic colliders must be treated with special care. In fact, the spin asymmetries change sign around  $\sqrt{s} \approx m_{\tilde{\nu}^\mu_\pm}$ . Since in hadronic collisions one has to integrate over  $\sqrt{s}$ , the spin asymmetries are reduced. To compensate this effect, one has to integrate the absolute values of the polarization asymmetries. Of course this demands a study, in a previous stage, of the  $\tau^+ \tau^-$  invariant mass distribution, which is needed to determine the  $m_{\tilde{\nu}^\mu_\pm}$  sneutrino mass. The maximum of the spin asymmetries reach 20 – 30% with a mass splitting  $\Delta m_{\tilde{\nu}^\mu} = \Gamma_{\tilde{\nu}^\mu}$  and 10 – 13% for  $\Delta m_{\tilde{\nu}^\mu} = \Gamma_{\tilde{\nu}^\mu}/4$ , throughout the mass range  $150 \text{ GeV} < m_{\tilde{\nu}^\mu_\pm} < 450 \text{ GeV}$ . At the Tevatron Run II (III) with  $\mathcal{L} = 2 \text{ fb}^{-1}$  ( $30 \text{ fb}^{-1}$ ) the CP conserving and CP violating asymmetries may be detected with a sensitivity above  $3\sigma$  over the mass range  $155 \text{ GeV} < m_{\tilde{\nu}^\mu_\pm} < 400 \text{ GeV}$  ( $155 \text{ GeV} < m_{\tilde{\nu}^\mu_\pm} < 300 \text{ GeV}$ ) if  $\Delta m_{\tilde{\nu}^\mu} = \Gamma_{\tilde{\nu}^\mu}$  ( $\Delta m_{\tilde{\nu}^\mu} = \Gamma_{\tilde{\nu}^\mu}/10$ ). Finally, the entire range of  $r$  (see CP violation in Section 1.7) can be practically covered for  $m_{\tilde{\nu}^\mu_-} = 200 \text{ GeV}$  at the Tevatron Run II (III) with at least  $3\sigma$  standard deviations, for  $\Delta m_{\tilde{\nu}^\mu} = \Gamma_{\tilde{\nu}^\mu}$  ( $\Delta m_{\tilde{\nu}^\mu} = \Gamma_{\tilde{\nu}^\mu}/4$ ). Those computations have been performed taking for  $\lambda'_{2jk}$  and  $|\lambda_{233}|$  the values of the low energy bounds, applying an upper cut on the  $\tau^+ \tau^-$  system invariant mass of  $M_{\tau^+ \tau^-}^+ = 500 \text{ GeV}$  and a lower cut of  $M_{\tau^+ \tau^-}^- = 150 \text{ GeV}$  and including all  $j, k$  combinations in  $d_j \bar{d}_k$  fusion. The results show that, contrary to the leptonic colliders framework [44], the CP odd and CP even spin asymmetries could be observed over a wide  $\tilde{\nu}^\mu$  sneutrino mass range, of about 300 GeV.

# References

- [1] J. Kalinowski, R. Rückl, H. Spiesberger and P. M. Zerwas, Phys. Lett. **B406** (1997) 314.
- [2] J. Kalinowski, eprint hep-ph/9712550, Acta Phys. Polon. **B28**, 2423 (1997).
- [3] J. Kalinowski, R. Rückl, H. Spiesberger and P. M. Zerwas, Z. Phys. **C74** (1997) 595.
- [4] D. Choudhury, Phys. Lett. **B376** (1996) 201.
- [5] P. J. Holt and P. B. Renton, DELPHI Collaboration, submitted to HEP'97 (Abstract Number 467), DELPHI 97-116, CONF 98 (1997), CERN-EP/99-05.
- [6] M. Acciari et al., L3 Collaboration, Phys. Lett. **B414** (1997) 373, updated with 183 GeV data in the contribution of L3 Collaboration to ICHEP'98 : L3 Note 2235.
- [7] OPAL Collaboration, CERN-EP/98-108.
- [8] Y. Arnoud et al., DELPHI Collaboration, submitted to HEP'97 (Abstract Number 589), DELPHI 97-119, CONF 101 (1997).
- [9] G. Altarelli et al., Preprint CERN-TH/97-40, March 1997; H. Dreiner and P. Morawitz, eprint hep-ph/9703279; J. Kalinowski, R. Rückl, H. Spiesberger and P. M. Zerwas, Preprint DESY 97-038, eprint hep-ph/9703288; J. Ellis, S. Lola and K. Sridhar, Preprint CERN-TH-97-109, eprint hep-ph/9706519.
- [10] F. Richard, Preprint DELPHI 97-46 PHYS 698 (1997).
- [11] J. Erler, J. Feng and N. Polonsky, Phys. Rev. Lett. **78** (1997) 3012.
- [12] J. Kalinowski, R. Rückl, H. Spiesberger and P. M. Zerwas, eprint hep-ph/9708272, Phys. Lett. **B414**, 297 (1997); J. Kalinowski, Proceedings of *"Beyond the Desert 97 – Accelerator and Non-Accelerator Approaches"*, Ringberg Castle, Germany, June 1997, eprint hep-ph/9708490.
- [13] H. Dreiner and G. G. Ross, Nucl. Phys. **B365** (1991) 597.
- [14] S. Dimopoulos and L. J. Hall, Phys. Lett. **B207** (1988) 210.
- [15] V. Barger, G. F. Giudice and T. Han, Phys. Rev. **D40** (1989) 2987.
- [16] H. E. Haber and G. L. Kane, Phys. Rep. **117** (1985) 175.
- [17] S. Lola, Presented at the 2nd ECFA/DESY study on Linear Colliders, Frascati, November 1998, LC note LC-TH-1999-021, hep-ph/9912217.
- [18] M. Chemtob and G. Moreau, Phys. Rev. **D59** (1999) 055003.
- [19] F. Ledroit-Guillon and R. López-Fernández, DELPHI Collaboration, DELPHI 98-165 PHYS 805.

- [20] ALEPH Collaboration, submitted to ICHEP'98 (Abstract Number 949), ALEPH 98-070, CONF 039 (1998).
- [21] F. Ledroit-Guillon and R. López-Fernández, DELPHI Collaboration, DELPHI 99-30, CONF 229 (1999).
- [22] N. Benekos et al., DELPHI Collaboration, submitted to HEP'99 (Abstract Number 7.209), DELPHI 99-79, CONF 266 (1999).
- [23] 'Conceptual Design Report of a 500GeV  $e^+e^-$  Linear Collider with Integrated X-ray Laser Facility', DESY 1997-048, ECFA 1997-182, Editors : R. Brinkmann, G. Materlik, J. Rossbach and A. Wagner, [www.desy.de/~schreibr/cdr/cdr.html](http://www.desy.de/~schreibr/cdr/cdr.html).  
See also [wwwhephy.oeaw.ac.at/susy/lcws/tdr.html](http://wwwhephy.oeaw.ac.at/susy/lcws/tdr.html).
- [24] J. A. Bagger, Nucl. Phys. (**Proc. Suppl.**)**62B** (1998) 23.
- [25] G. Moreau, in preparation.
- [26] H. Dreiner and S. Lola, published in "Munich-Annecy-Hamburg 1991/93, Proceedings,  $e^+e^-$  Collisions at 500 GeV : The Physics Potential ", DESY 92-123A+B, 93-123C; "Annecy-Gran Sasso-Hamburg 1995, Proceedings,  $e^+e^-$  Collisions at TeV Energies : The Physics Potential ", DESY 96-123D, ed. P. M. Zerwas; "Searches for New Physics ", contribution to the LEP II Workshop, 1996, eprint hep-ph/9602207; "Physics with  $e^+e^-$  Linear Colliders ", DESY-97-100, eprint hep-ph/9705442.
- [27] B. C. Allanach, H. Dreiner, P. Morawitz and M. D. Williams, eprint hep-ph/9708495.
- [28] A. Axelrod, Nucl. Phys. **B209** (1982) 349.
- [29] M. Clements et al., Phys. Rev. **D27** (1983) 570.
- [30] V. Ganapathi et al., Phys. Rev. **D27** (1983) 579.
- [31] M. J. Duncan, Phys. Rev. **D31** (1985) 1139.
- [32] B. Mukhopadhyaya and A. Raychaudhuri, Phys. Rev. **D39** (1989) 280.
- [33] U. Mahanta and A. Ghosal, Phys. Rev. **D57** (1998) 1735.
- [34] Y. Zeng-Hui, H. Pietschmann, M. Wen-Gan, H. Liang and J. Yi, eprint hep-ph/9910323.
- [35] M. Chemtob and G. Moreau, eprint hep-ph/9910543, Phys. Rev. **D61** (2000) 116004.
- [36] M. Chemtob and G. Moreau, Phys. Rev. **D59** (1999) 116012.
- [37] Y. Zeng-Hui, H. Pietschmann, M. Wen-Gan, Han Liang and J. Yi, eprint hep-ph/9903471.
- [38] M. Chemtob and G. Moreau, Phys. Lett. **B448** (1999) 57.
- [39] Particle Data Group, *Tests of Conservation Laws*, Phys. Rev. **D54** (1996) 60.
- [40] N. Arkani-Hamed, H. C. Cheng, J. L. Feng, L. J. Hall, Phys. Rev. Lett. **77** (1996) 1937.
- [41] J. Bernabéu, A. Santamaria and M.B. Gavela, Phys. Rev. Lett. **57** (1986) 1514.
- [42] W.-S. Hou, N.G. Deshpande, G. Eilam and A. Soni, Phys. Rev. Lett. **57** (1986) 1406.
- [43] G. Eilam, J. L. Hewett and A. Soni, Phys. Rev. Lett. **67** (1991) 1979; B. Grzadkowski, J. F. Gunion and P. Krawczyk, Phys. Lett. **B268** (1991) 106.

- [44] S. Bar-Shalom, G. Eilam and A. Soni, Phys. Rev. Lett. **80** (1998) 4629.
- [45] M. Hirsch, H. V. Klapdor-Kleingrothaus and S. G. Kovalenko, Phys. Lett. **B398** (1997) 311.
- [46] Y. Grossman and H. Haber, Phys. Rev. Lett. **78** (1997) 3438, Y. Grossman, hep-ph/9710276.
- [47] L. Hall, T. Moroi and H. Murayama, Phys. Lett. **B424** (1998) 305.
- [48] L. E. Ibañez and G. G. Ross, CERN-TH.6412/92, in *Perspectives in Higgs Physics*, G. Kane editor, World Scientific, Singapore, 1993.
- [49] S. Dimopoulos et al., Phys. Rev. **D41** (1990) 2099.
- [50] P. Binétruy et al., ECFA Large Hadron Collider (LHC) Workshop, Aachen, 1990, Vol. II.
- [51] J. L. Hewett and T. G. Rizzo, Proc. of 29th International Conference on High-Energy Physics (ICHEP 98), Vancouver, Canada (23-29 July) 1998, vol. 2 p.1698, eprint hep-ph/9809525.
- [52] F. Abe et al., Phys. Rev. Lett. **79** (1997) 2198.
- [53] H. L. Lai et al., Phys. Rev. **D51** (1995) 4763.
- [54] S. Bar-Shalom, G. Eilam and A. Soni, Phys. Rev. **D59** (1999) 055012.
- [55] D. K. Ghosh, S. Raychaudhuri and K. Sridhar, eprint hep-ph/9608352, Phys. Lett. **B396**, 177 (1997).
- [56] E. L. Berger and H. Contopanagos, Phys. Rev. **D54** (1996) 3085 and references therein.
- [57] P. Tipton, Talk presented at the International Conference on High Energy Physics, Warsaw (July 1996).
- [58] K. Hikasa, J. M. Yang and B. Young, Phys. Rev. **D60** (1999) 114041.
- [59] T. Stelzer and S. Willenbrock, Phys. Lett. **B357** (1995) 125.
- [60] A. Datta, J. M. Yang, B.-L. Young and X. Zhang, Phys. Rev. **D56** (1997) 3107.
- [61] R. J. Oakes, K. Whisnant, J. M. Yang, B.-L. Young and X. Zhang, Phys. Rev. **D57** (1998) 534.
- [62] P. Chiappetta, A. Deandrea, E. Nagy, S. Negroni, G. Polesello and J.M. Virey, Phys. Rev. **D61** (2000) 115008.
- [63] A. D. Martin, R. G. Roberts and W. J. Stirling, Phys. Lett. **B354** (1995) 155.
- [64] C. Quigg, *Gauge Interactions of the Strong, Weak, and Electromagnetic Interactions* (Benjamin-Cummings, Reading, Mass., 1983).
- [65] E. Eichten, I. Hinchliffe, K. Lane, and C. Quigg, Rev. Mod. Phys. **56** (1984) 579.
- [66] H. Dreiner, P. Richardson and M. H. Seymour, JHEP **0004** (2000) 008.
- [67] B. Abbott *et al.* [D0 Collaboration], hep-ex/0005034.
- [68] E. N. Argyres, C. G. Papadopoulos and S.D.P. Vlassopoulos, Phys. Lett. **B202** (1988) 425.
- [69] E.L.Berger, B. W. Harris and Z. Sullivan, Phys. Rev. Lett. **83** (1999) 4472.

- [70] CTEQ Collaboration, H. Lai et al., Phys. Rev. **D55** (1997) 1280.
- [71] H. Dreiner, P. Richardson and M. H. Seymour, eprint hep-ph/9903419, to be published in the Physics at Run II Workshop : Supersymmetry/Higgs, ed. H. Dreiner.
- [72] H. Dreiner, P. Richardson and M. H. Seymour, Proceedings of the Workshop “Physics at TeV Colliders”, Les Houches, France 8-18 June 1999, eprint hep-ph/0001224.
- [73] S. Abdullin et al., Report of the SUSY working group of the 1999 Les Houches Workshop “Physics at TeV Colliders”, Les Houches, France 8-18 June 1999, eprint hep-ph/0005142.
- [74] F. Déliot, G. Moreau and C. Royon, in preparation.
- [75] R. N. Mohapatra, Prog. Part. Nucl. Phys. **31** (1993) 39.
- [76] F. Déliot, G. Moreau, C. Royon, E. Perez and M. Chemtob, Phys. Lett. **B475**, 184 (2000).
- [77] G. Moreau, E. Perez and G. Polesello, Proceedings of the Workshop “Physics at TeV Colliders”, Les Houches, France 8-18 June 1999, eprint hep-ph/0002130.
- [78] G. Moreau, E. Perez and G. Polesello, eprint hep-ph/0003012.
- [79] V. Barger, W.Y. Keung, R.J.N. Phillips, Phys. Lett. **B364** (95) 27; *Erratum*, *ibid* Phys. Lett. **B377** (1996) 486.
- [80] T. Kon, T. Kobayashi, S. Kitamura, Phys. Lett. **B333** (94) 263.
- [81] E.A. Baltz, P. Gondolo; Phys. Rev. **D57** (1998) 2969.
- [82] OPAL collaboration, Phys. Lett. **B313** (1993) 333;  
ALEPH collaboration, Phys. Lett. **B349** (1995) 238.
- [83] Physics at LEP2, CERN Yellow Report 96-01, vol.1, p.207.
- [84] S. Katsanevas, P. Morawitz, Comp. Phys. Comm. **112** (1998) 227  
(<http://lyoinfo.in2p3.fr/susygen/susygen.html>)
- [85] S. Kawabata, Comp. Phys. Comm. **41** (1986) 127
- [86] J. Ellis and S. Rudaz, Phys. Lett. **B128** (1983) 248
- [87] A. Bartl et al., Z. Phys. **C76** (1997) 549
- [88] S. P. Martin, in *Perspectives on supersymmetry*, edited by G.L. Kane, 1-98; eprint hep-ph/9709356
- [89] M. Drees, “An introduction to supersymmetry” Lectures given at Inauguration Conference of the Asia Pacific Center for Theoretical Physics (APCTP), Seoul, Korea, 4-19 Jun 1996; eprint hep-ph/9611409
- [90] M. Drees and S.P. Martin, “Implications of SUSY model building,” eprint hep-ph/9504324.
- [91] M. Drees and K. Hikasa, Phys. Lett. **B252** (1990) 127
- [92] B. Allanach et al., “Searching for  $R$ -Parity Violation at RUN II of the TeVatron”, eprint hep-ph/9906224, to be published in the Physics at Run II Workshop : Supersymmetry/Higgs, ed. H. Dreiner.







## Publication II



# Resonant sneutrino production at Tevatron Run II

G. Moreau, M. Chemtob

*Service de Physique Théorique  
CE-Saclay F-91191 Gif-sur-Yvette, Cedex France*

F. Déliot, C. Royon, E. Perez

*Service de Physique des Particules, DAPNIA  
CE-Saclay F-91191 Gif-sur-Yvette, Cedex France*

Phys. Lett. **B475** (2000) 184, hep-ph/9910341

## Abstract

*We consider the single chargino production at Tevatron  $p\bar{p} \rightarrow \tilde{\nu}_i \rightarrow \tilde{\chi}_1^\pm l_i^\mp$  as induced by the resonant sneutrino production via a dominant  $R$ -parity violating coupling of type  $\lambda'_{ijk} L_i Q_j D_k^c$ . Within a supergravity model, we study the three leptons final state. The comparison with the expected background demonstrate that this signature allows to extend the sensitivity on the supersymmetric mass spectrum beyond the present LEP limits and to probe the relevant  $R$ -parity violating coupling down to values one order of magnitude smaller than the most stringent low energy indirect bounds. The trilepton signal offers also the opportunity to reconstruct the neutralino mass in a model independent way with good accuracy.*

In the minimal supersymmetric standard model (MSSM), the supersymmetric (SUSY) particles must be produced in pairs. In contrast, the single superpartner production which benefits from a larger phase space is allowed in the R-parity violating ( $\mathcal{R}_p$ ) extension of the MSSM. In particular the SUSY particle resonant production can reach high cross-sections either at leptonic [1] or hadronic colliders [2], even taking into account the strongest low-energy bounds on  $\mathcal{R}_p$  coupling constants [3]. Hadronic colliders provide an additional advantage in that they allow to probe a wide mass range of the new resonant particle, due to the continuous energy distribution of the colliding partons. Furthermore, since the resonant production has a cross-section which is proportional to the relevant coupling squared, this could allow an easier determination of the  $\mathcal{R}_p$  coupling than pair production reaction. Indeed in the latter case, the sensitivity on the  $\mathcal{R}_p$  coupling is mainly provided by the displaced vertex analysis for the Lightest Supersymmetric Particle (LSP) decay, which is difficult experimentally especially at hadronic colliders.

The SUSY particle produced at the resonance mainly decays through R-parity conserving interactions into the LSP, via cascade decays. In the case of a dominant  $\lambda''_{ijk} U_i^c D_j^c D_k^c$  coupling, the decay of the LSP leads to multi-jets final states, which have a high QCD background at hadronic colliders. Besides, at hadronic colliders, the  $\lambda_{ijk} L_i L_j E_k^c$  couplings do not contribute to resonant production. In this letter, we thus assume a dominant  $\lambda'_{ijk} L_i Q_j D_k^c$  coupling which initiates the resonant sneutrino production  $\bar{d}_j d_k \rightarrow \tilde{\nu}_i$  and hence the single chargino production at Tevatron through  $p\bar{p} \rightarrow \tilde{\nu}_i \rightarrow \tilde{\chi}_1^\pm l_i^\mp$ . We focus on the three leptons signature associated with the cascade decay  $\tilde{\chi}_1^\pm \rightarrow \tilde{\chi}_1^0 l_p^\pm \nu_p$ ,  $\tilde{\chi}_1^0 \rightarrow l_i^+ \bar{u}_j d_k + c.c.$ , assuming the  $\tilde{\chi}_1^0$  to be the LSP. The main motivation rests on the possibility to reduce the background. This is similar in spirit to a recent study [4] of the like sign dilepton signature from the single neutralino production at Tevatron via the resonant charged slepton production.

We concentrate on the  $\lambda'_{211}$  coupling. The associated hard scattering processes,  $d\bar{d} \rightarrow \tilde{\nu}_\mu \rightarrow \tilde{\chi}_1^\pm \mu^\mp$ ,  $d\bar{d} \rightarrow \tilde{\chi}_1^\pm \mu^\mp$  and  $u\bar{u} \rightarrow \tilde{\chi}_1^\pm \mu^\mp$  (see Fig.1), involve first generation quarks for the initial partons. The indirect constraint on this coupling is  $\lambda'_{211} < 0.09(\tilde{m}/100\text{GeV})$  [3].

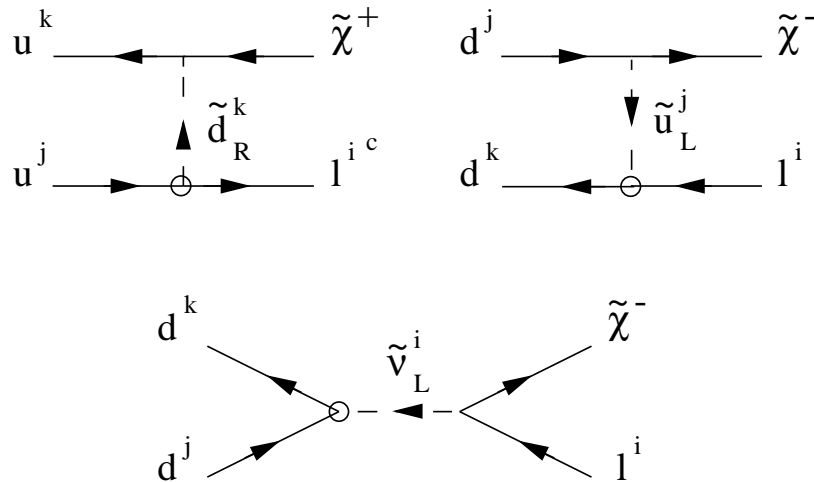


FIG. 1: Feynman diagrams for the single chargino production at Tevatron via the  $\lambda'_{ijk}$  coupling (symbolised by a circle in the figure). The arrows denote flow of the particle momentum.

While  $\lambda'_{111}$  is disfavored due to severe constraints [3], the case of a dominant  $\lambda'_{311}$  could also be of interest.

Our framework is the so-called minimal supergravity model (mSUGRA), in which the absolute value of the Higgsino mixing parameter  $|\mu|$  is determined by the radiative electroweak symmetry breaking condition. We restrict to the infrared fixed point region for the top quark Yukawa coupling, in which  $\tan\beta$  is fixed [5]. We shall present results for the low solution  $\tan\beta \simeq 1.5$  and for  $\text{sign}(\mu) = -1$ ,  $A = 0$ . In fact the cross-section for the single chargino production depends smoothly on the  $\mu$ ,  $A$  and  $\tan\beta$  parameters. The cross-section can reach values of order a few picobarns. For instance, choosing the mSUGRA point,  $M_2(m_Z) = 200\text{GeV}$ ,  $m_0 = 200\text{GeV}$ , and taking  $\lambda'_{211} = 0.09$  we find using CTEQ4 [6] parametrization for the parton densities a cross-section of  $\sigma(p\bar{p} \rightarrow \tilde{\chi}_1^\pm \mu^\mp) = 1.45\text{pb}$  at a center of mass energy  $\sqrt{s} = 2\text{TeV}$ . Choosing other parametrizations does not change significantly the results since mainly intermediate Bjorken  $x$  partons are involved in the studied process. The cross-section depends mainly on the  $m_{1/2}$  (or equivalently  $M_2$ ) and  $m_0$  soft SUSY breaking parameters. As  $M_2$  increases, the chargino mass increases reducing the single chargino production rate. At high values of  $m_0$ , the sneutrino mass is enhanced so that the resonant sneutrino production is reduced. This leads to a decrease of the single chargino production rate since the  $t$  and  $u$  channels contributions are small compared to the resonant sneutrino contribution. Finally, for values of  $m_{\tilde{\nu}_\mu}$  (which is related to  $m_0$ ) approaching  $m_{\tilde{\chi}_1^\pm}$  (which is related to  $M_2$ ), a reduction of the chargino production is caused by the decrease of the phase space factor associated to the decay  $\tilde{\nu}_\mu \rightarrow \chi_1^\pm \mu^\mp$ .

The single chargino production cross-section must be multiplied by the leptonic decays branching fractions which are  $B(\tilde{\chi}_1^\pm \rightarrow \tilde{\chi}_1^0 l_p^\pm \nu_p) = 33\%$  (summed over the three leptons species) and  $B(\tilde{\chi}_1^0 \rightarrow \mu u d) = 55\%$ , for the point chosen above of the mSUGRA parameter space. The leptonic decay of the chargino is typically of order 30% for  $m_{\tilde{l}}, m_{\tilde{q}}, m_{\tilde{\chi}_2^0} > m_{\tilde{\chi}_1^\pm}$ , and is smaller than the hadronic decay  $\tilde{\chi}_1^\pm \rightarrow \tilde{\chi}_1^0 \bar{q}_p q'_p$  because of the color factor. When  $\tilde{\chi}_1^0$  is the LSP, it decays via  $\lambda'_{211}$  either as  $\tilde{\chi}_1^0 \rightarrow \mu u d$  or as  $\tilde{\chi}_1^0 \rightarrow \nu_\mu d d$ , with branching ratios  $B(\tilde{\chi}_1^0 \rightarrow \mu u d)$  ranging between  $\sim 40\%$  and  $\sim 70\%$ .

The backgrounds for the three leptons signature at Tevatron are : (1) The top quark pair production followed by the top decays  $t \rightarrow bW$  where one of the charged leptons is generated in  $b$ -quark decay. (2) The  $W^\pm Z^0$  and  $Z^0 Z^0$  productions followed by leptonic decays of the gauge bosons. It has been pointed out recently [7, 8] that non negligible contributions can occur through virtual gauge boson, as for example the  $W^* Z^*$  or  $W\gamma^*$  productions. However, these contributions lead at most to one hard jet in the final state in contrast with the signal and have not been simulated. (3) Standard Model productions as for instance the  $W t \bar{t}$  production. These backgrounds have been estimated in [9] to be negligible at  $\sqrt{s} = 2\text{TeV}$ . We have checked that the  $Zb$  production gives a negligible contribution to the 3 leptons signature. (4) The fake backgrounds as,  $p\bar{p} \rightarrow Z + X$ ,  $Drell-Yan + X$ ,  $b\bar{b}b$ , where  $X$  and  $b$ -quarks fake a charged lepton. Monte Carlo simulations using simplified detector simulation cannot give a reliable estimate of this background. (5) The supersymmetric background generated by the superpartner pair production. This background is characterised by two cascade decays ending each with the decay of the LSP as  $\tilde{\chi}_1^0 \rightarrow \mu u d$  via the  $\lambda'_{211}$  coupling, and thus is suppressed compared to the signal due to the additional branching fraction factors. Moreover the SUSY background incurs a larger phase space suppression. In particular its main contribution, namely the squark and gluino pair productions, is largely suppressed for large  $\tilde{q}$  and  $\tilde{g}$

masses [10]. Although a detailed estimation has not been performed we expect that this background can be further reduced by analysis cuts, since at least four jets are expected in the final state and leptons should appear less isolated than in the signal.

We have simulated the single chargino production  $p\bar{p} \rightarrow \tilde{\chi}_1^\pm \mu^\mp$  with a modified version of the SUSYGEN event generator [11] and the Standard Model background ( $W^\pm Z^0$ ,  $Z^0 Z^0$  and  $t\bar{t}$  productions) with the PYTHIA event generator [12]. Both SUSYGEN and PYTHIA have been interfaced with the SHW detector simulation package [13], which mimics an average of the CDF and D0 Run II detector performance.

The following cuts aimed at enhancing the signal-to-background ratio have been applied. First, we have selected the events with at least three charged leptons ( $e^\pm$  or  $\mu^\pm$ ) with energies greater than  $10\text{GeV}$  for the softer of them and  $20\text{GeV}$  for the two others, namely,  $N_l \geq 3$  [ $l = e, \mu$ ] with  $E_{\min}(l) > 10\text{GeV}$ ,  $E_{\text{med}}(l) > 20\text{GeV}$  and  $E_{\max}(l) > 20\text{GeV}$ . In addition, since our final state is  $3l + 2\text{jets} + \cancel{E}$  we have required that the minimum number of jets should be equal to two, where the jets have an energy higher than  $10\text{GeV}$ , namely,  $N_j \geq 2$  with  $E_j > 10\text{GeV}$ . This selection criteria suppresses the background from the gauge bosons production which generates at most one hard jet. Note that these events requiring high energy charged leptons and jets are easily triggered at Tevatron. In order to eliminate poorly isolated leptons originating from the decays of hadrons (as in the  $t\bar{t}$  production), we have imposed the isolation cut  $\Delta R = \sqrt{\delta\phi^2 + \delta\theta^2} > 0.4$ , where  $\phi$  is the azimuthal angle and  $\theta$  the polar angle, between the 3 most energetic charged leptons and the 2 hardest jets. We have also demanded that  $\delta\phi > 70^\circ$  between the leading charged lepton and the 2 hardest jets. With the cuts described above and for an integrated luminosity of  $\mathcal{L} = 1\text{fb}^{-1}$  at  $\sqrt{s} = 2\text{TeV}$  for Tevatron Run II, the  $Z^0 Z^0$ ,  $W^\pm Z^0$ ,  $t\bar{t}$  productions lead to 0.22, 0.28, 1.1 events respectively.

In Fig.2, we present the  $3\sigma$  and  $5\sigma$  discovery contours and the limits at 95% confidence level in the  $\lambda'_{211}$ - $m_0$  plane, using a set of values for  $M_2$  and the luminosity. For a given value of  $M_2$ , we note that the sensitivity on the  $\lambda'_{211}$  coupling decreases at high and low values of  $m_0$ . At high values of  $m_0$ , the sneutrino mass is enhanced inducing a decrease of the sneutrino production cross-section. At low values of  $m_0$ , the sneutrino mass decreases leading to a reduction of the phase space factor for the decay  $\tilde{\nu}_\mu \rightarrow \tilde{\chi}_1^\pm \mu^\mp$  which follows the resonant sneutrino production. Similarly, we note the decrease of the sensitivity on the  $\lambda'_{211}$  coupling when  $M_2$  increases for a fixed value of  $m_0$ . This is due to the increase of the chargino mass which results also in a smaller phase space factor for the sneutrino decay.

In Fig.3, the discovery potential is shown in the plane  $m_0$  versus  $m_{1/2}$ , for different values of  $\lambda'_{211}$  and of luminosity. For the same reasons as above, we observe a reduction of the sensitivity on  $\lambda'_{211}$  when  $m_0$  (respectively,  $m_{1/2}$  or equivalently  $M_2$ ) increases for a fixed value of  $m_{1/2}$  (respectively  $m_0$ ).

An important improvement with respect to the limits derived recently from LEP data [14] can already be obtained within the first year of Run II at Tevatron ( $\mathcal{L} = 1\text{fb}^{-1}$ ). Even Run I data could probably lead to new limits on the supersymmetric parameters. The strongest bounds on the supersymmetric masses obtained at LEP in an  $\mathcal{R}_p$  model with non-vanishing  $\lambda'$  Yukawa coupling are  $m_{\tilde{\chi}_1^\pm} > 94\text{GeV}$ ,  $m_{\tilde{\chi}_1^0} > 30\text{GeV}$ ,  $m_{\tilde{l}} > 81\text{GeV}$  [14]. Note that for the minimum values of  $m_0$  and  $m_{1/2}$  spanned by the parameter space described in Fig.2 and Fig.3, namely  $m_0 = 100\text{GeV}$  and  $M_2 = 100\text{GeV}$ , the spectrum is  $m_{\tilde{\chi}_1^\pm} = 113\text{GeV}$ ,  $m_{\tilde{\chi}_1^0} = 54\text{GeV}$ ,  $m_{\tilde{\nu}_L} = 127\text{GeV}$ ,  $m_{\tilde{l}_L} = 137\text{GeV}$ ,  $m_{\tilde{l}_R} = 114\text{GeV}$ , so

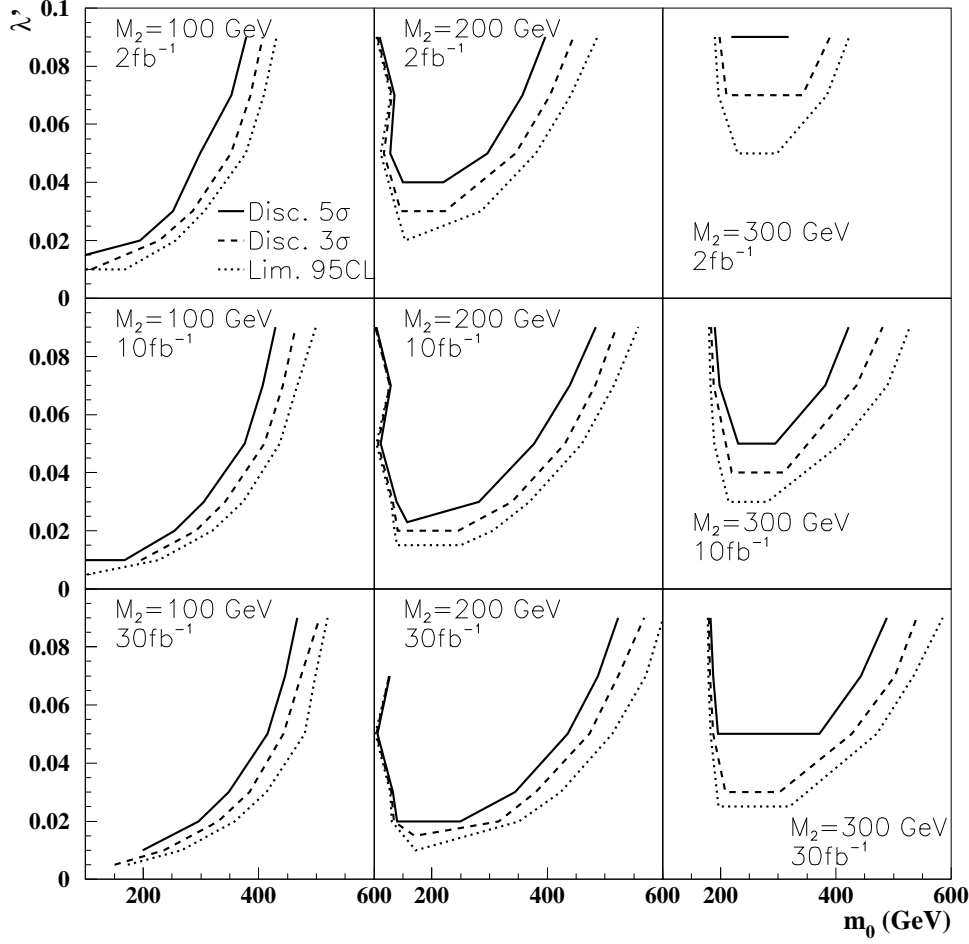


FIG. 2: Discovery contours at  $5\sigma$  (full line),  $3\sigma$  (dashed line) and limit at 95%  $C.L.$  (dotted line) presented in the plane  $\lambda'_{211}$  versus the  $m_0$  parameter, for different values of  $M_2$  and of luminosity.

that we are well above these limits. Since both the scalar and gaugino masses increase with  $m_0$  and  $m_{1/2}$ , the parameter space described in these figures lies outside the present forbidden range, in the considered framework.

With the luminosity of  $\mathcal{L} = 30 fb^{-1}$  expected at the end of the Run II,  $m_{1/2}$  values up to  $550 GeV$  ( $350 GeV$ ) corresponding to a chargino mass of about  $m_{\tilde{\chi}_1^\pm} \approx 500 GeV$  ( $300 GeV$ ) can be probed if the  $\lambda'_{211}$  coupling is 0.09 (0.03). The sensitivity on  $m_0$  reaches  $600 GeV$  ( $400 GeV$ ), which corresponds to a sneutrino mass of about  $m_{\tilde{\nu}_\mu} \approx 600 GeV$  ( $450 GeV$ ), for a value of the  $\lambda'_{211}$  coupling equal to 0.09 (0.03). Couplings down to a value of 0.005 can also be tested at Tevatron Run II, in the promising scenario where  $m_0 = 200 GeV$  and  $M_2 = 100 GeV$ , namely,  $m_{\tilde{\chi}_1^\pm} \approx 100 GeV$  and  $m_{\tilde{\nu}_\mu} \approx 200 GeV$ .

Let us make a few remarks on the model dependence of our results. First, as we have discussed above, the sensitivity reaches depend on the SUSY parameters mainly through the supersymmetric mass spectrum. Secondly, in the major part of the mSUGRA

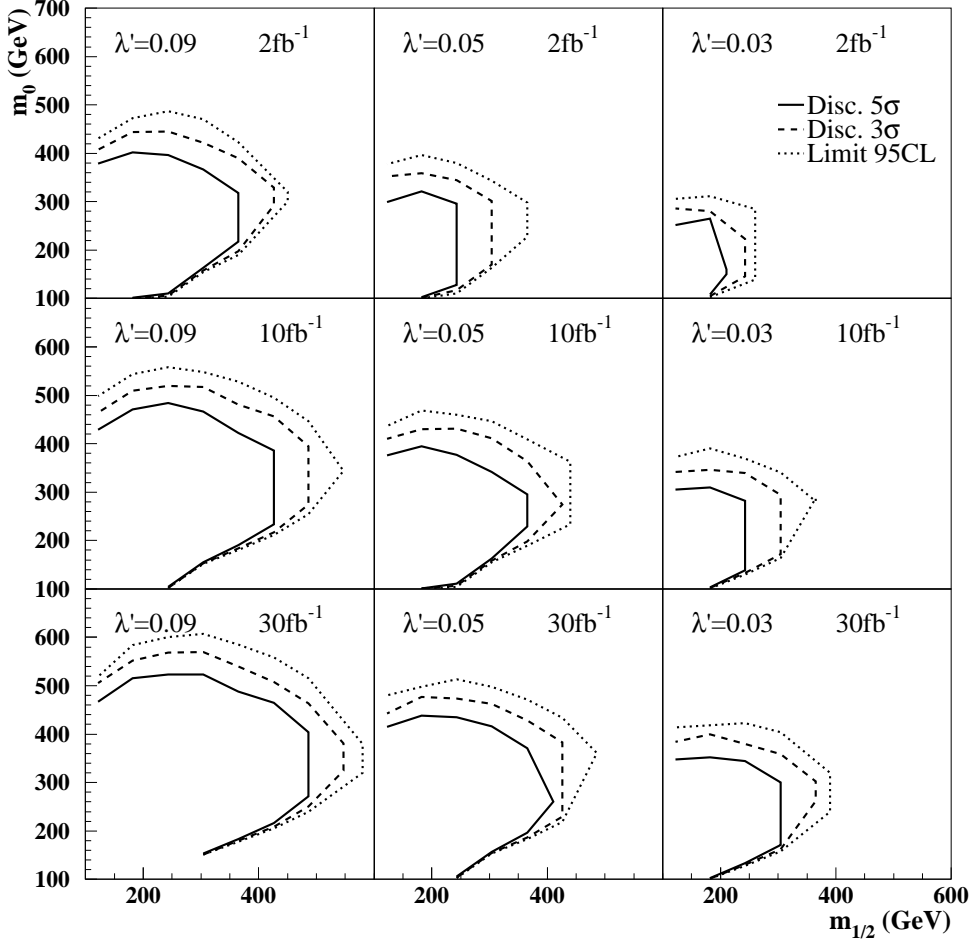


FIG. 3: Discovery contours at  $5\sigma$  (full line),  $3\sigma$  (dashed line) and limit at 95%  $C.L.$  (dotted line) presented in the plane  $m_0$  versus  $m_{1/2}$ , for different values of  $\lambda'_{211}$  and of luminosity.

parameter space, the LSP is the  $\tilde{\chi}_1^0$ . Besides, in the mSUGRA model, the mass difference between  $\tilde{\chi}_1^\pm$  and  $\tilde{\chi}_1^0$  is large enough not to induce a dominant  $\tilde{R}_p$  decay for the chargino. Notice also that we have chosen the scenario of low  $\tan\beta$ . For high  $\tan\beta$ , due to the slepton mixing in the third generation, the  $\tilde{\tau}$  slepton mass can be reduced down to  $\sim m_{\tilde{\chi}_1^\pm}$  so that the branching ratio of the  $\tilde{\chi}_1^\pm$  decay into tau-leptons  $\tilde{\chi}_1^\pm \rightarrow \tilde{\chi}_1^0 \tau_p^\pm \nu_\tau$  increases and exceeds that into  $e$  and  $\mu$  leptons, leading to a decrease of the efficiency after cuts. For example, the efficiency at the mSUGRA point  $m_0 = 200\text{GeV}$ ,  $M_2 = 150\text{GeV}$ ,  $\text{sign}(\mu) = -1$ ,  $A = 0$ , is 4.93% for  $\tan\beta = 1.5$  and 1.21% for  $\tan\beta = 50$ . However, for still decreasing  $\tilde{\tau}$  mass,  $\tilde{\chi}_1^\pm \rightarrow \tilde{\chi}_1^0 \tau_p^\pm \nu_\tau$  starts to dominate over the hadronic mode so that the efficiency loss is compensated by the leptonic decays of the  $\tau$ , and the branching of the  $\tilde{\chi}_1^\pm$  into  $e$  and  $\mu$  leptons can even increase up to 34%. For instance, the efficiency for  $m_0 = 300\text{GeV}$ ,  $M_2 = 300\text{GeV}$ ,  $\text{sign}(\mu) = -1$ ,  $A = 0$ , is 5% for the 2 values  $\tan\beta = 1.5$  and  $\tan\beta = 50$ .

Another particularly interesting aspect of our signal is the possibility of a  $\tilde{\chi}_1^0$  neutralino mass reconstruction in a model independent way. As a matter of fact, the invariant mass



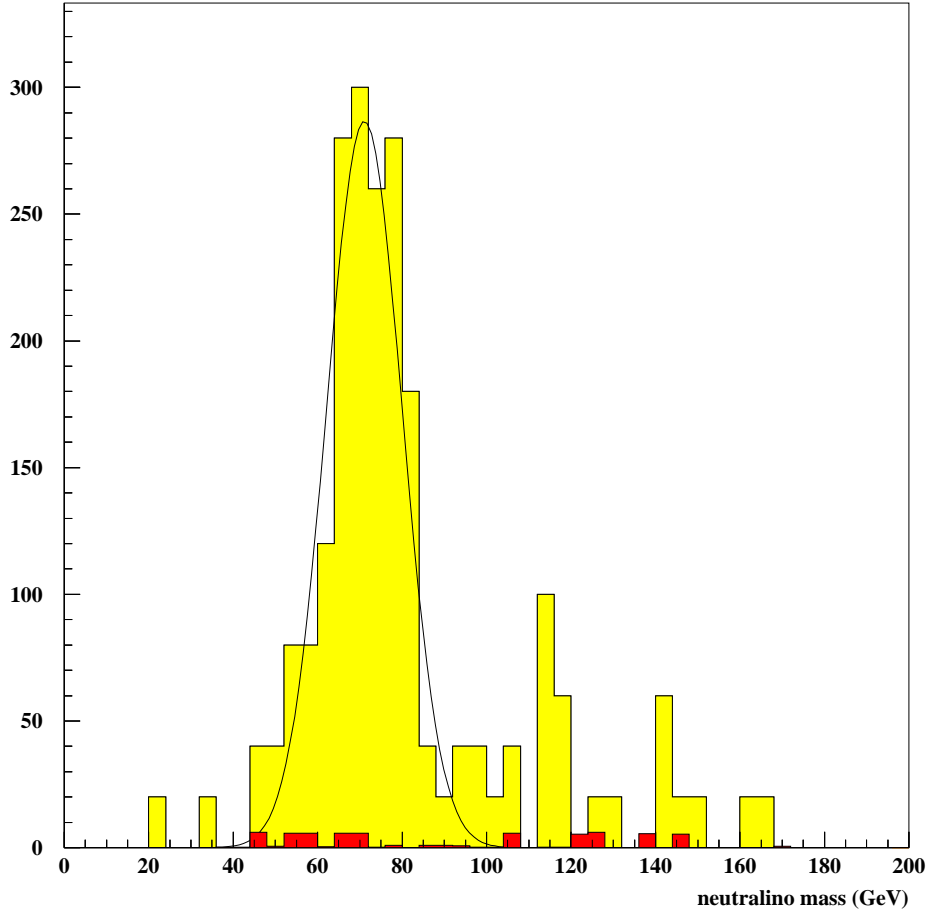


FIG. 4: Distribution for the invariant mass of the 2 jets and the lower energy muon in the  $e\mu\mu$  events, for a luminosity of  $\mathcal{L} = 30fb^{-1}$ . The sum of the  $WZ$ ,  $ZZ$  and  $t\bar{t}$  backgrounds is in black and the signal is grey. The mSUGRA point taken for this figure is,  $m_0 = 200GeV$ ,  $M_2 = 150GeV$  ( $m_{\tilde{\chi}_1^0} = 77GeV$ ), and the  $\mathcal{R}_p$  coupling is  $\lambda'_{211} = 0.09$ .

distribution of the charged lepton and the 2 jets coming from the neutralino decay  $\tilde{\chi}_1^0 \rightarrow \mu\mu d$  allows to perform a clear neutralino mass reconstruction. The 2 jets found in these events are generated in the  $\tilde{\chi}_1^0$  decay. In order to select the requisite charged lepton, we concentrate on the  $e\mu\mu$  events. In those events, we know that for a relatively important value of the mass difference,  $m_{\tilde{\nu}_\mu} - m_{\tilde{\chi}_1^\pm}$ , the leading muon comes from the decay,  $\tilde{\nu}_\mu \rightarrow \tilde{\chi}_1^\pm \mu^\mp$ , and the other one from the neutralino decay (the electron is generated in the decay  $\tilde{\chi}_1^\pm \rightarrow \tilde{\chi}_1^0 e^\pm \nu_e$ ). In Fig.4, we present the invariant mass distribution of the lepton and 2 jets selected through this method. The average reconstructed  $\tilde{\chi}_1^0$  mass is about  $71 \pm 9GeV$  to be compared with the generated mass of  $\tilde{\chi}_1^0 = 77GeV$ . In a more detailed analysis of this signal [15, 16], the neutralino mass can be reconstructed with higher precision using for e.g. constrained fit algorithms. This mass reconstruction is performed easily in contrast with the pair production analysis in  $\mathcal{R}_p$  scenarios [17] which suffers an higher combinatorial

background. Moreover, a reconstruction of the chargino and sneutrino masses is also possible. This invariant mass distribution would also allow to discriminate between the signal and the SUSY background.

As a conclusion, we have presented a new possibility of studying resonant sneutrino productions in  $R_p$  models at Tevatron. Results (see also [16]) lead to a sensitivity on the  $\lambda'_{211}$  coupling, on the sneutrino and chargino masses well beyond the present limits. Besides, a model-independent reconstruction of the neutralino mass can be performed easily with great accuracy. Our work leads to the interesting conclusion that the three leptons signature considered as a ‘gold plated’ channel for the discovery of supersymmetry at hadronic colliders [7, 8, 9], is also particularly attractive in an R-parity violation context.

We acknowledge C. Guyot, R. Peschanski, C. Savoy and X. Tata for useful discussions and reading the manuscript.

# References

- [1] V. Barger, G. F. Giudice and T. Han, Phys. Rev. **D40**, 2987 (1989).
- [2] S. Dimopoulos, R. Esmailzadeh, L.J. Hall, J. Merlo and G.D. Starkman, Phys. Rev. **D41**, 2099 (1990).
- [3] H. Dreiner, to be published in ‘Perspectives on Supersymmetry’, Ed. by G. L. Kane, World Scientific, hep-ph/9707435.
- [4] H. Dreiner, P. Richardson and M. H. Seymour, hep-ph/9903419.
- [5] M. Carena, M. Olechowski, S. Pokorski and C. E. M. Wagner, Nucl. Phys. **B419** (1994) 213.
- [6] CTEQ Coll., Phys. Rev. **D55**, 1280 (1997).
- [7] K. T. Matchev and D. M. Pierce, hep-ph/9904282, and references therein.
- [8] H. Baer, M. Drees, F. Paige, P. Quintana, X. Tata, hep-ph/9906233.
- [9] R. Barbieri, F. Caravaglios, M. Frigeni and M. Mangano, Nucl. Phys. **B 367**, 28 (1991).
- [10] H. Baer, C. Kao and X. Tata, Phys. Rev. **D51**, 2180 (1995).
- [11] SUSYGEN 3.0/06, N. Ghodbane, S. Katsanevas, P. Morawitz and E. Perez, lyoinfo.in2p3.fr/susygen/susygen3.html; N. Ghodbane, hep-ph/9909499.
- [12] T. Sjöstrand, Comp. Phys. Comm. **82**, 74 (1994); S. Mrenna, Comp. Phys. Comm. **101**, 232 (1997).
- [13] SHW, J. Conway, [www.physics.rutgers.edu/~jconway/soft/shw/shw.html](http://www.physics.rutgers.edu/~jconway/soft/shw/shw.html).
- [14] Y. Arnoud, talk given at the Moriond Conference, March 16, 1999.
- [15] G. Moreau, E. Perez, G. Polesello, in preparation.
- [16] M. Chemtob, F. Déliot, G. Moreau, E. Perez, C. Royon, in preparation.
- [17] ATLAS Coll., ATLAS TDR 15, Vol. II, 25 May 1999, CERN/LHCC 99-15.



## Publication III



# Single superpartner production at Tevatron Run II

G. Moreau

*Service de Physique Théorique  
CE-Saclay F-91191 Gif-sur-Yvette, Cedex France*

F. Déliot<sup>1</sup>, C. Royon<sup>1,2,3</sup>

*1 : Service de Physique des Particules, DAPNIA  
CE-Saclay F-91191 Gif-sur-Yvette, Cedex France*

*2 : Brookhaven National Laboratory, Upton, New York, 11973*

*3 : University of Texas, Arlington, Texas, 76019*

To appear in Eur. Phys. Jour. C, hep-ph/0007288

## Abstract

*We study the single productions of supersymmetric particles at Tevatron Run II which occur in the  $2 \rightarrow 2$ -body processes involving  $R$ -parity violating couplings of type  $\lambda'_{ijk} L_i Q_j D_k^c$ . We focus on the single gaugino productions which receive contributions from the resonant slepton productions. We first calculate the amplitudes of the single gaugino productions. Then we perform analyses of the single gaugino productions based on the three charged leptons and like sign dilepton signatures. These analyses allow to probe supersymmetric particles masses beyond the present experimental limits, and many of the  $\lambda'_{ijk}$  coupling constants down to values smaller than the low-energy bounds. Finally, we show that the studies of the single gaugino productions offer the opportunity to reconstruct the  $\tilde{\chi}_1^0$ ,  $\tilde{\chi}_1^\pm$ ,  $\tilde{\nu}_L$  and  $\tilde{l}_L^\pm$  masses with a good accuracy in a model independent way.*

# 1 Introduction

In the Minimal Supersymmetric Standard Model (MSSM), the supersymmetric (SUSY) particles must be produced in pairs. The phase space is largely suppressed in pair production of SUSY particles due to the large masses of the superpartners. The R-parity violating ( $\mathcal{R}_p$ ) extension of the MSSM contains the following additional terms in the superpotential, which are trilinear in the quarks and leptons superfields,

$$W_{\mathcal{R}_p} = \sum_{i,j,k} \left( \frac{1}{2} \lambda_{ijk} L_i L_j E_k^c + \lambda'_{ijk} L_i Q_j D_k^c + \frac{1}{2} \lambda''_{ijk} U_i^c D_j^c D_k^c \right), \quad (1.1)$$

where  $i, j, k$  are flavour indices. These  $\mathcal{R}_p$  couplings offer the opportunity to produce the scalar supersymmetric particles as resonances [1, 2]. Although the  $\mathcal{R}_p$  coupling constants are severely constrained by the low-energy experimental bounds [3, 4, 5, 6], the resonant superpartner production reaches high cross sections both at leptonic [7] and hadronic [8] colliders.

The resonant production of SUSY particle has another interest : since its cross section is proportional to a power 2 of the relevant  $\mathcal{R}_p$  coupling, this reaction would allow an easier determination of the  $\mathcal{R}_p$  couplings than the pair production provided the  $\mathcal{R}_p$  coupling is large enough. As a matter of fact in the pair production study, the sensitivity on the  $\mathcal{R}_p$  couplings is mainly provided by the displaced vertex analysis of the Lightest Supersymmetric Particle (LSP) decay which is difficult experimentally, especially at hadronic colliders. Besides, the displaced vertex analysis allows to test a limited range of couplings which is such that the LSP has a large enough life time to have a measurable decay length while still decaying inside the detector.

Neither the Grand Unified Theories (GUT), the string theories nor the study of the discrete gauge symmetries give a strong theoretical argument in favor of the R-parity violating or R-parity conserving scenarios [3]. Hence, the resonant production of SUSY particle through  $\mathcal{R}_p$  couplings is an attractive possibility which must be considered in the phenomenology of supersymmetry.

The hadronic colliders have an advantage in detecting new particles resonance. Indeed, due to the wide energy distribution of the colliding partons, the resonance can be probed in a wide range of the new particle mass at hadronic colliders. This is in contrast with the leptonic colliders where only large resonances can be probed through radiative returns.

At hadronic colliders, either a slepton or a squark can be produced at the resonance respectively through a  $\lambda'$  or a  $\lambda''$  coupling constant. In the hypothesis of a single dominant  $\mathcal{R}_p$  coupling constant, the resonant scalar particle can decay through the same  $\mathcal{R}_p$  coupling as in the production, leading to a two quark final state for the hard process [8, 9, 10, 11, 12, 13, 14, 15]. In the case where both  $\lambda'$  and  $\lambda$  couplings are non-vanishing, the slepton produced via  $\lambda'$  can decay through  $\lambda$  giving rise to the same final state as in Drell-Yan process, namely two leptons [8, 12, 13, 16, 18]. However, for reasonable values of the  $\mathcal{R}_p$  coupling constants, the decays of the resonant scalar particle via gauge interactions are typically dominant if kinematically allowed [7, 19].

The main decay of the resonant scalar particle through gauge interactions is the decay into its Standard Model partner plus a gaugino. Indeed, in the case where the resonant scalar particle is a squark, it is produced through  $\lambda''$  interactions so that it must be a Right squark  $\tilde{q}_R$  and thus it cannot decay into the  $W^\pm$ -boson, which is the only other



possible decay channel via gauge interactions. Besides, in the case where the resonant scalar particle is a slepton, it is a Left slepton produced via a  $\lambda'$  coupling but it cannot generally decay as  $\tilde{l}_L^\pm \rightarrow W^\pm \tilde{\nu}_L$  or as  $\tilde{\nu}_L \rightarrow W^\pm \tilde{l}_L^\mp$ . The reason is that in most of the SUSY models, as for example the supergravity or the gauge mediated models, the mass difference between the Left charged slepton and the Left sneutrino is due to the D-terms so that it is fixed by the relation  $m_{\tilde{l}_L^\pm}^2 - m_{\tilde{\nu}_L}^2 = \cos 2\beta M_W^2$  [20] and thus it does not exceed the  $W^\pm$ -boson mass. Nevertheless, we note that in the large  $\tan\beta$  scenario, a resonant scalar particle of the third generation can generally decay into the  $W^\pm$ -boson due to the large mixing in the third family sfermion sector. For instance, in the SUGRA model with a large  $\tan\beta$  a tau-sneutrino produced at the resonance can decay as  $\tilde{\nu}_\tau \rightarrow W^\pm \tilde{\tau}_1^\mp$ ,  $\tilde{\tau}_1^\mp$  being the lightest stau.

The resonant scalar particle production at hadronic colliders leads thus mainly to the single gaugino production, in case where the decay of the relevant scalar particle into gaugino is kinematically allowed. In this paper, we study the single gaugino productions at Tevatron Run II. The single gaugino productions at hadronic colliders were first studied in [2, 8]. Later, studies on the single neutralino [21] and single chargino [22] productions at Tevatron have been performed. The single neutralino [23]<sup>1</sup> and single chargino [25] productions have also been considered in the context of physics at LHC. In the present article, we also study the single superpartner productions at Tevatron Run II which occur via  $2 \rightarrow 2$  – *body* processes and do not receive contributions from resonant SUSY particle productions. The single slepton production in  $2 \rightarrow 3$  – *body* processes has been considered in [26] in the context of physics at Tevatron and LHC.

The singly produced superpartner initiates a cascade decay ended typically by the  $\mathcal{R}_p$  decay of the LSP. In case of a single dominant  $\lambda''$  coupling constant, the LSP decays into quarks so that this cascade decay leads to multijet final states having a large QCD background [8, 9]. Nevertheless, if some leptonic decays, as for instance  $\tilde{\chi}^\pm \rightarrow l^\pm \nu \tilde{\chi}^0$ ,  $\tilde{\chi}^\pm$  being the chargino and  $\tilde{\chi}^0$  the neutralino, enter the chain reaction, clearer leptonic signatures can be investigated [27]. In contrast, in the hypothesis of a single dominant  $\lambda'$  coupling constant, the LSP decay into charged leptons naturally favors leptonic signatures [2]. We will thus study the single superpartner production reaction at Tevatron Run II within the scenario of a single dominant  $\lambda'_{ijk}$  coupling constant.

In section 2, we define our theoretical framework. In section 3, we present the values of the cross sections for the various single superpartner productions via  $\lambda'_{ijk}$  at Tevatron Run II and we discuss the interesting multileptonic signatures that these processes can generate. In section 4, we analyse the three lepton signature induced by the single chargino production. In section 5, we study the like sign dilepton final state generated by the single neutralino and chargino productions.

## 2 Theoretical framework

Our framework throughout this paper will be the so-called minimal supergravity model (mSUGRA) which assumes the existence of a grand unified gauge theory and family universal boundary conditions on the supersymmetry breaking parameters. We choose

---

<sup>1</sup>After having submitted our paper, we noticed that resonant slepton production is also studied in [24].

the 5 following parameters :  $m_0$  the universal scalars mass at the unification scale  $M_X$ ,  $m_{1/2}$  the universal gauginos mass at  $M_X$ ,  $A = A_t = A_b = A_\tau$  the trilinear Yukawa coupling at  $M_X$ ,  $sign(\mu)$  the sign of the  $\mu(t)$  parameter ( $t = \log(M_X^2/Q^2)$ ,  $Q$  denoting the running scale) and  $\tan\beta = \langle H_u \rangle / \langle H_d \rangle$  where  $\langle H_u \rangle$  and  $\langle H_d \rangle$  denote the vacuum expectation values of the Higgs fields. In this model, the higgsino mixing parameter  $|\mu|$  is determined by the radiative electroweak symmetry breaking condition. Note also that the parameters  $m_{1/2}$  and  $M_2(t)$  ( $\tilde{W}$  wino mass) are related by the solution of the one loop renormalization group equations  $m_{1/2} = (1 - \beta_a t) M_a(t)$  with  $\beta_a = g_X^2 b_a / (4\pi)^2$ , where  $\beta_a$  are the beta functions,  $g_X$  is the coupling constant at  $M_X$  and  $b_a = [3, -1, -11]$ ,  $a = [3, 2, 1]$  corresponding to the gauge group factors  $SU(3)_c, SU(2)_L, SU(1)_Y$ . We shall set the unification scale at  $M_X = 2 \cdot 10^{16} GeV$  and the running scale at the  $Z^0$ -boson mass :  $Q = m_{Z^0}$ .

We also assume the infrared fixed point hypothesis for the top quark Yukawa coupling [28] that provides a natural explanation of a large top quark mass  $m_{top}$ . In the infrared fixed point approach,  $\tan\beta$  is fixed up to the ambiguity associated with large or low  $\tan\beta$  solutions. The low solution of  $\tan\beta$  is fixed by the equation  $m_{top} = C \sin\beta$ , where  $C \approx 190 - 210 GeV$  for  $\alpha_s(m_{Z^0}) = 0.11 - 0.13$ . For instance, with a top quark mass of  $m_{top} = 174.2 GeV$  [29], the low solution is given by  $\tan\beta \approx 1.5$ . The second important effect of the infrared fixed point hypothesis is that the dependence of the electroweak symmetry breaking constraint on the  $A$  parameter becomes weak so that  $|\mu|$  is a known function of the  $m_0$ ,  $m_{1/2}$  and  $\tan\beta$  parameters [28].

Finally, we consider the  $\mathcal{R}_p$  extension of the mSUGRA model characterised by a single dominant  $\mathcal{R}_p$  coupling constant of type  $\lambda'_{ijk}$ .

### 3 Single superpartner productions via $\lambda'_{ijk}$ at Tevatron Run II

#### 3.1 Resonant superpartner production

At hadronic colliders, either a sneutrino ( $\tilde{\nu}$ ) or a charged slepton ( $\tilde{l}$ ) can be produced at the resonance via the  $\lambda'_{ijk}$  coupling. As explained in Section 1, for most of the SUSY models, the slepton produced at the resonance has two possible gauge decays, namely a decay into either a chargino or a neutralino. Therefore, in the scenario of a single dominant  $\lambda'_{ijk}$  coupling and for most of the SUSY models, either a chargino or a neutralino is singly produced together with either a charged lepton or a neutrino, through the resonant superpartner production at hadronic colliders. There are thus four main possible types of single superpartner production reaction involving  $\lambda'_{ijk}$  at hadronic colliders which receive a contribution from resonant SUSY particle production. The diagrams associated to these four reactions are drawn in Fig.1. As can be seen in this figure, these single superpartner productions receive also some contributions from both the  $t$  and  $u$  channels. Note that all the single superpartner production processes drawn in Fig.1 have charge conjugated processes. We have calculated the amplitudes of the processes shown in Fig.1 and the results are given in Appendix 1.

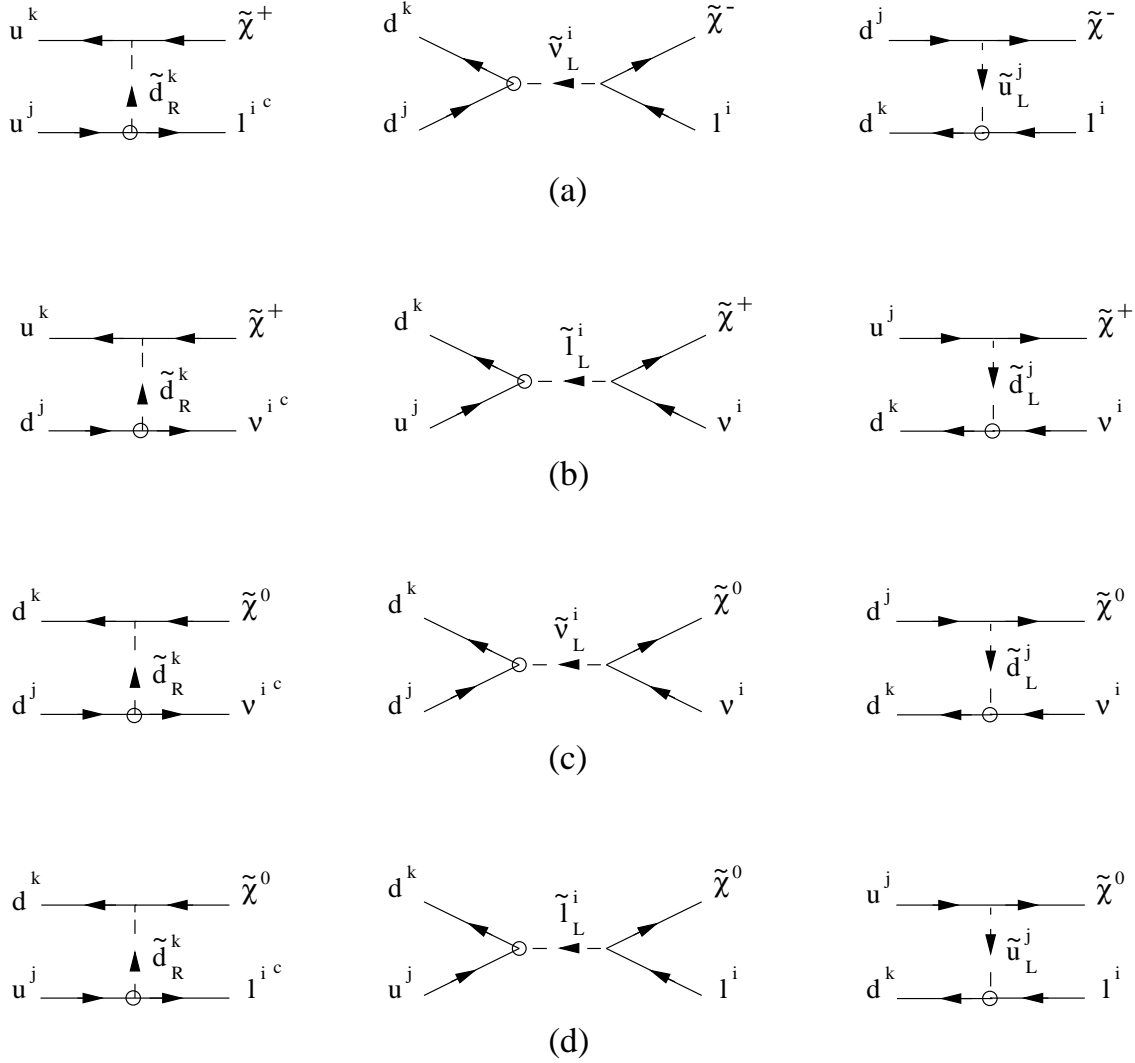


FIG. 1: Feynman diagrams for the 4 single production reactions involving  $\lambda'_{ijk}$  at hadronic colliders which receive a contribution from a resonant supersymmetric particle production. The  $\lambda'_{ijk}$  coupling constant is symbolised by a small circle and the arrows denote the flow of the particle momentum.

## Cross sections

In this section, we discuss the dependence of the single gaugino production cross sections on the various supersymmetric parameters. We will not assume here the radiative electroweak symmetry breaking condition in order to study the variations of the cross sections with the higgsino mixing parameter  $\mu$ .

First, we study the cross section of the single chargino production  $p\bar{p} \rightarrow \tilde{\chi}^+ l_i^-$  which occurs through the  $\lambda'_{ijk}$  coupling (see Fig.1(a)). The differences between the  $\tilde{\chi}^+ e^-$ ,  $\tilde{\chi}^+ \mu^-$  and  $\tilde{\chi}^+ \tau^-$  production (occurring respectively through the  $\lambda'_{1jk}$ ,  $\lambda'_{2jk}$  and  $\lambda'_{3jk}$  couplings with identical  $j$  and  $k$  indices) cross sections involve  $m_{l_i}$  lepton mass terms (see Appendix 1) and are thus negligible. The  $p\bar{p} \rightarrow \tilde{\chi}^+ l_i^-$  reaction receives contributions from the  $s$  channel sneutrino exchange and the  $t$  and  $u$  channels squark exchanges as shown in Fig.1. However, the  $t$  and  $u$  channels represent small contributions to the whole single chargino production cross section when the sneutrino exchanged in the  $s$  channel is real, namely

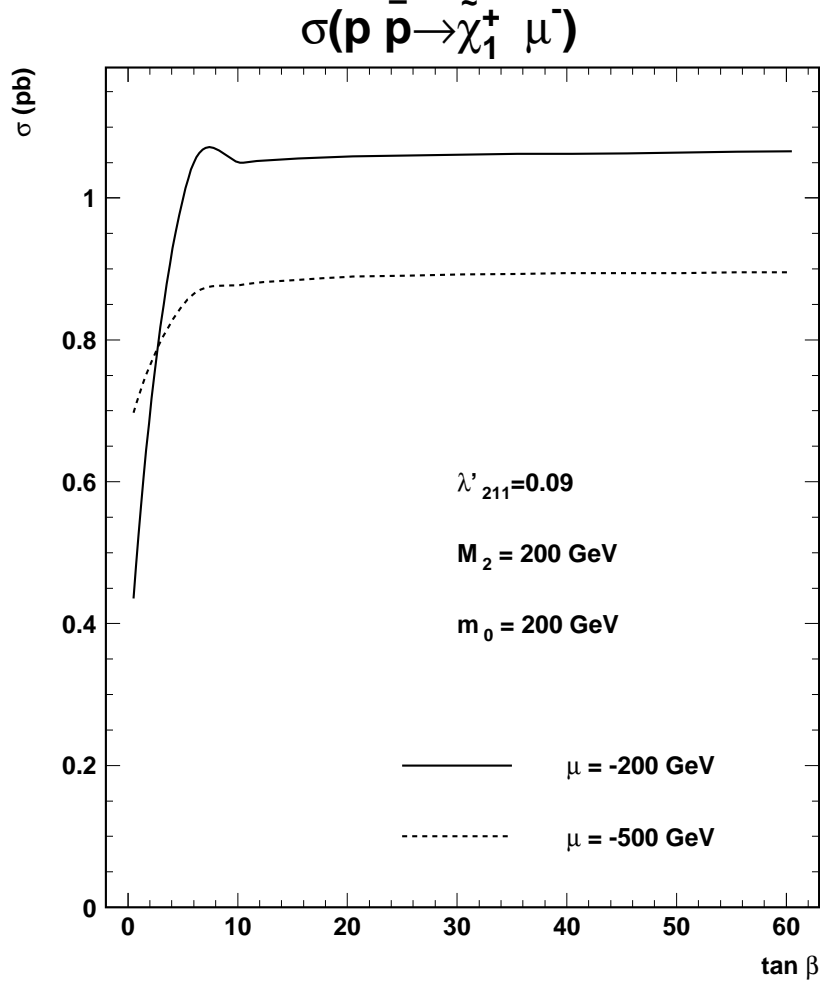


FIG. 2: Cross sections (in pb) of the single chargino production  $p\bar{p} \rightarrow \tilde{\chi}_1^+ \mu^-$  at a center of mass energy of 2TeV as a function of the  $\tan\beta$  parameter for  $\lambda'_{211} = 0.09$ ,  $M_2 = 200\text{GeV}$ ,  $m_0 = 200\text{GeV}$  and two values of the  $\mu$  parameter :  $\mu = -200\text{GeV}$ ,  $-500\text{GeV}$ .

for  $m_{\tilde{\nu}_{iL}} > m_{\tilde{\chi}^\pm}$ . The  $t$  and  $u$  channels cross sections will be relevant only when the produced sneutrino is virtual since the  $s$  channel contribution is small. In this situation the single chargino production rate is greatly reduced compared to the case where the exchanged sneutrino is produced as a resonance. Hence, The  $t$  and  $u$  channels do not represent important contributions to the  $\tilde{\chi}^+ l_i^-$  production rate.

The dependence of the  $\tilde{\chi}^+ l_i^-$  production rate on the  $A$  coupling is weak. Indeed, the rate depends on the  $A$  parameter only through the masses of the third generation squarks eventually exchanged in the  $t$  and  $u$  channels (see Fig.1). Similarly, the dependences on the  $A$  coupling of the rates of the other single gaugino productions shown in Fig.1 are weak. Therefore, in this article we present the results for  $A = 0$ . Later, we will discuss the effects of large  $A$  couplings on the cascade decays which are similar to the effects of large  $\tan\beta$  values.

**$\tan\beta$  dependence :** The dependence of the  $\tilde{\chi}^+ l_i^-$  production rate on  $\tan\beta$  is also weak,

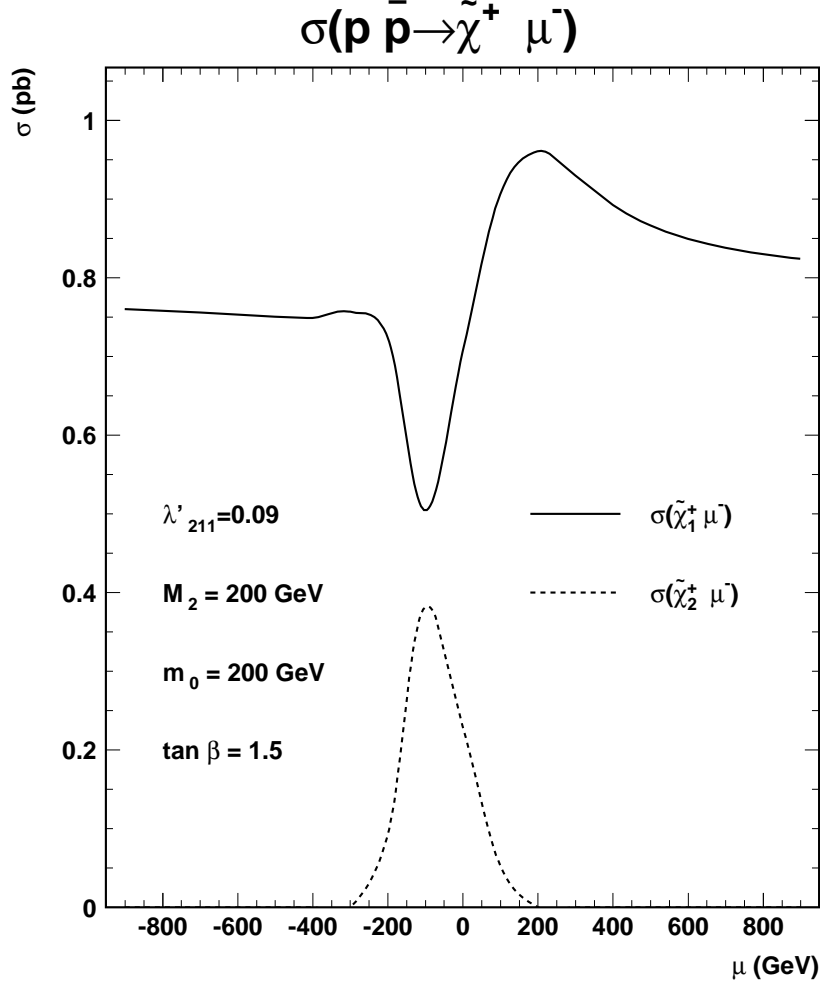


FIG. 3: Cross sections (in pb) of the single chargino productions  $p\bar{p} \rightarrow \tilde{\chi}_{1,2}^+ \mu^-$  as a function of the  $\mu$  parameter (in GeV) for  $\lambda'_{211} = 0.09$ ,  $M_2 = 200\text{GeV}$ ,  $\tan \beta = 1.5$  and  $m_0 = 200\text{GeV}$  at a center of mass energy of  $2\text{TeV}$ .

except for  $\tan \beta < 10$ . This can be seen in Fig.2 where the cross section of the  $p\bar{p} \rightarrow \tilde{\chi}_1^+ \mu^-$  reaction occurring through the  $\lambda'_{211}$  coupling is shown as a function of the  $\tan \beta$  parameter. The choice of the  $\lambda'_{211}$  coupling is motivated by the fact that the analysis in Sections 4 and 5 are explicitly made for this  $\mathcal{R}_p$  coupling. In Fig.2, we have taken the  $\lambda'_{211}$  value equal to its low-energy experimental bound for  $m_{\tilde{d}_R} = 100\text{GeV}$  which is  $\lambda'_{211} < 0.09$  [4]. At this stage, some remarks on the values of the cross sections presented in this section must be done. First, the single gaugino production rates must be multiplied by a factor 2 in order to take into account the charge conjugated process, which is for example in the present case  $p\bar{p} \rightarrow \tilde{\chi}^- \mu^+$ . Furthermore, the values of the cross sections for all the single gaugino productions are obtained using the CTEQ4L structure function [30]. Choosing other parametrizations does not change significantly the results since proton structure functions in our kinematical domain in Bjorken  $x$  are known and have been already measured. For instance, with the set of parameters  $\lambda'_{211} = 0.09$ ,  $M_2 = 100\text{GeV}$ ,

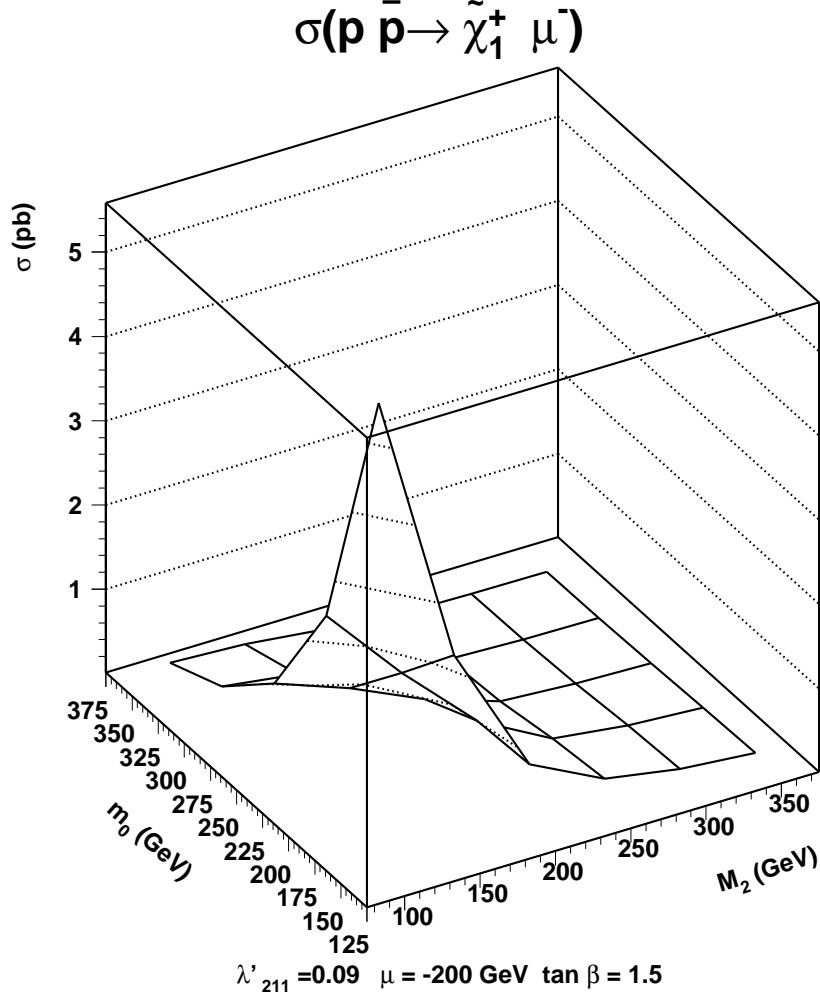


FIG. 4: Cross section (in pb) of the single chargino production  $p\bar{p} \rightarrow \tilde{\chi}_1^+ \mu^-$  as a function of the  $m_0$  (in GeV) and  $M_2$  (in GeV) parameters. The center of mass energy is  $\sqrt{s} = 2\text{TeV}$  and the other parameters are :  $\lambda'_{211} = 0.09$ ,  $\tan \beta = 1.5$  and  $\mu = -200\text{GeV}$ .

$\tan \beta = 1.5$ ,  $m_0 = 300\text{GeV}$  and  $\mu = -500\text{GeV}$ , the  $\tilde{\chi}_1^+ \mu^-$  production cross section is  $0.503\text{pb}$  for the CTEQ4L structure function [30],  $0.503\text{pb}$  for the BEP structure function [31],  $0.480\text{pb}$  for the MRS (R2) structure function [32] and  $0.485\text{pb}$  for the GRV LO structure function [33].

**$\mu$  dependence :** In Fig.3, we present the cross sections of the  $\tilde{\chi}_1^+ \mu^-$  and  $\tilde{\chi}_2^+ \mu^-$  productions as a function of the  $\mu$  parameter. We observe in this figure the weak dependence of the cross section  $\sigma(p\bar{p} \rightarrow \tilde{\chi}_1^+ \mu^-)$  on  $\mu$  for  $|\mu| > M_2$ . The reason is the smooth dependence of the  $\tilde{\chi}_1^\pm$  mass on  $\mu$  in this domain. However, the rate strongly decreases in the region  $|\mu| < M_2$  in which the  $\tilde{\chi}_1^\pm$  chargino is mainly composed by the higgsino. Nevertheless, the small  $|\mu|$  domain ( $|\mu|$  smaller than  $\sim 100\text{GeV}$  for  $\tan \beta = 1.41$ ,  $M_2 > 100\text{GeV}$ ,  $m_0 = 500\text{GeV}$  and  $\lambda' \neq 0$ ) is excluded by the present experimental limits derived from the LEP data [34].

In contrast, the cross section  $\sigma(p\bar{p} \rightarrow \tilde{\chi}_2^+ \mu^-)$  increases in the domain  $|\mu| < M_2$  due to the

fact that the  $\tilde{\chi}_2^\pm$  mass is enhanced as  $|\mu|$  increases and the  $\tilde{\chi}_2^\pm$  is primarily wino in the region  $|\mu| < M_2$ . The region in which  $\sigma(p\bar{p} \rightarrow \tilde{\chi}_2^\pm \mu^\mp)$  becomes important is at small values of  $|\mu|$ , near the LEP limits of [34]. We also remark in Fig.3 that the single  $\tilde{\chi}_1^+$  production rate values remain above the single  $\tilde{\chi}_2^+$  production rate values in all the considered range of  $\mu$ . In this figure, we also notice that the cross section is smaller when  $\mu$  is negative. To be conservative, we will take  $\mu < 0$  in the following.

**$m_0$  and  $M_2$  dependences :** In fact, the cross section  $\sigma(p\bar{p} \rightarrow \tilde{\chi}^+ l_i^-)$  depends mainly on the  $m_0$  and  $M_2$  parameters. We present in Fig.4 the rate of the  $\tilde{\chi}_1^+ \mu^-$  production as a function of the  $m_0$  and  $M_2$  parameters. The rate decreases at high values of  $m_0$  since the sneutrino becomes heavier as  $m_0$  increases and more energetic initial partons are required in order to produce the resonant sneutrino. The decrease of the rate at large values of  $M_2$  is due to the increase of the chargino mass and thus the reduction of the phase space factor.

In Fig.5, we show the variations of the  $\sigma(p\bar{p} \rightarrow \tilde{\chi}_1^+ \mu^-)$  cross sections with  $m_0$  for fixed values of  $M_2$ ,  $\mu$  and  $\tan\beta$ . The cross sections corresponding to the  $\tilde{\chi}_1^+ \mu^-$  production through various  $\mathcal{R}_p$  couplings of type  $\lambda'_{2jk}$  are presented. In this figure, we only consider the  $\mathcal{R}_p$  couplings giving the highest cross sections. The values of the considered  $\lambda'_{2jk}$  couplings have been taken at their low-energy limit [4] for a squark mass of  $100\text{GeV}$ . The rate of the  $\tilde{\chi}_2^+ \mu^-$  production through  $\lambda'_{211}$  is also shown in this figure. We already notice that the cross section is significant for many  $\mathcal{R}_p$  couplings and we will come back on this important statement in the following.

The  $\sigma(p\bar{p} \rightarrow \tilde{\chi}^+ \mu^-)$  rates decrease as  $m_0$  increases for the same reason as in Fig.4. A decrease of the rates also occurs at small values of  $m_0$ . The reason is the following. When  $m_0$  decreases, the  $\tilde{\nu}$  mass is getting closer to the  $\tilde{\chi}^\pm$  masses so that the phase space factor associated to the decay  $\tilde{\nu}_\mu \rightarrow \tilde{\chi}^\pm \mu^\mp$  decreases.

We also observe that the single  $\tilde{\chi}_2^+$  production rate is much smaller than the single  $\tilde{\chi}_1^+$  production rate, as in Fig.3.

Since the single chargino production rate scales as  $\lambda'^2$  (see Appendix 1), we easily see by doing a rescaling of the rates that the various  $\tilde{\chi}_1^+ \mu^-$  production rates presented in Fig.5 would still have different values for identical values of the involved  $\mathcal{R}_p$  coupling constants. These differences between the  $\tilde{\chi}_1^+ \mu^-$  production rates occurring via the various  $\lambda'_{2jk}$  couplings are explained by the different parton densities. Indeed, as shown in Fig.1 the hard processes associated to the  $\tilde{\chi}_1^+ \mu^-$  production occurring through the  $\lambda'_{2jk}$  coupling constant have a partonic initial state  $\bar{q}_j q_k$ . The influence of the parton density on the single chargino production rate can be observed on Fig.5 by comparing the  $\tilde{\chi}_1^+ \mu^-$  production rates occurring through the  $\lambda'_{211} = 0.09$  and  $\lambda'_{212} = 0.09$  coupling constants. For same values of the  $\lambda'_{2jk}$  coupling constants, the  $\tilde{\chi}_1^+ \mu^-$  production involving the  $\lambda'_{211}$  coupling constant has the highest cross section since the associated hard processes have first generation quarks in the initial state which provide the maximum parton density.

We now discuss the rate behaviours for the reactions  $p\bar{p} \rightarrow \tilde{\chi}^- \nu_\mu$ ,  $p\bar{p} \rightarrow \tilde{\chi}^0 \mu^-$  and  $p\bar{p} \rightarrow \tilde{\chi}^0 \nu_\mu$  which occur via  $\lambda'_{211}$ , in the SUSY parameter space. The dependences of these rates on the  $A$ ,  $\tan\beta$ ,  $\mu$  and  $M_2$  parameters are typically the same as for the  $\tilde{\chi}^+ \mu^-$  production rate. The variations of the  $\tilde{\chi}_1^- \nu_\mu$ ,  $\tilde{\chi}_{1,2}^0 \mu^-$  and  $\tilde{\chi}_1^0 \nu_\mu$  productions cross sections with the  $m_0$  parameter are shown in Fig.6. The  $\tilde{\chi}_2^- \nu_\mu$ ,  $\tilde{\chi}_{3,4}^0 \mu^-$  and  $\tilde{\chi}_{3,4}^0 \nu_\mu$  production rates are comparatively negligible and thus have not been represented. We observe in this figure that the cross sections decrease at large  $m_0$  values like the  $\tilde{\chi}^+ \mu^-$  production

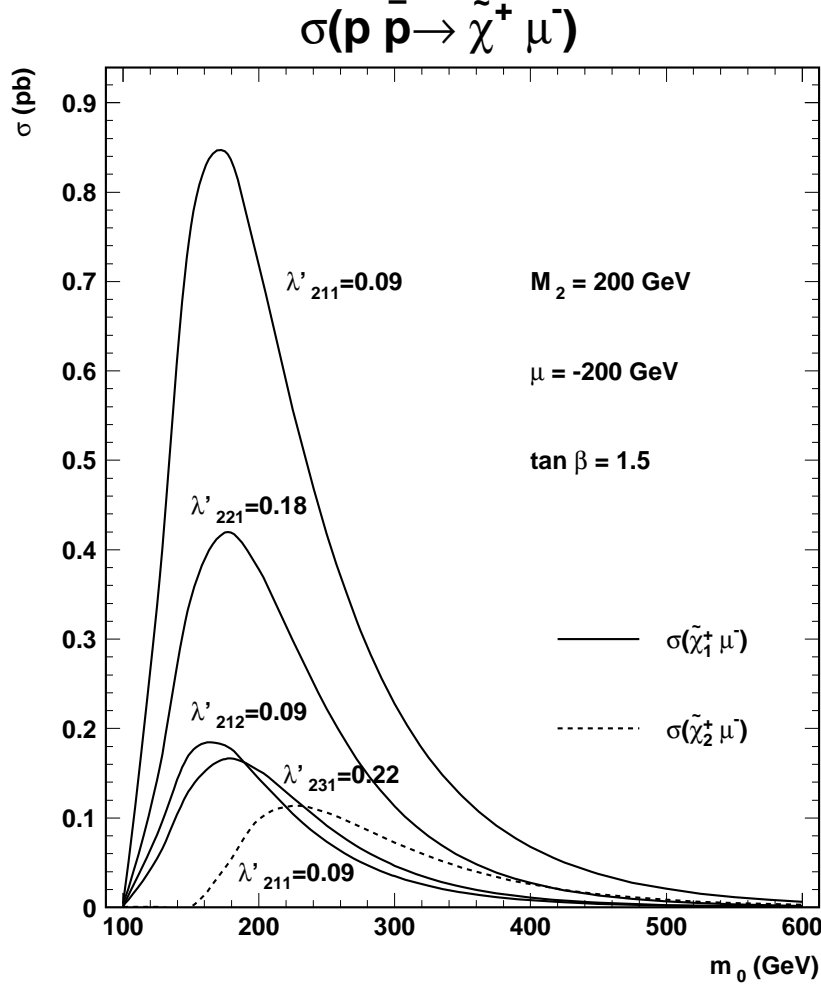


FIG. 5: Cross sections (in pb) of the single chargino productions  $p\bar{p} \rightarrow \tilde{\chi}_{1,2}^+ \mu^-$  as a function of the  $m_0$  parameter (in GeV). The center of mass energy is taken at  $\sqrt{s} = 2\text{TeV}$  and  $\lambda'_{211} = 0.09$ ,  $M_2 = 200\text{GeV}$ ,  $\tan\beta = 1.5$  and  $\mu = -200\text{GeV}$ . The rates of the single  $\tilde{\chi}_1^+$  production via the  $\tilde{R}_p$  couplings  $\lambda'_{212} = 0.09$ ,  $\lambda'_{221} = 0.18$  and  $\lambda'_{231} = 0.22$  are also shown. The chosen values of the  $\tilde{R}_p$  couplings correspond to the low-energy limits [4] for a squark mass of  $100\text{GeV}$ .

rate. However, while the single  $\tilde{\chi}_1^\pm$  productions rates decrease at small  $m_0$  values (see Fig.5 and Fig.6), this is not true for the single  $\tilde{\chi}_1^0$  productions (see Fig.6). The reason is that in mSUGRA the  $\tilde{\chi}_1^0$  and  $\tilde{l}_{iL}$  ( $l_i = l_i^\pm, \nu_i$ ) masses are never close enough to induce a significant decrease of the cross section associated to the reaction  $p\bar{p} \rightarrow \tilde{l}_{iL} \rightarrow \tilde{\chi}_1^0 l_i$ , where  $l_i = l_i^\pm, \nu_i$  (see Fig.1(c)(d)), caused by a phase space factor reduction. Therefore, the resonant slepton contribution to the single  $\tilde{\chi}_1^0$  production is not reduced at small  $m_0$  values like the resonant slepton contribution to the single  $\tilde{\chi}_1^\pm$  production. For the same reason, the single  $\tilde{\chi}_1^0$  productions have much higher cross sections than the single  $\tilde{\chi}_1^\pm$  productions in most of the mSUGRA parameter space, as illustrate Fig.5 and Fig.6. We note that in the particular case of a single dominant  $\lambda'_{3jk}$  coupling constant and of large  $\tan\beta$  values, the rate of the reaction  $p\bar{p} \rightarrow \tilde{\tau}_1^\pm \rightarrow \tilde{\chi}_1^0 \tau^\pm$  (see Fig.1(d)), where  $\tilde{\tau}_1^\pm$  is the



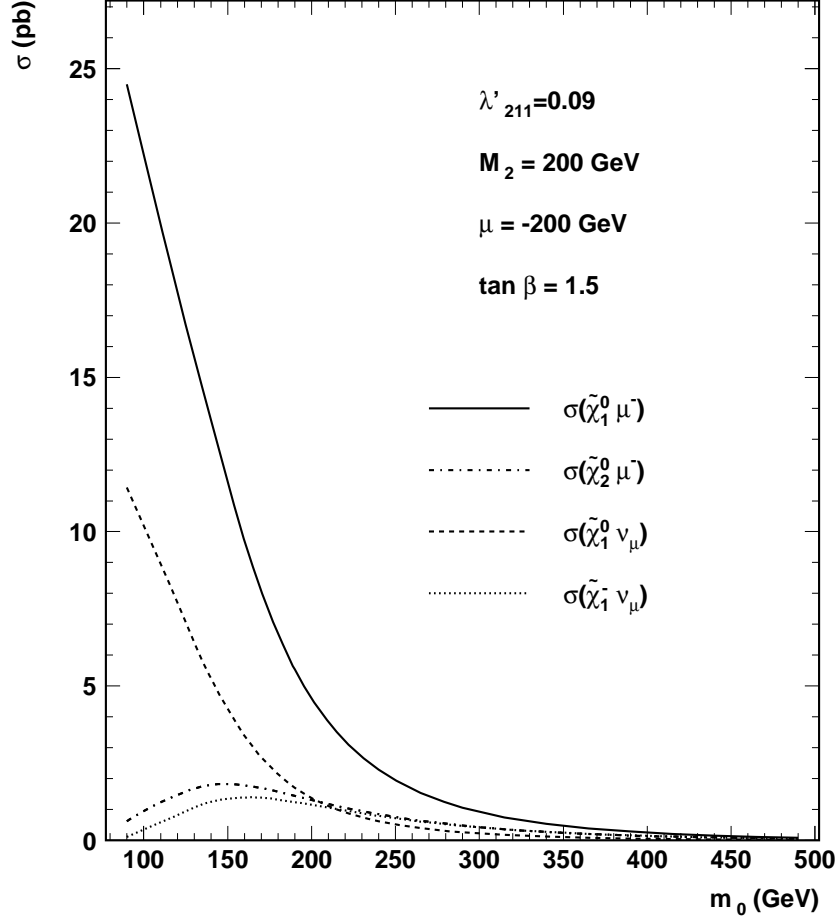


FIG. 6: Cross sections (in pb) of the reactions  $p\bar{p} \rightarrow \tilde{\chi}_1^- \nu$ ,  $p\bar{p} \rightarrow \tilde{\chi}_{1,2}^0 \mu^-$  and  $p\bar{p} \rightarrow \tilde{\chi}_1^0 \nu$  as a function of the  $m_0$  parameter (in GeV). The center of mass energy is taken at  $\sqrt{s} = 2\text{TeV}$  and the considered set of parameters is :  $\lambda'_{211} = 0.09$ ,  $M_2 = 200\text{GeV}$ ,  $\tan \beta = 1.5$  and  $\mu = -200\text{GeV}$ .

lightest tau-slepton, can be reduced at low  $m_0$  values since then  $m_{\tilde{\tau}_1^\pm}$  can be closed to  $m_{\tilde{\chi}_1^0}$  due to the large mixing occurring in the staus sector. By analysing Fig.5 and Fig.6, we also remark that the  $\tilde{\chi}^- \nu_\mu$  ( $\tilde{\chi}^0 \mu^-$ ) production rate is larger than the  $\tilde{\chi}^+ \mu^-$  ( $\tilde{\chi}^0 \nu_\mu$ ) one. The explanation is that in  $p\bar{p}$  collisions the initial states of the resonant charged slepton production  $u_j \bar{d}_k, \bar{u}_j d_k$  have higher partonic densities than the initial states of the resonant sneutrino production  $d_j \bar{d}_k, \bar{d}_j d_k$ . This phenomenon also increases the difference between the rates of the  $\tilde{\chi}_1^0 \mu^-$  and  $\tilde{\chi}_1^+ \mu^-$  productions at Tevatron.

Although the single  $\tilde{\chi}_1^\pm$  production cross sections are smaller than the  $\tilde{\chi}_1^0$  ones, it is interesting to study both of them since they have quite high values.

### 3.2 Non-resonant superpartner production

At hadronic colliders, the single productions of SUSY particle via  $\lambda'_{ijk}$  can occur through some  $2 \rightarrow 2$  – *body* processes which do not receive contributions from any resonant superpartner production. These non-resonant superpartner productions are (one must also add the charge conjugated processes) :

- The gluino production  $\bar{u}_j d_k \rightarrow \tilde{g} l_i$  via the exchange of a  $\tilde{u}_{jL}$  ( $\tilde{d}_{kR}$ ) squark in the  $t$  ( $u$ ) channel.
- The squark production  $\bar{d}_j g \rightarrow \tilde{d}_{kR}^* \nu_i$  via the exchange of a  $\tilde{d}_{kR}$  squark ( $d_j$  quark) in the  $t$  ( $s$ ) channel.
- The squark production  $\bar{u}_j g \rightarrow \tilde{d}_{kR}^* l_i$  via the exchange of a  $\tilde{d}_{kR}$  squark ( $u_j$  quark) in the  $t$  ( $s$ ) channel.
- The squark production  $d_k g \rightarrow \tilde{d}_{jL} \nu_i$  via the exchange of a  $\tilde{d}_{jL}$  squark ( $d_k$  quark) in the  $t$  ( $s$ ) channel.
- The squark production  $d_k g \rightarrow \tilde{u}_{jL} l_i$  via the exchange of a  $\tilde{u}_{jL}$  squark ( $d_k$  quark) in the  $t$  ( $s$ ) channel.
- The sneutrino production  $\bar{d}_j d_k \rightarrow Z \tilde{\nu}_{iL}$  via the exchange of a  $d_k$  or  $d_j$  quark ( $\tilde{\nu}_{iL}$  sneutrino) in the  $t$  ( $s$ ) channel.
- The charged slepton production  $\bar{u}_j d_k \rightarrow Z \tilde{l}_{iL}$  via the exchange of a  $d_k$  or  $u_j$  quark ( $\tilde{l}_{iL}$  slepton) in the  $t$  ( $s$ ) channel.
- The sneutrino production  $\bar{u}_j d_k \rightarrow W^- \tilde{\nu}_{iL}$  via the exchange of a  $d_j$  quark ( $\tilde{l}_{iL}$  sneutrino) in the  $t$  ( $s$ ) channel.
- The charged slepton production  $\bar{d}_j d_k \rightarrow W^+ \tilde{l}_{iL}$  via the exchange of a  $u_j$  quark ( $\tilde{\nu}_{iL}$  sneutrino) in the  $t$  ( $s$ ) channel.

The single gluino production cannot reach high cross sections due to the strong experimental limits on the squarks and gluinos masses which are typically about  $m_{\tilde{q}}, m_{\tilde{g}} \gtrsim 200 GeV$  [35]. Indeed, the single gluino production occurs through the exchange of squarks in the  $t$  and  $u$  channels, as described above, so that the cross section of this production decreases as the squarks and gluinos masses increase. For the value  $m_{\tilde{q}} = m_{\tilde{g}} = 250 GeV$  which is close to the experimental limits, we find the single gluino production rate  $\sigma(p\bar{p} \rightarrow \tilde{g}\mu) \approx 10^{-2} pb$  which is consistent with the results of [8]. The cross sections given in this section are computed at a center of mass energy of  $\sqrt{s} = 2 TeV$  using the version 33.18 of the COMPHEP routine [36] with the CTEQ4m structure function and an  $\mathcal{R}_p$  coupling  $\lambda'_{211} = 0.09$ . Similarly, the single squark production cross section cannot be large : for  $m_{\tilde{q}} = 250 GeV$ , the rate  $\sigma(p\bar{p} \rightarrow \tilde{u}_L \mu)$  is of order  $\sim 10^{-3} pb$ . The production of a slepton together with a massive gauge boson has a small phase space factor and does not involve strong interaction couplings. The cross section of this type of reaction is thus small. For instance, with a slepton mass of  $m_{\tilde{l}} = 100 GeV$  we find the cross section  $\sigma(p\bar{p} \rightarrow Z \tilde{\mu}_L)$  to be of order  $10^{-2} pb$ .

As a conclusion, the non-resonant single superpartner productions have small rates and will not be considered here. Nevertheless, some of these reactions are interesting as their cross section involves few SUSY parameters, namely only one scalar superpartner mass and one  $\mathcal{R}_p$  coupling constant.

## 4 Three lepton signature analysis

### 4.1 Signal

In this section, we study the three lepton signature at Tevatron Run II generated by the single chargino production through  $\lambda'_{ijk}$ ,  $p\bar{p} \rightarrow \tilde{\chi}^{\pm} l_i^{\mp}$ , followed by the cascade decay,  $\tilde{\chi}^{\pm} \rightarrow \tilde{\chi}_1^0 l^{\pm} \nu$ ,  $\tilde{\chi}_1^0 \rightarrow l_i u_j \bar{d}_k$ ,  $\bar{l}_i \bar{u}_j d_k$  (the indices  $i, j, k$  correspond to the indices of  $\lambda'_{ijk}$ ). In fact, the whole final state is 3 charged leptons + 2 hard jets + missing energy ( $\cancel{E}$ ). The two jets and the missing energy come respectively from the quarks and the neutrino produced in the cascade decay. In the mSUGRA model, which predicts the  $\tilde{\chi}_1^0$  as the LSP in most of the parameter space, the  $p\bar{p} \rightarrow \tilde{\chi}^{\pm} l_i^{\mp}$  reaction is the only single gaugino production allowing the three lepton signature to be generated in a significant way. Since the  $\tilde{\chi}_1^{\pm} l_i^{\mp}$  production rate is dominant compared to the  $\tilde{\chi}_2^{\pm} l_i^{\mp}$  production rate, as discussed in Section 3.1, we only consider the contribution to the three lepton signature from the single lightest chargino production.

For  $m_{\tilde{\nu}}, m_{\tilde{l}}, m_{\tilde{q}}, m_{\tilde{\chi}_2^0} > m_{\tilde{\chi}_1^{\pm}}$ , the branching ratio  $B(\tilde{\chi}_1^{\pm} \rightarrow \tilde{\chi}_1^0 l^{\pm} \nu)$  is typically of order 30% and is smaller than for the other possible decay  $\tilde{\chi}_1^{\pm} \rightarrow \tilde{\chi}_1^0 \bar{q}_p q'_p$  because of the color factor.

Since in our framework the  $\tilde{\chi}_1^0$  is the LSP, it can only decay via  $\lambda'_{ijk}$ , either as  $\tilde{\chi}_1^0 \rightarrow l_i u_j d_k$  or as  $\tilde{\chi}_1^0 \rightarrow \nu_i d_j d_k$ , with a branching ratio  $B(\tilde{\chi}_1^0 \rightarrow l_i u_j d_k)$  ranging between  $\sim 40\%$  and  $\sim 70\%$ .

The three lepton signature is particularly attractive at hadronic colliders because of the possibility to reduce the associated Standard Model background. In Section 4.2 we describe this Standard Model background and in Section 4.4 we show how it can be reduced.

### 4.2 Standard Model background of the 3 lepton signature at Tevatron

The first source of Standard Model background for the three leptons final state is the top quark pair production  $q\bar{q} \rightarrow t\bar{t}$  or  $gg \rightarrow t\bar{t}$ . Since the top quark life time is smaller than its hadronisation time, the top decays and its main channel is the decay into a  $W$  gauge boson and a bottom quark as  $t \rightarrow bW$ . The  $t\bar{t}$  production can thus give rise to a  $3l$  final state if the  $W$  bosons and one of the b-quarks undergo leptonic decays simultaneously. The cross section, calculated at leading order with PYTHIA [37] using the CTEQ2L structure function, times the branching fraction is  $\sigma(p\bar{p} \rightarrow t\bar{t}) \times B^2(W \rightarrow l_p \nu_p) \approx 863 fb$  ( $704 fb$ ) with  $p = 1, 2, 3$  at  $\sqrt{s} = 2TeV$  for a top quark mass of  $m_{top} = 170 GeV$  ( $175 GeV$ ).

The other major source of Standard Model background is the  $W^{\pm} Z^0$  production followed by the leptonic decays of the gauge bosons, namely  $W \rightarrow l\nu$  and  $Z \rightarrow l\bar{l}$ . The value for the cross section times the branching ratios is  $\sigma(p\bar{p} \rightarrow WZ) \times B(W \rightarrow l_p \nu_p) \times B(Z \rightarrow l_p \bar{l}_p) \approx 82 fb$  ( $p = 1, 2, 3$ ) at leading order with a center of mass energy of  $\sqrt{s} = 2TeV$ . The  $W^{\pm} Z^0$  production gives also a small contribution to the 3 leptons background through the decays :  $W \rightarrow bu_p$  and  $Z \rightarrow b\bar{b}$ ,  $W \rightarrow l\nu$  and  $Z \rightarrow b\bar{b}$  or  $W \rightarrow bu_p$  and  $Z \rightarrow l\bar{l}$ , if a lepton is produced in each of the b jets.

Similarly, the  $Z^0 Z^0$  production followed by the decays  $Z \rightarrow l\bar{l}$  ( $l = e, \mu$ ),  $Z \rightarrow \tau\bar{\tau}$ , where one of the  $\tau$  decays into lepton while the other decays into jet, leads to three

leptons in the final state. Within the same framework as above, the cross section is of order  $\sigma(p\bar{p} \rightarrow ZZ \rightarrow 3l) \approx 2fb$ .

The  $Z^0 Z^0$  production can also contribute weakly to the 3 leptons background via the decays :  $Z \rightarrow l\bar{l}$  and  $Z \rightarrow b\bar{b}$  or  $Z \rightarrow b\bar{b}$  and  $Z \rightarrow b\bar{b}$ , since a lepton can be produced in a b jet.

It has been pointed out recently that the  $WZ^*$  (throughout this paper a star indicates a virtual particle) and the  $W\gamma^*$  productions could represent important contributions to the trilepton background [38, 39]. The complete list of contributions to the 3 leptons final state from the  $WZ, W\gamma^*$  and  $ZZ$  productions, including cases where either one or both of the gauge bosons can be virtual, has been calculated in [40]. The authors of [40] have found that the  $WZ, W\gamma^*$  and  $ZZ$  backgrounds (including virtual boson(s)) at the upgraded Tevatron have together a cross section of order  $0.5fb$  after the following cuts have been implemented :  $P_t(l_1) > 20GeV$ ,  $P_t(l_2) > 15GeV$ ,  $P_t(l_3) > 10GeV$ ;  $|\eta(l_1, l_{2,3})| < 1.0, 2.0$ ;  $ISO_{\delta R=0.4} < 2GeV$ ;  $\cancel{E}_T > 25GeV$ ;  $81GeV < M_{inv}(l\bar{l}) < 101GeV$ ;  $12GeV < M_{inv}(l\bar{l})$ ;  $60GeV < m_T(l, \cancel{E}_T) < 85GeV$ .

We note that there is at most one hard jet in the 3 leptons backgrounds generated by the  $WZ, W\gamma^*$  and  $ZZ$  productions (including virtual boson(s)). Since the number of hard jets is equal to 2 in our signal (see Section 4.1), a jet veto can thus reduce this Standard Model background with respect to the signal.

Other small sources of Standard Model background have been estimated in [41] : The productions like  $Zb, Wt$  or  $Wt\bar{t}$ . After applying cuts on the geometrical acceptance, the transverse momentum and the isolation, these backgrounds are expected to be at most of order  $10^{-4}pb$  in  $p\bar{p}$  collisions with a center of mass energy of  $\sqrt{s} = 2TeV$ . We have checked that the  $Zb$  production gives a negligible contribution to the 3 lepton signature.

There are finally some non-physics sources of background. First, the 4 leptons signal, which can be generated by the  $Z^0 Z^0$  and  $t\bar{t}$  productions, appears as a 3 leptons signature if one of the leptons is missed. Besides, the processes  $p\bar{p} \rightarrow Z + X$ ,  $Drell-Yan + X$  would mimic a trilepton signal if  $X$  fakes a lepton. Monte Carlo simulations using simplified detector simulation, like for example SHW [42] as in the present study (see Section 4.4), cannot give a reliable estimate of this background. A knowledge of the details of the detector response as well as the jet fragmentation is necessary in order to determinate the probability to fake a lepton. In [43], using standard cuts the background coming from  $p\bar{p} \rightarrow Z + X$ ,  $Drell-Yan + X$  has been estimated to be of order  $2fb$  at Tevatron with  $\sqrt{s} = 2TeV$ . The authors of [43] have also estimated the background from the three-jet events faking trilepton signals to be around  $10^{-3}fb$ .

Hence for the study of the Standard Model background associated to the 3 lepton signature at Tevatron Run II, we consider the  $W^\pm Z^0$  production and both the physics and non-physics contributions generated by the  $Z^0 Z^0$  and  $t\bar{t}$  productions.

### 4.3 Supersymmetric background of the 3 lepton signature at Tevatron

If an excess of events is observed in the three lepton channel at Tevatron, one would wonder what is the origin of those anomalous events. One would thus have to consider all of the supersymmetric productions leading to the three lepton signature. In the present context of R-parity violation, multileptonic final states can be generated by the single

$m_{1/2} \setminus m_0$	100GeV	200GeV	300GeV	400GeV	500GeV
100GeV	6.359	3.846	3.369	3.567	3.849
200GeV	0.179	0.149	0.151	0.160	0.170
300GeV	$2.2 \cdot 10^{-2}$	$1.6 \cdot 10^{-2}$	$1.5 \cdot 10^{-2}$	$1.5 \cdot 10^{-2}$	$1.6 \cdot 10^{-2}$

TAB. 3: Cross section (in  $pb$ ) of the sum of all the superpartners pair productions at Tevatron Run II as a function of the  $m_0$  and  $m_{1/2}$  parameters for  $\tan\beta = 1.5$ ,  $\text{sign}(\mu) < 0$  and  $\lambda'_{211} = 0.05$  at a center of mass energy of  $\sqrt{s} = 2TeV$ . These rates have been calculated with HERWIG [48] using the CTEQ4m structure function.

chargino production involving  $R_p$  couplings, but also by the supersymmetric particle pair production which involves only gauge couplings [44, 13]. In  $R_p$  models, the superpartner pair production can even lead to the trilepton signature [45, 46, 47]. As a matter of fact, both of the produced supersymmetric particles decay, either directly or through cascade decays, into the LSP which is the neutralino in our framework. In the hypothesis of a dominant  $\lambda'$  coupling constant, each of the 2 produced neutralinos can decay into a charged lepton and two quarks : at least two charged leptons and four jets in the final state are produced. The third charged lepton can be generated in the cascade decays as for example at the level of the chargino decay  $\tilde{\chi}^\pm \rightarrow \tilde{\chi}^0 l^\pm \nu$ .

In Table 3, we show for different mSUGRA points the cross section of the sum of all superpartner pair productions, namely the  $R_p$  conserving SUSY background of the 3 lepton signature generated by the single chargino production. As can be seen in this table, the summed superpartner pair production rate decreases as  $m_0$  and  $m_{1/2}$  increase. This is due to the increase of the superpartner masses as the  $m_0$  or  $m_{1/2}$  parameter increases. The SUSY background will be important only for low values of  $m_0$  and  $m_{1/2}$  as we will see in the following.

## 4.4 Cuts

In order to simulate the single chargino production  $p\bar{p} \rightarrow \tilde{\chi}_1^\pm l^\mp$  at Tevatron, the matrix elements (see Appendix 1) of this process have been implemented in a version of the SUSYGEN event generator [49] allowing the generation of  $p\bar{p}$  reactions [50]. The Standard Model background ( $W^\pm Z^0$ ,  $Z^0 Z^0$  and  $t\bar{t}$  productions) has been simulated using the PYTHIA event generator [37] and the SUSY background (all SUSY particles pair productions) using the HERWIG event generator [48]. SUSYGEN, PYTHIA and HERWIG have been interfaced with the SHW detector simulation package [42], which mimics an average of the CDF and D0 Run II detector performance.

We have developed a series of cuts in order to enhance the signal-to-background ratio. First, we have selected the events with at least three leptons where the leptons are either an electron, a muon or a tau reconstructed from a jet, namely  $N_l \geq 3$  [ $l = e, \mu, \tau$ ]. We have also considered the case where the selected leptons are only electrons and muons, namely  $N_l \geq 3$  [ $l = e, \mu$ ].

The selection criteria on the jets was to have a number of jets greater or equal to two, where the jets have a transverse momentum higher than 10GeV, namely  $N_j \geq 2$  with  $P_t(j) > 10GeV$ . This jet veto reduces the 3 lepton backgrounds coming from the  $W^\pm Z^0$  and  $Z^0 Z^0$  productions. Indeed, the  $W^\pm Z^0$  production generates no hard jets and

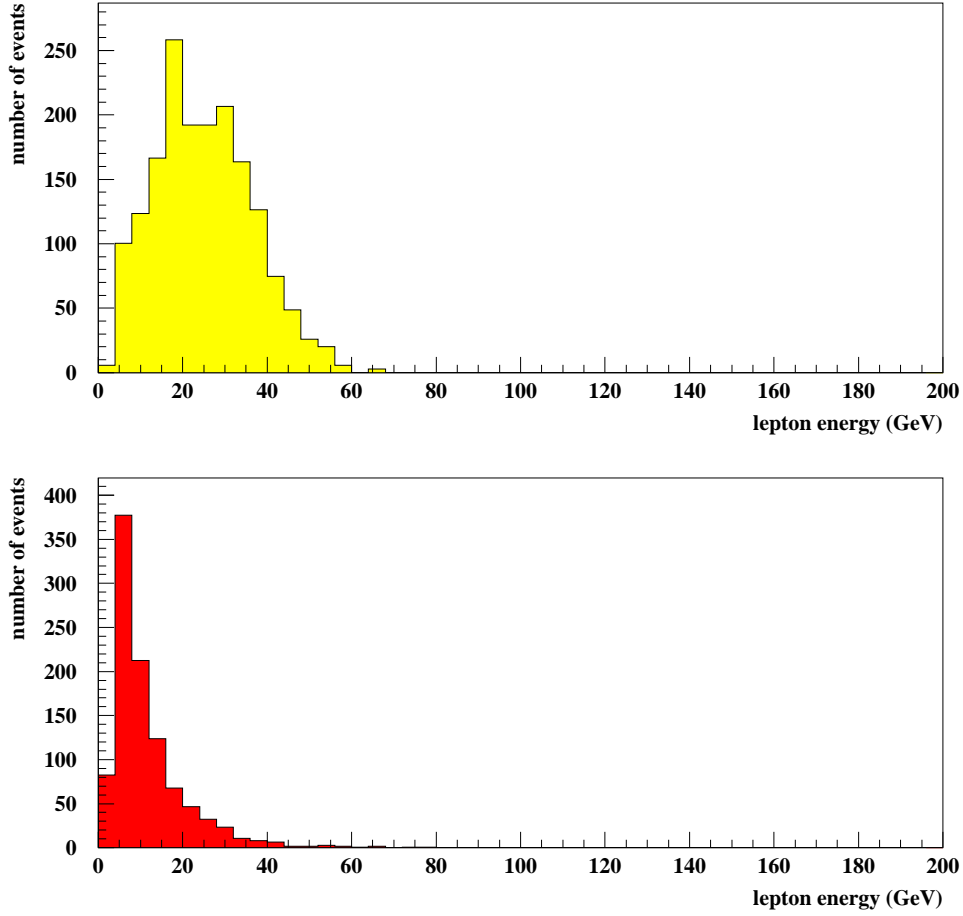


FIG. 7: Distributions of the lowest lepton energy (in GeV) among the energies of the 3 leading leptons (electrons and muons) in the events containing at least 3 charged leptons and 2 jets generated by the Standard Model background (lower curve), namely the  $W^\pm Z^0$ ,  $Z^0 Z^0$  and  $t\bar{t}$  productions, and the SUSY signal (upper curve), for  $\lambda'_{211} = 0.09$ ,  $M_2 = 150\text{GeV}$ ,  $m_0 = 200\text{GeV}$ ,  $\tan\beta = 1.5$  and  $\text{sign}(\mu) < 0$ . The numbers of events correspond to an integrated luminosity of  $\mathcal{L} = 10\text{fb}^{-1}$ .

the  $Z^0 Z^0$  production generates at most one hard jet. Moreover, the hard jet produced in the  $Z^0 Z^0$  background is generated by a tau decay (see Section 4.2) and can thus be identified as a tau.

Besides, some effective cuts concerning the energies of the produced leptons have been applied. In Fig.7, we show the distributions of the third leading lepton energy in the 3 lepton events produced by the Standard Model background ( $W^\pm Z^0$ ,  $Z^0 Z^0$  and  $t\bar{t}$ ) and the SUSY signal. Based on those kinds of distributions, we have chosen the following cut on the third leading lepton energy :  $E(l_3) > 10\text{GeV}$ . Similarly, we have required that the energies of the 2 leading leptons verify  $E(l_2) > 20\text{GeV}$  and  $E(l_1) > 20\text{GeV}$ .

We will refer to all the selection criteria described above, namely  $N_l \geq 3$  [ $l = e, \mu, \tau$ ] with  $E(l_1) > 20\text{GeV}$ ,  $E(l_2) > 20\text{GeV}$ ,  $E(l_3) > 10\text{GeV}$ , and  $N_j \geq 2$  with  $P_t(j) > 10\text{GeV}$ ,

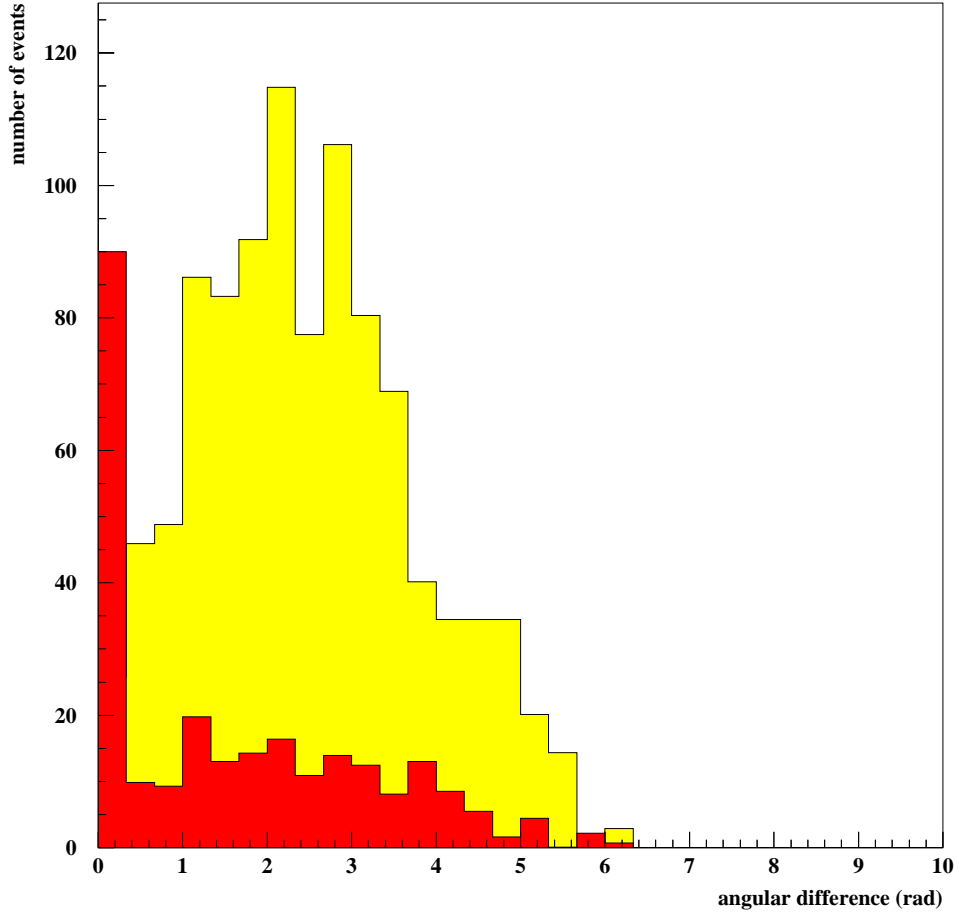


FIG. 8: Distributions of the  $\Delta R$  angular difference (in rad) between the third leading lepton (electron or muon) and the second leading jet in the 3 leptons events selected by applying cut 1 and produced by the Standard Model background (curve in black), namely the  $W^\pm Z^0$ ,  $Z^0 Z^0$  and  $t\bar{t}$  productions, and the SUSY signal (curve in grey), for  $\lambda'_{211} = 0.09$ ,  $M_2 = 150\text{GeV}$ ,  $m_0 = 200\text{GeV}$ ,  $\tan\beta = 1.5$  and  $\text{sign}(\mu) < 0$ . The numbers of events correspond to an integrated luminosity of  $\mathcal{L} = 10\text{fb}^{-1}$ .

as cut 1.

Finally, since the leptons originating from the hadron decays (as in the  $t\bar{t}$  production) are not well isolated, we have applied some cuts on the lepton isolation. We have imposed the isolation cut  $\Delta R = \sqrt{\delta\phi^2 + \delta\theta^2} > 0.4$  where  $\phi$  is the azimuthal angle and  $\theta$  the polar angle between the 3 most energetic charged leptons and the 2 hardest jets. Such a cut is for instance motivated by the distributions shown in Fig.8 of the  $\Delta R$  angular difference between the third leading lepton and the second leading jet, in the 3 lepton events generated by the SUSY signal and Standard Model background. We call cut  $\Delta R > 0.4$  together with cut 1, cut 2.

In order to eliminate poorly isolated leptons, we have also required that  $E < 2\text{GeV}$ , where  $E$  represents the summed energies of the jets being close to a muon or an electron,

	$W^\pm Z^0$	$Z^0 Z^0$	$t\bar{t}$	Total
cut 1	$1.39 \pm 0.11$	$1.37 \pm 0.11$	$39.80 \pm 1.00$	$42.56 \pm 1.01$
cut 2	$0.26 \pm 0.05$	$0.21 \pm 0.04$	$4.23 \pm 0.39$	$4.70 \pm 0.40$
cut 3	$0.24 \pm 0.04$	$0.17 \pm 0.04$	$1.14 \pm 0.17$	$1.55 \pm 0.18$
cut 1*	$0.51 \pm 0.06$	$0.73 \pm 0.08$	$27.80 \pm 0.80$	$29.04 \pm 0.80$
cut 2*	$0.26 \pm 0.05$	$0.21 \pm 0.04$	$2.92 \pm 0.27$	$3.39 \pm 0.28$
cut 3*	$0.23 \pm 0.04$	$0.17 \pm 0.04$	$0.64 \pm 0.13$	$1.04 \pm 0.14$

TAB. 4: Numbers of three lepton events generated by the Standard Model background ( $W^\pm Z^0$ ,  $Z^0 Z^0$  and  $t\bar{t}$  productions) at Tevatron Run II for the cuts described in the text, assuming an integrated luminosity of  $\mathcal{L} = 1fb^{-1}$  and a center of mass energy of  $\sqrt{s} = 2TeV$ . The cuts marked by a  $\star$  do not include the reconstruction of the tau-jets. These results have been obtained by generating and simulating  $3 \cdot 10^5$  events for the  $W^\pm Z^0$  production,  $10^4$  events for the  $Z^0 Z^0$  and  $3 \cdot 10^5$  events for the  $t\bar{t}$ .

namely the jets contained in the cone centered on a muon or an electron and defined by  $\Delta R < 0.25$ . This cut is not applied for taus candidates as they have hadronic decays. It is quite efficient (see Fig.21 for the 2 lepton case) since we sum over all jet energies in the cone. The Standard Model background shows more jets and less separation between jets and leptons in  $(\theta, \phi)$  in final state than the single productions<sup>2</sup>. We denote cut  $E < 2GeV$  plus cut 2 as cut 3<sup>3</sup>.

The selected events require high energy charged leptons and jets and can thus easily be triggered at Tevatron. This is illustrated in Fig.9 where we show the energy distributions of the 3 leptons and the second leading jet in the 3 leptons events selected by applying cut 3 and generated by the SUSY signal and Standard Model background.

In Table 4, we give the numbers of three lepton events expected from the Standard Model background at Tevatron Run II with the various cuts described above. We see in Table 4 that the main source of Standard Model background to the three lepton signature at Tevatron is the  $t\bar{t}$  production. This is due to the important cross section of the  $t\bar{t}$  production compared to the other Standard Model backgrounds (see Section 4.2). Table 4 also shows that the  $t\bar{t}$  background is relatively more suppressed than the other sources of Standard Model background by the lepton isolation cuts. The reason is that in the  $t\bar{t}$  background, one of the 3 charged leptons of the final state is generated in a  $b$ -jet and is thus not well isolated.

In Table 5, we give the number of three lepton events generated by the SUSY background (all superpartners pair productions) at Tevatron Run II as a function of the  $m_0$  and  $m_{1/2}$  parameters for the cut 3. This number of events decreases as  $m_0$  and  $m_{1/2}$  increase due to the behaviour of the summed superpartners pair productions cross section in the SUSY parameter space (see Section 4.3).

<sup>2</sup>This cut will have to be fine tuned with real events since it will depend on the energy flow inside the detector, the overlap and minimum biased events.

<sup>3</sup>Although it has not been applied, we mention another kind of isolation cut which allows to further reduce the Standard Model background :  $\delta\phi > 70^\circ$  between the leading charged lepton and the 2 hardest jets.



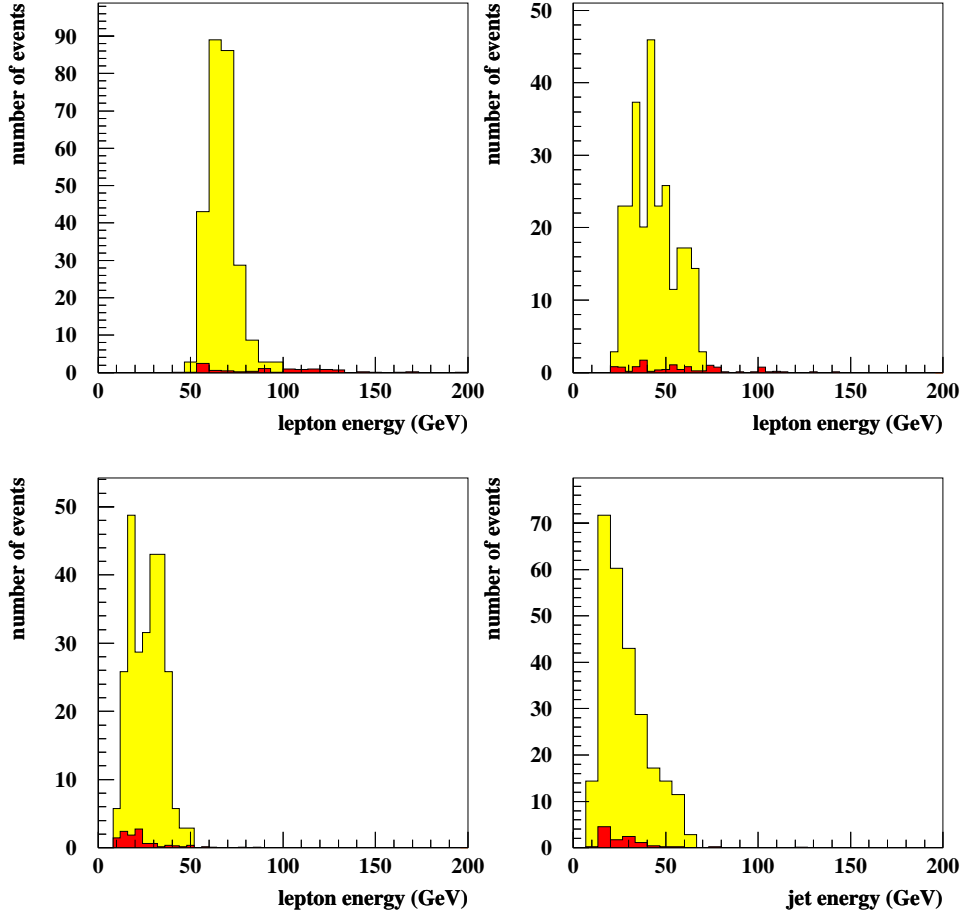


FIG. 9: Energy distributions (in GeV) of the 3 leading charged leptons and the second leading jet in the events containing at least 3 charged leptons selected by applying cut 3 and produced by the Standard Model background (curve in black), namely the  $W^\pm Z^0$ ,  $Z^0 Z^0$  and  $t\bar{t}$  productions, and the SUSY signal (curve in grey), for  $\lambda'_{211} = 0.09$ ,  $M_2 = 150\text{GeV}$ ,  $m_0 = 200\text{GeV}$ ,  $\tan\beta = 1.5$  and  $\text{sign}(\mu) < 0$ . The upper left plot represents the leading lepton distribution, the upper right plot the second leading lepton distribution and the lower left plot the third leading lepton distribution. The numbers of events correspond to an integrated luminosity of  $\mathcal{L} = 10\text{fb}^{-1}$ .

## 4.5 Results

### Discovery potential for the $\lambda'_{2jk}$ coupling constant

We first present the reach in the mSUGRA parameter space obtained from the analysis of the trilepton signature at Tevatron Run II generated by the single chargino production through the  $\lambda'_{211}$  coupling, namely  $p\bar{p} \rightarrow \tilde{\chi}_1^\pm \mu^\mp$ . The sensitivity that can be obtained on the  $\lambda'_{2jk}$  ( $j$  and  $k$  being not equal to 1 simultaneously) couplings based on the  $\tilde{\chi}_1^\pm \mu^\mp$  production analysis will be discussed at the end of this section for a given mSUGRA point. We give more detailed results for the case of a single dominant  $\lambda'_{211}$  coupling since this

$m_{1/2} \setminus m_0$	100GeV	200GeV	300GeV	400GeV	500GeV
100GeV	93.94	125.59	80.53	66.62	63.90
200GeV	5.11	4.14	3.86	4.02	4.26
300GeV	2.26	0.66	0.52	0.55	0.55

TAB. 5: Number of 3 lepton events generated by the SUSY background (all superpartners pair productions) at Tevatron Run II as a function of the  $m_0$  and  $m_{1/2}$  parameters for  $\tan\beta = 1.5$ ,  $\text{sign}(\mu) < 0$  and  $\lambda'_{211} = 0.05$ . Cut 3 (see text) has been applied. These results have been obtained by generating 7500 events and correspond to an integrated luminosity of  $\mathcal{L} = 1fb^{-1}$  and a center of mass energy of  $\sqrt{s} = 2TeV$ .

$\mathcal{R}_p$  coupling gives the highest partonic luminosity to the  $\tilde{\chi}_1^\pm \mu^\mp$  production (see Section 3.1) and leads thus to the highest sensitivities.

In Fig.10, we present the  $3\sigma$  and  $5\sigma$  discovery contours and the limits at 95% confidence level in the plane  $m_0$  versus  $m_{1/2}$ , for  $\text{sign}(\mu) < 0$ ,  $\tan\beta = 1.5$  and using a set of values for  $\lambda'_{211}$  and the luminosity. This discovery potential was obtained by considering the  $\tilde{\chi}_1^\pm \mu^\mp$  production and the background originating from the Standard Model. The signal and background were selected by using cut 3 described in Section 4.4. The results presented for a luminosity of  $\mathcal{L} = 0.5fb^{-1}$  in Fig.10 and Fig.11 were obtained with cut 2 only in order to optimize the sensitivity on the SUSY parameters. The reduction of the sensitivity on  $\lambda'_{211}$  observed in Fig.10 when either  $m_0$  or  $m_{1/2}$  increases is due to the decrease of the  $\tilde{\chi}_1^\pm \mu^\mp$  production cross section with  $m_0$  or  $m_{1/2}$  (or equivalently  $M_2$ ), which can be observed in Fig.4. In Fig.10, we also see that for all the considered values of  $\lambda'_{211}$  and the luminosity, the sensitivity on  $m_{1/2}$  is reduced to low masses in the domain  $m_0 \lesssim 200GeV$ . This important reduction of the sensitivity as  $m_0$  decreases is due to the decrease of the phase space factor associated to the decay  $\tilde{\nu}_\mu \rightarrow \tilde{\chi}_1^\pm \mu^\mp$  (see Section 3.1). Finally, we note from Fig.3 that for  $\text{sign}(\mu) > 0$  the  $\tilde{\chi}_1^\pm \mu^\mp$  production cross section, and thus the sensitivities presented in Fig.10, would incur a little increase compared to the case  $\text{sign}(\mu) < 0$ .

In Fig.11, the discovery potential is shown in the  $\lambda'_{211}$ - $m_0$  plane for different values of  $M_2$  and the luminosity. For a given value of  $M_2$ , we note that the sensitivity on the  $\lambda'_{211}$  coupling decreases at high and low values of  $m_0$ . The main explanation is the decrease of the  $p\bar{p} \rightarrow \tilde{\chi}_1^\pm \mu^\mp$  rate at high and low values of  $m_0$  which appears clearly in Fig.5. We also observe, as in Fig.10, a decrease of the sensitivity on the  $\lambda'_{211}$  coupling when  $M_2$  (or equivalently  $m_{1/2}$ ) increases for a fixed value of  $m_0$ .

The strongest bounds on the supersymmetric masses obtained at LEP in an  $\mathcal{R}_p$  model with a non-vanishing  $\lambda'$  Yukawa coupling are  $m_{\tilde{\chi}_1^0} > 26GeV$  (for  $m_0 = 200GeV$  and  $\tan\beta = \sqrt{2}$  [51]),  $m_{\tilde{\chi}_1^\pm} > 100GeV$ ,  $m_{\tilde{l}} > 93GeV$ ,  $m_{\tilde{\nu}} > 86GeV$  [34]. For the minimum values of  $m_0$  and  $m_{1/2}$  spanned by the parameter space described in Figures 10 and 11, namely  $m_0 = 100GeV$  and  $M_2 = 100GeV$ , the mass spectrum is  $m_{\tilde{\chi}_1^\pm} = 113GeV$ ,  $m_{\tilde{\chi}_1^0} = 54GeV$ ,  $m_{\tilde{\nu}_L} = 127GeV$ ,  $m_{\tilde{l}_L} = 137GeV$ ,  $m_{\tilde{l}_R} = 114GeV$ , so that we are well above these limits. Since both the scalar and gaugino masses increase with  $m_0$  and  $m_{1/2}$ , the parameter space described in Figures 10 and 11 lies outside the SUSY parameters ranges excluded by LEP data [34, 51]. Therefore, the discovery potential of Figures 10 and 11 represents an important improvement with respect to the supersymmetric masses limits derived from LEP data [34, 51]. Figures 10 and 11 show also that the low-energy

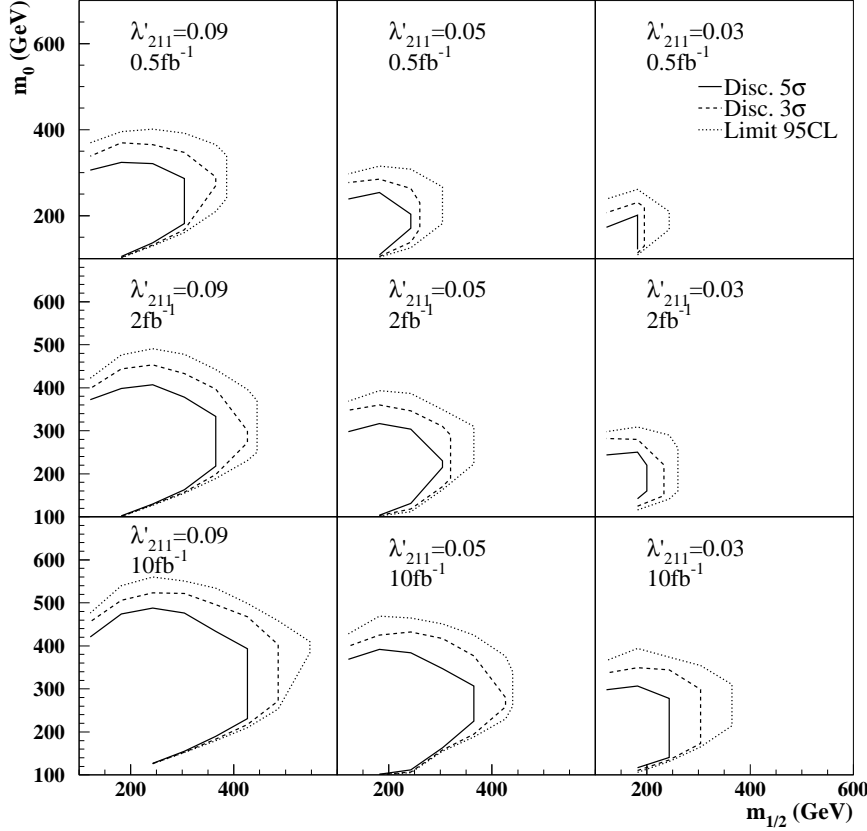


FIG. 10: Discovery contours at  $5\sigma$  (full line),  $3\sigma$  (dashed line) and limit at 95%  $C.L.$  (dotted line) obtained from the trilepton signature analysis at Tevatron Run II assuming a center of mass energy of  $\sqrt{s} = 2TeV$ . This discovery reach is presented in the plane  $m_0$  versus  $m_{1/2}$ , for  $sign(\mu) < 0$ ,  $\tan\beta = 1.5$  and different values of  $\lambda'_{211}$  and of luminosity.

bound on the considered  $\mathcal{R}_p$  coupling,  $\lambda'_{211} < 0.09(m_{\tilde{d}_R}/100GeV)$  at  $1\sigma$  (from  $\pi$  decay) [4], can be greatly improved.

Interesting sensitivities on the SUSY parameters can already be obtained within the first year of Run II at Tevatron with a low luminosity ( $\mathcal{L} = 0.5fb^{-1}$ ) and no reconstruction of the tau-jets. To illustrate this point, we present in Fig.12 and Fig.13 the same discovery potentials as in Fig.10 and Fig.11, respectively, obtained without reconstruction of the tau leptons decaying into jets. By comparing Fig.10, Fig.11 and Fig.12, Fig.13, we observe that the sensitivity on the SUSY parameters is weakly affected by the reconstruction of the tau-jets <sup>4</sup>.

<sup>4</sup>This is actually an artefact of the method : cut 3 is our most efficient cut to reduce the Standard Model background with electrons and muons but is not applied with taus. Thus, the relative ratio signal over background is not so good with taus. Finding another efficient cut could improve our discovery

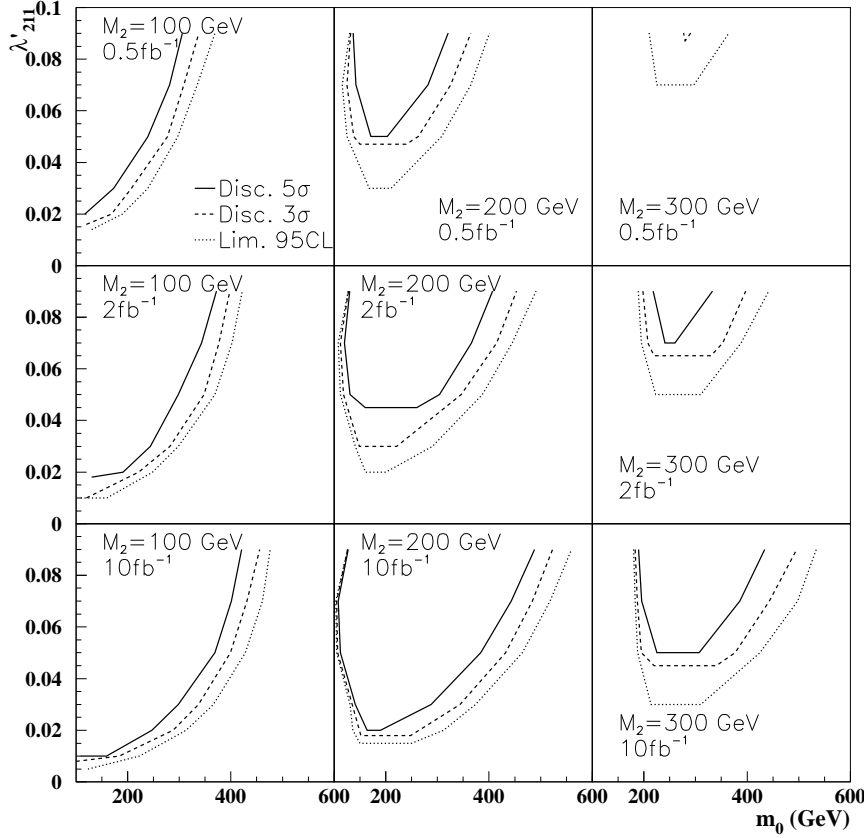


FIG. 11: Discovery contours at  $5\sigma$  (full line),  $3\sigma$  (dashed line) and limit at 95%  $C.L.$  (dotted line) presented in the plane  $\lambda'_{211}$  versus the  $m_0$  parameter, for  $sign(\mu) < 0$ ,  $\tan\beta = 1.5$  and different values of  $M_2$  and of luminosity.

Using the ratios of the cross sections for the  $\tilde{\chi}_1^+ \mu^-$  productions via different  $\lambda'_{2jk}$  couplings, one can deduce from the sensitivity obtained on  $\lambda'_{211}$  via the 3 lepton final state analysis an estimation of the sensitivity on any  $\lambda'_{2jk}$  coupling. For instance, let us consider the SUSY point  $m_0 = 180 GeV$ ,  $M_2 = 200 GeV$ ,  $\tan\beta = 1.5$  and  $\mu = -200 GeV$  ( $m_{\tilde{u}_L} = 601 GeV$ ,  $m_{\tilde{d}_L} = 603 GeV$ ,  $m_{\tilde{u}_R} = 582 GeV$ ,  $m_{\tilde{d}_R} = 580 GeV$ ,  $m_{\tilde{t}_L} = 253 GeV$ ,  $m_{\tilde{t}_R} = 205 GeV$ ,  $m_{\tilde{\nu}_L} = 248 GeV$ ,  $m_{\tilde{\chi}_1^\pm} = 199 GeV$ ,  $m_{\tilde{\chi}_1^0} = 105 GeV$ ) which corresponds, as can be seen in Fig.11, to the point where the sensitivity on  $\lambda'_{211}$  is maximized for  $M_2 = 200 GeV$ . We can see on Fig.5 that for this SUSY point, the ratio between the rates of the  $\tilde{\chi}_1^+ \mu^-$  productions via  $\lambda'_{211}$  and  $\lambda'_{221}$  is  $\sigma(\lambda'_{211})/\sigma(\lambda'_{221}) \approx 7.9$  for same values of the  $\mathcal{R}_p$  couplings. Therefore, since the single chargino production rate scales as  $\lambda^2$  (see Appendix 1), the sensitivity on  $\lambda'_{221}$  at this SUSY point is equal to the sensitivity obtained on  $\lambda'_{211}$  ( $\sim 0.02$  at 95% $C.L.$  with  $\mathcal{L} = 2 fb^{-1}$  as shows Fig.11) multiplied by the factor  $\sqrt{7.9}$ , potential and limits using taus.

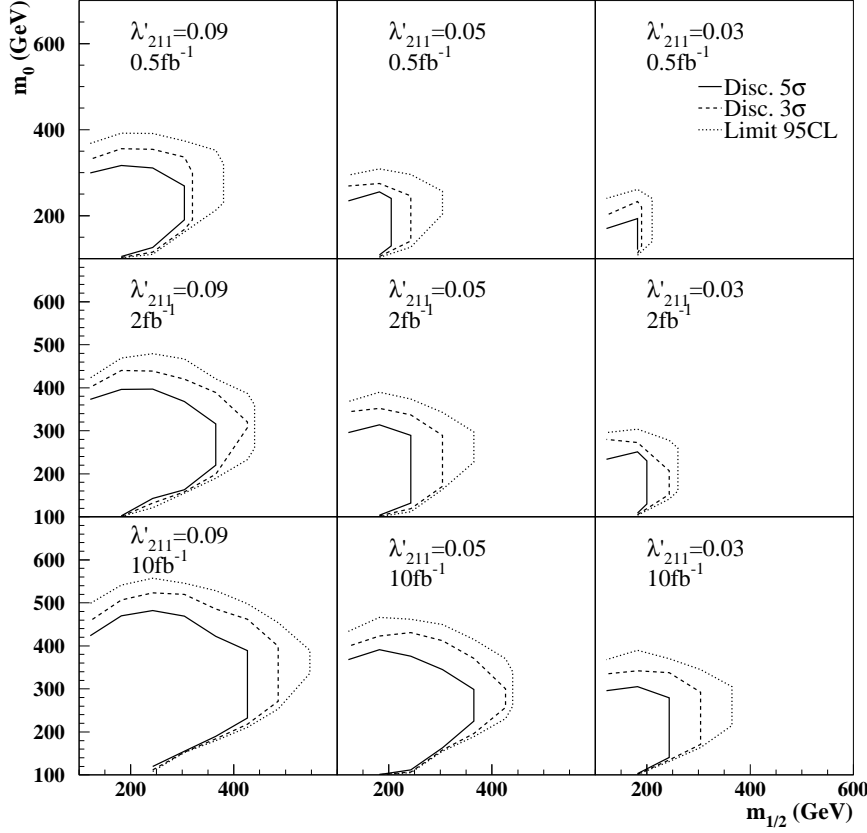


FIG. 12: Discovery contours at  $5\sigma$  (full line),  $3\sigma$  (dashed line) and limit at 95%  $C.L.$  (dotted line) presented in the plane  $m_0$  versus  $m_{1/2}$  and obtained without reconstruction of the tau leptons decaying into jets for  $sign(\mu) < 0$ ,  $\tan\beta = 1.5$  and different values of  $\lambda'_{211}$  and of luminosity.

$\lambda'_{212}$	$\lambda'_{213}$	$\lambda'_{221}$	$\lambda'_{222}$	$\lambda'_{223}$	$\lambda'_{231}$	$\lambda'_{232}$	$\lambda'_{233}$
0.04	0.07	0.05	0.12	0.21	0.10	0.36	0.63

TAB. 6: Sensitivities at 95%CL on the  $\lambda'_{2jk}$  coupling constants derived from the sensitivity on  $\lambda'_{211}$  for a luminosity of  $\mathcal{L} = 2fb^{-1}$  and the following set of SUSY parameters,  $\tan\beta = 1.5$ ,  $M_2 = 200GeV$ ,  $\mu = -200GeV$  and  $m_0 = 180GeV$ .

namely  $\sim 0.05$ . This result represents a significant improvement with respect to the low-energy indirect limit  $\lambda'_{221} < 0.18(m_{\tilde{d}_R}/100GeV)$  [4]. Using the same method, we find at the same SUSY point the sensitivities on the  $\lambda'_{2jk}$  coupling constants given in Table 6. All the sensitivities on the  $\lambda'_{2jk}$  coupling constants given in Table 6 are stronger than the low-energy bounds of [4] which we rewrite here :  $\lambda'_{21k} < 0.09(m_{\tilde{d}_{kR}}/100GeV)$  at  $1\sigma$  ( $\pi$

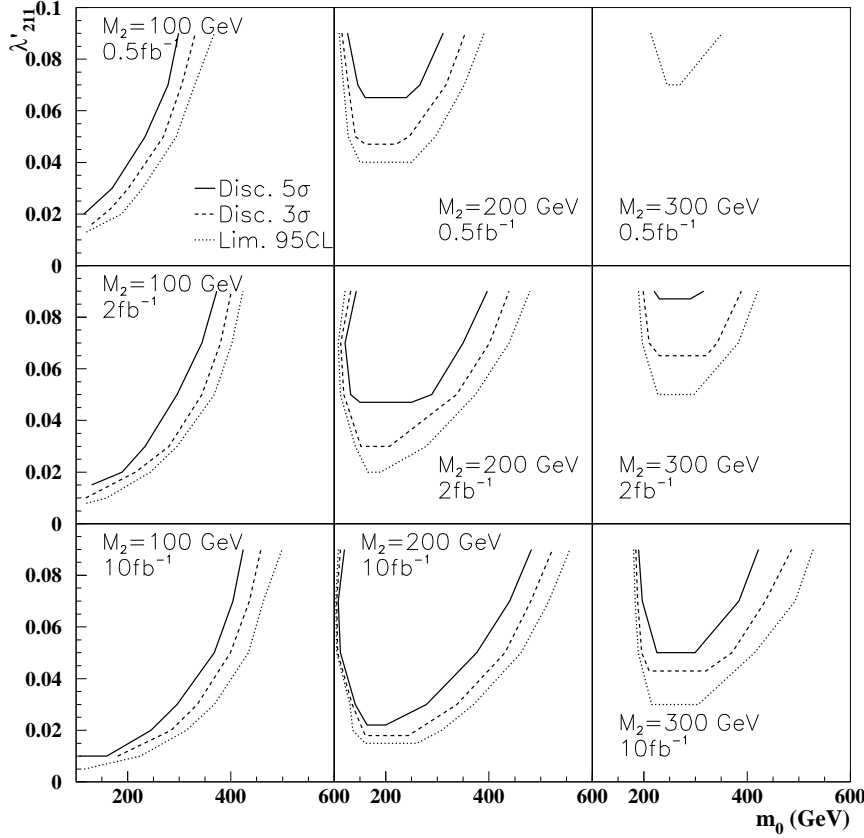


FIG. 13: Discovery contours at  $5\sigma$  (full line),  $3\sigma$  (dashed line) and limit at 95%  $C.L.$  (dotted line) presented in the plane  $\lambda'_{211}$  versus the  $m_0$  parameter and obtained without reconstruction of the tau leptons decaying into jets for  $sign(\mu) < 0$ ,  $\tan\beta = 1.5$  and different values of  $M_2$  and of luminosity.

decay),  $\lambda'_{22k} < 0.18(m_{\tilde{d}_{kR}}/100GeV)$  at  $1\sigma$  ( $D$  decay),  $\lambda'_{231} < 0.22(m_{\tilde{b}_L}/100GeV)$  at  $2\sigma$  ( $\nu_\mu$  deep inelastic scattering),  $\lambda'_{232} < 0.36(m_{\tilde{q}}/100GeV)$  at  $1\sigma$  ( $R_\mu$ ),  $\lambda'_{233} < 0.36(m_{\tilde{q}}/100GeV)$  at  $1\sigma$  ( $R_\mu$ ).

In the case of a single dominant  $\lambda'_{2j3}$  coupling, the neutralino decays as  $\tilde{\chi}_1^0 \rightarrow \mu u_j b$  and the semileptonic decay of the b-quark could affect the analysis efficiency. Therefore in this case, the precise sensitivity cannot be simply calculated by scaling the value obtained for  $\lambda'_{211}$ . Nevertheless, the order of magnitude of the sensitivity which can be inferred from our analysis should be correct.

The range of SUSY parameters in which the constraint on a given  $\lambda'_{2jk}$  coupling constant obtained via the three leptons analysis is stronger than the relevant low-energy bound depends on the low-energy bound itself as well as on the values of the cross section for the single chargino production via the considered  $\lambda'_{2jk}$  coupling.

Finally, we remark that while the low-energy constraints on the  $\lambda'_{2jk}$  couplings become weaker as the squark masses increase, the sensitivities on those couplings obtained from the three leptons analysis are essentially independent of the squark masses as long as  $m_{\tilde{q}} > m_{\tilde{\chi}_1^\pm}$  (recall that the branching ratio of the decay  $\tilde{\chi}_1^\pm \rightarrow q\bar{q}\tilde{\chi}_1^0$  is greatly enhanced when  $m_{\tilde{q}} < m_{\tilde{\chi}_1^\pm}$ ).

We end this section by some comments on the effect of the supersymmetric  $R_p$  conserving background to the 3 lepton signature. In order to illustrate this discussion, we consider the results on the  $\lambda'_{211}$  coupling constant.

We see from Table 5 that the SUSY background to the 3 lepton final state can affect the sensitivity on the  $\lambda'_{211}$  coupling constant obtained by considering only the Standard Model background, which is shown in Fig.10, only in the region of small superpartner masses, namely in the domain  $m_{1/2} \lesssim 300\text{GeV}$  for  $\tan\beta = 1.5$ ,  $\text{sign}(\mu) < 0$  and assuming a luminosity of  $\mathcal{L} = 1\text{fb}^{-1}$ .

In contrast with the SUSY signal amplitude which is increased if  $\lambda'_{211}$  is enhanced, the SUSY background amplitude is typically independent on the value of the  $\lambda'_{211}$  coupling constant since the superpartner pair production does not involve  $R_p$  couplings. Therefore, even if we consider the SUSY background in addition to the Standard Model one, it is still true that large values of the  $\lambda'_{211}$  coupling can be probed over a wider domain of the SUSY parameter space than low values, as can be observed in Fig.10 for  $m_{1/2} \gtrsim 300\text{GeV}$ . Note that in Fig.10 larger values of  $\lambda'_{211}$  could have been considered as the low-energy bound on this  $R_p$  coupling, namely  $\lambda'_{211} < 0.09(m_{\tilde{d}_R}/100\text{GeV})$  [4], is proportional to the squark mass.

Finally, we mention that further cuts, as for instance some cuts based on the superpartner mass reconstructions (see Section 4.5), could allow to reduce the SUSY background to the 3 lepton signature.

## High $\tan\beta$ scenario

In mSUGRA, for large values of  $\tan\beta$  and small values of  $m_0$  compared to  $m_{1/2}$ , due to the large mixing in the third generation sfermions, the mass of the lighter  $\tilde{\tau}_1$  slepton can become smaller than  $m_{\tilde{\chi}_1^\pm}$ , with the sneutrino remaining heavier than the  $\tilde{\chi}_1^\pm$  so that the  $\tilde{\chi}_1^\pm l^\mp$  production rate can still be significant. In this situation, the efficiency for the 3 lepton signature arising mainly through,  $\tilde{\chi}_1^\pm \rightarrow \tilde{\tau}_1^\pm \nu_\tau$ ,  $\tilde{\tau}_1^\pm \rightarrow \tilde{\chi}_1^0 \tau^\pm$ ,  $\tilde{\chi}_1^0 \rightarrow l_i^\pm u_j d_k$ , can be enhanced compared to the case where the 3 lepton signal comes from,  $\tilde{\chi}_1^\pm \rightarrow \tilde{\chi}_1^0 l^\pm \nu$ ,  $\tilde{\chi}_1^0 \rightarrow l_i^\pm u_j d_k$ . Indeed, the branching ratio  $B(\tilde{\chi}_1^\pm \rightarrow \tilde{\tau}_1^\pm \nu_\tau)$  can reach  $\sim 100\%$ ,  $B(\tilde{\tau}_1^\pm \rightarrow \tilde{\chi}_1^0 \tau^\pm) \approx 100\%$ , since the  $\tilde{\chi}_1^0$  is the LSP,  $B(\tau \rightarrow l \nu_l \nu_\tau) = 35\%$  ( $l = e, \mu$ ) and the  $\tau$ -jets can be reconstructed at Tevatron Run II. However, in such a scenario the increased number of tau leptons in the final state leads to a softer charged lepton spectrum which tends to reduce the efficiency after cuts. Therefore, for relatively small values of  $m_0$  compared to  $m_{1/2}$ , the sensitivity obtained in the high  $\tan\beta$  scenario is essentially unaffected with respect to the low  $\tan\beta$  situation, unless  $m_0$  is small enough to render  $m_{\tilde{\tau}_1}$  and  $m_{\tilde{\chi}_1^0}$  almost degenerate. As a matter of fact, in such a situation, the energy of the tau produced in the decay  $\tilde{\tau}_1^\pm \rightarrow \tilde{\chi}_1^0 \tau^\pm$  often falls below the analysis cuts. Therefore, this degeneracy results in a loss of signal efficiency after cuts, at small values of  $m_0$  compared to  $m_{1/2}$ , and thus in a loss of sensitivity, with respect to the low  $\tan\beta$  situation. This can be seen by comparing Fig.10, Fig.11 and Fig.14, Fig.15. Indeed, the decrease of the sensitivity on  $m_{1/2}$  at low  $m_0$  is stronger for

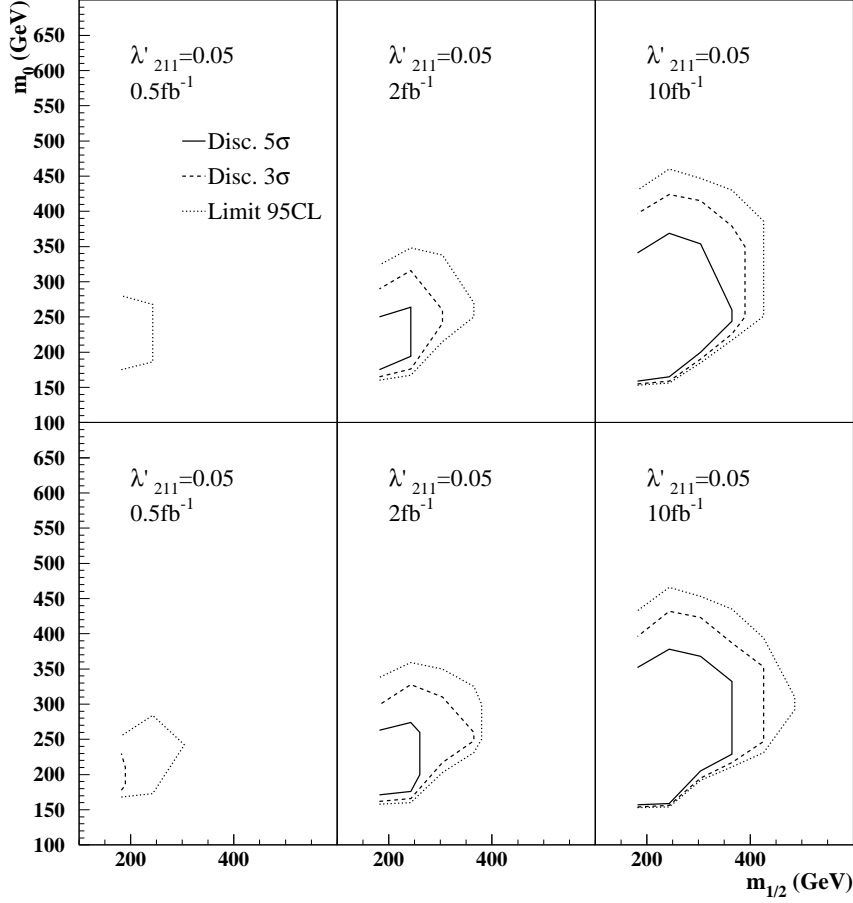


FIG. 14: Discovery contours at  $5\sigma$  (full line),  $3\sigma$  (dashed line) and limit at 95%  $C.L.$  (dotted line) presented in the plane  $m_0$  versus  $m_{1/2}$ , for  $sign(\mu) < 0$ ,  $\tan\beta = 50$ ,  $\lambda'_{211} = 0.09$  and different values of luminosity. The upper (lower) curves are obtained without (with) the reconstruction of the tau-jets.

high  $\tan\beta$  (see Fig.14) than for low  $\tan\beta$  (see Fig.10). Similarly, the decrease of the sensitivity on  $\lambda'_{211}$  at low  $m_0$  is stronger for high  $\tan\beta$  (see Fig.15) than for low  $\tan\beta$  (see Fig.11).

The effect on the discovery potential of the single chargino production rate increase at large  $\tan\beta$  values shown in Fig.2 is hidden by the large  $\tan\beta$  scenario influences on the cascade decays described above.

In contrast with the low  $\tan\beta$  scenario (see Section 4.5), the sensitivity on the SUSY parameters depends in a significant way on the reconstruction of the tau-jets in case where  $\tan\beta$  is large, as can be seen in Fig.14 and Fig.15. The reason is the increased number of tau leptons among the final state particles in a large  $\tan\beta$  model. This is due to the decrease of the lighter stau mass which tends to increase the  $B(\tilde{\chi}_1^\pm \rightarrow \tilde{\chi}_1^0 \tau^\pm \nu_\tau)$  branching ratio.



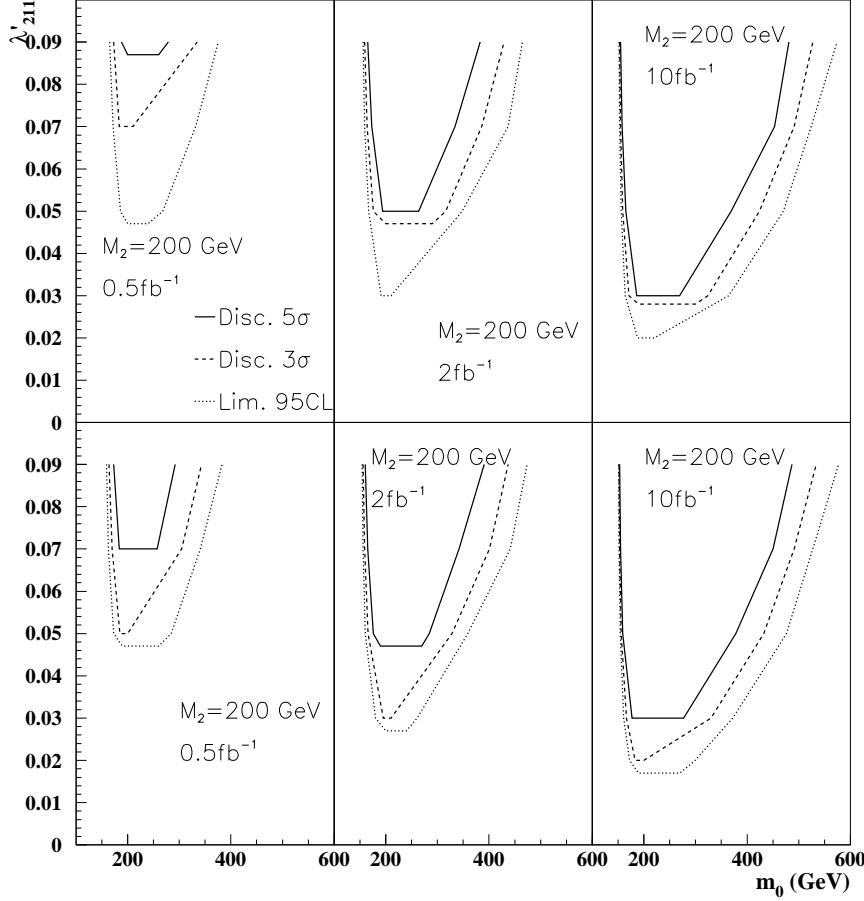


FIG. 15: Discovery contours at  $5\sigma$  (full line),  $3\sigma$  (dashed line) and limit at 95%  $C.L.$  (dotted line) presented in the plane  $\lambda'_{211}$  versus the  $m_0$  parameter, for  $sign(\mu) < 0$ ,  $\tan\beta = 50$ ,  $M_2 = 200\text{GeV}$  and different values of luminosity. The upper (lower) curves are obtained without (with) the reconstruction of the tau-jets.

### Discovery potential for the $\lambda'_{1jk}$ and $\lambda'_{3jk}$ coupling constants

In Fig.16, we present the  $3\sigma$  and  $5\sigma$  discovery contours and the limits at 95% confidence level in the plane  $m_0$  versus  $m_{1/2}$ , for  $sign(\mu) < 0$ ,  $\tan\beta = 1.5$ ,  $\lambda'_{311} = 0.10$  and various values of the luminosity. In Fig.17, the discovery potential is shown in the  $\lambda'_{311}$ - $m_0$  plane for  $M_2 = 200\text{GeV}$ . Comparing Fig.16, Fig.17 and Fig.10, Fig.11, we see that the sensitivity on the SUSY parameters is weaker in the case of a single dominant  $\lambda'_{311}$  coupling than in the case of a single dominant  $\lambda'_{211}$  coupling. The reason is that in the case of a single dominant  $\lambda'_{3jk}$  coupling constant, tau leptons are systematically produced at the chargino production level  $p\bar{p} \rightarrow \tilde{\chi}_1^\pm \tau^\mp$  (see Fig.1(a)) as well as in the LSP decay  $\tilde{\chi}_1^0 \rightarrow \tau u_j d_k$  (see Section 4.1), so that the number of tau leptons among the 3 charged leptons of the final state is increased compared to the dominant  $\lambda'_{2jk}$  case. The decrease in sensitivity is due to the fact that a lepton (electron or muon) generated in a tau decay

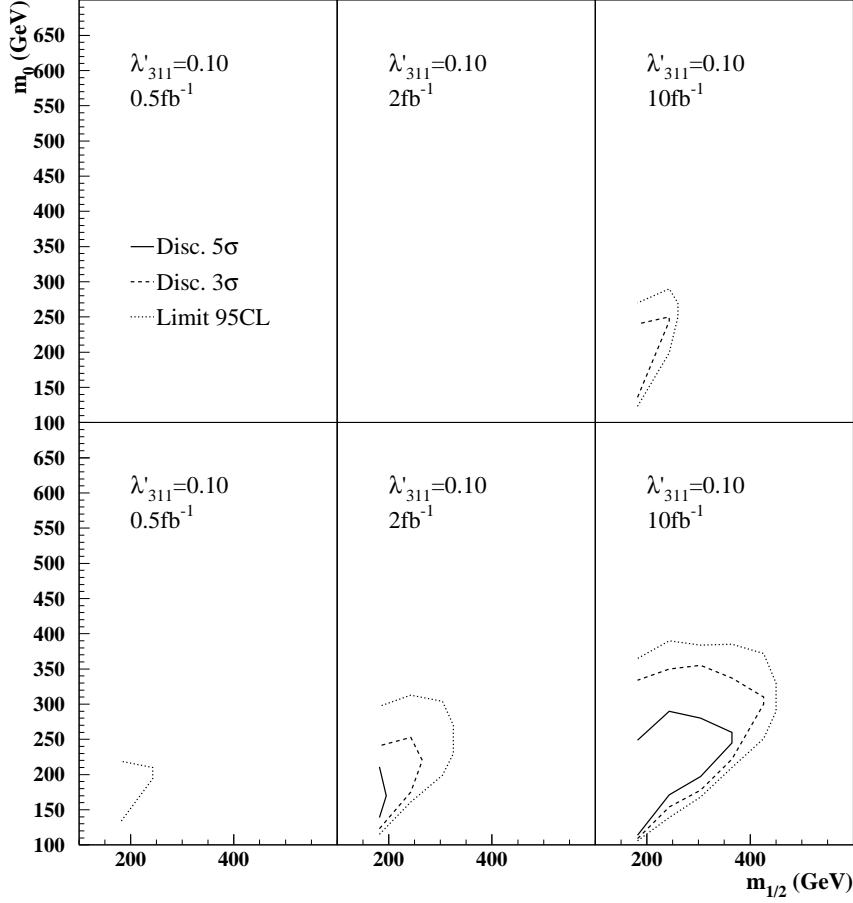


FIG. 16: Discovery contours at  $5\sigma$  (full line),  $3\sigma$  (dashed line) and limit at 95%  $C.L.$  (dotted line) presented in the plane  $m_0$  versus  $m_{1/2}$ , for  $sign(\mu) < 0$ ,  $\tan\beta = 1.5$ ,  $\lambda'_{311} = 0.10$  and different values of luminosity. The upper (lower) curves are obtained without (with) the reconstruction of the tau-jets.

has an higher probability not to pass the analysis requirements concerning the particle energy and that the reconstruction efficiency for a tau decaying into a jet is limited. Nevertheless, the discovery potentials of Fig.16 and Fig.17 represent also an important improvement with respect to the experimental mass limits from LEP measurements [34, 51] and to the low-energy indirect constraint  $\lambda'_{311} < 0.10(m_{\tilde{d}_R}/100GeV)$  at  $1\sigma$  (from  $\tau^- \rightarrow \pi^- \nu_\tau$ ) [4].

We also observe in Fig.16 and Fig.17 that the results obtained from the  $\tilde{\chi}_1^\pm \tau^\mp$  production analysis in the case of a single dominant  $\lambda'_{3jk}$  coupling depend strongly on the reconstruction of the tau-jets. This is due to the large number of tau leptons among the 3 charged leptons of the considered final state.

Using the same method and same SUSY point as in Section 4.5, we have estimated the sensitivity on all the  $\lambda'_{3jk}$  coupling constants from the sensitivity obtained on  $\lambda'_{311}$

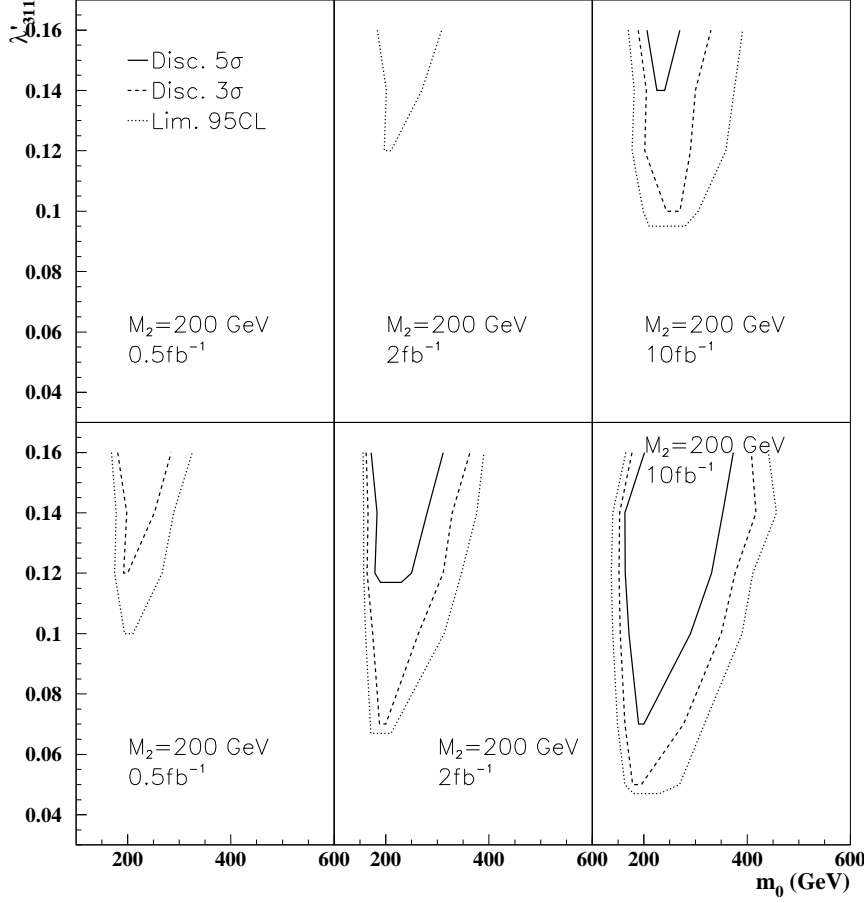


FIG. 17: Discovery contours at  $5\sigma$  (full line),  $3\sigma$  (dashed line) and limit at 95%  $C.L.$  (dotted line) presented in the plane  $\lambda'_{311}$  versus the  $m_0$  parameter, for  $sign(\mu) < 0$ ,  $\tan\beta = 1.5$ ,  $M_2 = 200\text{GeV}$  and different values of luminosity. The upper (lower) curves are obtained without (with) the reconstruction of the tau-jets.

$\lambda'_{312}$	$\lambda'_{313}$	$\lambda'_{321}$	$\lambda'_{322}$	$\lambda'_{323}$	$\lambda'_{331}$	$\lambda'_{332}$	$\lambda'_{333}$
0.13	0.23	0.18	0.41	0.70	0.33	1.17	2.05

TAB. 7: Sensitivities at 95% $CL$  on the  $\lambda'_{3jk}$  coupling constants derived from the sensitivity on  $\lambda'_{311}$  for a luminosity of  $\mathcal{L} = 2\text{fb}^{-1}$  and the following set of SUSY parameters,  $\tan\beta = 1.5$ ,  $M_2 = 200\text{GeV}$ ,  $\mu = -200\text{GeV}$  and  $m_0 = 180\text{GeV}$ .

at 95% $CL$  for a luminosity of  $\mathcal{L} = 2\text{fb}^{-1}$ . The results are given in Table 7. All the sensitivities on the  $\mathcal{R}_p$  couplings presented in Table 7, except those on  $\lambda'_{32k}$ , are stronger than the present indirect limits on the same  $\mathcal{R}_p$  couplings :  $\lambda'_{31k} < 0.10(m_{\tilde{d}_{kR}}/100\text{GeV})$  at  $1\sigma$  ( $\tau^- \rightarrow \pi^- \nu_\tau$ ),  $\lambda'_{32k} < 0.20$  (for  $m_{\tilde{l}} = m_{\tilde{q}} = 100\text{GeV}$ ) at  $1\sigma$  ( $D^0 - \bar{D}^0$  mix),  $\lambda'_{33k} < 0.48(m_{\tilde{q}}/100\text{GeV})$  at  $1\sigma$  ( $R_\tau$ ) [4].

We mention that in the case of a single dominant  $\lambda'_{3j3}$  coupling, the neutralino decays as  $\tilde{\chi}_1^0 \rightarrow \tau u_j b$  so that the b semileptonic decay could affect a little the analysis efficiency.

We discuss now the sensitivities that could be obtained on a single dominant  $\lambda'_{1jk}$  coupling constant via the analysis of the reaction  $p\bar{p} \rightarrow \tilde{\chi}_1^\pm e^\mp$  (see Fig.1(a)). Since the cross section of the  $\tilde{\chi}_1^\pm e^\mp$  production through  $\lambda'_{1jk}$  is equal to the rate of the  $\tilde{\chi}_1^\pm \mu^\mp$  production via  $\lambda'_{2jk}$ , for same  $j$  and  $k$  indices (see Section 3.1), the sensitivity obtained on a  $\lambda'_{1jk}$  coupling constant is expected to be identical to the sensitivity on  $\lambda'_{2jk}$ . If we assume that the sensitivities obtained on the  $\lambda'_{1jk}$  couplings are equal to those presented in Table 6, we remark that for the SUSY point chosen in this table only the sensitivities expected for the  $\lambda'_{112}$ ,  $\lambda'_{113}$ ,  $\lambda'_{121}$ ,  $\lambda'_{131}$  and  $\lambda'_{132}$  couplings are stronger than the corresponding low-energy bounds :  $\lambda'_{11k} < 0.02(m_{\tilde{d}_{kR}}/100GeV)$  at  $2\sigma$  (Charged current universality),  $\lambda'_{1j1} < 0.035(m_{\tilde{q}_{jL}}/100GeV)$  at  $2\sigma$  (Atomic parity violation),  $\lambda'_{132} < 0.34$  at  $1\sigma$  for  $m_{\tilde{q}} = 100GeV$  ( $R_e$ ) [4]. The reason is that the low-energy constraints on the  $\lambda'_{1jk}$  couplings are typically more stringent than the limits on the  $\lambda'_{2jk}$  couplings [4].

## Mass reconstructions

The  $\tilde{\chi}_1^0$  neutralino decays in our framework as  $\tilde{\chi}_1^0 \rightarrow l_i u_j d_k$  through the  $\lambda'_{ijk}$  coupling constant. The invariant mass distribution of the lepton and the 2 jets coming from this decay channel is peaked at the  $\tilde{\chi}_1^0$  mass. The experimental analysis of this invariant mass distribution would thus be particularly interesting since it would allow a model independent determination of the lightest neutralino mass.

We have performed the  $\tilde{\chi}_1^0$  mass reconstruction based on the 3 lepton signature analysis. The difficulty of this mass reconstruction lies in the selection of the lepton and the 2 jets coming from the  $\tilde{\chi}_1^0$  decay. In the signal we are considering, the only jets come from the  $\tilde{\chi}_1^0$  decay, and of course from the initial and final QCD radiations. Therefore, if there are more than 2 jets in the final state we have selected the 2 hardest ones. It is more subtle for the selection of the lepton since our signal contains 3 leptons. We have considered the case of a single dominant coupling of type  $\lambda'_{2jk}$  and focused on the  $e\mu\mu$  final state. In these events, one of the  $\mu^\pm$  is generated in the decay of the produced sneutrino as  $\tilde{\nu}_\mu \rightarrow \tilde{\chi}_1^\pm \mu^\mp$  and the other one in the decay of the  $\tilde{\chi}_1^0$  as  $\tilde{\chi}_1^0 \rightarrow \mu^\pm u_j d_k$ , while the electron comes from the chargino decay  $\tilde{\chi}_1^\pm \rightarrow \tilde{\chi}_1^0 e^\pm \nu_e$ . Indeed, the dominant contribution to the single chargino production is the resonant sneutrino production (see Fig.1). In order to select the muon from the  $\tilde{\chi}_1^0$  decay we have chosen the softer muon, since for relatively important values of the  $m_{\tilde{\nu}_\mu} - m_{\tilde{\chi}_1^\pm}$  mass difference the muon generated in the sneutrino decay is the most energetic. Notice that when the  $\tilde{\nu}_\mu$  and  $\tilde{\chi}_1^\pm$  masses are close to one another, the sensitivity on the SUSY parameters suffers a strong decrease as shown in Section 4.5.

We present in Fig.18 the invariant mass distribution of the muon and the 2 jets produced in the  $\tilde{\chi}_1^0$  decay. This distribution has been obtained by using the selection criteria described above and by considering the mSUGRA point :  $m_0 = 200GeV$ ,  $M_2 = 150GeV$ ,  $\tan\beta = 1.5$ ,  $sign(\mu) < 0$  and  $\lambda'_{211} = 0.09$  ( $m_{\tilde{\chi}_1^0} = 77.7GeV$ ,  $m_{\tilde{\chi}_1^\pm} = 158.3GeV$ ,  $m_{\tilde{\nu}_L} = 236GeV$ ). We also show on the plot of Fig.18 the fit of the invariant mass distribution. As can be seen from this fit, the distribution is well peaked around the  $\tilde{\chi}_1^0$  generated mass. The average reconstructed  $\tilde{\chi}_1^0$  mass is of  $71 \pm 9GeV$ .

We have also performed the  $\tilde{\chi}_1^\pm$  and  $\tilde{\nu}_\mu$  mass reconstructions based on the 3 lepton signature analysis in the scenario of a single dominant coupling of type  $\lambda'_{2jk}$ . The  $\tilde{\chi}_1^\pm$  and

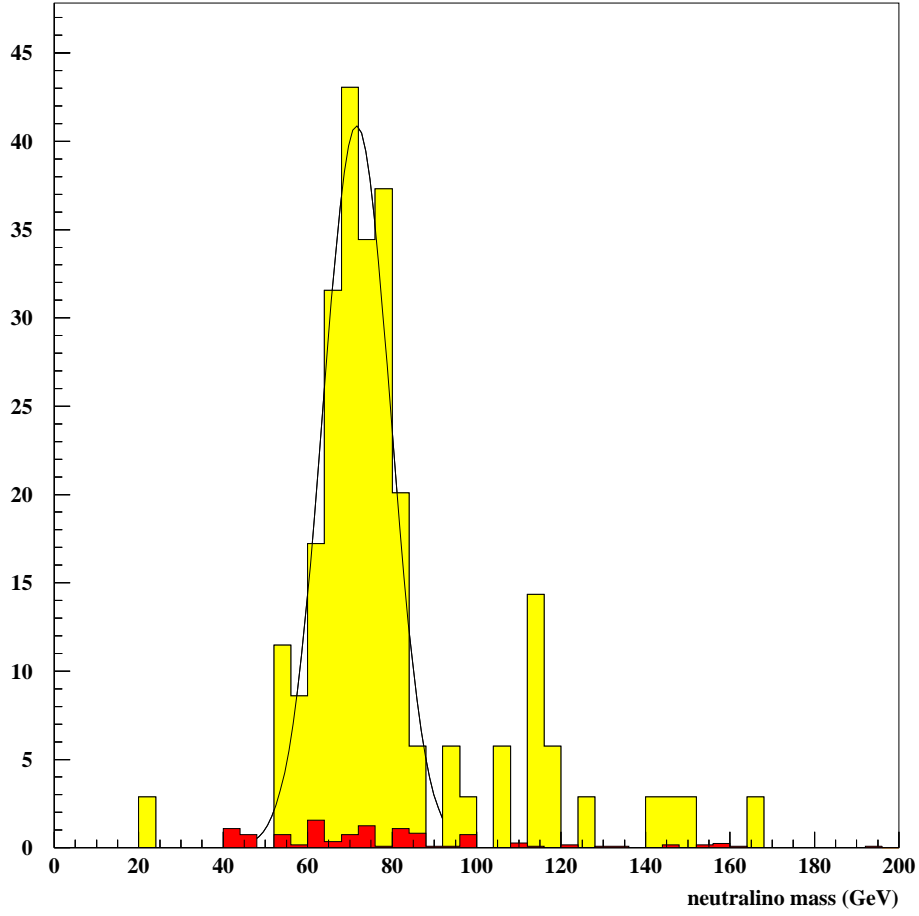


FIG. 18: Distribution of the *softer*  $\mu + 2j$  invariant mass in the  $e + \mu + \mu + 2j + \nu$  events, for a luminosity of  $\mathcal{L} = 10 fb^{-1}$ . The sum of the  $WZ$ ,  $ZZ$  and  $t\bar{t}$  backgrounds is in black and the SUSY signal is in grey. The mSUGRA point taken for this figure is  $m_0 = 200 GeV$ ,  $M_2 = 150 GeV$ ,  $\tan\beta = 1.5$  and  $sign(\mu) < 0$  ( $m_{\tilde{\chi}_1^0} = 77.7 GeV$ ) and the considered  $\mathcal{R}_p$  coupling is  $\lambda'_{211} = 0.09$ . The average reconstructed  $\tilde{\chi}_1^0$  mass is  $71 \pm 9$  GeV.

$\tilde{\nu}_\mu$  masses reconstructions are based on the 4-momentum of the neutrino present in the  $3l + 2j + \nu$  final state (see Section 4.1). The transverse component of this momentum can be deduced from the momentum of the charged leptons and jets present in the final state. However, the longitudinal component of the neutrino momentum remains unknown due to the poor detection at small polar angle values. Therefore, in this study we have assumed a vanishing longitudinal component of the neutrino momentum. Besides, we have focused on the  $e\mu\mu$  events as in the  $\tilde{\chi}_1^0$  mass reconstruction study. In this context, the cascade decay initiated by the produced lightest chargino is  $\tilde{\chi}_1^\pm \rightarrow \tilde{\chi}_1^0 e^\pm \nu_e$ ,  $\tilde{\chi}_1^0 \rightarrow \mu^\pm u_j d_k$ . Therefore, the  $\tilde{\chi}_1^\pm$  has been reconstructed from the softer muon, the 2 jets, the electron and the neutrino present in the final state, since the softer muon is mainly generated in the  $\tilde{\chi}_1^0$  decay as explained above. The  $\tilde{\nu}_\mu$  has then been reconstructed from the  $\tilde{\chi}_1^\pm$  and

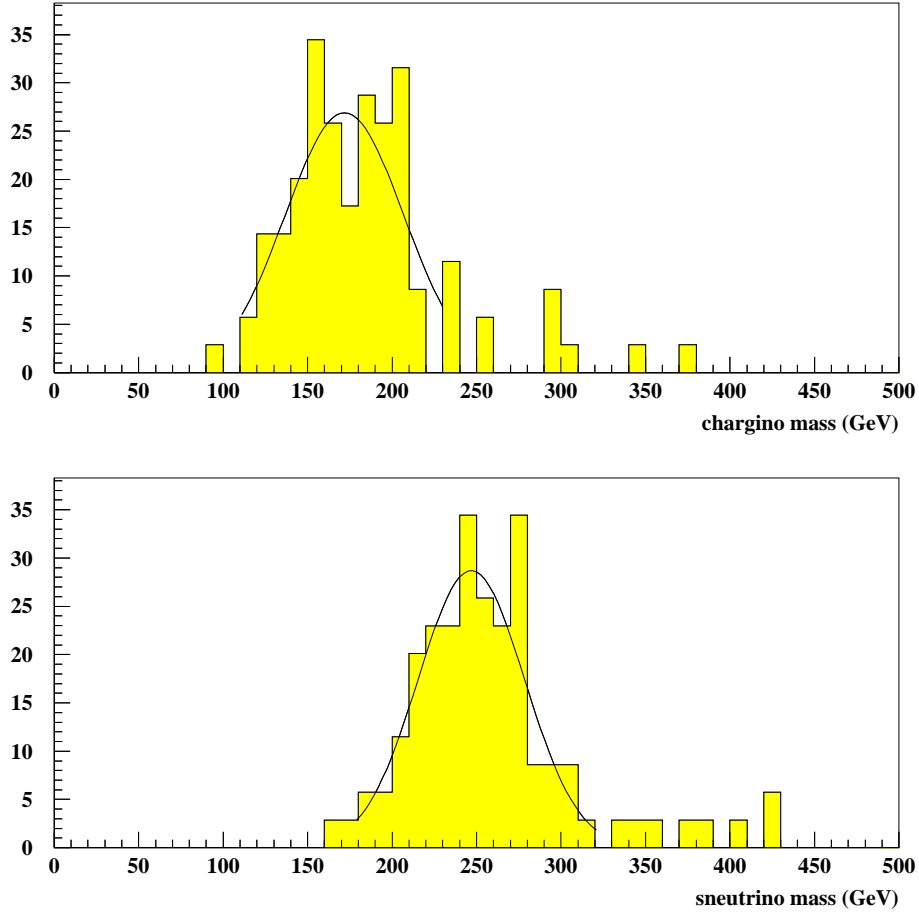


FIG. 19: Distributions of the  $e + \text{softer } \mu + 2j + \nu$  (upper plot) and  $e + \mu + \mu + 2j + \nu$  (lower plot) invariant masses in the  $e + \mu + \mu + 2j + \nu$  events, for a luminosity of  $\mathcal{L} = 10fb^{-1}$ . The mSUGRA point taken for these figures is  $m_0 = 200GeV$ ,  $M_2 = 150GeV$ ,  $\tan\beta = 1.5$  and  $sign(\mu) < 0$  ( $m_{\tilde{\chi}_1^\pm} = 158.3GeV$ ,  $m_{\tilde{\nu}_{\mu L}} = 236GeV$ ) and the considered  $\mathcal{R}_p$  coupling is  $\lambda'_{211} = 0.09$ . The average reconstructed masses are  $m_{\tilde{\chi}_1^\pm} = 171 \pm 35GeV$  and  $m_{\tilde{\nu}_{\mu L}} = 246 \pm 32GeV$ .

the leading muon of the final state. This was motivated by the fact that the dominant contribution to the single chargino production is the reaction  $p\bar{p} \rightarrow \tilde{\nu}_\mu \rightarrow \tilde{\chi}_1^\pm \mu^\mp$  (see Fig.1).

In Fig.19, we present the  $\tilde{\chi}_1^\pm$  and  $\tilde{\nu}_\mu$  mass reconstructions performed through the method presented above. We also show on the plots of Fig.19 the fits of the invariant mass distributions. As can be seen from those fits, the distributions are well peaked around the  $\tilde{\chi}_1^\pm$  and  $\tilde{\nu}_{\mu L}$  generated masses. The average reconstructed masses are  $m_{\tilde{\chi}_1^\pm} = 171 \pm 35GeV$  and  $m_{\tilde{\nu}_{\mu L}} = 246 \pm 32GeV$ . This study on the  $\tilde{\chi}_1^\pm$  and  $\tilde{\nu}_{\mu L}$  masses shows that based on a simplified mass reconstruction analysis promising results are obtained from the 3 lepton signature generated by the single  $\tilde{\chi}_1^\pm$  production. The  $\tilde{\chi}_1^\pm$  and  $\tilde{\nu}_{\mu L}$  mass reconstructions

can be improved using constrained fits.

In the hypothesis of a single dominant coupling constant of type  $\lambda'_{1jk}$ , exactly the same kind of  $\tilde{\chi}_1^0$ ,  $\tilde{\chi}_1^\pm$  and  $\tilde{\nu}_\mu$  mass reconstructions can be performed by selecting the  $e + e + \mu + 2j + \nu$  events. In contrast, the case of a single dominant  $\lambda'_{3jk}$  coupling requires more sophisticated methods.

As a conclusion, in the case of a single dominant coupling constant of type  $\lambda'_{1jk}$  or  $\lambda'_{2jk}$ , the  $\tilde{\chi}_1^0$ ,  $\tilde{\chi}_1^\pm$  and  $\tilde{\nu}_\mu$  mass reconstructions based on the 3 lepton signature generated by the single  $\tilde{\chi}_1^\pm$  production at Tevatron can easily give precise results, in contrast with the mass reconstructions performed in the superpartner pair production analysis at hadronic colliders which suffer a high combinatorial background [44].

## Model dependence of the results

In this Section, we discuss qualitatively the impact on our results of the choice of our theoretical model, namely mSUGRA with the infrared fixed point hypothesis for the top quark Yukawa coupling. We focus on the discovery potentials obtained in Sections 4.5, 4.5 and 4.5, since the choice of the theoretical framework does not influence the study of the neutralino mass reconstruction made in Section 4.5 which is model independent.

The main effect of the infrared fixed point approach is to fix the value of the  $\tan\beta$  parameter, up to the ambiguity on the low or high solution. Therefore, the infrared fixed point hypothesis has no important effects on the results since the dependences of the single gaugino productions rates on  $\tan\beta$  are smooth, in the high  $\tan\beta$  scenario (see Section 3.1).

As we have mentioned in Section 2, in the mSUGRA scenario, the  $|\mu|$  parameter is fixed. This point does not influence much our results since the single gaugino production cross sections vary weakly with  $|\mu|$  as shown in Section 3.1.

Another particularity of the mSUGRA model is that the LSP is the  $\tilde{\chi}_1^0$  in most of the parameter space. For instance, in a model where the LSP would be the lightest chargino or a squark, the contribution to the three lepton signature from the  $\tilde{\chi}_1^\pm l^\mp$  production would vanish.

Finally in mSUGRA, the squark masses are typically larger than the lightest chargino mass so that the decay  $\tilde{\chi}_1^\pm \rightarrow \tilde{\chi}_1^0 l^\pm \nu$  has a branching ratio of at least  $\sim 30\%$  (see Section 4.1). In a scenario where  $m_{\tilde{\chi}_1^\pm} > m_{\tilde{q}}$ , the two-body decay  $\tilde{\chi}_1^\pm \rightarrow \tilde{q} q$  would be dominant so that the contribution to the three lepton signature from the  $\tilde{\chi}_1^\pm l^\mp$  production would be small. Besides, in mSUGRA, the  $\tilde{\chi}_1^\pm - \tilde{\chi}_1^0$  mass difference is typically large enough to avoid significant branching ratio for the  $\tilde{R}_p$  decay of the lightest chargino which would result in a decrease of the sensitivities on the SUSY parameters presented in Sections 4.5, 4.5 and 4.5.

In a model where the contribution to the three lepton signature from the  $\tilde{\chi}^\pm l^\mp$  production would be suppressed, the three lepton final state could be generated in a significant way by other single gaugino productions, namely the  $\tilde{\chi}^\pm \nu$ ,  $\tilde{\chi}^0 l^\mp$  or  $\tilde{\chi}^0 \nu$  productions.

## 5 Like sign dilepton signature analysis

### 5.1 Signal

Within the context of the mSUGRA model, three of the single gaugino productions via  $\lambda'_{ijk}$  presented in Section 3.1 can generate a final state containing a pair of same sign leptons. As a matter of fact, the like sign dilepton signature can be produced through the reactions  $p\bar{p} \rightarrow \tilde{\chi}_1^0 l_i^\pm$ ;  $p\bar{p} \rightarrow \tilde{\chi}_2^0 l_i^\pm$ ,  $\tilde{\chi}_2^0 \rightarrow \tilde{\chi}_1^0 + X$  ( $X \neq l^\pm$ );  $p\bar{p} \rightarrow \tilde{\chi}_1^\pm l_i^\mp$ ,  $\tilde{\chi}_1^\pm \rightarrow \tilde{\chi}_1^0 q\bar{q}$  and  $p\bar{p} \rightarrow \tilde{\chi}_1^\pm \nu_i$ ,  $\tilde{\chi}_1^\pm \rightarrow \tilde{\chi}_1^0 l^\pm \nu$ ,  $i$  corresponding to the flavour index of the  $\lambda'_{ijk}$  coupling. Indeed, since the  $\tilde{\chi}_1^0$  is a Majorana particle, it decays via  $\lambda'_{ijk}$  into a lepton, as  $\tilde{\chi}_1^0 \rightarrow l_i u_j \bar{d}_k$ , and into an anti-lepton, as  $\tilde{\chi}_1^0 \rightarrow \bar{l}_i \bar{u}_j d_k$ , with the same probability. The  $\tilde{\chi}_{3,4}^0 l_i^\pm$ ,  $\tilde{\chi}_2^\pm l_i^\mp$  and  $\tilde{\chi}_2^\pm \nu_i$  productions do not bring significant contributions to the like sign dilepton signature due to their relatively small cross sections (see Section 3.1).

In mSUGRA, the most important contribution to the like sign dilepton signature originates from the  $\tilde{\chi}_1^0 l_i^\pm$  production since this reaction has a dominant cross section in most of the mSUGRA parameter space, as shown in Section 3.1. The other reason is that if  $\tilde{\chi}_1^0$  is the LSP, the  $\tilde{\chi}_1^0 l_i^\pm$  production rate is not affected by branching ratios of any cascade decay since the  $\tilde{\chi}_1^0$  only decays through  $\mathcal{R}_p$  coupling.

### 5.2 Standard Model background of the like sign dilepton signature at Tevatron

The  $b\bar{b}$  production can lead to the like sign dilepton signature if both of the  $b$  quarks decay semi-leptonically. The leading order cross section of the  $b\bar{b}$  production at Tevatron for an energy of  $\sqrt{s} = 2TeV$  is  $\sigma(p\bar{p} \rightarrow b\bar{b}) \approx 4.654 \cdot 10^{10} fb$ . This rate has been calculated with PYTHIA [37] using the CTEQ2L structure function.

The  $t\bar{t}$  production, followed by the decays  $t \rightarrow W^+ b \rightarrow l^+ \nu b$ ,  $\bar{t} \rightarrow W^- \bar{b} \rightarrow \bar{q} q \bar{b} \rightarrow \bar{q} q l^+ \nu \bar{c}$ , or  $t \rightarrow W^+ b \rightarrow \bar{q} q b \rightarrow \bar{q} q l^- \bar{\nu} c$ ,  $\bar{t} \rightarrow W^- \bar{b} \rightarrow l^- \bar{\nu} \bar{b}$ , also generates a final state with two same sign leptons. The leading order cross section of the  $t\bar{t}$  production at  $\sqrt{s} = 2TeV$ , including the relevant branching ratios, is  $\sigma(p\bar{p} \rightarrow t\bar{t}) \times 2 \times B(W \rightarrow l_p \nu_p) \times B(W \rightarrow q_p \bar{q}_{p'}) \approx 3181 fb$  ( $2800 fb$ ) for  $m_{top} = 170 GeV$  ( $175 GeV$ ) with  $p, p' = 1, 2, 3$ .

The third important source of Standard Model background is the  $t\bar{b}/\bar{t}b$  production since the (anti-) $b$  quark can undergo a semi-leptonic decay as  $b \rightarrow l^- \bar{\nu} c$  ( $\bar{b} \rightarrow l^+ \nu \bar{c}$ ) and the (anti-) top quark can decay simultaneously as  $t \rightarrow b W^+ \rightarrow b l^+ \nu$  ( $\bar{t} \rightarrow \bar{b} W^- \rightarrow \bar{b} l^- \bar{\nu}$ ). The leading order cross section at  $\sqrt{s} = 2TeV$  including the branching fraction is  $\sigma(p\bar{p} \rightarrow t\bar{q}, \bar{t}q) \times B(W \rightarrow l_p \nu_p) \approx 802 fb$  ( $687 fb$ ) for  $m_{top} = 170 GeV$  ( $175 GeV$ ) with  $p = 1, 2, 3$ .

Other small sources of Standard Model background are the  $W^\pm W^\mp$  production, followed by the decays :  $W \rightarrow l\nu$  and  $W \rightarrow bu_p$  ( $p = 1, 2$ ) or  $W \rightarrow bu_p$  and  $W \rightarrow bu_p$  ( $p = 1, 2$ ), the  $W^\pm Z^0$  production, followed by the decays :  $W \rightarrow l\nu$  and  $Z \rightarrow b\bar{b}$  or  $W \rightarrow q_p \bar{q}_{p'}$  and  $Z \rightarrow b\bar{b}$ , and the  $Z^0 Z^0$  production, followed by the decays :  $Z \rightarrow l\bar{l}$  and  $Z \rightarrow b\bar{b}$  or  $Z \rightarrow q_p \bar{q}_p$  and  $Z \rightarrow b\bar{b}$ .

Finally, the 3 lepton final states generated by the  $Z^0 Z^0$  and  $W^\pm Z^0$  productions (see Section 4.2) can be mistaken for like sign dilepton events in case where one of the leptons is lost in the detection. Non-physics sources of background can also be caused by some fake leptons or by the misidentification of the charge of a lepton.

Therefore for the study of the Standard Model background associated to the like sign dilepton signal at Tevatron Run II, we consider the  $b\bar{b}$ , the  $t\bar{t}$ , the  $W^\pm W^\mp$  and the single



top production and both the physics and non-physics contributions generated by the  $W^\pm Z^0$  and  $Z^0 Z^0$  productions.

### 5.3 Supersymmetric background of the like sign dilepton signature at Tevatron

All the pair productions of superpartners are a source of SUSY background for the like sign dilepton signature originating from the single gaugino productions. Indeed, both of the produced superpartners initiate a cascade decay ended by the  $\tilde{R}_p$  decay of the LSP through  $\lambda'_{ijk}$ , and if the two LSP's undergo the same decay  $\tilde{\chi}_1^0 \rightarrow l_i u_j \bar{d}_k$  or  $\tilde{\chi}_1^0 \rightarrow \bar{l}_i \bar{u}_j d_k$ , two same sign charged leptons are generated. Another possible way for the SUSY pair production to generate the like sign dilepton signature is that only one of the LSP's decays into a charged lepton of a given sign, the other decaying as  $\tilde{\chi}_1^0 \rightarrow \nu_i d_j d_k$ , and a second charged lepton of the same sign is produced in the cascade decays.

The cross sections of the superpartners pair productions have been studied in Section 4.3.

### 5.4 Cuts

In order to simulate the single chargino productions  $p\bar{p} \rightarrow \tilde{\chi}_1^\pm l^\mp$ ,  $p\bar{p} \rightarrow \tilde{\chi}_1^\pm \nu$  and the single neutralino production  $p\bar{p} \rightarrow \tilde{\chi}_1^0 l^\mp$  at Tevatron, the matrix elements (see Appendix 1) of these processes have been implemented in a version of the SUSYGEN event generator [49] allowing the generation of  $p\bar{p}$  reactions [50]. The Standard Model background ( $W^\pm W^\mp$ ,  $W^\pm Z^0$ ,  $Z^0 Z^0$ ,  $t\bar{b}/\bar{t}b$ ,  $t\bar{t}$  and  $b\bar{b}$  productions) has been simulated using the PYTHIA event generator [37] and the SUSY background (all SUSY particles pair productions) using the HERWIG event generator [48]. SUSYGEN, PYTHIA and HERWIG have been interfaced with the SHW detector simulation package [42] (see Section 4.4).

Several selection criteria have been applied in order to reduce the background. First, we have selected the events containing two same sign muons. The reason is that in the like sign dilepton signature analysis we have focused on the case of a single dominant  $\tilde{R}_p$  coupling constant of the type  $\lambda'_{2jk}$ . In such a scenario, the two same charge leptons generated in the  $\tilde{\chi}_1^0 l^\mp$  production, which represents the main contribution to the like sign dilepton final state (see Section 5.1), are muons (see Fig.1 and Section 5.1). This requirement that the 2 like sign leptons have the same flavour allows to reduce the Standard Model background with respect to the signal.

We require a number of jets greater or equal to two with a transverse momentum higher than  $10\text{GeV}$ , namely  $N_j \geq 2$  with  $P_t(j) > 10\text{GeV}$ . This jet veto reduces the non-physics backgrounds generated by the  $W^\pm Z^0$  and  $Z^0 Z^0$  productions (see Section 5.2) which produce at most one hard jet (see Section 4.4).

Besides, some effective cuts concerning the energies of the 2 selected muons have been applied. In Fig.20, we present the distributions of the 2 muon energies in the like sign dimuon events generated by the Standard Model background ( $W^\pm W^\mp$ ,  $W^\pm Z^0$ ,  $Z^0 Z^0$ ,  $t\bar{t}$ ,  $t\bar{b}/\bar{t}b$  and  $b\bar{b}$ ) and the SUSY signal. Based on these distributions, we have chosen the following cuts on the muon energies :  $E(\mu_2) > 20\text{GeV}$  and  $E(\mu_1) > 20\text{GeV}$ .

We will refer to all the selection criteria described above, namely 2 same sign muons with  $E(\mu_2) > 20\text{GeV}$  and  $E(\mu_1) > 20\text{GeV}$ , and  $N_j \geq 2$  with  $P_t(j) > 10\text{GeV}$ , as cut 1.

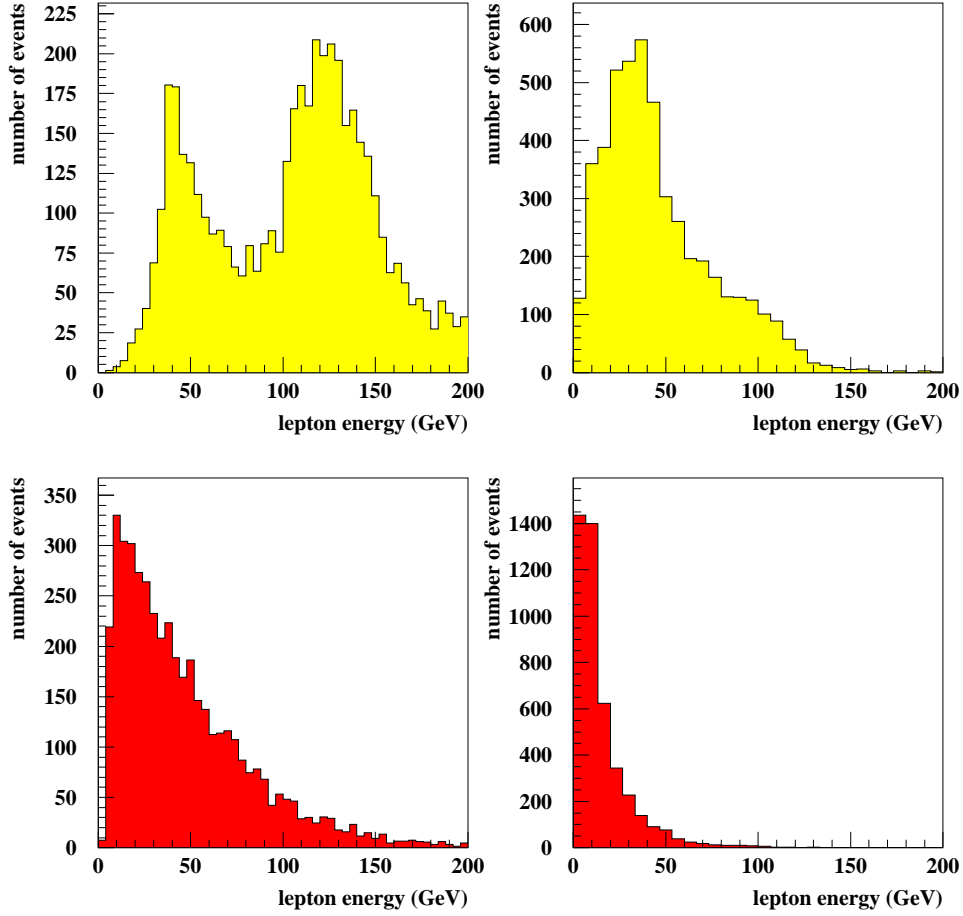


FIG. 20: Distributions of the 2 muon energies (in GeV) in the events containing 2 same sign muons and at least 2 jets generated by the Standard Model background (lower curve), namely the  $W^\pm W^\mp$ ,  $W^\pm Z^0$ ,  $Z^0 Z^0$ ,  $t\bar{t}$ ,  $t\bar{b}/t\bar{b}$  and  $b\bar{b}$  productions, and the SUSY signal (upper curve), for  $\lambda'_{211} = 0.05$ ,  $M_2 = 250\text{GeV}$ ,  $m_0 = 200\text{GeV}$ ,  $\tan\beta = 1.5$  and  $\text{sign}(\mu) < 0$ . The left plots represent the leading muon distributions and the right plots the second leading muon distributions. The numbers of events correspond to an integrated luminosity of  $\mathcal{L} = 10\text{fb}^{-1}$ .

Let us explain the origin of the two peaks in the upper left plot of Fig.20. This will be helpful for the mass reconstruction study of Section 5.5.

The main contribution to the like sign dimuon signature from the SUSY signal is the  $\tilde{\chi}_1^0 \mu^\pm$  production (see Section 5.1) in the case of a single dominant  $\lambda'_{2jk}$  coupling. Furthermore, the dominant contribution to this production is the reaction  $p\bar{p} \rightarrow \tilde{\mu}_L^\pm \rightarrow \tilde{\chi}_1^0 \mu^\pm$ . In this reaction, the  $\mu^\pm$  produced together with the  $\tilde{\chi}_1^0$  has an energy around  $E(\mu^\pm) \approx (m_{\tilde{\mu}_L^\pm}^2 + m_{\mu^\pm}^2 - m_{\tilde{\chi}_1^0}^2)/2m_{\tilde{\mu}_L^\pm} = 121.9\text{GeV}$  for the SUSY point considered in Fig.20, namely  $M_2 = 250\text{GeV}$ ,  $m_0 = 200\text{GeV}$ ,  $\tan\beta = 1.5$  and  $\text{sign}(\mu) < 0$ , which gives rise to the mass spectrum :  $m_{\tilde{\chi}_1^0} = 127.1\text{GeV}$ ,  $m_{\tilde{\chi}_2^0} = 255.3\text{GeV}$ ,  $m_{\tilde{\chi}_1^\pm} = 255.3\text{GeV}$ ,  $m_{\tilde{t}_L^\pm} = 298\text{GeV}$  and  $m_{\tilde{b}_L^\pm} = 294\text{GeV}$ . This energy value corresponds approximatively to the mean value of the

right peak of the leading muon energy distribution presented in the upper left plot of Fig.20. This is due to the fact that the leading muon in the dimuon events generated by the reaction  $p\bar{p} \rightarrow \tilde{\chi}_1^0 \mu^\pm$  is the  $\mu^\pm$  produced together with the  $\tilde{\chi}_1^0$  for relatively important values of the  $m_{\tilde{\mu}_L^\pm} - m_{\tilde{\chi}_1^0}$  mass difference. The right peak in the upper left plot of Fig.20 is thus associated to the  $\tilde{\chi}_1^0 \mu^\pm$  production.

Similarly, the left peak in the upper left plot of Fig.20 corresponds to the reactions  $p\bar{p} \rightarrow \tilde{\mu}_L^\pm \rightarrow \tilde{\chi}_2^0 \mu^\pm$  and  $p\bar{p} \rightarrow \tilde{\nu}_{\mu L} \rightarrow \tilde{\chi}_1^\pm \mu^\mp$  which produce  $\mu^\pm$  of energies around  $E(\mu^\pm) \approx (m_{\tilde{\mu}_L^\pm}^2 + m_{\tilde{\chi}_2^0}^2)/2m_{\tilde{\mu}_L^\pm} = 39.6\text{GeV}$  and  $E(\mu^\pm) \approx (m_{\tilde{\nu}_{\mu L}}^2 + m_{\tilde{\chi}_1^\pm}^2)/2m_{\tilde{\nu}_{\mu L}} = 36.2\text{GeV}$ , respectively. The  $\tilde{\chi}_1^\pm \nu_\mu$  production represents a less important contribution to the like sign dimuon events compared to the 3 above single gaugino productions since the 2 same sign leptons generated in this production are not systematically muons and the involved branching ratios have smaller values (see Section 5.1).

Finally, since the leptons produced in the quark  $b$  decays are not well isolated (as in the  $W^\pm W^\mp$ ,  $W^\pm Z^0$ ,  $Z^0 Z^0$ ,  $t\bar{t}$ ,  $t\bar{b}/\bar{t}b$  and  $b\bar{b}$  productions), we have applied some cuts on the lepton isolation. We have imposed the isolation cut  $\Delta R = \sqrt{\delta\phi^2 + \delta\theta^2} > 0.4$  where  $\phi$  is the azimuthal angle and  $\theta$  the polar angle between the 2 same sign muons and the 2 hardest jets. This cut is for example motivated by the distributions shown in Fig.21 of the  $\Delta R$  angular difference between the second leading muon and the second leading jet, in the like sign dimuons events generated by the SUSY signal and Standard Model background. We call cut  $\Delta R > 0.4$  together with cut 1, cut 2.

In order to eliminate poorly isolated muons, we have also imposed that  $E < 2\text{GeV}$ , where  $E$  represents the summed energies of the jets being close to a muon, namely the jets contained in the cone centered on a muon and defined by  $\Delta R < 0.25$ . This cut is for instance motivated by the distributions shown in Fig.22 which represent the summed energies  $E$  of the jets being close to the second leading muon in the like sign dimuons events generated by the SUSY signal and Standard Model background. We denote cut  $E < 2\text{GeV}$  plus cut 2 as cut 3.

The selected events require high energy charged leptons and jets and can thus be easily triggered at Tevatron. Moreover, the considered charged leptons and jets are typically emitted at intermediate polar angles and would thus be often detected at Tevatron. These points are illustrated in Fig.23 where are shown the energy and polar angle distributions of the leading muon and the leading jet in the like sign dimuons events selected by applying cut 3 and generated by the SUSY signal and Standard Model background.

In Table 8, we give the numbers of like sign dilepton events expected from the Standard Model background at Tevatron Run II with the various cuts described above. We see in Table 8 that the main source of Standard Model background to the like sign dilepton signature at Tevatron is the  $t\bar{t}$  production. This is due to its important cross section compared to the other Standard Model backgrounds (see Section 5.2) and to the fact that in the  $t\bar{t}$  background, in contrast with the  $b\bar{b}$  background, only one charged lepton of the final state is produced in a  $b$ -jet and is thus not isolated.

In Table 9, we give the number of like sign dilepton events generated by the SUSY background (all superpartners pair productions) at Tevatron Run II as a function of the  $m_0$  and  $m_{1/2}$  parameters for cut 3. This number of events decreases as  $m_0$  and  $m_{1/2}$  increase due to the behaviour of the summed superpartners pair production cross section in the SUSY parameter space (see Section 4.3).

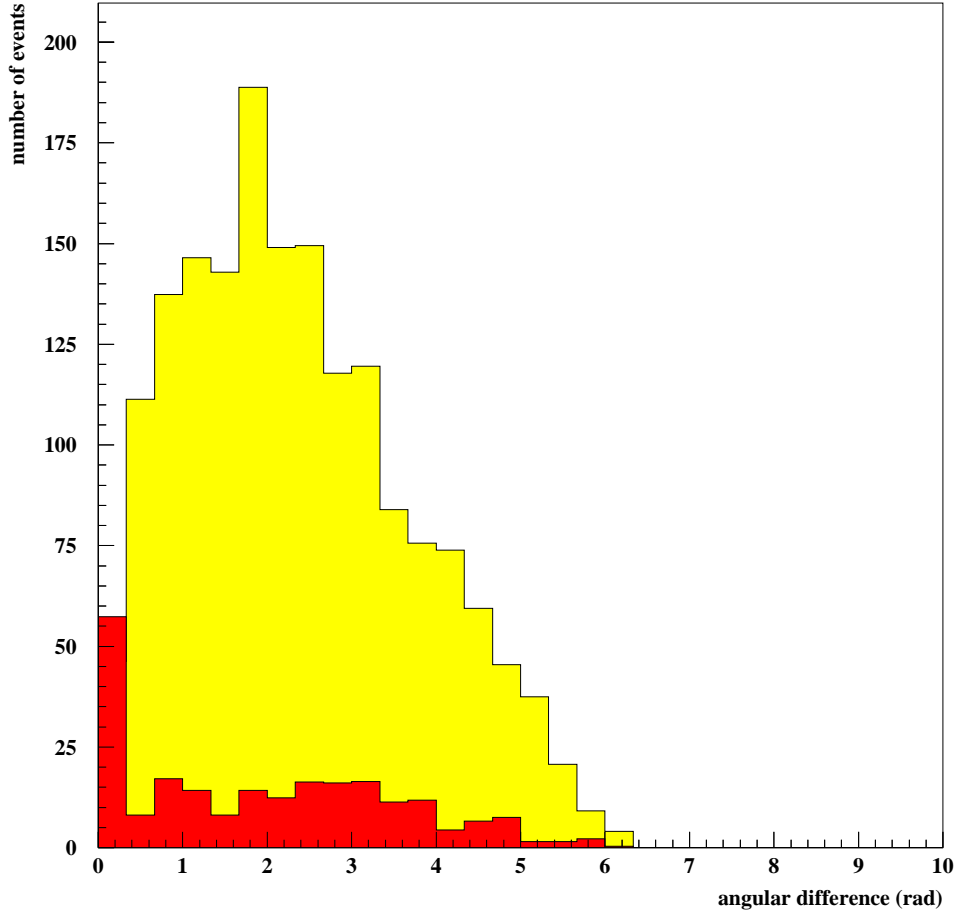


FIG. 21: Distributions of the  $\Delta R$  angular difference (in rad) between the second leading muon and the second leading jet in the like sign dimuons events selected by applying cut 1 and generated by the Standard Model background (curve in black), namely the  $W^\pm W^\mp$ ,  $W^\pm Z^0$ ,  $Z^0 Z^0$ ,  $t\bar{t}$ ,  $t\bar{b}/\bar{t}b$  and  $b\bar{b}$  productions, and the SUSY signal (curve in grey), for  $\lambda'_{211} = 0.05$ ,  $M_2 = 250\text{GeV}$ ,  $m_0 = 200\text{GeV}$ ,  $\tan\beta = 1.5$  and  $\text{sign}(\mu) < 0$ . The numbers of events correspond to an integrated luminosity of  $\mathcal{L} = 10\text{fb}^{-1}$ .

## 5.5 Results

### Discovery potential

We first present the reach in the mSUGRA parameter space obtained from the analysis of the like sign dilepton final state at Tevatron Run II produced by the single neutralino and chargino productions via  $\lambda'_{211} : p\bar{p} \rightarrow \tilde{\chi}_{1,2}^0 \mu^\pm$ ,  $p\bar{p} \rightarrow \tilde{\chi}_1^\pm \mu^\mp$  and  $p\bar{p} \rightarrow \tilde{\chi}_1^\pm \nu_\mu$ . The sensitivities that can be obtained on the  $\lambda'_{2jk}$  ( $j$  and  $k$  being not equal to 1 simultaneously),  $\lambda'_{1jk}$  and  $\lambda'_{3jk}$  coupling constants will be discussed at the end of this section.

In Fig.24, we present the  $3\sigma$  and  $5\sigma$  discovery contours and the limits at 95% confidence level in the plane  $m_0$  versus  $m_{1/2}$ , for  $\text{sign}(\mu) < 0$ ,  $\tan\beta = 1.5$ ,  $\lambda'_{211} = 0.05$  and using a set of values for the luminosity. Those discovery potentials were obtained by considering the

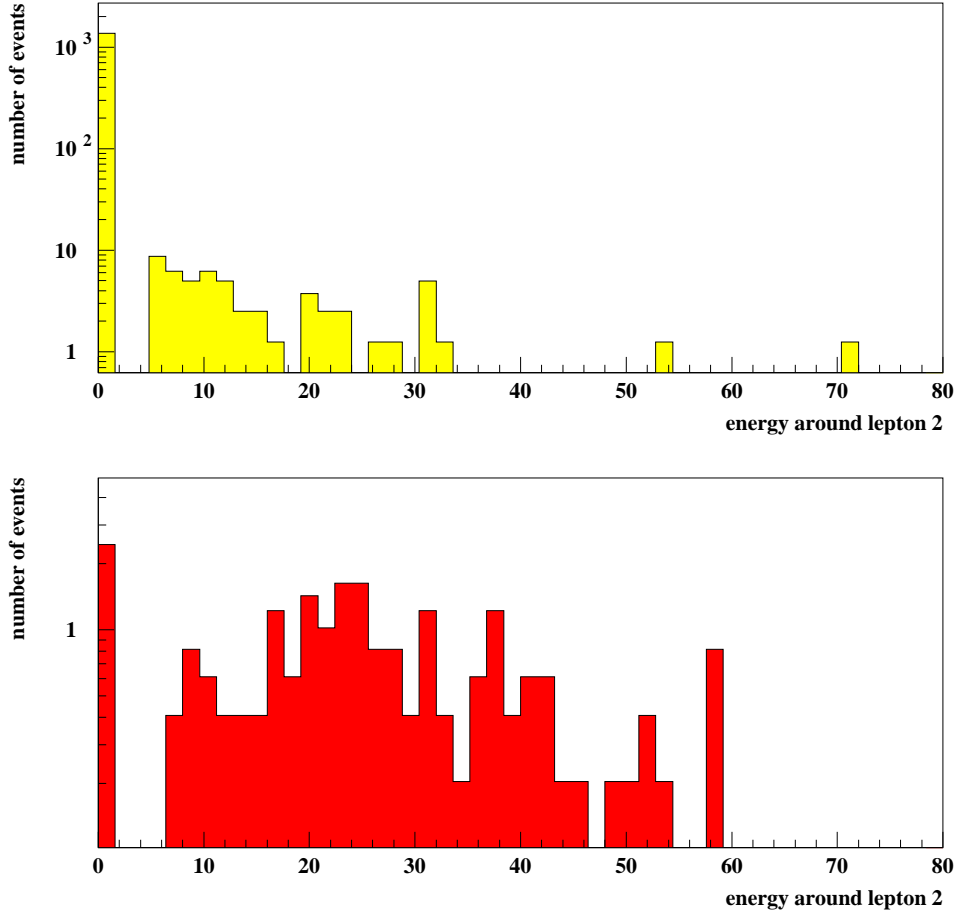


FIG. 22: Distributions of the summed energies ( $E$ , in GeV) of the jets being close to the second leading muon, namely the jets contained in the cone centered on the second leading muon and defined by  $\Delta R < 0.25$ , in the like sign dimuons events selected by applying cut 2 and generated by the Standard Model background (lower curve), namely the  $W^\pm W^\mp$ ,  $W^\pm Z^0$ ,  $Z^0 Z^0$ ,  $t\bar{t}$ ,  $t\bar{b}/\bar{t}b$  and  $b\bar{b}$  productions, and the SUSY signal (upper curve), for  $\lambda'_{211} = 0.05$ ,  $M_2 = 250\text{GeV}$ ,  $m_0 = 200\text{GeV}$ ,  $\tan\beta = 1.5$  and  $\text{sign}(\mu) < 0$ . These distributions were obtained after cut  $E < 2\text{GeV}$ , where  $E$  represents the summed energies of the jets being close to the leading muon, has been applied in these like sign dimuons events. The numbers of events correspond to an integrated luminosity of  $\mathcal{L} = 10\text{fb}^{-1}$ .

$\tilde{\chi}_{1,2}^0 \mu^\pm$ ,  $\tilde{\chi}_1^\pm \mu^\mp$  and  $\tilde{\chi}_1^\pm \nu_\mu$  productions and the background originating from the Standard Model. The signal and background were selected by using cut 3 described in Section 5.4. The reduction of the sensitivity on  $m_{1/2}$  observed in Fig.24 as  $m_0$  increases is due to the decrease of the  $\tilde{\chi}_{1,2}^0 \mu^\pm$ ,  $\tilde{\chi}_1^\pm \mu^\mp$  and  $\tilde{\chi}_1^\pm \nu_\mu$  productions cross sections with the  $m_0$  increase observed in Fig.5 and Fig.6. In Fig.24, we also see that the sensitivity on  $m_{1/2}$  is reduced in the domain  $m_0 \lesssim 200\text{GeV}$ . This reduction of the sensitivity is due to the fact that in mSUGRA at low  $\tan\beta$  and for large values of  $m_{1/2}$  and small values of  $m_0$ , the LSP is the Right slepton  $\tilde{l}_{iR}^\pm$  ( $i = 1, 2, 3$ ). Therefore, in this mSUGRA region the dominant decay

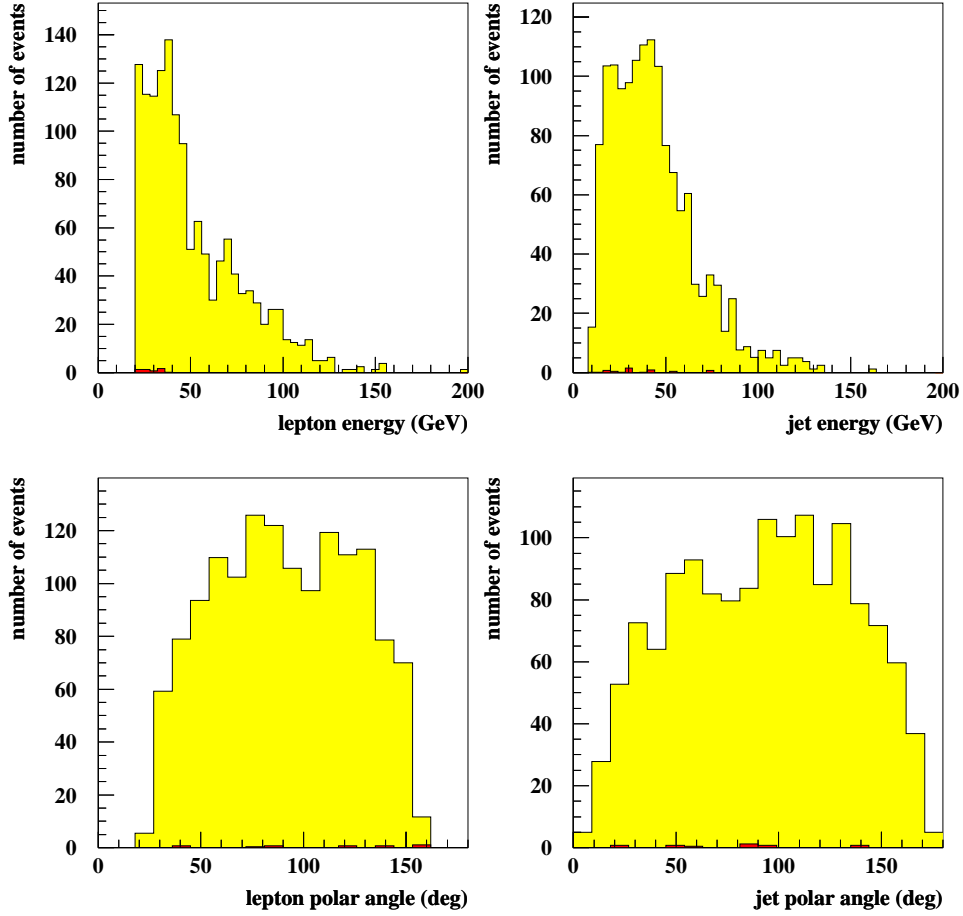


FIG. 23: Energy (in GeV) and polar angle ( $\theta$ , in deg) distributions of the leading muon and the leading jet in the like sign dimuon events selected by applying cut 3 and generated by the Standard Model background (curve in black), namely the  $W^\pm W^\mp$ ,  $W^\pm Z^0$ ,  $Z^0 Z^0$ ,  $t\bar{t}$ ,  $t\bar{b}/\bar{t}b$  and  $b\bar{b}$  productions, and the SUSY signal (curve in grey), for  $\lambda'_{211} = 0.05$ ,  $M_2 = 250\text{GeV}$ ,  $m_0 = 200\text{GeV}$ ,  $\tan\beta = 1.5$  and  $\text{sign}(\mu) < 0$ . The numbers of events correspond to an integrated luminosity of  $\mathcal{L} = 10\text{fb}^{-1}$ .

channel of the lightest neutralino is  $\tilde{\chi}_1^0 \rightarrow \tilde{l}_{iR}^\pm l_i^\mp$  ( $i = 1, 2, 3$ ) so that the  $\tilde{\chi}_1^0 \mu^\pm$  production, which is the main contribution to the like sign dilepton signature, leads to the  $2\mu^\pm + 2\text{ jets}$  final state only in a few cases. There are two reasons. First, in this mSUGRA scenario the charged lepton produced in the main  $\tilde{\chi}_1^0$  decay is not systematically a muon. Secondly, if the LSP is the Right slepton  $\tilde{l}_{iR}^\pm$  it cannot decay in the case of a single dominant  $\lambda'_{ijk}$  coupling constant and it is thus a stable particle.

The sensitivities presented in the discovery reach of Fig.24 which are obtained from the like sign dilepton signature analysis are higher than the sensitivities shown in Fig.10 which correspond to the trilepton final state analysis. This is due to the 3 following points. First, the rate of the  $\tilde{\chi}_1^0 \mu^\pm$  production (recall that it represents the main contribution to the like sign dilepton final state) is larger than the  $\sigma(p\bar{p} \rightarrow \tilde{\chi}_1^\pm \mu^\mp)$  cross section in most

	$W^\pm Z^0$	$Z^0 Z^0$	$t\bar{t}$	$t\bar{b}/\bar{t}b$	Total
cut 1	$0.21 \pm 0.06$	$0.11 \pm 0.04$	$21.80 \pm 0.70$	$0.69 \pm 0.13$	$22.81 \pm 0.71$
cut 2	$0.05 \pm 0.03$	$0.03 \pm 0.03$	$8.80 \pm 0.50$	$0.28 \pm 0.08$	$9.16 \pm 0.51$
cut 3	$0.03 \pm 0.03$	$0.01 \pm 0.02$	$0.64 \pm 0.13$	$0.10 \pm 0.05$	$0.78 \pm 0.14$

TAB. 8: Numbers of like sign dilepton events generated by the Standard Model background ( $W^\pm W^\mp$ ,  $W^\pm Z^0$ ,  $Z^0 Z^0$ ,  $t\bar{t}$ ,  $t\bar{b}/\bar{t}b$  and  $b\bar{b}$  productions) at Tevatron Run II for the cuts described in the text, assuming an integrated luminosity of  $\mathcal{L} = 1fb^{-1}$  and a center of mass energy of  $\sqrt{s} = 2TeV$ . The numbers of events coming from the  $W^\pm W^\mp$  and  $b\bar{b}$  backgrounds have been found to be negligible after cut 3 is applied. These results have been obtained by generating  $2 \cdot 10^4$  events for the  $W^\pm Z^0$  production,  $10^4$  events for the  $W^\pm Z^0$  (non-physics contribution),  $3 \cdot 10^4$  events for the  $Z^0 Z^0$ ,  $10^4$  events for the  $Z^0 Z^0$  (non-physics contribution),  $3 \cdot 10^5$  events for the  $t\bar{t}$  and  $10^5$  events for the  $t\bar{b}/\bar{t}b$ .

$m_{1/2} \setminus m_0$	100GeV	200GeV	300GeV	400GeV	500GeV
100GeV	101.64	54.92	44.82	39.26	38.77
200GeV	3.74	4.08	4.33	4.56	4.99
300GeV	1.04	0.63	0.61	0.70	0.66

TAB. 9: Number of like sign dilepton events generated by the SUSY background (all superpartner pair productions) at Tevatron Run II as a function of the  $m_0$  and  $m_{1/2}$  parameters for  $\tan\beta = 1.5$ ,  $sign(\mu) < 0$  and  $\lambda'_{211} = 0.05$ . Cut 3 (see text) has been applied. These results have been obtained by generating 7500 events and correspond to an integrated luminosity of  $\mathcal{L} = 1fb^{-1}$  and a center of mass energy of  $\sqrt{s} = 2TeV$ .

of the mSUGRA parameter space (see Section 3.1). Secondly, the  $\tilde{\chi}_1^0$  decay leading to the like sign dilepton final state in the case of the  $\tilde{\chi}_1^0 \mu^\pm$  production has a larger branching ratio than the cascade decay initiated by the  $\tilde{\chi}_1^\pm$  which generates the trilepton final state (see Sections 4.1 and 5.1). Finally, at Tevatron Run II the Standard Model background of the like sign dilepton signature is weaker than the trilepton Standard Model background (see Tables 4 and 8).

It is clear from Fig.24 that at low values of the  $m_0$  and  $m_{1/2}$  parameters, high sensitivities can be obtained on the  $\lambda'_{211}$  coupling constant. We have found that for instance at the mSUGRA point defined as  $m_0 = 200GeV$ ,  $m_{1/2} = 200GeV$ ,  $sign(\mu) < 0$  and  $\tan\beta = 1.5$ ,  $\lambda'_{211}$  values of  $\sim 0.03$  can be probed through the like sign dilepton analysis at Tevatron Run II assuming a luminosity of  $\mathcal{L} = 1fb^{-1}$ . This result was obtained by applying cut 3 described in Section 5.4 on the SUSY signal ( $\tilde{\chi}_{1,2}^0 \mu^\pm$ ,  $\tilde{\chi}_1^\pm \mu^\mp$  and  $\tilde{\chi}_1^\pm \nu_\mu$  productions) and the Standard Model background.

We expect that, as in the three lepton signature analysis, interesting sensitivities could be obtained on other  $\lambda'_{2jk}$  coupling constants.

The sensitivities obtained on the  $\lambda'_{3jk}$  couplings from the like sign dilepton signature analysis should be weaker than the sensitivities on the  $\lambda'_{2jk}$  couplings deduced from the same study. Indeed, in the case of a single dominant  $\lambda'_{3jk}$  coupling the same sign leptons generated by the  $\tilde{\chi}_1^0 \tau^\pm$  production would be 2 tau leptons (see Fig.1(d) and Section 5.1). Therefore, the like sign dileptons ( $e^\pm e^\pm$  or  $\mu^\pm \mu^\pm$ ) produced by the  $\mathcal{R}_p$  signal would be mainly generated in tau decays and would thus have higher probabilities to not pass the

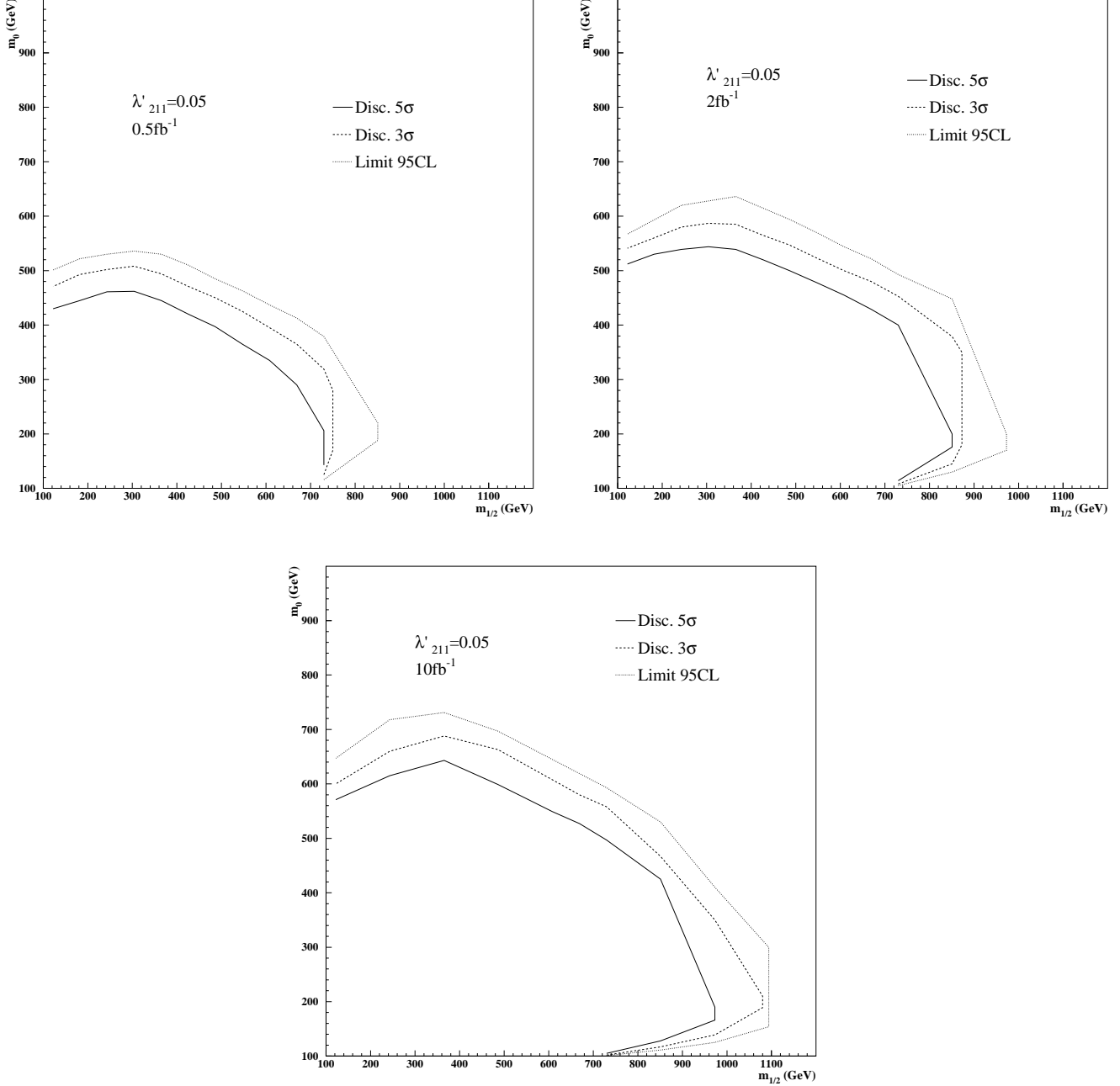


FIG. 24: Discovery contours at  $5\sigma$  (full line),  $3\sigma$  (dashed line) and limit at 95%  $C.L.$  (dotted line) obtained from the like sign dilepton signature analysis at Tevatron Run II assuming a center of mass energy of  $\sqrt{s} = 2TeV$ . These discovery potentials are presented in the plane  $m_0$  versus  $m_{1/2}$ , for  $sign(\mu) < 0$ ,  $\tan\beta = 1.5$ ,  $\lambda'_{211} = 0.05$  and different values of luminosity.

analysis cuts on the particle energy. Moreover, the requirement of  $e^\pm e^\pm$  or  $\mu^\pm \mu^\pm$  events would decrease the efficiency after cuts of the  $\mathcal{R}_p$  signal due to the hadronic decay of the tau. Finally, the selection of two same flavour like sign dileptons ( $e^\pm e^\pm$  or  $\mu^\pm \mu^\pm$ ) would reduce the  $\mathcal{R}_p$  signal, since each of the 2 produced taus could decay either into an electron



or a muon, and hence would not be an effective cut anymore.

The sensitivities obtained on the  $\lambda'_{1jk}$  couplings from the like sign dilepton signature study are expected to be identical to the sensitivities on the  $\lambda'_{2jk}$  couplings obtained from the same study. Indeed, in the case of a single dominant  $\lambda'_{1jk}$  coupling constant, the only difference in the like sign dilepton signature analysis would be that  $e^\pm e^\pm$  events should be selected instead of  $\mu^\pm \mu^\pm$  events (see Fig.1(d) and Section 5.1). Nevertheless, a smaller number of  $\lambda'_{1jk}$  couplings is expected to be probed since the low-energy constraints on the  $\lambda'_{1jk}$  couplings are generally stronger than the limits on the  $\lambda'_{2jk}$  couplings [4].

In the high  $\tan\beta$  case, the lightest stau  $\tilde{\tau}_1$  can become the LSP instead of the lightest neutralino, due to a large mixing in the third generation of charged sleptons. In such a situation, the dominant decay channel of the lightest neutralino is  $\tilde{\chi}_1^0 \rightarrow \tilde{\tau}_1^\pm \tau^\mp$ . Two scenarios must then be discussed : if the single dominant  $\mathcal{R}_p$  coupling is not of the type  $\lambda'_{3jk}$ , the  $\tilde{\tau}_1^\pm$ -LSP is a stable particle so that the reaction  $p\bar{p} \rightarrow \tilde{\chi}_1^0 l_i^\pm$ , representing the main contribution to the like sign dilepton final state, does not often lead to the  $2\mu^\pm + 2 jets$  signature. If the single dominant  $\mathcal{R}_p$  coupling is of the type  $\lambda'_{3jk}$ , the  $\tilde{\chi}_1^0 \tau^\pm$  production can receive a contribution from the resonant  $\tilde{\tau}_2^\pm$  production (see Fig.1(d)) and the  $\tilde{\tau}_1^\pm$ -LSP decays via  $\lambda'_{3jk}$  as  $\tilde{\tau}_1^\pm \rightarrow u_j d_k$  so that the  $2\mu^\pm + 2 jets$  signature can still be generated in a significant way by the  $p\bar{p} \rightarrow \tilde{\chi}_1^0 \tau^\pm$  reaction.

We end this Section by some comments on the effect of the supersymmetric  $\mathcal{R}_p$  conserving background to the like sign dilepton signature. In order to illustrate this discussion, we consider the results on the  $\lambda'_{211}$  coupling constant.

We see from Table 9 that the SUSY background to the like sign dilepton final state can affect the sensitivity on the  $\lambda'_{211}$  coupling constant obtained by considering only the Standard Model background, which is shown in Fig.24, only in the region of small superpartners masses, namely in the domain  $m_{1/2} \lesssim 300 GeV$  for  $\tan\beta = 1.5$ ,  $sign(\mu) < 0$  and assuming a luminosity of  $\mathcal{L} = 1 fb^{-1}$ .

In contrast with the SUSY signal amplitude which is increased if  $\lambda'_{211}$  is enhanced, the SUSY background amplitude is typically independent on the value of the  $\lambda'_{211}$  coupling constant since the superpartner pair production does not involve  $\mathcal{R}_p$  couplings. Therefore, even if we consider the SUSY background in addition to the Standard Model one, it is still true that large values of the  $\lambda'_{211}$  coupling can be probed over a wider domain of the SUSY parameter space than low values, as can be observed in Fig.24 for  $m_{1/2} \gtrsim 300 GeV$ . Note that in Fig.24 larger values of  $\lambda'_{211}$  still respecting the indirect limit could have been considered.

Finally, we mention that further cuts, as for instance some cuts based on the superpartners mass reconstructions (see Section 5.5), could allow to reduce the SUSY background to the like sign dilepton signature.

## Mass reconstructions

The  $\tilde{\chi}_1^0$  and  $\tilde{l}_L^\pm$  mass reconstructions can be performed in a model independent way via the like sign dilepton analysis. We have simulated these mass reconstructions based on the like sign dimuon events generated in the scenario of a single dominant  $\lambda'_{2jk}$  coupling constant. In this scenario, the main SUSY contribution to the like sign dilepton signature, namely the  $\tilde{\chi}_1^0 \mu^\pm$  production, has the final state  $\mu^\pm + \mu^\pm + 2jets$  (see Section 5.1). Indeed, the produced  $\tilde{\chi}_1^0$  decays into  $\mu^\pm u_j d_k$  through  $\lambda'_{2jk}$ . The muon generated together with the

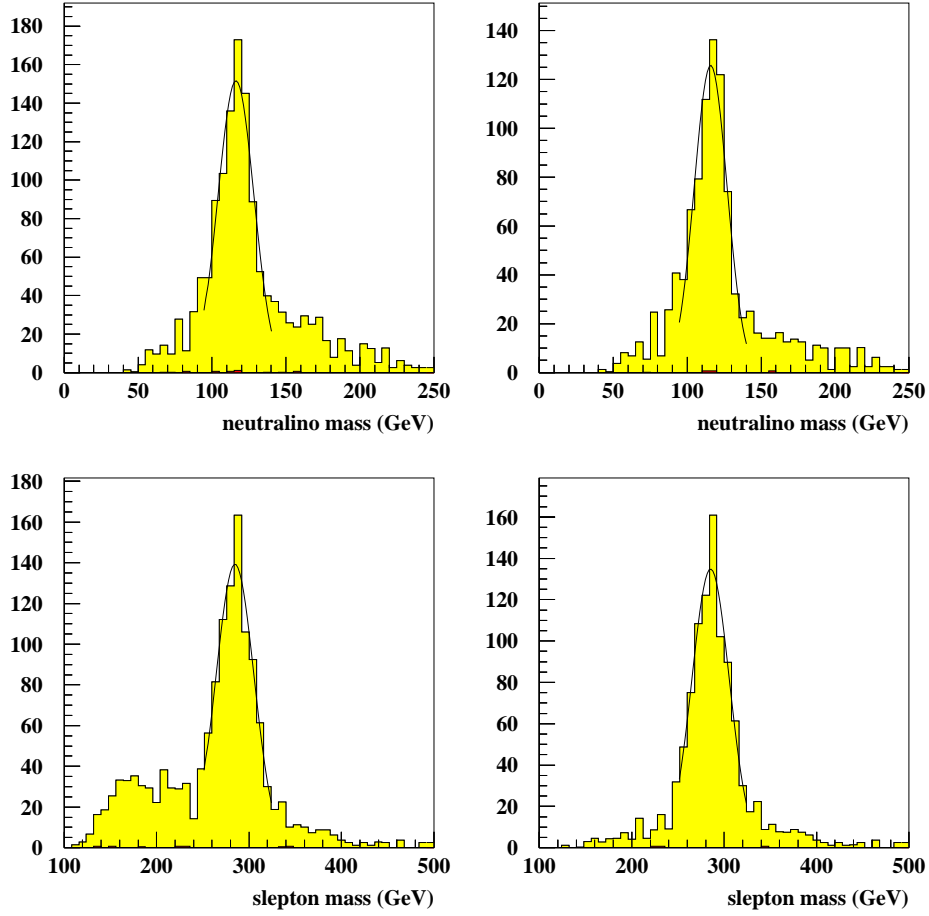


FIG. 25: Distributions of the *softer*  $\mu^\pm + 2 \text{ leading jets}$  (upper plots) and  $\mu^\pm + \mu^\pm + 2 \text{ leading jets}$  (lower plots) invariant masses in the  $\mu^\pm + \mu^\pm + jets + \cancel{E}$  events generated by the SUSY signal ( $\tilde{\chi}_{1,2}^0 \mu^\pm$ ,  $\tilde{\chi}_1^\pm \mu^\mp$  and  $\tilde{\chi}_1^\pm \nu_\mu$  productions), for a luminosity of  $\mathcal{L} = 10 fb^{-1}$ . The 2 right plots are obtained by applying a cut in the upper left plot of Fig.20 selecting only the peak associated to the  $\tilde{\chi}_1^0 \mu^\pm$  production. The mSUGRA point taken for this figure is,  $m_0 = 200 GeV$ ,  $M_2 = 250 GeV$ ,  $\tan \beta = 1.5$  and  $sign(\mu) < 0$  ( $m_{\tilde{\chi}_1^0} = 127.1 GeV$ ,  $m_{\tilde{\mu}_L^\pm} = 298.0 GeV$ ) and the considered  $\mathcal{R}_p$  coupling is  $\lambda'_{211} = 0.05$ . The average reconstructed masses are  $m_{\tilde{\chi}_1^0} = 116 \pm 11 GeV$  and  $m_{\tilde{\mu}_L^\pm} = 285 \pm 20 GeV$ .

$\tilde{\chi}_1^0$  can be identified as the leading muon for relatively large  $m_{\tilde{\mu}_L^\pm} - m_{\tilde{\chi}_1^0}$  mass differences (see Section 5.4). Note that for nearly degenerate values of  $m_{\tilde{\mu}_L^\pm}$  and  $m_{\tilde{\chi}_1^0}$  the  $\tilde{\chi}_1^0 \mu^\pm$  production rate and thus the sensitivity on the SUSY parameters would be reduced (see Section 3.1). The muon created in the  $\tilde{\chi}_1^0$  decay can thus be identified as the softer muon so that the  $\tilde{\chi}_1^0$  can be reconstructed from the the softer muon and the 2 jets present in the  $\tilde{\chi}_1^0 \mu^\pm$  production final state. The other contributions to the like sign dimuons events can lead to some missing energy and at most 4 jets in the final state (see Section 5.1). Hence, we have

chosen to reconstruct the  $\tilde{\chi}_1^0$  from the 2 leading jets when the final state contains more than 2 jets. Once the  $\tilde{\chi}_1^0$  has been reconstructed, the  $\tilde{\mu}_L^\pm$  has been reconstructed from the  $\tilde{\chi}_1^0$  and the leading muon since the dominant contribution to the  $\tilde{\chi}_1^0\mu^\pm$  production is the reaction  $p\bar{p} \rightarrow \tilde{\mu}_L^\pm \rightarrow \tilde{\chi}_1^0\mu^\pm$ . These mass reconstructions are represented in Fig.25. In this figure, we also represent the same mass reconstructions obtained by applying a cut in the upper left plot of Fig.20 excluding the peak associated to the  $\tilde{\chi}_2^0\mu^\pm$  and  $\tilde{\chi}_1^\pm\mu^\mp$  productions (see Section 5.4). The interest of this cut, as can be seen in Fig.25, is to select the  $\tilde{\chi}_1^0\mu^\pm$  production and thus to improve the accuracy on the  $\tilde{\chi}_1^0$  and  $\tilde{\mu}_L^\pm$  reconstructions which are based on this production. We observe in Fig.25 that the  $\tilde{\chi}_1^0$  reconstruction has less combinatorial background than the  $\tilde{\mu}_L^\pm$  reconstruction. This comes from the fact that the selection of the softer muon and the 2 leading jets allows to reconstruct the  $\tilde{\chi}_1^0$  even in the dimuon events generated by the  $\tilde{\chi}_2^0\mu^\pm$  and  $\tilde{\chi}_1^\pm\mu^\mp$  productions, while the selection of the 2 muons and the 2 leading jets does not allow to reconstruct the  $\tilde{\mu}_L^\pm$  in the dimuon events generated by the  $\tilde{\chi}_2^0\mu^\pm$  and  $\tilde{\chi}_1^\pm\mu^\mp$  productions (see Section 5.1). We have represented on the plots of Fig.25 the fits of the invariant mass distributions. We see from these fits that the distributions are well peaked around the  $\tilde{\chi}_1^0$  and  $\tilde{\mu}_L^\pm$  generated masses. The average reconstructed masses are  $m_{\tilde{\chi}_1^0} = 116 \pm 11 GeV$  and  $m_{\tilde{\mu}_L^\pm} = 285 \pm 20 GeV$ .

We note that the accuracy on the  $\tilde{\chi}_1^0$  (and thus on the  $\tilde{\mu}_L^\pm$ ) mass reconstruction could be improved if the distributions in the upper plots of Fig.25 were recalculated by selecting the muon giving the  $\tilde{\chi}_1^0$  mass the closer to the mean value of the peak obtained in the relevant upper plot of Fig.25.

In the hypothesis of a single dominant coupling constant of type  $\lambda'_{1jk}$  or  $\lambda'_{3jk}$ , exactly the same kind of  $\tilde{\chi}_1^0$  and  $\tilde{\mu}_L^\pm$  mass reconstructions can be performed by selecting the  $e^\pm + e^\pm + jets + \cancel{E}$  or  $l_i^\pm + l_j^\pm + jets + \cancel{E}$  events, respectively.

As a conclusion, the  $\tilde{\chi}_1^0$  and  $\tilde{\mu}_L^\pm$  mass reconstructions based on the like sign dilepton signature generated by the  $\tilde{\chi}_{1,2}^0\mu^\pm$ ,  $\tilde{\chi}_1^\pm\mu^\mp$  and  $\tilde{\chi}_1^\pm\nu_\mu$  productions at Tevatron can easily give precise results, in contrast with the mass reconstructions performed in the super-partner pair production analysis at hadronic colliders which suffer an high combinatorial background [44].

## Model dependence of the results

In our theoretical framework (see Section 2), the values of the  $|\mu|$  and  $\tan\beta$  (up to the ambiguity of low/high solution) parameters are predicted. This has no important effects on the results presented in Sections 5.5 as the single gaugino production cross sections vary weakly with these parameters (see Section 3.1).

However, since we have worked within the mSUGRA model, the  $\tilde{l}_L^\pm$  mass was typically larger than the  $\tilde{\chi}_1^0$  mass. In a situation where  $m_{\tilde{l}_L^\pm}$  would approach  $m_{\tilde{\chi}_1^0}$ , the rate of the  $\tilde{\chi}_1^0\tilde{l}_i^\pm$  production, representing in mSUGRA the main contribution to the like sign dilepton signature (see Section 5.1), would decrease. Therefore, within a model allowing degenerate  $\tilde{l}_L^\pm$  and  $\tilde{\chi}_1^0$  masses or even a  $\tilde{l}_L^\pm$  lighter than the  $\tilde{\chi}_1^0$ , other single gaugino productions than the  $p\bar{p} \rightarrow \tilde{\chi}_1^0\tilde{l}_i^\pm$  reaction could represent the major contribution to the like sign dilepton signature in some parts of the SUSY parameter space.

Besides, in a situation where the LSP would not be the  $\tilde{\chi}_1^0$ , the branching ratios of the  $\tilde{\chi}_1^0$  decays violating  $R_p$  would be reduced with respect to the case where the LSP is the  $\tilde{\chi}_1^0$ , as often occurs in mSUGRA. However, in such a situation, the like sign dilepton

signature could receive a significant contribution from a decay of the  $\tilde{\chi}_1^0$  different from the  $\mathcal{R}_p$  channel. In those kinds of scenarios where the LSP is not the  $\tilde{\chi}_1^0$ , the  $\tilde{\chi}_1^0 l_i^\pm$  production would not represent systematically the main contribution to the like sign dilepton signature.

In the several scenarios described above where the  $\tilde{\chi}_1^0 l_i^\pm$  production is not the major contribution to the like sign dilepton signature, this signature could receive quite important contribution from the other single gaugino productions described in Section 3.1.

## 6 Conclusion

The single gaugino productions at Tevatron reach important cross sections thanks to the contributions of the resonant slepton productions. Hence, the analysis of the 3 charged leptons and like sign dilepton signatures generated by the single gaugino productions at Tevatron Run II would allow to obtain high sensitivities on many  $\mathcal{R}_p$  coupling constants, compared to the low-energy limits, in wide domains of the SUSY parameter space. This is also due to the fact that the Standard Model backgrounds associated to the 3 charged leptons and like sign dilepton final states at Tevatron can be greatly suppressed.

From the supersymmetry discovery point of view, superpartner masses well beyond the present experimental limits could be tested through the analysis of the the 3 charged leptons and like sign dilepton signatures generated by the single gaugino productions at Tevatron Run II. If some of the  $\mathcal{R}_p$  coupling constants values were close to their low-energy bounds, the single gaugino productions study based on the 3 charged leptons and like sign dilepton signatures would even allow to extend the region in the  $m_0$ - $m_{1/2}$  plane probed by the superpartner pair production analyses in the 3 charged leptons and like sign dilepton channels at Tevatron Run II. The reason is that the single superpartner production has a larger phase space factor than the superpartner pair production. Besides, the 3 charged leptons and like sign dilepton signatures generated by the single gaugino productions at Tevatron Run II would allow to reconstruct in a model independent way the  $\tilde{\chi}_1^0$ ,  $\tilde{\chi}_1^\pm$ ,  $\tilde{\nu}_L$  and  $\tilde{l}_L^\pm$  masses with a smaller combinatorial background than in the superpartner pair production analysis.

We end this summary by a comparison between the results obtained from the studies of the 3 charged lepton and like sign dilepton signatures generated by the single gaugino productions at Tevatron Run II. In the mSUGRA model, the like sign dilepton signature analysis would give rise to higher sensitivities on the SUSY parameters than the study of the 3 charged lepton final state. This comes notably from the fact that in mSUGRA, the  $\tilde{\chi}_1^0$  is lighter than the  $\tilde{\chi}_1^\pm$  so that the cross section of the  $\tilde{\chi}_1^0 l^\pm$  production, which is the main contribution to the like sign dilepton signature, reaches larger values than the cross section of the  $\tilde{\chi}_1^\pm l^\mp$  production, representing the main contribution to the 3 charged lepton final state.

Other interesting prospective studies concerning hadronic colliders are the analyses of the single gaugino productions occurring through resonant squark productions via  $\lambda''$  coupling constants which we will perform in the next future.

## 7 Acknowledgments

We would like to thank Emmanuelle Perez, Robi Peschanski and Auguste Besson for fruitful discussions and reading the manuscript.

# 1 Formulas for spin summed amplitudes

In this Appendix, we give the amplitudes for all the single productions of supersymmetric particle at hadronic colliders, which can receive a contribution from a slepton resonant production. These single productions occur via the  $\mathcal{R}_p$  coupling  $\lambda'_{ijk}$  and correspond to the four reactions,  $q\bar{q} \rightarrow \tilde{\chi}_a^+ \bar{\nu}_i$ ,  $q\bar{q} \rightarrow \tilde{\chi}_a^0 \bar{\nu}_i$ ,  $q\bar{q} \rightarrow \tilde{\chi}_a^0 \bar{l}_i$ ,  $q\bar{q} \rightarrow \tilde{\chi}_a^- \bar{l}_i$ . Each of those four processes receives contributions from both the t and u channel (see Fig.1) and have charge conjugated diagrams. Note also that the contributions coming from the exchange of a right squark in the u channel involve the higgsino components of the gauginos. These contributions, in the case of the single chargino production, do not interfere with the s channel slepton exchange since the initial or final states are different (see Fig.1). In the following, we give the formulas for the probability amplitudes, squared and summed over the polarizations. Our notations closely follow the notations of [52]. In particular, the matrix elements  $N'_{ij}$  are defined in the basis of the photino and the zino, as in [52].

$$\begin{aligned}
& |M_s(u^j \bar{d}^k \rightarrow \tilde{\chi}_a^+ \bar{\nu}_i)|^2 = \\
& \frac{\lambda'_{ijk}{}^2 g^2 |U_{a1}|^2}{12(s - m_{\tilde{l}_L}^2)^2} (m_{u^j}^2 + m_{d^k}^2 - s)(m_{\tilde{\chi}_a^+}^2 - s) \\
& |M_t(u^j \bar{d}^k \rightarrow \tilde{\chi}_a^+ \bar{\nu}_i)|^2 = \\
& \frac{\lambda'_{ijk}{}^2 g^2}{12(t - m_{\tilde{d}_L}^2)^2} (m_{d^k}^2 - t) \left[ (|U_{a1}|^2 + \frac{m_{u^j}^2 |V_{a2}|^2}{2m_W^2 \sin^2 \beta}) (m_{u^j}^2 + m_{\tilde{\chi}_a^+}^2 - t) \right. \\
& \left. - \frac{4m_{u^j}^2 m_{\tilde{\chi}_a^+} Re(U_{a1} V_{a2})}{\sqrt{2}m_W \sin \beta} \right] \\
& |M_u(u^k \bar{d}^j \rightarrow \tilde{\chi}_a^+ \nu_i)|^2 = \\
& \frac{\lambda'_{ijk}{}^2 g^2 m_{d^k}^2 |U_{a2}|^2}{24m_W^2 \cos^2 \beta^2 (u - m_{\tilde{d}_R}^2)^2} (m_{\tilde{\chi}_a^+}^2 + m_{u^k}^2 - u)(m_{d^j}^2 - u) \\
& 2Re[M_s M_t^* (\tilde{\chi}_a^+ \bar{\nu}_i)] = \\
& \frac{\lambda'_{ijk}{}^2 g^2}{6(s - m_{\tilde{l}_L}^2)(t - m_{\tilde{d}_L}^2)} \left[ \frac{|U_{a1}|^2}{2} [(m_{u^j}^2 + m_{\tilde{\chi}_a^+}^2 - t)(m_{d^k}^2 - t) \right. \\
& + (m_{u^j}^2 + m_{d^k}^2 - s)(m_{\tilde{\chi}_a^+}^2 - s) - (m_{u^j}^2 - u)(m_{\tilde{\chi}_a^+}^2 + m_{d^k}^2 - u)] \\
& \left. - (m_{d^k}^2 - t) \frac{Re(U_{a1} V_{a2}) m_{\tilde{\chi}_a^+} m_{u^j}^2}{\sqrt{2}m_W \sin \beta} \right], \tag{1.1}
\end{aligned}$$

where,  $s = (p(u^j) - p(\bar{d}_k))^2$ ,  $t = (p(u^j) - p(\tilde{\chi}_a^+))^2$  and  $u = (p(\bar{d}^j) - p(\nu_i))^2$ .

$$\begin{aligned}
& |M_s(d_j \bar{d}_k \rightarrow \tilde{\chi}_a^0 \bar{\nu}_i)|^2 = \\
& \frac{\lambda'_{ijk}{}^2 g^2 |N'_{a2}|^2}{24 \cos^2 \theta_W (s - m_{\tilde{\nu}_L}^2)^2} (s - m_{d^k}^2 - m_{d^j}^2)(s - m_{\tilde{\chi}_a^0}^2)
\end{aligned}$$

$$\begin{aligned}
& |M_t(d_j \bar{d}_k \rightarrow \tilde{\chi}_a^0 \bar{\nu}_i)|^2 = \\
& \frac{\lambda'_{ijk}{}^2 g^2}{6(t - m_{\tilde{d}_L}^2)^2} (m_{d^k}^2 - t) \left[ (m_{d^j}^2 + m_{\tilde{\chi}_a^0}^2 - t) \left( \frac{g^2 m_{d^j}^2 |N'_{a3}|^2}{4m_W^2 \cos^2 \beta} + \frac{e^2 |N'_{a1}|^2}{9} \right. \right. \\
& + \frac{g^2 |N'_{a2}|^2 (\sin^2 \theta_W / 3 - 1/2)^2}{\cos^2 \theta_W} - \frac{2eg \operatorname{Re}(N'_{a1} N'_{a2}) (\sin^2 \theta_W / 3 - 1/2)}{3 \cos \theta_W} \Big) \\
& + \left. \frac{2m_{\tilde{\chi}_a^0} m_{d^j}^2 g}{m_W \cos \beta} \left( -\frac{e \operatorname{Re}(N'_{a1} N'_{a3})}{3} + \frac{g \operatorname{Re}(N'_{a2} N'_{a3})}{\cos \theta_W} \left( \frac{\sin^2 \theta_W}{3} - \frac{1}{2} \right) \right) \right]
\end{aligned}$$

$$\begin{aligned}
& |M_u(d_j \bar{d}_k \rightarrow \tilde{\chi}_a^0 \bar{\nu}_i)|^2 = \\
& \frac{\lambda'_{ijk}{}^2}{6(u - m_{\tilde{d}_R}^2)^2} (m_{d^j}^2 - u) \left[ (m_{\tilde{\chi}_a^0}^2 + m_{d^k}^2 - u) \left( \frac{g^2 m_{d^k}^2 |N'_{a3}|^2}{4m_W^2 \cos^2 \beta} + \frac{e^2 |N'_{a1}|^2}{9} \right. \right. \\
& + \frac{g^2 \sin^4 \theta_W |N'_{a2}|^2}{9 \cos^2 \theta_W} - \frac{2eg \operatorname{Re}(N'_{a1} N'_{a2}) \sin^2 \theta_W}{9 \cos \theta_W} \Big) \\
& - \left. \frac{2m_{\tilde{\chi}_a^0} m_{d^k}^2 g}{m_W \cos \beta} \left( -\frac{e \operatorname{Re}(N'_{a1} N'_{a3})}{3} + \frac{g \sin^2 \theta_W \operatorname{Re}(N'_{a2} N'_{a3})}{3 \cos \theta_W} \right) \right]
\end{aligned}$$

$$\begin{aligned}
& 2\operatorname{Re}[M_s M_t^*(\tilde{\chi}_a^0 \bar{\nu}_i)] = \\
& -\frac{\lambda'_{ijk}{}^2 g}{12 \cos \theta_W (s - m_{\tilde{\nu}_L}^2)(t - m_{\tilde{d}_L}^2)} \left[ (m_{d^k}^2 - t) \frac{m_{\tilde{\chi}_a^0} m_{d^j}^2 g \operatorname{Re}(N'_{a2} N'_{a3})}{m_W \cos \beta} \right. \\
& + \left( -\frac{e \operatorname{Re}(N'_{a1} N'_{a2})}{3} + \frac{g |N'_{a2}|^2}{\cos \theta_W} \left( \frac{\sin^2 \theta_W}{3} - \frac{1}{2} \right) \right) [(m_{d^j}^2 + m_{\tilde{\chi}_a^0}^2 - t)(m_{d^k}^2 - t) \\
& + (m_{d^j}^2 + m_{d^k}^2 - s)(m_{\tilde{\chi}_a^0}^2 - s) - (m_{\tilde{\chi}_a^0}^2 + m_{d^k}^2 - u)(m_{d^j}^2 - u)] \Big]
\end{aligned}$$

$$\begin{aligned}
& 2\operatorname{Re}[M_t M_u^*(\tilde{\chi}_a^0 \bar{\nu}_i)] = \\
& \frac{\lambda'_{ijk}{}^2}{6(u - m_{\tilde{d}_R}^2)(t - m_{\tilde{d}_L}^2)} \left[ (m_{d^k}^2 - t) \frac{gm_{\tilde{\chi}_a^0} m_{d^j}^2}{m_W \cos \beta} \left( \frac{g \sin^2 \theta_W \operatorname{Re}(N'_{a2} N'_{a3})}{3 \cos \theta_W} - \frac{e \operatorname{Re}(N'_{a1} N'_{a3})}{3} \right) \right. \\
& + [(m_{d^j}^2 - u)(m_{\tilde{\chi}_a^0}^2 + m_{d^k}^2 - u) + (m_{d^k}^2 - t)(m_{d^j}^2 + m_{\tilde{\chi}_a^0}^2 - t) - (m_{\tilde{\chi}_a^0}^2 - s)(m_{d^j}^2 + m_{d^k}^2 - s)] \\
& \left( -\frac{eg \operatorname{Re}(N'_{a1} N'_{a2})}{3 \cos \theta_W} \left( \frac{2 \sin^2 \theta_W}{3} - \frac{1}{2} \right) + \frac{e^2 |N'_{a1}|^2}{9} + \frac{g^2 \sin^2 \theta_W |N'_{a2}|^2}{3 \cos^2 \theta_W} \left( \frac{\sin^2 \theta_W}{3} - \frac{1}{2} \right) \right) \\
& - \frac{m_{\tilde{\chi}_a^0} m_{d^k}^2 g}{m_W \cos \beta} \left( -\frac{e \operatorname{Re}(N'_{a1} N'_{a3})}{3} + \frac{g \operatorname{Re}(N'_{a2} N'_{a3})}{\cos \theta_W} \left( \frac{\sin^2 \theta_W}{3} - \frac{1}{2} \right) \right) (m_{d^j}^2 - u) \\
& + \left. \frac{m_{d^j}^2 m_{d^k}^2 g^2 |N'_{a3}|^2}{2m_W^2 \cos^2 \beta} (m_{\tilde{\chi}_a^0}^2 - s) \right]
\end{aligned}$$

$$\begin{aligned}
& 2\operatorname{Re}[M_s M_u^*(\tilde{\chi}_a^0 \bar{\nu}_i)] = \\
& \frac{\lambda'_{ijk}{}^2 g}{12 \cos \theta_W (s - m_{\tilde{\nu}_L}^2)(u - m_{\tilde{d}_R}^2)} \left[ -\frac{m_{\tilde{\chi}_a^0} m_{d^k}^2 g \operatorname{Re}(N'_{a2} N'_{a3})}{m_W \cos \beta} (m_{d^j}^2 - u) \right. \\
& + \left( -\frac{e \operatorname{Re}(N'_{a1} N'_{a2})}{3} + \frac{|N'_{a2}|^2 g \sin^2 \theta_W}{3 \cos \theta_W} \right) [(m_{d^j}^2 + m_{d^k}^2 - s)(m_{\tilde{\chi}_a^0}^2 - s)
\end{aligned}$$

$$+ (m_{\tilde{\chi}_a^0}^2 + m_{d^k}^2 - u)(m_{d^j}^2 - u) - (m_{d^j}^2 + m_{\tilde{\chi}_a^0}^2 - t)(m_{d^k}^2 - t)] \Big], \quad (1.2)$$

where,  $s = (p(d^j) - p(\bar{d}_k))^2$ ,  $t = (p(d^j) - p(\tilde{\chi}_a^0))^2$  and  $u = (p(d^j) - p(\bar{\nu}_i))^2$ .

$$\begin{aligned} |M_s(u_j \bar{d}_k \rightarrow \tilde{\chi}_a^0 \bar{l}_i)|^2 = & \frac{\lambda'_{ijk}}{6(s - m_{\tilde{l}_L}^2)^2} (s - m_{u^j}^2 - m_{d^k}^2) \left[ \left( \frac{g^2 m_{l_i}^2 |N'_{a3}|^2}{4m_W^2 \cos^2 \beta} + e^2 |N'_{a1}|^2 + \frac{g^2 |N'_{a2}|^2}{\cos^2 \theta_W} (\sin^2 \theta_W - \frac{1}{2})^2 \right. \right. \\ & - \left. \frac{2eg \operatorname{Re}(N'_{a1} N'_{a2})}{\cos \theta_W} (\sin^2 \theta_W - \frac{1}{2}) \right) (s - m_{l_i}^2 - m_{\tilde{\chi}_a^0}^2) - \frac{2gm_{\tilde{\chi}_a^0} m_{l_i}^2}{m_W \cos \beta} \left( -e \operatorname{Re}(N'_{a1} N'_{a3}) \right. \\ & \left. \left. + \frac{g \operatorname{Re}(N'_{a2} N'_{a3})}{\cos \theta_W} (\sin^2 \theta_W - \frac{1}{2}) \right) \right] \end{aligned}$$

$$\begin{aligned} |M_t(u_j \bar{d}_k \rightarrow \tilde{\chi}_a^0 \bar{l}_i)|^2 = & \frac{\lambda'_{ijk}}{6(t - m_{\tilde{u}_L}^2)^2} (-t + m_{l_i}^2 + m_{d^k}^2) \left[ \left( \frac{g^2 m_{u^j}^2 |N'_{a4}|^2}{4m_W^2 \sin^2 \beta} + \frac{4e^2 |N'_{a1}|^2}{9} \right. \right. \\ & + \left. \frac{g^2 |N'_{a2}|^2}{\cos^2 \theta_W} \left( \frac{1}{2} - \frac{2 \sin^2 \theta_W}{3} \right)^2 + \frac{4eg \operatorname{Re}(N'_{a1} N'_{a2})}{3 \cos \theta_W} \left( \frac{1}{2} - \frac{2 \sin^2 \theta_W}{3} \right) \right) (-t + m_{u^j}^2 + m_{\tilde{\chi}_a^0}^2) \\ & \left. + \frac{2gm_{u^j} m_{\tilde{\chi}_a^0}}{m_W \sin \beta} \left( \frac{2e \operatorname{Re}(N'_{a1} N'_{a4})}{3} + \frac{g \operatorname{Re}(N'_{a2} N'_{a4})}{\cos \theta_W} \left( \frac{1}{2} - \frac{2 \sin^2 \theta_W}{3} \right) \right) \right] \end{aligned}$$

$$\begin{aligned} |M_u(u_j \bar{d}_k \rightarrow \tilde{\chi}_a^0 \bar{l}_i)|^2 = & \frac{\lambda'_{ijk}}{6(u - m_{\tilde{d}_R}^2)^2} (m_{u^j}^2 + m_{l_i}^2 - u) \left[ \left( \frac{e^2 |N'_{a1}|^2}{9} + \frac{g^2 \sin^4 \theta_W |N'_{a2}|^2}{9 \cos^2 \theta_W} - \frac{2eg \operatorname{Re}(N'_{a1} N'_{a2}) \sin^2 \theta_W}{9 \cos \theta_W} \right. \right. \\ & + \left. \frac{g^2 m_{d^k}^2 |N'_{a3}|^2}{4m_W^2 \cos^2 \beta} \right) (m_{\tilde{\chi}_a^0}^2 + m_{d^k}^2 - u) - \frac{2gm_{d^k} m_{\tilde{\chi}_a^0}}{m_W \cos \beta} \left( -\frac{e \operatorname{Re}(N'_{a1} N'_{a3})}{3} \right. \\ & \left. \left. + \frac{g \sin^2 \theta_W \operatorname{Re}(N'_{a2} N'_{a3})}{3 \cos \theta_W} \right) \right] \end{aligned}$$

$$\begin{aligned} 2\operatorname{Re}[M_s M_t^*(\tilde{\chi}_a^0 \bar{l}_i)] = & -\frac{\lambda'_{ijk}}{6(s - m_{\tilde{l}_L}^2)(t - m_{\tilde{u}_L}^2)} \left[ -\frac{m_{l_i}^2 m_{u^j}^2 g^2 \operatorname{Re}(N'_{a3} N_{a4}^*)}{2m_W^2 \sin \beta \cos \beta} (m_{\tilde{\chi}_a^0}^2 + m_{d^k}^2 - u) \right. \\ & + \left( \frac{-2e^2 |N'_{a1}|^2}{3} + \frac{eg \operatorname{Re}(N'_{a1} N'_{a2})}{3 \cos \theta_W} (4 \sin^2 \theta_W - \frac{5}{2}) \right. \\ & + \left. \frac{g^2 |N'_{a2}|^2}{\cos^2 \theta_W} \left( \frac{1}{2} - \frac{2 \sin^2 \theta_W}{3} \right) (\sin^2 \theta_W - \frac{1}{2}) \right) \\ & [ (m_{u^j}^2 + m_{d^k}^2 - s)(m_{\tilde{\chi}_a^0}^2 + m_{l_i}^2 - s) + (m_{u^j}^2 + m_{\tilde{\chi}_a^0}^2 - t)(m_{l_i}^2 + m_{d^k}^2 - t) \\ & - (m_{u^j}^2 + m_{l_i}^2 - u)(m_{\tilde{\chi}_a^0}^2 + m_{d^k}^2 - u) ] + \frac{gm_{u^j} m_{\tilde{\chi}_a^0}}{m_W \sin \beta} \left( -e \operatorname{Re}(N'_{a1} N'_{a4}) + \frac{g \operatorname{Re}(N'_{a2} N'_{a4})}{\cos \theta_W} \right. \\ & \left. (\sin^2 \theta_W - \frac{1}{2}) \right) (m_{l_i}^2 + m_{d^k}^2 - t) - (s - m_{u^j}^2 - m_{d^k}^2) \frac{gm_{l_i}^2 m_{\tilde{\chi}_a^0}}{m_W \cos \beta} \left( \frac{2e \operatorname{Re}(N'_{a1} N'_{a3})}{3} \right. \\ & \left. \left. + \frac{g \operatorname{Re}(N'_{a2} N'_{a3})}{\cos \theta_W} \left( \frac{1}{2} - \frac{2 \sin^2 \theta_W}{3} \right) \right) \right] \end{aligned}$$



$$\begin{aligned}
2\text{Re}[M_t M_u^* (\tilde{\chi}_a^0 \bar{l}_i)] = & \frac{\lambda'_{ijk}{}^2}{6(u - m_{\tilde{d}_R}^2)(t - m_{\tilde{u}_L}^2)} \left[ \frac{gm_{u^j}^2 m_{\tilde{\chi}_a^0}}{m_W \sin \beta} (m_{l^i}^2 + m_{d^k}^2 - t) \left( -\frac{e\text{Re}(N'_{a1} N'_{a4})}{3} \right. \right. \\
+ & \left. \frac{g \sin^2 \theta_W \text{Re}(N'_{a2} N'_{a4})}{3 \cos \theta_W} \right) - \frac{m_{\tilde{\chi}_a^0} g m_{d^k}^2}{m_W \cos \beta} \left( \frac{2e\text{Re}(N'_{a1} N'_{a3})}{3} + \frac{g\text{Re}(N'_{a2} N'_{a3})}{\cos \theta_W} \left( \frac{1}{2} - \frac{2 \sin^2 \theta_W}{3} \right) \right) \\
& (m_{l^i}^2 + m_{u^j}^2 - u) - \frac{g^2 \text{Re}(N'_{a3} N_{a4}^*) m_{u^j}^2 m_{d^k}^2}{2m_W^2 \cos \beta \sin \beta} (s - m_{l^i}^2 - m_{\tilde{\chi}_a^0}^2) + \left( -\frac{2e^2 |N'_{a1}|^2}{9} \right. \\
+ & \left. \frac{eg\text{Re}(N_{a1}^* N'_{a2})}{3 \cos \theta_W} \left( -\frac{1}{2} + \frac{4 \sin^2 \theta_W}{3} \right) + \frac{g^2 \sin^2 \theta_W |N'_{a2}|^2}{3 \cos^2 \theta_W} \right. \\
& \left. \left( \frac{1}{2} - \frac{2 \sin^2 \theta_W}{3} \right) \right] [(m_{l^i}^2 + m_{u^j}^2 - u)(m_{\tilde{\chi}_a^0}^2 + m_{d^k}^2 - u) + (m_{l^i}^2 + m_{d^k}^2 - t)(m_{\tilde{\chi}_a^0}^2 + m_{u^j}^2 - t) \\
- & (m_{l^i}^2 + m_{\tilde{\chi}_a^0}^2 - s)(m_{d^k}^2 + m_{u^j}^2 - s)]
\end{aligned}$$

$$\begin{aligned}
2\text{Re}[M_s M_u^* (\tilde{\chi}_a^0 \bar{l}_i)] = & \frac{\lambda'_{ijk}{}^2}{6(s - m_{\tilde{l}_L}^2)(u - m_{\tilde{d}_R}^2)} \left[ -\frac{gm_{l^i}^2 m_{\tilde{\chi}_a^0}}{m_W \cos \beta} \left( -\frac{e\text{Re}(N'_{a1} N'_{a3})}{3} + \frac{g \sin^2 \theta_W \text{Re}(N'_{a2} N'_{a3})}{3 \cos \theta_W} \right) \right. \\
& (s - m_{d^k}^2 - m_{u^j}^2) - \frac{gm_{d^k}^2 m_{\tilde{\chi}_a^0}}{m_W \cos \beta} \left( -e\text{Re}(N'_{a1} N'_{a3}) + \frac{g\text{Re}(N'_{a2} N'_{a3})}{\cos \theta_W} (\sin^2 \theta_W - \frac{1}{2}) \right) \\
& (m_{l^i}^2 + m_{u^j}^2 - u) + \frac{g^2 m_{l^i}^2 m_{d^k}^2 |N'_{a3}|^2}{2m_W^2 \cos^2 \beta} (m_{\tilde{\chi}_a^0}^2 + m_{u^j}^2 - t) + \left( \frac{e^2 |N'_{a1}|^2}{3} \right. \\
- & \left. \frac{eg\text{Re}(N_{a1}^* N'_{a2})}{3 \cos \theta_W} (2 \sin^2 \theta_W - \frac{1}{2}) + \frac{g^2 |N'_{a2}|^2 \sin^2 \theta_W}{3 \cos^2 \theta_W} (\sin^2 \theta_W - \frac{1}{2}) \right) \\
& [(m_{l^i}^2 + m_{u^j}^2 - u)(m_{\tilde{\chi}_a^0}^2 + m_{d^k}^2 - u) - (m_{l^i}^2 + m_{d^k}^2 - t)(m_{\tilde{\chi}_a^0}^2 + m_{u^j}^2 - t) \\
+ & (m_{l^i}^2 + m_{\tilde{\chi}_a^0}^2 - s)(m_{d^k}^2 + m_{u^j}^2 - s)] \Big], \tag{1.3}
\end{aligned}$$

where,  $s = (p(u^j) - p(\bar{d}_k))^2$ ,  $t = (p(u^j) - p(\tilde{\chi}_a^0))^2$  and  $u = (p(u^j) - p(\bar{l}_i))^2$ .

$$\begin{aligned}
|M_s(d_j \bar{d}_k \rightarrow \tilde{\chi}_a^- \bar{l}_i)|^2 = & \frac{g^2 \lambda'_{ijk}{}^2}{6(s - m_{\tilde{\nu}_L^i}^2)^2 (s - m_{d^j}^2 - m_{d^k}^2)} \left[ \left( \frac{m_{l^i}^2 |U_{a2}|^2}{4m_W^2 \cos^2 \beta} + \frac{|V_{a1}|^2}{2} \right) (s - m_{\tilde{\chi}_a^+}^2 - m_{l^i}^2) \right. \\
+ & \left. \frac{\sqrt{2} \text{Re}(V_{a1} U_{a2}) m_{l^i}^2 m_{\tilde{\chi}_a^+}}{m_W \cos \beta} \right]
\end{aligned}$$

$$\begin{aligned}
|M_t(d_j \bar{d}_k \rightarrow \tilde{\chi}_a^- \bar{l}_i)|^2 = & \frac{g^2 \lambda'_{ijk}{}^2}{3(t - m_{\tilde{u}_L^j}^2)^2 (t - m_{d^k}^2 - m_{l^i}^2)} \left[ (t - m_{\tilde{\chi}_a^+}^2 - m_{d^j}^2) \left( \frac{|V_{a1}|^2}{4} + \frac{m_{d^j}^2 |U_{a2}|^2}{8M_W^2 \cos^2 \beta} \right) \right. \\
+ & \left. \frac{\text{Re}(V_{a1} U_{a2}) m_{\tilde{\chi}_a^+} m_{d^j}^2}{\sqrt{2} m_W \cos \beta} \right]
\end{aligned}$$

$$|M_u(\bar{u}_k u_j \rightarrow \tilde{\chi}_a^- \bar{l}_i)|^2 = \frac{g^2 \lambda'_{ijk}{}^2}{24(u - m_{d_R}^2)^2} (m_{\tilde{\chi}_a^+}^2 + m_{u^k}^2 - u)(m_{l^i}^2 + m_{u^j}^2 - u) \frac{|U_{a2}|^2 m_{d^k}^2}{m_W^2 \cos^2 \beta}$$

$$\begin{aligned} 2\text{Re}[M_s M_t^* (\tilde{\chi}_a^- \bar{l}_i)] = & \frac{g^2 \lambda'_{ijk}{}^2}{12(s - m_{\tilde{\nu}_L^i}^2)(t - m_{\tilde{u}_L^j}^2)} \left[ |V_{a1}|^2 [-(m_{l^i}^2 + m_{d^j}^2 - u)(m_{\tilde{\chi}_a^+}^2 + m_{d^k}^2 - u) \right. \\ + & (m_{l^i}^2 + m_{d^k}^2 - t)(m_{\tilde{\chi}_a^+}^2 + m_{d^j}^2 - t) + (m_{l^i}^2 + m_{\tilde{\chi}_a^+}^2 - s)(m_{d^k}^2 + m_{d^j}^2 - s)] \\ + & \frac{\text{Re}(V_{a1} U_{a2}) m_{\tilde{\chi}_a^+} \sqrt{2}}{m_W \cos \beta} [m_{l^i}^2 (s - m_{d^j}^2 - m_{d^k}^2) - m_{d^j}^2 (m_{l^i}^2 + m_{d^k}^2 - t)] \\ - & \left. \frac{|U_{a2}|^2 m_{l^i}^2 m_{d^j}^2}{m_W^2 \cos^2 \beta} (m_{\tilde{\chi}_a^+}^2 + m_{d^k}^2 - u) \right], \end{aligned} \quad (1.4)$$

where,  $s = (p(d^j) - p(\bar{d}_k))^2$ ,  $t = (p(d^j) - p(\tilde{\chi}_a^-))^2$  and  $u = (p(u^j) - p(\bar{l}_i))^2$ .

# References

- [1] S. Dimopoulos and L.J. Hall, Phys. Lett. **B 207**, 210 (1988).
- [2] H. Dreiner and G. G. Ross, Nucl. Phys. **B 365**, 597 (1991).
- [3] H. Dreiner, published in *Perspectives on Supersymmetry*, ed. by G.L. Kane, World Scientific (1998), hep-ph/9707435.
- [4] G. Bhattacharyya, Invited talk presented at ‘Beyond the Desert’, Castle Ringberg, Tegernsee, Germany, 8-14 June 1997; Susy ’96, Nucl. Phys. B (Proc. Suppl.) **52A** 83 (1997).
- [5] R. Barbier et al., Report of the Group on the R-parity Violation, hep-ph/9810232.
- [6] B. C. Allanach, A. Dedes, H. K. Dreiner, Phys. Rev. **D60**, 075014 (1999).
- [7] V. Barger, G. F. Giudice and T. Han, Phys. Rev. **D 40**, 2987 (1989).
- [8] S. Dimopoulos, R. Esmailzadeh, L.J. Hall, J. Merlo and G.D. Starkman, Phys. Rev. **D41**, 2099 (1990).
- [9] P. Binétruy et al., ECFA Large Hadron Collider (LHC) Workshop, Aachen, 1990, Vol. II.
- [10] A. Datta, J. M. Yang, B.-L. Young and X. Zhang, Phys. Rev. **D56**, 3107 (1997).
- [11] R. J. Oakes, K. Whisnant, J. M. Yang, B.-L. Young and X. Zhang, Phys. Rev. **D57**, 534 (1998).
- [12] J. L. Hewett and T. G. Rizzo, “Proceedings of the XXIX International Conference on High Energy Physics”, Vancouver, CA, 23-29 July 1998, hep-ph/9809525.
- [13] B. Allanach et al., ‘Searching for R-Parity Violation at Run-II of Tevatron’, hep-ph/9906224.
- [14] P. Chiappetta, A. Deandrea, E. Nagy, S. Negroni, G. Polesello and J.M. Virey, Phys. Rev. **D61**, 115008 (2000).
- [15] H. Dreiner, P. Richardson, M. H. Seymour, JHEP **0004**, 008 (2000).
- [16] J. Kalinowski, R. Rückl, H. Spiesberger and P. M. Zerwas, Phys. Lett. **B414**, 297 (1997).
- [17] J. Kalinowski, Proceedings of “*Beyond the Desert 97 – Accelerator and Non-Accelerator Approaches*”, Ringberg Castle, Germany, June 1997, hep-ph/9708490.
- [18] S. Bar-Shalom, G. Eilam and A. Soni, Phys. Rev. **D59**, 055012 (1999).
- [19] S. Lola, Presented at the 2nd ECFA/DESY study on Linear Colliders, Frascati, November 1998, LC note LC-TH-1999-021, hep-ph/9912217.
- [20] L. E. Ibañez and G. G. Ross, CERN-TH.6412/92, in *Perspectives in Higgs Physics*, G. Kane editor, World Scientific, Singapore, 1993.

- [21] H. Dreiner, P. Richardson and M. H. Seymour, to appear in the proceedings of the BTMSSM subgroup of the Physics at Run II Workshop on Supersymmetry/Higgs, hep-ph/9903419.
- [22] F. Déliot, G. Moreau, C. Royon, E. Perez and M. Chemtob, Phys. Lett. **B475**, 184 (2000).
- [23] H. Dreiner, P. Richardson and M. H. Seymour, hep-ph/0001224.
- [24] H. Dreiner, P. Richardson and M. H. Seymour, hep-ph/0007228.
- [25] G. Moreau, E. Perez and G. Polesello, hep-ph/0003012, subm. to Nucl. Phys. **B**; G. Moreau, E. Perez and G. Polesello, Proceedings of the Workshop ‘*Physics at TeV Colliders*’, 8-18 June, 1999, Les Houches, France, hep-ph/0002130.
- [26] F. Borzumati, J.-L. Kneur, N. Polonsky, Phys. Rev. **D60**, 115011 (1999).
- [27] E. L. Berger, B. W. Harris and Z. Sullivan, Phys. Rev. Lett. **83**, 4472 (1999).
- [28] M. Carena, M. Olechowski, S. Pokorski and C. E. M. Wagner, Nucl. Phys. **B419** (1994) 213.
- [29] Top averaging group, preprint Fermilab **TM-2084** (1999) D0 Collab., Phys. Rev. **D58**, 052001 (1998), Phys. Rev. Lett. **79**, 1197 (1997), Phys. Rev. **D60**, 052001 (1999), CDF Collab., Phys. Rev. Lett. **80**, 2767 (1998), Phys. Rev. Lett. **82**, 271, (1999).
- [30] CTEQ Coll., Phys. Rev. **D55**, 1280 (1997).
- [31] R. Baier, J. Engels, B. Petersson, Z Phys. **C2**, 265 (1979).
- [32] E. W. N. Glover, A. D. Martin, R. G. Roberts, W. J. Stirling, Phys. Lett. **B381**, 353 (1996).
- [33] M. Glück, E. Reya, A. Vogt, Z Phys. **C53**, 127 (1992).
- [34] ALEPH Collaboration, ALEPH 2000-013, CONF 010 (2000).
- [35] C. Caso et al., The European Physical Journal **C3**, 1 (1998).
- [36] A. Pukhov, E. Boos, M. Dubinin, V. Edneral, V. Ilyin, D. Kovalenko, A. Kryukov, V. Savrin, S. Shichanin, and A. Semenov, ”CompHEP - a package for evaluation of Feynman diagrams and integration over multi-particle phase space. User’s manual for version 33.”, Preprint INP MSU 98-41/542, hep-ph/9908288.
- [37] T. Sjöstrand, Comp. Phys. Comm. **82**, 74 (1994); S. Mrenna, Comp. Phys. Comm. **101**, 232 (1997).
- [38] J. Lykken and K. T. Matchev, preprint FERMILAB-PUB-99/034-T, Phys. Rev. **D61**, 015001 (2000).
- [39] K. T. Matchev and D. M. Pierce, preprint FERMILAB-PUB-99/078-T, Phys. Rev. **D60**, 075004 (1999).
- [40] H. Baer, M. Drees, F. Paige, P. Quintana, X. Tata, hep-ph/9906233.
- [41] R. Barbieri, F. Caravaglios, M. Frigeni and M. Mangano, Nucl. Phys. **B 367**, 28 (1991).
- [42] J. Conway, talk given at the SUSY/Higgs Workshop Meeting, Fermilab, May 14-16, 1998.  
See also [www.physics.rutgers.edu/jconway/soft/shw/shw.html](http://www.physics.rutgers.edu/jconway/soft/shw/shw.html).

- [43] T. Kamon, J. L. Lopez, P. McIntyre, and J. T. White, Phys. Rev. **D50**, 5676 (1994).
- [44] ATLAS Coll., ‘ATLAS Detector and Physics Performance Technical Design Report’, Vol. II, ATLAS TDR 15, 25 May 1999, CERN/LHCC 99-15.  
See also [atlasinfo.cern.ch/Atlas/GROUPS/PHYSICS/TDR/access.html](http://atlasinfo.cern.ch/Atlas/GROUPS/PHYSICS/TDR/access.html).
- [45] V. Barger et al., Phys. Rev. **D50**, 4299 (1994).
- [46] H. Baer, C. Kao and X. Tata, Phys. Rev. **D51**, 2180 (1995).
- [47] H. Baer, C.-H. Chen and X. Tata, Phys. Rev. **D55**, 1466 (1997).
- [48] HERWIG 6.1 Release Note, hep-ph/9912396; G. Marchesini, B. R. Webber, G. Abbiendi, I. G. Knowles, M. H. Seymour and L. Stanco, Computer Phys. Commun. **67**, 465 (1992).
- [49] SUSYGEN 3.0/06, ‘A Monte Carlo Event generator for MSSM sparticle production for  $e^+e^-$ ,  $\mu^+\mu^-$  and  $ep$  colliders’, N. Ghodbane, S. Katsanevas, P. Morawitz and E. Perez, [lyoinfo.in2p3.fr/susygen/susygen3.html](http://lyoinfo.in2p3.fr/susygen/susygen3.html); N. Ghodbane, hep-ph/9909499.
- [50] E. Perez, private communication.
- [51] ALEPH Collaboration, ALEPH 98-017, CONF 007 (1998).
- [52] J. F. Gunion and H. E. Haber, Nucl. Phys. **B272**, 1 (1986); Erratum-ibid **B402**, 567 (1993).



# Publication IV





# Resonant sneutrino production in Supersymmetry with R-parity violation at the LHC

G. Moreau

*Service de Physique Théorique  
CE-Saclay F-91191 Gif-sur-Yvette, Cedex France*

E. Perez

*Service de Physique des Particules, DAPNIA  
CE-Saclay, F-91191, Gif-sur-Yvette, Cedex France*

G. Polesello

*INFN, Sezione di Pavia  
Via Bassi 6, Pavia, Italy*

To appear in Nucl. Phys. **B**, hep-ph/0003012

Abstract

*The resonant production of sneutrinos at the LHC via the R-parity violating couplings  $\lambda'_{ijk} L_i Q_j D_k^c$  is studied through its three-leptons signature. A detailed particle level study of signal and background is performed using a fast simulation of the ATLAS detector. Through the full reconstruction of the cascade decay, a model-independent and precise measurement of the masses of the involved sparticles can be performed. Besides, this signature can be detected for a broad class of supersymmetric models, and for a wide range of values of several  $\lambda'_{ijk}$  coupling constants. Within the MSSM, the production of a 900 GeV sneutrino for  $\lambda'_{211} > 0.05$ , and of a 350 GeV sneutrino for  $\lambda'_{211} > 0.01$  can be observed within the first three years of LHC running.*

# 1 Introduction

The most general superpotential respecting the gauge symmetries of the Standard Model (SM) contains bilinear and trilinear terms which are not taken into account in the Minimal Supersymmetric Standard Model (MSSM). Restricting to the trilinear part, these additional terms read as :

$$W \supset \sum_{i,j,k} \left( \frac{1}{2} \lambda_{ijk} L_i L_j E_k^c + \lambda'_{ijk} L_i Q_j D_k^c + \frac{1}{2} \lambda''_{ijk} U_i^c D_j^c D_k^c \right), \quad (1.1)$$

where  $i, j, k$  are generation indices,  $L$  ( $Q$ ) denote the left-handed leptons (quarks) superfields, and  $E^c$ ,  $D^c$  and  $U^c$  are right-handed superfields for charged leptons, down and up-type quarks, respectively.

The first two terms in Eq.(1.1) lead to violation of the lepton number ( $\mathbb{L}$ ), while the last one implies violation of the baryon number ( $\mathbb{B}$ ). Since the simultaneous presence of  $\mathbb{L}$  and  $\mathbb{B}$  couplings could lead to a too fast proton decay, a discrete multiplicative symmetry which forbids the above terms in the superpotential has been imposed by hand in the MSSM. This symmetry, called R-parity ( $R_p$ ), is defined as  $R_p = (-1)^{3B+L+2S}$ , where  $B$ ,  $L$  and  $S$  respectively denote the baryon number, the fermion number and the spin, such that  $R_p = -1$  ( $R_p = 1$ ) for all supersymmetric (SM) particles. However other solutions can ensure the proton stability, e.g. if  $L$  only is violated, or if only  $U_i^c D_j^c D_k^c$  interactions are allowed and the proton is lighter than the Lightest Supersymmetric Particle (LSP). Moreover, on the theoretical point of view, there is no clear preference, e.g. in models inspired by Grand Unified or string theories, between  $\mathbb{R}_p$  and  $R_p$  conservation [1]. It is thus mandatory to search for SUSY in both scenarios.

On the experimental side, the main consequence of  $\mathbb{R}_p$  lies in the possibility for the LSP to decay into ordinary matter. This is in contrast to scenarios where  $R_p$  is conserved, in which the LSP is stable and escapes detection, leading to the characteristic search for missing energy signals in direct collider searches. Moreover, while in  $R_p$  conserved models, the supersymmetric (SUSY) particles must be produced in pairs,  $\mathbb{R}_p$  allows the single production of superpartners, thus enlarging the mass domain where SUSY could be discovered. In particular,  $\mathbb{R}_p$  couplings offer the opportunity to resonantly produce supersymmetric particles [2, 3]. Although the  $\mathbb{R}_p$  coupling constants are severely constrained by the low-energy experimental bounds [1, 4, 5, 6, 7, 8], the superpartner resonant production can have significant cross-sections both at leptonic [4] and hadronic [9] colliders. This is this possibility which is exploited throughout this paper.

The resonant production of supersymmetric particles is attractive for another reason : Since its rate is proportional to a power 2 of the relevant  $\mathbb{R}_p$  coupling, this reaction would allow an easier determination of the  $\mathbb{R}_p$  couplings than the pair production. In fact in the latter case, the sensitivity on the  $\mathbb{R}_p$  coupling is mainly provided by the displaced vertex analysis for the LSP decay, which is difficult experimentally especially at hadronic colliders.

In this paper, we focus on the resonant SUSY particle production at the Large Hadron Collider (LHC) operating at a center of mass energy of 14 TeV with special reference to the ATLAS detector. At the LHC due to the continuous distribution of the centre of mass energy of the colliding partons, a parton-parton resonance can be probed over a wide mass domain. This is a distinct advantage over the situation at lepton colliders, where

the search for narrow resonances requires lengthy scans over the centre of mass energy of the machine.

At hadronic colliders, either a slepton or a squark can be produced at the resonance through a  $\lambda'$  or a  $\lambda''$  coupling constant, respectively. In the hypothesis of a single dominant  $\mathcal{R}_p$  coupling constant, the resonant SUSY particle could decay through the same  $\mathcal{R}_p$  coupling as in the production, leading then to a two quarks final state for the hard process [10, 11, 12, 13, 14]. In the case where both  $\lambda'$  and  $\lambda$  couplings are non-vanishing, the slepton produced via  $\lambda'$  can decay through  $\lambda$  giving rise to the same final state as in Drell-Yan process, namely two leptons [13, 15, 16, 17]. However, for most of the values of the  $\mathcal{R}_p$  coupling constants allowed by present indirect searches, the decays of the resonant SUSY particle via gauge interactions are dominant if kinematically accessible [4]. In this favoured situation, typically, the produced superpartner initiates a cascade decay ended by the  $\mathcal{R}_p$  decay of the LSP. In case of a dominant  $\lambda''$  coupling constant, due to the  $\mathcal{R}_p$  decay of the LSP into quarks, this cascade decay leads to multijet final states which have a large QCD background [9, 10]. Only if leptonic decays such as for instance  $\tilde{\chi}_1^+ \rightarrow \bar{l}_i \nu_i \tilde{\chi}_1^0$  enter the cascade clearer signatures can be investigated [18]. The situation is more favourable in the hypothesis of a single  $\lambda'$  coupling constant, where the LSP can decay into a charged lepton, allowing then multileptonic final states to be easily obtained. We will thus assume a dominant  $\lambda'_{ijk}$  coupling constant. At hadronic colliders, either a  $\tilde{\nu}_i$  sneutrino or a  $\tilde{l}_i$  charged slepton can be produced at the resonance via  $\lambda'_{ijk}$  and the initial states are  $d_j \bar{d}_k$  and  $u_j \bar{d}_k$ , respectively. The slepton produced at the resonance has two possible gauge decays, either into a chargino or a neutralino. In both cases particularly clean signatures can be observed. For example, the production of a neutralino together with a charged lepton resulting from the resonant charged slepton production can lead to the interesting like-sign dilepton topology [19, 20] since, due to its Majorana nature, the neutralino decays via  $\lambda'_{ijk}$  into a lepton as  $\tilde{\chi}^0 \rightarrow l_i u_j \bar{d}_k$  and into an anti-lepton as  $\tilde{\chi}^0 \rightarrow \bar{l}_i \bar{u}_j d_k$  with the same probability.

In this article, we consider the single lightest chargino production at LHC as induced by the resonant sneutrino production  $pp \rightarrow \tilde{\nu}_i \rightarrow \tilde{\chi}_1^\pm l_i$ . The single  $\tilde{\chi}_1^\pm$  production also receives contributions from the  $t$  and  $u$  channel squark exchange diagrams shown in Figure 1. In many models, the  $\tilde{\chi}_1^0$  neutralino is the LSP for most of the SUSY parameter space. In the hypothesis of a  $\tilde{\chi}_1^0$  LSP, the produced  $\tilde{\chi}_1^\pm$  chargino mainly decays into the neutralino as  $\tilde{\chi}_1^\pm \rightarrow \tilde{\chi}_1^0 q_p \bar{q}'_p$  or as  $\tilde{\chi}_1^\pm \rightarrow \tilde{\chi}_1^0 l_p^\pm \nu_p$ . The neutralino then decays via  $\lambda'_{ijk}$  as  $\tilde{\chi}_1^0 \rightarrow l_i u_j \bar{d}_k$ ,  $\bar{l}_i \bar{u}_j d_k$  or as  $\tilde{\chi}_1^0 \rightarrow \nu_i d_j \bar{d}_k$ ,  $\bar{\nu}_i \bar{d}_j d_k$ . We concentrate on the decays of both the chargino and the neutralino into charged leptons, which lead to a three leptons final state. This signature has a low Standard Model background, and allows the reconstruction of the whole decay chain, thus providing a measurement of some parameters of the SUSY model.

## 2 The signal

### 2.1 Theoretical framework

Our theoretical framework in sections 2 and 3 will be the  $\mathcal{R}_p$  extension of the Minimal Supersymmetric Standard Model. In Section 4 we will also give results in the Minimal Supergravity (mSUGRA) model. The MSSM parameters are the following.  $M_1$ ,  $M_2$  and

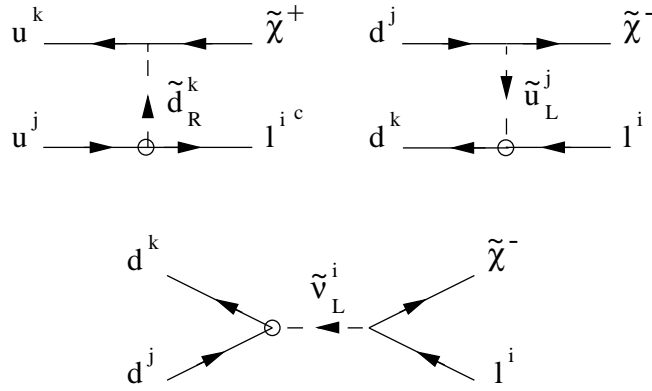


FIG. 1: *Feynman diagrams for the single chargino production at hadronic colliders via the  $\lambda'_{ijk}$  coupling (symbolised by a circle in the figure). The arrows denote the flow of the particle momentum.*

$M_3$  are the soft-SUSY breaking mass terms for the bino, the wino and the gluino, respectively.  $\mu$  is the Higgs mass parameter.  $\tan \beta = \langle H_u \rangle / \langle H_d \rangle$  is the ratio of the vacuum expectation values (vev) for the two-Higgs doublet fields.  $A_t$ ,  $A_b$  and  $A_\tau$  are the third generation soft-SUSY breaking trilinear couplings. In fact, since these trilinear couplings are proportional to the fermion masses one can neglect the first two generations couplings without any phenomenological consequence in this context. Finally,  $m_{\tilde{q}}$ ,  $m_{\tilde{l}}$  and  $m_{\tilde{\nu}}$  are the squark, slepton and sneutrino mass, respectively. The value of the squark mass enters our study mainly in the determination of the relative branching ratios of the  $\tilde{\chi}^0$  into lepton or neutrino and of the  $\tilde{\chi}^\pm$  into  $\tilde{\chi}^0 + \text{quarks}$  or  $\tilde{\chi}^0 + \text{leptons}$ . The remaining three parameters  $m_{H_u}^2$ ,  $m_{H_d}^2$  and the soft-SUSY breaking bilinear coupling  $B$  are determined through the electroweak symmetry breaking conditions which are two necessary minimisation conditions of the Higgs potential.

We choose to study the case of a single dominant  $\lambda'_{2jk}$  allowing the reactions  $pp \rightarrow \tilde{\chi}^\pm \mu^\mp$ . In section 3 the analysis will be performed explicitly for the  $\lambda'_{211}$  coupling, since it corresponds to the hard subprocess  $d\bar{d} \rightarrow \tilde{\chi}_1^\pm \mu^\mp$  which offers the highest partonic luminosity. We will take  $\lambda'_{211}=0.09$ , the upper value allowed by indirect bound :  $\lambda'_{211} < 0.09(m_{\tilde{d}_R}/100\text{GeV})$  [1] for a squark mass of 100 GeV. A quantitative discussion will be given below for the general case of a single dominant  $\lambda'_{2jk}$  coupling constant. We will not treat explicitly the  $\lambda'_{1jk}$  couplings which are associated to the  $\tilde{\chi}^\pm - e^\mp$  production, since the low-energy bounds on these couplings are rather more stringent than the constraints on  $\lambda'_{2jk}$  and  $\lambda'_{3jk}$  [1]. However, the three-leptons analysis from sneutrino production should give similar sensitivities on the  $\lambda'_{1jk}$  and  $\lambda'_{2jk}$  couplings since isolation cuts will be included in the selection criteria for the leptons. We will not perform the analysis of the  $\lambda'_{3jk}$  couplings which correspond to the  $\tilde{\chi}^\pm - \tau^\mp$  production. A technique for mass reconstruction in the ATLAS detector using the hadronic decays of the  $\tau$  has been demonstrated in [21]. The detailed experimental analysis needed to extract a signal is beyond the scope of this work. Besides, in this case the sneutrino and chargino mass reconstruction studied in Section 3.1 is spoiled by the neutrinos produced in the  $\tau$  decay.

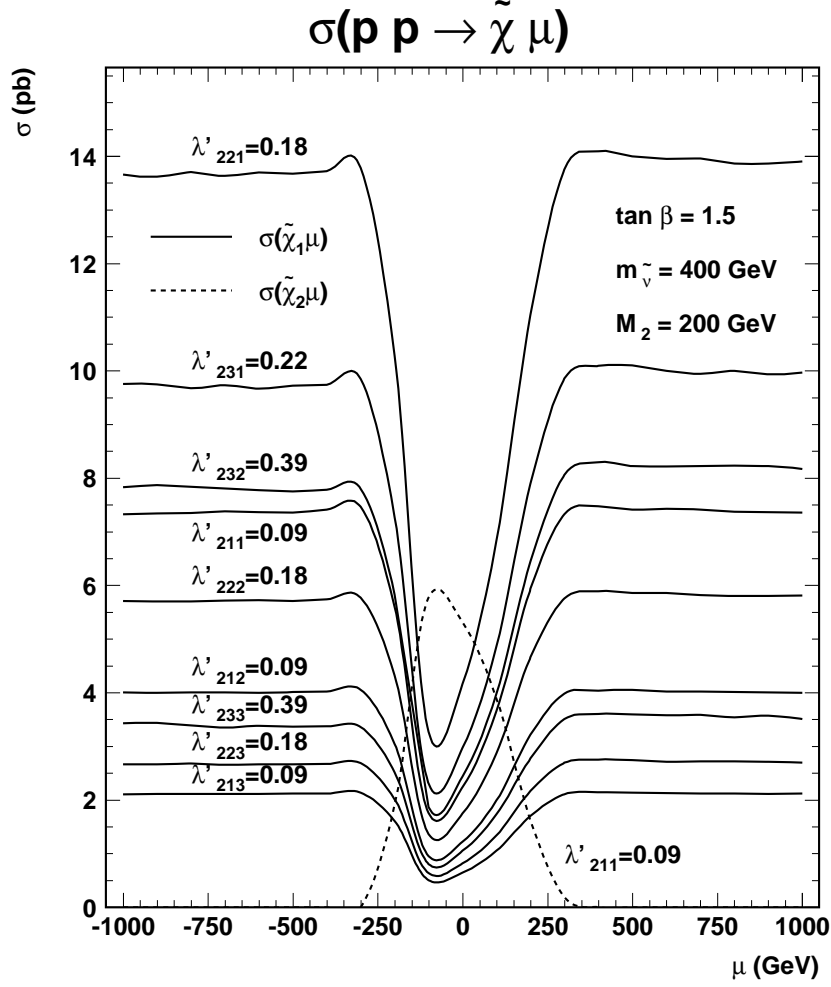


FIG. 2: Cross-sections for the  $\tilde{\chi}_1^\pm\text{-}\mu^\mp$  production as a function of the  $\mu$  parameter through various  $\lambda'_{2jk}$  couplings, for  $\tan\beta=1.5$ ,  $M_2 = 200$  GeV and  $m_{\tilde{\nu}} = 400$  GeV. In the case of  $\lambda'_{211}$  the cross-section for  $\tilde{\chi}_2^\pm\text{-}\mu^\mp$  is also shown as the dashed line. The values of the  $R_p$  couplings have been chosen equal to :  $\lambda'_{211} = 0.09$ ,  $\lambda'_{212} = 0.09$ ,  $\lambda'_{213} = 0.09$ ,  $\lambda'_{221} = 0.18$ ,  $\lambda'_{222} = 0.18$ ,  $\lambda'_{223} = 0.18$ ,  $\lambda'_{231} = 0.22$ ,  $\lambda'_{232} = 0.39$  and  $\lambda'_{233} = 0.39$ , which correspond to the low-energy limits for a sfermion mass of 100 GeV [1].

## 2.2 Single chargino production cross-section

In order to establish the set of models in which the analysis presented below can be performed, we need to study the variations of the single chargino production rate  $\sigma(pp \rightarrow \tilde{\chi}^\pm \mu^\mp)$  with the MSSM parameters.

In Figure 2, we present the cross-sections for the  $\tilde{\chi}_1^\pm\text{-}\mu^\mp$  production through several  $\lambda'_{2jk}$  couplings as a function of the  $\mu$  parameter for the fixed values :  $\tan\beta=1.5$ ,  $M_2 = 200$  GeV, and  $m_{\tilde{\nu}} = 400$  GeV. For this choice of parameters and independently of  $\mu$ , the chargino  $\tilde{\chi}_1^\pm$  is lighter than the  $\tilde{\nu}$ . In this case the contributions of squark exchange in the  $t$  and  $u$  channels are negligible compared to the resonant process so that the  $\tilde{\chi}_1^\pm\text{-}$

$\mu^\mp$  production cross-section does not depend on the squark mass. The values for the considered  $\mathcal{R}_p$  coupling constants have been conservatively taken equal to the low-energy limits for a sfermion mass of 100 GeV [1]. The cross-sections scale as  $\lambda_{2jk}^{\prime 2}$ .

We see on this Figure that the dependence of the rates on  $\mu$  is smooth for  $|\mu| > M_2$ . This is due to the weak dependence of the  $\tilde{\chi}_1^\pm$  mass on  $\mu$  in this domain. In contrast, we observe a strong decrease of the rate in the region  $|\mu| < M_2$  where the  $\tilde{\chi}_1^\pm$  chargino is mainly composed by the higgsino. Most of the small  $|\mu|$  domain ( $|\mu|$  smaller than  $\sim 100$  GeV for  $\tan\beta = 1.41$  and  $m_0 = 500$  GeV) is however excluded by the present LEP limits [30].

We also show as a dashed line on the plot the rate for the  $\tilde{\chi}_2^\pm$ - $\mu^\mp$  production through the  $\lambda'_{211}$  coupling. The decrease of the  $\tilde{\chi}_2^\pm$  production rate with increasing  $|\mu|$  is due to an increase of the  $\tilde{\chi}_2^\pm$  mass. We will not consider the contribution to the three-leptons final state from the  $\tilde{\chi}_2^\pm$  production since the rate becomes important only for a very limited range of small  $|\mu|$  values not yet excluded by LEP data.

Figure 2 also allows to compare the sensitivities that can be reached on various  $\lambda'_{2jk}$  couplings using the single chargino production. If we compare for instance the cross-sections of the  $\tilde{\chi}_1^\pm$  production via  $\lambda'_{211}$  and  $\lambda'_{221}$  at  $\mu = -500$  GeV, we can see that for equal values of the  $\mathcal{R}_p$  couplings the ratios between the cross-sections associated to  $\lambda'_{211}$  and  $\lambda'_{221}$  is  $\sim 2.17$ . Therefore, the sensitivity that can be obtained on  $\lambda'_{221}$  is only  $\sim \sqrt{2.17}$  times weaker than the sensitivity on  $\lambda'_{211}$ , for a 400 GeV sneutrino. Note that the cross-section ratio, and hence the scaling to be applied, in order to infer from the reach on  $\lambda'_{211}$  the sensitivity on another coupling  $\lambda'_{2jk}$ , depends on the sneutrino mass. The reason is that the evolution of the parton densities with the  $x$ -Bjorken variable is different for sea quark and valence quark and for different quark flavours.

In order to study the dependence of the cross-section on the masses of the involved particles, the parameters  $m_{\tilde{\nu}}$  and  $M_2$  were varied, and the other model parameters affecting the cross-section were fixed at the values :  $\lambda'_{211} = 0.09$ ,  $\mu = -500$  GeV and  $\tan\beta = 1.5$ . The cross-section for  $\tilde{\chi}_1^\pm$ - $\mu^\mp$  production as a function of  $m_{\tilde{\nu}}$  and  $m_{\tilde{\chi}_1^\pm}$  is shown in Figure 3. Since the  $\tilde{\chi}_1^\pm$  mass is approximately equal to  $M_2$  as long as  $M_2 < |\mu|$ , and becomes equal to  $|\mu|$  for  $M_2 > |\mu|$ , we studied  $\tilde{\nu}$  masses between 100 and 950 GeV, and values of  $M_2$  between 100 and 500 GeV. For increasing  $m_{\tilde{\nu}}$  the cross-section decreases due to a reduction of the partonic luminosity. A decrease of the cross-section is also observed for  $m_{\tilde{\chi}_1^\pm}$  approaching  $m_{\tilde{\nu}}$ , since the phase space factor of the decay  $\tilde{\nu} \rightarrow \tilde{\chi}_1^\pm \mu^\mp$  following the resonant sneutrino production is then suppressed. In the region  $m_{\tilde{\chi}_1^\pm} > m_{\tilde{\nu}}$ , the chargino production still receives contributions from the  $s$  channel exchange of a virtual sneutrino, as well as from the  $t$  and  $u$  channels squark exchange which in that case also contribute significantly. However, in this phase space domain where the resonant sneutrino production is not accessible, the cross-section is considerably reduced.

Finally, the single chargino production rate depends weakly on the  $A$  trilinear couplings. Indeed, only the  $t$  and  $u$  channels squark exchange, varying with the squark mass which can be influenced by  $A$ , depends on these couplings. The dependence of the rate on the  $\tan\beta$  parameter is also weak.

## 2.3 Three leptons branching ratio

We calculate the total three leptons rate by multiplying the single chargino cross-section by the chargino branching ratio, since we neglect the width of the chargino. The

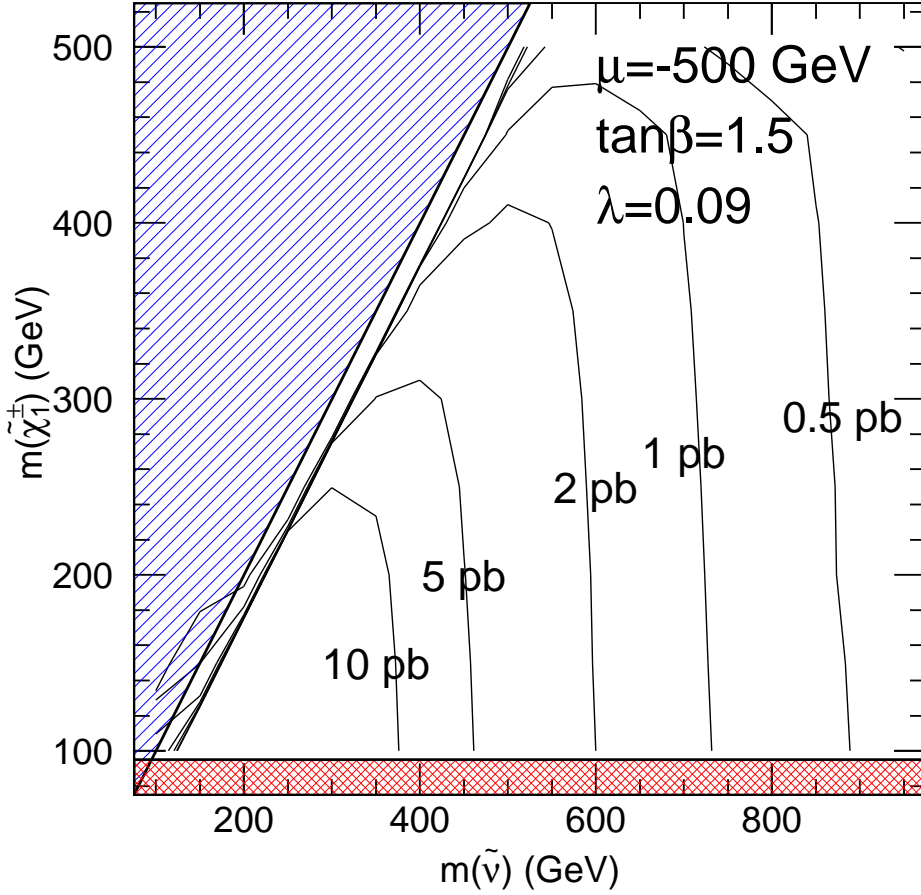


FIG. 3: Cross-section for  $\tilde{\chi}_1^\pm\text{-}\mu^\mp$  production as a function of  $m_{\tilde{\nu}}$  and  $m_{\tilde{\chi}_1^\pm}$  in the MSSM for the choice of values  $\mu = -500$  GeV,  $\tan\beta = 1.5$  and  $\lambda'_{211} = 0.09$ . The hatched region at the upper left corresponds to  $m_{\tilde{\nu}} < m_{\tilde{\chi}_1^\pm}$ . The cross-hatched region at low  $m_{\tilde{\chi}_1^\pm}$  is excluded by the preliminary LEP results at  $\sqrt{s} = 196$  GeV [30].

three-leptons final state is generated by the cascade decay  $\tilde{\chi}_1^\pm \rightarrow \tilde{\chi}_1^0 l_p^\pm \nu_p$ ,  $\tilde{\chi}_1^0 \rightarrow \mu u d$ . For  $m_{\tilde{\nu}}, m_{\tilde{l}}, m_{\tilde{q}}, m_{\tilde{\chi}_2^0} > m_{\tilde{\chi}_1^\pm}$ , the chargino decays mainly into a real or virtual  $W$  and a  $\tilde{\chi}_1^0$  and hence its branching fraction for the decay into leptons (lepton= $e, \mu$ ) is  $\sim 22\%$ .

In particular kinematic configurations, the  $\mathcal{R}_p$  modes can compete with the gauge couplings, affecting the  $\tilde{\chi}_1^\pm$  branching fractions. However, this does not happen as long as the chargino is sufficiently heavier than the neutralino, as is the case for example in supergravity inspired models. When  $\tilde{\chi}_1^0$  is the LSP, the branching ratio  $B(\tilde{\chi}_1^0 \rightarrow \mu u d)$  ranges between  $\sim 40\%$  and  $\sim 70\%$ . For values of  $|\mu|$  much smaller than  $M_2$  the other allowed decay  $\tilde{\chi}_1^0 \rightarrow \nu_\mu d d$  becomes dominant, spoiling the three-leptons signature.

## 3 Experimental analysis

### 3.1 Mass reconstruction

The analysis strategy is based on the exploitation of the decay chain :

$$\begin{array}{lcl} \tilde{\nu}_\mu & \rightarrow & \tilde{\chi}_1^+ \mu^- \\ & \searrow & \tilde{\chi}_1^0 W^+ \rightarrow e^+(\mu^+)\nu \\ & \searrow & \mu^\pm q \bar{q}' \end{array} \quad (3.1)$$

which presents a sequence of three decays which can be fully reconstructed. The strong kinematic constraint provided by the masses of the three particles in the cascade is sufficient to reduce the contribution of the different background sources well below the signal rate.

The signal events were generated with a version of the SUSYGEN MonteCarlo [22] modified to allow the generation of  $pp$  processes. The hard-subprocess  $q\bar{q}' \rightarrow \tilde{\chi}^\pm \mu^\mp$  is first generated according to the full lowest order matrix elements corresponding to the diagrams depicted in Figure 1. Cascade decays of the  $\tilde{\chi}$ 's are performed according to the relevant matrix elements. The parton showers approach [23] relying on the DGLAP [24] evolution equations is used to simulate QCD radiations in the initial and final states, and the non-perturbative part of the hadronization is modeled using string fragmentation [23]. The events were then processed through the program ATLFast [25], a parameterized simulation of the ATLAS detector response.

In this section, the analysis will be performed for the  $\mathcal{R}_p$  coupling  $\lambda'_{211} = 0.09$  and for the following MSSM point :

$M_1 = 75$  GeV,  $M_2 = 150$  GeV,  $\mu = -200$  GeV,  $\tan\beta = 1.5$ ,  $A_t = A_b = A_\tau = 0$ ,  $m_{\tilde{f}} = 300$  GeV.

For this set of MSSM parameters, the masses of the relevant gauginos are :

$$m_{\tilde{\chi}_1^0} = 79.9 \text{ GeV} \quad m_{\tilde{\chi}_1^\pm} = 162.3 \text{ GeV}$$

and the  $\tilde{\chi}_1^\pm$  decay into an on shell  $W$  has a branching ratio of order 100%. The total cross-section for the resonant sneutrino production  $pp \rightarrow \tilde{\nu}$  is 37 pb. If we include the branching fractions into the three leptons, the cross-section is 3.3 pb, corresponding to  $\sim 100000$  events for the standard integrated luminosity of  $30 \text{ fb}^{-1}$  for the first three years of LHC data taking.

The signal is characterised by the presence of three isolated leptons and two jets. For the initial sample selection we require that :

- Exactly three isolated leptons are found in the event, with  $p_T^1 > 20$  GeV,  $p_T^{2,3} > 10$  GeV, where  $p_T$  is the momentum component in the plane perpendicular to the beam direction, and pseudorapidity  $|\eta| < 2.5$ .
- At least two of the three leptons must be muons.
- At least two jets with  $p_T > 15$  GeV are found.
- The invariant mass of any  $\mu^+ \mu^-$  pair is outside  $\pm 6.5$  GeV of the  $Z$  mass.

The isolation prescription on the leptons is necessary to reduce the background from the semileptonic decays of heavy quarks, and consists in requiring an energy deposition of less



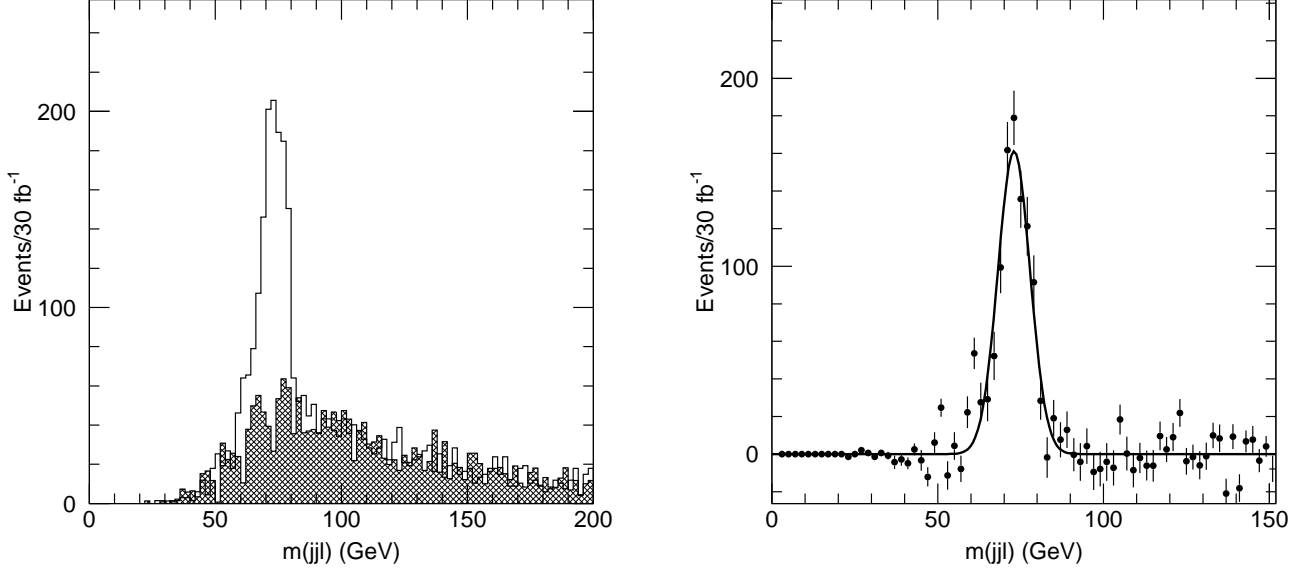


FIG. 4:  $\mu$ -jet-jet invariant mass for events in configuration 1. (see text) Left : exclusive two jet events with superimposed (hatched) the combinatorial background Right :  $\tilde{\chi}_1^0$  peak after background subtraction.

than 10 GeV not associated with the lepton in a pseudorapidity-azimuth ( $\eta - \phi$ ) cone of opening  $\Delta R = 0.2$  around the lepton direction.

The efficiency for these cuts, after the branching fractions have been taken into account, is  $\sim 25\%$ , where half of the loss comes from requiring three isolated leptons, and the other half is the loss of jets from  $\tilde{\chi}_1^0$  decay either because they are not reconstructed, or because the two jets from the decay are reconstructed as a single jet. The  $Z$  mass cut gives a 10% loss in statistics. In order to avoid the combinatorial background from additional QCD events we further require that no third jet with  $p_T > 15$  GeV is reconstructed in the event. The efficiency after this cut is  $\sim 15\%$ .

The reconstruction of the sparticle masses could be performed either starting from the  $\tilde{\chi}_1^0$  reconstruction and going up the decay chain, or trying to exploit the three mass constraints at the same time. We choose the first approach which is not optimal, but allows a clearer insight into the kinematics of the events.

The first step in reconstruction of the  $\tilde{\chi}_1^0 \rightarrow \mu \text{ jet jet}$  is the choice of the correct muon to attempt the reconstruction. The three leptons come in the following flavour-sign configurations (+ charge conjugates) :

1.  $\mu^- e^+ \mu^+$
2.  $\mu^- e^+ \mu^-$
3.  $\mu^- \mu^+ \mu^+$
4.  $\mu^- \mu^+ \mu^-$

where the first lepton comes from the  $\tilde{\nu}_\mu$ , the second one from the  $W$ , and the third one from the  $\tilde{\chi}_1^0$  decay, corresponding to three final state signatures : 1) two opposite sign

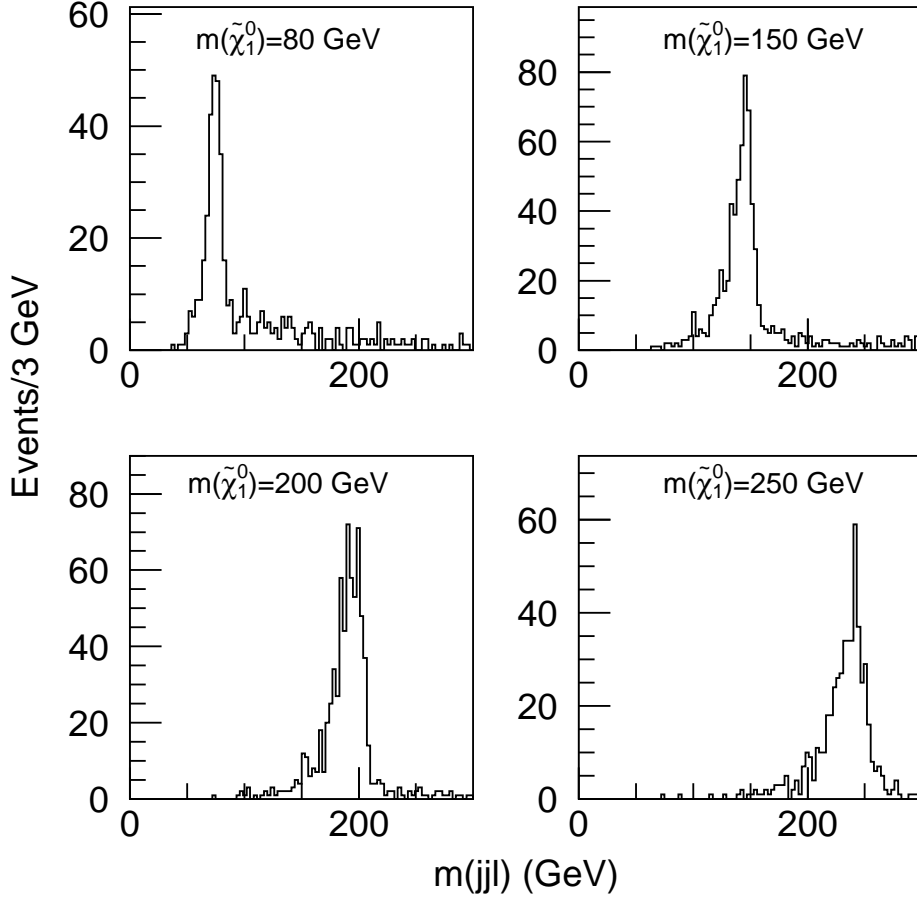


FIG. 5: *Lepton-jet-jet invariant mass for exclusive two-jet events where the  $\tilde{\chi}_1^0$  lepton is uniquely defined, for four different values of the  $\tilde{\chi}_1^0$  mass :  $m_{\tilde{\chi}_1^0}=80, 150, 200$  and  $250$  GeV. In all cases the sneutrino mass is set at  $500$  GeV,  $-\mu = M_2 = 2M_1$ , and  $\tan\beta = 1.5$ , yielding a  $\tilde{\chi}_1^\pm$  mass twice the  $\tilde{\chi}_1^0$  mass. All the sfermion masses are set to  $500$  GeV. The normalisation is arbitrary.*

muons and an electron <sup>5</sup>, 2) two same-sign muons and an electron, 3-4) three muons. The configuration with three same-sign muons does not correspond to the required signature and is rejected in the analysis. For signature 1) the muon produced in the  $\tilde{\chi}_1^0$  decay is defined as the one which has the same sign as the electron. For configuration 2) both muons must be tested to reconstruct the  $\tilde{\chi}_1^0$ . For configuration 3-4), the  $\tilde{\chi}_1^0$  muon must be one of the two same-sign ones.

In order to minimise the combinatorial background we start the reconstruction from signature 1) where each lepton is unambiguously attributed to a step in the decay. The distribution of the  $\mu$ -jet-jet invariant mass is shown in the left plot of Figure 4. A clear

<sup>5</sup>Here and in the following, “electron” stands for both  $e^+$  and  $e^-$ .

peak is visible corresponding to the  $\tilde{\chi}_1^0$  mass superimposed to a combinatorial background of events where one of the two jets from the  $\tilde{\chi}_1^0$  was lost and a jet from initial state radiation was picked up. The combinatorial background can be evaluated using three-jet events, where at least one jet is guaranteed to come from initial state radiation. The shape of the combinatorial background estimated with this method is shown as the shaded histogram superimposed to the signal peak. After background subtraction, an approximately gaussian peak with a width of  $\sim 4.5$  GeV, and a statistics of about 1050 events is reconstructed, shown in the right of Figure 4. If we consider a window of  $\pm 12$  GeV around the peak, corresponding to  $\sim 2.5\sigma$  of the gaussian,  $\sim 1500$  events are observed in the sample, and the combinatorial contamination is approximately  $\sim 30\%$ . A tail towards low mass values is observed, corresponding to events where a fraction of the parton energy is lost in the jet reconstruction. From this distribution the  $\tilde{\chi}_1^0$  mass can be measured with a statistical error of  $\sim 100$  MeV. The measurement error will in this case be dominated by the systematic error on the jet energy scale which in ATLAS is estimated to be at the level of 1% [31].

The 30% combinatorial background is due to the 'soft' kinematics of the chosen example point, with a  $\tilde{\chi}_1^0$  which is both light and produced with a small boost. In order to show the effect of the mass hierarchy of the involved sparticles, the shape of the  $\tilde{\chi}_1^0$  mass peak is shown in Figure 5 for a sneutrino mass of 500 GeV and different choices for the  $\tilde{\chi}_1^0$  mass. In all cases the  $\tilde{\chi}_1^\pm$  mass is twice the  $\tilde{\chi}_1^0$  mass, corresponding to the gauge unification condition and to  $|\mu|$  values of the same order as  $M_2$ . The combinatorial background is in general smaller than for a 300 GeV sneutrino, due to the higher boost imparted to the  $\tilde{\chi}_1^0$ , and it decreases with increasing  $\tilde{\chi}_1^0$  masses, due to the higher efficiency for reconstructing both jets from the  $\tilde{\chi}_1^0$  decay. For this analysis no attempt has been done for the recalibration of the jet energy. This results in the skewing of the distributions towards low masses, and in the peak value being slightly displaced with respect to the nominal mass value.

Once the position of the  $\tilde{\chi}_1^0$  mass peak is known, the reconstructed  $\tilde{\chi}_1^0$  statistics can be increased by also considering signatures 2) and 3-4). For events coming from signatures 2 to 4, the  $\tilde{\chi}_1^0$  candidate is defined as the muon-jet-jet combination which gives a mass nearest to the mass peak determined from signature 1) events. In all cases the reconstructed mass is required to be within  $\pm 12$  GeV of the peak position to define a  $\tilde{\chi}_1^0$  candidate. In 83% of the events containing at least a combination satisfying this requirement, only one  $\tilde{\chi}_1^0$  candidate is found, and this sample can be used to improve the statistical precision on the  $\tilde{\chi}_1^0$  mass measurement.

Using the above definition of the  $\tilde{\chi}_1^0$ , we can go further in the mass reconstruction of the involved sparticles. Only configurations 1) and 2) are used, i.e. the events containing two muons and an electron in order to avoid ambiguities in the choice of the lepton from the  $W$  decay. The preliminary step for the reconstruction of the  $\tilde{\chi}_1^\pm$  is the reconstruction of the  $W$  boson from its leptonic decay. The longitudinal momentum of the neutrino from the  $W$  decay is calculated from the missing transverse momentum of the event (considered as  $p_T^\nu$ ) and the requirement that the electron-neutrino invariant mass gives the  $W$  mass. The resulting neutrino longitudinal momentum, has a twofold ambiguity. We therefore build the invariant  $W - \tilde{\chi}_1^0$  mass candidate using both solutions for the  $W$  boson momentum. The resulting spectrum is shown in Figure 6, as the full line histogram. A clear peak is seen, superimposed on a combinatorial background. If only the solution yielding the  $\tilde{\chi}_1^\pm$  mass nearest to the measured mass peak is retained, the mass spectrum corresponding to

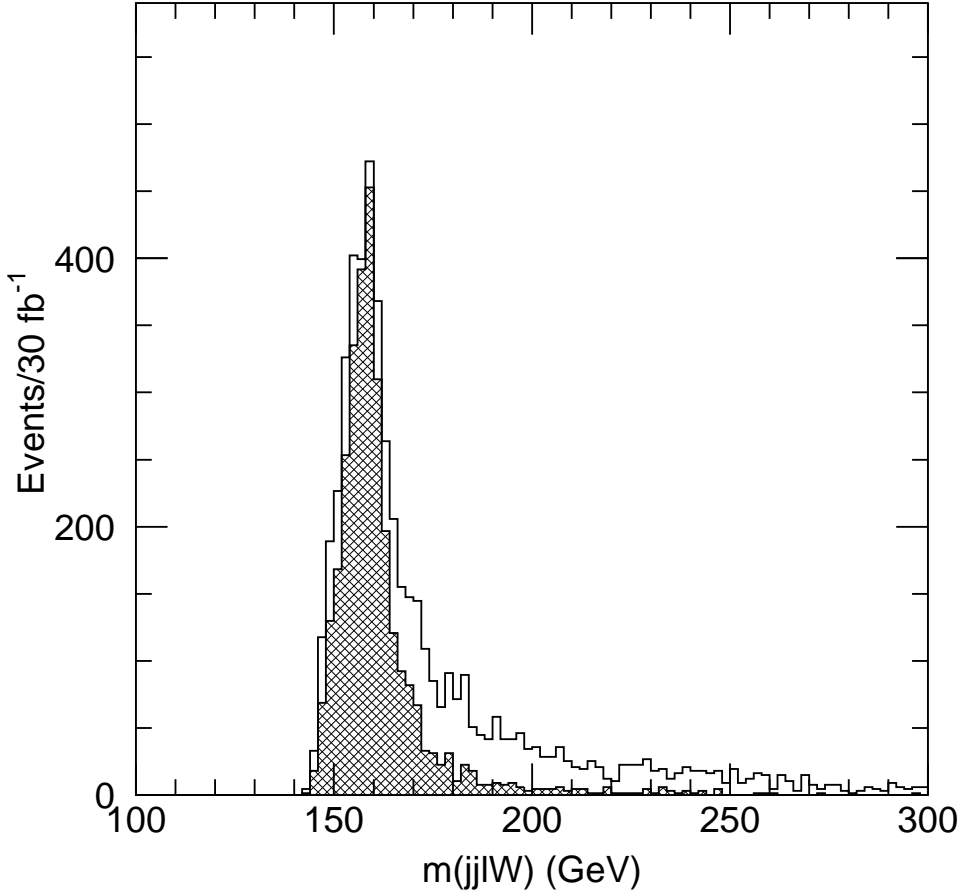


FIG. 6: Invariant mass of the  $\tilde{\chi}_1^0$  with the  $W$  candidate. The full line histogram includes both solutions for the neutrino longitudinal momentum, the grey one only includes the solution which gives the mass nearest to the measured peak.

the shaded histogram is obtained. The peak in the unbiased histogram can be fitted with a gaussian shape, with a width of  $\sim 6$  GeV.

The combination with the mass nearest to the measured peak is taken as  $\tilde{\chi}_1^\pm$  candidate, provided that the reconstructed mass is within 15 GeV of the peak. For 80% of the  $e\mu\mu$  events where a  $\tilde{\chi}_1^0$  candidate is found, a  $W - \tilde{\chi}_1^0$  combination satisfying this requirement is reconstructed.

Finally the  $\tilde{\chi}_1^\pm$  candidates are combined with the leftover muon, yielding the mass spectrum shown in Figure 7. The  $\tilde{\nu}$  mass peak at this point presents very limited tails, and has a width of  $\sim 10$  GeV. We define fully reconstructed events as those for which this mass lies within 25 GeV of the measured  $\tilde{\nu}$  peak. From the estimate of the combinatorial under the  $\tilde{\chi}_1^0$  peak, we expect approximately  $2 \times 1050 = 2100$  events where all the jets and leptons are correctly assigned over a total of 2450 events observed in the peak. The

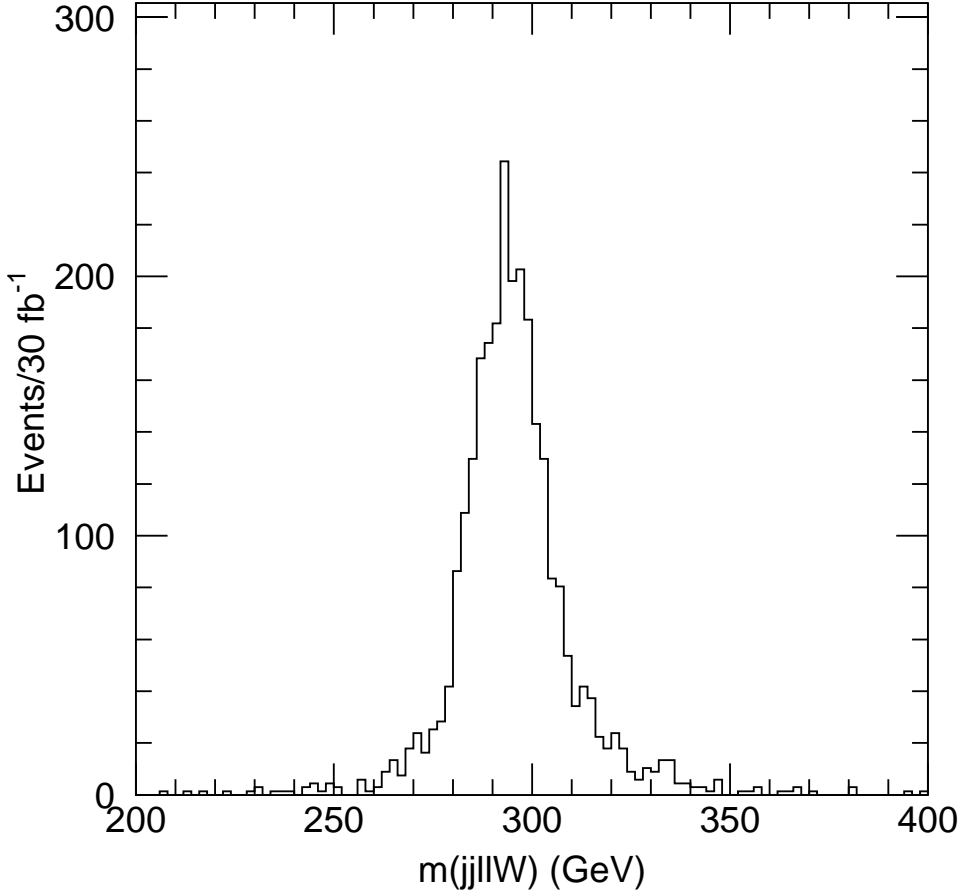


FIG. 7: *Invariant mass of the third lepton in the event with the  $\tilde{\chi}_1^\pm$  candidate.*

difference between the two numbers are events for which one of the two jets used for the  $\tilde{\chi}_1^0$  reconstruction comes from initial state radiation. These jets are typically soft, and therefore the reconstructed  $\tilde{\chi}_1^0$  candidate very often has a momentum which both in magnitude and direction is close to the momentum of the original  $\tilde{\chi}_1^0$ . Therefore for such events the reconstructed  $\tilde{\chi}_1^0$  behaves in the further steps in the reconstruction as the real one, only inducing some widening in the  $\tilde{\chi}_1^\pm$  and  $\tilde{\nu}$  peaks.

The statistics available at the different steps in the analysis for an integrated luminosity of  $30 \text{ fb}^{-1}$  is given in the first column of Table 10. For the assumed value of the coupling,  $\lambda'_{211} = 0.09$ , the uncertainty on the measurement of all the three masses involved will be dominated by the 1% uncertainty on the jet energy scale.

The efficiency for the reconstruction of the full decay chain with the analysis described above is  $\sim 2.5\%$ . A more sophisticated analysis using also the three-muons events should approximately double this efficiency.

From the observed number of events and the  $\tilde{\nu}$  mass a measurement of the quantity

Process	Signal	$\bar{t}t$	$WZ$	$Wbb$	$Wt$	$Zb$
$\sigma$ (pb)	3.3	590	26	300	60	7000
$N_{ev}(30 \text{ fb}^{-1})$	$1 \times 10^5$	$1.7 \times 10^7$	$8 \times 10^5$	$9 \times 10^6$	$1.8 \times 10^6$	$2.1 \times 10^8$
Loose cuts	23600	2900	53	2.4	3.5	56
Jet veto	14200	1450	38	-	-	30
$\tilde{\chi}_1^0$	6750	158	4	-	-	-
$\tilde{\chi}_1^\pm$	2700	8	0.4	-	-	-
$\tilde{\nu}_\mu$	2450	0	0.25	-	-	-

TAB. 10: *Cross-sections and expected numbers of events after cuts for the signal and the different Standard Model background contributions considered in the analysis. The “Loose cuts” are described at the beginning of section 3.1, and the “Jet veto” consists in adding the requirement that no third jet with  $p_T > 15$  GeV is reconstructed in the event. The line labelled “ $\tilde{\chi}_1^0$ ” gives the number of events from signatures 1 to 4 ( $e\mu\mu$  and  $\mu\mu\mu$ ) for which a  $\tilde{\chi}_1^0$  candidate is found. The line labelled “ $\tilde{\chi}_1^\pm$ ” shows the number of events from signatures 1 and 2 ( $e\mu\mu$ ) where a  $\tilde{\chi}_1^\pm$  candidate is found in addition, and the last line indicates the number of fully reconstructed events. In the case of the signal, we give the cross-section for the resonant sneutrino production multiplied by the branching ratios into three leptons.*

$\lambda_{211}^2 \times BR$ , where  $BR$  is the product of the branching ratios of the decays shown in equation 3.1, is possible. The measurement of additional SUSY processes will be needed to disentangle the two terms of this product.

### 3.2 Standard Model Background

The requirement of three isolated leptons in the events strongly reduces the possible background sources. The following processes were considered as a background :

- $\bar{t}t$  production, followed by  $t \rightarrow Wb$ , where the two  $W$  and one of the  $b$  quarks decay leptonically.
- $WZ$  production, where both bosons decay leptonically.
- $Wt$  production
- $Wbb$  production
- $Zb$  production

These backgrounds were generated with the PYTHIA MonteCarlo [26], except  $Wt$  and  $Wbb$  for which the ONETOP parton level generator [27] was used, interfaced to PYTHIA for hadronisation and fragmentation. The cross-sections for the various processes, and the number of total expected events for an integrated luminosity of  $30 \text{ fb}^{-1}$  are given in Table 10, according to the cross-section numbers used in the ATLAS physics performance TDR [31]. In particular, even when the cross-section is known at NLO, as in the case of the top, the Born cross-section is taken for internal consistency of the study.

For each of the background processes a sample of events between one seventh and a few times the expected statistics was generated and passed through the simplified simulation of the ATLAS detector.

After the loose selection cuts described in Section 3.1, the background is dominated by top production, as can be seen from the numbers shown in Table 10. The distribution

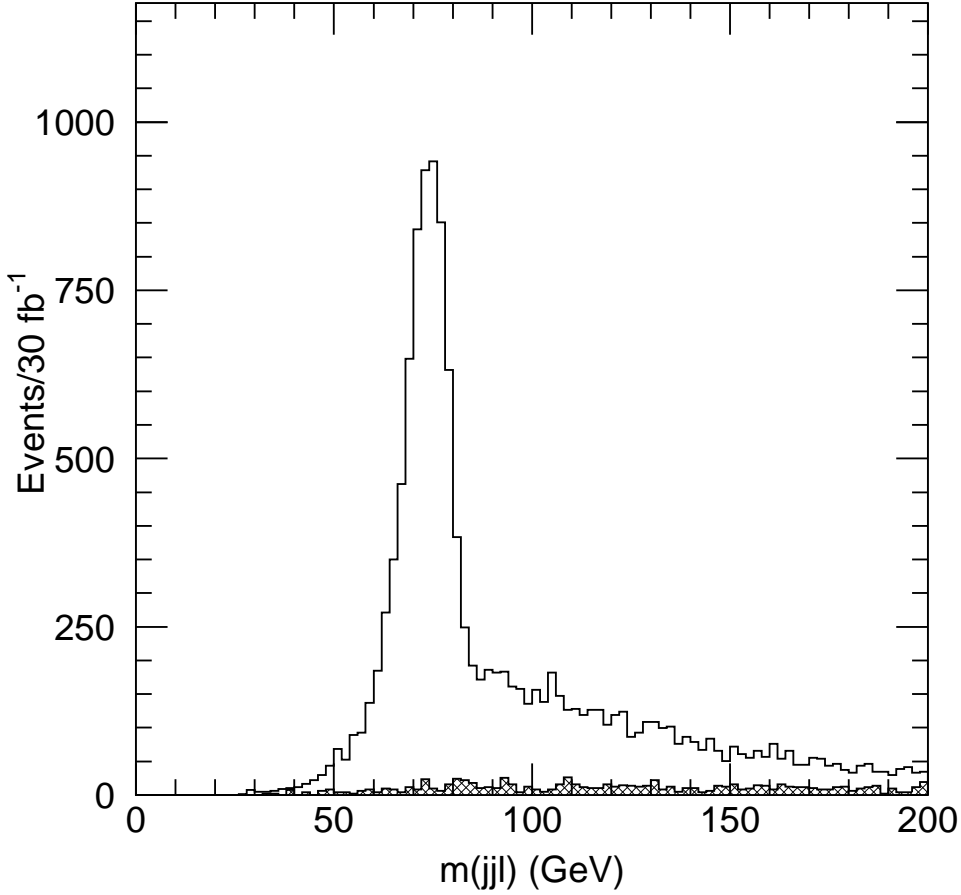


FIG. 8: *Invariant mass of the  $\tilde{\chi}_1^0$  candidates entering the kinematic analysis superimposed to the Standard Model background (hatched).*

of the  $\mu$ -jet-jet invariant mass for background events, obtained as in Section 3.1 and corresponding to the  $\tilde{\chi}_1^0$  candidates selection, is shown as the hatched histogram in Figure 8. In this figure we have superimposed the same distribution for the signal. Already at this level, the signal stands out very clearly from the background, and in the following steps of the reconstruction the background becomes almost negligible. The numbers of background and signal events expected at the various steps of the reconstruction can be compared in Table 10. The full analysis was performed only for the  $t\bar{t}$  and  $WZ$  background because for the other channels the background is essentially negligible compared to top production, and in most cases the MonteCarlo statistics after the initial selection was too low to allow a detailed study. For the SUSY model considered and the chosen value of the  $\lambda'$  coupling constant, even the loose selection applied allows to efficiently separate the signal from the background.

### 3.3 Sensitivity on $\lambda'$

From these results, it is possible to evaluate the minimum value of the  $\lambda'_{211}$  coupling for which it will be possible to discover the signal. The starting point in the analysis is the observation of a peak in the muon-jet-jet invariant mass over an essentially flat background. All of the further analysis steps of the cascade reconstruction rely on the possibility of selecting the events with a mass around the  $\tilde{\chi}_1^0$  peak.

For the observation of the peak, the best signal/background ratio is obtained using the three-muons sample (configurations 3 and 4 above). In the Standard Model, which incorporates lepton universality, about one eighth of the three-leptons events present a three-muons configuration, whereas about half of the signal events come in this configuration, thereby granting an improvement of a factor 4 in signal over background, with respect to the full sample. The three muons come either in the  $'-++'$  or in the  $'-+-'$  sign configuration, because the two muons from the decay chain  $\tilde{\nu}(\tilde{\bar{\nu}}) \rightarrow \tilde{\chi}_1^\pm \mu^\mp \rightarrow \tilde{\chi}_1^0 \mu^\pm \mu^\mp$  must have opposite sign, whereas the  $\tilde{\chi}_1^0$  can decay to muons of either sign. Therefore the muon for the  $\tilde{\chi}_1^0$  reconstruction must be chosen between the two same-sign ones. The distribution for the  $\mu$ -jet-jet invariant mass, for events containing two jets and three muons is shown in Figure 9, scaled down by a factor 25, corresponding to a  $\lambda'$  value of 0.018, superimposed to the expected top background. In the distribution each event enters twice, for each of the two same-sign muons which can be used to reconstruct the  $\tilde{\chi}_1^0$ . We expect, however, that the combination with the “wrong” muon gives in most cases a reconstructed mass outside of the  $\tilde{\chi}_1^0$  peak.

A statistical prescription is needed to define the fact that a peak structure is seen in the signal+background distribution. Given the exploratory nature of the work, we adopt the naive approach of calculating the  $\lambda'$  value for which  $S/\sqrt{B} = 5$ , where  $S$  and  $B$  are respectively the number of signal and background candidates counted in an interval of  $\pm 15$  GeV around the measured  $\tilde{\chi}_1^0$  peak. The window for the definition of a  $\tilde{\chi}_1^0$  candidate is enlarged with respect to the analysis described in Section 3.1, in order to recover the non-gaussian tail of the signal peak, thus increasing the analysis efficiency. In this interval, for the chosen point, for an integrated luminosity of  $30 \text{ fb}^{-1}$ ,  $S = 580000 \times (\lambda')^2$  and  $B = 46$  events. In the hypothesis that the  $t\bar{t}$  background can be precisely measured from data, the lower limit on  $\lambda'_{211}$  is :

$$\lambda'_{211} > 0.0075$$

The pair production of SUSY particles through standard  $R_p$ -conserving processes is another possible source of background, due to the possibility to obtain final states with high lepton multiplicity, and the high production cross-sections. This background can only be evaluated inside models providing predictions for the whole SUSY spectrum. As a preliminary study, a sample of events were generated with the HERWIG 6.0 MonteCarlo [29] by setting the slepton masses at 300 GeV, the masses of squarks and gluinos at 1000 GeV and the chargino-neutralino spectrum as for the example model. The total  $R_p$ -conserving cross-section is in this case  $\sim 6$  pb. A total of 60 SUSY background events which satisfy the requirements used above to define  $S$  and  $B$  are observed. All the events surviving the cuts are from direct chargino and neutralino production, with a small contribution from Drell-Yan slepton production. Since the contributions from squark and gluino decays are strongly suppressed by the jet veto requirements, this result can be considered as a correct



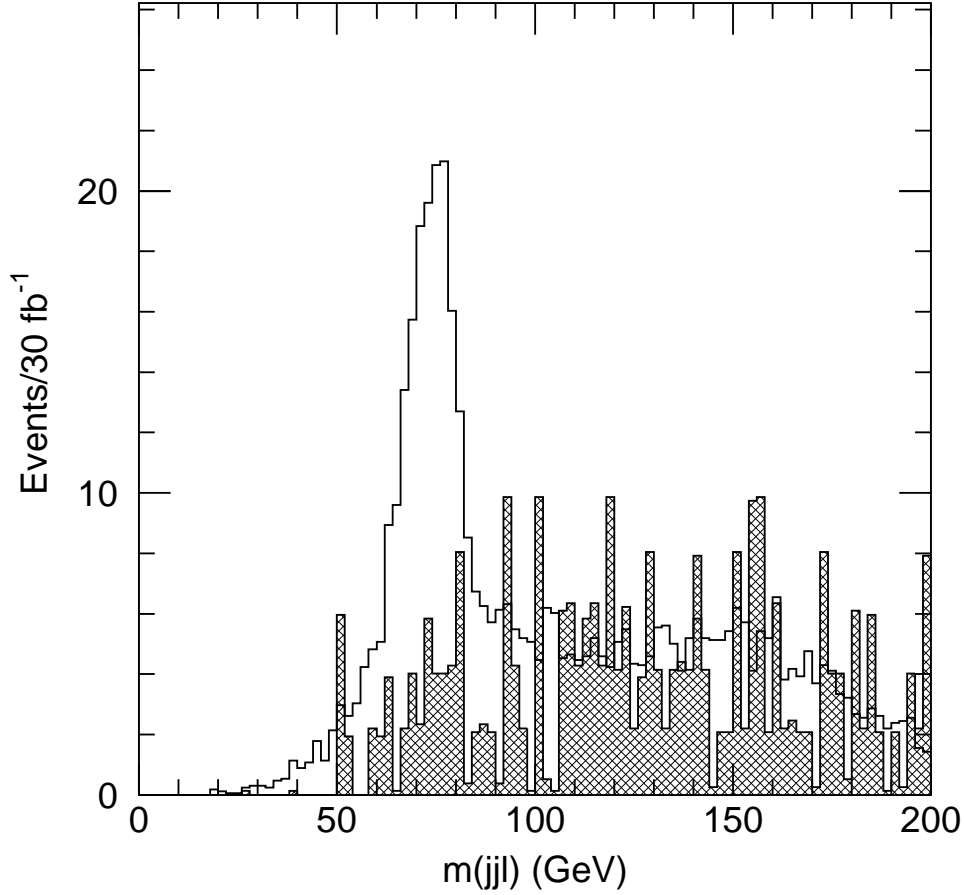


FIG. 9: *Invariant mass of the  $\tilde{\chi}_1^0$  candidates from three-muon events scaled down by a factor 25, corresponding to a  $\lambda'$  value of 0.018, superimposed to the Standard Model background (hatched).*

order of magnitude estimate, independently from the assumed values for the squark and gluino masses. Moreover, the reconstructions of the chargino and sneutrino masses can also be used in order to reduce the SUSY background. A more thorough discussion of the SUSY background will be given below in the framework of the mSUGRA model.

## 4 Analysis reach in various models

For the example case studied in Section 3.1 it was shown that the sneutrino production signal can be easily separated from the background, and allows to perform precision measurements of the masses of the sparticles involved in the decay chain.

The analysis can be generalised to investigate the range of SUSY parameters in which this kind of analysis is possible, and to define the minimum value of the  $\lambda'$  constant which

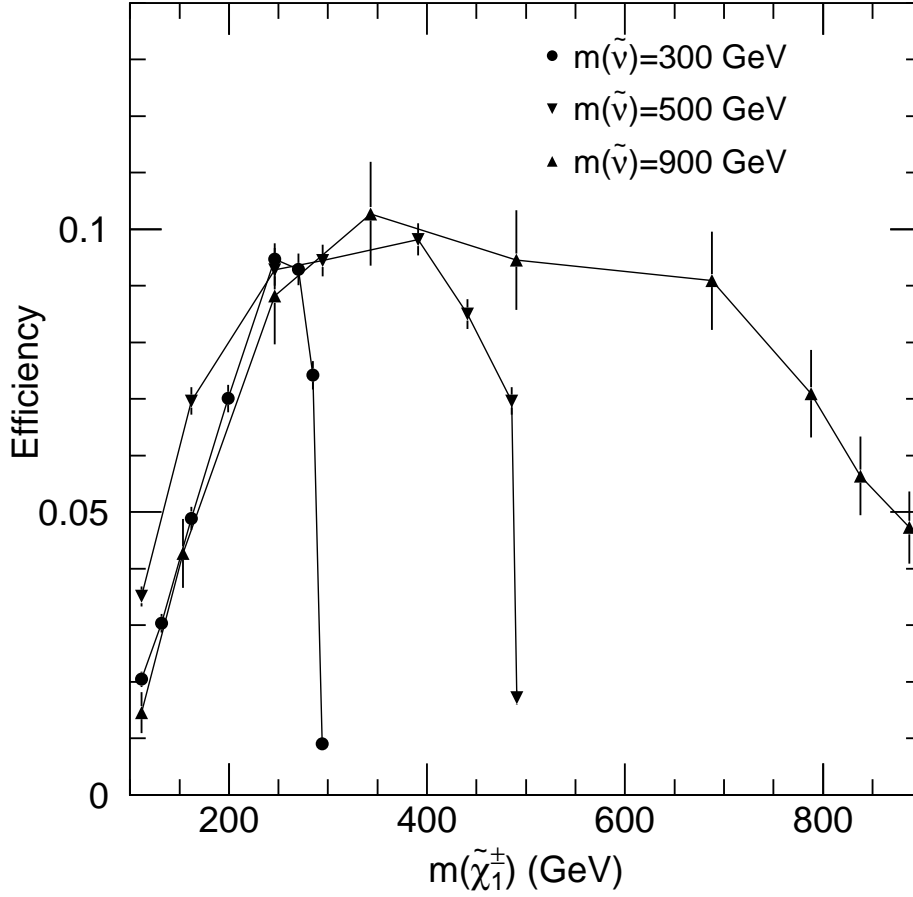


FIG. 10: *Efficiency for reconstructing a  $\mu$ -jet-jet invariant mass within 15 GeV of the  $\tilde{\chi}_1^0$  mass in three-muons events, as a function of the  $\tilde{\chi}_1^\pm$  mass. The shown points were generated with the following parameters :  $-\mu = M_2 = 2M_1$ ,  $\tan\beta = 1.5$ . All the sfermion masses are set equal to the sneutrino mass. Points for  $m_{\tilde{\nu}} = 300, 500$  and  $900$  GeV are shown.*

gives a detectable signal in a given SUSY scenario. The different model parameters enter the definition of the detectability at different levels :

- The sneutrino production cross-section is a function only of the sneutrino mass and of the square of the R-parity violating coupling constant.
- The branching fraction of the sneutrino decay into three leptons is a function of all the SUSY parameters.
- The analysis efficiency is a function of the masses of the three supersymmetric particles involved in the decay.

The dependences of the cross-section and branching ratios on the SUSY parameters were discussed in Section 2 for the MSSM, and are summarised in Figures 2 and 3. We only

need at this point to parameterize the analysis efficiency as a function of the sparticle masses. The number of signal events for each considered model will then be obtained by multiplying the expected number of three-lepton events by the parameterized efficiency.

## 4.1 Efficiency of the three-muon analysis

According to the discussion presented in Section 3.3, we need to calculate the efficiency for the signal process to satisfy the following requirements :

- to pass the initial selection cuts described in Section 3.1 (Loose cuts), including the veto on the third jet (Jet veto) ;
- to contain three reconstructed muons, with one of the  $\mu$ -jet-jet invariant masses within 15 GeV of the  $\tilde{\chi}_1^0$  mass.

Three sneutrino masses,  $m_{\tilde{\nu}} = 300, 500$  and  $900$  GeV were considered, and for each of these the evolution of the efficiency with the  $\tilde{\chi}_1^\pm$  mass was studied. The mass of the  $\tilde{\chi}_1^0$  was assumed to be half of the mass of the  $\tilde{\chi}_1^\pm$ , relation which is in general valid in SUGRA inspired models and correspond to a choice of values for  $|\mu|$  of the same order as  $M_2$ .

The analysis efficiency is shown in Figure 10 as a function of the  $\tilde{\nu}_\mu$  mass and of the  $\tilde{\chi}_1^\pm$  mass. The efficiency values are calculated with respect to the number of events which at generation level did contain the three leptons, therefore they only depend on the event kinematics and not on the branching ratios. The loss of efficiency at the lower end of the  $\tilde{\chi}_1^\pm$  mass spectrum is due to the inefficiency for detecting two jets from the  $\tilde{\chi}_1^0$  decay, either because the two jets are reconstructed as a single jet, or because one of the two jets is below the detection threshold of 15 GeV. The efficiency then becomes approximately independent of the masses of the sneutrino and of the  $\tilde{\chi}_1^\pm$ , up to the point where the  $\tilde{\nu}$  and  $\tilde{\chi}_1^\pm$  masses become close enough to affect the efficiency for the detection of the muon from the  $\tilde{\nu} \rightarrow \tilde{\chi}_1^\pm \mu$  decay ; for  $m_{\tilde{\nu}} - m_{\tilde{\chi}_1^\pm} < 10$  GeV the analysis efficiency rapidly drops to zero. The moderate decrease in efficiency at high  $\tilde{\chi}_1^\pm$  masses for  $m_{\tilde{\nu}} = 900$  GeV can be ascribed to the fact that one of two energetic jets from the  $\tilde{\chi}_1^0$  decay radiates a hard gluon, three jets are reconstructed, and the event is rejected by the jet veto.

At this point all the ingredients are available to study the reach in the parameter space for the analysis presented in Section 3 within different SUSY models.

## 4.2 Analysis reach in the MSSM

The region in the  $m_{\tilde{\nu}}-m_{\tilde{\chi}_1^\pm}$  plane for which the signal significance is greater than  $5\sigma$ , as defined in Section 3.3, and at least 10 signal events are observed for an integrated luminosity of  $30 \text{ fb}^{-1}$  is shown in Figure 11 for different choices of the  $\lambda'_{211}$  constant. The behaviours of the sensitivity curves in the  $m_{\tilde{\nu}}-m_{\tilde{\chi}_1^\pm}$  plane are well explained by the variations of the single chargino production cross-section shown in Figure 3 in the same plane of parameters. The SUSY background is not considered in the plot, as it depends on all the model parameters. It was however verified in a few example cases that for our analysis cuts this background is dominated by direct chargino and neutralino production, and it becomes negligible in the limit of high  $\tilde{\chi}_1^0$  and  $\tilde{\chi}^\pm$  masses. The main effect of taking into account this background will be to reduce the significance of the signal for  $\tilde{\chi}_1^\pm$  masses lower than 200 GeV.

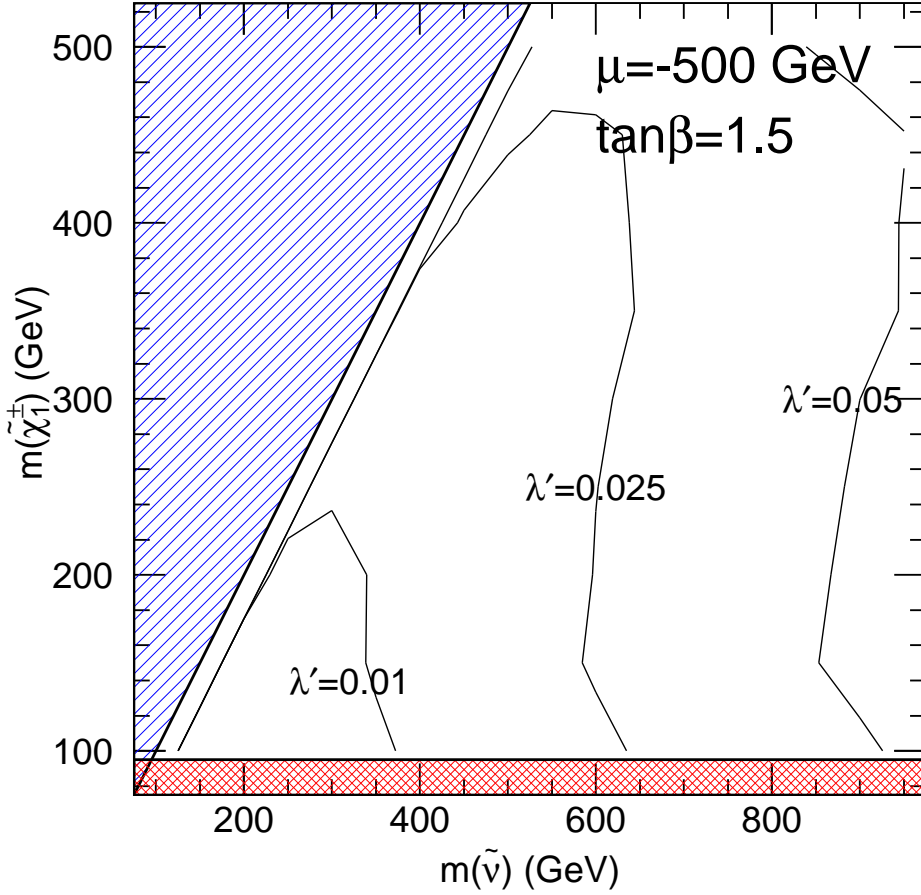


FIG. 11:  $5\sigma$  reach in the  $m_{\tilde{\nu}}-m_{\tilde{\chi}_1^\pm}$  plane for three different choices of the  $\lambda'_{211}$  coupling for an integrated luminosity of  $30 \text{ fb}^{-1}$  at the LHC. The chosen model parameters were :  $\mu = -500 \text{ GeV}$ ,  $\tan\beta=1.5$ ,  $m_{\tilde{q}} = m_{\tilde{l}} = 300 \text{ GeV}$ ,  $A_t = A_b = A_\tau = 0$ ,  $M_2 = 2M_1$ . The significance is defined only considering the Standard Model background, and a signal of at least ten events is required. The hatched region at the upper left corresponds to  $m_{\tilde{\nu}} < m_{\tilde{\chi}_1^\pm}$ . The cross-hatched region at low  $m_{\tilde{\chi}_1^\pm}$  is excluded by the preliminary LEP results at  $\sqrt{s} = 196 \text{ GeV}$  [30].

From the curves in Figure 11 we can conclude that within the MSSM, the production of a 900 GeV sneutrino for  $\lambda'_{211} > 0.05$ , and of a 350 GeV sneutrino for  $\lambda'_{211} > 0.01$  can be observed within the first three years of LHC running, provided that the sneutrino is heavier than the lightest chargino.

The sensitivity on an  $\mathcal{R}_p$  coupling of type  $\lambda'_{2jk}$  can be derived from the sensitivity obtained for  $\lambda'_{211}$ , as explained in Section 2.2. For example, we have seen that the sensitivity on  $\lambda'_{221}$  was  $\sim 1.5$  times weaker than the sensitivity on  $\lambda'_{211}$ , for  $\tan\beta=1.5$ ,  $M_2 = 200 \text{ GeV}$ ,  $\mu = -500 \text{ GeV}$  and  $m_{\tilde{\nu}} = 400 \text{ GeV}$ . This set of parameters leads to a sensitivity on  $\lambda'_{211}$

$\lambda'_{211}$	$\lambda'_{212}$	$\lambda'_{213}$	$\lambda'_{221}$	$\lambda'_{222}$	$\lambda'_{223}$	$\lambda'_{231}$	$\lambda'_{232}$	$\lambda'_{233}$
0.01	0.02	0.02	0.02	0.03	0.05	0.03	0.06	0.09

TAB. 11: Sensitivities on the  $\lambda'_{2jk}$  coupling constants deduced from the sensitivity on  $\lambda'_{211}$  for  $\tan\beta=1.5$ ,  $M_1 = 100$  GeV,  $M_2 = 200$  GeV,  $\mu = -500$  GeV,  $m_{\tilde{q}} = m_{\tilde{l}} = 300$  GeV and  $m_{\tilde{\nu}} = 400$  GeV.

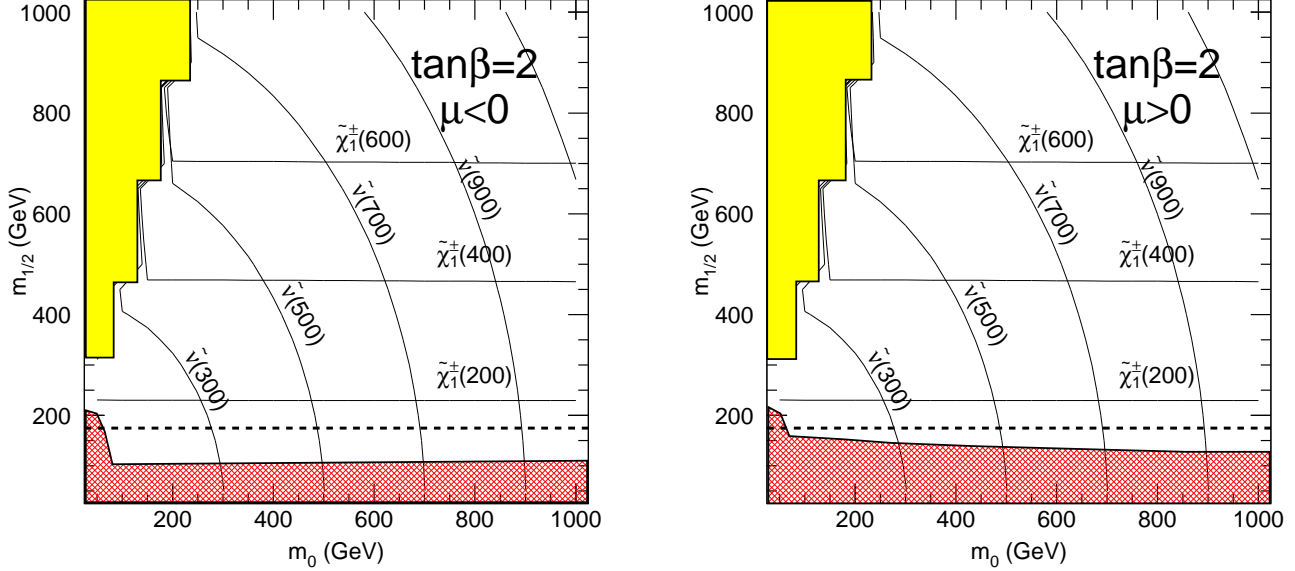


FIG. 12: Curves of equal mass for  $\tilde{\nu}$  and  $\tilde{\chi}_1^\pm$  in the  $m_0 - m_{1/2}$  plane for  $\tan\beta = 2$ . The grey region at the upper left indicates the domain where the  $\tilde{\chi}_1^0$  is not the LSP. The cross-hatched region for low  $m_{1/2}$  gives the kinematic limit for the discovery of  $\tilde{\chi}_1^\pm$  or  $\tilde{l}$  by LEP running at  $\sqrt{s} = 200$  GeV. The dotted line shows the region below which the  $\tilde{\chi}_1^\pm$  decays to a virtual  $W$ .

of about 0.015 as can be seen in Figure 11, and hence to a sensitivity on  $\lambda'_{221}$  of  $\sim 0.022$ . In Table 11, we present the sensitivity on any  $\lambda'_{2jk}$  coupling estimated using the same method and for the same MSSM parameters. Those sensitivities represent an important improvement with respect to the low-energy limits of [1].

In the case of a single dominant  $\lambda'_{2j3}$  coupling the neutralino decays as  $\tilde{\chi}_1^0 \rightarrow \mu u_j b$  and the semileptonic decay of the b-quark could affect the analysis efficiency. Hence in this case, the precise sensitivity cannot be simply calculated by scaling the value obtained for  $\lambda'_{211}$ . The order of magnitude of the sensitivity which can be inferred from our analysis should however be correct.

### 4.3 Analysis reach in mSUGRA

Our framework throughout this Section will be the so-called minimal supergravity model. In this model the parameters obey a set of boundary conditions at the Grand Uni-

fication Theory (GUT) scale  $M_x$ . These conditions appear to be natural in supergravity scenario since the supersymmetry breaking occurs in an hidden sector which communicates with the visible sector only through gravitational interactions. First, mSUGRA contains the gauge coupling unification at  $M_x$ , such an unification being suggested by the experimental results obtained at LEP I. One can view the gauge coupling unification assumption as a fixing of the GUT scale  $M_x$ . Second, the gaugino (bino, wino and gluino) masses at  $M_x$  are given by the universal mass  $m_{1/2}$ . the parameters  $m_{1/2}$  and  $M_i$  [ $i = 1, 2, 3$ ] are thus related by the solutions of the renormalization group equations (RGE). Besides, since the gaugino masses and the gauge couplings are governed by the same RGE, one has the well-known relation :  $M_1 = \frac{5}{3} \tan^2 \theta_W M_2$ . Similarly, at  $M_x$ , the universal scalars mass is  $m_0$  and the trilinear couplings are all equal to  $A_0$ . Finally, in mSUGRA the absolute value of the higgsino mixing parameter  $|\mu|$  as well as the bilinear coupling  $B$  are determined by the radiative electroweak symmetry breaking conditions. Therefore, mSUGRA contains only the five following parameters :  $sign(\mu)$ ,  $\tan \beta$ ,  $A_0$ ,  $m_0$  and  $m_{1/2}$ .

Due to the small dependence of the single chargino production rate on the  $\mu$  parameter for  $M_2 \leq |\mu|$  (see Section 2), the study of the mSUGRA model in which  $|\mu|$  is fixed by the electroweak symmetry breaking condition provides information on a broader class of models. The single chargino production rate depends mainly on the values of  $m_0$  and  $m_{1/2}$  (see Section 2). We will set  $A_0 = 0$ , and study the detectability of the signal in the  $m_0 - m_{1/2}$  plane. We show in Figure 12 the curves of equal mass for  $\tilde{\nu}$  and  $\tilde{\chi}_1^\pm$  for  $\tan \beta = 2$  calculated with the ISASUSY [28] package which uses one-loop RGE to get the SUSY spectrum from the mSUGRA parameters.

The signal reach can be easily evaluated from the sparticle mass spectrum and branching fractions by using the parameterization of the analysis efficiency shown in Figure 10.

## Supersymmetric background

In the case of a well constrained model as mSUGRA, the SUSY background can in principle be evaluated in each considered point in the parameter space. For this evaluation the full SUSY sample must be generated for each point, requiring the generation of a large number of events.

The sparticle masses for the model studied in detail in Section 3 uniquely define a model in the mSUGRA framework. Therefore, as a first approach to the problem, a full analysis was performed for this model, corresponding to the parameter values :

$$m_0 = 275 \text{ GeV}, \quad m_{1/2} = 185 \text{ GeV}, \quad \tan \beta = 1.5, \quad \mu < 0, \quad A_0 = 0.$$

For this mSUGRA point, the mass scale for squarks/gluinos is in the proximity of 500 GeV, and the total cross-section for all the SUSY particles pair productions is approximately 130 pb, yielding a signal of  $\sim 4 \cdot 10^6$  events for the first three years of data-taking at the LHC. A total of 400k events were generated and analysed. The number of surviving events after cuts in the three-muons sample was  $47 \pm 21$  for an integrated luminosity of  $30 \text{ fb}^{-1}$ . All the background events come from direct chargino and neutralino production, as it was the case for the MSSM point studied in Section 3.3. As a cross-check, we generated for the same mSUGRA point only the processes of the type  $pp \rightarrow \tilde{\chi} + X$ , where  $\tilde{\chi}$  denotes either  $\tilde{\chi}^0$  or  $\tilde{\chi}^\pm$ , and  $X$  any other SUSY particle. The cross-section is in this case

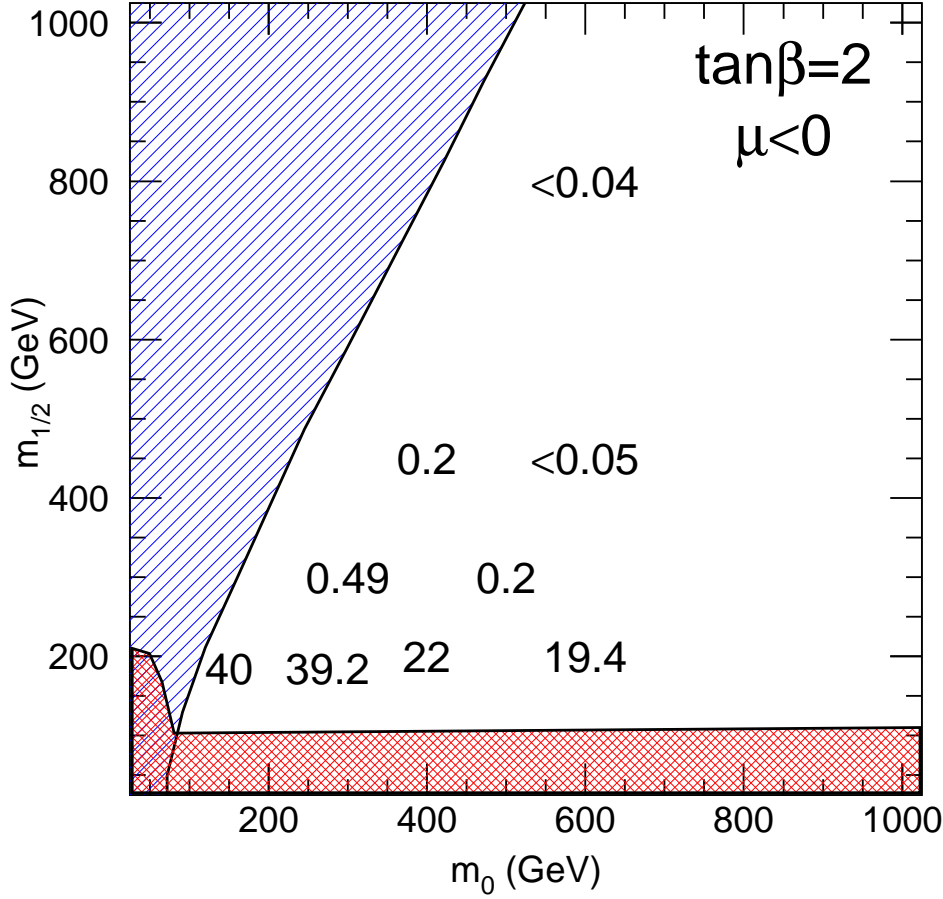


FIG. 13: Number of SUSY background events for an integrated luminosity of  $30 \text{ fb}^{-1}$  in the  $m_0 - m_{1/2}$  plane with  $\tan \beta = 2$  for a few selected test models. The hatched region at the upper left corresponds to  $m_{\tilde{\nu}} < m_{\tilde{\chi}_1^\pm}$ . The cross-hatched region for low  $m_{1/2}$  gives the kinematic limit for the discovery of  $\tilde{\chi}_1^\pm$  or  $\tilde{l}$  by LEP running at  $\sqrt{s} = 200 \text{ GeV}$ .

$\sim 6 \text{ pb}$ , and the number of background events is  $39 \pm 7$  events, in good agreement with the number evaluated generating all the SUSY processes.

Based on this result, we have performed a scan in the  $m_0 - m_{1/2}$  plane the fixed values  $\tan \beta = 2$ ,  $\mu < 0$ . On a grid of points we generated event samples for the  $pp \rightarrow \tilde{\chi} + X$  processes with the HERWIG 6.0 MonteCarlo [29]. The number of SUSY events with a  $\mu$ -jet-jet combination with an invariant mass within 15 GeV of the  $\tilde{\chi}_1^0$  mass is shown in Figure 13 in the  $m_0 - m_{1/2}$  plane for an integrated luminosity of  $30 \text{ fb}^{-1}$ . The background is significant for a  $\tilde{\chi}_1^\pm$  mass of 175 GeV ( $m_{1/2} = 200 \text{ GeV}$ ), and becomes essentially negligible for  $\tilde{\chi}_1^\pm$  mass of 260 GeV ( $m_{1/2} = 300 \text{ GeV}$ ). This behaviour is due to the combination of two effects : the  $\tilde{\chi}^\pm \tilde{\chi}^\pm$  production cross-section decreases with increasing  $\tilde{\chi}^\pm$  mass, and the probability of losing two of the four jets from the decay of the two  $\tilde{\chi}_1^0$  in the event

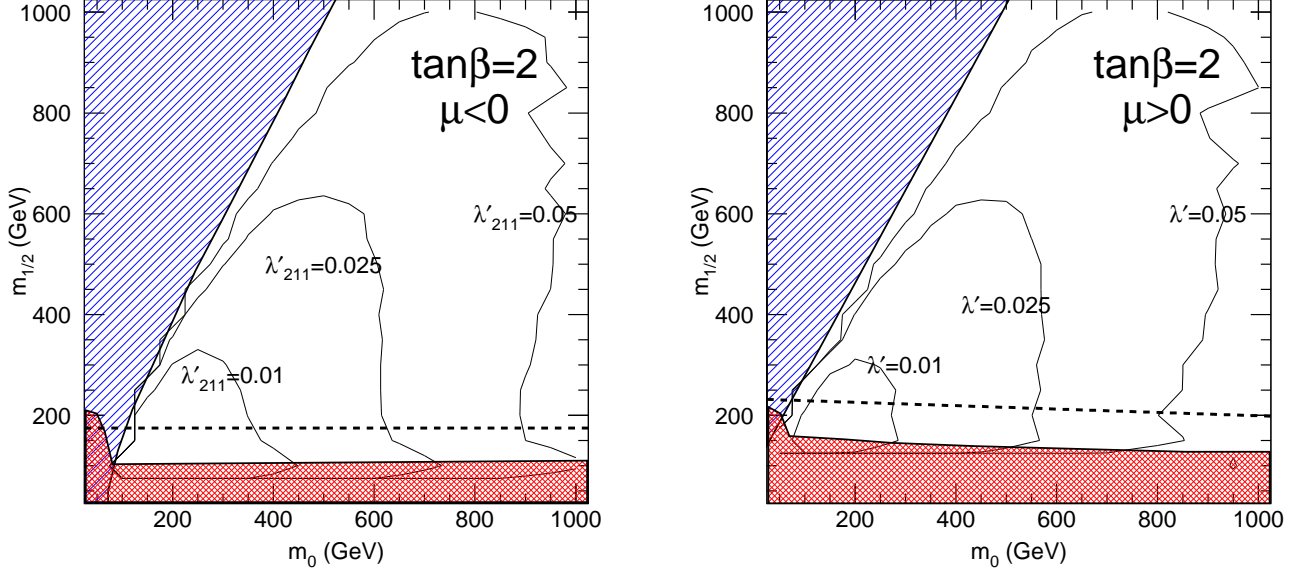


FIG. 14:  $5\sigma$  reach in the  $m_0 - m_{1/2}$  plane for  $\tan\beta=2$  and three different choices of the  $\lambda'_{211}$  coupling for an integrated luminosity of  $30 \text{ fb}^{-1}$  at the LHC. The significance is defined only considering the Standard Model background, and a signal of at least ten events is required. The dotted line shows the region below which the  $\tilde{\chi}_1^\pm$  decays to a virtual  $W$ .

becomes very small for a  $\tilde{\chi}_1^\pm$  mass of  $\sim 220$  GeV. Indeed, the suppression of the SUSY background is mainly due to the Jet veto cut.

Given the high SUSY cross-section, and the high lepton multiplicity from  $\tilde{\chi}_1^0$  decays, a prominent signal should manifest itself through R-conserving sparticle pair production in this scenario. Single resonant sneutrino production will then be used as a way of extracting information on the value of the  $R_p$ -violating coupling constant, and of precisely measuring the masses of  $\tilde{\nu}_\mu$ ,  $\tilde{\chi}_1^\pm$ ,  $\tilde{\chi}_1^0$ . Moreover, thanks to the very high number of produced  $\tilde{\chi}_1^0$  expected from  $\tilde{q}/\tilde{g}$  pair production, the  $\tilde{\chi}_1^0$  mass will be directly reconstructed from  $\tilde{q}$  and  $\tilde{g}$  decays, as shown in [31]. So, for the present analysis it can be assumed that the  $\tilde{\chi}_1^0$  mass is approximately known, and an attempt to reconstruct the  $\tilde{\chi}_1^\pm$  peak can be performed even if the  $\tilde{\chi}_1^0$  reconstruction does not yield a significant peak over the SUSY+SM background. In order to perform the full reconstruction, one just needs to observe a statistically significant excess of events over what is expected from the Standard Model background in the mass region corresponding to the known  $\tilde{\chi}_1^0$  mass. The full kinematic reconstruction described in Section 3.1 above will then easily allow to separate the process of interest from the SUSY background.

## Results

Based on the discussion in the previous section we calculate the signal significance as  $S/\sqrt{B}$ , where for the signal  $S$  we only consider the resonant sneutrino production, and for the background  $B$  we only consider the SM background. We show in Figure 14 for



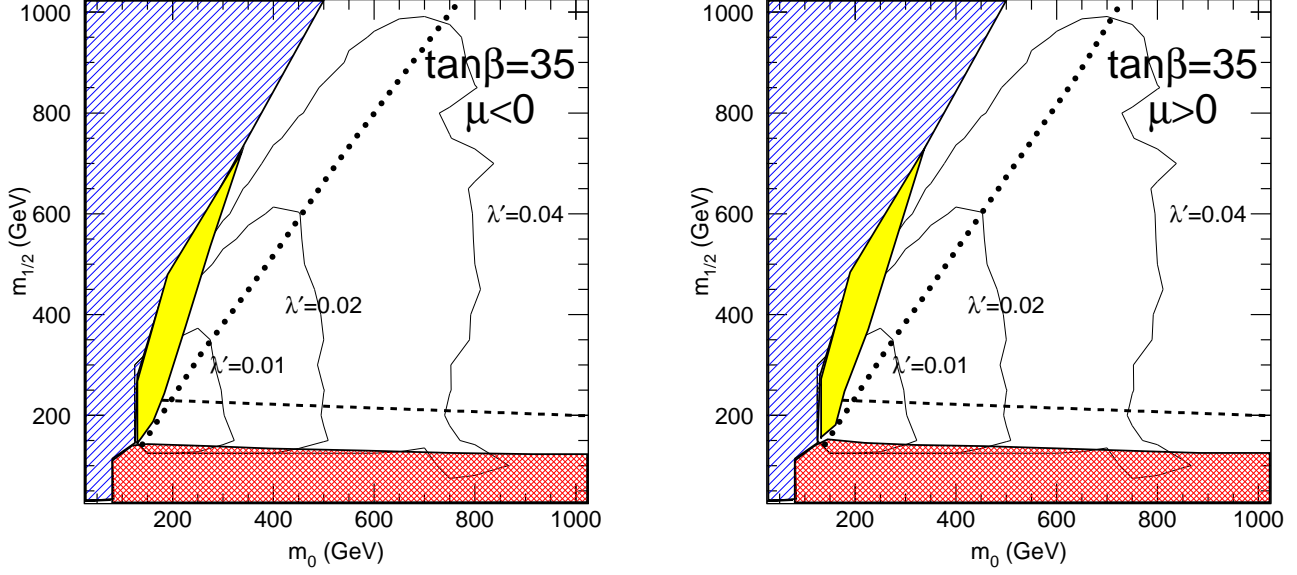


FIG. 15:  $5\sigma$  reach in the  $m_0 - m_{1/2}$  plane for  $\tan\beta=35$  and three different choices of the  $\lambda'_{211}$  coupling for an integrated luminosity of  $30 \text{ fb}^{-1}$  at the LHC. The significance is defined only considering the Standard Model background, and a signal of at least ten events is required. The dashed line shows the region below which the  $\tilde{\chi}_1^\pm$  decays to a virtual  $W$ . The region to the left of the dotted lines has a branching ratio for  $\tilde{\chi}_1^\pm \rightarrow \tilde{\tau}_1 \nu_\tau$  larger than 50%, and the grey area indicates the region for which a low signal efficiency is expected.

$\tan\beta = 2$  and for the two signs of  $\mu$  the regions in the  $m_0 - m_{1/2}$  plane for which the signal significance exceeds  $5\sigma$  and the number of signal events is larger than 10, for an integrated luminosity of  $30 \text{ fb}^{-1}$ . The reach is shown for three different choices of the  $\lambda'_{211}$  parameter :  $\lambda'_{211} = 0.01, 0.025, 0.05$ . Even for the lowest considered coupling the signal can be detected in a significant fraction of the parameter space. The dotted line shows the region below which the  $\tilde{\chi}_1^\pm$  decays to the  $\tilde{\chi}_1^0$  and a virtual  $W$ , thus making the kinematic reconstruction of the decay chain described in Section 3.1 impossible. The reconstruction of the  $\tilde{\chi}_1^0$  is however still possible, but the reconstruction efficiency drops rapidly due to the difficulty to separate the two soft jets from the  $\tilde{\chi}_1^0$  decay. A detailed study involving careful consideration of jet identification algorithms is needed to assert the LHC reach in that region.

As observed in [32], the efficiencies quoted for this analysis rely on a branching ratio of  $\sim 100\%$  for the decay  $\tilde{\chi}_1^\pm \rightarrow W\tilde{\chi}_1^0$ . This is in general true in SUGRA models as long as the  $\tilde{\tau}_1$  is heavier than the  $\tilde{\chi}_1^\pm$ , corresponding to moderate values for  $\tan\beta$ . For high  $\tan\beta$ , the decay  $\tilde{\chi}_1^\pm \rightarrow \tilde{\tau}_1 \nu_\tau$  can become kinematically possible, and its branching ratio can dominate the standard  $\tilde{\chi}_1^\pm \rightarrow W\tilde{\chi}_1^0$ . The stau in turns typically decays as  $\tilde{\tau}_1 \rightarrow \tau \tilde{\chi}_1^0$ . The three-leptons signature is in this case even enhanced, due to the higher branching fraction into electrons and muons for the  $\tau$  compared to the  $W$ , at the price of a softer lepton spectrum. The  $\tilde{\chi}_1^0$  reconstruction is still possible but the presence of three neutrinos (two

additional neutrinos come from the leptonic  $\tau$  decay) renders the reconstruction of the particles earlier in the decay chain difficult. The analysis efficiency is essentially unaffected with respect to the low  $\tan\beta$  case as long as the mass difference between the  $\tilde{\tau}_1$  and the  $\tilde{\chi}_1^0$  is larger than  $\sim 50$  GeV. For  $\tilde{\tau}_1$  and  $\tilde{\chi}_1^0$  masses too much degenerate, the transverse momentum of the charged lepton coming from the  $\tau$  decay would often fall below the analysis requirements, leading thus to a reduction of the signal efficiency. The reach in the  $m_0 - m_{1/2}$  plane is shown in Figure 15 for  $\tan\beta = 35$  and three different choices of the  $\lambda'_{211}$  coupling. The branching fraction for the decay  $\tilde{\chi}_1^\pm \rightarrow \tilde{\tau}_1 \nu_\tau$  is higher than 50% to the left of the dotted line, and the region for which a reduced signal efficiency is expected is displayed as a grey area. The reach for  $\tilde{\chi}_1^0$  detection is similar to the low  $\tan\beta$  case, but the region in which the full reconstruction of the sneutrino decay chain is possible is severely restricted.

## 5 Conclusions

We have analysed the resonant sneutrino production at LHC in supersymmetric models with R-parity violation. We have focused on the three-leptons signature which has a small Standard Model background, and allows a model-independent mass reconstruction of the full sneutrino decay chain.

A detailed study for an example MSSM point has shown that the mass reconstruction analysis has an efficiency of a few percent, and that a precise measurement of the masses of  $\tilde{\nu}$ ,  $\tilde{\chi}_1^\pm$ ,  $\tilde{\chi}_1^0$  can be performed. Both the Standard Model background and the backgrounds from other SUSY pair productions were studied in detail, and shown to be well below the expected signal for a value of the considered  $\mathcal{R}_p$  coupling  $\lambda'_{211}$  taken at the present low-energy limit.

The trilepton signal from sneutrino production was then studied as a function of the model parameters under different model assumptions, and sensitivity over a significant part of the parameter space was found. Within the MSSM, the production of a 900 GeV sneutrino for  $\lambda'_{211} > 0.05$ , and of a 350 GeV sneutrino for  $\lambda'_{211} > 0.01$  can be observed in the first three years of LHC running. In the framework of the mSUGRA model, the region in the  $m_0 - m_{1/2}$  space accessible to the analysis was mapped as a function of the value of the  $R_p$ -violating coupling for representative values of  $\tan\beta$ . A significant part of the  $m_0 - m_{1/2}$  plane will be accessible for  $\lambda'_{211} > 0.01$ .

Although the detailed study was focused on the case of a single dominant  $\lambda'_{211}$  coupling, we have found that the resonant sneutrino production analysis can bring interesting sensitivities on all the  $\mathcal{R}_p$  couplings of the type  $\lambda'_{2jk}$ , compared to the low-energy constraints. The resonant sneutrino production should also allow to test most of the  $\lambda'_{1jk}$  coupling constants.

In conclusion we have demonstrated that if minimal supersymmetry with R-parity violation is realised in nature, the three-leptons signature from sneutrino decay will be a privileged channel for the precision measurement of sparticle masses and for studying the SUSY parameter space, over a broad spectrum of models. Analyses based on the study of events including three leptons, were often advocated in the literature [33]-[46] as a particularly sensitive way of attacking the search for SUSY at the LHC in the standard R-conserving scenario. The higher lepton multiplicity and the possibility to perform precise measurements of the model parameters make this kind of analyses an even more attractive

possibility in the case of R-parity violation with dominant  $\lambda'$  couplings.

## 6 Acknowledgements

This work was initiated during a workshop held in Les Houches. We warmly thank Patrick Aurenche and all of the organising team for the stimulating program, the excellent atmosphere and the outstanding computing facilities. We are also deeply indebted to the HERWIG team for allowing us to use a prerelease of the HERWIG 6.0 MonteCarlo.

# References

- [1] H. Dreiner, published in *Perspectives on Supersymmetry*, ed. by G.L. Kane, World Scientific (1998), hep-ph/9707435.
- [2] S. Dimopoulos and L.J. Hall, Phys. Lett. **B 207**, 210 (1988).
- [3] H. Dreiner and G. G. Ross, Nucl. Phys. **B 365**, 597 (1991).
- [4] V. Barger, G. F. Giudice and T. Han, Phys. Rev. **D 40**, 2987 (1989).
- [5] G. Bhattacharyya, Invited talk presented at ‘Beyond the Desert’, Castle Ringberg, Tegernsee, Germany, 8-14 June 1997; Susy ’96, Nucl. Phys. B (Proc. Suppl.) **52A** 83 (1997).
- [6] R. Barbier et al., Report of the Group on the R-parity Violation, hep-ph/9810232.
- [7] F. Ledroit and G. Sajot, GDR-S-008 (ISN, Grenoble, 1998).
- [8] B. C. Allanach, A. Dedes, H. Dreiner, Phys. Rev. **D60**, 075014 (1999).
- [9] S. Dimopoulos, R. Esmailzadeh, L.J. Hall, J. Merlo and G.D. Starkman, Phys. Rev. **D41**, 2099 (1990).
- [10] P. Binetruy et al., ECFA Large Hadron Collider (LHC) Workshop, Aachen, 1990, Vol. II.
- [11] A. Datta, J. M. Yang, B.-L. Young and X. Zhang, Phys. Rev. **D56**, 3107 (1997).
- [12] R. J. Oakes, K. Whisnant, J. M. Yang, B.-L. Young and X. Zhang, Phys. Rev. **D57**, 534 (1998).
- [13] J. L. Hewett and T. G. Rizzo, “Proceedings of the XXIX International Conference on High Energy Physics”, Vancouver, CA, 23-29 July 1998, hep-ph/9809525.
- [14] P. Chiappetta et al., hep-ph/9910483.
- [15] J. Kalinowski, R. Rückl, H. Spiesberger and P. M. Zerwas, Phys. Lett. **B414**, 297 (1997).
- [16] J. Kalinowski, Proceedings of “*Beyond the Desert 97 – Accelerator and Non-Accelerator Approaches*”, Ringberg Castle, Germany, June 1997, hep-ph/9708490.
- [17] S. Bar-Shalom, G. Eilam and A. Soni, Phys. Rev. **D59**, 055012 (1999).
- [18] E. L. Berger, B. W. Harris and Z. Sullivan, Phys. Rev. Lett. **83**, 4472 (1999).
- [19] H. Dreiner, P. Richardson and M. H. Seymour, to appear in the proceedings of the BTMSSM subgroup of the Physics at Run II Workshop on Supersymmetry/Higgs, hep-ph/9903419.
- [20] H. Dreiner, P. Richardson and M. H. Seymour, hep-ph/0001224.
- [21] I. Hinchliffe and F. Paige, hep-ph/9907919.

- [22] SUSYGEN 3.0/06 N. Ghodbane, S. Katsanevas, P. Morawitz and E. Perez, [lyoinfo.in2p3.fr/susygen/susygen3.html](http://lyoinfo.in2p3.fr/susygen/susygen3.html); N. Ghodbane, hep-ph/9909499.
- [23] JETSET 7.3 and 7.4; T. Sjöstrand, Lund Univ. preprint LU-TP-95-20 (August 1995) 321pp; *idem*, CERN preprint TH-7112-93 (February 1994) 305pp.
- [24] V.N. Gribov et L.N. Lipatov, Sov. Journ. Nucl. Phys. 15 (1972) 78;  
G. Altarelli et G. Parisi, Nucl. Phys. B126 (1977) 298;  
Y.L. Dokshitzer, JETP 46 (1977) 641.
- [25] E. Richter-Was, D. Froidevaux, L. Poggioli, 'ATLFAST 2.0 : a fast simulation package for ATLAS', ATLAS Internal Note ATL-PHYS-98-131 (1998).
- [26] T. Sjöstrand, Comp. Phys. Comm. **82**, 74 (1994).
- [27] D.O. Carlson, S. Mrenna, C.P. Yuan, private communication;  
D.O. Carlson and C.P. Yuan, Phys. Lett. **B306**, 386 (1993).
- [28] H. Baer, F.E. Paige, S.D. Protopopescu, and X. Tata, hep-ph/9305342; *ibid.*, hep-ph/9804321 (1998).
- [29] HERWIG 6.1 Release Note, hep-ph/9912396; G. Marchesini, B. R. Webber, G. Abbiendi, I. G. Knowles, M. H. Seymour and L. Stanco, Computer Phys. Commun. **67**, 465 (1992).
- [30] The ALEPH Collaboration, Internal Note ALEPH 99-078, CONF 99-050 (1999), contributed to HEP-EPS 99.
- [31] The ATLAS Collaboration, 'ATLAS Detector and Physics Performance Technical Design Report', ATLAS TDR 15, CERN/LHCC/99-15 (1999).
- [32] G. Moreau et al., To appear in Phys. Lett. **B**, hep-ph/9910341.
- [33] P. Nath and R. Arnowitt, Mod. Phys. Lett. **A 2**, 331 (1987).
- [34] R. Arnowitt, R. Barnett, P. Nath and F. Paige, Int. J. Mod. Phys. **A 2**, 1113 (1987).
- [35] H. Baer, K. Hagiwara and X. Tata, Phys. Rev. **D35**, 1598 (1987).
- [36] R. Barbieri, F. Caravaglios, M. Frigeni and M. Mangano, Nucl. Phys. **B 367**, 28 (1991).
- [37] T. Kamon, J. L. Lopez, P. McIntyre, and J. T. White, Phys. Rev. **D50**, 5676 (1994).
- [38] H. Baer, C.-H. Chen, C. Kao and X. Tata, Phys. Rev. **D52**, 1565 (1995).
- [39] S. Mrenna, G. Kane, G. Kribs and J. Wells, Phys. Rev. **D53**, 1168 (1996).
- [40] H. Baer, C.-H. Chen, M. Drees, F. Paige and X. Tata, Phys. Rev. Lett. **79**, 986 (1997).
- [41] H. Baer, C.-H. Chen, M. Drees, F. Paige and X. Tata, Phys. Rev. **D58**, 075008 (1998).
- [42] V. Barger, C. Kao and T.-J. Li., Phys. Lett. **B433**, 328 (1998).
- [43] V. Barger and C. Kao, preprint FERMILAB-PUB-98/342-T, Phys. Rev. **D60**, 115015 (1999).
- [44] J. Lykken and K. T. Matchev, preprint FERMILAB-PUB-99/034-T, Phys. Rev. **D61**, 015001 (2000).
- [45] K. T. Matchev and D. M. Pierce, preprint FERMILAB-PUB-99/078-T, Phys. Rev. **D60**, 075004 (1999).
- [46] H. Baer, M. Drees, F. Paige, P. Quintana, X. Tata, hep-ph/9906233.



# Publication V





# Systematics of single superpartners production at leptonic colliders

M. Chemtob, G. Moreau

*Service de Physique Théorique  
CE-Saclay F-91191 Gif-sur-Yvette, Cedex France*

Phys. Rev. **D59** (1999) 055003, hep-ph/9807509

## Abstract

*We examine the effects of the lepton number violating  $R$  parity odd superpotential,  $W = \lambda_{ijk} L_i L_j E_k^c$ , on single production of fermion (charginos and neutralinos) and scalar (sleptons and sneutrinos) superpartners at leptonic colliders for center of mass energies up to  $500\text{GeV} - 1\text{TeV}$ . The probability amplitudes for all the five  $2 \rightarrow 2$  body processes :  $l_J^+ l_J^- \rightarrow \tilde{\chi}_1^\pm l_m^\mp$ ,  $\tilde{\chi}_1^0 \nu_m$  ( $\tilde{\chi}_1^0 \tilde{\nu}_m$ ),  $\tilde{l}_m^\mp W^\pm$ ,  $\tilde{\nu}_m Z^0$  ( $\tilde{\nu}_m \tilde{Z}^0$ ),  $\tilde{\nu}_m \gamma$  ( $\tilde{\nu}_m \tilde{\gamma}$ ), and the decays branching ratios for the produced superpartners are calculated at tree level. The rates for all five reactions are proportionnal to  $\lambda_{mJJ}^2$  where  $J = 1, 2$  for  $e^-e^+$  and  $\mu^-\mu^+$  colliders, respectively. A semi-quantitative discussion is presented within a supergravity model assuming grand unification of gauge interactions and universal (flavor independent) soft supersymmetry breaking parameters  $m_0$  (scalars),  $m_{1/2}$  (gauginos) at the unification scale. The predictions obtained for the total and partial rates show that the single production reactions have a good potential of observability at the future  $e^-e^+$  and  $\mu^-\mu^+$  supercolliders. For values of the  $R$  parity violating coupling constant of order 0.05, the  $\tilde{\chi}^{\pm,0}$  productions could probe all the relevant intervals for  $\tan\beta$  and  $m_0$  and broad regions of the parameter space for the  $\mu$  (Higgs mixing) and  $m_{1/2}$  parameters ( $|\mu| < 400\text{GeV}$ ,  $m_{1/2} < 240\text{GeV}$ ), while the  $\tilde{\nu}$  and  $\tilde{l}$  productions could probe sneutrinos and sleptons masses up to the kinematical limits ( $m_{\tilde{\nu}} < 500\text{GeV}$ ,  $m_{\tilde{l}} < 400\text{GeV}$ ). Using the hypothesis of a single dominant  $R$  parity violating coupling constant, a Monte Carlo events simulation for the reactions,  $l_J^+ l_J^- \rightarrow \tilde{\chi}_1^\pm l_m^\mp$ ,  $\tilde{\chi}_{1,2}^0 \nu_m$ ,  $\tilde{\chi}_{1,2}^0 \tilde{\nu}_m$ , is employed to deduce some characteristic dynamical distributions of the final states.*

# 1 Introduction

Should R parity turn out to be an approximate symmetry of the minimal supersymmetric standard model, the truly quantitative tests of such a possibility would have to be sought in high energy colliders physics, as was first emphasized in [1, 2, 3]. The great majority of the existing theoretical studies for the LEP or the Tevatron accelerators physics have focused on signals associated with the LSP (lightest supersymmetric particle) decays and certain rare decays of the standard model particles (gauge [2, 4, 5, 6] or Higgs [2] bosons or top-quark [7]). A few experimental searches have been attempted for  $Z^0$  boson decays [8, 9], for inos decays [10, 11] and also in more general settings [12, 13]. Proceeding one step further, interesting proposals were made recently to explain the so-called ALEPH anomalous four-jets events [14] on the basis of R parity violating decays of neutralinos or charginos [15, 16, 17], squarks [18, 19], sleptons [20] or sneutrinos [21] produced in pairs through the two-body processes,  $e^+e^- \rightarrow \tilde{\chi}^{0,+}\tilde{\chi}^{0,-}$  or  $e^+e^- \rightarrow \tilde{f}\tilde{f}$ . (See [22] for recent updates and lists of references.)

Apart from precursor studies devoted to the HERA collider [23, 24, 25], little consideration was given in the past to single production of supersymmetric particles in spite of the potential interest of a discovery of supersymmetry that might be accessible at lower incident energies. The reason, of course, is the lack of information about the size of the R parity odd coupling constants other than the large number of indirects bounds deduced from low and intermediate energy phenomenology [26]. Therefore, for obvious reasons, the existing single production studies have rather focused on resonant production of sneutrinos, charged sleptons [1, 2, 12, 27, 28, 29, 30, 31, 32] or squarks [3, 23, 27, 28, 29]. The interpretation of the anomalous high  $Q^2$  events recently observed at HERA by the ZEUS [33] and H1 [34] Collaborations, in terms of squark resonant production, has also stimulated a renewed interest in R parity violation phenomenology [35].

The collider physics tests of supersymmetric models without R parity entail an important change in focus with respect to the conventional tests : degraded missing energy, diluted signals, additional background from the minimal supersymmetric standard model interactions and uncertainties from the R parity violation coupling constants compounded with those from the superpartners mass spectra. Our purpose in this work is to discuss semi quantitatively the potential for a discovery and the tests of supersymmetry with  $2 \rightarrow 2$  body single superpartner production. Although several order of magnitudes in rates are lost with respect to the resonant single production, one can dispose here of a rich variety of phenomena with multilepton final states non diagonal in flavor. Besides, one may also test larger ranges of the sneutrino mass since this need not be restricted by the center of mass energy value. Encouraged by the recent developments on R parity violation and by the prospects of high precision measurements at supercolliders [36], we propose to study single production at leptonic (electron and muon) colliders for the set of five  $2 \rightarrow 2$  body reactions,  $l_J^+ l_J^- \rightarrow \tilde{\chi}^\pm l_m^\mp$ ,  $l_J^+ l_J^- \rightarrow \tilde{\chi}^0 \nu_m$  ( $\tilde{\chi}^0 \bar{\nu}_m$ ),  $l_J^+ l_J^- \rightarrow \tilde{l}_m^\mp W^\pm$ ,  $l_J^+ l_J^- \rightarrow \tilde{\nu}_{mL} Z^0$  ( $\tilde{\nu}_{mL} \bar{Z}^0$ ),  $l_J^+ l_J^- \rightarrow \tilde{\nu}_{mL} \gamma$  ( $\tilde{\nu}_{mL} \bar{\gamma}$ ) [ $J = 1, 2$ ], in a more systematic way than has been attempted so far. We limit ourselves to the lowest inos eigenstates. Let us note here that precursor indicative studies of the inos single production reactions were already presented in [37, 38] and that recent discussions concerning the reactions,  $e^\pm \gamma \rightarrow e^\pm \tilde{\nu}$  and  $e^\pm \gamma \rightarrow \tilde{l}^\pm \nu$ , where the photon flux is radiated by one of the two beams, were presented in [39]. We shall restrict our study to the lepton number violating interactions  $L_i L_j E_k^c$  in

association with the familiar gauge and Yukawa couplings of the minimal supersymmetric standard model. The final states consist then of multileptons with or without hadronic jets.

This paper contains four sections. In section 2, we present the main formalism for superpartners production cross sections and decay rates. In section 4, based on the supergravity approach to supersymmetry soft breaking parameters, we present numerical results for the total rates and the various branching ratios in wide regions of the parameter space. In section 5, we show results for final states distributions of the processes,  $l_J^+ l_J^- \rightarrow \tilde{\chi}^\pm l^\mp, \tilde{\chi}^0 \nu, \tilde{\chi}^0 \bar{\nu}$ , obtained by means of a Monte Carlo events simulation, using the SUSYGEN routine [40]. In section 6, we state our conclusions.

## 2 General Formalism

Five  $2 \rightarrow 2$  body single production reactions may be observed at leptonic colliders. We shall use the following short hand notation to denote the associated probability amplitudes :

$$\begin{aligned} M(\tilde{\chi}_a^- + l_m^+) &= M(l_J^- + l_J^+ \rightarrow \tilde{\chi}_a^- + l_m^+), \\ M(\tilde{\chi}_a^0 + \bar{\nu}_m) &= M(l_J^- + l_J^+ \rightarrow \tilde{\chi}_a^0 + \bar{\nu}_m), \\ M(\tilde{l}_{mL}^- + W^+) &= M(l_J^- + l_J^+ \rightarrow \tilde{l}_{mL}^- + W^+), \\ M(\tilde{\nu}_m + Z) &= M(l_J^- + l_J^+ \rightarrow \tilde{\nu}_m + Z), \\ M(\tilde{\nu}_m + \gamma) &= M(l_J^- + l_J^+ \rightarrow \tilde{\nu}_m + \gamma), \end{aligned} \quad (2.1)$$

where  $J = 1, 2$  is a flavor index for the initial state leptons (electrons and muons, respectively), the index  $a$  labels the charginos or neutralinos eigenvalues and the index  $m$  the sleptons or sneutrinos families. Our theoretical framework is the minimal supersymmetric standard model supplemented by the lepton number violating R parity odd superpotential,  $W = \frac{1}{2} \sum_{ijk} \lambda_{ijk} L_i L_j E_k^c$ . This yields the sfermion-fermion Yukawa interactions,

$$L = \frac{1}{2} \sum_{[i \neq j, k]=1}^3 \lambda_{ijk} [\tilde{\nu}_{iL} \bar{e}_{kR} e_{jL} + \tilde{e}_{jL} \bar{\nu}_{iL} + \tilde{e}_{kR}^* \bar{\nu}_{iR}^c e_{jL} - (i \rightarrow j)] + h.c. \quad (2.2)$$

where the sums labelled by indices,  $i, j, k$ , run over the three leptons and neutrinos families with the condition  $i \neq j$  following from the antisymmetry property,  $\lambda_{ijk} = -\lambda_{jik}$ .

### 2.1 Production Cross Sections

Each of the processes in eq.(2.1) has a charge conjugate partner such that the transformation between pairs of conjugate amplitudes can be formally described by applying a CP transformation to the S-matrix. The relationship is most easily described at the level of the amplitudes squared obtained after summation over the spins. Because of the simple action of CP on the initial state,  $l_J^+(k) l_J^-(k')$ , it can be seen that the amplitudes for the pairs of charge conjugated processes are related by the substitutions,  $k \leftrightarrow k'$  and  $\lambda_{ijk} \leftrightarrow \lambda_{ijk}^*$ . The tree level probability amplitudes are easily calculated by inspection of the Feynman diagrams given in Fig.1. The formulas for the amplitudes are consigned in Appendix 1. A few observations are in order at this point. First, the same configurations of lepton flavor indices, namely,  $\lambda_{mJJ}$  with  $J = 1, m = 2, 3$  for  $e^- e^+$  colliders

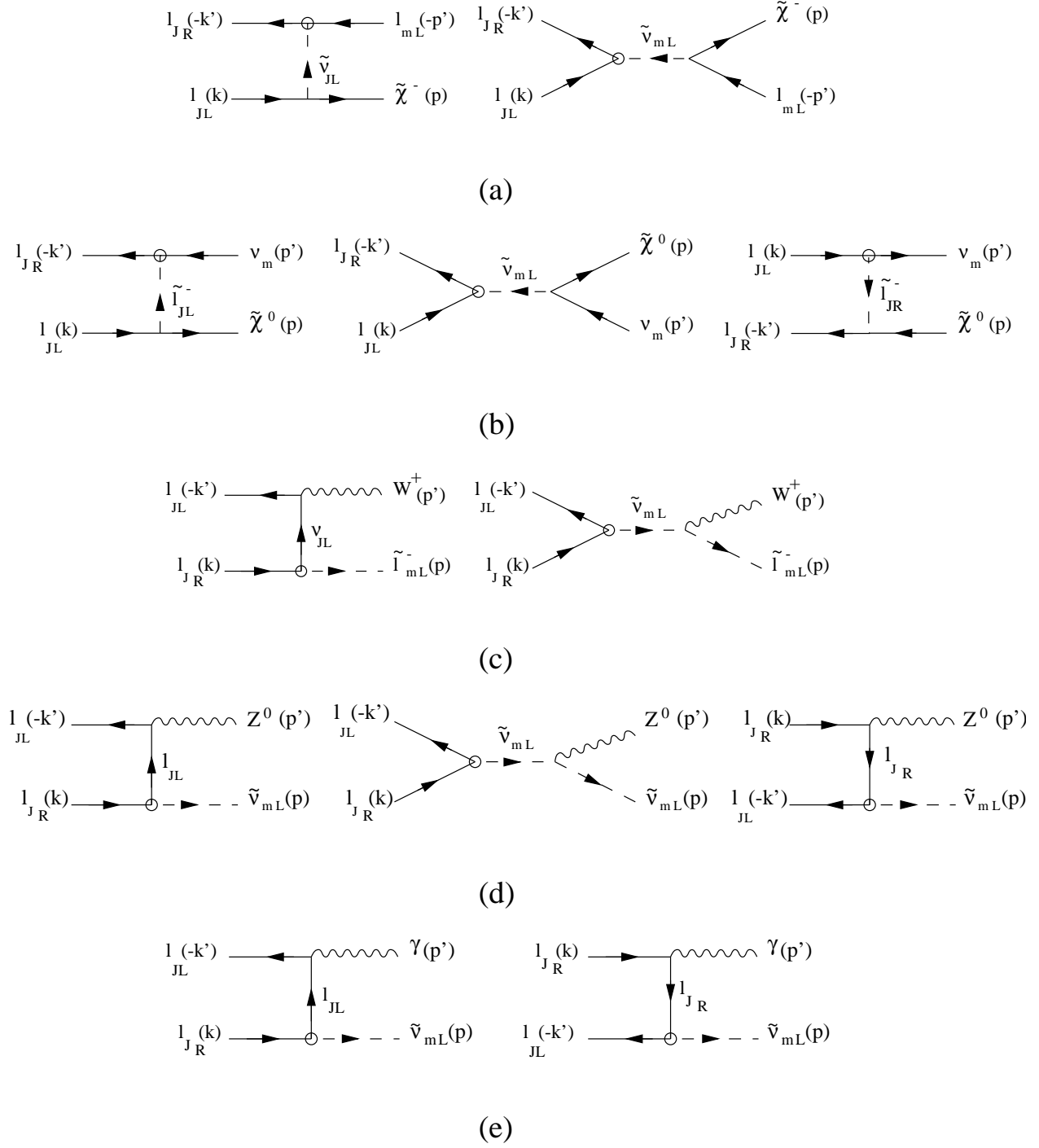


FIG. 1: Feynman diagrams for the processes,  $l_J^+ l_J^- \rightarrow \tilde{\chi}^- l_m^+$  (a),  $l_J^+ l_J^- \rightarrow \tilde{\chi}^0 \bar{\nu}_m$  (b),  $l_J^+ l_J^- \rightarrow \tilde{l}_{mL}^- W^+$  (c),  $l_J^+ l_J^- \rightarrow \tilde{\nu}_{mL} Z^0$  (d) and  $l_J^+ l_J^- \rightarrow \tilde{\nu}_{mL} \gamma$  (e). The circled vertex correspond to the RPV interaction, with the coupling constant  $\lambda_{mJJ}$ , and the arrows denote flow of momentum.

Mass Intervals	Decays	Final State	$\lambda_{m11}$
$m_{\tilde{l}^-} > m_{\tilde{\chi}^-}$ (1) $m_{\tilde{l}^-} < m_{\tilde{\chi}^-}$ (2)	$\bullet \tilde{\chi}^- \rightarrow \bar{\nu}_i \bar{\nu}_j l_k$ $\bullet \tilde{\chi}^- \rightarrow \bar{\nu}_i \tilde{l}_i^- \rightarrow \bar{\nu}_i l_k \bar{\nu}_j$	(A) $l_m^+ l_k^- \cancel{E}$	$l_m^+ e^-$
$m_{\tilde{\nu}} > m_{\tilde{\chi}^-}$ (3) $m_{\tilde{\nu}} < m_{\tilde{\chi}^-}$ (4)	$\bullet \tilde{\chi}^- \rightarrow l_j \bar{l}_k l_i$ $\bullet \tilde{\chi}^- \rightarrow l_i \tilde{\nu}_i \rightarrow l_i l_j \bar{l}_k$	(B) $l_m^+ l_k^+ l_i^- l_j^-$	$l_m^+ l_m^- e^+ e^-$
$m_{\tilde{l}}, m_{\tilde{\nu}} > m_{\tilde{\chi}^-} > m_{\tilde{\chi}^0}$ (5) $m_{\tilde{\chi}^-} > m_{\tilde{l}} > m_{\tilde{\chi}^0}$ (6) $m_{\tilde{\chi}^-} > m_{\tilde{\nu}} > m_{\tilde{\chi}^0}$ (7)	$\bullet \tilde{\chi}^- \rightarrow \tilde{\chi}^0 l_p \bar{\nu}_p \rightarrow l_p \bar{\nu}_p \nu_i l_j \bar{l}_k$ $\bullet \tilde{\chi}^- \rightarrow \bar{\nu}_p \tilde{l}_p^- \rightarrow \bar{\nu}_p l_p \tilde{\chi}^0 \rightarrow l_p \bar{\nu}_p \nu_i l_j \bar{l}_k$ $\bullet \tilde{\chi}^- \rightarrow l_p \tilde{\nu}_p \rightarrow l_p \bar{\nu}_p \tilde{\chi}^0 \rightarrow l_p \bar{\nu}_p \nu_i l_j \bar{l}_k$	(C) $l_m^+ l_p^- l_k^\pm l_i^\mp \cancel{E}$	$l_m^+ l_p^- e^+ e^-$ , $l_m^+ l_p^- e^\pm l_m^\mp$
$m_{\tilde{q}} > m_{\tilde{\chi}^-} > m_{\tilde{\chi}^0}$ (8) $m_{\tilde{\chi}^-} > m_{\tilde{q}} > m_{\tilde{\chi}^0}$ (9)	$\bullet \tilde{\chi}^- \rightarrow \tilde{\chi}^0 q_p \bar{q}_p \rightarrow q_p \bar{q}_p \nu_i l_j \bar{l}_k$ $\bullet \tilde{\chi}^- \rightarrow \bar{q}_p \tilde{q}_p \rightarrow q_p \bar{q}_p \tilde{\chi}^0 \rightarrow q_p \bar{q}_p \nu_i l_j \bar{l}_k$	(D) $l_m^+ l_k^\pm l_i^\mp \cancel{E} + 2jet$	$l_m^+ e^+ e^-$ , $l_m^+ e^\pm l_m^\mp$
$m_{\tilde{\chi}^-} > m_{\tilde{\chi}^0} + m_W$ (10)	$\bullet \tilde{\chi}^- \rightarrow \tilde{\chi}^0 W^- \rightarrow W^- \nu_i l_j \bar{l}_k$	(E) $l_m^+ l_k^\pm l_i^\mp W^- \cancel{E}$	$l_m^+ e^+ e^-$ , $l_m^+ e^\pm l_m^\mp$

TAB. 12: The allowed chargino decays for different relative orderings of the superpartners masses. The column fields give the mass intervals, the decay schemes, the final states corresponding to the process,  $l_j^+ l_j^- \rightarrow \tilde{\chi}^- l_m^+$ , with a single dominant coupling constant  $\lambda_{ijk}$  and the leptonic components of the final states in the case of a single dominant coupling constant  $\lambda_{m11}$  [ $m = 2, 3$ ]. The notation  $\cancel{E}$  stands for missing energy associated with neutrinos.

and  $J = 2$ ,  $m = 1, 3$  for  $\mu^- \mu^+$  colliders, occur in all cases. Second, the amplitude for right chirality slepton  $\tilde{l}_{mR}$  production has not been included in the above list of formulas for the reason that this is proportional to the coupling constants  $\lambda_{11m}$  which vanishes by the antisymmetry property,  $\lambda_{ijk} = -\lambda_{jik}$ . Thirdly, all five processus can appear only in a single helicity configuration for the initial fermions (assumed massless), corresponding to identical helicities, namely, either  $l_L^+ l_L^-$  or  $l_R^+ l_R^-$  (recall that physical helicity for anti-particle is opposite to chirality). Lastly, we observe that the relative signs between the  $s, t$  and  $u$  channels contributions are dictated by both the structure of the interaction Lagrangian and the signs of the Wick contractions for fermions. The results for the spin summed squared amplitudes are given by somewhat complicated formulas which we have assembled in Appendix 1. We have checked that our formulas for  $\tilde{\chi}^0$  and  $\tilde{\chi}^\pm$  productions agree with the results provided in [37, 38] and [41].

## 2.2 Decays

In order to exhibit the possible physical final states, we need to consider the decays of the produced supersymmetric particles, taking into account both the minimal supersymmetric standard model interactions (denoted RPC or R parity conserving) and the R parity odd interactions (denoted RPV or R parity violating).

Mass Intervals	Decays	Final State	$\lambda_{m11}$
$m_{\tilde{\nu}} < m_{\tilde{\chi}^+}$ (1)	$\bullet \tilde{\nu}_m \rightarrow l_k \bar{l}_j$	(A) $l_k^- l_j^+ Z^0$	$e^+ e^-$
$m_{\tilde{\nu}} > m_{\tilde{\chi}^+}$ (2)	$\bullet \tilde{\nu}_m \rightarrow l_m \tilde{\chi}^+ \rightarrow l_m \bar{l}_i \bar{l}_j l_k$	(B) $l_i^+ l_j^+ l_k^- l_m^- Z^0$	$e^+ e^- l_m^+ l_m^-$
$m_{\tilde{\nu}}, m_{\tilde{l}} > m_{\tilde{\chi}^+}$ (3) $m_{\tilde{\nu}} > m_{\tilde{\chi}^+} > m_{\tilde{l}}$ (4)	$\bullet \tilde{\nu}_m \rightarrow l_m \tilde{\chi}^+ \rightarrow l_m \nu_i \nu_j \bar{l}_k$ $\bullet \tilde{\nu}_m \rightarrow l_m \tilde{\chi}^+ \rightarrow l_m \tilde{l}_j^+ \nu_j \rightarrow l_m \nu_j \nu_i \bar{l}_k$	(C) $l_k^+ l_m^- \cancel{E} Z^0$	$e^+ l_m^-$
$m_{\tilde{\nu}} > m_{\tilde{\chi}^0}$ (5)	$\bullet \tilde{\nu}_m \rightarrow \nu_m \tilde{\chi}^0 \rightarrow \nu_m \nu_i l_j \bar{l}_k$	(D) $l_k^\pm l_i^\mp \cancel{E} Z^0$	$e^+ e^-, e^\pm l_m^\mp$
$m_{\tilde{\nu}} > m_{\tilde{\chi}^+} > m_{\tilde{\chi}^0}$ (6) $m_{\tilde{\nu}} > m_{\tilde{\chi}^+} > m_{\tilde{l}} > m_{\tilde{\chi}^0}$ (7)	$\bullet \tilde{\nu}_m \rightarrow \tilde{\chi}^+ l_m \rightarrow l_m \tilde{\chi}^0 \bar{l}_p \nu_p \rightarrow l_m \bar{l}_p \nu_p \nu_i l_j \bar{l}_k$ $\bullet \tilde{\nu}_m \rightarrow \tilde{\chi}^+ l_m \rightarrow l_m \nu_p \tilde{l}_p^+ \rightarrow l_m \nu_p \bar{l}_p \tilde{\chi}^0 \rightarrow l_m \nu_p \bar{l}_p \nu_i l_j \bar{l}_k$	(E) $l_p^+ l_m^- l_k^\pm l_i^\mp \cancel{E} Z^0$	$l_p^+ l_m^- e^+ e^-, l_p^+ l_m^- e^\pm l_m^\mp$
$m_{\tilde{\nu}} > m_{\tilde{\chi}^+} > m_{\tilde{\chi}^0}$ (8) $m_{\tilde{\nu}} > m_{\tilde{\chi}^+} > m_{\tilde{q}} > m_{\tilde{\chi}^0}$ (9)	$\bullet \tilde{\nu}_m \rightarrow \tilde{\chi}^+ l_m \rightarrow l_m \tilde{\chi}^0 q_p \bar{q}_p \rightarrow l_m q_p \bar{q}_p \nu_i l_j \bar{l}_k$ $\bullet \tilde{\nu}_m \rightarrow \tilde{\chi}^+ l_m \rightarrow l_m \bar{q}_p \tilde{q}_p \rightarrow l_m \bar{q}_p q_p \tilde{\chi}^0 \rightarrow l_m q_p \bar{q}_p \nu_i l_j \bar{l}_k$	(F) $l_m^- l_k^\pm l_i^\mp Z^0 + 2jet$	$l_m^- e^+ e^-, l_m^- e^\pm l_m^\mp$
$m_{\tilde{\nu}} > m_{\tilde{\chi}^+} > m_{\tilde{\chi}^0} + m_W$ (10)	$\bullet \tilde{\nu}_m \rightarrow \tilde{\chi}^+ l_m \rightarrow l_m \tilde{\chi}^0 W^+ \rightarrow l_m W^+ \nu_i l_j \bar{l}_k$	(G) $l_m^- l_k^\pm l_i^\mp \cancel{E} W^+ Z^0$	$l_m^- e^+ e^-, l_m^- e^\pm l_m^\mp$

TAB. 13: The allowed sneutrino decays for different relative orderings of the superpartners masses. The column fields give the mass intervals, the decay schemes, the final states corresponding to the process,  $l_j^+ l_j^- \rightarrow Z^0 \tilde{\nu}_m$ , with a single dominant coupling constant  $\lambda_{ijk}$  and the leptonic components of the final states in the case of a single dominant coupling constant  $\lambda_{m11}$  [ $m = 2, 3$ ]. The notation  $\cancel{E}$  stands for missing energy associated with neutrinos.

A number of hypotheses and approximations, which we list below, will be employed in the evaluation of partial rates.

- 1) Supersymmetric particles decays are assumed to have narrow widths (compared to their masses) and are produced on-shell with negligible spin correlations between the production and decay stages. This allows us to apply the familiar phase space factorisation formula for the production cross sections.
- 2) Spin correlations are neglected at all stages of the cascade decays such that the branching ratios in single or double cascades can be obtained by applying recursively the standard factorisation formula.
- 3) Sleptons belonging to all three families and squarks belonging to the first two families are degenerate in mass. Therefore, for a given decay process as, for instance,  $\tilde{\chi}^- \rightarrow \tilde{\nu}_p l_p$ , either all three generations will be energetically allowed or forbidden. Furthermore, flavor off-diagonal channels such as,  $\tilde{l}_1 \rightarrow \tilde{l}_2 + Z^0, \dots$  are closed.
- 4) The lowest eigenstates of neutralinos  $\tilde{\chi}_a^0$  and charginos  $\tilde{\chi}_a^\pm$  ( $a = 1$ ) are excited in the cascade chains.

Mass Intervals	Decays	Final State	$\lambda_{m11}$
$m_{\tilde{l}^-} < m_{\tilde{\chi}^-}$ (1)	$\bullet \tilde{l}_m^- \rightarrow l_k \bar{\nu}_i$	(A) $l_k^- \cancel{W}^+$	$e^-$
$m_{\tilde{l}^-} > m_{\tilde{\chi}^-}$ (2)	$\bullet \tilde{l}_m^- \rightarrow \nu_m \tilde{\chi}^- \rightarrow \nu_m l_k \bar{\nu}_j \bar{\nu}_i$	(B) $l_k^- \cancel{W}^+$	$e^-$
$m_{\tilde{l}^-}, m_{\tilde{\nu}} > m_{\tilde{\chi}^-}$ (3)	$\bullet \tilde{l}_m^- \rightarrow \nu_m \tilde{\chi}^- \rightarrow \nu_m l_j \bar{l}_k l_i$	(C) $l_k^+ l_i^- l_j^- \cancel{W}^+$	$e^+ e^- l_m^-$
$m_{\tilde{l}^-} > m_{\tilde{\chi}^-} > m_{\tilde{\nu}}$ (4)	$\bullet \tilde{l}_m^- \rightarrow \nu_m \tilde{\chi}^- \rightarrow \nu_m \tilde{\nu}_i l_i$ $\rightarrow \nu_m l_i l_j \bar{l}_k$		
$m_{\tilde{l}^-} > m_{\tilde{\chi}^0}$ (5)	$\bullet \tilde{l}_m^- \rightarrow l_m \tilde{\chi}^0 \rightarrow l_m \nu_i l_j \bar{l}_k$	(D) $l_m^- l_k^\pm l_i^\mp \cancel{W}^+$	$l_m^- e^+ e^-$ , $l_m^- e^\pm l_m^\mp$
$m_{\tilde{l}^-} > m_{\tilde{\chi}^-} > m_{\tilde{\chi}^0}$ (6)	$\bullet \tilde{l}_m^- \rightarrow \tilde{\chi}^- \nu_m \rightarrow \nu_m \tilde{\chi}^0 l_p \bar{\nu}_p$ $\rightarrow \nu_m l_p \bar{\nu}_p \nu_i l_j \bar{l}_k$	(E) $l_p^- l_k^\pm l_i^\mp \cancel{W}^+$	$l_p^- e^+ e^-$ , $l_p^- e^\pm l_m^\mp$
$m_{\tilde{l}^-} > m_{\tilde{\chi}^-} > m_{\tilde{\chi}^0}$ (7)	$\bullet \tilde{l}_m^- \rightarrow \tilde{\chi}^- \nu_m \rightarrow \nu_m l_p \tilde{\nu}_p$ $\rightarrow \nu_m l_p \bar{\nu}_p \tilde{\chi}^0 \rightarrow \nu_m l_p \bar{\nu}_p \nu_i l_j \bar{l}_k$		
$m_{\tilde{l}^-} > m_{\tilde{\chi}^-} > m_{\tilde{\chi}^0}$ (8)	$\bullet \tilde{l}_m^- \rightarrow \tilde{\chi}^- \nu_m \rightarrow \nu_m \tilde{\chi}^0 q_p \bar{q}_p$ $\rightarrow \nu_m q_p \bar{q}_p \nu_i l_j \bar{l}_k$	(F) $l_k^\pm l_i^\mp \cancel{W}^+ + 2jet$	$e^+ e^-$ , $e^\pm l_m^\mp$
$m_{\tilde{l}^-} > m_{\tilde{\chi}^-} > m_{\tilde{q}}$ (9)	$\bullet \tilde{l}_m^- \rightarrow \tilde{\chi}^- \nu_m \rightarrow \nu_m \bar{q}_p \tilde{q}_p$ $\rightarrow \nu_m \bar{q}_p q_p \tilde{\chi}^0 \rightarrow \nu_m \bar{q}_p q_p \nu_i l_j \bar{l}_k$		
$m_{\tilde{l}^-} > m_{\tilde{\chi}^-} > m_{\tilde{\chi}^0} + m_W$ (10)	$\bullet \tilde{l}_m^- \rightarrow \tilde{\chi}^- \nu_m \rightarrow \nu_m \tilde{\chi}^0 W^-$ $\rightarrow \nu_m W^- \nu_i l_j \bar{l}_k$	(G) $l_k^\pm l_i^\mp W^- \cancel{W}^+$	$e^+ e^-$ , $e^\pm l_m^\mp$

TAB. 14: The allowed slepton decays for different relative orderings of the superpartners masses. The column fields give the mass intervals, the decay schemes, the final states corresponding to the process,  $l_j^+ l_j^- \rightarrow W^+ \tilde{l}_m^-$ , with a single dominant coupling constant  $\lambda_{ijk}$  and the leptonic components of the final states in the case of a single dominant coupling constant  $\lambda_{m11}$  [ $m = 2, 3$ ]. The notation  $\cancel{E}$  stands for missing energy associated with neutrinos.

- 5) All superpartners decay inside the detector volume. In the presence of broken R parity, the condition for electric charge neutral LSPs to decay inside the detector yields comfortable lower bounds of order  $\lambda > 10^{-7}$  [3, 43].
- 6) Either a single RPV coupling constant is dominant in both the production and decay stages, or a pair of RPV coupling constants are dominant, one in the production stage ( $\lambda_{mJJ}$ ) and the other in the decay stage ( $\lambda_{ijk}$ ). The latter case with two dominant RPV coupling constants may be of interest since strong bounds on quadratic products exist only for a few family configurations. The strongest bounds arise from the  $\mu \rightarrow 3e$  decay [42] :  $\lambda_{p11}\lambda_{p12} < 6.5 \cdot 10^{-7}$ ,  $\lambda_{p21}\lambda_{p11} < 6.5 \cdot 10^{-7}$  [ $p = 2, 3$ ], while other quadratic product bounds are of order  $10^{-3}$ ,  $10^{-4}$ . Besides, as long as the coupling constant  $\lambda$ , which controls the RPV decays, is small in comparison with the gauge coupling constants but not very much smaller (so that the LSP decays inside the detector), then the branching ratio will depend weakly on  $\lambda$  since the last stage of the decay chain (LSP decay) is independent of  $\lambda$ .
- 7) The widths for the decays with four and higher body final states are neglected, such as those which occur in slepton (sneutrino) decays for,  $m_{\tilde{\chi}^-}, m_{\tilde{\chi}^0} > m_{\tilde{l}}^-$  ( $m_{\tilde{\chi}^-}, m_{\tilde{\chi}^0} > m_{\tilde{\nu}}$ ), mediated by virtual charginos or neutralinos, namely,  $\tilde{l}_m^- \rightarrow \nu_m l_k \bar{\nu}_j \bar{\nu}_i$  and  $\tilde{l}_m^- \rightarrow l_m \bar{l}_k l_j \nu_i$  ( $\tilde{\nu}_m \rightarrow l_m l_k \bar{l}_j \bar{l}_i$  and  $\tilde{\nu}_m \rightarrow \nu_m \bar{l}_k l_j \nu_i$ ).
- 8) A supergravity model for the soft supersymmetry breaking parameters is used where,

generically,  $\tilde{\chi}_1^0$  is the LSP.

The consideration of the various order relations in the superpartners mass spectrum leads to a list of decay schemes for the initially produced superparticles. These are displayed in Tables 12, 13 and 14, for  $\tilde{\chi}^\pm$ ,  $\tilde{\nu}_L$  and  $\tilde{l}_L$ , respectively. The signals for the  $\tilde{\chi}_1^0$  decays are very few in number and will be discussed separately in section 4.2. Some comments on these tables are in order. Except for hadronic dijet pairs from the decay processes,  $\tilde{\chi}^\pm \rightarrow \tilde{\chi}^0 \bar{q} q'$ , all other final particles will consists of multileptons and missing energy associated with neutrinos. In the hypothesis of a single dominant RPV coupling constant in the decays stage, one can deduce the various final states flavor configurations by an inspection of the tables (cf. tables captions). The produced  $\tilde{\chi}^0$ ,  $\tilde{\chi}^\pm$ ,  $\tilde{\nu}$ ,  $\tilde{l}^\pm$  will decay according to cascade schemes dictated by the superpartners mass spectrum. It is important to distinguish the direct RPV induced decays :  $\tilde{\chi}^- \rightarrow \bar{\nu}_i \bar{\nu}_j l_k$ ,  $\tilde{\chi}^- \rightarrow l_i l_j \bar{l}_k$ ,  $\tilde{\chi}^0 \rightarrow \nu_i l_j \bar{l}_k$ ,  $\tilde{\chi}^0 \rightarrow \bar{\nu}_i \bar{l}_j l_k$ ,  $\tilde{\nu}_i \rightarrow l_k \bar{l}_j$ ,  $\tilde{l}_{kR}^- \rightarrow l_j \nu_i$ , and  $\tilde{l}_{jL}^- \rightarrow l_k \bar{\nu}_i$ , from the indirect RPC induced decays :  $\tilde{l}_L^- \rightarrow \tilde{\chi}^- \bar{\nu}$ ,  $\tilde{\nu}_L \rightarrow \tilde{\chi}^+ l$ ,  $\tilde{l}_{L,R}^- \rightarrow \tilde{\chi}^0 l$ ,  $\tilde{\nu}_L \rightarrow \tilde{\chi}^0 \nu$ ,  $\tilde{\chi}^0 \rightarrow \tilde{l}^- \bar{l}$ ,  $\tilde{\chi}^0 \rightarrow l \bar{l}^+$ ,  $\tilde{\chi}^- \rightarrow \tilde{l}^- \bar{\nu}$ ,  $\tilde{\chi}^- \rightarrow \tilde{l} \bar{\nu}$  and  $\tilde{\chi}^\pm \rightarrow \tilde{\chi}^0 W^\pm$  for two-body final states and,  $\tilde{\chi}^- \rightarrow \tilde{\chi}^0 f \bar{f}$  (f=leptons or quarks), for three-body final states. All the formulas needed to evaluate the partial decay widths are quoted in the Appendix 2. As can be seen from Tables 12,13,14, a given final state can arise from different processes, depending on the relative orderings of the masses. A reaction chain occuring through an intermediate particle which is produced on-shell leads obviously to the same final state when the production of this particle is kinematically forbidden and it must then occur through a virtual intermediate state. In the approximation of family degenerate sleptons, sneutrinos and squarks, the index  $p$  in the tables runs over the three generations. A single exception is the hadronic decay,  $\tilde{\chi}^\pm \rightarrow \tilde{\chi}^0 u_p \bar{d}_p$  ( $\tilde{\chi}^0 d_p \bar{u}_p$ ), which is restricted to the first two families because of the large top-quark mass.

Another subtle point concerns the multiplicity of a given signal, namely, the number of different configurations which can lead to the same final state. Due to the antisymmetry property of  $\lambda_{ijk}$ , the final states from chargino RPV decays (cf. A and B in Table 12) have a multiplicity of two. The reason is that these decays proceed through the exchanges of the sleptons (or sneutrinos) in families  $i$  and  $j$ , for a given  $\lambda_{ijk}$ . This fact is already accounted for in the virtual  $\tilde{\chi}^\pm$  three-body decays (A(1),B(1),Table 12), but must be put by hand in the  $\tilde{\chi}^\pm$  cascade decays proceeding through the on-shell production of sleptons or sneutrinos which decay subsequently (A(2),B(2),Table 12).

To get a better understanding of the interplay between RPC and RPV decays, it is helpful to note that the branching ratios can be written formally as,  $B_D = \frac{\lambda^2}{c g^2 + \lambda^2}$ , for direct decays and,  $B_I = \frac{g^2 B}{c_0 g^2 + \lambda^2}$ , for two-stages indirect decays, where  $B = \frac{\lambda^2}{c g^2 + \lambda^2}$  is the LSP branching ratio,  $\lambda$  and  $g$  are symbolic notations for the RPV and RPC coupling constants and  $c, c_0$  are calculable constants. Of course,  $B = 1$ , if the last decaying particle is the LSP, which is the generical case. For values of the RPV coupling constants small with respect to the gauge coupling constants ( $\lambda \leq 0.05$ ), namely,  $g^2 \gg \lambda^2$ , the dependence on  $\lambda$  of the indirect decays branching ratios is weak and we have,  $B_I \gg B_D$ . For large enough RPV coupling constant (for example,  $\lambda = 0.1$ ) or for suppressed indirect decays (due for example to kinematical reasons), the direct decays may become competitive and both the direct and indirect branching ratios depend strongly on  $\lambda$ .



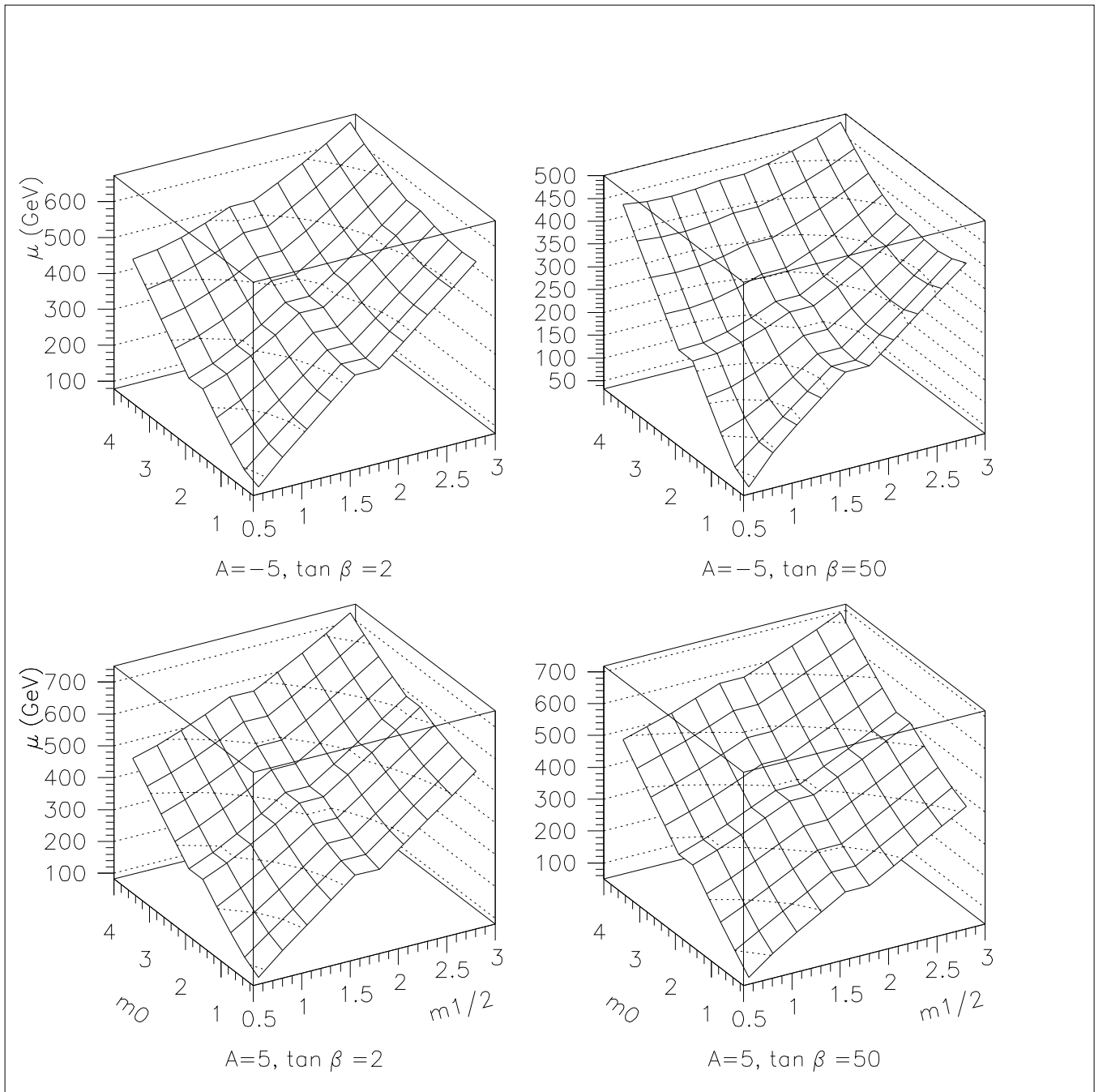


FIG. 2: The solution  $\mu(t_Z)$ , at scale  $m_Z$ , for the electroweak symmetry radiative breaking equations, at running top-quark mass,  $m_t(m_t) = 171 \text{ GeV}$  ( $m_t^{\text{pole}} = 180 \text{ GeV}$ ), is plotted as a function of  $\frac{m_0}{100 \text{ GeV}}$  and  $\frac{m_{1/2}}{100 \text{ GeV}}$  for four values of the pair of parameters,  $A$  and  $\tan \beta$ .

### 3 The model and its parameter space

We shall develop the study of single superpartner production within a non minimal supergravity framework, assuming the existence of a grand unified gauge theory and of family universal boundary conditions on the supersymmetry breaking parameters. The renormalization group improved classical spectrum of the scalar superpartners is deter-

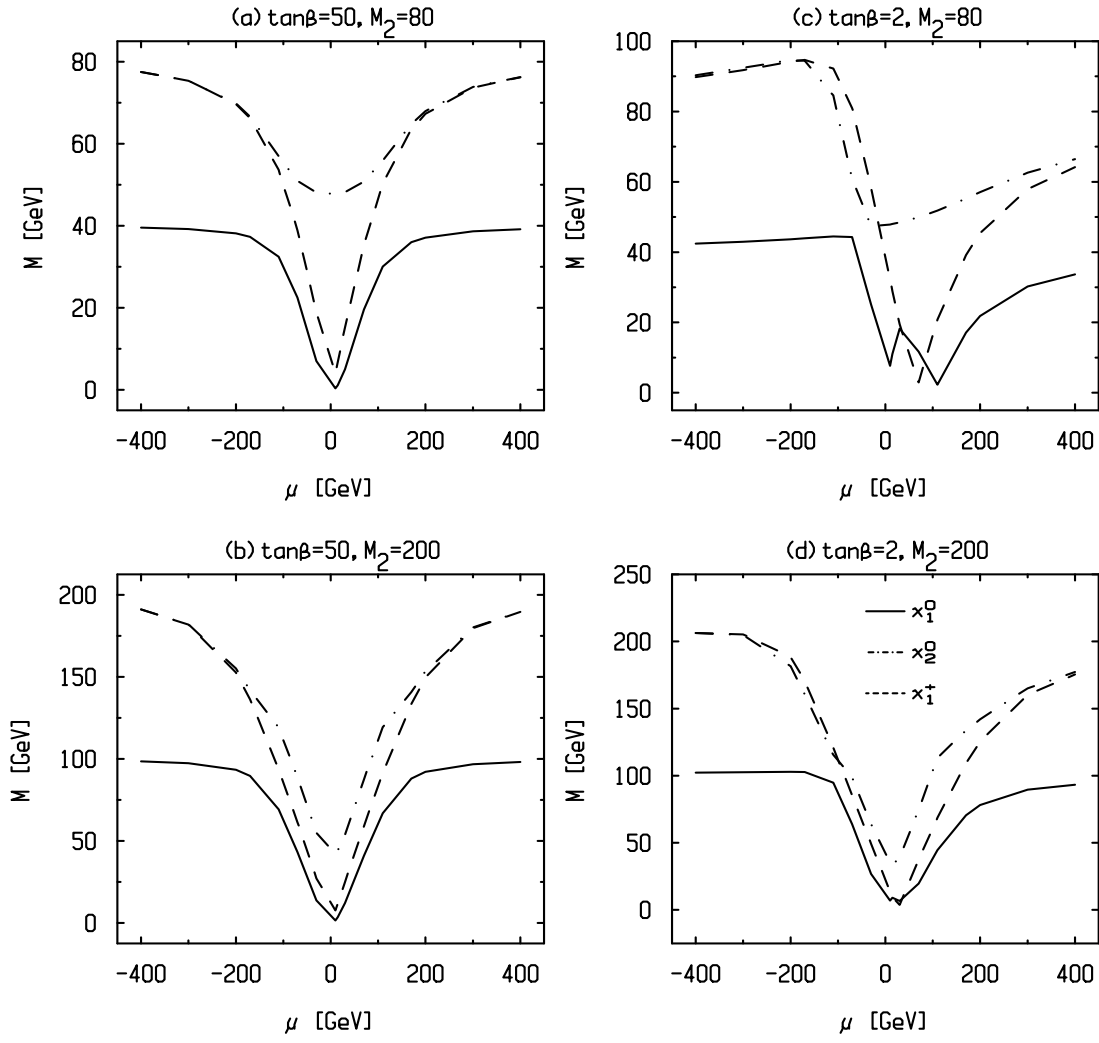


FIG. 3: Mass spectrum for the chargino  $\tilde{\chi}_1^\pm$  and the first two lowest mass neutralinos,  $\tilde{\chi}_1^0$  and  $\tilde{\chi}_2^0$ , as a function of  $\mu$ . Four choices of the parameters,  $\tan\beta$  and  $M_2$  (in GeV), are used, as indicated on top of each window.

mined in principle by the full set of soft supersymmetry breaking parameters at the unification scale,  $M_X$ , namely,  $m_0$  (common scalars mass),  $m_{1/2}$  (common gauginos mass),  $A$  (trilinear Yukawa interactions),  $B_\mu$  (bilinear Higgs interaction); by the parameters  $\tan\beta = \frac{v_u}{v_d} = \frac{\langle H_u \rangle}{\langle H_d \rangle}$  and  $\mu(t)$ , where  $t$  denotes the running scale; and by the gauge coupling constants,  $g_a(t)$ , along with fermions masses,  $m_f^2(t)$ . If one neglects the Yukawa interactions of quarks and leptons with the Higgs bosons, then the running masses of all sfermions remain family degenerate down to the electroweak breaking scale where they are described by the familiar additive formula,

$$m_{\tilde{f}}^2(t) = m_f^2(t) + m_0^2 + c_f(t)m_{1/2}^2 \pm m_{Z^0}^2 \cos(2\beta)(T_3^f - Q^f x_W), \quad (3.1)$$

where  $c_f(t)$  are calculable coefficients depending on the gauge interactions parameters and the last term represents the D-term contribution, the upper and lower sign being for the left and right chirality sfermions, respectively. The most relevant Yukawa coupling

constants, namely, those of the third family of up-quarks or, for large  $\tan\beta$ , of d-quarks and leptons, are expected to induce downwards shifts for the third family squarks (up and down) and sleptons, which depend non trivially on the parameters  $A$  and  $\mu$ . In this work, we shall restrict consideration to the simple case of family independent running masses and employ the approximate representation in eq.(3.1) with the numerical values quoted in [44]. Note that the total rates do not depend on the squarks masses and, as already remarked in section 2.2, the third families of squarks are not considered in the cascade decays. The charginos and neutralinos classical mass spectra are determined by the subset of parameters :  $M_1(t)$ ,  $M_2(t)$ ,  $\mu(t)$  and  $\tan\beta$ . For fixed  $m_{1/2}$ , the solution of the one loop renormalization group equations is given explicitly by,  $m_{1/2} = (1 - \beta_a t)M_a(t)$ , where  $t = \log(\frac{M_X^2}{Q^2})$ ,  $Q$  denoting the running scale,  $\beta_a = \frac{g_X^2 b_a}{(4\pi)^2}$ ,  $b_a = (3, -1, -11)$  with  $a = (3, 2, 1)$ , corresponding to the beta functions parameters for the gauge group factors,  $SU(3)$ ,  $SU(2)_L$ ,  $U(1)_Y$ , and  $g_X$  is the coupling constant at unification scale. Note that the wino and bino masses are related as,  $M_1(t) = \frac{5}{3}M_2(t)\tan^2\theta_W$ . It is useful here to comment on the relation of our framework with the so-called minimal supergravity framework in which one assumes a constrained parameter space compatible with electroweak symmetry breaking. Let us follow here the so-called ambidextrous minimal supergravity approach [45], where one chooses  $[m_0, m_{1/2}, A, \text{sign}(\mu), \tan\beta]$  as the free parameters set and derives  $\mu(t_Z)$ ,  $B_\mu(t_Z)$ , at the electroweak symmetry breaking scale,  $t_Z = \ln M_X^2/m_Z^2$ , through the minimisation equations for the Higgs bosons potential. For fixed  $m_0, m_{1/2}$  and  $\tan\beta$ , varying  $A$  will let the parameter  $\mu(t_Z)$  span finite intervals of relatively restricted sizes. In figure 2, we give results of a numerical resolution of the renormalization group equations which show the variation of  $|\mu(t_Z)|$  as a function of  $m_0$  and  $m_{1/2}$ , and also exhibit its dependence on  $A$ . Note that the equations admit the symmetry,  $\mu(t_Z) \rightarrow -\mu(t_Z)$ . Observing that  $\mu(t_Z)$  is typically a monotonous increasing function of  $A$ , we see from Fig.2 that the corresponding incremental increase,  $\delta\mu(t_Z)/\mu(t_Z)$ , as one spans the wide interval,  $A \in [-5, +5]$ , is small and of order 20%.

In the infrared fixed point approach for the top-quark Yukawa coupling,  $\tan\beta$  is fixed (up to the ambiguity associated with large or low  $\tan\beta$  solutions) in terms of the top-quark mass,  $m_t = C \sin\beta$ , with,  $C \simeq 190 - 210 \text{ GeV}$ , for,  $\alpha_3(m_{Z^0}) = 0.11 - 0.13$  [46]. The dependence on  $A$  of the electroweak constraint also becomes very weak, so that  $\mu(t_Z)$  is a known function of  $m_0, m_{1/2}$  and  $\tan\beta$  [46] :

$$\mu^2 + \frac{m_Z^2}{2} = m_0^2 \frac{1 + 0.5 \tan^2 \beta}{\tan^2 \beta - 1} + m_{1/2}^2 \frac{0.5 + 3.5 \tan^2 \beta}{\tan^2 \beta - 1}. \quad (3.2)$$

In section 4.2, we will discuss results for the branching ratios in this constrained model. The total rates are not affected in any significant way by which version of the supergravity models is used, since, as we will see, their dependence on  $\tan\beta$  and  $m_0$  turns out to be smooth.

The main uncertain inputs are the superpartners mass spectrum and the coupling constants  $\lambda_{ijk}$ . To survey the characteristic properties of single production over a broad region of parameter space, we found it convenient to consider a continuous interval of variation for  $\mu(t_Z)$ , namely,  $\mu(t_Z) \in [-400, +400] \text{ GeV}$ , while choosing suitable discrete values for the other parameters :  $M_2(t_Z) = 50, 80, 100, 150, 200 \text{ GeV}$ ,  $m_0 = 20, 50, 150 \text{ GeV}$  and  $\tan\beta = 2, 50$ . We shall set the unification scale at  $M_X = 2 \cdot 10^{16} \text{ GeV}$  and the running

scale at  $Q^2 = m_Z^2$ . For definiteness, we choose the coupling constant, which controls the size of the production cross section, at the reference value :  $\lambda_{mJJ} = 0.05$ . This is the strongest bound for a slepton mass of  $100\text{GeV}$  [26]. The dependence of integrated total rates on  $\lambda_{mJJ}$  is then given by a simple rescaling  $(\frac{\lambda_{mJJ}}{0.05})^2$  but that of branching ratios on  $\lambda_{ijk}$  (which may or may not be identified with  $\lambda_{mJJ}$ ) is more complicated because of the interplay between the RPC and RPV contributions which add up in the total decay widths. The reference value used here,  $\lambda_{ijk} = 0.05$ , is also an interesting borderline value since below this value the dependence of branching fractions on  $\lambda_{ijk}$  becomes negligible in generic cases.

It will prove helpful in the following discussion to keep within sight the spectrum for the low-lying inos. We display in Figure 3 the results obtained by solving numerically the eigenvalues problem for the charginos and neutralinos mass matrices. Recall the current experimental bounds [47],  $m_{\tilde{\chi}_1^0} > 23\text{GeV}$ ,  $m_{\tilde{\chi}_1^\pm} > 45\text{GeV}$ ,  $m_{\tilde{\nu}} > 37.1\text{GeV}$  and  $m_{\tilde{l}} > 45\text{GeV}$ . The following remarks about Figure 3 will prove relevant for the discussion on branching fractions : (i) The symmetry of the spectra under,  $\mu \leftrightarrow -\mu$ , is spoilt at low  $\tan\beta$  as can be seen on the explicit expression for the inos masses in [48] ; (ii) The mass differences  $\tilde{\chi}^+ - \tilde{\chi}^0$  increase with  $|\mu|$  with a steep rise appearing at,  $\mu = M_2$ , the borderline between the Higgsino and gaugino dominant regimes ; (iii) The spacings  $\tilde{\chi}_2^0 - \tilde{\chi}_1^0$  and  $\tilde{\chi}_1^+ - \tilde{\chi}_1^0$  decrease in magnitudes, relatively to the  $\tilde{\chi}_1^0$  mass, with increasing  $M_2$ . Although we show here the results for  $\tilde{\chi}_2^0$  mass, the interesting possibility of exciting the second neutralino  $\tilde{\chi}_2^0$  is not considered in the subsequent discussion.

## 4 Results and discussion

### 4.1 Total production rates

The total production rates are evaluated by taking the angular integral,  $\sigma = \int_{-x_m}^{+x_m} \frac{d\sigma}{dx} dx$ , [ $x = \cos\theta$ ], over the differential cross sections which are given explicitly in eqs.(1.2)-(1.6) in Appendix 1. To follow the usual practice we shall set an angular cut-off to account for the poor detection condition along the beam pipe :  $170^\circ > \theta_m > 10^\circ$ , corresponding to  $x_m = \cos\theta_m = 0.9848$ .

#### Inos production

The results for the integrated rates of the production of the lowest mass eigenstates  $\tilde{\chi}_1^-$  and  $\tilde{\chi}_1^0$ , at LEP II energies, are displayed in Figures 4 and 6, respectively. The inos production rates depend smoothly on  $\tan\beta$ , and on the mass parameters,  $\mu$ ,  $m_0$ ,  $M_2$ , in a way which closely reflects on the mass spectrum. Thus, the symmetry under  $\mu \leftrightarrow -\mu$  is upset only for low  $\tan\beta$  and the rates decrease with increasing  $M_2$ . The only cases where fast variations of rates arise are for values of  $m_0$  and  $M_2$  at which the center of mass energy hits on the sneutrino s-channel pole,  $\sqrt{s} = m_{\tilde{\nu}}$ . As  $m_0$  increases, the resonance occurs at smaller values of  $M_2$  since the sneutrino mass depends on  $M_2$ ,  $m_0$  and  $\tan\beta$  (see eq.(3.1)). The pole cross sections themselves, as parametrized by the conventional formula,

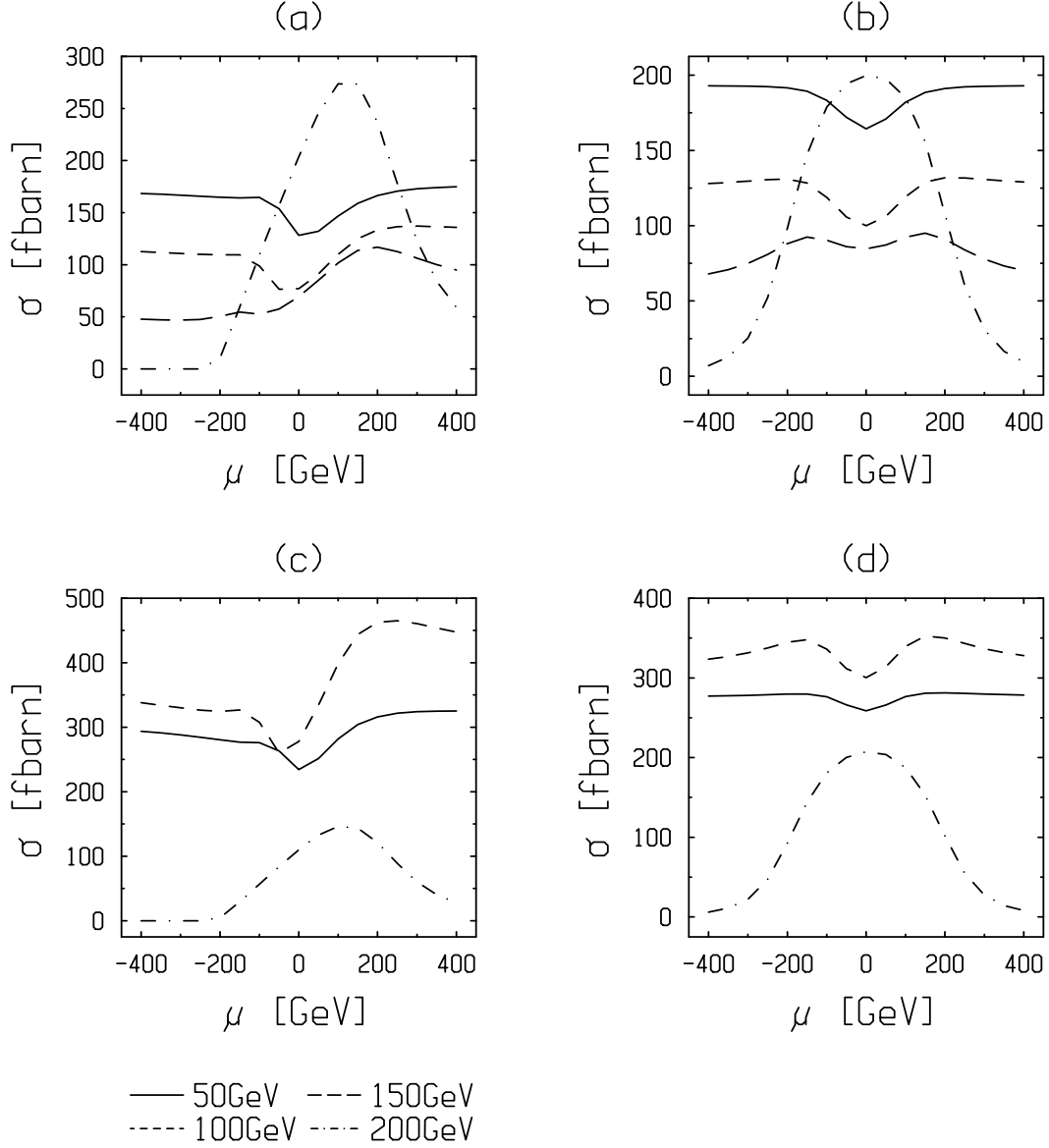


FIG. 4: The integrated cross sections for the process,  $l_J^+ l_J^- \rightarrow \tilde{\chi}_1^- l_m^+$ , at a center of mass energy of  $200\text{GeV}$ , are shown as a function of  $\mu$  for discrete choices of the remaining parameters : (a)  $\tan\beta = 2$ ,  $m_0 = 50\text{GeV}$ , (b)  $\tan\beta = 50$ ,  $m_0 = 50\text{GeV}$ , (c)  $\tan\beta = 2$ ,  $m_0 = 150\text{GeV}$  and (d)  $\tan\beta = 50$ ,  $m_0 = 150\text{GeV}$ , with  $\lambda_{mJJ} = 0.05$ . The windows conventions are such that  $\tan\beta = 2, 50$  horizontally and  $m_0 = 50, 150\text{GeV}$  vertically. The different curves refer to the values of  $M_2$  of  $50\text{GeV}$  (continuous line),  $100\text{GeV}$  (dot-dashed line),  $150\text{GeV}$  (dashed line) and  $200\text{GeV}$  (dotted line), as indicated at the bottom of the figure.

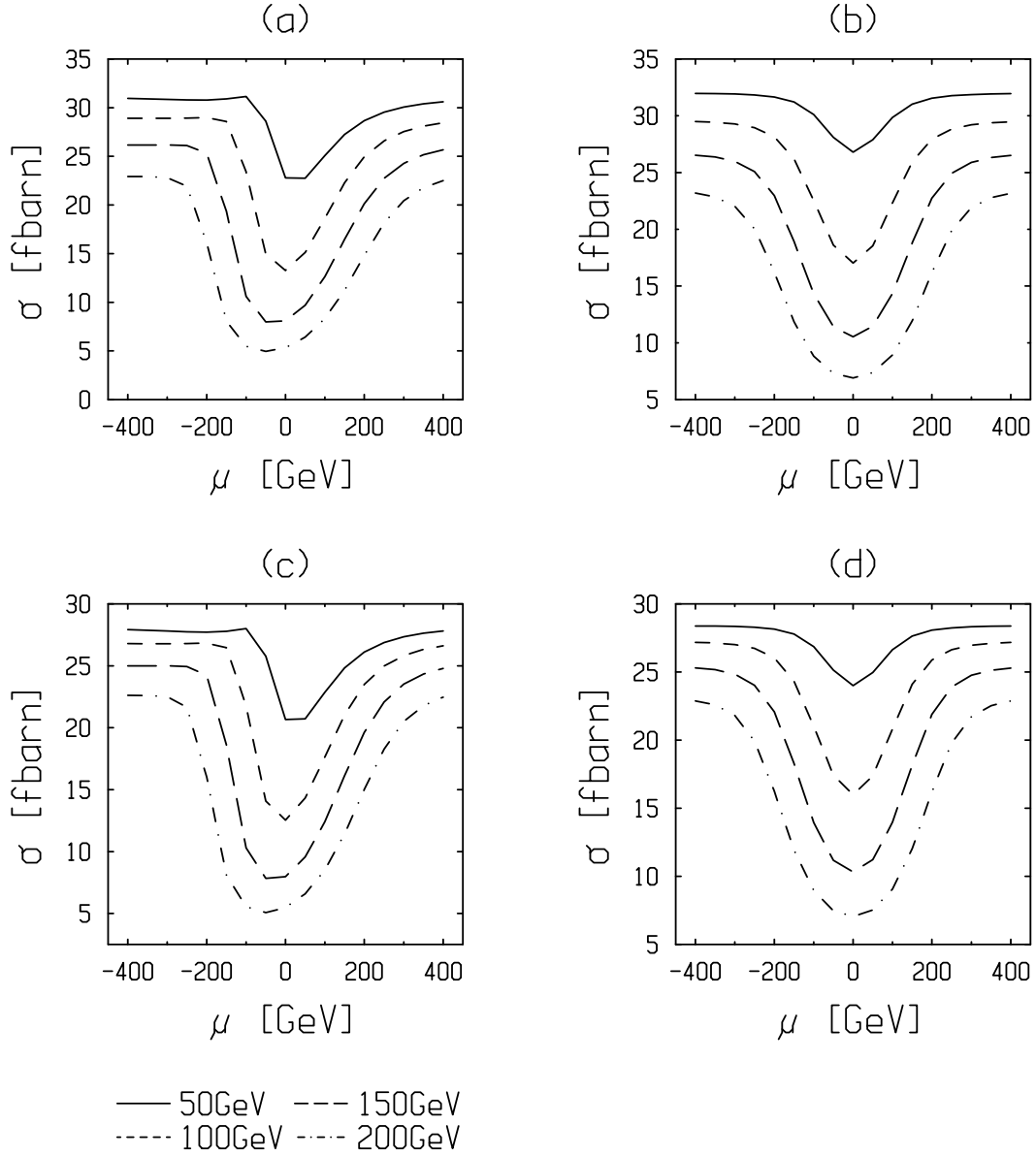


FIG. 5: The integrated cross sections for the process,  $l_J^+ l_J^- \rightarrow \tilde{\chi}_1^- l_m^+$ , at a center of mass energy of 500 GeV, are shown as a function of  $\mu$  for discrete choices of the remaining parameters : (a)  $\tan \beta = 2$ ,  $m_0 = 50 \text{ GeV}$ , (b)  $\tan \beta = 50$ ,  $m_0 = 50 \text{ GeV}$ , (c)  $\tan \beta = 2$ ,  $m_0 = 150 \text{ GeV}$  and (d)  $\tan \beta = 50$ ,  $m_0 = 150 \text{ GeV}$ , with  $\lambda_{mJJ} = 0.05$ . The windows conventions are such that  $\tan \beta = 2, 50$  horizontally and  $m_0 = 50, 150 \text{ GeV}$  vertically. The different curves refer to the values of  $M_2$  of 50 GeV (continuous line), 100 GeV (dot-dashed line), 150 GeV (dashed line) and 200 GeV (dotted line), as indicated at the bottom of the figure.

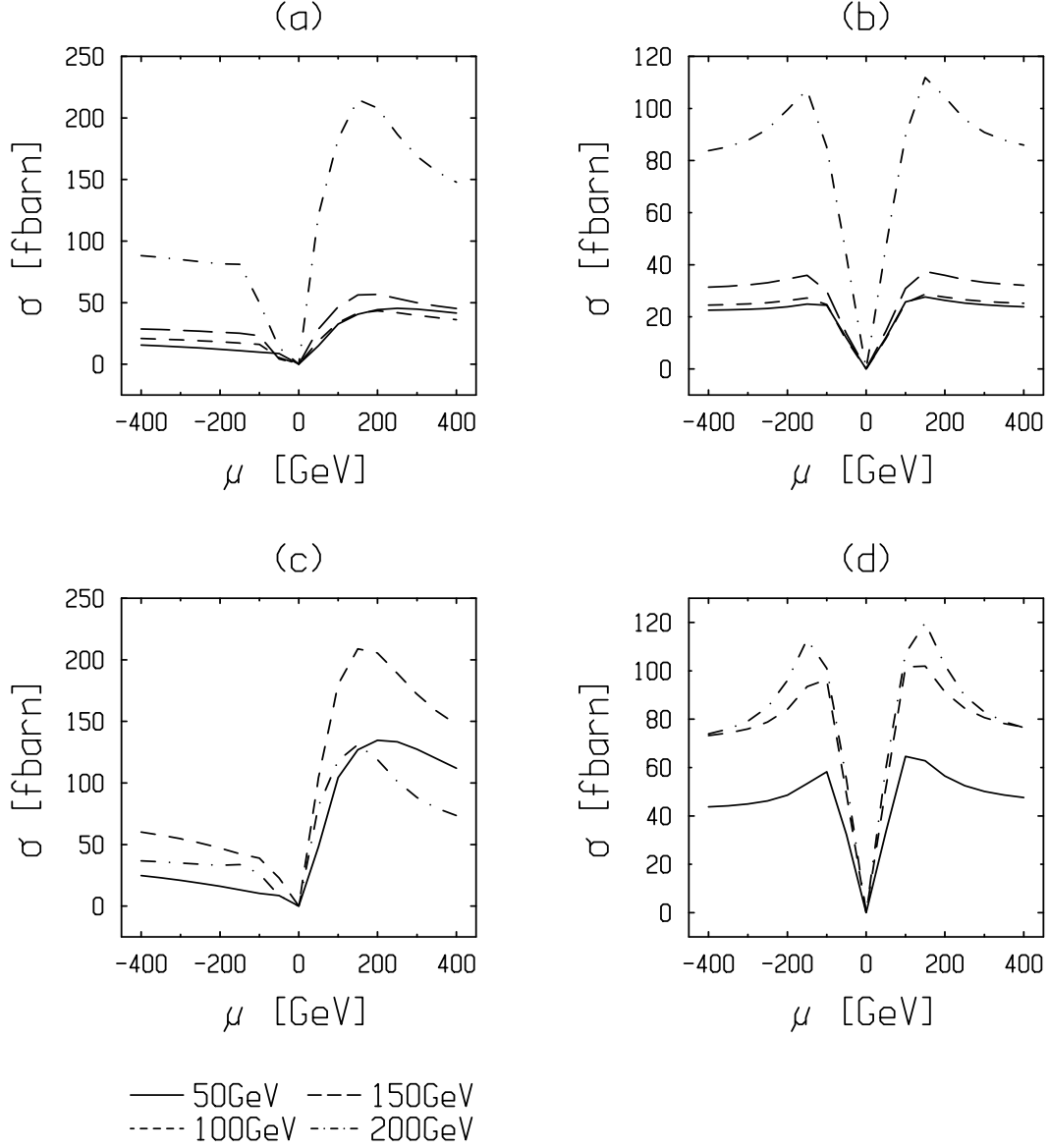


FIG. 6: The integrated cross sections for the process,  $l_J^+ l_J^- \rightarrow \tilde{\chi}_1^0 \bar{\nu}_m$ , at a center of mass energy of  $200\text{GeV}$ , are shown as a function of  $\mu$  for discrete choices of the remaining parameters : (a)  $\tan\beta = 2$ ,  $m_0 = 50\text{GeV}$ , (b)  $\tan\beta = 50$ ,  $m_0 = 50\text{GeV}$ , (c)  $\tan\beta = 2$ ,  $m_0 = 150\text{GeV}$  and (d)  $\tan\beta = 50$ ,  $m_0 = 150\text{GeV}$ , with  $\lambda_{mJJ} = 0.05$ . The windows conventions are such that  $\tan\beta = 2, 50$  horizontally and  $m_0 = 50, 150\text{GeV}$  vertically. The different curves refer to the values of  $M_2$  of  $50\text{GeV}$  (continuous line),  $100\text{GeV}$  (dot-dashed line),  $150\text{GeV}$  (dashed line) and  $200\text{GeV}$  (dotted line), as indicated at the bottom of the figure.

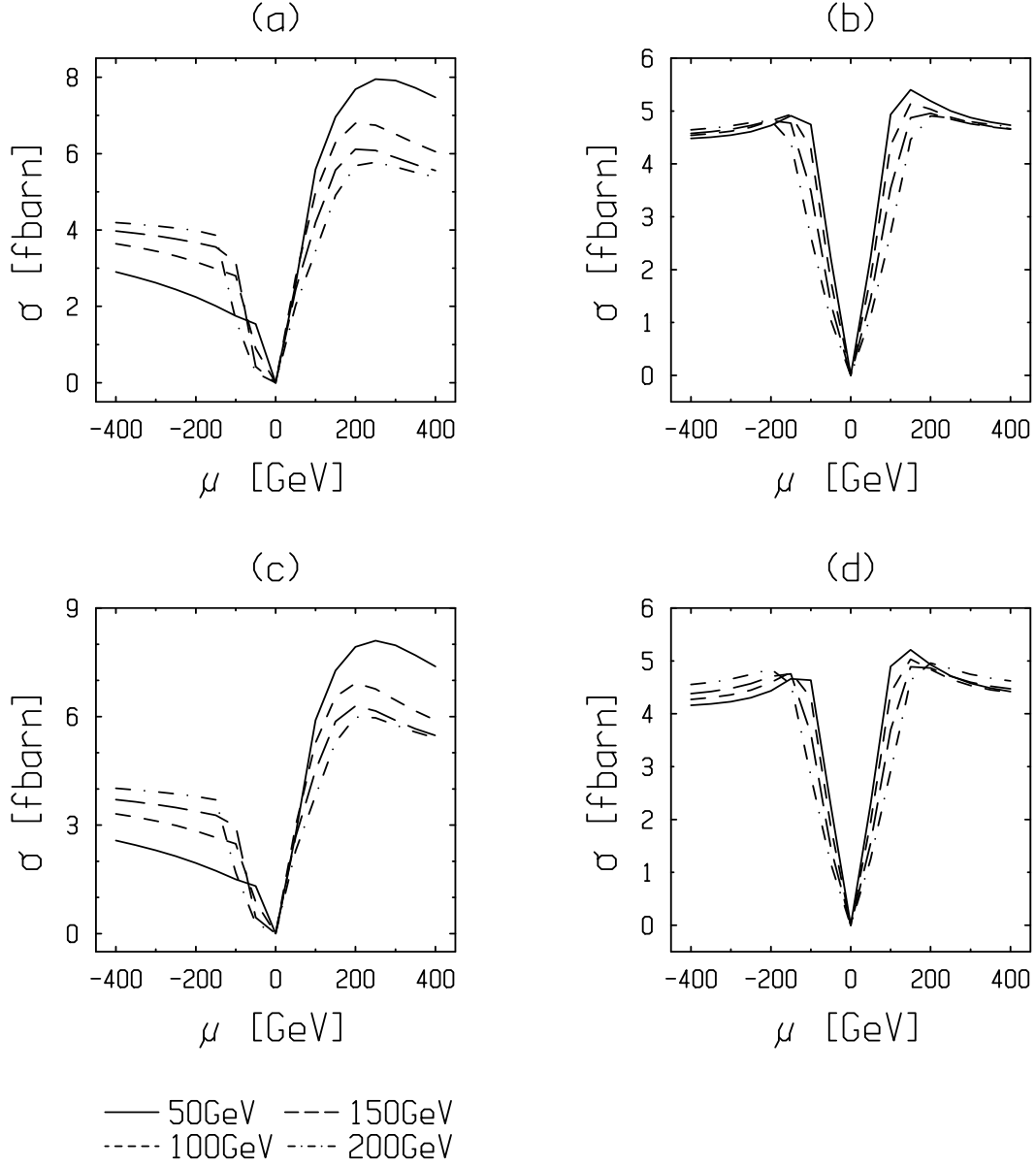


FIG. 7: The integrated cross sections for the process,  $l_J^+ l_J^- \rightarrow \tilde{\chi}_1^0 \bar{\nu}_m$ , at a center of mass energy of 500GeV, are shown as a function of  $\mu$  for discrete choices of the remaining parameters : (a)  $\tan \beta = 2$ ,  $m_0 = 50\text{GeV}$ , (b)  $\tan \beta = 50$ ,  $m_0 = 50\text{GeV}$ , (c)  $\tan \beta = 2$ ,  $m_0 = 150\text{GeV}$  and (d)  $\tan \beta = 50$ ,  $m_0 = 150\text{GeV}$ , with  $\lambda_{mJJ} = 0.05$ . The windows conventions are such that  $\tan \beta = 2, 50$  horizontally and  $m_0 = 50, 150\text{GeV}$  vertically. The different curves refer to the values of  $M_2$  of 50GeV (continuous line), 100GeV (dot-dashed line), 150GeV (dashed line) and 200GeV (dotted line), as indicated at the bottom of the figure.



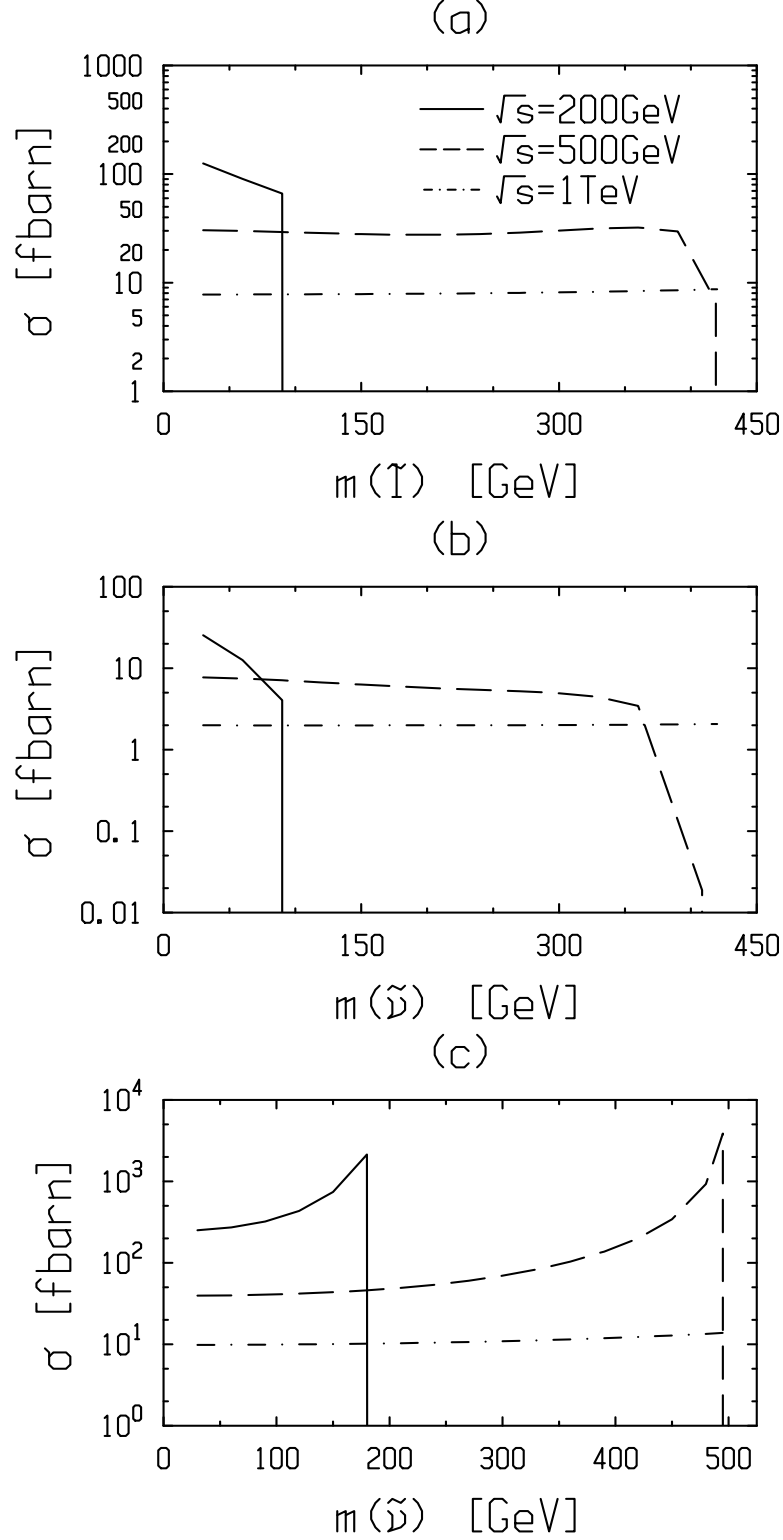


FIG. 8: The cross sections for the processes,  $l_J^+ l_J^- \rightarrow \tilde{l}_m^- W^+$  (a),  $l_J^+ l_J^- \rightarrow \tilde{\nu}_m Z^0$  (b) and  $l_J^+ l_J^- \rightarrow \tilde{\nu}_m \gamma$  (c), are shown as a function of the slepton mass and the sneutrino mass, for  $\lambda_{mJJ} = 0.05$ . The three values of the center of mass energies considered are 200, 500 and 1000 GeV, as quoted in the top window.

$$\begin{aligned}
\sigma(l^+l^- \rightarrow X) &= \frac{8\pi s \Gamma(\tilde{\nu} \rightarrow l^+l^-)\Gamma(\tilde{\nu} \rightarrow X)}{m_{\tilde{\nu}}^2 \left[ (s - m_{\tilde{\nu}}^2)^2 + \Gamma_{\tilde{\nu}}^2 \right]} \\
&\approx 4 \cdot 10^8 \left( \frac{100 \text{ GeV}}{m_{\tilde{\nu}}} \right)^2 B(\tilde{\nu} \rightarrow l^+l^-) B(\tilde{\nu} \rightarrow X) \text{ fbarns}, \quad (4.1)
\end{aligned}$$

can grow to values several order of magnitudes higher. For clarity, we have refrained from drawing the cross sections close to the resonant energy in the same plot. This is the reason why the curves corresponding to  $M_2 = 150 \text{ GeV}$  do not appear in Figures 4(c)(d) and 6(c)(d). The effect of the pole can be seen for  $M_2 = 200 \text{ GeV}$  in Figures 4(a)(b) and 6(a)(b). We note also that for  $\mu = 0$ ,  $\tilde{\chi}_1^0$  is a pure higgsino and the  $\tilde{\chi}_1^0$  production cross section vanishes. The results for inos production rates at NLC or  $\mu^+\mu^-$  colliders center of mass energies are displayed in Figures 5 and 7. The drop with respect to the LEP II energies is nearly by one order of magnitude. The second neutralino production rates,  $\sigma(\tilde{\chi}_2^0) = \sigma(l_J^+ l_J^- \rightarrow \tilde{\chi}_2^0 \nu_m)$ , when this is kinematically allowed, turns out to be of the same order of magnitude as  $\sigma(\tilde{\chi}_1^0)$ . For  $\sqrt{s} = 500 \text{ GeV}$ ,  $\sigma(\tilde{\chi}_1^0)$  and  $\sigma(\tilde{\chi}_2^0)$  are numerically close throughout the parameter space of our model. However, for  $\sqrt{s} = 200 \text{ GeV}$ , there are regions (large  $\tan\beta$ ,  $\mu < 0$ ) where one has  $\sigma(\tilde{\chi}_2^0) \approx 2\sigma(\tilde{\chi}_1^0)$  and other regions (low  $\tan\beta$ ,  $\mu > 0$ ) where one rather has  $\sigma(\tilde{\chi}_2^0) \approx \frac{1}{2}\sigma(\tilde{\chi}_1^0)$ . As for the production rate of the second chargino,  $\sigma(\tilde{\chi}_2^\pm)$ , this is always nearly an order of magnitude below  $\sigma(\tilde{\chi}_1^\pm)$ .

## Sleptons production

The slepton and sneutrino production rates depend solely on the sleptons masses and  $\lambda_{mJJ}$ . The results, obtained by setting  $m_{\tilde{l}} = m_{\tilde{\nu}}$ , are displayed in Figure 8 for three values of the center of mass energies. An account of the mass difference between  $m_{\tilde{l}}$  and  $m_{\tilde{\nu}}$  would not change the numerical results in any significant way.

The differential cross section for the reaction  $l_J^+ l_J^- \rightarrow \tilde{\nu} \gamma$  must be treated with special care because of its extreme sensitivity at the end points,  $x = \pm 1$ , in the limit of vanishing electron mass,  $m_e \rightarrow 0$ . As appears clearly on the expression of the squared momentum transfer variable,  $t = (k' - p')^2 = m_\gamma^2 - \frac{1}{2}(s - m_{\tilde{\nu}}^2 + m_\gamma^2)(1 - \frac{k}{E_k} \frac{p}{E_p} x)$ , for  $m_\gamma = 0$ , the t-channel amplitude has a collinear singularity,  $t \rightarrow 0$  as  $x \rightarrow 1$ . An analogous collinear singularity occurs for the u-channel amplitude,  $u = (k - p')^2 \rightarrow 0$  as  $x \rightarrow -1$ . Imposing the cut-off on the center of mass angle  $\theta$  makes the regularisation of collinear singularities pointless.

In the limit of vanishing  $m_\gamma$ , independently of  $x$  and  $m_e$ , the sneutrino production cross section becomes infinite at the limiting energy point,  $\sqrt{s} = m_{\tilde{\nu}}$ . This accounts for the property of the numerical results for the integrated cross section to rise with  $m_{\tilde{\nu}}$ , as seen in Figure 8(c). However, if one were to set  $m_\gamma$  at, say, the  $\rho$ -meson mass, in line with the vector meson dominance hypothesis, one would rather find the opposite behaviour with respect to the dependence on  $m_{\tilde{\nu}}$ . Observe that the increase of the cross section with  $m_{\tilde{\nu}}$  corresponds to the fact that, for  $m_{\tilde{\nu}} \approx \sqrt{s}$ , the process  $l_J^+ l_J^- \rightarrow \tilde{\nu} \gamma$  behaves like a sneutrino resonant production, accompanied by the initial state radiation of a soft photon.

## Discussion

In summary, the single production rates range from several 10's of  $fbarns$  to a few 100's of  $fbarns$  at LEP energies and several units to a few 10's of  $fbarns$  at NLC energies. Therefore, the superpartners single production are at the limit of observability for LEP II assuming an integrated luminosity per year of  $200pb^{-1}$  at  $\sqrt{s} = 200GeV$ . The prospects for single production should be rather good at NLC [49] and  $\mu^+\mu^-$  colliders [50] since the assumed integrated luminosity per year is expected to be about  $50fb^{-1}$  at  $\sqrt{s} = 500GeV$ . Moreover, it is important to note here that had we considered for the RPV coupling constants, constant values for the product  $\lambda_{mJJ}(\frac{m_{\tilde{l}_R}}{100GeV})$ , rather than for  $\lambda_{mJJ}$ , the rates would get an important amplification factor  $(\frac{m_{\tilde{l}_R}}{100GeV})^2$  for increasing superpartners masses. Note that the slepton involved in the bound is of right chirality and thus is of opposite chirality than the slepton involved in the rate. Of course, the masses of  $\tilde{l}_L$  and  $\tilde{l}_R$  are related in a given model. At  $\sqrt{s} = 500GeV$  and assuming  $\lambda_{ijk} \geq 0.05$ , all the single production reactions should be potentially observable over a broad region of parameter space. The slepton production reactions could then probe slepton masses up to  $400GeV$  (Figure 8(a)) and sneutrino masses up to  $500GeV$  (Figure 8(c)). The ino production reactions could probe a large region of the parameter plane  $(\mu, M_2)$ , since the dependence on the parameters  $m_0$  and  $\tan\beta$  is smooth. To strengthen our conclusions, it is necessary to examine the signatures associated with the final states, which is the subject of the next section.

## 4.2 Branching Ratios

In the narrow resonance approximation, the partial transition rates are readily obtained by multiplying the total rates for each reaction with the decay branching fractions. The various final states for each of the  $2 \rightarrow 2$  single production reactions have been listed in Tables 12, 13 and 14. The leptons family configurations in the final states will depend on the hypothesis for the RPV coupling constant (single or pair dominance).

With the purpose of testing characteristic points of the parameter space, we have evaluated the branching ratios for the decays of the superpartners, namely,  $\tilde{\chi}_1^\pm, \tilde{l}^\pm$  and  $\tilde{\nu}$ , for variable  $\mu$  at discrete choices of  $M_2, m_0$  and  $\tan\beta$ , such that the main typical cases in the ordering of the masses  $m_{\tilde{\chi}_1^0}, m_{\tilde{\chi}_1^\pm}, m_{\tilde{l}}, m_{\tilde{\nu}}$ , can be explored. The results are shown in Figures 9, 10 and 11, for the chargino, the sneutrino and the slepton decays, respectively. The curves for the various branching ratios are distinguished by the same letters (numbers) as those used in Tables 12, 13 and 14 to label the various final states (decay processes). We shall now discuss in turn the various superpartner decay schemes corresponding to the five single production reactions.

### Lowest mass Neutralino

The branching ratios for the  $\tilde{\chi}_1^0$  desintegrations are best analysed separately. For convenience, we do not treat the cases,  $m_{\tilde{\chi}_1^0} > m_{\tilde{q}}$  and  $m_{\tilde{\chi}_1^0} > m_{\tilde{\chi}_1^\pm}$ , since these arise marginally in most of the currently favored models (supergravity or gauge mediated soft supersymmetry breaking). The cascade decays which occur if  $m_{\tilde{\chi}_1^\pm} < m_{\tilde{\chi}_1^0}$  are also not considered since the corresponding region of the parameter space (Figure 3(c)) is forbidden by the experimental constraints on the inos masses. Thus, the process  $l_J^+ l_J^- \rightarrow \tilde{\chi}_1^0 \nu_m$  will only

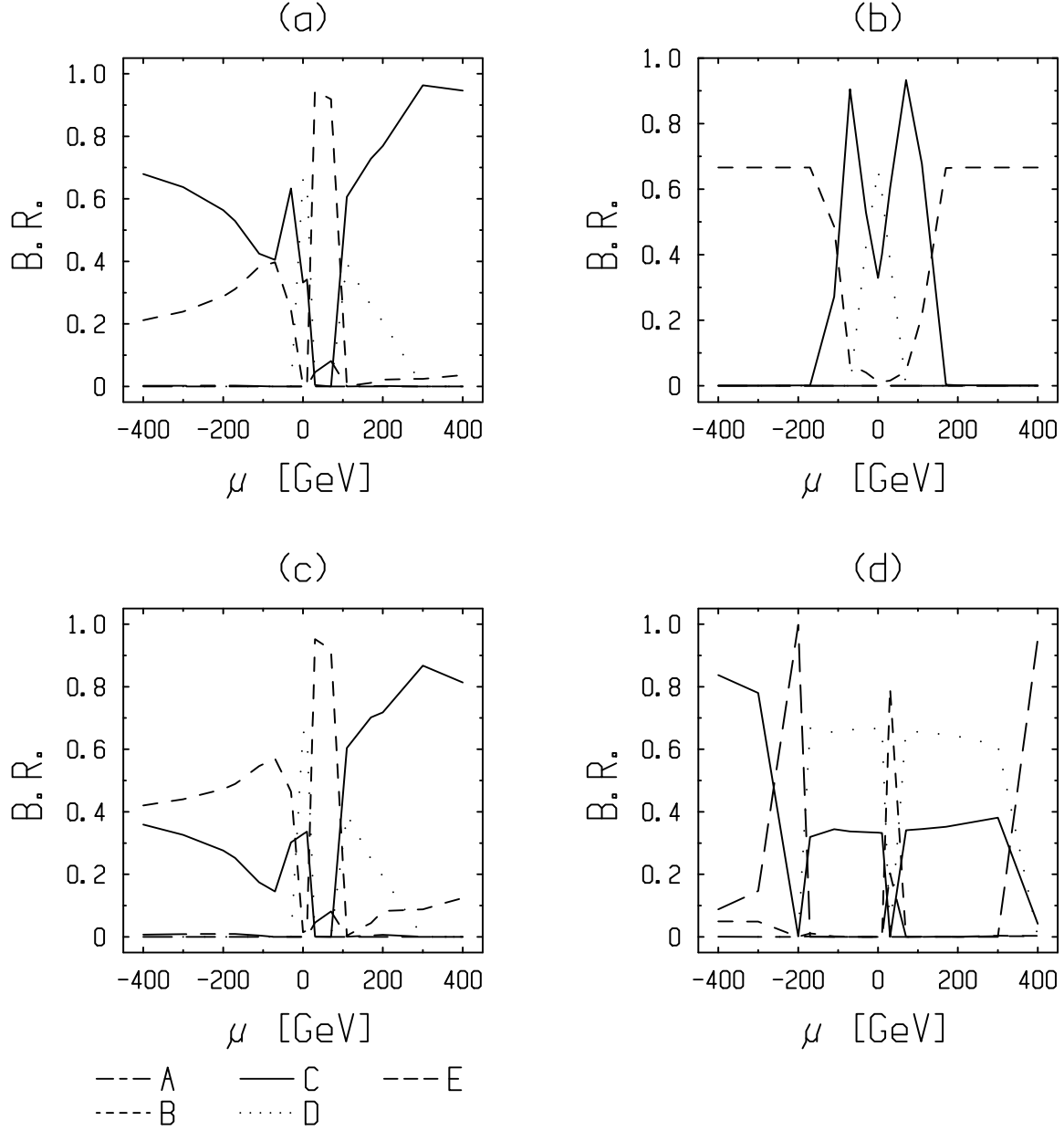


FIG. 9: Branching ratios for the chargino  $\tilde{\chi}_1^-$  decays as a function of  $\mu$ . The results in the four windows are obtained with the following choices for the parameters,  $[(M_2(\text{GeV}), m_0(\text{GeV}), \tan\beta, \lambda_{ijk}), m_{\tilde{\nu}_L}(\text{GeV}), m_{\tilde{L}}(\text{GeV})]$  : (a)  $[(80, 20, 2, 0.05), 53.19, 81.66]$ , (b)  $[(80, 20, 50, 0.05), 34.20, 86.97]$ , (c)  $[(80, 20, 2, 0.1), 53.19, 81.66]$ , (d)  $[(200, 100, 2, 0.05), 195.6, 205.2]$ . The final states are labeled by the letters, A, B, C, D, E, which have the same meaning as in Table 12.

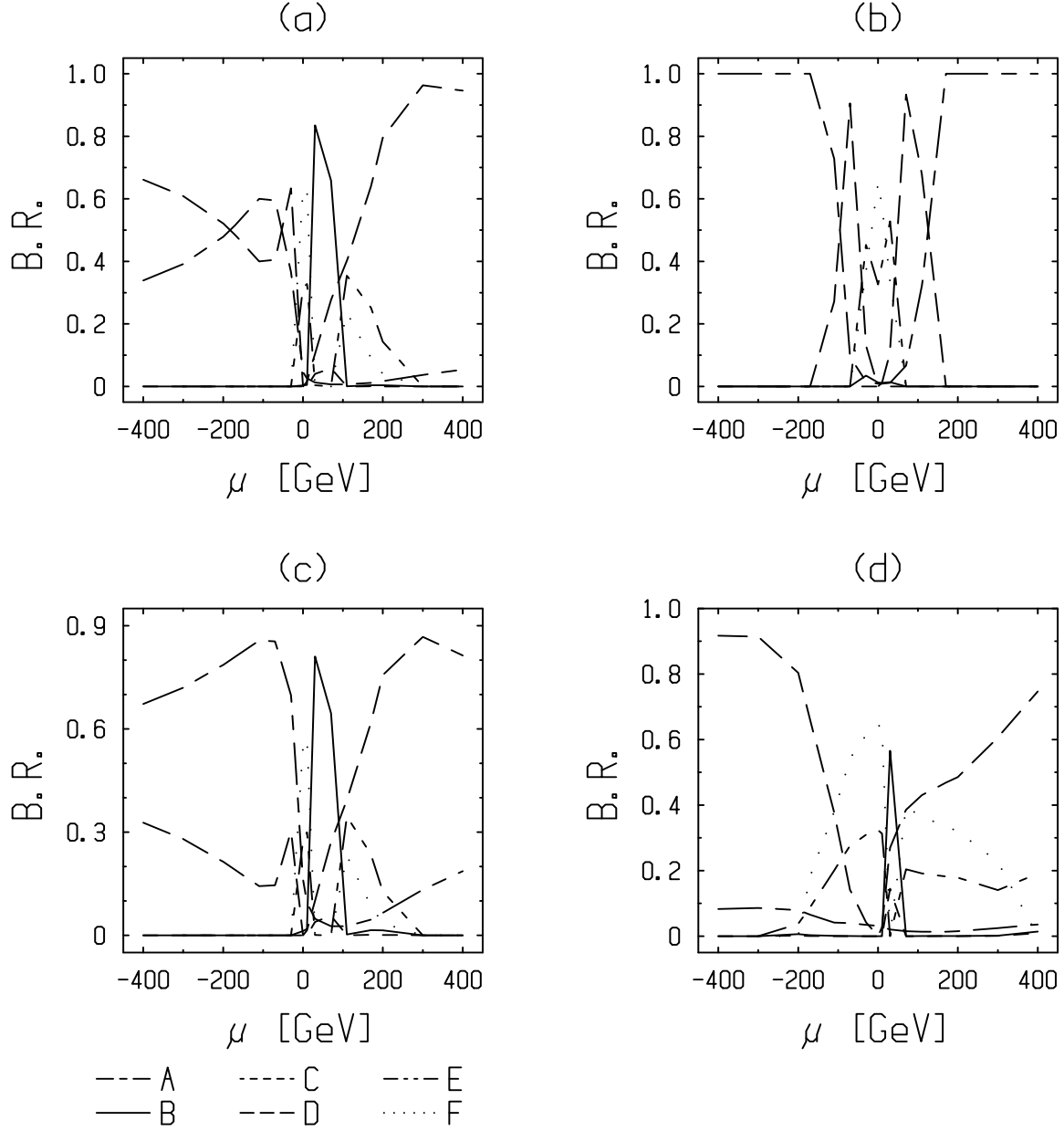


FIG. 10: Branching ratios of the sneutrino decays as a function of  $\mu$ . The results in the four windows are obtained with the following choices for the parameters,  $[(M_2(\text{GeV}), m_0(\text{GeV}), \tan\beta, \lambda_{ijk}), m_{\tilde{\nu}_L}(\text{GeV}), m_{\tilde{l}_L}(\text{GeV})]$  : (a)  $[(80, 20, 2, 0.05), 53.19, 81.66]$ , (b)  $[(80, 20, 50, 0.05), 34.20, 86.97]$ , (c)  $[(80, 20, 2, 0.1), 53.19, 81.66]$ , (d)  $[(200, 100, 2, 0.05), 195.6, 205.2]$ . The final states are labeled by the letters, A, B, C, D, E, F, which have the same meaning as in Table 13.

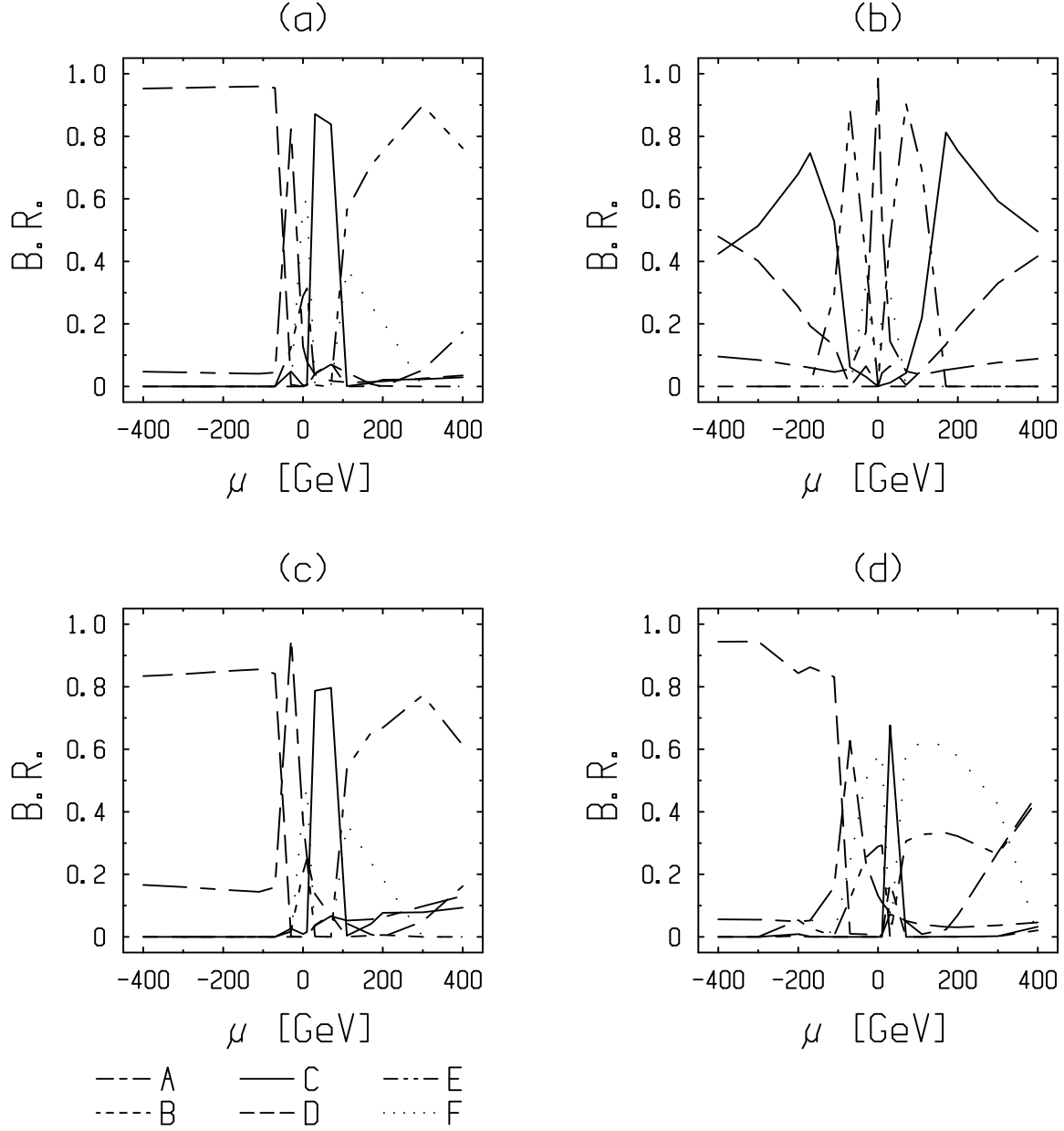


FIG. 11: Branching ratios of the slepton decays as a function of  $\mu$ . The results in the four windows are obtained with the following choices for the parameters,  $[(M_2(\text{GeV}), m_0(\text{GeV}), \tan\beta, \lambda_{ijk}), m_{\tilde{\nu}_L}(\text{GeV}), m_{\tilde{l}_L}(\text{GeV})]$  : (a)  $[(80, 20, 2, 0.05), 53.19, 81.66]$ , (b)  $[(80, 20, 50, 0.05), 34.20, 86.97]$ , (c)  $[(80, 20, 2, 0.1), 53.19, 81.66]$ , (d)  $[(200, 100, 2, 0.05), 195.6, 205.2]$ . The final states are labeled by the letters, A, B, C, D, E, F, which have the same meaning as in Table 14.

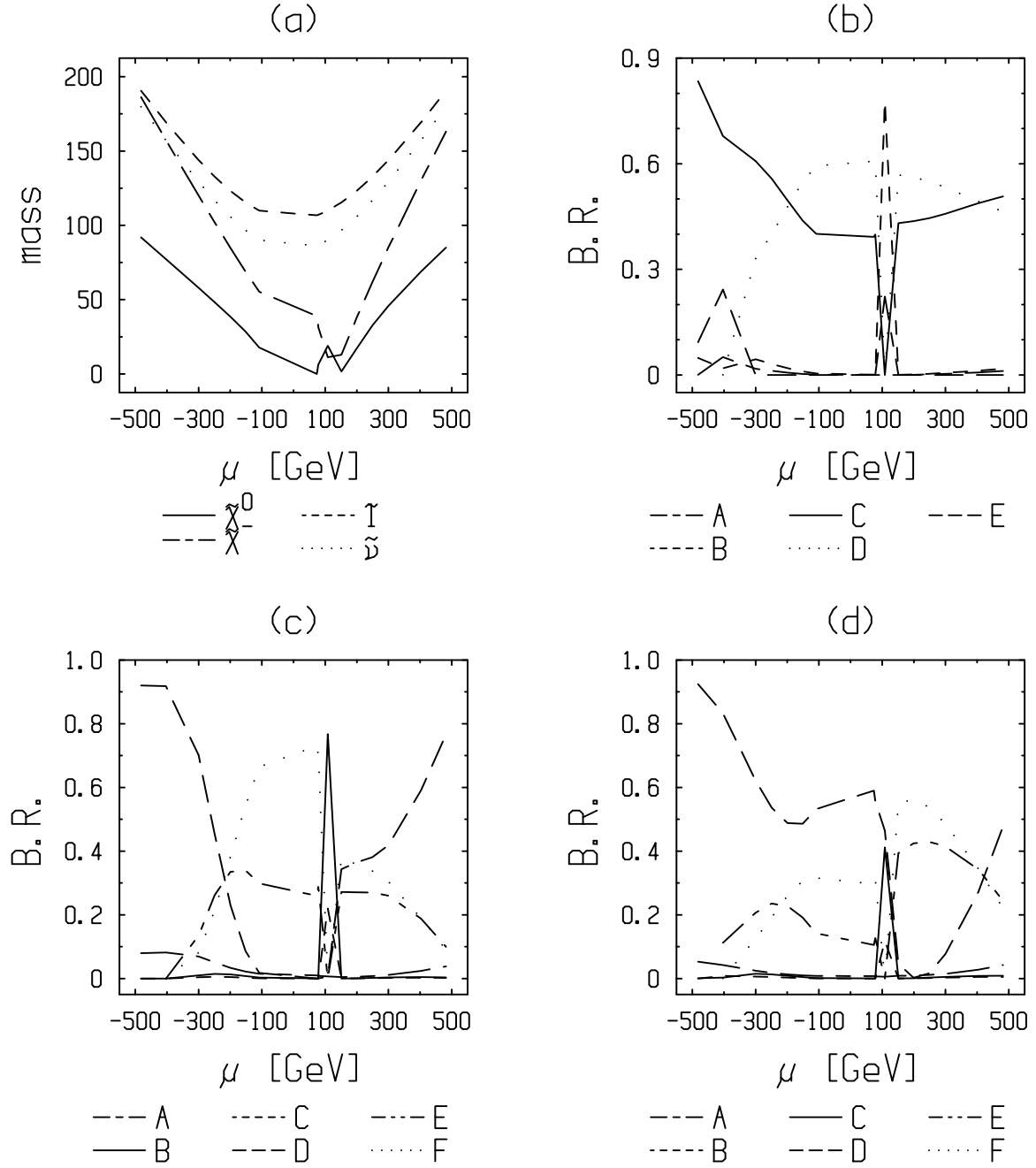


FIG. 12: Mass spectrum of the supersymmetric particles (a), in GeV, and branching ratios for the decays of the chargino (b), sneutrino (c) and slepton (d), as a function of  $\mu$ . The results are obtained for  $m_0 = 100\text{GeV}$ , using equation (3.2). The final states in figures (b),(c),(d) are labeled by the letters, A,B,... which have the same meaning as in tables 12,13,14, respectively.

generate events with 2 leptons +  $\cancel{E}$ . At this point, it is necessary to specialize our discussion to a single dominant coupling constant hypothesis, assuming  $\lambda_{ijk} \neq 0$  not necessarily identical to  $\lambda_{mJJ}$ . One may distinguish the following four distinct cases. For an LSP  $\tilde{\chi}_1^0$ , namely,  $m_{\tilde{\chi}_1^0} < m_{\tilde{l}}, m_{\tilde{\nu}}$  (Case 1), only the direct RPV three-body decays,  $\tilde{\chi}_1^0 \rightarrow \bar{\nu}_i \bar{l}_j l_k$ ,  $\tilde{\chi}_1^0 \rightarrow \nu_i l_j \bar{l}_k$ , are allowed. The branching ratios are then determined on the basis of simple combinatoric arguments. For a dominant coupling constant, say,  $\lambda_{m11}$ , there are four final states :  $\nu_1 l_m^- e^+$ ,  $\bar{\nu}_1 l_m^+ e^-$ ,  $\nu_m e^- e^+$  and  $\bar{\nu}_m e^+ e^-$ . Accordingly, the branching ratios of  $\tilde{\chi}_1^0$  into two charged leptons will depend on the type (flavor, charge) of the final state : The branching ratios equal  $\frac{1}{2}$  for the flavor diagonal  $e^+ e^-$  or flavor non diagonal  $l^\pm e^\mp$  channels,  $\frac{1}{4}$  for the fixed charges and flavors  $l^+ e^-$  or  $l^- e^+$  channels and 1 for the lepton-antilepton pairs of unspecified flavors. For a dominant coupling constant  $\lambda_{ijk} \neq \lambda_{m11}$ , an analogous result is obtained. For  $m_{\tilde{\chi}_1^0} > m_{\tilde{l}}, m_{\tilde{\nu}}$  (Case 2), the branching ratio for  $\tilde{\chi}_1^0$  decay is,

$$B(\tilde{\chi}_1^0 \rightarrow \bar{\nu}_i \bar{l}_j l_k) = \frac{\Gamma(\tilde{\chi}_1^0 \rightarrow \tilde{l}_j \bar{l}_j) B(\tilde{l}_j \rightarrow \bar{\nu}_i l_k) + \Gamma(\tilde{\chi}_1^0 \rightarrow \tilde{\nu}_i \bar{\nu}_i) B(\tilde{\nu}_i \rightarrow \bar{l}_j l_k)}{3\Gamma(\tilde{\chi}_1^0 \rightarrow \tilde{l}_j l_j) + 3\Gamma(\tilde{\chi}_1^0 \rightarrow \tilde{\nu}_i \nu_i)} = \frac{1}{3}, \quad (4.2)$$

where we have used the fact that in the present case, assuming a dominant coupling constant  $\lambda_{ijk}$ ,  $B(\tilde{l}_j \rightarrow \bar{\nu}_i l_k) = B(\tilde{\nu}_i \rightarrow \bar{l}_j l_k) = 1$ . The factors 3 in the denominator account for the number of families. For the intermediate case,  $m_{\tilde{\nu}} > m_{\tilde{\chi}_1^0} > m_{\tilde{l}}$  (Case 3), there occur contributions from 2-body RPC decays and 3-body RPV decays, such that :

$$B(\tilde{\chi}_1^0 \rightarrow \bar{\nu}_i \bar{l}_j l_k) = \frac{\Gamma'(\tilde{\chi}_1^0 \rightarrow \bar{\nu}_i \bar{l}_j l_k) + \Gamma(\tilde{\chi}_1^0 \rightarrow \tilde{l}_j \bar{l}_j) B(\tilde{l}_j \rightarrow \bar{\nu}_i l_k)}{\Gamma'(\tilde{\chi}_1^0 \rightarrow \bar{\nu}_i \bar{l}_j l_k) + 3\Gamma(\tilde{\chi}_1^0 \rightarrow \tilde{l}_j l_j)} \simeq \frac{1}{3}, \quad (4.3)$$

where the prime on  $\Gamma'$  is a reminder to indicate that the decay width includes only the contribution from a virtual sneutrino exchange. The approximate equality in eq.(4.3) derives from the fact that  $\Gamma'(\tilde{\chi}_1^0 \rightarrow \bar{\nu}_i \bar{l}_j l_k) \ll \Gamma(\tilde{\chi}_1^0 \rightarrow \tilde{l}_j \bar{l}_j)$ , based on the expectation that an RPV 3-body decay should be much smaller than an RPC 2-body decay. An analogous argument to that of case 3 holds for the other intermediate case,  $m_{\tilde{l}} > m_{\tilde{\chi}_1^0} > m_{\tilde{\nu}}$  (Case 4). For the cases 2, 3 and 4, the multiplicity factors are the same as for the case 1. The  $\tilde{\chi}_1^0$  process may occur at the end stage in the decays of  $\tilde{\chi}_1^-$ ,  $\tilde{l}$  and  $\tilde{\nu}$ , to be discussed below. The associated  $\tilde{\chi}_1^0$  decay multiplicity factors for the two leptons final states will then take the same values as quoted above for the various selection criteria. In quoting numerical results below, we shall, for convenience, assume the case of unspecified lepton flavor and charge and thus will set the multiplicity factors to unity.

## Lowest mass Chargino

The results in Fig. 9 for the high  $\tan\beta$  case show a high degree of symmetry with respect to  $\mu \leftrightarrow -\mu$ , which arises from the symmetry in the inos mass spectrum (Figure 3(a)(b)). As can be seen from Figure 9(a), a dominant mode for the chargino at high values of  $|\mu|$  is the cascade decay,  $\tilde{\chi}^- \rightarrow \tilde{\chi}^0 l^- \bar{\nu}$ , since this occurs via the two-body decay,  $\tilde{\chi}^- \rightarrow l^- \tilde{\nu}$  (C(7)). Indeed, for these high values of  $\mu$ , one has  $m_{\tilde{\nu}} < m_{\tilde{\chi}^-}$ . This two-body decay competes with the other two-body decay E,  $\tilde{\chi}^- \rightarrow \tilde{\chi}^0 W^-$ , when the latter is kinematically allowed, as is the case for  $\mu < -200 GeV$  in Figure 9(d). The difference between the values of the branching ratios C(7) and E is explained by the relative phase space factors of the associated rates. The RPV direct decays (A and B) are three-body decays with small



coupling constant and are thus suppressed. In the case,  $m_{\tilde{\nu}} < m_{\tilde{\chi}^0} < m_{\tilde{\chi}^\pm}$ , the only open channel for the sneutrino is,  $\tilde{\nu} \rightarrow \ell\bar{\ell}$ , so that the dominant mode for the chargino decay is the RPV decay B(4) (high values of  $|\mu|$  in Figure 9(b)). Even for  $m_{\tilde{\nu}} \approx m_{\tilde{\chi}^0}$ , the channel B(4) is competitive due to a small phase space ( $\mu \simeq -100\text{GeV}$  in Figure 9(a)). In this case, for  $\lambda_{ijk} = 0.1$ , the direct RPV decay B(4) can become dominant (moderate negative values of  $\mu$  in Figure 9(c)). For small values of  $|\mu|$ , the difference between the two dominant leptonic (C) and hadronic (D) cascade decays is due to the flavor and color factors. We note also that in a small interval of  $\mu$  near  $\mu = 0$ ,  $m_{\tilde{\chi}_1^0} > m_{\tilde{\chi}_1^\pm}$  (see Figure 3), and consequently the only open channels are the direct RPV decays (Figure 9(a)(c)(d)). In this region, the direct RPV decay A(1) is negligible because the branching ratio depends on  $U_{11}$  which is small [51]. In conclusion, the highest branching ratios are associated with the cascade decays, C,D and E, except for the case in which the sneutrino is the LSP, where they are associated with the RPV decays B. The range of  $\mu$  for which the chargino  $\tilde{\chi}_1^-$  is the LSP is excluded by the experimental constraints on the inos masses (see Figure 3).

## Sneutrino

We turn now our attention to the sneutrino decays. For high values of  $\mu$ , the cascade decay D has the highest probability (Figure 10(a)(d)) since the decay into chargino is either kinematically forbidden or suppressed by a small phase space. As for the chargino study, the RPV direct decay A is of course small except when the competitive channel is reduced by a small phase space factor ( $\mu \approx -100\text{GeV}$  in Figure 10(a)). In such a case, the RPV direct decay A may be important for values of  $\lambda_{ijk}$  near 0.1 (negative  $\mu$  in Figure 10(c)). When the sneutrino is the LSP, the RPV direct decay has a branching ratio equal to unity (Figure 10(b)). For small  $|\mu|$ , the decays E(6) and F(8) through charginos dominate the decay D through neutralinos. The reason is that for  $\mu = 0$ ,  $\tilde{\chi}_1^0$  is a pure higgsino, whose couplings are weak. In the so called higgsino limit,  $\mu \rightarrow 0$  [51], the decays B and C(3) are small since they occur through the  $\tilde{\chi}^-$  RPV direct decays. However, they have the highest probability if,  $m_{\tilde{\chi}_1^0} > m_{\tilde{\chi}_1^\pm}$  (Figure 10(a)(c)(d)). The relation between the leptonic (E) and hadronic (F) cascade decays can be explained in the light of the study on the chargino. We conclude that the cascade decays, B, D, E and F, are always the dominant modes, except when the sneutrino is the LSP.

## Slepton

Finally, we concentrate on slepton decays. For high values of  $\mu$ , the cascade decays via charginos are reduced because of a small phase space ( $|\mu| \approx 400\text{GeV}$  in Figure 11(b) or for  $\mu < 0$  in Figures 11(c)(d)) or even closed (for  $\mu < 0$  in Figure 11(a)). In these cases, the decay D via neutralinos dominates. Elsewhere, the decays via charginos have higher branching ratios (for  $\mu > 0$  in Figures 11(a)(d)) since larger coupling constants are involved. In the higgsino limit, the slepton cascade decay D via  $\tilde{\chi}_1^0$  is suppressed for the same reason as in the sneutrino study. The decay via  $\tilde{\chi}_1^-$  is then dominating. The interpretation of the difference between the decays, B, C, E and F, via charginos is based on the specific behaviours of the chargino branching ratios which have already been described above. We see in Figure 11(c), that for  $\lambda_{ijk} = 0.1$ , the RPV direct decay A is still very reduced. This is due to the important phase space for the slepton decay

into neutralino. Lastly, a new phenomenon appears for the slepton case. In the higgsino limit ( $\mu \rightarrow 0$ ) at large  $\tan\beta$ , the matrix element  $U_{11} \rightarrow 0$  which forces the vertex  $\tilde{l} \tilde{\chi}^\pm \nu$  (see eq.2.3 in Appendix 2) and the branching ratios for the cascade decays through the chargino to vanish [51]. This is the explanation of the fact that for  $\mu \simeq 0$ , one observes a peak of the direct RPV decay branching fraction (Figure 11(b)). Similar peaks are also observed at shifted  $\mu < 0$  for the low  $\tan\beta$  cases (Figures 11(a)(c)(d)). However this behaviour appears for ranges of the parameters which are forbidden by the bounds on the inos masses (Figure 3). The conclusion is that the cascade decays have always the highest probability for the reason that the L-chirality slepton cannot be the LSP in generic supergravity models.

## Discussion

In summary, we have learned that the general behaviour of branching ratios is mainly determined by the phase space and thus by the ordering of the supersymmetric particles masses. We have explored all the characteristic cases,  $m_{\tilde{\nu}} > m_{\tilde{\chi}_1^-} > m_{\tilde{\chi}_1^0}$ ,  $m_{\tilde{\chi}_1^-} > m_{\tilde{\nu}} > m_{\tilde{\chi}_1^0}$  and  $m_{\tilde{\chi}_1^-} > m_{\tilde{\chi}_1^0} > m_{\tilde{\nu}}$ . For high values of  $m_0$  lying above  $M_2$ , the sleptons would have masses greater than the inos masses. We have not analysed this case since one has then the same situation in the mass ordering as for the case of small values of  $|\mu|$  (except for large enough values of  $m_0$  where the on-shell  $W^\pm$  production can take place in  $\tilde{l}$  and  $\tilde{\nu}$  decays G). In this situation, as we have explained above, the charginos principally decay into neutralinos, while the sleptons and sneutrinos decay into charginos. The main conclusion is that the cascade decays are the dominant modes except if the sneutrino is the LSP. In this case, the RPV decay,  $\tilde{\chi}_1^- \rightarrow l_i \tilde{\nu}_i \rightarrow l_i l_j \bar{l}_k$ , is dominant for the chargino decays, and the only open channel for the sneutrino is of course the direct RPV decay. Besides, for values of  $\lambda_{ijk}$  higher than 0.05, the RPV direct decay branching ratios can reach significant levels for the case where the cascade decays are suppressed due to small phase space factors.

The excitation of the second neutralino  $\tilde{\chi}_2^0$  deserves some attention since this may have in certain regions of the parameter space comparable, if not larger, production rates than the excitation of  $\tilde{\chi}_1^0$ . Assuming that the direct RPV widths are small enough so that the decay chain is initiated by the RPC contributions, then the desintegration mode,  $\tilde{\chi}_2^0 \rightarrow (\tilde{\chi}_1^0 + l^+ l^-), (\tilde{\chi}_1^0 + \bar{\nu} \nu)$ , will also yield  $2l + \cancel{E}$  and  $4l + \cancel{E}$  final states, respectively, and the other desintegration modes,  $\tilde{\chi}_2^0 \rightarrow (\tilde{\chi}_1^+ + l^- \bar{\nu}, \tilde{\chi}_1^- + l^+ \nu), (\tilde{\nu} \nu, \tilde{\nu} \bar{\nu}), (\tilde{l}^\pm l^\mp)$ , will yield  $2l + \cancel{E}$  and  $4l + \cancel{E}$  final states according to decay schemes similar to those given in Tables 13,14,12. In our supergravity models, the  $\tilde{\chi}_2^0$  decay into  $\tilde{\chi}_1^\pm$  should be suppressed by a small phase space (Fig.3). To determine which of the decay modes,  $\tilde{\chi}_2^0 \rightarrow \tilde{\chi}_1^0, \tilde{l}$  or  $\tilde{\nu}$ , leads to the dominant signal would require a detailed comparison of branching ratios at the initial as well as the subsequent stages.

Let us ask in what way would alternate hypotheses on the family dependence affect our conclusions. Especially regarding the multiplicities of final states, this is relevant for the cases,  $m_{\tilde{\chi}_1^-} > m_{\tilde{l}}, m_{\tilde{\nu}}$ , where the chargino can cascade decay to on-shell sleptons or sneutrinos (A(2) and B(4) in Table 12). As we have emphasized in the last paragraph of Section 2.2, the chargino decays have a multiplicity of 2 for three degenerate families of sleptons. For the case of two degenerate families, labeled by the indices,  $m, n$ , assuming a dominant RPV coupling constant  $\lambda_{ijk}$ , the multiplicity equals 2 for  $(m, n) = (i, j)$ , since the two sleptons from families  $i$  and  $j$  can be produced on-shell, and equals 1 for  $m = k$  or

$n = k$ . For the physically interesting case of a single low mass family, labeled by the index,  $m$ , one finds that the multiplicity equals 1 for  $m \neq k$  and 0 otherwise. The conclusion is that the RPV contributions A and B (in Table 12) to the chargino branching ratios increase as the number of slepton families, which are lower in mass than the chargino, becomes higher. This effect, which is quite small, would affect the branching ratios in parameters regions for which the RPV contributions A and B are not weak, that is for  $\mu < 0$  in Figures 9(a)(b)(c).

In Figure 12, we present results for the branching fractions for fixed  $m_0$  in the infrared fixed point model with electroweak symmetry breaking. In this constrained version, where  $m_{1/2}$  varies with  $\mu$ , the dependence on  $\mu$  is rather similar to that of the non minimal model where we worked instead with fixed  $m_0$  and  $m_{1/2}$ . However, as we see from the mass spectrum, here the LSP is the neutralino  $\tilde{\chi}_1^0$  for all the physical ranges of the parameters. Due to the large mass difference between the  $\tilde{\chi}_1^0$  LSP and the NLSP (next to LSP), the cascade decays are the only dominant modes and the branching ratios for the RPV direct decays are very weak.

Let us add a few qualitative remarks on the predictions of gauge mediated supersymmetry breaking models. In order for the production rates in the minimal model [52] to have the same order of magnitude as those obtained in the supergravity model of section 4, one needs a parameter  $\Lambda = \frac{F}{M} \simeq 10^4 GeV$ , using familiar notations for the supersymmetry breaking scale ( $\sqrt{F}$ ) and messenger scale ( $M$ ). Concerning the signals, by comparing the mean free paths for  $\tilde{\chi}_1^0$  (favourite candidate for LSP) in both models, one finds that the decay channel to the gravitino,  $\tilde{\chi}_1^0 \rightarrow \gamma \tilde{G}$ , becomes competitive with the RPV decay channel,  $\tilde{\chi}_1^0 \rightarrow \nu l \bar{l}$ , for,  $\frac{\sqrt{\langle F \rangle}}{100 TeV} \leq \frac{10^{-2}}{\sqrt{\Lambda}}$ .

Let us also comment briefly on some of the experimental issues. A given final state can possibly arise simultaneously from several of the single production processes. The important  $4l + \cancel{E}$  signal which occurs for  $\tilde{\chi}^\pm, \tilde{l}^\pm, \tilde{\nu}$  productions is one such example where one may be forced to add all three types of cross sections in comparing with some given experimental data sample. Similarly, for most signals, one must typically add the contributions from the two charge conjugate partner processes. Concerning the competition with the standard model background, one expects that the most important contributions to the final states,  $2l + \cancel{E}$  and  $4l$ , will arise from the reactions,  $l_J^+ l_J^- \rightarrow W^+ l^- \bar{\nu}, W^- l^+ \nu, W^+ W^-, Z^0 l^+ l^-, Z^0 Z^0, Z^0 \gamma$ . In spite of the large standard model rates of order one picobarn at  $\sqrt{s} = 500 GeV$  [38], one should be able to distinguish the single production signals by exploiting their specific non diagonal flavor character (final state B in Table 14 and A in Table 13). The other multileptons final states, generated by the cascade decays,  $4l + \cancel{E}, 4l + Z^0, 3l + Z^0 + W^\pm + \cancel{E}, \dots$  have a standard model background which is negligible. The potentially large two photons background processes, induced by  $\gamma\gamma$  photons pairs radiated by the initial leptons, can be significantly reduced by imposing suitable cuts on the leptons transverse momenta. Finally, we note that the selection by the RPV single production of identical helicities for the initial state,  $l_H^+ l_H^-$ , can be exploited to discriminate against the minimal supersymmetric standard model and also the standard model, for which the identical helicities configuration only appears with the t-channel Z-boson exchange.

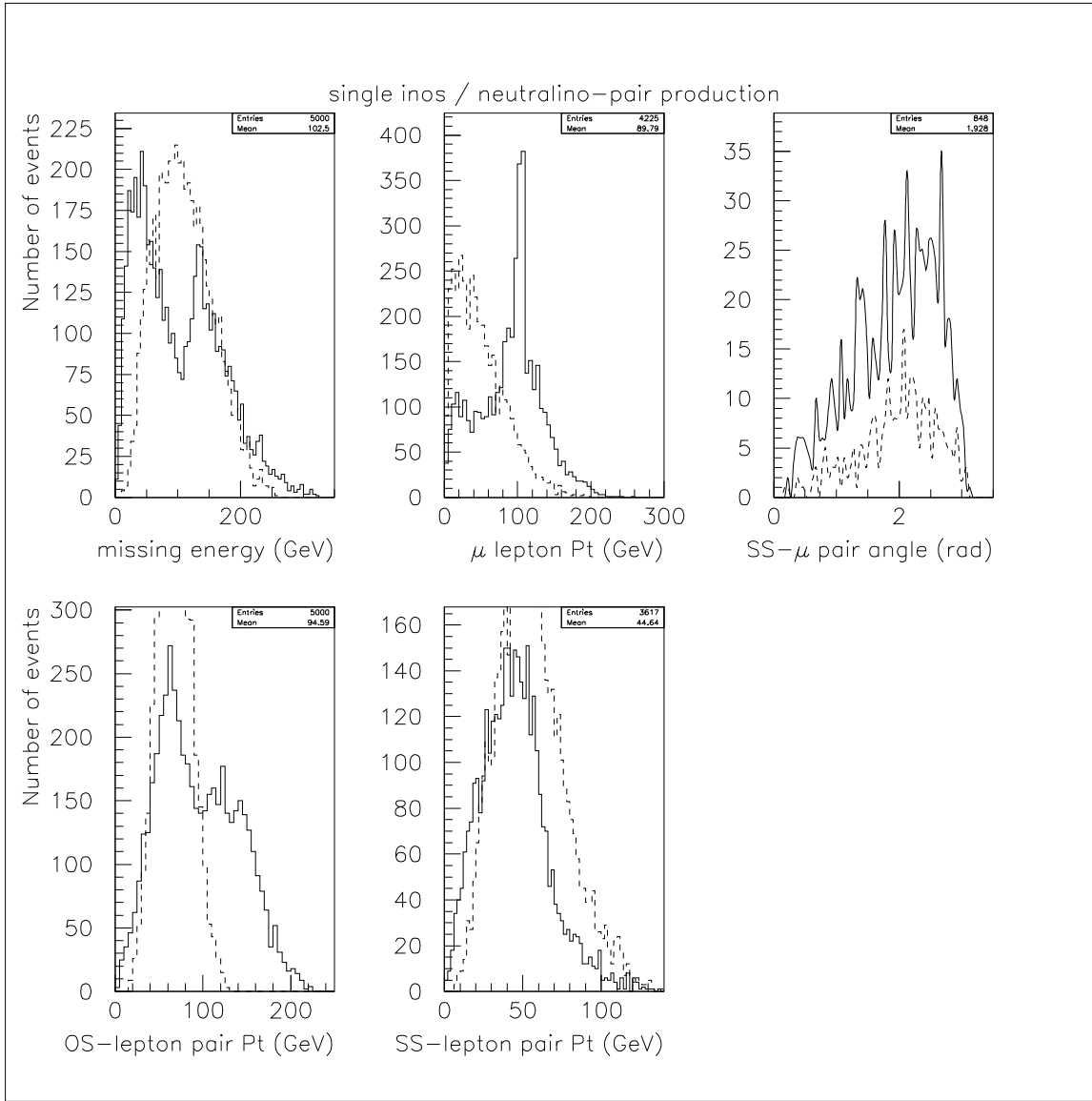


FIG. 13: Distributions of missing energy, muon transverse momentum, same sign muon pair angle, summed transverse momentum for opposite sign (OS) and same sign (SS) leptons pairs (electrons and muons) for the single production processes,  $l_J^+ l_J^- \rightarrow \tilde{\chi}_1^\pm l^\mp, \tilde{\chi}_1^0 \nu_\mu, \tilde{\chi}_1^0 \bar{\nu}_\mu, \tilde{\chi}_2^0 \nu_\mu, \tilde{\chi}_2^0 \bar{\nu}_\mu$  (solid line), and the pair production process,  $l_J^+ l_J^- \rightarrow \tilde{\chi}_1^0 \tilde{\chi}_1^0$  (dashed line), at a center of mass energy of 350 GeV. The parameters values are,  $M_2 = 250 \text{ GeV}$ ,  $m_0 = 70 \text{ GeV}$ ,  $\mu = 400 \text{ GeV}$ ,  $\tan \beta = 2$ ,  $\lambda_{211} = 0.05$ . Events samples, consisting of 5000 events each, are generated for the inos single production and neutralino pair production, respectively.

## 5 Dynamical distributions

The distributions of rates with respect to kinematical variables associated with the final states offer helpful means to characterize the underlying production processes. As an indicative study we shall present here some characteristic dynamical distributions obtained for the production reactions,  $l_J^+ l_J^- \rightarrow \tilde{\chi}_1^\pm l^\mp, \tilde{\chi}_1^0 \nu, \tilde{\chi}_1^0 \bar{\nu}, \tilde{\chi}_2^0 \nu, \tilde{\chi}_2^0 \bar{\nu}$ , from a Monte Carlo events simulation for which we have used the event generator SUSYGEN [41].

We concentrate on the final state signals of  $2l+\cancel{E}$ ,  $4l$  and  $4l+\cancel{E}$ . Note that for high values of  $\mu$ , the final state  $4l+\cancel{E}$  is the dominant mode for the chargino, slepton and sneutrino decays. This signal also receives contributions from the reactions,  $l_J^+ l_J^- \rightarrow \tilde{\nu} Z^0 (\tilde{\nu} Z^0), \tilde{\nu} \gamma (\tilde{\nu} \gamma), \tilde{l}^\pm W^\mp$ , which however are not included in the simulation. The standard model background is expected to be small for the  $4l+\cancel{E}$  signal. The main background from the minimal supersymmetric standard model interactions arises from the neutralino RPC pair production,  $l_J^+ l_J^- \rightarrow \tilde{\chi}_1^0 \tilde{\chi}_1^0$ . Following the analysis in [53], we consider an incident energy of  $\sqrt{s} = 350 \text{ GeV}$  and use a non minimal supergravity model for which we choose the set of parameters,  $M_2 = 250 \text{ GeV}, \mu = 400 \text{ GeV}, m_0 = 70 \text{ GeV}, \tan \beta = 2$ , which yields the spectrum,  $m_{\tilde{\chi}_1^0} = 118.5 \text{ GeV}, m_{\tilde{\chi}_2^0} = 221.4 \text{ GeV}, m_{\tilde{\chi}_1^\pm} = 219.1 \text{ GeV}, m_{\tilde{\nu}_L} = 225 \text{ GeV}, m_{\tilde{l}_L} = 233 \text{ GeV}, m_{\tilde{l}_R} = 141 \text{ GeV}$ . The integrated rates (ignoring acceptance cuts) are, for  $\lambda_{mJJ} = 0.05$  [ $m = 2$ ],  $\sigma(\tilde{\chi}_1^+ \mu^-) = 30.9 \text{ fb}, \sigma(\tilde{\chi}_1^0 \nu_\mu) = 4.8 \text{ fb}, \sigma(\tilde{\chi}_2^0 \nu_\mu) = 12.1 \text{ fb}$  and  $\sigma(\tilde{\chi}_1^0 \tilde{\chi}_1^0) = 238.9 \text{ fb}$ . We consider the following five dynamical variables for all types of final states : Invariant missing energy,  $E_m = \sum_{i \in \nu} E_i$  where the sum is over the neutrinos, as appropriate to a broken R parity situation ; Average per event of the  $\mu^\pm$  lepton transverse momentum,  $P_t(\mu^\pm) = \frac{\sum_i |p_t(\mu_i^\pm)|}{N_\mu}$ , where  $N_\mu$  is the number of muons ; Angle between the momenta of same electric charge sign (SS) muons pairs ; Average per event of the summed transverse momenta for leptons pairs of same sign (SS) or opposite sign (OS),  $P_t^{SS,OS}(ll) = \sum_{(i,j)} \frac{p_t(l_i^{\pm,\mp}) + p_t(l_j^\pm)}{N}$ , where  $N$  is the number of configurations and  $l = e, \mu$ .

We have generated the inos single production and the  $\tilde{\chi}_1^0$  pair production in separate samples of 5000 events each. Our choice of using equal number of events for both reactions has been made on the basis of the following three somewhat qualitative considerations, none of which is compelling. First, the single production reactions occur in company of their charge conjugate partners, which multiplies rates by a factor 2. Second, the other  $\tilde{\nu}$  and  $\tilde{l}$  single production reactions, which have not been included, would be expected to add contributions of similar size to the leptonic distributions. Third, assuming for the RPV coupling constant the alternative bound,  $\lambda_{mJJ} \frac{100 \text{ GeV}}{m_{\tilde{l}_R}} < 0.05$ , there would result a relative enhancement for single production over pair production by a factor,  $(\frac{m_{\tilde{l}_R}}{100 \text{ GeV}})^2$ . The above three points motivate our rough guess that the number of events chosen for the five single production processes (together with their charge conjugate partners) should be of comparable size to that of the  $\tilde{\chi}_1^0$  pair production process.

The results are shown in Figure 13. The single production reactions present certain clear characteristic features : Concentration of missing energy  $E_m$  at low energies ; pronounced peaks in the muon transverse momentum  $P_t(\mu^\pm)$  and in the angular distribution for the same sign muons pairs ; and a double peak in the transverse momentum distribution for the opposite sign leptons pairs,  $P_t^{OS}(ll)$ . The large transverse momentum components present in the single production distributions in  $P_t^{OS}(ll)$  and in  $P_t(\mu^\pm)$  are explained by the fact that one of the two leptons (namely,  $l_m^\pm$ ) is created at the production stage. Similarly, the existence of a strong angular correlation between same sign muons pairs is interpreted naturally by the momentum conservation balance between the lepton  $l_m^\pm$  produced in the initial stage and the other lepton produced at the decay stage. Although there are certain distinguishing properties between the single and pair production processes, the discrimination between the two may depend crucially on the relative sizes of the associated event samples. Of course, the best possible situation would be for an energetically forbidden neutralino pair production.

Finally, we comment on the effect of eventually excluding the  $\tilde{\chi}_2^0$  single production component. In that case, most of the signals for single production would become less diluted in comparison with neutralino pair production, the large missing energy signal would be removed while the large OS lepton pair  $P_t^{OS}(ll)$  signal would become amplified.

## 6 Conclusions

We have analysed the full set of  $2 \rightarrow 2$  single production processes at leptonic colliders induced by the RPV interactions  $LL\tilde{E}^c$ , within a supergravity model. Although our approximate study has obvious limitations (factorisation and narrow resonance approximation, neglect of the spin correlations and omission of acceptance cuts), it uncovers the general trends of all the 5 single production reactions. Over the whole parameter space, for an RPV coupling constant  $\lambda_{mJJ}$  of order 0.05, the integrated rates are of comparable order of magnitudes although  $\tilde{\chi}_1^\pm$  and  $\tilde{\nu}$  are typically larger by factors of 2 compared to  $\tilde{l}$  production and by factors of 5 compared to  $\tilde{\chi}_1^0$  production. The detectability for each single production separately is modest at LEP II but comfortable at NLC, corresponding to a few events and a few thousands of events per year, respectively. A wide region of the parameter space can be probed at  $\lambda_{mJJ} > 0.05$ . In spite of the rich variety of final states, the dominant signals arise from the single or double RPC induced cascade decays to the LSP, which are also favored by phase space arguments. For the minimal supergravity model, assuming electroweak symmetry breaking, large mass differences occur between the scalar superpartners and the  $\tilde{\chi}_1^0$  LSP, leading to dominant cascade decays modes with weak competitiveness from the RPV direct decays. The signals,  $4l + \cancel{E}$ ,  $6l + \cancel{E}$ , arising from cascade decays are free from standard model background which make them quite interesting signatures for the discovery of supersymmetry and R parity violation. Even the  $4l$  signal arising from direct RPV decays could be observable due to a characteristic non diagonal flavor configuration. For center of mass energies well above all the thresholds, the  $4l + \cancel{E}$  signal receives contributions from all five single production processes and hence should be strongly amplified. We have presented some dynamical distributions for the final states which could characterise the single production reactions.

## 7 Acknowledgments

We are grateful to R. Barbier and S. Katsanevas for guidance in using the events generator SUSYGEN, to P. Lutz and the Direction of the DAPNIA at Saclay for providing us, through the DELPHI Collaboration, an access to the ANASTASIE computer network at Lyon and to P. Micout for his technical help on that matter. We thank M. Besançon, F. Ledroit, R. Lopez and G. Sajot for helpful discussions.

# 1 Formulas for spin summed amplitudes

We discuss the five  $2 \rightarrow 2$  body single production processes given by eq.(2.1). The formulas for the probability amplitudes are :

$$\begin{aligned}
M(\tilde{\chi}_a^- + l_m^+) &= \frac{g\lambda_{mJJ}V_{a1}^*}{s - m_{\tilde{\nu}_{mL}}^2} \bar{v}(k') P_L u(k) \bar{u}^c(p) P_L v(p') - \frac{g\lambda_{mJJ}V_{a1}^*}{t - m_{\tilde{\nu}_{JL}}^2} \bar{u}^c(p) P_L u(k) \bar{v}(k') P_L v(p'), \\
M(\tilde{\chi}_a^0 + \bar{\nu}_m) &= + \frac{\sqrt{2}g\lambda_{mJJ}}{s - m_{\tilde{\nu}_{mL}}^2} \frac{1}{2} (N_{a2}^* - tg\theta_W N_{a1}^*) \bar{u}(p) P_L v(p') \bar{v}(k') P_L u(k) \\
&\quad + \frac{\sqrt{2}g\lambda_{mJJ}}{t - m_{\tilde{l}_{JL}}^2} \frac{1}{2} (N_{a2}^* + tg\theta_W N_{a1}^*) \bar{u}(p) P_L u(k) \bar{v}(k') P_L v(p') \\
&\quad + \frac{\sqrt{2}g\lambda_{mJJ}}{u - m_{\tilde{l}_{JR}}^2} (tg\theta_W N_{a2}^*) \bar{v}^c(p') P_L u(k) \bar{v}(k') P_L v(p), \\
M(\tilde{l}_{mL}^-(p) + W^+(p')) &= \frac{g\lambda_{mJJ}^*}{\sqrt{2}(s - m_{\tilde{\nu}_{mL}}^2)} 2p \cdot \epsilon(p') \bar{v}(k') P_R u(k) + \frac{g\lambda_{mJJ}^*}{\sqrt{2}t} \bar{v}(k') \gamma \cdot \epsilon(p') (\not{p} - \not{k}) P_R u(k), \\
M(\tilde{\nu}_{mL}(p) + Z(p')) &= \frac{g\lambda_{mJJ}^*}{2\cos\theta_W} \left[ \frac{\bar{v}(k') \gamma \cdot \epsilon(p') (\not{k} - \not{p}) a_L(e) P_R u(k)}{t - m_{\tilde{l}_J}^2} \right. \\
&\quad \left. + \frac{\bar{v}(k') a_R(e) P_R (\not{k} - \not{p}') \gamma \cdot \epsilon(p') u(k)}{u - m_{\tilde{l}_J}^2} + \frac{\bar{v}(k') a_L(\tilde{\nu}) P_R u(k) 2p \cdot \epsilon(p')}{s - m_{\tilde{\nu}_{mL}}^2} \right], \\
M(\tilde{\nu}_{mL}(p) + \gamma(p')) &= -e\lambda_{mJJ}^* \left[ \frac{\bar{v}(k') \gamma \cdot \epsilon(p') (\not{k} - \not{p}) P_R u(k)}{t - m_{\tilde{l}_J}^2} + \frac{\bar{v}(k') (\not{k} - \not{p}') \gamma \cdot \epsilon(p') P_R u(k)}{u - m_{\tilde{l}_J}^2} \right].
\end{aligned} \tag{1.1}$$

In deriving the results for the inos production amplitudes, we have systematically neglected their higgsino components. The parameters in the  $Z^0 f \bar{f}$  and  $Z^0 \tilde{f} \tilde{\bar{f}}$  vertices denoted as,  $a_H(f) = a(f_H)$  and  $a_H(\tilde{f}) = a(\tilde{f}_H)$ , are defined by,  $a(f_H) = a(\tilde{f}_H) = 2T_3^H(f) - 2Qx_W$ , with  $H = [L, R]$  and  $x_W = \sin^2 \theta_W$ . Throughout this work, our notations follow closely the Haber-Kane conventions [48].

The unpolarized cross sections in the center of mass frame are given by the familiar formula,  $d\sigma/d\cos\theta = p/(128\pi ks) \sum_{pol} |M|^2$ , where the sums over polarizations for the probability amplitudes squared are given by :

$$\begin{aligned}
\sum_{pol} |M(\tilde{\chi}_a^- + l_m^+)|^2 &= |\lambda_{mJJ} g V_{a1}^*|^2 \left[ \frac{s(s - m_{\tilde{\chi}_a^-}^2 - m_{l_m}^2)}{|R_s(\tilde{\nu}_{mL})|^2} + \frac{(m_{\tilde{\chi}_a^-}^2 - t)(m_{l_m}^2 - t)}{|R_t(\tilde{\nu}_{JL})|^2} \right. \\
&\quad \left. - Re \left( \frac{(s(s - m_{\tilde{\chi}_a^-}^2 - m_{l_m}^2) + (m_{\tilde{\chi}_a^-}^2 - t)(m_{l_m}^2 - t) - (m_{\tilde{\chi}_a^-}^2 - u)(m_{l_m}^2 - u))}{R_s(\tilde{\nu}_{mL}) R_t^*(\tilde{\nu}_{JL})} \right) \right],
\end{aligned} \tag{1.2}$$

$$\begin{aligned}
\sum_{pol} |M(\tilde{\chi}_a^0 + \bar{\nu}_m)|^2 &= \frac{g^2}{2} |\lambda_{mJJ}|^2 \left[ |N_{a2} + tg\theta_W N_{a1}|^2 \frac{t(t - m_{\tilde{\chi}_a^0}^2)}{|R_t(\tilde{l}_{JL})|^2} \right. \\
&\quad \left. + 4|tg\theta_W N_{a2}|^2 \frac{u(u - m_{\tilde{\chi}_a^0}^2)}{|R_u(\tilde{l}_{JR})|^2} + |N_{a2} - tg\theta_W N_{a1}|^2 \frac{s(s - m_{\tilde{\chi}_a^0}^2)}{|R_s(\tilde{\nu}_{mL})|^2} \right]
\end{aligned}$$

$$\begin{aligned}
& - \operatorname{Re} \left( (N_{a2}^* - t g \theta_W N_{a1}^*) (-N_{a2} - t g \theta_W N_{a1}) \frac{(s(s - m_{\tilde{\chi}_a^0}^2) - t(m_{\tilde{\chi}_a^0}^2 - t) + u(m_{\tilde{\chi}_a^0}^2 - u))}{R_s(\tilde{\nu}_{mL}) R_t^*(\tilde{l}_{JL})} \right. \\
& + 2(N_{a2}^* - t g \theta_W N_{a1}^*) (-t g \theta_W N_{a2}) \frac{(s(s - m_{\tilde{\chi}_a^0}^2) - u(m_{\tilde{\chi}_a^0}^2 - u) + t(m_{\tilde{\chi}_a^0}^2 - t))}{R_s(\tilde{\nu}_{mL}) R_u^*(\tilde{l}_{JR})} \\
& \left. + 2(-N_{a2}^* - t g \theta_W N_{a1}^*) (-t g \theta_W N_{a2}) \frac{(-u(m_{\tilde{\chi}_a^0}^2 - u) - t(m_{\tilde{\chi}_a^0}^2 - t) - s(s - m_{\tilde{\chi}_a^0}^2))}{R_t(\tilde{l}_{JL}) R_u^*(\tilde{l}_{JR})} \right), \quad (1.3)
\end{aligned}$$

$$\begin{aligned}
\sum_{pol} |M(\tilde{l}_{mL}^- + W^+)|^2 &= \frac{sg^2 |\lambda_{mJJ}|^2}{2|R_s(\tilde{\nu}_{mL})|^2} \left( \frac{(s - m_{\tilde{l}_{mL}}^2 - m_W^2)^2}{m_W^2} - 4m_{\tilde{l}_{mL}}^2 \right) - \frac{g^2 |\lambda_{mJJ}|^2}{2|t|^2} \\
&\times [(m_{\tilde{l}_{mL}}^2 - t)(m_W^2 - t) + st + \frac{m_W^2 - t}{m_W^2} ((m_{\tilde{l}_{mL}}^2 - t)(m_W^2 + t) + t(m_W^2 - u))] \\
&- g^2 \operatorname{Re} \frac{\lambda_{mJJ} \lambda_{mJJ}^*}{t R_s^*(\tilde{\nu}_{mL})} [(m_{\tilde{l}_{mL}}^2 - t)(m_{\tilde{l}_{mL}}^2 - u) + s(m_{\tilde{l}_{mL}}^2 - u) + (m_{\tilde{l}_{mL}}^2 - t)(m_W^2 - t) \\
&- \frac{s(s - m_W^2 - m_{\tilde{l}_{mL}}^2)(m_W^2 - t)}{m_W^2}], \quad (1.4)
\end{aligned}$$

$$\begin{aligned}
\sum_{pol} |M(\tilde{\nu}_{mL} + Z)|^2 &= \frac{g^2 |\lambda_{mJJ}|^2}{\cos^2 \theta_W} \operatorname{Re} \left[ \frac{s}{|R_s(\tilde{\nu}_{mL})|^2} \left( \frac{(s - m_{\tilde{\nu}_{mL}}^2 - m_Z^2)^2}{4m_Z^2} - m_{\tilde{\nu}_{mL}}^2 \right) \right. \\
&- \frac{(\sin^2 \theta_W)^2}{|R_u(l_J)|^2} \left( (m_{\tilde{\nu}_{mL}}^2 - u)(m_Z^2 - u) + su + \frac{m_Z^2 - u}{m_Z^2} ((m_{\tilde{\nu}_{mL}}^2 - u)(m_Z^2 + t) + u(m_Z^2 - t)) \right) \\
&- \frac{(2 \sin^2 \theta_W - 1)^2}{4|R_t(l_J)|^2} \left( (m_{\tilde{\nu}_{mL}}^2 - t)(m_Z^2 - t) + st + \frac{m_Z^2 - t}{m_Z^2} ((m_{\tilde{\nu}_{mL}}^2 - t)(m_Z^2 + t) + t(m_Z^2 - u)) \right) \\
&- \frac{(\sin^2 \theta_W)}{R_u(l_J) R_s^*(\tilde{\nu}_{mL})} \left( (m_{\tilde{\nu}_{mL}}^2 - t)(m_{\tilde{\nu}_{mL}}^2 - u) + s(m_{\tilde{\nu}_{mL}}^2 - t) + (m_{\tilde{\nu}_{mL}}^2 - u)(m_Z^2 - u) \right. \\
&- \left. \frac{s}{m_Z^2} (s - m_{\tilde{\nu}_{mL}}^2 - m_Z^2)(m_Z^2 - u) \right) + \frac{(2 \sin^2 \theta_W - 1)}{2 R_t(l_J) R_s^*(\tilde{\nu}_{mL})} \left( (m_{\tilde{\nu}_{mL}}^2 - t)(m_{\tilde{\nu}_{mL}}^2 - u) + s(m_{\tilde{\nu}_{mL}}^2 - u) \right. \\
&+ (m_Z^2 - t)(m_{\tilde{\nu}_{mL}}^2 - t) - \frac{s}{m_Z^2} (m_Z^2 - t)(s - m_{\tilde{\nu}_{mL}}^2 - m_Z^2) \left. \right) + \frac{(2 \sin^2 \theta_W - 1)(\sin^2 \theta_W)}{R_t(l_J) R_u^*(l_J)} \\
&\times \left( (m_{\tilde{\nu}_{mL}}^2 - u)(m_{\tilde{\nu}_{mL}}^2 - t) + s m_{\tilde{\nu}_{mL}}^2 - \frac{1}{M_Z^2} \left( -\frac{(s - m_{\tilde{\nu}_{mL}}^2 - m_Z^2)}{2} ((m_{\tilde{\nu}_{mL}}^2 - u)(m_Z^2 - u) \right. \right. \\
&+ \left. \left. (m_{\tilde{\nu}_{mL}}^2 - t)(m_Z^2 - t) - s(s - m_{\tilde{\nu}_{mL}}^2 - m_Z^2)) + (m_Z^2 - u)(m_Z^2 - t) m_{\tilde{\nu}_{mL}}^2 \right) \right], \quad (1.5)
\end{aligned}$$

$$\begin{aligned}
\sum_{pol} |M(\tilde{\nu}_{mL} + \gamma)|^2 &= 2e^2 |\lambda_{mJJ}|^2 ((m_{\tilde{\nu}_{mL}}^2 - t)(m_{\tilde{\nu}_{mL}}^2 - u) - s m_{\tilde{\nu}_{mL}}^2) \left[ \frac{1}{|R_t(l_J)|^2} + \frac{1}{|R_u(l_J)|^2} \right] \\
&+ 4e^2 |\lambda_{mJJ}|^2 \operatorname{Re} \frac{(m_{\tilde{\nu}_{mL}}^2 - t)(m_{\tilde{\nu}_{mL}}^2 - u)}{R_t(l_J) R_u^*(l_J)}, \quad (1.6)
\end{aligned}$$

where  $\operatorname{Re}$  stands for the real part,  $R_s(\tilde{\nu}_i) = s - m_{\tilde{\nu}_i}^2 + i m_{\tilde{\nu}_i} \Gamma_{\tilde{\nu}_i}$ ,  $R_t(\tilde{\nu}_i) = t - m_{\tilde{\nu}_i}^2$  and  $R_u(\tilde{\nu}_i) = u - m_{\tilde{\nu}_i}^2$ ,  $[s = (k + k')^2, t = (k - p)^2, u = (k - p')^2]$ , with similar definitions applying for the propagator factors  $R_{s,t,u}(l_i, \tilde{l}_i)$ .



## 2 Formulas for partial decay widths

The formulas for the various two-body decay widths are quoted below.

$$\Gamma(\tilde{\nu} \rightarrow \tilde{\chi}_a^+ + l^-) = \frac{g^2}{16\pi} |V_{a1}|^2 m_{\tilde{\nu}} \left(1 - \frac{m_{\tilde{\chi}_a}^2}{m_{\tilde{\nu}}^2}\right)^2 \quad (2.1)$$

$$\Gamma(\tilde{\nu} \rightarrow \tilde{\chi}_a^0 + \nu) = \frac{g^2}{32\pi} |N_{a2} - N_{a1} \tan \theta_W|^2 m_{\tilde{\nu}} \left(1 - \frac{m_{\tilde{\chi}_a}^2}{m_{\tilde{\nu}}^2}\right)^2 \quad (2.2)$$

$$\Gamma(\tilde{l}_L^+ \rightarrow \tilde{\chi}_a^+ \bar{\nu}) = \frac{g^2}{16\pi} |U_{a1}|^2 m_{\tilde{l}_L} \left(1 - \frac{m_{\tilde{\chi}_a}^2}{m_{\tilde{l}_L}^2}\right)^2 \quad (2.3)$$

$$\Gamma(\tilde{l}_{[L,R]}^- \rightarrow \tilde{\chi}_a^0 + l^-) = \frac{g^2}{32\pi} [|N_{a2} + N_{a1} \tan \theta_W|^2, |N_{a2} \tan \theta_W|^2] m_{\tilde{l}_H} \left(1 - \frac{m_{\tilde{\chi}_a}^2}{m_{\tilde{l}_H}^2}\right)^2 \quad (2.4)$$

$$\begin{aligned} \Gamma(\tilde{\nu}_i(M) \rightarrow l_k^-(m_1) + l_j^+(m_2)) &= \Gamma(\tilde{l}_{jL}^-(M) \rightarrow \bar{\nu}_i(m_1) + l_k^-(m_2)) \\ &= \Gamma(\tilde{l}_{kR}^-(M) \rightarrow \nu_i(m_1) + l_j^-(m_2)) \\ &= \frac{|\lambda_{ijk}|^2}{8\pi} k \left(1 - \frac{m_1^2 + m_2^2}{M^2}\right) \end{aligned} \quad (2.5)$$

$$\begin{aligned} \Gamma(\tilde{\chi}_m^\pm(M_\pm) \rightarrow \tilde{\chi}_l^0(M_0) + W^\pm(m_W)) &= \frac{g^2 |k|}{16\pi M_\pm^2} \left[ (|O_L|^2 + |O_R|^2) \left( (M_\pm^2 + M_0^2 - m_W^2) \right. \right. \\ &\quad \left. \left. + \frac{1}{m_W^2} (M_\pm^2 - M_0^2 - m_W^2) (M_\pm^2 - M_0^2 + m_W^2) \right) \right. \\ &\quad \left. - 12 M_0 M_\pm \text{Re}(O_L O_R^*) \right] \end{aligned} \quad (2.6)$$

$$\Gamma(\tilde{\chi}_a^0 \rightarrow \tilde{f}_{[L,R]} f') = \frac{g^2 M_0}{16\pi} \left(1 - \frac{m_{\tilde{f}}^2}{M_0^2}\right)^2 \frac{1}{[|T_3^f N_{a2} - \tan \theta_W (T_3^f - Q^f) N_{a1}|^2, |\tan \theta_W N_{a2}|^2]} \quad (2.7)$$

$$\Gamma(\tilde{\chi}_a^\pm \rightarrow \tilde{f}_{[T_3^f=-1/2, 1/2]} f') = \frac{g^2 M_\pm}{32\pi} \left(1 - \frac{m_{\tilde{f}}^2}{M_\pm^2}\right)^2 [|U_{a1}|^2, |V_{a1}|^2]. \quad (2.8)$$

We use the notations :  $O^L = O_{lm}^L = N_{l2} V_{m1}^* - \frac{1}{\sqrt{2}} N_{l4} V_{m2}^*$ ,  $O^R = O_{lm}^R = N_{l2} U_{m1} + \frac{1}{\sqrt{2}} N_{l3}^* U_{m2}$ ,  $M_\pm = m_{\tilde{\chi}_a^\pm}$ ,  $M_0 = m_{\tilde{\chi}_a^0}$  and  $k = \lambda^{\frac{1}{2}}(M^2, m_1^2, m_2^2)/2M$  with  $\lambda(a, b, c) = a^2 + b^2 + c^2 + ab + bc + ac$ . The notations,  $T_3^f$ ,  $Q^f$ , stand for the third component of the  $SU(2)_L$  group and the electric charge of the fermion  $f$ . We have omitted the higgsino components of the inos. We shall use the simplified formulas for the RPC three-body decays,  $\tilde{\chi}_m^- \rightarrow \tilde{\chi}_l^0 + l\bar{\nu}$ ,  $q\bar{q}$ , obtained by neglecting the three-momenta in the W and

$\tilde{l}$  propagators, as quoted in [54]. We have set in these formulas, the flavor and color parameters to,  $N_f = 2$ ,  $N_c = 3$  for quarks and  $N_f = 3$ ,  $N_c = 1$  for leptons. The formulas for the spin summed amplitudes of the RPV decays  $\tilde{\chi}_a^- \rightarrow \bar{\nu}_i \bar{\nu}_j l_k^-$ ,  $\tilde{\chi}_a^- \rightarrow l_k^+ l_j^- l_i^-$ , associated to the coupling constants  $\lambda_{ijk}$ , were first derived in [15] (see the appendix). The integrated decay rates are given by familiar formulas [47] involving twofold integrals over the final state three-body phase space. If we neglect the final particles masses, an analytic formula can be derived for the integral giving the contributions to the charginos partial rates associated with the gauginos components only (neglecting the higgsino components contribution). For completeness, we display the final results :

$$\begin{aligned}
\Gamma(\tilde{\chi}_a^-) = & M_{\tilde{\chi}_a^-} \frac{g^2 X_{a1}^2 |\lambda_{ijk}|^2}{128\pi^3} \left[ \frac{1}{8} \left( -5 + 6\mu_i + (2 - 8\mu_i + 6\mu_i^2) \log\left(1 - \frac{1}{\mu_i}\right) \right. \right. \\
& - \left. 5 + 6\mu_j + (2 - 8\mu_j + 6\mu_j^2) \log\left(1 - \frac{1}{\mu_j}\right) \right) \\
& + \frac{1}{2} \left( \mu_i + \mu_j - \frac{1}{2} + (\mu_i^2 - \mu_i) \log\left(1 - \frac{1}{\mu_i}\right) + (\mu_j^2 - \mu_j) \log\left(1 - \frac{1}{\mu_j}\right) \right. \\
& - \left. \mu_i \mu_j \log\left(1 - \frac{1}{\mu_i}\right) \log\left(\frac{\mu_i + \mu_j - 1}{\mu_j}\right) \right. \\
& - \left. \mu_i \mu_j \log\left(1 - \frac{1}{\mu_j}\right) \log\left(\frac{\mu_i + \mu_j - 1}{\mu_i}\right) \right. \\
& \left. \left. + \mu_i \mu_j \left[ Sp\left(\frac{\mu_i}{\mu_j}\right) + Sp\left(\frac{\mu_j}{\mu_i}\right) - Sp\left(\frac{1 - \mu_i}{\mu_j}\right) - Sp\left(\frac{1 - \mu_j}{\mu_i}\right) \right] \right) \right], \quad (2.9)
\end{aligned}$$

where  $Sp(x) = Polylog(x) = Li_2(x)$  is the Spence or Polylog function. We use the notations  $\mu_\alpha = m_{\tilde{\nu}_\alpha}^2 / M_{\tilde{\chi}_a^-}^2$ ,  $[\alpha = i, j]$ ,  $X_{a1} = U_{a1}$  for the decay  $\tilde{\chi}_a^- \rightarrow l_k^+ l_j^- l_i^-$ , and  $\mu_\alpha = m_{l_\alpha}^2 / M_{\tilde{\chi}_a^-}^2$ ,  $[\alpha = i, j]$ ,  $X_{a1} = V_{a1}$  for the decay  $\tilde{\chi}_a^- \rightarrow \bar{\nu}_i \bar{\nu}_j l_k^-$ .

# References

- [1] S. Dimopoulos and L. J. Hall, Phys. Lett. **B207** (1988) 210
- [2] V. Barger, G. F. Giudice and T. Han, Phys. Rev. **D40** (1989) 2987
- [3] H. Dreiner and G. G. Ross, Nucl. Phys. **B365** (1991) 597
- [4] R. Barbieri, D. E. Brahm, L. J. Hall and S. D. H. Hsu, Phys. Lett. **B238** (1990) 86
- [5] D. E. Brahm and L. J. Hall, Phys. Rev. **D40** (1989) 2449
- [6] S. Lola and J. Mc Curry, Nucl. Phys. **B381** (1992) 559
- [7] H. Dreiner and R. J. N. Phillips, Nucl. Phys. **B367** (1991) 591
- [8] Opal Coll., Phys. Lett., **B313** (1993) 333
- [9] Aleph Coll., Phys. Lett., **B349** (1995) 238
- [10] D. P. Roy, Phys. Lett., **B283** (1992) 270
- [11] Aleph Coll., Phys. Lett., **B384** (1996) 461
- [12] Delphi Coll., Y. Arnoud et al., 20 July 1997, DELPHI 97-119, CONF 101, Hep'97
- [13] Aleph Coll., R. Barate et al., Eur. Phys. J., **C4** (1998) 433
- [14] D. Buskulic et al., Aleph Coll., Z. Phys. **C71** (1996) 179; F. Ragusa, for the Aleph Coll., talk at the LEPC Meeting, November 19, 1996
- [15] H. Dreiner, S. Lola and P. Morawitz, Phys. Lett. **B389** (1996) 62
- [16] D. Choudhury and D. P. Roy, Phys. Rev. **D54** (1996) 6797; D. K. Ghosh, R. M. Godbole and S. Raychaudhuri, Z. Phys. **C 75** (1997) 357
- [17] P. Chankowski, D. Choudhuri and S. Pokorski, Phys. Lett. **B389** (1996) 677
- [18] A. K. Grant, R. D. Peccei, T. Veletto and K. Wang, Phys. Lett. **B379** (1996) 272
- [19] G. R. Farrar, Phys. Rev. Lett. **76** (1996) 4115
- [20] M. Carena, G. F. Giudice, S. Lola, C. E. M. Wagner, Phys. Lett. **B395** (1997) 225
- [21] V. Barger, W.-Y. Keung and R. J. N. Phillips, Phys. Lett. **B364** (1995) 27
- [22] R. Barate et al., (Aleph Coll.) Phys. Lett. **B420** (1998) 196; K. Ackerstaff et al., (Opal Coll.) Phys. Lett. **B429** (1998) 399
- [23] J. Butterworth and H. Dreiner, Nucl. Phys. **B397** (1993) 3
- [24] E. Perez, Y. Sirois and H. Dreiner, hep-ph/9703444
- [25] H1 Coll., S. Aid et al, Z.Phys. **C71**, 211 (1996)
- [26] G. Bhattacharyya, Invited talk presented at 'Beyond the Desert', Castle Ringberg, Tegemsee, Germany, 8-14 June 1997; Susy '96, Nucl. Phys. B (Proc. Suppl.) **52A** (1997) 83

- [27] S. Dimopoulos, R. Esmailzadeh, L.J. Hall, J. Merlo and G.D. Starkman, Phys. Rev. **D41** (1990) 2099
- [28] A. Datta, J. M. Yang, B.-L. Young and X. Zhang, Phys. Rev **D 56** (1997) 3107
- [29] R. J. Oakes, K. Whisnant, J. M. Yang, B.-L. Young and X. Zhang, Phys. Rev. **D 57** (1998) 534
- [30] J. Erler, J.L. Feng and N. Polonsky, Phys. Rev. Lett. **78** (1997) 3063
- [31] J. Kalinowski, R. R ueckl, H. Spiesberger and P.M. Zerwas, Phys. Lett. **B406** (1997) 314
- [32] J. Kalinowski, R. R ueckl, H. Spiesberger and P.M. Zerwas, Phys. Lett. **B414** (1997) 297
- [33] J. Breitweg and al, Zeus Coll., DESY 97-025 and Z. Phys. **C74** (1997) 207
- [34] C. Adloff and al, H1 Coll., DESY 97-024 and Z. Phys. **C74** (1997) 191
- [35] D. Choudhury and S. Raychaudhuri, Phys.Lett. **B401**, 54 (1997); G. Altarelli, J. Ellis, G. F. Giudice, S. Lola, M. L. Mangano, Nucl.Phys. **B506**, 3 (1997); H. Dreiner and P. Morawitz, Nucl.Phys. **B503**, 55 (1997); J. Kalinowski, R. R ueckl, H. Spiesberger and P.M. Zerwas, Z.Phys. **C74**, 595 (1997); T. Kon and T. Kobayashi, Phys.Lett. **B409**, 265 (1997)
- [36] H. Murayama and M. E. Peskin, Ann. Rev. Nucl. Part. Science **46** (1996) 533
- [37] H.Dreiner and S. Lola, published in “Munich /Annecy/Hamburg 1991, Proceedings,  $e^+e^-$  collisions at 500 GeV”; “Searches for New Physics”, contribution to the LEPII workshop, 1996, hep-ph/9602207
- [38] E. Accomando et al., “Physics with  $e^+e^-$  Linear Colliders”, DESY-97-100, hep-ph/9705442
- [39] B.C. Allanach, H. Dreiner, P. Morawitz and M.D. Williams, hep-ph/9708495
- [40] SUSYGEN 2.2 - A Monte Carlo Event Generator for MSSM Sparticle Production at  $e^+e^-$  colliders, S. Katsanevas and P. Morawitz, IC/HEP/97-5, IFAE-UAB/97-01, LYCEN 9744, submitted to Physics Communications, location : <http://lyohp5.in2p3.fr/delphi/katsan/susygen.html>
- [41] S. Katsanevas and P. Morawitz, IC/HEP/97-5, IFAE-UAB/97-01, LYCEN 9744, submitted to Physics Communications
- [42] D. Choudhury and D. P. Roy, Phys. Lett. **B378** (1996) 153
- [43] S. Dawson, Nucl. Phys. **B261** (1985) 297
- [44] M. Drees and M. M. Nojiri, Nucl. Phys. **B369** (1992) 54
- [45] V. Barger, M. S. Berger and P. Ohmann, Phys. Rev. **D49** (1994) 4908
- [46] M. Carena, M. Olechowski, S. Pokorski and C. E. M. Wagner, Nucl. Phys. **B419** (1994) 213
- [47] Particle Data Group, R. M. Barnett et al., Phys. Rev. **D54** (1996) 1
- [48] H.E. Haber and G.L. Kane, Phys. Rep. **117** (1985) 175
- [49] J. A. Bagger, Nucl. Phys. B (Proc. Suppl.) **62** (1998) 23
- [50] V. Barger, M. S. Berger, J. F. Gunion and T. Han, MADPHY-96-939, Nucl. Phys. (Proc. Suppl.) **51A** (1996) 13; V. Barger, MADPHY-98-1038, hep-ph/9802355

- [51] B. Grinstein, J. Polchinski and M. B. Wise, Phys. Lett. **B130** (1983) 285
- [52] S. Dimopoulos, S. Thomas and J. D. Wells, Nucl. Phys. **B488** (1997) 39
- [53] K. Fujii, Susy'95, eds. I. Antoniadis and H. Videau (Editions Frontieres, Gif-sur-Yvette,1996) 123
- [54] J. L. Feng and M. J. Strassler, Phys. Rev. **D51** (1995) 4661



# Publication VI





# Single chargino production at linear colliders

G. Moreau

*Service de Physique Théorique  
CE-Saclay F-91191 Gif-sur-Yvette, Cedex France*

Linear Collider note LC-TH-2000-040, hep-ph/0009140

## Abstract

*We study the single chargino production  $e^+e^- \rightarrow \tilde{\chi}^\pm \mu^\mp$  at linear colliders which occurs through the  $\lambda_{121}$   $R$ -parity violating coupling constant. We focus on the final state containing 4 leptons and some missing energy. The largest background is supersymmetric and can be reduced using the initial beam polarization and some cuts based on the specific kinematics of the single chargino production. Assuming the highest allowed supersymmetric background, a center of mass energy of  $\sqrt{s} = 500\text{GeV}$  and a luminosity of  $\mathcal{L} = 500\text{fb}^{-1}$ , the sensitivities on the  $\lambda_{121}$  coupling constant obtained from the single chargino production study improve the low-energy experimental limit over a range of  $\Delta m_{\tilde{\nu}} \approx 500\text{GeV}$  around the sneutrino resonance, and reach values of  $\sim 10^{-4}$  at the  $\tilde{\nu}$  pole. The single chargino production also allows to reconstruct the  $\tilde{\chi}_1^\pm$ ,  $\tilde{\chi}_2^\pm$  and  $\tilde{\nu}$  masses. The initial state radiation plays a fundamental role in this study.*

# 1 Introduction

In supersymmetric theories, there is no clear theoretical argument in favor of the conservation of the so-called R-parity symmetry, either from the point of view of grand unified models, string theories or scenarios with discrete gauge symmetries [1]. The phenomenology of supersymmetry (SUSY) at futur colliders would change fundamentally if the R-parity symmetry were violated. Indeed, in such a scenario the typical missing energy signature caused by the stable nature of the Lightest Supersymmetric Particle (LSP) would be replaced by multijet or multileptonic signals, depending on what are the dominant R-parity violating ( $\mathcal{R}_p$ ) couplings. The reason is that the  $\mathcal{R}_p$  terms of the superpotential trilinear in the quarks and leptons superfields (see Eq.(1.1)) allow the LSP, whatever it is, to decay.

$$W_{\mathcal{R}_p} = \sum_{i,j,k} \left( \frac{1}{2} \lambda_{ijk} L_i L_j E_k^c + \lambda'_{ijk} L_i Q_j D_k^c + \frac{1}{2} \lambda''_{ijk} U_i^c D_j^c D_k^c \right). \quad (1.1)$$

The effects of the  $\mathcal{R}_p$  decays of the LSP on the study of SUSY particles pair production have been considered in the context of linear colliders [2] and futur hadronic colliders, namely the Tevatron (Run II) [3, 4, 5, 6] and the LHC [7].

The measure of the  $\mathcal{R}_p$  coupling constants of Eq.(1.1) could be performed via the detection of the displaced vertex associated to the decay of the LSP. The sensitivities on the  $\mathcal{R}_p$  couplings obtained through this method depend on the detector geometry and performances. Let us estimate the largest values of the  $\mathcal{R}_p$  coupling constants that can be measured via the displaced vertex analysis. We suppose that the LSP is the lightest neutralino ( $\tilde{\chi}_1^0$ ). The flight length of the LSP in the laboratory frame is then given in meters by [8],

$$c\gamma\tau \sim 3\gamma \cdot 10^{-3} m \left( \frac{\tilde{m}}{100\text{GeV}} \right)^4 \left( \frac{1\text{GeV}}{m_{LSP}} \right)^5 \left( \frac{1}{\Lambda} \right)^2, \quad (1.2)$$

where  $\Lambda = \lambda, \lambda'$  or  $\lambda''$ ,  $c$  is the light speed,  $\gamma$  the Lorentz boost factor,  $\tau$  the LSP life time,  $m_{LSP}$  the LSP mass and  $\tilde{m}$  the mass of the supersymmetric scalar particle involved in the three-body decay of the LSP. Since the displaced vertex analysis is an experimental challenge at hadronic colliders, we consider here the linear colliders. Assuming that the minimum distance between two vertex necessary to distinguish them experimentally is of order  $2 \cdot 10^{-5} m$  at linear colliders, we see from Eq.(1.2) that the  $\mathcal{R}_p$  couplings could be measured up to the values,

$$\Lambda < 1.2 \cdot 10^{-4} \gamma^{1/2} \left( \frac{\tilde{m}}{100\text{GeV}} \right)^2 \left( \frac{100\text{GeV}}{m_{LSP}} \right)^{5/2}. \quad (1.3)$$

There is a gap between these values and the low-energy experimental constraints on the  $\mathcal{R}_p$  couplings which range typically in the interval  $\Lambda < 10^{-1} - 10^{-2}$  for superpartners masses of  $100\text{GeV}$  [1, 9, 10]. However, the domain lying between these low-energy bounds and the values of Eq.(1.3) can be tested through another way : The study of the production of either Standard Model or SUSY particles involving  $\mathcal{R}_p$  couplings. Indeed, the cross sections of such productions are directly proportional to a power of the relevant  $\mathcal{R}_p$  coupling constant(s), which allows to determine the values of the  $\mathcal{R}_p$  couplings. Therefore, there exists a complementarity between the displaced vertex analysis and the study

of reactions involving  $\mathcal{R}_p$  couplings, since these two methods allow to investigate different ranges of values of the  $\mathcal{R}_p$  coupling constants.

The studies of the  $\mathcal{R}_p$  contributions to Standard Model particle productions have been performed both at leptonic [11]-[28] and hadronic [29]-[35] colliders. Those contributions generally involve two  $\mathcal{R}_p$  vertex and have thus some rates proportional to  $\Lambda^4$ . The processes involving only one  $\mathcal{R}_p$  vertex are less suppressed since the  $\mathcal{R}_p$  couplings incur stringent experimental limits [1, 9, 10]. Those reactions correspond to the single production of supersymmetric particle. Another interest of the single superpartner production is the possibility to produce SUSY particles at lower energies than through the superpartner pair production, which is the favored reaction in R-parity conserved models.

At hadronic colliders, the single superpartner production involves either  $\lambda'$  or  $\lambda''$  coupling constants [8, 29, 36, 37, 38, 39, 40, 41]. The test of the  $\lambda$  couplings via the single superpartner production can only be performed at leptonic colliders. At leptonic colliders, either gaugino (not including gluino) [12, 42, 43, 44] or slepton (charged or neutral) [44] can be singly produced in the simple  $e^+e^- \rightarrow 2 - \text{body}$  reactions. The single production of slepton has a reduced phase space, since the slepton is produced together with a  $Z$  or  $W$  gauge boson. In contrast, the  $\tilde{\chi}_1^0$  is produced together with a neutrino. Nevertheless, if the  $\tilde{\chi}_1^0$  is the LSP, as in many supersymmetric scenarios, it undergoes an  $\mathcal{R}_p$  decay which reads as  $\tilde{\chi}_1^0 \rightarrow l\bar{l}\nu$  if one assumes a dominant  $\lambda$  Yukawa coupling. Therefore, the single  $\tilde{\chi}_1^0$  production leads typically to the  $2l + \cancel{E}$  final state which has a large Standard Model background. In this paper, we focus on the single chargino production  $e^+e^- \rightarrow \tilde{\chi}^\pm l_m^\mp$ , which occurs through the  $\mathcal{R}_p$  coupling constants  $\lambda_{1m1}$  ( $m = 2$  or  $3$ ). There are several motivations. First, the single chargino production has an higher cross section than the single neutralino production [44]. Moreover, it can lead to particularly interesting multileptonic signatures due to the cascade decay initiated by the chargino.

The single gaugino productions at  $e^+e^-$  colliders have  $t$  and  $u$  channels and can also receive a contribution from the resonant sneutrino production. At  $\sqrt{s} = 200\text{GeV}$ , the off-resonance rates of the single chargino and neutralino productions are typically of order  $100\text{fb}$  and  $10\text{fb}$ , respectively [44], for a value of the relevant  $\mathcal{R}_p$  coupling constant equal to its low-energy bound for  $m_{\tilde{e}_R} = 100\text{GeV}$  :  $\lambda_{1m1} = 0.05$  [9]. The off-pole effects of the single gaugino production are thus at the limit of observability at LEP II assuming an integrated luminosity of  $\mathcal{L} \approx 200\text{pb}^{-1}$ . At the sneutrino resonance, the single gaugino production has higher cross section values. For instance with  $\lambda_{1m1} = 0.01$ , the chargino production rate can reach  $2 \cdot 10^{-1}\text{pb}$  at the resonance [42]. This is the reason why the experimental analysis of the single gaugino production at the LEP collider [20, 21, 22, 23, 24] allows to test  $\mathcal{R}_p$  couplings values smaller than the low-energy bounds only at the sneutrino resonance  $\sqrt{s} = m_{\tilde{\nu}}$  and, due to the Initial State Radiation (ISR) effect, in a range of typically  $\sim 50\text{GeV}$  around the  $\tilde{\nu}$  pole. The sensitivities on the  $\lambda_{1m1}$  couplings obtained at LEP reach values of order  $10^{-3}$  at the sneutrino resonance.

The experimental analysis of the single gaugino production at futur linear colliders should be interesting due to the high luminosities and energies expected at these futur colliders [45, 46]. However, the single gaugino production might suffer a large SUSY background at linear colliders. Indeed, due to the high energies reached at these colliders, the pair productions of SUSY particles may have important cross sections.

In this article, we study the single chargino production via the  $\lambda_{121}$  coupling at linear colliders and we consider the final state containing 4 leptons plus some missing energy ( $\cancel{E}$ ).

We show that the SUSY background can be greatly reduced with respect to the signal. This discrimination is based on the two following points : First, the SUSY background can be suppressed by making use of the beam polarization capability of the linear colliders. Secondly, the specific kinematics of the single chargino production reaction allows to put some efficient cuts on the transverse momentum of the lepton produced together with the chargino. We find that, by consequence of this background reduction, the sensitivity on the  $\lambda_{121}$  coupling obtained at the  $\tilde{\nu}$  resonance at linear colliders for  $\sqrt{s} = 500\text{GeV}$  and  $\mathcal{L} = 500\text{fb}^{-1}$  [45] would be of order  $10^{-4}$ , namely one order of magnitude better than the results of the LEP analysis [20, 21, 22, 23, 24], assuming the largest supersymmetric background allowed by the experimental limits on the SUSY masses.

Besides, in the scenario of a single dominant  $\mathcal{R}_p$  coupling of type  $\lambda$  with  $\tilde{\chi}_1^0$  as the LSP, the experimental superpartner mass reconstruction from the SUSY particle pair production suffers an high combinatorial background both at linear colliders [2] and LHC [7]. The reason is that all the masses reconstructions are based on the  $\tilde{\chi}_1^0$  reconstruction which is degraded by the imperfect identification of the charged leptons generated in the decays of the 2 neutralinos as  $\tilde{\chi}_1^0 \rightarrow l\bar{l}\nu$ , and the presence of missing energy in the final state. In particular, the chargino mass reconstruction in the leptonic channel is difficult since the presence of an additional neutrino, coming from the decay  $\tilde{\chi}^\pm \rightarrow \tilde{\chi}^0 l\nu$ , renders the control on the missing energy more challenging. In this paper, we show that through the study of the  $4l + \cancel{E}$  final state, the specific kinematics of the single chargino production reaction at linear colliders allows to determine the  $\tilde{\chi}_{1,2}^\pm$  and  $\tilde{\nu}$  masses.

In Section 2 we define the theoretical framework. In Sections 3 and 4 we describe the signal and the several backgrounds. In Section 5, we present the sensitivity on the SUSY parameters that can be obtained in an  $e^+e^-$  machine allowing an initial beam polarization. In this last section, we also show how some information on the SUSY mass spectrum can be derived from the study of the single chargino production, and we comment on another kind of signature : the  $3l + 2jets + \cancel{E}$  final state.

## 2 Theoretical framework

We work within the Minimal Supersymmetric Standard Model (MSSM) which has the minimal particle content and the minimal gauge group  $SU(3)_C \times SU(2)_L \times U(1)_Y$ , namely the Standard Model gauge symmetry. The supersymmetric parameters defined at the electroweak scale are the Higgsino mixing parameter  $\mu$ , the ratio of the vacuum expectation values of the two Higgs doublet fields  $\tan\beta = \langle H_u \rangle / \langle H_d \rangle$  and the soft SUSY breaking parameters, namely the bino ( $\tilde{B}$ ) mass  $M_1$ , the wino ( $\tilde{W}$ ) mass  $M_2$ , the gluino ( $\tilde{g}$ ) mass  $M_3$ , the sfermion masses  $m_{\tilde{f}}$  and the trilinear Yukawa couplings  $A$ . The remaining three parameters  $m_{H_u}^2$ ,  $m_{H_d}^2$  and the soft SUSY breaking bilinear coupling  $B$  are determined through the electroweak symmetry breaking conditions, which are two necessary minimization conditions of the Higgs potential.

We assume that all phases in the soft SUSY breaking potential are equal to zero in order to eliminate all new sources of CP violation which are constrained by extremely tight experimental limits on the electron and neutron electric moments. Furthermore, to avoid any problem of Flavor Changing Neutral Currents, we take the matrices in flavor space of the sfermion masses and  $A$  couplings close to the unit matrix. In particular, for simplification reason we consider vanishing  $A$  couplings. This last assumption concerns

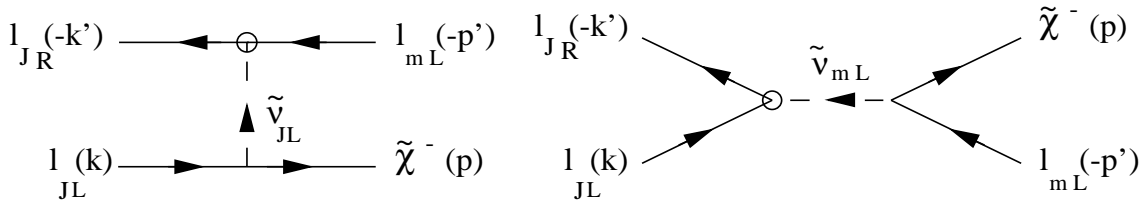


FIG. 1: Feynman diagrams of the single chargino production process at leptonic colliders. The  $\mathcal{R}_p$  coupling constant  $\lambda_{JmJ}$  ( $J = 1, m = 2$  or  $3$  for  $e^+e^-$  colliders and  $J = 2, m = 1$  or  $3$  for  $\mu^+\mu^-$  colliders) is symbolised by a small circle, and the arrows denote the flow of momentum of the corresponding particles. The Left and Right helicities of the particles are denoted by L and R, respectively, and the momentum of the particles by  $k, k', p$  and  $p'$ . The higgsino contribution as well as the charge conjugated process are not represented.

the splitting between the Left and Right sfermions masses and does not affect our analysis which depends mainly on the relative values of the sleptons, squarks and gauginos masses as we will discuss in next sections.

Besides, we suppose the R-parity symmetry to be violated so that the interactions written in the superpotential of Eq.(1.1) are present. The existence of a hierarchy among the values of the  $\mathcal{R}_p$  couplings is suggested by the analogy of those couplings with the Yukawa couplings. We thus assume a single dominant  $\mathcal{R}_p$  coupling of the type  $\lambda_{1m1}$  which allows the single chargino production at  $e^+e^-$  colliders.

Finally, we choose the LSP to be the  $\tilde{\chi}_1^0$  neutralino since it is often real in many models, such as the supergravity inspired models.

### 3 Signal

The single chargino production  $e^+e^- \rightarrow \tilde{\chi}^\pm l_m^\mp$  occurs via the  $\lambda_{1m1}$  coupling constant either through the exchange of a  $\tilde{\nu}_{mL}$  sneutrino in the  $s$  channel or a  $\tilde{\nu}_{eL}$  sneutrino in the  $t$  channel (see Fig.1). Due to the antisymmetry of the  $\lambda_{ijk}$  Yukawa couplings in the  $i$  and  $j$  indices, only a muon or a tau-lepton can be produced together with the chargino, namely  $m = 2$  or  $3$ . The produced chargino can decay into the LSP as  $\tilde{\chi}^\pm \rightarrow \tilde{\chi}_1^0 l \nu$  or as  $\tilde{\chi}^\pm \rightarrow \tilde{\chi}_1^0 u d$ . Then the LSP decays as  $\tilde{\chi}_1^0 \rightarrow \bar{e} e \nu_m, \bar{e} e \bar{\nu}_m, l_m \bar{e} \bar{\nu}_e$  or  $\bar{l}_m e \nu_e$  through  $\lambda_{1m1}$ . Each of these 4  $\tilde{\chi}_1^0$  decay channels has a branching ratio exactly equal to 25%. In this paper, we study the  $4l + \cancel{E}$  final state generated by the decay  $\tilde{\chi}^\pm \rightarrow \tilde{\chi}_1^0 l \nu$  of the produced chargino.

The single chargino production has a specific feature which is particularly attractive : Because of the simple kinematics of  $2 \rightarrow 2$  - *body* type reaction, the energy of the lepton produced with the chargino, which we write  $E(l_m)$ , is completely fixed by the center of mass energy  $\sqrt{s}$ , the lepton mass  $m_{l_m}$  and the chargino mass  $m_{\tilde{\chi}^\pm}$  :

$$E(l_m) = \frac{s + m_{l_m}^2 - m_{\tilde{\chi}^\pm}^2}{2\sqrt{s}}. \quad (3.1)$$

The lepton momentum  $P(l_m)$ , which is related to the lepton energy by  $P(l_m) = (E(l_m)^2 - m_{l_m}^2 c^4)^{1/2}/c$ , is thus also fixed. Therefore, the momentum distribution of the produced

lepton is peaked and offers the opportunity to put some cuts allowing an effective discrimination between the signal and the several backgrounds. Besides, the momentum value of the produced lepton gives the  $\tilde{\chi}^\pm$  mass through Eq.(3.1). Nevertheless, for a significant ISR effect the radiated photon carries a non negligible energy and the single chargino production must be treated as a three-body reaction of the type  $e^+e^- \rightarrow \tilde{\chi}^\pm l_m^\mp \gamma$ . Therefore, the energy of the produced lepton is not fixed anymore by the SUSY parameters. As we will show in Section 5.3, in this situation the transverse momentum of the produced lepton is more appropriate to apply some cuts and reconstruct the  $\tilde{\chi}^\pm$  mass.

In the case where the produced lepton is a tau, the momentum of the lepton ( $e^\pm$  or  $\mu^\pm$ ) coming from the  $\tau$ -decay is of course not peaked at a given value. Moreover, in contrast with the muon momentum, the precise determination of the tau-lepton momentum is difficult experimentally due to the unstable nature of the  $\tau$ . From this point of view, the case of a single dominant  $\lambda_{121}$  coupling constant is a more promising scenario than the situation in which  $\lambda_{131}$  is the dominant coupling. Hence, from now on we focus on the single dominant  $\mathcal{R}_p$  coupling  $\lambda_{121}$  and consider the single chargino production  $e^+e^- \rightarrow \tilde{\chi}^\pm \mu^\mp$ .

At this stage, an important remark can be made concerning the initial state. As can be seen from Fig.1, in the single  $\tilde{\chi}^-$  production the initial electron and positron have the same helicity, namely, they are both Left-handed. Similarly in the  $\tilde{\chi}^+$  production, the electron and the positron are both Right-handed. The incoming lepton and anti-lepton have thus in any case the same helicity. This is due to the particular structure of the trilinear  $\mathcal{R}_p$  couplings which flips the chirality of the fermion. The incoming electron and positron could also have identical helicities. However, this contribution involves the higgsino component of the chargino and is thus suppressed by the coupling of the higgsino to leptons which is proportional to  $m_l/(m_W \cos \beta)$ . This same helicity property, which is characteristic of all type of single superpartner production at leptonic colliders [44], allows to increase the single chargino production rate by selecting same helicities initial leptons.

## 4 Background

### 4.1 Non-physic background

First, one has to consider the non-physic background for the  $4l + \cancel{E}$  signature. The main source of such a background is the  $Z$ -boson pair production with ISR. Indeed, the ISR photons have an high probability to be colinear to the beam axis. They will thus often be missed experimentally becoming then a source of missing energy. The four leptons can come from the leptonic decays of the 2  $Z$ -bosons. This background can be greatly reduced by excluding the same flavor opposite-sign dileptons which have an invariant mass in the range,  $10GeV < |M_{inv}(l_p \bar{l}_p) - M_Z|$ ,  $p = 1, 2, 3$  being the generation indice. Furthermore, the missing energy coming from the ISR is mainly present at small angles with respect to the beam axis. This point can be exploited to perform a better selection of the signal. As a matter of fact, the missing energy coming from the signal has a significant transverse component since it is caused by the presence of neutrinos in the final state. In Fig.2, we present the distribution of the transverse missing energy in the  $4l + \cancel{E}$  events generated by the single  $\tilde{\chi}_1^\pm$  production for a sneutrino mass of  $m_{\tilde{\nu}} = 240GeV$  and for the point A of the SUSY parameter space defined as :  $M_1 = 200GeV$ ,  $M_2 = 250GeV$ ,  $\mu = 150GeV$ ,  $\tan \beta = 3$ ,  $m_{\tilde{l}^\pm} = 300GeV$  and  $m_{\tilde{q}} = 600GeV$  ( $m_{\tilde{\chi}_1^\pm} = 115.7GeV$ ,  $m_{\tilde{\chi}_1^0} = 101.9GeV$ ,

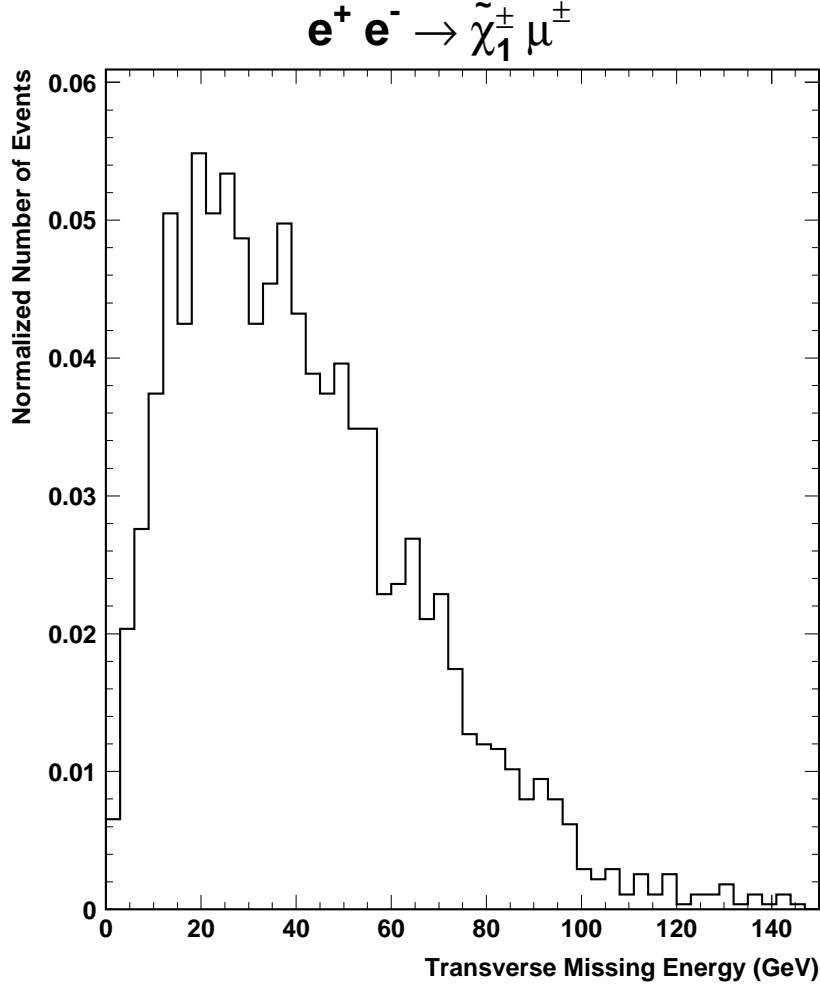


FIG. 2: Distribution of the transverse missing energy (in GeV) in the  $4l + \cancel{E}$  events generated by the single  $\tilde{\chi}_1^\pm$  production at a center of mass energy of 500 GeV and for the point A of the SUSY parameter space with  $m_{\tilde{\nu}} = 240$  GeV. The number of events has been normalized to unity.

$m_{\tilde{\chi}_2^0} = 154.5$  GeV). The cut on the lepton momentum mentioned in Section 3 can also enhance the signal-to-background ratio. Finally, the beam polarization may be useful in reducing this source of background. Indeed, the initial leptons in the  $ZZ$  production process have opposite helicities. The reason is that the  $Z - f - \bar{f}$  vertex conserves the fermion chirality. Furthermore, recall that in our signal, the initial electron and positron have similar helicities. Thus if the beam polarization at linear collider were chosen in order to favor opposite helicities initial states, the signal would be enhanced while the  $ZZ$  background would be suppressed. Since the polarization expected at linear colliders is of order 85% for the electron and 60% for the positron [45], the  $ZZ$  background would not be entirely eliminated by the beam polarization effect.

## 4.2 Standard Model background

The Standard Model backgrounds for the  $4l + \cancel{E}$  signal come from  $2 \rightarrow 3$  - *body* processes. For example, the  $e^+e^- \rightarrow Z^0 Z^0 Z^0$  reaction can give rise to the four leptons plus missing energy signature. Another source of Standard Model background is the  $e^+e^- \rightarrow Z^0 W^+ W^-$  reaction. The rates for those backgrounds have been calculated in [2] after the cuts on the charged lepton rapidity,  $|\eta(l)| < 3$ , the charged lepton transverse momentum,  $P_t(l) > 10 \text{ GeV}$ , and the missing transverse energy,  $\cancel{E}_t > 20 \text{ GeV}$ , have been applied. The results are the followings. The  $ZZZ$  production cross section does not exceed  $1 \text{ fb}$ . The  $ZWW$  production has a cross section of  $0.4 \text{ fb}$  ( $0.1 \text{ fb}$ ) at  $\sqrt{s} = 500 \text{ GeV}$  ( $350 \text{ GeV}$ ) after convoluting with the branching fractions for the leptonic decays of the gauge bosons. This rate value is obtained without the ISR effect which should reduce the cross section of the  $ZWW$  production dominated by the  $t$  channel exchange contribution [2]. As before, the  $ZWW$  production can be reduced using simultaneously the cut on the lepton momentum indicated in Section 3, the dilepton invariant mass cut and the beam polarization effect. Indeed, the initial leptons have opposite helicities in both the  $s$  and  $t$  channels of the process  $e^+e^- \rightarrow Z^0 W^+ W^-$ , as in the  $ZZ$  production process.

## 4.3 Supersymmetric background

The main sources of supersymmetric background to the  $4l + \cancel{E}$  signature are the neutralinos and sneutrinos pair productions.

First, the reaction,

$$e^+e^- \rightarrow \tilde{\chi}_1^0 + \tilde{\chi}_1^0, \quad (4.1)$$

represents a background for the  $4l + \cancel{E}$  signature since the  $\tilde{\chi}_1^0$ , which is the LSP in our framework, decays as  $\tilde{\chi}_1^0 \rightarrow \bar{e}e\nu_\mu$ ,  $\bar{e}e\bar{\nu}_\mu$ ,  $\mu\bar{e}\bar{\nu}_e$  or  $\bar{\mu}e\nu_e$  through the  $\lambda_{121}$  coupling. Therefore, the  $\tilde{\chi}_i^0 \tilde{\chi}_j^0$  productions (where  $i = 1, \dots, 4$  and  $j = 1, \dots, 4$  are not equal to 1 simultaneously) leading through cascade decays to a pair of  $\tilde{\chi}_1^0$  accompanied by some neutrinos give also rise to the final state with 4 leptons plus some missing energy. These reactions are the following,

$$e^+e^- \rightarrow \tilde{\chi}_i^0 + \tilde{\chi}_1^0 \rightarrow \tilde{\chi}_1^0 \nu_p \bar{\nu}_p + \tilde{\chi}_1^0, \quad (4.2)$$

$$e^+e^- \rightarrow \tilde{\chi}_i^0 + \tilde{\chi}_j^0 \rightarrow \tilde{\chi}_1^0 \nu_p \bar{\nu}_p + \tilde{\chi}_1^0 \nu_{p'} \bar{\nu}_{p'}, \quad (4.3)$$

where  $i, j = 2, 3, 4$  and  $p, p' = 1, 2, 3$ . Besides, the pair productions of neutralinos followed by their  $\cancel{R}_p$  decays through  $\lambda_{121}$  :

$$e^+e^- \rightarrow \tilde{\chi}_i^0 + \tilde{\chi}_1^0 \rightarrow \bar{l}l\nu + \tilde{\chi}_1^0, \quad (4.4)$$

$$e^+e^- \rightarrow \tilde{\chi}_i^0 + \tilde{\chi}_j^0 \rightarrow \bar{l}l\nu + \tilde{\chi}_1^0 \nu_p \bar{\nu}_p, \quad (4.5)$$

$$e^+e^- \rightarrow \tilde{\chi}_i^0 + \tilde{\chi}_j^0 \rightarrow \bar{l}l\nu + \bar{l}l\nu, \quad (4.6)$$

where  $i, j = 2, 3, 4$ , are also a source of background.



Secondly, the  $4l + \cancel{E}$  signature can arise in the sneutrino pair production through the reactions,

$$e^+e^- \rightarrow \tilde{\nu}_p + \tilde{\nu}_p^* \rightarrow \tilde{\chi}_i^0 \nu_p + \tilde{\chi}_j^0 \bar{\nu}_p, \quad (4.7)$$

where  $i, j = 1, \dots, 4$ , if the produced neutralinos decay as above, namely either as  $\tilde{\chi}_i^0 \rightarrow \tilde{\chi}_1^0 \nu_p \bar{\nu}_p$  (if  $i \neq 1$ ) or as  $\tilde{\chi}_i^0 \rightarrow l\bar{l}\nu$ .

The neutralinos and sneutrinos pair productions also lead to the  $4l + \cancel{E}$  final state via more complex cascade decays such as  $\tilde{\chi}_i^0 \rightarrow \tilde{\chi}_j^0 \nu_p \bar{\nu}_p \rightarrow \tilde{\chi}_1^0 \nu_{p'} \bar{\nu}_{p'} \nu_p \bar{\nu}_p$  ( $i, j = 2, 3, 4$  and  $i > j$ ) or  $\tilde{\nu} \rightarrow l^\mp \tilde{\chi}_1^\pm \rightarrow l^\mp e^\pm \nu_e \nu_\mu$  where the chargino decays through the  $\lambda_{121}$  coupling.

At the high energies available at linear colliders [45, 46], the rates of the neutralinos and sneutrinos pair productions (see Section 5.2) are typically quite larger than the cross sections of the Standard Model background reactions (see Section 4.2). We however note that in the regions of large  $\tilde{\chi}_i^0$  and  $\tilde{\nu}_p$  masses with respect to the center of mass energy  $\sqrt{s}$ , the  $\tilde{\chi}_i^0 \tilde{\chi}_j^0$  and  $\tilde{\nu}_p \tilde{\nu}_p^*$  productions cross sections, respectively, are suppressed by the phase space factor. In the kinematic domain  $2m_{\tilde{\chi}_i^0}, 2m_{\tilde{\nu}_p} > \sqrt{s} > m_{\tilde{\chi}_1^\pm} > m_{\tilde{\chi}_1^0}$  ( $i = 1, \dots, 4$  and  $p = 1, 2, 3$ ), all the neutralinos and sneutrinos pair productions are even kinematically closed while the single chargino production remains possible. In such a situation, the only background to the  $4l + \cancel{E}$  final state would be the Standard Model background so that the sensitivity on the  $\lambda_{121}$  coupling would be greatly improved. Nevertheless, the kinematic domain described above is restrictive and not particularly motivated. As a conclusion, except in some particular kinematic domains, the main background to the  $4l + \cancel{E}$  final state is supersymmetric.

In Section 5, we will focus on the largest allowed SUSY background. Indeed, the various considered domains of the SUSY parameter space will be chosen such that the  $\tilde{\chi}_1^0$  mass is around the value  $m_{\tilde{\chi}_1^0} \approx 100 \text{ GeV}$  which is close to the experimental limit  $m_{\tilde{\chi}_1^0} > 52 \text{ GeV}$  (for  $\tan \beta = 20$  and any  $\lambda_{ijk}$  coupling) [24] in order to maximize the phase space factors of the  $\tilde{\chi}_i^0 \tilde{\chi}_j^0$  productions and the decays  $\tilde{\nu}_p \rightarrow \tilde{\chi}_i^0 \nu_p$ .

The SUSY background could be suppressed by the cut on the lepton momentum mentioned in Section 3. The selection of initial leptons of same helicities would also reduce the SUSY background. Indeed, the neutralino (sneutrino) pair production occurs through the exchange of either a  $Z$ -boson in the  $s$  channel or a charged slepton (chargino) in the  $t$  channel, and the helicities of the initial electron and positron are opposite in all those channels. The  $t$  channels of the SUSY background processes allow however same helicity leptons in the initial state but this contribution entails the higgsino component of the relevant gaugino and is thus suppressed by powers of  $m_l/(m_W \cos \beta)$ .

## 5 Analysis

In this part, we determine the sensitivity on the  $\lambda_{121}$  coupling constant expected from the study of the single chargino production  $e^+e^- \rightarrow \tilde{\chi}_1^\pm \mu^\mp$  based on the analysis of the  $4l + \cancel{E}$  final state at linear colliders, assuming a center of mass energy of  $\sqrt{s} = 500 \text{ GeV}$  and a luminosity of  $\mathcal{L} = 500 \text{ fb}^{-1}$ . For this purpose, we study the SUSY background and show how it can be reduced with respect to the signal. At the end of this part, we also discuss the determination of the  $\tilde{\chi}_1^\pm$ ,  $\tilde{\chi}_2^\pm$  and  $\tilde{\nu}$  masses, the single chargino production at different center of mass energies and via other  $\mathcal{R}_p$  couplings, the  $3l + 2j + \cancel{E}$  final state and the single neutralino production.

We have simulated the signal and the supersymmetric background with the new version of the SUSYGEN event generator [47] including the beam polarization effects.

## 5.1 Polarization

The signal-to-noise ratio could be enhanced by making use of the capability of the linear colliders to polarize the initial beams.

First, as we have seen in Section 4.3 the SUSY background would be reduced if initial leptons of similar helicities were selected. Hence, we consider in this study the selection of the  $e_L^- e_L^+$  initial state, namely Left-handed initial electron and positron. In order to illustrate the effect of this polarization on the SUSY background, let us consider for example the  $\tilde{\chi}_1^0 \tilde{\chi}_2^0$  production. At the point A of the SUSY parameter space, the unpolarized cross section is  $\sigma(e^+ e^- \rightarrow \tilde{\chi}_1^0 \tilde{\chi}_2^0) = 153.99 fb$  for a center of mass energy of  $\sqrt{s} = 500 GeV$ . Selecting now the  $e_L^- e_L^+$  initial beams and assuming a value of 85% (60%) for the electron (positron) polarization, the production rate becomes  $\sigma_{polar}(e^+ e^- \rightarrow \tilde{\chi}_1^0 \tilde{\chi}_2^0) = 82.56 fb$ .

Secondly, the selection of same helicities initial leptons would increase the signal rate as mentioned in Section 3. We discuss here the effect of the considered  $e_L^- e_L^+$  beam polarization on the signal rate. As explained in Section 3, the single chargino production occurs through the process  $e_L^- e_L^+ \rightarrow \tilde{\chi}_1^- \mu^+$  (see Fig.1) or through its charge conjugated process  $e_R^- e_R^+ \rightarrow \tilde{\chi}_1^+ \mu^-$ . These charge conjugated processes have the same cross section :  $\sigma(e_L^- e_L^+ \rightarrow \tilde{\chi}_1^- \mu^+) = \sigma(e_R^- e_R^+ \rightarrow \tilde{\chi}_1^+ \mu^-)$ . The whole cross section is thus  $\sigma = [\sigma(e_L^- e_L^+ \rightarrow \tilde{\chi}_1^- \mu^+) + \sigma(e_R^- e_R^+ \rightarrow \tilde{\chi}_1^+ \mu^-)]/4 = \sigma(e_L^- e_L^+ \rightarrow \tilde{\chi}_1^- \mu^+)/2$ . The chosen beam polarization favoring Left-handed initial leptons, only the process  $e_L^- e_L^+ \rightarrow \tilde{\chi}_1^- \mu^+$  would be selected if the polarization were total. The polarized cross section would then be  $\sigma_{polar}^{total} = \sigma(e_L^- e_L^+ \rightarrow \tilde{\chi}_1^- \mu^+) = 2 \sigma$ . Hence, the signal would be increased by a factor of 2 with respect to the whole cross section. In fact, due to the limited expected efficiency of the beam polarization, the chargino production can also receive a small contribution from the process  $e_R^- e_R^+ \rightarrow \tilde{\chi}_1^+ \mu^-$ . The polarized cross section is thus replaced by  $\sigma_{polar} = \sigma_{polar}(\tilde{\chi}_1^- \mu^+) + \sigma_{polar}(\tilde{\chi}_1^+ \mu^-)$  where  $\sigma_{polar}(\tilde{\chi}_1^- \mu^+) = P(e_L^-)P(e_L^+)\sigma(e_L^- e_L^+ \rightarrow \tilde{\chi}_1^- \mu^+)$  and  $\sigma_{polar}(\tilde{\chi}_1^+ \mu^-) = P(e_R^-)P(e_R^+)\sigma(e_R^- e_R^+ \rightarrow \tilde{\chi}_1^+ \mu^-)$ ,  $P(e_L^-)$  being for example the probability to have a Left-handed initial positron. Assuming a polarization efficiency of 85% (60%) for the electron (positron) and selecting Left-handed initial leptons, the probabilities are  $P(e_L^-) = (1 + 0.85)/2 = 0.925$ ,  $P(e_L^+) = (1 + 0.60)/2 = 0.8$ ,  $P(e_R^-) = (1 - 0.85)/2 = 0.075$  and  $P(e_R^+) = (1 - 0.60)/2 = 0.2$ . Hence, the polarized cross section reads as  $\sigma_{polar} = [P(e_L^-)P(e_L^+) + P(e_R^-)P(e_R^+)]\sigma(e_L^- e_L^+ \rightarrow \tilde{\chi}_1^- \mu^+) = 0.755 \sigma(e_L^- e_L^+ \rightarrow \tilde{\chi}_1^- \mu^+) = 1.51 \sigma$ . The signal rate is thus enhanced by a factor of 1.51 with respect to the whole cross section if the  $e_L^- e_L^+$  beam polarization is applied.

## 5.2 Cross sections and branching ratios

### Signal

The single  $\tilde{\chi}_1^\pm$  chargino production has a cross section typically of order  $10 fb$  at  $\sqrt{s} = 500 GeV$  for  $\lambda_{121} = 0.05$  [44]. The single  $\tilde{\chi}_1^\pm$  production rate is reduced in the higgsino dominated region  $|\mu| \ll M_1, M_2$  where the  $\tilde{\chi}_1^\pm$  is dominated by its higgsino component, compared to the wino dominated domain  $|\mu| \gg M_1, M_2$  in which the  $\tilde{\chi}_1^\pm$  is mainly composed by the charged higgsino [44]. Besides, the single  $\tilde{\chi}_1^\pm$  production cross section

depends weakly on the sign of the  $\mu$  parameter at large values of  $\tan\beta$ . However, as  $\tan\beta$  decreases the rate increases (decreases) for  $\text{sign}(\mu) > 0$  ( $< 0$ ). This evolution of the rate with the  $\tan\beta$  and  $\text{sign}(\mu)$  parameters is explained by the evolution of the  $\tilde{\chi}_1^\pm$  mass in the SUSY parameter space [44]. Finally, when the sneutrino mass approaches the resonance ( $m_{\tilde{\nu}} = \sqrt{s}$ ) by lower values, the single  $\tilde{\chi}_1^\pm$  production cross section is considerably increased due to the ISR effect [43]. For instance, at the point A of the SUSY parameter space, the rate is equal to  $\sigma(e^+e^- \rightarrow \tilde{\chi}_1^\pm \mu^\mp) = 353.90 fb$  for a center of mass energy of  $\sqrt{s} = 500 GeV$  and a sneutrino mass of  $m_{\tilde{\nu}} = 240 GeV$ . At the resonance, the single chargino production rate reaches high values. For example at  $m_{\tilde{\nu}} = \sqrt{s} = 500 GeV$ , the cross section is  $\sigma(e^+e^- \rightarrow \tilde{\chi}_1^\pm \mu^\mp) = 30.236 pb$  for the same MSSM point A.

Since we consider the  $4l + \cancel{E}$  final state and the chargino width is neglected, the single chargino production rate must be multiplied by the branching ratio of the leptonic chargino decay  $B(\tilde{\chi}_1^\pm \rightarrow \tilde{\chi}_1^0 l_p \nu_p)$  ( $p = 1, 2, 3$ ). The leptonic decay of the chargino is typically of order 30% for  $m_{\tilde{\nu}}, m_{\tilde{l}^\pm}, m_{\tilde{q}} > m_{\tilde{\chi}_1^\pm}$ . This leptonic decay is suppressed compared to the hadronic decay  $\tilde{\chi}_1^\pm \rightarrow \tilde{\chi}_1^0 d_p u_{p'}$  ( $p = 1, 2, 3; p' = 1, 2$ ) because of the color factor. Indeed for  $m_{\tilde{\nu}}, m_{\tilde{l}^\pm}, m_{\tilde{q}} > m_{\tilde{\chi}_1^\pm}$  the hadronic decay is typically  $B(\tilde{\chi}_1^\pm \rightarrow \tilde{\chi}_1^0 d_p u_{p'}) \approx 70\%$  ( $p = 1, 2, 3; p' = 1, 2$ ). In the case where  $m_{\tilde{q}} > m_{\tilde{\chi}_1^\pm} > m_{\tilde{\nu}}, m_{\tilde{l}^\pm}$ , the decay  $\tilde{\chi}_1^\pm \rightarrow \tilde{\chi}_1^0 l_p \nu_p$  occurs through the two-body decays  $\tilde{\chi}_1^\pm \rightarrow \tilde{\nu} l^\pm$  and  $\tilde{\chi}_1^\pm \rightarrow \tilde{l}^\pm \nu$  and is thus the dominant channel. In such a scenario, the branching ratio of the  $4l + \cancel{E}$  final state for the single  $\tilde{\chi}_1^\pm$  production is close to 100%. In contrast, for  $m_{\tilde{\nu}}, m_{\tilde{l}^\pm} > m_{\tilde{\chi}_1^\pm} > m_{\tilde{q}}$ , the decay  $\tilde{\chi}_1^\pm \rightarrow \tilde{\chi}_1^0 d_p u_{p'}$  dominates, as it occurs through the two-body decay  $\tilde{\chi}_1^\pm \rightarrow \tilde{q} q'$ , and the signal is negligible. The  $\tilde{R}_p$  decays of the chargino via  $\lambda_{121}, \tilde{\chi}_1^\pm \rightarrow e^\pm \mu^\pm e^\mp, e^\pm \nu_e \nu_\mu$ , have generally negligible branching fractions due to the small values of the  $\tilde{R}_p$  coupling constants. Nevertheless, in the case of nearly degenerate  $\tilde{\chi}_1^\pm$  and  $\tilde{\chi}_1^0$  masses, those  $\tilde{R}_p$  decays can become dominant spoiling then the  $4l + \cancel{E}$  signature.

## SUSY background

In this part, we discuss the variations and the order of magnitude of the cross sections and branching ratios on which the whole SUSY background depends.

- **Neutralino pair production** The neutralinos pair productions represent a SUSY background for the present study of the R-parity violation. A detailed description of the neutralinos pair productions cross sections at linear colliders for an energy of  $\sqrt{s} = 500 GeV$  has recently been performed in [2]. In order to consider in our analysis the main variations of the neutralinos pair productions rates, we have generated all the  $\tilde{\chi}_i^0 \tilde{\chi}_j^0$  productions ( $i$  and  $j$  both varying between 1 and 4) at some points belonging to characteristic regions of the MSSM parameter space. The points chosen for the analysis respect the experimental limits derived from the LEP data on the lightest chargino and neutralino masses,  $m_{\tilde{\chi}_1^0} > 52 GeV$  ( $\tan\beta = 20$ ) and  $m_{\tilde{\chi}_1^\pm} > 94 GeV$  [24], as well as the excluded regions in the  $\mu - M_2$  plane [24]. Besides, since the neutralinos pair productions rates depend weakly on  $\tan\beta$  and  $\text{sign}(\mu)$  [2], we have fixed those SUSY parameters at  $\tan\beta = 3$  and  $\text{sign}(\mu) > 0$ .

We present now the characteristic domains of the MSSM parameter space considered in our analysis. For each of those domains, we will describe the behaviour of all the  $\tilde{\chi}_i^0 \tilde{\chi}_j^0$  productions cross sections except the  $\tilde{\chi}_i^0 \tilde{\chi}_4^0$  productions ( $i = 1, \dots, 4$ ). This is justified by the fact that at a center of mass energy of  $500 GeV$ , the dominant neutralinos productions are the  $\tilde{\chi}_1^0 \tilde{\chi}_1^0, \tilde{\chi}_1^0 \tilde{\chi}_2^0$  and  $\tilde{\chi}_2^0 \tilde{\chi}_2^0$  productions in most parts of the SUSY parameter space.

We will also discuss in each of the considered regions the values of the branching ratios  $B(\tilde{\chi}_2^0 \rightarrow \tilde{\chi}_1^0 \nu_p \bar{\nu}_p)$  and  $B(\tilde{\chi}_2^0 \rightarrow l \bar{l} \nu)$  (for  $\lambda_{121} = 0.05$ ) which determine the contribution of the  $\tilde{\chi}_1^0 \tilde{\chi}_2^0$  and  $\tilde{\chi}_2^0 \tilde{\chi}_2^0$  productions to the  $4l + \cancel{E}$  signature. The restriction of the discussion to the  $\tilde{\chi}_2^0$  decays is justified by the hierarchy mentioned above between the  $\tilde{\chi}_i^0 \tilde{\chi}_j^0$  productions rates, and by the fact that the  $\tilde{\chi}_3^0$  and  $\tilde{\chi}_4^0$  cascade decays have many possible combinations, due to the large  $\tilde{\chi}_3^0$  and  $\tilde{\chi}_4^0$  masses with respect to the  $\tilde{\chi}_1^0$  and  $\tilde{\chi}_2^0$  masses, so that the contributions of the  $\tilde{\chi}_i^0 \tilde{\chi}_j^0$  productions (with  $i$  or  $j$  equal to 3 or 4) to the  $4l + \cancel{E}$  signature are suppressed by small branching ratio factors. We will also not discuss the complex cascade decays mentioned in Section 4.3 since the associated branching ratios are typically small. However, all the  $\tilde{\chi}_i^0 \tilde{\chi}_j^0$  productions as well as all the cascade decays of the four neutralinos are taken into account in the analysis.

First, we consider the higgsino dominated region characterised by  $|\mu| \ll M_1, M_2$  where the  $\tilde{\chi}_1^0$  and  $\tilde{\chi}_2^0$  neutralinos are predominantly composed by the higgsinos. In this higgsino region, due to the weak couplings of the higgsinos to charged leptons, the  $\tilde{\chi}_1^0 \tilde{\chi}_i^0$  and  $\tilde{\chi}_2^0 \tilde{\chi}_i^0$  productions ( $i = 1, 2, 3$ ) are reduced. However, the  $\tilde{\chi}_1^0 \tilde{\chi}_2^0$  production rate reaches its larger values in this domain because of the  $Z \tilde{\chi}_i^0 \tilde{\chi}_j^0$  coupling. At  $\sqrt{s} = 500 \text{ GeV}$ , the  $\tilde{\chi}_3^0 \tilde{\chi}_3^0$  production is suppressed by a small phase space factor (when kinematically allowed). For the MSSM point A which belongs to this higgsino region, the cross sections including the beam polarization described in Section 5.1 are  $\sigma(\tilde{\chi}_1^0 \tilde{\chi}_1^0) = 0.29 \text{ fb}$ ,  $\sigma(\tilde{\chi}_1^0 \tilde{\chi}_2^0) = 82.56 \text{ fb}$ ,  $\sigma(\tilde{\chi}_2^0 \tilde{\chi}_2^0) = 0.11 \text{ fb}$ ,  $\sigma(\tilde{\chi}_1^0 \tilde{\chi}_3^0) = 6.62 \text{ fb}$ ,  $\sigma(\tilde{\chi}_2^0 \tilde{\chi}_3^0) = 6.31 \text{ fb}$ ,  $\sigma(\tilde{\chi}_3^0 \tilde{\chi}_3^0) = 13.57 \text{ fb}$ ,  $\sigma(\tilde{\chi}_1^0 \tilde{\chi}_4^0) = 1.11 \text{ fb}$  and  $\sigma(\tilde{\chi}_2^0 \tilde{\chi}_4^0) = 9.59 \text{ fb}$  for the kinematically open neutralinos productions at  $\sqrt{s} = 500 \text{ GeV}$ .

The  $\tilde{\chi}_1^0 \tilde{\chi}_2^0$  production gives rise to the  $4l + \cancel{E}$  final state if the second lightest neutralino decays as  $\tilde{\chi}_2^0 \rightarrow \tilde{\chi}_1^0 \bar{\nu}_p \nu_p$ . In the higgsino region, due to the various decay channels of the  $\tilde{\chi}_2^0$ , the branching ratio  $B(\tilde{\chi}_2^0 \rightarrow \tilde{\chi}_1^0 \bar{\nu}_p \nu_p)$  reaches values only about 15%. At the point A of the MSSM parameter space, this branching is  $B(\tilde{\chi}_2^0 \rightarrow \tilde{\chi}_1^0 \bar{\nu}_p \nu_p) = 15.8\%$  for  $m_{\tilde{\nu}} = 450 \text{ GeV}$ . For a  $\tilde{\nu}$  lighter than the  $\tilde{\chi}_2^0$ , the branching  $B(\tilde{\chi}_2^0 \rightarrow \tilde{\chi}_1^0 \bar{\nu}_p \nu_p)$  is enhanced as this decay occurs via the two-body decay  $\tilde{\chi}_2^0 \rightarrow \tilde{\nu} \nu$ . At the point A with  $m_{\tilde{\nu}} = 125 \text{ GeV}$ ,  $B(\tilde{\chi}_2^0 \rightarrow \tilde{\chi}_1^0 \bar{\nu}_p \nu_p) = 62.3\%$ .

Secondly, we consider the wino dominated region  $|\mu| \gg M_1, M_2$  where  $\tilde{\chi}_1^0$  and  $\tilde{\chi}_2^0$  are primarily bino and wino, respectively. In this wino region, the  $\tilde{\chi}_3^0 \tilde{\chi}_i^0$  productions are reduced since the  $\tilde{\chi}_3^0$  mass strongly increases with the absolute value of the parameter  $|\mu|$ . Therefore in the wino region, the main neutralinos productions are the  $\tilde{\chi}_1^0 \tilde{\chi}_1^0$ ,  $\tilde{\chi}_1^0 \tilde{\chi}_2^0$  and  $\tilde{\chi}_2^0 \tilde{\chi}_2^0$  productions. In this part of the MSSM parameter space and for  $m_{\tilde{l}^\pm} = 300 \text{ GeV}$ , the  $\tilde{\chi}_1^0 \tilde{\chi}_1^0$  production can reach  $\sim 30 \text{ fb}$ , after the beam polarization described in Section 5.1 has been applied. Moreover in this region, while the  $\tilde{\chi}_1^0 \tilde{\chi}_2^0$  production cross section is typically smaller than the  $\tilde{\chi}_1^0 \tilde{\chi}_1^0$  production rate, the  $\tilde{\chi}_2^0 \tilde{\chi}_2^0$  production cross section can reach higher values. At the point B belonging to this wino region and defined as  $M_1 = 100 \text{ GeV}$ ,  $M_2 = 200 \text{ GeV}$ ,  $\mu = 600 \text{ GeV}$ ,  $\tan \beta = 3$ ,  $m_{\tilde{l}^\pm} = 300 \text{ GeV}$  and  $m_{\tilde{q}} = 600 \text{ GeV}$  ( $m_{\tilde{\chi}_1^\pm} = 189.1 \text{ GeV}$ ,  $m_{\tilde{\chi}_1^0} = 97.3 \text{ GeV}$ ,  $m_{\tilde{\chi}_2^0} = 189.5 \text{ GeV}$ ), the cross sections (including the beam polarization described in Section 5.1) for the allowed neutralinos productions at  $\sqrt{s} = 500 \text{ GeV}$  are  $\sigma(\tilde{\chi}_1^0 \tilde{\chi}_1^0) = 32.21 \text{ fb}$ ,  $\sigma(\tilde{\chi}_1^0 \tilde{\chi}_2^0) = 25.60 \text{ fb}$  and  $\sigma(\tilde{\chi}_2^0 \tilde{\chi}_2^0) = 26.40 \text{ fb}$ .

In the wino region and for  $M_1 < M_2$ , the difference between the  $\tilde{\chi}_2^0$  and the  $\tilde{\chi}_1^0$  masses increases with  $|\mu|$  [44] and can reach high values. Thus, the decay  $\tilde{\chi}_2^0 \rightarrow \tilde{\chi}_1^0 + Z^0$  is often dominant. At the point B and with  $m_{\tilde{\nu}} = 450 \text{ GeV}$ , this channel has a branching fraction of  $B(\tilde{\chi}_2^0 \rightarrow \tilde{\chi}_1^0 Z^0) = 79.9\%$ . The decay of the  $Z$ -boson into neutrinos has a branching

fraction of  $B(Z^0 \rightarrow \nu_p \bar{\nu}_p) = 20.0\%$ . In the wino region and for  $M_1 > M_2$ , the mass difference  $m_{\tilde{\chi}_2^0} - m_{\tilde{\chi}_1^\pm}$  is larger than the  $W^\pm$  mass as long as  $M_1 - M_2$  is larger than  $\sim 75\text{GeV}$ . In this case, the dominant channel is  $\tilde{\chi}_2^0 \rightarrow \tilde{\chi}_1^\pm W^\mp$ . For  $M_1 - M_2$  smaller than  $\sim 75\text{GeV}$ ,  $m_{\tilde{\chi}_2^0} - m_{\tilde{\chi}_1^\pm}$  remains large enough to allow a dominant decay of type  $\tilde{\chi}_2^0 \rightarrow \tilde{\chi}_1^\pm f \bar{f}$ ,  $f$  being a fermion. As a conclusion, in the wino region the decay  $\tilde{\chi}_2^0 \rightarrow \tilde{\chi}_1^0 \bar{\nu}_p \nu_p$  can have a significant branching ratio for  $M_1 < M_2$ .

We also consider some intermediate domains. At the point C defined as  $M_1 = 100\text{GeV}$ ,  $M_2 = 400\text{GeV}$ ,  $\mu = 400\text{GeV}$ ,  $\tan\beta = 3$ ,  $m_{\tilde{t}^\pm} = 300\text{GeV}$  and  $m_{\tilde{q}} = 600\text{GeV}$  ( $m_{\tilde{\chi}_1^\pm} = 329.9\text{GeV}$ ,  $m_{\tilde{\chi}_1^0} = 95.5\text{GeV}$ ,  $m_{\tilde{\chi}_2^0} = 332.3\text{GeV}$ ) with  $m_{\tilde{\nu}} = 450\text{GeV}$ , the cross sections (including beam polarization) for the allowed neutralinos productions at  $\sqrt{s} = 500\text{GeV}$  are  $\sigma(\tilde{\chi}_1^0 \tilde{\chi}_1^0) = 32.18\text{fb}$ ,  $\sigma(\tilde{\chi}_1^0 \tilde{\chi}_2^0) = 6.64\text{fb}$  and  $\sigma(\tilde{\chi}_1^0 \tilde{\chi}_3^0) = 0.17\text{fb}$ , and the branching ratio of the  $\tilde{\chi}_2^0$  decay into neutrinos is  $B(\tilde{\chi}_2^0 \rightarrow \tilde{\chi}_1^0 \bar{\nu}_p \nu_p) = 0.9\%$ . The branching ratio of the decay  $\tilde{\chi}_2^0 \rightarrow \tilde{\chi}_1^0 \bar{\nu}_p \nu_p$  is small for this point C since the  $\tilde{\chi}_2^0$  mass is large which favors other  $\tilde{\chi}_2^0$  decays.

At the point D given by  $M_1 = 150\text{GeV}$ ,  $M_2 = 300\text{GeV}$ ,  $\mu = 200\text{GeV}$ ,  $\tan\beta = 3$ ,  $m_{\tilde{t}^\pm} = 300\text{GeV}$  and  $m_{\tilde{q}} = 600\text{GeV}$  ( $m_{\tilde{\chi}_1^\pm} = 165.1\text{GeV}$ ,  $m_{\tilde{\chi}_1^0} = 121.6\text{GeV}$ ,  $m_{\tilde{\chi}_2^0} = 190.8\text{GeV}$ ), the cross sections (including beam polarization) for the allowed neutralinos productions at  $\sqrt{s} = 500\text{GeV}$  are  $\sigma(\tilde{\chi}_1^0 \tilde{\chi}_1^0) = 7.80\text{fb}$ ,  $\sigma(\tilde{\chi}_1^0 \tilde{\chi}_2^0) = 13.09\text{fb}$ ,  $\sigma(\tilde{\chi}_2^0 \tilde{\chi}_2^0) = 10.08\text{fb}$ ,  $\sigma(\tilde{\chi}_1^0 \tilde{\chi}_3^0) = 35.69\text{fb}$ ,  $\sigma(\tilde{\chi}_2^0 \tilde{\chi}_3^0) = 41.98\text{fb}$ ,  $\sigma(\tilde{\chi}_3^0 \tilde{\chi}_3^0) = 0.02\text{fb}$  and  $\sigma(\tilde{\chi}_1^0 \tilde{\chi}_4^0) = 0.42\text{fb}$ . Since this point D lies in a particular region between the higgsino region and the domain of large  $|\mu|$  (or equivalently large  $m_{\tilde{\chi}_3^0}$ ), the  $\tilde{\chi}_1^0 \tilde{\chi}_3^0$  and  $\tilde{\chi}_2^0 \tilde{\chi}_3^0$  productions become relatively important. At the MSSM point D and for  $m_{\tilde{\nu}} = 450\text{GeV}$ , the branching ratio of the  $\tilde{\chi}_2^0$  decay into neutrinos is  $B(\tilde{\chi}_2^0 \rightarrow \tilde{\chi}_1^0 \bar{\nu}_p \nu_p) = 10.6\%$ .

Finally, in the domain of low charged slepton masses the  $\tilde{\chi}_i^0 \tilde{\chi}_j^0$  productions are increased due to the  $t$  channel  $\tilde{l}^\pm$  exchange contribution. At the point E, defined as the point B with a lower  $\tilde{l}^\pm$  mass, namely  $M_1 = 100\text{GeV}$ ,  $M_2 = 200\text{GeV}$ ,  $\mu = 600\text{GeV}$ ,  $\tan\beta = 3$ ,  $m_{\tilde{t}^\pm} = 150\text{GeV}$  and  $m_{\tilde{q}} = 600\text{GeV}$ , the polarized neutralinos pair productions rates which read as  $\sigma(\tilde{\chi}_1^0 \tilde{\chi}_1^0) = 67.06\text{fb}$ ,  $\sigma(\tilde{\chi}_1^0 \tilde{\chi}_2^0) = 57.15\text{fb}$  and  $\sigma(\tilde{\chi}_2^0 \tilde{\chi}_2^0) = 69.56\text{fb}$  are increased compared to the point B.

For  $m_{\tilde{\chi}_2^0} > m_{\tilde{t}^\pm}$  or  $m_{\tilde{\chi}_2^0} > m_{\tilde{q}}$ , the dominant  $\tilde{\chi}_2^0$  decays are  $\tilde{\chi}_2^0 \rightarrow \tilde{\chi}_1^0 \bar{l}_p l_p$  or  $\tilde{\chi}_2^0 \rightarrow \tilde{\chi}_1^0 \bar{q}_p q_p$ , respectively, and the decay  $\tilde{\chi}_2^0 \rightarrow \tilde{\chi}_1^0 \bar{\nu}_p \nu_p$  is typically negligible except for  $m_{\tilde{\chi}_2^0} > m_{\tilde{\nu}}$ . At the point E for  $m_{\tilde{\nu}} > m_{\tilde{\chi}_2^0}$ , the  $\tilde{\chi}_2^0$  mainly decays into  $\tilde{\chi}_1^0 \bar{l}_p l_p$  via an on shell  $\tilde{l}_p^\pm$  and the decay into neutrinos has a branching ratio of  $B(\tilde{\chi}_2^0 \rightarrow \tilde{\chi}_1^0 \bar{\nu}_p \nu_p) \sim 0\%$ . In contrast, at the point E with  $m_{\tilde{\nu}} = 160\text{GeV}$ ,  $B(\tilde{\chi}_2^0 \rightarrow \tilde{\chi}_1^0 \bar{\nu}_p \nu_p) = 32.0\%$ . Of course for  $m_{\tilde{t}^\pm}, m_{\tilde{q}} > m_{\tilde{\chi}_2^0} > m_{\tilde{\nu}}$ , the decay  $\tilde{\chi}_2^0 \rightarrow \tilde{\chi}_1^0 \bar{\nu}_p \nu_p$  is dominant.

• **Sneutrino pair production** The other source of SUSY background is the sneutrino pair production. We discuss here the main variations of this background in the SUSY parameter space. First, we note that the  $\tilde{\nu}_1$  pair production has the highest cross section among the  $\tilde{\nu}_p \tilde{\nu}_p^*$  ( $p = 1, 2, 3$  being the family index) productions since it receives a contribution from the  $t$  channel exchange of charginos. Besides, the main contribution to the  $4l + \cancel{E}$  signature from the sneutrino pair production is the reaction  $e^+ e^- \rightarrow \tilde{\nu}_p + \tilde{\nu}_p^* \rightarrow \tilde{\chi}_1^0 \nu_p + \tilde{\chi}_1^0 \bar{\nu}_p$ . Indeed, this contribution has the simplest cascade decays and furthermore the decay  $\tilde{\nu}_p \rightarrow \tilde{\chi}_1^0 \nu_p$  is favored by the phase space factor. Hence, we restrict the discussion of the  $\tilde{\nu}_p \tilde{\nu}_p^*$  background to this reaction, although all contributions from the sneutrino pair productions to the  $4l + \cancel{E}$  signature are included in our analysis.

The  $\tilde{\nu}_p$  pair production rate is reduced in the higgsino region like the  $\tilde{\chi}_1^0\tilde{\chi}_1^0$  production. For instance, at the point A with  $m_{\tilde{\nu}} = 175\text{GeV}$  the sneutrino pair production cross section including the beam polarization effect described in Section 5.1 is  $\sigma(e^+e^- \rightarrow \tilde{\chi}_1^0\nu_p\tilde{\chi}_1^0\bar{\nu}_p) = 75.26\text{fb}$  ( $1.96\text{fb}$ ) for  $p = 1$  ( $2, 3$ ), while it is  $\sigma(e^+e^- \rightarrow \tilde{\chi}_1^0\nu_p\tilde{\chi}_1^0\bar{\nu}_p) = 501.55\text{fb}$  ( $10.29\text{fb}$ ) for  $p = 1$  ( $2, 3$ ) at the point B with the same sneutrino mass. These values of the cross sections are obtained with SUSYGEN [47] and include the spin correlations effect. Besides, the  $\tilde{\nu}_p$  pair production rates strongly decrease as the sneutrino mass increases. Considering once more the point B, we find that the rate is reduced to  $\sigma(e^+e^- \rightarrow \tilde{\chi}_1^0\nu_p\tilde{\chi}_1^0\bar{\nu}_p) = 232.92\text{fb}$  ( $4.59\text{fb}$ ) for  $p = 1$  ( $2, 3$ ) if we take now  $m_{\tilde{\nu}} = 200\text{GeV}$ .

The branching ratio  $B(\tilde{\nu} \rightarrow \tilde{\chi}_1^0\nu)$  decreases as the sneutrino mass increases, since the phase space factors associated to the decays of the sneutrino into other SUSY particles than the  $\tilde{\chi}_1^0$ , like  $\tilde{\nu} \rightarrow \tilde{\chi}_1^\pm l^\mp$ , increase with  $m_{\tilde{\nu}}$ . For example, at the point B the branching ratio  $B(\tilde{\nu}_e \rightarrow \tilde{\chi}_1^0\nu_e)$  is equal to 93.4% for  $m_{\tilde{\nu}} = 175\text{GeV}$  and to 82.6% for  $m_{\tilde{\nu}} = 200\text{GeV}$ .

## 5.3 Cuts

### General selection criteria

First, we select the events without jets containing 4 charged leptons and missing energy. In order to take into account the observability of leptons at a  $500\text{GeV}$   $e^+e^-$  machine, we apply the following cuts on the transverse momentum and rapidity of all the charged leptons :  $P_t(l) > 3\text{GeV}$  and  $|\eta(l)| < 3$ . This should simulate the detector acceptance effects in a first approximation. In order to reduce the supersymmetric background, we also demand that the number of muons is at least equal to one. Since we consider the  $\tilde{\chi}_1^\pm\mu^\mp$  production, this does not affect the signal.

### Kinematics of the muon produced with the chargino

We now discuss in details the most important cut concerning the momentum of the muon which is produced together with the chargino. For a negligible ISR effect, this muon momentum is completely determined by the values of the chargino mass and the center of mass energy through Eq.(3.1), as explained in Section 3. Hence, some cuts on the muon momentum should be efficient to enhance the signal-to-noise ratio since the muon momentum distribution is perfectly peaked at a given value.

For a significant ISR effect, the energy of the photon generated via the ISR must be taken into account. Hence, the muon energy  $E(\mu)$  must be calculated through the three-body kinematics of the reaction  $e^+e^- \rightarrow \tilde{\chi}_1^\pm\mu^\mp\gamma$ . Since this kinematics depends on the angle between the muon and the photon, the muon energy  $E(\mu)$  is not completely fixed by the SUSY parameters anymore. Therefore, the distribution obtained experimentally of the muon momentum  $P(\mu) = (E(\mu)^2 - m_{\mu^\pm}^2 c^4)^{1/2}/c$  would appear as a peaked curve instead of a Dirac peak. Although the momentum of the produced muon remains a good selection criteria, we have found that in this case the transverse momentum distribution of the produced muon was more peaked, and thus more appropriate to apply some cuts. We explain the reasons why in details below.

We have thus chosen to apply cuts on the distribution of the muon transverse momentum instead of the whole muon momentum, even if for a negligible ISR effect the transverse momentum distribution is not peaked as well as the whole momentum distribution. The

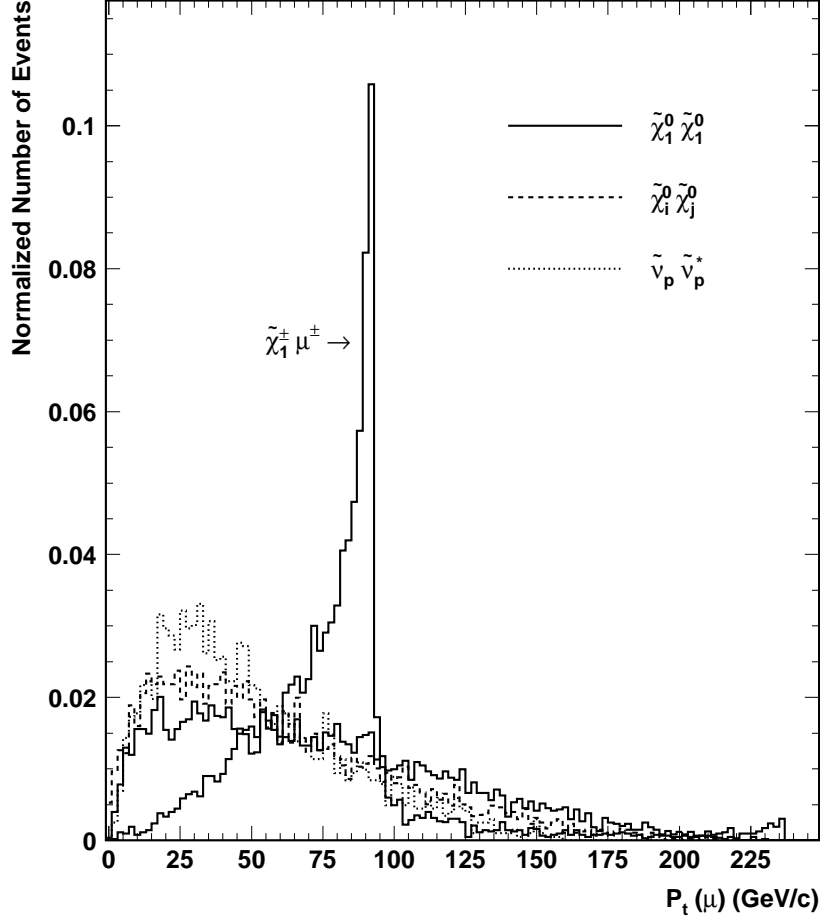


FIG. 3: Distributions of the highest muon transverse momentum  $P_t(\mu)$  (in  $\text{GeV}/c$ ) for the  $4l + \cancel{E}$  events generated by the single  $\tilde{\chi}_1^\pm$  production and the SUSY background which is divided into the  $\tilde{\chi}_1^0 \tilde{\chi}_1^0$ ,  $\tilde{\chi}_i^0 \tilde{\chi}_j^0$  and  $\tilde{\nu}_p \tilde{\nu}_p^*$  productions. The number of events for each distribution is normalized to the unity, the center of mass energy is fixed at  $500\text{GeV}$  and the point A of the SUSY parameter space is considered with  $\lambda_{121} = 0.05$  and  $m_{\tilde{\nu}} = 240\text{GeV}$ .

amplitude of the ISR effect depends on the SUSY mass spectrum as we will discuss below. The cuts on the muon transverse momentum have been applied on the muon with the highest transverse momentum which can be identified as the muon produced together with the chargino in the case of the signal. Indeed, the muon produced together with the chargino is typically more energetic than the 3 other leptons generated in the chargino cascade decay. We will come back on this point later.

In Fig.3, we show the distribution of the highest muon transverse momentum  $P_t(\mu)$  in the  $4l + \cancel{E}$  events generated by the single  $\tilde{\chi}_1^\pm$  production and the SUSY background at  $\sqrt{s} = 500\text{GeV}$  for the point A of the SUSY parameter space with  $\lambda_{121} = 0.05$  and  $m_{\tilde{\nu}} = 240\text{GeV}$ . For these SUSY parameters, the cross sections, polarized as in Section 5.1, and the branching ratios are  $\sigma(\tilde{\chi}_1^\pm \mu^\mp) = 534.39\text{fb}$ ,  $B(\tilde{\chi}_1^\pm \rightarrow \tilde{\chi}_1^0 l_p \nu_p) = 34.3\%$ ,  $\sigma(e^+e^- \rightarrow$

$\tilde{\nu}_p + \tilde{\nu}_p^* \rightarrow \tilde{\chi}_1^0 \nu_p + \tilde{\chi}_1^0 \bar{\nu}_p = 3.81 fb$  and  $B(\tilde{\chi}_2^0 \rightarrow \tilde{\chi}_1^0 \bar{\nu}_p \nu_p) = 16\%$  (see Section 5.2 for the values of  $\sigma(\tilde{\chi}_i^0 \tilde{\chi}_j^0)$ ). In Fig.3, the cuts described in Section 5.3 have not been applied and in order to perform a separate analysis for each of the main considered backgrounds, the SUSY background has been decomposed into three components : the  $\tilde{\chi}_1^0 \tilde{\chi}_1^0$ ,  $\tilde{\chi}_i^0 \tilde{\chi}_j^0$  ( $i, j = 1, \dots, 4$  with  $i$  and  $j$  not equal to 1 simultaneously) and  $\tilde{\nu}_p \tilde{\nu}_p^*$  productions. The number of  $4l + \cancel{E}$  events for each of those 3 SUSY backgrounds and the single chargino production has been normalized to the unity. Our motivation for such a normalization is that the relative amplitudes of the 3 SUSY backgrounds and the single chargino production, which depend strongly on the SUSY parameters, were discussed in detail in Sections 5.2 and 5.2, and in this section we focus on the shapes of the various distributions.

We see in the highest muon transverse momentum distribution of Fig.3 that, as expected, a characteristic peak arises for the single chargino production. Therefore, some cuts on the highest muon transverse momentum  $P_t(\mu)$  would greatly increase the signal with respect to the backgrounds. For instance, the selection criteria suggested by the Fig.3 are something like  $60 GeV \lesssim P_t(\mu) \lesssim 100 GeV$ . We can also observe in Fig.3 that the distributions of the  $\tilde{\chi}_i^0 \tilde{\chi}_j^0$  and  $\tilde{\nu}_p \tilde{\nu}_p^*$  productions are concentrated at lower transverse momentum values than the  $\tilde{\chi}_1^0 \tilde{\chi}_1^0$  distribution. This is due to the energy carried away by the neutrinos in the cascade decays of the reactions (4.2), (4.3), (4.5) and (4.7). The main variation of the highest muon transverse momentum distributions of the SUSY backgrounds with the SUSY parameters is the following : The SUSY backgrounds distributions spread to larger values of the muon transverse momentum as the  $\tilde{\chi}_1^0$  mass increases, since then the charged leptons coming from the decay  $\tilde{\chi}_1^0 \rightarrow l \bar{l} \nu$  reach higher energies.

Fig.3 shows also clearly that the peak in the transverse momentum distribution of the muon produced with the chargino exhibits an upper limit which we note  $P_t^{lim}(\mu)$ . This bound  $P_t^{lim}(\mu)$  is a kinematic limit and thus its value depends on the SUSY masses. The consequence on our analysis is that the cuts on the muon transverse momentum are modified as the SUSY mass spectrum is changing. Note that the kinematic limit of the whole muon momentum depends also on the SUSY masses, so that our choice of working with the transverse momentum remains judicious. For a better understanding of the analysis and in view of the study on the SUSY mass spectrum of Section 5.5, we now determine the value of the muon transverse momentum kinematic limit  $P_t^{lim}(\mu)$  as a function of the SUSY parameters. For this purpose we divide the discussion into 2 scenarios.

First, we consider the situation where  $m_{\tilde{\nu}_\mu} > m_{\tilde{\chi}_1^\pm} + m_{\mu^\mp}$  and  $m_{\tilde{\nu}_\mu} < \sqrt{s}$ . In this case, the dominant  $s$  channel contribution to the three-body reaction  $e^+e^- \rightarrow \tilde{\chi}_1^\pm \mu^\mp \gamma$ , where the photon is generated by the ISR, can be decomposed into two levels. First, a sneutrino is produced together with a photon in the two-body reaction  $e^+e^- \rightarrow \gamma \tilde{\nu}_\mu$  and then the sneutrino decays as  $\tilde{\nu}_\mu \rightarrow \tilde{\chi}_1^\pm \mu^\mp$ . Thus, the muon energy in the center of mass of the sneutrino  $E^*(\mu)$  (throughout this article a  $\star$  indicates that the variable is defined in the center of mass of the produced sneutrino) is equal to,

$$E^*(\mu) = \frac{m_{\tilde{\nu}_\mu}^2 + m_\mu^2 - m_{\tilde{\chi}_1^\pm}^2}{2m_{\tilde{\nu}_\mu}}. \quad (5.1)$$

The transverse momentum limit of the produced muon in the center of mass of the sneutrino  $P_t^{lim\star}(\mu)$  is given by  $P_t^{lim\star}(\mu) = (E^*(\mu)^2 - m_{\mu^\pm}^2 c^4)^{1/2}/c$  since  $P_t^*(\mu) \leq P^*(\mu)$  and  $P^*(\mu) = (E^*(\mu)^2 - m_{\mu^\pm}^2 c^4)^{1/2}/c$ . The important point is that the sneutrino rest frame is



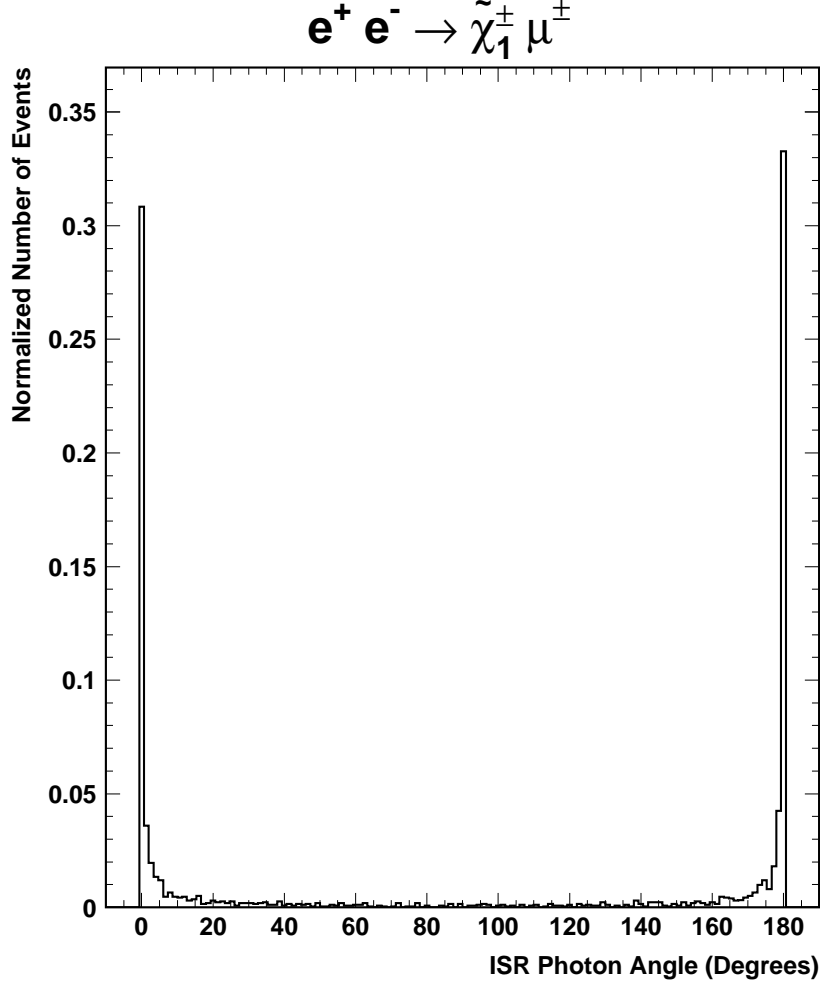


FIG. 4: Distribution of the angle (in Degrees) between the beam axis and the photon radiated from the initial state of the single  $\tilde{\chi}_1^\pm$  production process at a center of mass energy of 500GeV and for the point A of the SUSY parameter space with  $m_{\tilde{\nu}} = 240\text{GeV}$ . The number of events has been normalized to the unity.

mainly boosted in the direction of the beam axis. This is due to the fact that the produced photon is mainly radiated at small angles with respect to the initial colliding particles direction (see Fig.4). The consequence is that the transverse momentum of the produced muon is mainly the same in the sneutrino rest frame and in the laboratory frame. In conclusion, the transverse momentum limit of the produced muon in the laboratory frame is given by  $P_t^{lim}(\mu) \approx P_t^{lim*}(\mu) = (E^*(\mu)^2 - m_{\mu^\pm}^2 c^4)^{1/2}/c$ ,  $E^*(\mu)$  being calculated through Eq.(5.1). We see explicitly through Eq.(5.1) that the value of  $P_t^{lim}(\mu) \approx (E^*(\mu)^2 - m_{\mu^\pm}^2 c^4)^{1/2}/c$  increases with the sneutrino mass.

In this first situation, where  $m_{\tilde{\nu}_\mu} > m_{\tilde{\chi}_1^\pm} + m_{\mu^\mp}$  and  $m_{\tilde{\nu}_\mu} < \sqrt{s}$ , the ISR effect is large so that the single chargino production cross section is enhanced. The distributions of Fig.3 are obtained for the point A (for which  $m_{\tilde{\chi}_1^\pm} = 115.7\text{GeV}$ ) with  $m_{\tilde{\nu}_\mu} = 240\text{GeV}$  which corresponds to this situation of large ISR. The distribution of Fig.3 gives a value

for the transverse momentum kinematic limit of  $P_t^{lim}(\mu) = 92.3 GeV/c$  which is well approximately equal to  $(E^*(\mu)^2 - m_{\mu^\pm}^2 c^4)^{1/2}/c = 92.1 GeV/c$  where  $E^*(\mu)$  is calculated using Eq.(5.1).

Based on this explanation, we can now understand why for large ISR the transverse momentum of the produced muon  $P_t(\mu)$  is more peaked than its whole momentum  $P(\mu)$ : As we have discussed above, the muon transverse momentum  $P_t(\mu)$  is controlled by the two-body kinematics of the decay  $\tilde{\nu}_\mu \rightarrow \tilde{\chi}_1^\pm \mu^\mp$ . For a set of SUSY parameters, the muon transverse momentum is thus fixed if only the absolute value of the cosinus of the angle that makes the muon with the initial beam direction in the sneutrino rest frame is given. In contrast, the whole muon momentum  $P(\mu)$  is given by the three-body kinematics of the reaction  $e^+e^- \rightarrow \tilde{\chi}_1^\pm \mu^\mp \gamma$  and thus depends on the cosinus of the angle between the muon and the photon (recall that the photon is mainly emitted along the beam axis) in the laboratory frame. Therefore, the muon transverse momentum  $P_t(\mu)$  is less dependent on the muon angle than the whole muon momentum  $P(\mu)$ , leading thus to a more peaked distribution.

We consider now the scenario where  $m_{\tilde{\nu}_\mu} < m_{\tilde{\chi}_1^\pm} + m_{\mu^\mp}$  or  $m_{\tilde{\nu}_\mu} > \sqrt{s}$ . In such a situation, the kinematics is different since the sneutrino cannot be produced on shell. The single chargino production  $e^+e^- \rightarrow \tilde{\chi}_1^\pm \mu^\mp \gamma$  can thus not occur through the two-body reaction  $e^+e^- \rightarrow \gamma \tilde{\nu}_\mu$ . In fact in this situation, the energy of the radiated photon becomes negligible so that the muon energy  $E(\mu)$  is given in a good approximation by the two-body kinematics formula of Eq.(3.1). The kinematic limit of the muon transverse momentum is related to this energy through  $P_t^{lim}(\mu) = P(\mu) = (E(\mu)^2 - m_{\mu^\pm}^2 c^4)^{1/2}/c$ .

In this second scenario where  $m_{\tilde{\nu}_\mu} < m_{\tilde{\chi}_1^\pm} + m_{\mu^\mp}$  or  $m_{\tilde{\nu}_\mu} > \sqrt{s}$ , the ISR effect is negligible and the single chargino production rate is thus not increased. In Fig.5, we show the transverse momentum distribution (without the cuts of Section 5.3) of the produced muon in such a situation, namely at  $\sqrt{s} = 500 GeV$  for the point A of the SUSY parameter space with  $\lambda_{121} = 0.05$  and  $m_{\tilde{\nu}_\mu} = 550 GeV$ . For these SUSY parameters, the cross sections, polarized as in Section 5.1, and the branching ratios are  $\sigma(\tilde{\chi}_1^\pm \mu^\mp) = 91.05 fb$ ,  $B(\tilde{\chi}_1^\pm \rightarrow \tilde{\chi}_1^0 l_p \nu_p) = 33.9\%$  and  $B(\tilde{\chi}_2^0 \rightarrow \tilde{\chi}_1^0 \bar{\nu}_p \nu_p) = 15.7\%$  (see Section 5.2 for the values of  $\sigma(\tilde{\chi}_i^0 \tilde{\chi}_j^0)$ ). We check that the value of the muon transverse momentum kinematic limit  $P_t^{lim}(\mu) = 236.7 GeV/c$  obtained from the distribution of Fig.5 is well approximately equal to  $(E(\mu)^2 - m_{\mu^\pm}^2 c^4)^{1/2}/c = 236.6 GeV/c$  where  $E(\mu)$  is obtained from Eq.(3.1).

At this stage, we can make a comment on the variation of the muon transverse momentum distribution associated to the single  $\tilde{\chi}_1^\pm$  production with the value of the transverse momentum limiy  $P_t^{lim}(\mu)$ . As can be seen by comparing Fig.3 and Fig.5, this distribution is more peaked for small values of  $P_t^{lim}(\mu)$  due to an higher concentration of the distribution at low muon transverse momentum values. This effect is compensated by the fact that at low muon transverse momentum values the SUSY background is larger, as can be seen in Fig.3.

The determination of  $P_t^{lim}(\mu)$  performed in this section allows us to verify that the muon produced with the chargino is well often the muon of highest transverse momentum. Indeed, we have checked that in the two situations of large (point A with  $m_{\tilde{\nu}_\mu} = 240 GeV$ ) and negligible (point A with  $m_{\tilde{\nu}_\mu} = 550 GeV$ ) ISR effect, the calculated values of  $P_t^{lim}(\mu)$  for the produced muon were consistent with the values of  $P_t^{lim}(\mu)$  obtained with the highest muon transverse momentum distributions (Fig.3 and Fig.5). Therefore, the identification of the produced muon with the muon of highest transverse momentum is correct for

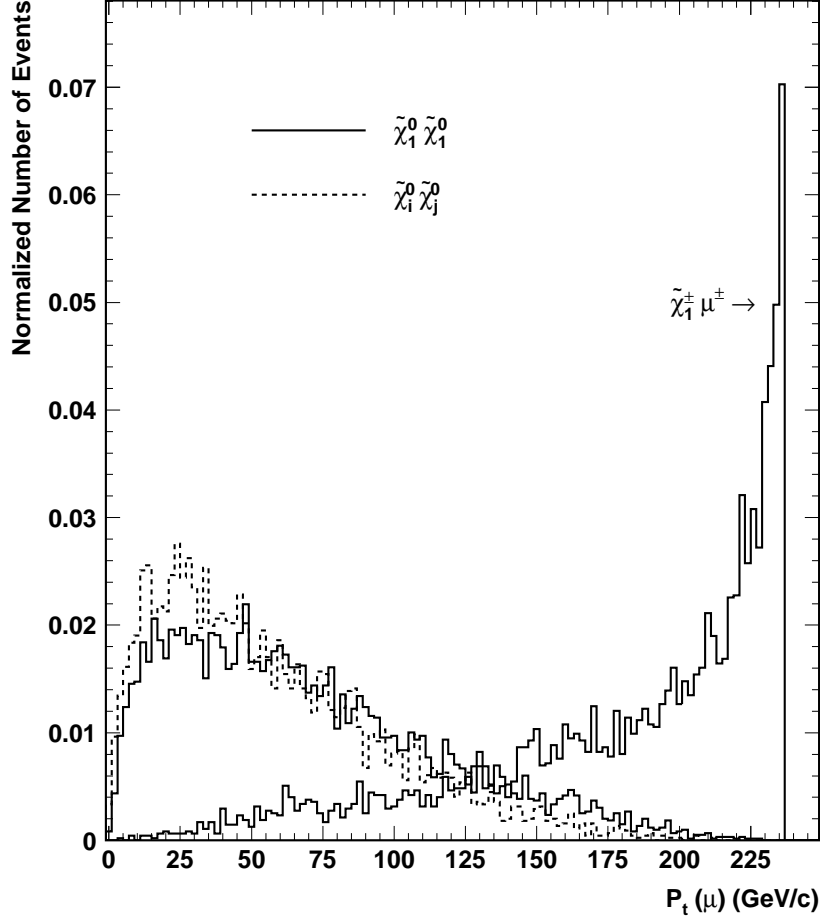


FIG. 5: Distributions of the highest muon transverse momentum  $P_t(\mu)$  (in  $\text{GeV}/c$ ) for the  $4l + \cancel{E}$  events generated by the single  $\tilde{\chi}_1^\pm$  production and the SUSY background which is divided into the  $\tilde{\chi}_1^0 \tilde{\chi}_1^0$  and  $\tilde{\chi}_i^0 \tilde{\chi}_j^0$  productions. The number of events for each distribution is normalized to the unity, the center of mass energy is fixed at  $500\text{GeV}$  and the point A of the SUSY parameter space is considered with  $\lambda_{121} = 0.05$  and  $m_{\tilde{\nu}} = 550\text{GeV}$ .

the two MSSM points considered above. The well peaked shapes of the highest muon transverse momentum distributions for the point A with  $m_{\tilde{\nu}_\mu} = 240\text{GeV}$  and  $m_{\tilde{\nu}_\mu} = 550\text{GeV}$  are another confirmation of the validity of this identification. Nevertheless, one must wonder what is the domain of validity of this identification. In particular, the transverse momentum of the produced muon can be small since  $P_t^{lim}(\mu)$  which is determined via Eq.(3.1) or Eq.(5.1) can reach low values. As a matter of fact,  $P_t^{lim}(\mu)$  can reach small values in the scenario where  $m_{\tilde{\nu}_\mu} > m_{\tilde{\chi}_1^\pm} + m_{\mu^\mp}$  and  $m_{\tilde{\nu}_\mu} < \sqrt{s}$  for  $m_{\tilde{\nu}_\mu}$  close to  $m_{\tilde{\chi}_1^\pm}$  (see Eq.(5.1)), as well as in the scenario where  $m_{\tilde{\nu}_\mu} < m_{\tilde{\chi}_1^\pm} + m_{\mu^\mp}$  or  $m_{\tilde{\nu}_\mu} > \sqrt{s}$  for  $\sqrt{s}$  close to  $m_{\tilde{\chi}_1^\pm}$  (see Eq.(3.1)). Moreover, the leptons generated in the cascade decay initiated by the  $\tilde{\chi}_1^\pm$  become more energetic, and can thus have larger transverse momentum, for either larger  $\tilde{\chi}_1^0$  masses or higher mass differences between the  $\tilde{\chi}_1^\pm$  and  $\tilde{\chi}_1^0$ . We have found that

for produced muons of small transverse momentum corresponding to  $P_t^{lim}(\mu) \approx 10\text{GeV}$  the identification remains valid for neutralino masses up to  $m_{\tilde{\chi}_1^0} \approx 750\text{GeV}$  and mass differences up to  $m_{\tilde{\chi}_1^\pm} - m_{\tilde{\chi}_1^0} \approx 750\text{GeV}$ .

## 5.4 Discovery potential

In Fig.6, we present exclusion plots at the  $5\sigma$  level in the plane  $\lambda_{121}$  versus  $m_{\tilde{\nu}_\mu}$  based on the study of the  $4l + \cancel{E}$  final state for several points of the SUSY parameter space and at a center of mass energy of  $\sqrt{s} = 500\text{GeV}$  assuming a luminosity of  $\mathcal{L} = 500\text{fb}^{-1}$  [45]. The considered signal and backgrounds are respectively the single  $\tilde{\chi}_1^\pm$  production and the pair productions of all the neutralinos and sneutrinos. The curves of Fig.6 correspond to a number of signal events larger than 10. An efficiency of 30% has been assumed for the reconstruction of the tau-lepton from its hadronic decay. The experimental LEP limit on the sneutrino mass  $m_{\tilde{\nu}} > 78\text{GeV}$  [24] has been respected. We have included the ISR effects as well as the effects of the polarization described in Section 5.1, assuming an electron (positron) polarization efficiency of 85% (60%). The cuts described in Section 5.3 have also been applied. In particular, we have applied some cuts on the transverse momentum of the produced muon. Since the value of the muon transverse momentum depends on the sneutrino and chargino masses (see Section 5.3), different cuts have been chosen which were appropriate to the different values of  $m_{\tilde{\nu}_\mu}$  and  $m_{\tilde{\chi}_1^\pm}$  considered in Fig.6.

We can observe in Fig.6 that the sensitivity on the  $\lambda_{121}$  coupling constant typically increases as the sneutrino mass approaches the resonance point  $m_{\tilde{\nu}} = \sqrt{s} = 500\text{GeV}$ . This is due to the ISR effect which increases the single chargino production rate as discussed in Section 5.2. While the ISR effect is significant in the domain where  $m_{\tilde{\nu}_\mu} > m_{\tilde{\chi}_1^\pm} + m_{\mu^\mp}$  and  $m_{\tilde{\nu}_\mu} < \sqrt{s}$ , it is small for  $m_{\tilde{\nu}_\mu} < m_{\tilde{\chi}_1^\pm} + m_{\mu^\mp}$  or  $m_{\tilde{\nu}_\mu} > \sqrt{s}$ , the reason being that in the former case the single chargino production occurs through the production of an on shell sneutrino as explained in Section 5.3. This results in a decrease of the sensitivity on the  $\lambda_{121}$  coupling at  $m_{\tilde{\nu}_\mu} \gtrsim \sqrt{s}$  and  $m_{\tilde{\nu}_\mu} \gtrsim m_{\tilde{\chi}_1^\pm}$  as illustrate the various curves of Fig.6. The decrease of the sensitivity corresponding to  $m_{\tilde{\nu}_\mu} \gtrsim m_{\tilde{\chi}_1^\pm}$  occurs at larger sneutrino masses for the point C compared to the other SUSY points, since for this set of SUSY parameters the chargino mass is larger :  $m_{\tilde{\chi}_1^\pm} = 329.9\text{GeV}$ .

For  $m_{\tilde{\nu}} < m_{\tilde{\chi}_1^\pm}$  the decay  $\tilde{\chi}_1^\pm \rightarrow \tilde{\chi}_1^0 l_p \nu_p$  becomes dominant as explained in Section 5.2. This results in an increase of the sensitivity on  $\lambda_{121}$  which can be seen for the point C between  $m_{\tilde{\nu}} \approx 330\text{GeV}$  and  $m_{\tilde{\nu}} \approx 260\text{GeV}$  and for the points B and E between  $m_{\tilde{\nu}} \approx 190\text{GeV}$  and  $m_{\tilde{\nu}} \approx 160\text{GeV}$ .

Additional comments must be made concerning the exclusion curve obtained for the point C : The decrease of sensitivity in the interval  $260\text{GeV} \gtrsim m_{\tilde{\nu}} \gtrsim 200\text{GeV}$  comes from the increase of the sneutrino pair production cross section (see Section 5.2), while the increase of sensitivity in the range  $200\text{GeV} \gtrsim m_{\tilde{\nu}} \gtrsim 160\text{GeV}$  is due to an increase of the single chargino production rate which receives in this domain an important  $t$  channel contribution. The significant sensitivity on the  $\lambda_{121}$  coupling obtained for the point C in the interval  $330\text{GeV} \gtrsim m_{\tilde{\nu}} \gtrsim 160\text{GeV}$  emphasizes the importance of the off-resonance contribution in the single chargino production study at linear colliders. For  $m_{\tilde{\nu}} > 500\text{GeV}$ , the sensitivity obtained with the point C is weak with respect to the other SUSY points due to the high chargino mass which suppresses the signal cross section.

We also see in Fig.6 that there are no important differences between the exclusion curves

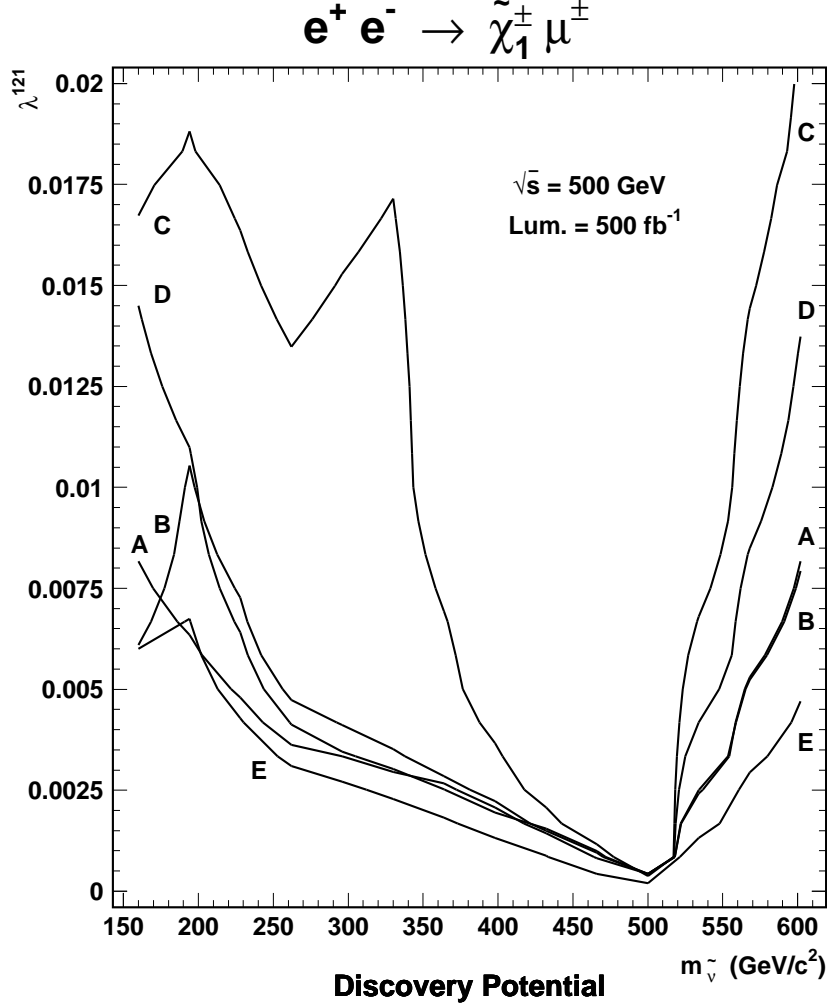


FIG. 6: Discovery potential at the  $5\sigma$  level in the plane  $\lambda_{121}$  versus  $m_{\tilde{\nu}}$  (in  $\text{GeV}/c^2$ ) for the points A, B, C, D, E of the SUSY parameter space (see text) at a center of mass energy of  $500\text{GeV}$  and assuming a luminosity of  $\mathcal{L} = 500\text{fb}^{-1}$ . The domains of the SUSY parameter space situated above the curves correspond to  $S/\sqrt{B} \geq 5$  where  $S$  is the  $4l + \cancel{E}$  signal generated by the single  $\tilde{\chi}_1^\pm$  production and  $B$  is the  $R_p$ -conserving SUSY background.

obtained for the SUSY points belonging to the higgsino region (point A), the wino region (point B) and the intermediate domain (point D). The reason is the following. The single chargino production has a cross section which decreases as going from the wino region to the higgsino region (see Section 5.2). However, this is also true for the  $\tilde{\nu}_p \tilde{\nu}_p^*$  and most of the  $\tilde{\chi}_i^0 \tilde{\chi}_j^0$  productions (see Section 5.2). Therefore, the sensitivities on the  $\lambda_{121}$  coupling obtained in the higgsino and wino region are of the same order.

Finally, we discuss the sensitivity obtained for the point E which is defined as the point B but with a smaller charged slepton mass. Although the neutralino pair production rate is larger for the point E than for the point B (see Section 5.2), the sensitivity obtained on  $\lambda_{121}$  is higher for the point E in all the considered range of sneutrino mass. This is due to the branching ratio  $B(\tilde{\chi}_1^\pm \rightarrow \tilde{\chi}_1^0 l_p \nu_p)$  which becomes important at the point E due to the

hierarchy  $m_{\tilde{\chi}_1^\pm} > m_{\tilde{l}^\pm}$  (see Section 5.2).

We mention that the sensitivity on the  $\lambda_{121}$  coupling tends to decrease as  $\tan\beta$  increases (for  $\text{sign}(\mu) > 0$ ) and is weaker for  $\text{sign}(\mu) < 0$  (with  $\tan\beta = 3$ ) due to the evolution of the single chargino production rate which was described in Section 5.2. However, the order of magnitude of the sensitivity on  $\lambda_{121}$  found in Fig.6 remains correct for either large  $\tan\beta$ , as for instance  $\tan\beta = 50$ , or negative  $\mu$ .

Let us make some concluding remarks. We see in Fig.6 that the sensitivity on the  $\lambda_{121}$  coupling reaches values typically of order  $10^{-4}$  at the sneutrino resonance. We also observe that for each SUSY point the  $5\sigma$  limit on the  $\lambda_{121}$  coupling remains more stringent than the low-energy limit at  $2\sigma$ , namely  $\lambda_{121} < 0.05$  ( $m_{\tilde{e}_R}/100\text{GeV}$ ) [9], over an interval of the sneutrino mass of  $\Delta m_{\tilde{\nu}} \approx 500\text{GeV}$  around the  $\tilde{\nu}$  pole. Therefore, the sensitivities on the SUSY parameters obtained via the single chargino production analysis at linear colliders would greatly improve the results derived from the LEP analysis (see Section 1). Besides, the range of  $\lambda_{121}$  coupling constant values investigated at linear colliders through the single chargino production analysis (see Fig.6) would be complementary to the sensitivities obtained via the displaced vertex analysis (see Eq.(1.3)).

## 5.5 SUSY mass spectrum

### Lightest chargino and sneutrino

First, the sneutrino mass can be determined through the study of the  $4l + \cancel{E}$  final state by performing a scan on the center of mass energy in order to find the value of  $\sqrt{s}$  at which hold the peak of the cross section associated to the sneutrino resonance. The accuracy on the measure of the sneutrino mass should be of order  $\delta m_{\tilde{\nu}} \sim \sigma_{\sqrt{s}}$ , where  $\sigma_{\sqrt{s}}$  is the root mean square spread in center of mass energy given in terms of the beam resolution  $R$  by [48],

$$\sigma_{\sqrt{s}} = (7\text{MeV}) \left( \frac{R}{0.01\%} \right) \left( \frac{\sqrt{s}}{100\text{GeV}} \right). \quad (5.2)$$

The values of the beam resolution at linear colliders are expected to verify  $R > 1\%$ .

Besides, the  $\tilde{\chi}_1^\pm$  mass can be deduced from the transverse momentum distribution of the muon produced with the chargino. The reason is that, as we have explained in Section 5.3, the value of the muon transverse momentum limit  $P_t^{\text{lim}}(\mu)$  is a function of the  $\tilde{\chi}_1^\pm$  and  $\tilde{\nu}$  masses. In order to discuss the experimental determination of the chargino mass, we consider separately the scenarios of negligible and significant ISR effect.

In the scenario where the ISR effect is negligible ( $m_{\tilde{\nu}_\mu} < m_{\tilde{\chi}_1^\pm} + m_{\mu^\mp}$  or  $m_{\tilde{\nu}_\mu} > \sqrt{s}$ ), the value of the muon transverse momentum limit  $P_t^{\text{lim}}(\mu)$  is equal to  $(E(\mu)^2 - m_{\mu^\pm}^2 c^4)^{1/2}/c$ ,  $E(\mu)$  being calculated in a good approximation with Eq.(3.1), as described in Section 5.3. Since Eq.(3.1) gives  $E(\mu)$  as a function of the center of mass energy and the chargino mass, the experimental value of  $P_t^{\text{lim}}(\mu)$  would allow to determine the  $\tilde{\chi}_1^\pm$  mass.

We now estimate the accuracy on the chargino mass measured through this method. In this method, the first source of error comes from the fact that to calculate the value of  $E(\mu)$  in  $P_t^{\text{lim}}(\mu) = (E(\mu)^2 - m_{\mu^\pm}^2 c^4)^{1/2}/c$ , we use the two-body kinematics formula of Eq.(3.1) so that the small ISR effect is neglected. In order to include this error, we rewrite the transverse momentum kinematic limit as  $P_t^{\text{lim}}(\mu) \pm \delta P_t^{\text{lim}}(\mu) = (E(\mu)^2 - m_{\mu^\pm}^2 c^4)^{1/2}/c$ ,  $E(\mu)$  being calculated using Eq.(3.1). By comparing the value of  $E(\mu)$  calculated with

Eq.(3.1) and the value of  $P_t^{lim}(\mu)$  obtained from the transverse momentum distribution, we have found that  $\delta P_t^{lim}(\mu) \sim 1 GeV$ . One must also take into account the experimental error on the measure of the muon transverse momentum expected at linear colliders which is given by :  $\delta P_t^{exp}(\mu)/P_t(\mu)^2 \leq 10^{-4}(GeV/c)^{-1}$  [45]. Hence, we take  $\delta P_t^{lim}(\mu) \sim 1 GeV + P_t^{lim}(\mu)^2 10^{-4}(GeV/c)^{-1}$ . The experimental error on the muon transverse momentum limit depends on the value of  $P_t^{lim}(\mu)$  itself and thus on the SUSY parameters and on the center of mass energy. However, we have found that in the single chargino production analysis at  $\sqrt{s} = 500 GeV$ , the experimental error on the muon transverse momentum limit never exceeds  $\sim 5 GeV$ . Another source of error in the measure of the  $\tilde{\chi}_1^\pm$  mass is the root mean square spread in center of mass energy  $\sigma_{\sqrt{s}}$  which is given by Eq.(5.2).

For instance, at the point A with  $m_{\tilde{\nu}} = 550 GeV$  and an energy of  $\sqrt{s} = 500 GeV$ , the muon transverse momentum distribution, which is shown in Fig.5, gives a value for the transverse momentum limit of  $P_t^{lim}(\mu) = 236.7 GeV/c$ . This value leads through Eq.(3.1) to a chargino mass of  $m_{\tilde{\chi}_1^\pm} = 115.3 \pm 29.7 GeV$  taking into account the different sources of error and assuming a beam resolution of  $R = 1\%$  at linear colliders. Here, the uncertainty on the chargino mass is important due to the large value of  $P_t^{lim}(\mu)$  which increases the error  $\delta P_t^{lim}(\mu)$ .

In the scenario where the ISR effect is important ( $m_{\tilde{\nu}_\mu} > m_{\tilde{\chi}_1^\pm} + m_{\mu^\mp}$  and  $m_{\tilde{\nu}_\mu} < \sqrt{s}$ ), the three-body kinematics of the reaction  $e^+e^- \rightarrow \tilde{\chi}_1^\pm \mu^\mp \gamma$  leaves the muon energy and thus the whole muon momentum  $P(\mu) = (E(\mu)^2 - m_{\mu^\pm}^2 c^4)^{1/2}/c$  unfixed by the SUSY parameters, since the muon energy depends also on the angle between the muon and the photon. Hence,  $P(\mu)$  cannot bring any information on the SUSY mass spectrum. In contrast, the experimental measure of the muon transverse momentum limit  $P_t^{lim}(\mu)$  would give the  $\tilde{\chi}_1^\pm$  mass as a function of the  $\tilde{\nu}_\mu$  mass since  $P_t^{lim}(\mu) \approx (E^*(\mu)^2 - m_{\mu^\pm}^2 c^4)^{1/2}/c$  (see Section 5.3) and  $E^*(\mu)$  is a function of  $m_{\tilde{\chi}_1^\pm}$  and  $m_{\tilde{\nu}_\mu}$  (see Eq.(5.1)). Assuming that the  $\tilde{\nu}_\mu$  mass has been deduced from the scan on the center of mass energy mentioned above, one could thus determine the  $\tilde{\chi}_1^\pm$  mass.

Let us evaluate the degree of precision in the measure of  $m_{\tilde{\chi}_1^\pm}$  through this calculation. First, we rewrite the transverse momentum limit as  $P_t^{lim}(\mu) \pm \delta P_t^{lim}(\mu) = (E^*(\mu)^2 - m_{\mu^\pm}^2 c^4)^{1/2}/c$  to take into account the error  $\delta P_t^{lim}(\mu)$  coming from the fact that the emission angle of the radiated photon with the beam axis is neglected (see Section 5.3). By comparing the value of  $E^*(\mu)$  calculated with Eq.(5.1) and the value of  $P_t^{lim}(\mu)$  obtained from the transverse momentum distribution, we have found that  $\delta P_t^{lim}(\mu) \sim 1 GeV$ . In order to consider the experimental error on  $P_t^{lim}(\mu)$ , we take as before  $\delta P_t^{lim}(\mu) \sim 1 GeV + P_t^{lim}(\mu)^2 10^{-4}(GeV/c)^{-1}$ . One must also take into account the error on the sneutrino mass. We assume that this mass has been preliminary determined up to an accuracy of  $\delta m_{\tilde{\nu}} \sim \sigma_{\sqrt{s}}$ .

For example, the transverse momentum distribution of Fig.3, which has been obtained for the point A with  $m_{\tilde{\nu}} = 240 GeV$  and  $\sqrt{s} = 500 GeV$ , gives a value for the transverse momentum limit of  $P_t^{lim}(\mu) = 92.3 GeV$ . The chargino mass derived from this value of  $P_t^{lim}(\mu)$  via Eq.(5.1) is  $m_{\tilde{\chi}_1^\pm} = 115.3 \pm 5.9 GeV$ , if the various uncertainties are considered and assuming that  $\sigma_{\sqrt{s}} \sim 3.5 GeV$  which corresponds to  $R = 1\%$  and  $\sqrt{s} = 500 GeV$  (see Eq.(5.2)).

Hence, the  $\tilde{\chi}_1^\pm$  mass can be determined from the study of the peak in the muon transverse momentum distribution in the two scenarios of negligible and significant ISR effect. The regions in the SUSY parameter space where a peak associated to the signal

can be observed over the SUSY background at the  $5\sigma$  level are shown in Fig.6. These domains indicate for which SUSY parameters  $P_t^{lim}(\mu)$  and thus the chargino mass can be determined, if we assume that as soon as a peak is observed in the muon transverse momentum distribution the upper kinematic limit of this peak  $P_t^{lim}(\mu)$  can be measured.

## Heaviest chargino

The single  $\tilde{\chi}_2^\pm$  production  $e^+e^- \rightarrow \tilde{\chi}_2^\pm \mu^\mp$  is also of interest at linear colliders. This reaction, when kinematically open, has a smaller phase space factor than the single  $\tilde{\chi}_1^\pm$  production. Hence, the best sensitivity on the  $\lambda_{121}$  coupling is obtained from the study of the single  $\tilde{\chi}_1^\pm$  production. However, for sufficiently large values of the  $\lambda_{121}$  coupling, the  $e^+e^- \rightarrow \tilde{\chi}_2^\pm \mu^\mp$  reaction would allow to determine either the  $\tilde{\chi}_2^\pm$  mass or a relation between the  $\tilde{\chi}_2^\pm$  and  $\tilde{\nu}$  masses. As described in Section 5.5, those informations could be derived from the upper kinematic limit  $P_t^{lim}(\mu)$  of the peak associated to the single  $\tilde{\chi}_2^\pm$  production observed in the muon transverse momentum distribution. Indeed, the method presented in the study of the single  $\tilde{\chi}_1^\pm$  production remains valid for the single  $\tilde{\chi}_2^\pm$  production analysis.

The simultaneous determination of the  $\tilde{\chi}_1^\pm$  and  $\tilde{\chi}_2^\pm$  masses is possible since the peaks in the muon transverse momentum distribution corresponding to the single  $\tilde{\chi}_1^\pm$  and  $\tilde{\chi}_2^\pm$  productions can be distinguished and identified. In order to discuss this point, we present in Fig.7 the muon transverse momentum distribution for the  $4l + \cancel{E}$  events generated by the reactions  $e^+e^- \rightarrow \tilde{\chi}_1^\pm \mu^\mp$  and  $e^+e^- \rightarrow \tilde{\chi}_2^\pm \mu^\mp$  and by the SUSY background at the MSSM point A (for which  $m_{\tilde{\chi}_1^\pm} = 115.7 GeV$  and  $m_{\tilde{\chi}_2^\pm} = 290.6 GeV$ ) with  $\lambda_{121} = 0.05$  and  $m_{\tilde{\nu}} = 450 GeV$ . The cuts described in Section 5.3 have not been applied. In this Figure, we observe that the peak associated to the single  $\tilde{\chi}_2^\pm$  production appears at smaller values of the transverse momentum than the peak caused by the single  $\tilde{\chi}_1^\pm$  production. This is due to the hierarchy of the chargino masses. Indeed, the chargino masses enter the formula of Eq.(5.1) which gives the values of  $P_t^{lim}(\mu) \approx (E^*(\mu)^2 - m_{\mu^\pm}^2 c^4)^{1/2}/c$  for the point A with  $m_{\tilde{\nu}} = 450 GeV$ . The same difference between the two peaks is observed in the scenario where the values of  $P_t^{lim}(\mu) \approx (E(\mu)^2 - m_{\mu^\pm}^2 c^4)^{1/2}/c$  are calculated using the formula of Eq.(3.1), namely for  $m_{\tilde{\nu}_\mu} < m_{\tilde{\chi}_1^\pm} + m_{\mu^\mp}$  and  $m_{\tilde{\nu}_\mu} < m_{\tilde{\chi}_2^\pm} + m_{\mu^\mp}$ , or  $m_{\tilde{\nu}_\mu} > \sqrt{s}$ . Fig.7 also illustrates the fact that the peaks associated to the single  $\tilde{\chi}_1^\pm$  and  $\tilde{\chi}_2^\pm$  productions can be easily identified thanks to their relative heights. The difference between the heights of the two peaks is due to the relative values of the cross sections and branching ratios which read for instance with the SUSY parameters of Fig.7 as (including the beam polarization described in Section 5.1) :  $\sigma(\tilde{\chi}_1^\pm \mu^\mp) = 620.09 fb$ ,  $\sigma(\tilde{\chi}_2^\pm \mu^\mp) = 605.48 fb$ ,  $B(\tilde{\chi}_1^\pm \rightarrow \tilde{\chi}_1^0 l^\pm \cancel{E}) = 33.9\%$  and  $B(\tilde{\chi}_2^\pm \rightarrow \tilde{\chi}_1^0 l^\pm \cancel{E}) = 10.8\%$ .

## 5.6 Extension of the analysis to different center of mass energies

In this section, we comment on a similar study of the reaction  $e^+e^- \rightarrow \tilde{\chi}^\pm \mu^\mp$  based on the  $4l + \cancel{E}$  events at center of mass energies different from  $\sqrt{s} = 500 GeV$ .

First, the muon transverse momentum distributions depend mainly on the relative values of the center of mass energy and of the various SUSY masses, so that the discussion on the cuts given in Section 5.3 still hold for different energies. The reconstruction of the  $\tilde{\chi}_{1,2}^\pm$  and  $\tilde{\nu}$  masses through the methods exposed in Section 5.5 is possible at any center of mass energy. We thus discuss in this section the sensitivity on the  $\lambda_{121}$  coupling that would be obtained at other center of mass energies than  $\sqrt{s} = 500 GeV$ .



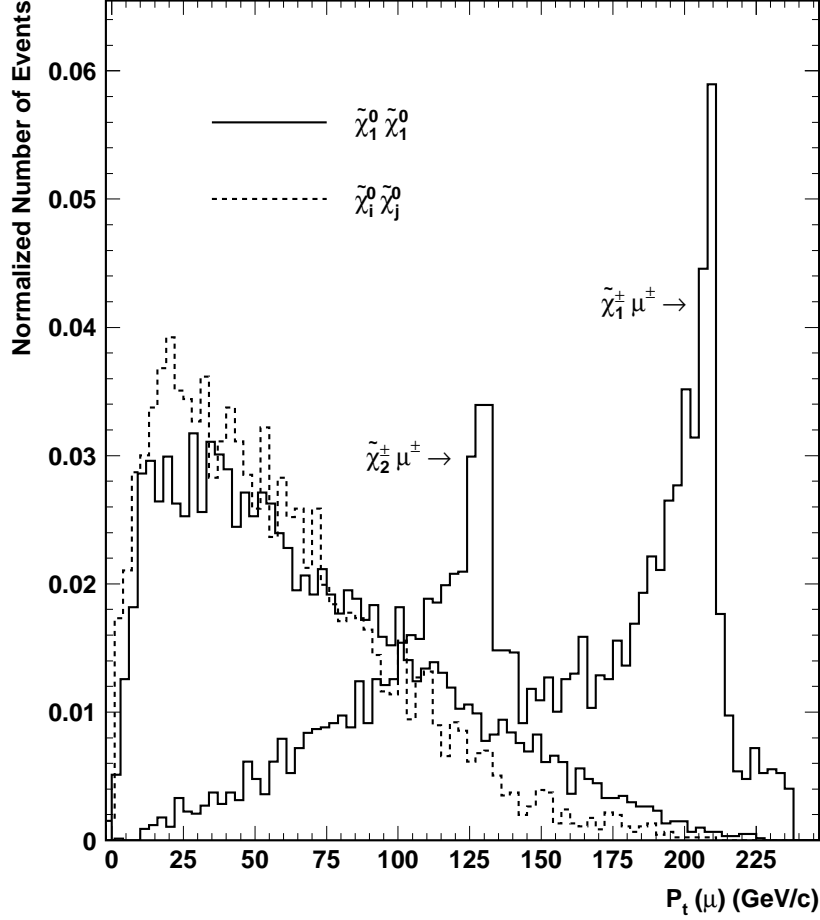


FIG. 7: Distributions of the highest muon transverse momentum  $P_t(\mu)$  (in  $\text{GeV}/c$ ) for the  $4l + \cancel{E}$  events generated by the single chargino productions ( $\tilde{\chi}_1^\pm + \tilde{\chi}_2^\pm$ ) and the SUSY background which is divided into the  $\tilde{\chi}_1^0 \tilde{\chi}_1^0$  and  $\tilde{\chi}_i^0 \tilde{\chi}_j^0$  productions. The number of events for each distribution is normalized to the unity, the center of mass energy is fixed at  $500\text{GeV}$  and the point A of the SUSY parameter space is considered with  $\lambda_{121} = 0.05$  and  $m_{\tilde{\nu}} = 450\text{GeV}$ .

Similarly, the values of the branching ratios are function of the SUSY mass spectrum, as shown in Sections 5.2 and 5.2, and thus do not change if the center of mass energy is modified.

Besides, the amplitude of the ISR effect on the signal cross section depends on the relative values of  $m_{\tilde{\nu}}$ ,  $m_{\tilde{\chi}_1^\pm}$  and  $\sqrt{s}$  (see Section 5.3). The shapes of the exclusion curves obtained at different center of mass energies would thus be similar to the shapes of the exclusion plots presented in Fig.6 for same relative values of  $m_{\tilde{\nu}}$ ,  $m_{\tilde{\chi}_1^\pm}$  and  $\sqrt{s}$ .

However, the cross sections of the SUSY backgrounds, namely the  $\tilde{\nu}_p \tilde{\nu}_p^*$  and  $\tilde{\chi}_i^0 \tilde{\chi}_j^0$  productions, depend strongly on the center of mass energy which determines the phase space factors of the superpartners pair productions.

Therefore, the sensitivity on the  $\lambda_{121}$  coupling tends to decrease (increase) at higher

(smaller) center of mass energies due to the increase (decrease) of the SUSY background rates.

## 5.7 Study based on the $3l + 2jets + \cancel{E}$ final state

In this Section, we would like to emphasize the interest of the  $3l + 2jets + \cancel{E}$  final state for the study of the reaction  $e^+e^- \rightarrow \tilde{\chi}^\pm \mu^\mp$  at linear colliders.

First, the  $3l + 2jets + \cancel{E}$  final state is generated by the decay  $\tilde{\chi}^\pm \rightarrow \tilde{\chi}_1^0 d_p u_{p'}$  which has a larger branching ratio than the decay  $\tilde{\chi}^\pm \rightarrow \tilde{\chi}_1^0 l_p \nu_p$  for the hierarchy  $m_{\tilde{\nu}}, m_{\tilde{t}^\pm}, m_{\tilde{q}} > m_{\tilde{\chi}_1^\pm}$ , as mentioned in Section 5.2.

Secondly, the Standard Model background of the  $3l + 2jets + \cancel{E}$  signature is the  $WWZ$  production. The rate of the  $3l + 2jets + \cancel{E}$  production from the  $e^+e^- \rightarrow WWZ$  reaction is  $1.5fb$  ( $0.5fb$ ) at  $\sqrt{s} = 500GeV$  ( $350GeV$ ) including the cuts  $|\eta(l)| < 3$ ,  $P_t(l) > 10GeV$  and neglecting the ISR [2]. This background can be further reduced as explained in Section 4.2. Besides, the  $3l + 2jets + \cancel{E}$  signature has no  $R_p$ -conserving SUSY background if one assumes that the LSP is the  $\tilde{\chi}_1^0$  and that the single dominant  $R_p$  coupling is  $\lambda_{121}$ . Indeed, the pair productions of SUSY particles typically lead to final states which contain at least 4 charged leptons due to the decay of the two LSP's through  $\lambda_{121}$  as  $\tilde{\chi}_1^0 \rightarrow \bar{l}l\nu$ .

Therefore, the sensitivity on the  $\lambda_{121}$  coupling obtained from the study of the single chargino production based on the  $3l + 2jets + \cancel{E}$  final state should be greatly enhanced with respect to the analysis of the  $4l + \cancel{E}$  signature.

The  $3l + 2jets + \cancel{E}$  final state is also attractive from the mass reconstruction point of view. Indeed, the full decay chain  $\tilde{\chi}_1^\pm \rightarrow \tilde{\chi}_1^0 d_p u_{p'}$ ,  $\tilde{\chi}_1^0 \rightarrow \bar{l}l\nu$  can be reconstructed. The reason is that, since the muon produced together with the chargino in the reaction  $e^+e^- \rightarrow \tilde{\chi}_1^\pm \mu^\mp$  can be identified (see Section 5.3) the origin of each particle in the final state can be known. First, the  $\tilde{\chi}_1^0$  mass can be measured with the distribution of the invariant mass of the two charged leptons coming from the  $\tilde{\chi}_1^0$  decay : The value of the  $\tilde{\chi}_1^0$  mass is readen at the upper endpoint of this distribution. Similarly, the upper endpoint of the invariant mass distribution of the two jets coming from the chargino decay gives the mass difference  $m_{\tilde{\chi}_1^\pm} - m_{\tilde{\chi}_1^0}$ . Since  $m_{\tilde{\chi}_1^0}$  has already been determined from the dilepton invariant mass, we can deduce from this mass difference the  $\tilde{\chi}_1^\pm$  mass.

Besides, the  $\tilde{\nu}$  and  $\tilde{\chi}_{1,2}^\pm$  masses can be measured as explained in Section 5.5.

Hence, in the case of a non-vanishing  $\lambda$  coupling with  $\tilde{\chi}_1^0$  as the LSP, the combinatorial background for the  $\tilde{\chi}_1^0$  mass reconstruction from the study of the single chargino production based on the  $3l + 2jets + \cancel{E}$  final state is expected to be greatly reduced with respect to the analysis based on the pair production of SUSY particles [7], due to the better identification of the charged leptons coming from the  $\tilde{\chi}_1^0$  decay. Furthermore, while the  $\tilde{\chi}_{1,2}^\pm$  and  $\tilde{\nu}$  masses reconstructions are possible via the single chargino production, these reconstructions appear to be more difficult with the pair production of SUSY particles. Indeed, the  $\tilde{\chi}^\pm$  and  $\tilde{\nu}$  masses reconstructions from the superpartner pair production are based on the  $\tilde{\chi}_1^0$  reconstruction, and moreover in the pair production the  $\tilde{\chi}^\pm$  or  $\tilde{\nu}$  decays lead to either an additional uncontrolled missing energy or an higher number of charged particles (or both) in the final state with respect to the single chargino production signature.

## 5.8 Study of the single chargino production through various $R_p$ couplings

The single chargino production at muon colliders  $\mu^+\mu^- \rightarrow \tilde{\chi}^\pm l_m^\mp$  (see Fig.1) would allow to study the  $\lambda_{2m2}$  coupling,  $m$  being equal to either 1 or 3 due to the antisymmetry of the  $\lambda_{ijk}$  couplings.

The study of the  $\lambda_{212}$  coupling would be essentially identical to the study of  $\lambda_{121}$ . Only small modifications would enter the analysis : Since an electron/positron would be produced together with the chargino, one should require that the final state contains at least one electron instead of one muon as in the  $\lambda_{121}$  case (Section 5.3). Besides, one should study the distribution of the highest electron transverse momentum instead of the highest muon transverse momentum. The particularities of the muon colliders would cause other differences in the study : First, the analysis would suffer an additional background due to the  $\mu$  decays in the detector. Secondly, large polarization would imply sacrifice in luminosity since at muon colliders this is achieved by keeping only the larger  $p_z$  muons emerging from the target [49]. Therefore, one expects an interesting sensitivity on the  $\lambda_{212}$  coupling from the single  $\tilde{\chi}_1^\pm$  production at muon colliders although this sensitivity should not be as high as in the study of the  $\lambda_{121}$  coupling at linear colliders.

Besides, the  $\mu^+\mu^- \rightarrow \tilde{\chi}^\pm e^\mp$  reaction occuring through  $\lambda_{212}$  would allow to determine the  $\tilde{\chi}_1^0$ ,  $\tilde{\chi}_1^\pm$ ,  $\tilde{\chi}_2^\pm$  and  $\tilde{\nu}$  masses as described in Sections 5.5 and 5.7 for the single chargino production at linear colliders. The main difference would be the following. The accuracy in the determination of the sneutrino mass performed through a scan over the center of mass energy would be higher at muon colliders than at linear colliders. The reason is the high beam resolution  $R$  expected at muon colliders (see Section 5.5). For instance, at muon colliders the beam resolution should reach  $R \sim 0.14\%$  for a luminosity of  $\mathcal{L} = 10fb^{-1}$  and an energy of  $\sqrt{s} = 300 - 500GeV$  [49].

The production of a single chargino together with a tau-lepton occurs through the  $\lambda_{131}$  coupling at linear colliders and via  $\lambda_{232}$  at muon coliders. Due to the  $\tau$ -decay, the transverse momentum distribution of the produced  $\tau$ -lepton cannot be obtained with a good accuracy. The strong cut on the transverse momentum described in Section 5.3 is thus difficult to apply in that case, and one must think of other discrimination variables such as the total transverse momentum of the event, the total missing energy, the rapidity, the polar angle, the isolation angle, the acoplanarity, the acollinearity or the event sphericity. Therefore, the sensitivities on the  $\lambda_{131}$  and  $\lambda_{232}$  couplings obtained from the  $\tilde{\chi}^\pm \tau^\mp$  production should be weaker than the sensitivities expected for  $\lambda_{121}$  and  $\lambda_{212}$  respectively. Furthermore, the lack of precision in the  $\tau$  transverse momentum distribution renders the reconstructions of the  $\tilde{\chi}_1^0$ ,  $\tilde{\chi}_1^\pm$  and  $\tilde{\chi}_2^\pm$  masses from the  $\tilde{\chi}^\pm \tau^\mp$  production (see Sections 5.5 and 5.7) difficult.

## 5.9 Single neutralino production

We have seen in Sections 5.3 and 5.4 that when the sneutrino mass is smaller than the lightest chargino mass (case of small ISR effect), the single chargino production cross section is greatly reduced at linear colliders. The reason is that in this situation the radiative return to the sneutrino resonance allowed by the ISR is not possible anymore. The interesting point is that for  $m_{\tilde{\chi}_1^0} < m_{\tilde{\nu}} < m_{\tilde{\chi}_1^\pm}$ , the radiative return to the sneutrino

resonance remains possible in the single  $\tilde{\chi}_1^0$  production through  $\lambda_{1m1} : e^+e^- \rightarrow \tilde{\chi}_1^0\nu_m$ . Therefore, in the region  $m_{\tilde{\chi}_1^0} < m_{\tilde{\nu}} < m_{\tilde{\chi}_1^\pm}$  the single  $\tilde{\chi}_1^0$  production has a larger rate than the single  $\tilde{\chi}_1^\pm$  production and is thus attractive to test the  $\lambda_{1m1}$  couplings.

We give now some qualitative comments on the backgrounds of the single neutralino production. If we assume that the  $\tilde{\chi}_1^0$  is the LSP, the  $\tilde{\chi}_1^0\nu_m$  production leads to the  $2l + \cancel{E}$  final state due to the  $\tilde{R}_p$  decay  $\tilde{\chi}_1^0 \rightarrow l\bar{l}\nu$ . This signature is free of  $R_p$ -conserving SUSY background since the pair production of SUSY particles produces at least 4 charged leptons due to the presence of the LSP at the end of each of the 2 cascade decays. The Standard Model background is strong as it comes from the  $WW$  and  $ZZ$  productions but it can be reduced by some kinematic cuts.

Therefore, in the region  $m_{\tilde{\chi}_1^0} < m_{\tilde{\nu}} < m_{\tilde{\chi}_1^\pm}$ , one expects an interesting sensitivity on  $\lambda_{1m1}$  from the single neutralino production study which was for instance considered in [26] for muon colliders.

The single  $\tilde{\chi}_1^0$  production allows also to reconstruct the  $\tilde{\chi}_1^0$  mass. Indeed, the neutralino mass is given by the endpoint of the distribution of the 2 leptons invariant mass in the  $2l + \cancel{E}$  final state generated by the single  $\tilde{\chi}_1^0$  production. The combinatorial background is extremely weak since the considered final state contains only 2 charged leptons.

If the sneutrino is the LSP, when it is produced at the resonance through  $\lambda_{1m1}$  as  $e^+e^- \rightarrow \tilde{\nu}_m$ , it can only decay as  $\tilde{\nu}_m \rightarrow e^+e^-$  assuming a single dominant  $\tilde{R}_p$  coupling constant. Hence, in this scenario, the sneutrino resonance must be studied through its effect on the Bhabha scattering [14, 15, 18, 19]. This conclusion also holds in the case of nearly degenerate  $\tilde{\nu}$  and  $\tilde{\chi}_1^0$  masses since then the decay  $\tilde{\nu}_m \rightarrow e^+e^-$  is dominant compared to the decay  $\tilde{\nu}_m \rightarrow \tilde{\chi}_1^0\nu_m$ .

## 6 Conclusion

The study at linear colliders of the single chargino production via the single dominant  $\lambda_{121}$  coupling  $e^+e^- \rightarrow \tilde{\chi}^\pm\mu^\mp$  is promising, due to the high luminosities and energies expected at these colliders. Assuming that the  $\tilde{\chi}_1^0$  is the LSP, the singly produced chargino has 2 main decay channels :  $\tilde{\chi}^\pm \rightarrow \tilde{\chi}_1^0 l^\pm \nu$  and  $\tilde{\chi}^\pm \rightarrow \tilde{\chi}_1^0 u d$ .

The leptonic decay of the produced chargino  $\tilde{\chi}^\pm \rightarrow \tilde{\chi}_1^0 l^\pm \nu$  (through, virtual or real, sleptons and  $W$ -boson) leads to the clean  $4l + \cancel{E}$  final state which is almost free of Standard Model background. This signature suffers a large SUSY background in some regions of the MSSM parameter space but this SUSY background can be controlled using the initial beam polarization and some cuts based on the specific kinematics of the single chargino production. Therefore, considering a luminosity of  $\mathcal{L} = 500 fb^{-1}$  at  $\sqrt{s} = 500 GeV$  and assuming the largest SUSY background, values of the  $\lambda_{121}$  coupling smaller than the present low-energy bound could be probed over a range of the sneutrino mass of  $\Delta m_{\tilde{\nu}} \approx 500 GeV$  around the sneutrino resonance and at the  $\tilde{\nu}$  pole the sensitivity on  $\lambda_{121}$  could reach values of order  $10^{-4}$ . Besides, the  $4l + \cancel{E}$  channel could allow to reconstruct the  $\tilde{\chi}_1^\pm$ ,  $\tilde{\chi}_2^\pm$  and  $\tilde{\nu}$  masses.

The hadronic decay of the produced chargino  $\tilde{\chi}^\pm \rightarrow \tilde{\chi}_1^0 u d$  (through, virtual or real, squarks and  $W$ -boson) gives rise to the  $3l + 2j + \cancel{E}$  final state. This signature, free from SUSY background, has a small Standard Model background and should thus also give a good sensitivity on the  $\lambda_{121}$  coupling constant. This hadronic channel should allow to

reconstruct the  $\tilde{\chi}_1^0$ ,  $\tilde{\chi}_1^\pm$ ,  $\tilde{\chi}_2^\pm$  and  $\tilde{\nu}$  masses.

The sensitivity on the  $\lambda_{131}$  coupling constant, obtained from the  $\tilde{\chi}^\pm \tau^\mp$  production study, is expected to be weaker than the sensitivity found on  $\lambda_{121}$  due to the decays of the tau-lepton.

## 7 Acknowledgments

The author is grateful to M. Chemtob, H.-U. Martyn and Y. Sirois for helpful discussions and having encouraged this work. It is also a pleasure to thank N. Ghodbane and M. Boonekamp for instructive conversations.

# References

- [1] H. Dreiner, published in *Perspectives on Supersymmetry*, ed. by G.L. Kane, World Scientific (1998), hep-ph/9707435.
- [2] D. K. Ghosh, R. M. Godbole, S. Raychaudhuri, hep-ph/9904233.
- [3] V. Barger et al., Phys. Rev. **D50**, 4299 (1994).
- [4] H. Baer, C. Kao and X. Tata, Phys. Rev. **D51**, 2180 (1995).
- [5] H. Baer, C.-H. Chen and X. Tata, Phys. Rev. **D55**, 1466 (1997).
- [6] B. Allanach et al., ‘Searching for R-Parity Violation at Run-II of the Tevatron’, hep-ph/9906224.
- [7] ATLAS Coll., ‘ATLAS Detector and Physics Performance Technical Design Report’, Vol. II, ATLAS TDR 15, 25 May 1999, CERN/LHCC 99-15, atlasinfo.cern.ch/Atlas-/GROUPS/PHYSICS/TDR/access.html.
- [8] H. Dreiner and G. G. Ross, Nucl. Phys. **B 365**, 597 (1991).
- [9] G. Bhattacharyya, Invited talk presented at ‘Beyond the Desert’, Castle Ringberg, Tegernsee, Germany, 8-14 June 1997; Susy ’96, Nucl. Phys. B (Proc. Suppl.) **52A** 83 (1997).
- [10] R. Barbier et al., Report of the Group on the R-parity Violation, hep-ph/9810232.
- [11] S. Dimopoulos and L.J. Hall, Phys. Lett. **B 207**, 210 (1988).
- [12] V. Barger, G. F. Giudice and T. Han, Phys. Rev. **D 40**, 2987 (1989).
- [13] D. Choudhury, Phys. Lett. **B 376**, 201 (1996).
- [14] J. Kalinowski, R. Rückl, H. Spiesberger and P. M. Zerwas, Z. Phys. **C 74**, 595 (1997).
- [15] J. Kalinowski, R. Rückl, H. Spiesberger and P. M. Zerwas, Phys. Lett. **B406**, 314 (1997).
- [16] J. Kalinowski, Talk presented at the 5th International Workshop on “*Deep Inelastic Scattering and QCD*” (DIS’97), Chicago, Illinois, USA, April 14-18, 1997, hep-ph/9706203.
- [17] J. Kalinowski, R. Rückl, H. Spiesberger and P. M. Zerwas, Phys. Lett. **B414**, 297 (1997).
- [18] J. Kalinowski, Proceedings of “*Beyond the Desert 97 – Accelerator and Non-Accelerator Approaches*”, Ringberg Castle, Germany, June 1997, hep-ph/9708490.
- [19] J. Kalinowski, Acta Phys. Polon. **B28**, 2423 (1997).
- [20] ALEPH Collaboration, submitted to ICHEP’98 (Abstract Number 949), ALEPH 98-070, CONF 039 (1998).

- [21] Y. Arnoud et al., DELPHI Collaboration, submitted to HEP'97 (Abstract Number 589), DELPHI 97-119, CONF 101 (1997).
- [22] F. Ledroit-Guillon and R. López-Fernández, DELPHI Collaboration, DELPHI 98-165, PHYS 805.
- [23] F. Ledroit-Guillon and R. López-Fernández, DELPHI Collaboration, DELPHI 99-30, CONF 229 (1999).
- [24] N. Benekos et al., DELPHI Collaboration, submitted to HEP'99 (Abstract Number 7\_209), DELPHI 99-79, CONF 266 (1999).
- [25] J. Erler, J. L. Feng and N. Polonsky, Phys. Rev. Lett. **78**, 3063 (1997).
- [26] J. L. Feng, J. F. Gunion and T. Han, Phys. Rev. **D58**, 071701 (1998); J. L. Feng, Proceedings of the Workshop on Physics at the First Muon Collider and at the Front End of a Muon Collider, Fermi National Accelerator Laboratory, 6-9 november 1997, hep-ph/9801248.
- [27] S. Bar-Shalom, G. Eilam and A. Soni, Phys. Rev. Lett. **80**, 4629 (1998).
- [28] D. Choudhury and S. Raychaudhuri, hep-ph/9807373.
- [29] S. Dimopoulos, R. Esmailzadeh, L.J. Hall, J. Merlo and G.D. Starkman, Phys. Rev. **D41**, 2099 (1990).
- [30] P. Binétruy et al., ECFA Large Hadron Collider (LHC) Workshop, Aachen, 1990, Vol. II.
- [31] D. K. Ghosh, S. Raychaudhuri and K. Sridhar, Phys. Lett. **B396**, 177 (1997).
- [32] A. Datta, J. M. Yang, B.-L. Young and X. Zhang, Phys. Rev. **D56**, 3107 (1997).
- [33] R. J. Oakes, K. Whisnant, J. M. Yang, B.-L. Young and X. Zhang, Phys. Rev. **D57**, 534 (1998).
- [34] S. Bar-Shalom, G. Eilam and A. Soni, Phys. Rev. **D59**, 055012 (1999).
- [35] J. L. Hewett and T. G. Rizzo, "Proceedings of the XXIX International Conference on High Energy Physics", Vancouver, CA, 23-29 July 1998, hep-ph/9809525.
- [36] H. Dreiner, P. Richardson and M. H. Seymour, to appear in the proceedings of the BTMSSM subgroup of the Physics at Run II Workshop on Supersymmetry/Higgs, hep-ph/9903419.
- [37] E. L. Berger, B. W. Harris and Z. Sullivan, Phys. Rev. Lett. **83**, 4472 (1999).
- [38] F. Déliot, G. Moreau, C. Royon, E. Perez and M. Chemtob, Phys. Lett. **B475**, 184 (2000).
- [39] H. Dreiner, P. Richardson and M. H. Seymour, hep-ph/0001224.
- [40] G. Moreau, E. Perez and G. Polesello, Proceedings of the Workshop '*Physics at TeV Colliders*', 8-18 June, 1999, Les Houches, France, hep-ph/0002130.
- [41] G. Moreau, E. Perez and G. Polesello, hep-ph/0003012.
- [42] H. Dreiner and S. Lola, published in "Munich-Annecy-Hamburg 1991/93, Proceedings,  $e^+e^-$  Collisions at 500 GeV : The Physics Potential ", DESY 92-123A+B, 93-123C; "Annecy-Gran Sasso-Hamburg 1995, Proceedings,  $e^+e^-$  Collisions at TeV Energies : The Physics Potential ", DESY 96-123D, ed. P. M. Zerwas; "Searches for New Physics", contribution to the LEPII Workshop, 1996, hep-ph/9602207; "Physics with  $e^+e^-$  Linear Colliders", DESY-97-100, hep-ph/9705442.

- [43] S. Lola, Presented at the 2nd ECFA/DESY study on Linear Colliders, Frascati, November 1998, LC note LC-TH-1999-021, hep-ph/9912217.
- [44] M. Chemtob and G. Moreau, Phys. Rev. **D 59**, 055003 (1999).
- [45] ‘Conceptual Design Report of a 500GeV  $e^+e^-$  Linear Collider with Integrated X-ray Laser Facility’, DESY 1997-048, ECFA 1997-182, Editors : R. Brinkmann, G. Materlik, J. Rossbach and A. Wagner, [www.desy.de/~schreibr/cdr/cdr.html](http://www.desy.de/~schreibr/cdr/cdr.html).  
See also [wwwhephy.oeaw.ac.at/susy/lcws/tdr.html](http://wwwhephy.oeaw.ac.at/susy/lcws/tdr.html).
- [46] J. A. Bagger, Nucl. Phys. (Proc. Suppl.) **B 62**, 23 (1998).
- [47] SUSYGEN 3.0/06, ‘A Monte Carlo Event generator for MSSM sparticle production for  $e^+e^-$ ,  $\mu^+\mu^-$  and  $ep$  colliders’, N. Ghodbane, S. Katsanevas, P. Morawitz and E. Perez, [lyoinfo.in2p3.fr/susygen/susygen3.html](http://lyoinfo.in2p3.fr/susygen/susygen3.html); N. Ghodbane, hep-ph/9909499.
- [48] V. Barger, ‘Physics at Muon Colliders’, Talk present at FCP97, Workshop on Fundamental Particles and Interactions, Vanderbilt University, May 1997, hep-ph/9801441.
- [49] J. F. Gunion, ‘Muon Colliders : The Machine and The Physics’, Proceedings of “*Beyond the Standard Model V*”, Balholm, Norway, May, 1997, hep-ph/9707379.







## Publication VII



# Broken R parity contributions to flavor changing rates and CP asymmetries in fermion pair production at leptonic colliders

M. Chemtob, G. Moreau

*Service de Physique Théorique  
CE-Saclay F-91191 Gif-sur-Yvette, Cedex France*

Phys. Rev. **D59** (1999) 116012, hep-ph/9806494

## Abstract

*We examine the effects of the R parity odd renormalizable interactions on flavor changing rates and CP asymmetries in the production of fermion-antifermion pairs at leptonic (electron and muon) colliders. In the reactions,  $l^- + l^+ \rightarrow f_J + \bar{f}_{J'}$ , [ $l = e, \mu$ ;  $J \neq J'$ ] the produced fermions may be leptons, down-quarks or up-quarks, and the center of mass energies may range from the Z-boson pole up to 1000 GeV. Off the Z-boson pole, the flavor changing rates are controlled by tree level amplitudes and the CP asymmetries by interference terms between tree and loop level amplitudes. At the Z-boson pole, both observables involve loop amplitudes. The lepton number violating interactions, associated with the coupling constants,  $\lambda_{ijk}$ ,  $\lambda'_{ijk}$ , are only taken into account. The consideration of loop amplitudes is restricted to the photon and Z-boson vertex corrections. We briefly review flavor violation physics at colliders. We present numerical results using a single, species and family independent, mass parameter,  $\tilde{m}$ , for all the scalar superpartners and considering simple assumptions for the family dependence of the R parity odd coupling constants. Finite non diagonal rates (CP asymmetries) entail non vanishing products of two (four) different coupling constants in different family configurations. For lepton pair production, the Z-boson decays branching ratios,  $B_{JJ'} = B(Z \rightarrow l_J^- + l_{J'}^+)$ , scale in order of magnitude as,  $B_{JJ'} \approx (\frac{\lambda}{0.1})^4 (\frac{100\text{GeV}}{\tilde{m}})^{2.5} 10^{-9}$ , with coupling constants  $\lambda = \lambda_{ijk}$  or  $\lambda'_{ijk}$  in appropriate family configurations. The corresponding results for d- and u-quarks are larger, due to an extra color factor,  $N_c = 3$ . The flavor non diagonal rates, at energies well above the Z-boson pole, slowly decrease with the center of mass energy and scale*

with the mass parameter approximately as,  $\sigma_{JJ'} \approx (\frac{\lambda}{0.1})^4 (\frac{100\text{GeV}}{\tilde{m}})^2 \sim 3(1 - 10)\text{fbarns}$ . Including the contributions from an sneutrino  $s$ -channel exchange could raise the rates for leptons or  $d$ -quarks by one order of magnitude. The  $CP$ -odd asymmetries at the  $Z$ -boson pole,  $\mathcal{A}_{JJ'} = \frac{B_{JJ'} - B_{J'J}}{B_{JJ'} + B_{J'J}}$ , vary inside the range,  $(10^{-1} - 10^{-3}) \sin \psi$ , where  $\psi$  is the  $CP$ -odd phase. At energies higher than the  $Z$ -boson pole,  $CP$ -odd asymmetries for leptons,  $d$ -quarks and  $u$ -quarks pair production lie approximately at,  $(10^{-2} - 10^{-3}) \sin \psi$ , irrespective of whether one deals with light or heavy flavors.

# 1 Introduction

An approximate R parity symmetry could greatly enhance our insight into the supersymmetric flavor problem. As is known, the dimension four R parity odd superpotential trilinear in the quarks and leptons superfields,

$$W_{R-odd} = \sum_{i,j,k} \left( \frac{1}{2} \lambda_{ijk} L_i L_j E_k^c + \lambda'_{ijk} Q_i L_j D_k^c + \frac{1}{2} \lambda''_{ijk} U_i^c D_j^c D_k^c \right), \quad (1.1)$$

adds new dimensionless couplings in the family spaces of the quarks and leptons and their superpartners. Comparing with the analogous situation for the Higgs-meson-matter Yukawa interactions, one naturally expects the set of 45 dimensionless coupling constants,  $\lambda_{ijk} = -\lambda_{jik}$ ,  $\lambda'_{ijk}$ ,  $\lambda''_{ijk} = -\lambda''_{ikj}$ , to exhibit a non-trivial hierarchical structure in the families spaces. Our goal in this work will be to examine a particular class of tests at high energy colliders by which one could access a direct information on the family structure of these coupling constants.

The R parity symmetry has inspired a vast literature since the pioneering period of the early 80's [1, 2, 3, 4, 5, 6, 7, 8] and the maturation period of the late 80's and early 90's [9, 10, 11, 12, 13, 14]. This subject is currently witnessing a renewed interest [15, 16]. As is well known, the R parity odd interactions can contribute at tree level, by exchange of the scalar superpartners, to processes which violate the baryon and lepton numbers as well as the leptons and quarks flavors. The major part of the existing experimental constraints on coupling constants is formed from the indirect bounds gathered from the low energy phenomenology. Most often, these have been derived on the basis of the so-called single coupling hypothesis, where a single one of the coupling constants is assumed to dominate over all the others, so that each of the coupling constants contributes once at a time. Apart from a few isolated cases, the typical bounds derived under this assumption, assuming a linear dependence on the superpartner masses, are of order,  $[\lambda, \lambda', \lambda''] < (10^{-1} - 10^{-2}) \frac{\tilde{m}}{100 GeV}$ .

One important variant of the single coupling hypothesis can be defined by assuming that the dominance of single operators applies at the level of the gauge (current) basis fields rather than the mass eigenstate fields, as was implicit in the above original version. This appears as a more natural assumption in models where the presumed hierarchies in coupling constants originate from physics at higher scales (gauge, flavor, or strings). Flavor changing contributions may then be induced even when a single R parity odd coupling constant is assumed to dominate [17]. While the redefined mass basis superpotential may then depend on the various unitary transformation matrices,  $V_{L,R}^{u,d}$ , [18], two distinguished predictive choices are those where the generation mixing is represented solely in terms of the CKM (Cabibbo-Kobayashi-Maskawa) matrix, with flavor changing effects appearing in either up-quarks or down-quarks flavors [17]. A similar situation holds for leptons with respect to the couplings,  $\lambda_{ijk}$ , and transformations,  $V_{L,R}^{l,\nu}$ .

A large set of constraints has also been obtained by applying an extended hypothesis of dominance of coupling constants by pairs (or more). Several analyses dealing with hadron flavor changing effects (mixing parameters for the neutral light and heavy flavored mesons, rare mesons decays such as,  $K \rightarrow \pi + \nu + \bar{\nu}$ , ...) [17]; lepton flavor changing effects (leptons decays,  $l_i^\pm \rightarrow l_k^\pm + l_n^- + l_p^+$ , [19]  $\mu^- \rightarrow e^-$  conversion processes, [20], neutrinos Majorana mass [21], ...) ; lepton number violating effects (neutrinoless double beta decay

[22, 23, 24]); or baryon number violating effects (proton decay partial branchings [25], rare non-leptonic decays of heavy mesons [26], nuclei desintegration [27],...) have led to strong bounds on a large number of quadratic products of the coupling constants. All of the above low energy works, however, suffer from one or other form of model dependence, whether they rely on the consideration of loop diagrams [25], on additional assumptions concerning the flavor mixing [17, 19, 20], or on hadronic wave functions inputs [26, 27].

Proceeding further with a linkage of R parity with physics beyond the standard model, our main observation in this work is that the R parity odd coupling constants could by themselves be an independent source of CP violation. Of course, the idea that the RPV interactions could act as a source of superweak CP violation is not a new one in the supersymmetry literature. The principal motivation is that, whether the RPV interactions operate by themselves or in association with the gauge interactions, by exploiting the absence of strong constraints on violations with respect to the flavors of quarks, leptons and the scalar superpartners by the RPV interactions, one could greatly enhance the potential for observability of CP violation. To our knowledge, one of the earliest discussion of this possibility is contained in ref.[8], where the rôle of a relative complex phase in a pair of  $\lambda'_{ijk}$  coupling constants was analyzed in connection with the neutral  $K$ ,  $\bar{K}$  mesons mixing and decays and also with the neutron electric dipole moment. This subject has attracted increased interest in the recent literature [28, 29, 30, 31, 32, 33, 34, 35, 36, 37]. Thus, the rôle of complex  $\lambda'_{ijk}$  coupling constants was considered in an analysis of the muon polarization in the decay,  $K^+ \rightarrow \mu^+ + \nu + \gamma$  [33], and also of the neutral  $B$ ,  $\bar{B}$  meson CP-odd decays asymmetries [29, 31, 32]; that of complex  $\lambda_{ijk}$  interactions was considered in a study of the spin-dependent asymmetries of sneutrino-antisneutrino resonant production of  $\tau$ -lepton pairs,  $l^- l^+ \rightarrow \tilde{\nu}, \tilde{\bar{\nu}} \rightarrow \tau^+ \tau^-$  [35]; and that of complex  $\lambda''_{ijk}$  interactions was considered as a possible explanation for the cosmological baryon asymmetry [34], as well as in the neutral  $B$ ,  $\bar{B}$  decays asymmetries [32]. An interesting alternative proposal [30] is to embed the CP-odd phase in the scalar superpartner interactions corresponding to interactions of  $A'_{ijk} \lambda'_{ijk}$  type. Furthermore, even if one assumes that the R parity odd interactions are CP conserving, these could still lead, in combination with the other possible sources of complex phases in the minimal supersymmetric standard model, to new tests of CP violation. Thus, in the hypothesis of pair of dominant coupling constants new contributions involving the coupling constants  $\lambda'_{ijk}$  and the CKM complex phase can arise for CP-odd observables associated with the neutral mesons mixing parameters and decays [29, 31, 32]. Also, through the interference with the extra CP-odd phases present in the soft supersymmetry parameters,  $A$ , the interactions  $\lambda_{ijk}$  and  $\lambda'_{ijk}$  may induce new contributions to electric dipole moments [38].

We propose in this work to examine the effect that R parity odd CP violating interactions could have on flavor non-diagonal rates and CP asymmetries in the production at high energy colliders of fermion-antifermion pairs of different families. We consider the two-body reactions,  $l^-(k) + l^+(k') \rightarrow f_J(p) + \bar{f}_{J'}(p')$ ,  $[J \neq J']$  where  $l$  stands for electron or muon, the produced fermions are leptons, down-quarks or up-quarks and the center of mass energies span the relevant range of existing and planned leptonic (electron or muon) colliders, namely, from the Z-boson pole up to 1000 GeV. High energy colliders tests of the RPV contributions to the flavor diagonal reactions were recently examined in [39, 40, 41, 42] and for flavor non-diagonal reactions in [43].

The physics of CP non conservation at high energy colliders has motivated a wide



variety of proposals in the past [44] and is currently the focus of important activity. In this work we shall limit ourselves to the simplest kind of observable, namely, the spin independent observable involving differences in rates between a given flavor non-diagonal process and its CP conjugated process. While the R parity odd interactions contribute to flavor changing amplitudes already at tree level, their contribution to spin independent CP-odd observables entails the consideration of loop diagrams. Thus, the CP asymmetries in the Z-boson pole branching fractions,  $B(Z \rightarrow f_J + \bar{f}_{J'})$ , are controlled by a complex phase interference between non-diagonal flavor contributions to loop amplitudes, whereas the off Z-boson pole asymmetries are controlled instead by a complex phase interference between tree and loop amplitudes. Finite contributions at tree level order can arise for spin dependent CP-odd observables, as discussed in refs. [35, 36].

It is useful to recall at this point that contributions in the standard model to the flavor changing rates and/or CP asymmetries can only appear through loop diagrams involving the quarks-gauge bosons interactions. Corresponding contributions involving squarks-gauginos or sleptons-gauginos interactions also arise in the minimal supersymmetric standard model. In studies performed some time ago within the standard model, the flavor non diagonal vector bosons (Z-boson and/or W-bosons) decay rates asymmetries [45, 46, 47] and CP-odd asymmetries [48, 49] were found to be exceedingly small. (Similar conclusions were reached in top-quark phenomenology [50].) On the other hand, in most proposals of physics beyond the standard model, the prospects for observing flavor changing effects in rates [45, 46, 47, 48, 49, 51] or in CP asymmetries [44, 52] are on the optimistic side. Large effects were reported for the supersymmetric corrections in flavor changing Z-boson decay rates arising from squarks flavor mixings [53], but the conclusions from this initial work have been challenged in a subsequent work [54] involving a more complete calculation.

The possibility that the R parity odd interactions could contribute to the CP asymmetries at observable levels depends in the first place on the accompanying mechanisms responsible for the flavor changing rates. Our working assumption in this work will be that the R parity odd interactions are the dominant contributors to flavor non-diagonal amplitudes.

The contents of this paper are organized into 4 sections. In Section 2, we develop the basic formalism for describing the scattering amplitudes at tree and one-loop levels. We discuss the case of leptons, down-quarks and up-quarks successively in subsections 2.1, 2.2 and 2.3. The evaluation of the one-loop loop diagrams is based on the standard formalism of [56]. Our calculations here closely parallel similar ones developed [57, 58] in connection with corrections to the Z-boson partial widths. In Section 3, we first briefly review the physics of flavor violation and next present our numerical results for the integrated cross sections (rates) and CP asymmetries for fermion pair production at and off the Z-boson pole. In Section 4, we state our main conclusions and discuss the impact of our results on possible experimental measurements.

## 2 Production of fermion pairs of different flavors

In this section we shall examine the contributions induced by the RPV (R parity violating) couplings on the flavor changing processes,  $l^-(k) + l^+(k') \rightarrow f_J(p) + \bar{f}_{J'}(p')$ , [ $l =$

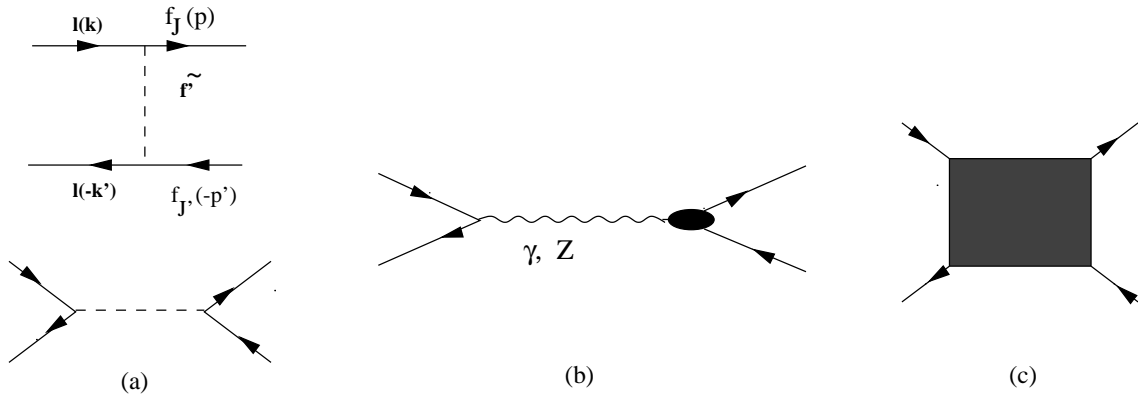


FIG. 1: Flavor non-diagonal process of  $l^-l^+$  production of a fermion-antifermion pair,  $l^-(k) + l^+(k') \rightarrow f_J(p) + \bar{f}_{J'}(p')$ . The tree level diagrams in (a) represent t- and s-channel exchange amplitudes. The loop level diagrams represent  $\gamma$  and  $Z$  gauge boson exchange amplitudes with dressed vertices in (b) and box amplitudes in (c).

$e, \mu; J \neq J'$ ] where  $f$  stands for leptons or quarks and  $J, J'$  are family indices. The relevant tree and one-loop level diagrams are shown schematically in Fig. 1. At one-loop order, there arise  $\gamma$ - and  $Z$ -boson exchange triangle diagrams as well as box diagrams. In the sequel, for clarity, we shall present the formalism for the one-loop contributions only for the dressed  $Zf\bar{f}$  vertex in the  $Z$ -boson exchange amplitude. The dressed  $\gamma$ -exchange amplitude has a similar structure and will be added in together with the  $Z$ -boson exchange amplitude at the level of the numerical results. Since we shall repeatedly refer in the text to the R parity odd effective Lagrangian for the fermions-sfermion Yukawa interactions, we quote below its full expression,

$$\begin{aligned}
L = & \sum_{ijk} \left\{ \frac{1}{2} \lambda_{ijk} [\tilde{\nu}_{iL} \bar{e}_{kR} e_{jL} + \tilde{e}_{jL} \bar{e}_{kR} \nu_{iL} + \tilde{e}_{kR}^* \bar{\nu}_{iR}^c e_{jL} - (i \rightarrow j)] \right. \\
& + \lambda'_{ijk} [\tilde{\nu}_{iL} \bar{d}_{kR} d_{jL} + \tilde{d}_{jL} \bar{d}_{kR} \nu_{iL} + \tilde{d}_{kR}^* \bar{\nu}_{iR}^c d_{jL} - \tilde{e}_{iL} \bar{d}_{kR} u_{jL} - \tilde{u}_{jL} \bar{d}_{kR} e_{iL} - \tilde{d}_{kR}^* \bar{e}_{iR}^c u_{jL}] \\
& \left. + \frac{1}{2} \lambda''_{ijk} \epsilon_{\alpha\beta\gamma} [\tilde{u}_{i\alpha R}^* \bar{d}_{j\beta R} d_{k\gamma L}^c + \tilde{d}_{j\beta R}^* \bar{u}_{i\alpha R} d_{k\gamma L}^c + \tilde{d}_{k\gamma R}^* \bar{u}_{i\alpha R} d_{j\beta L}^c - (j \rightarrow k)] \right\} + h.c. ,
\end{aligned} \tag{2.1}$$

noting that the summations run over the (quarks and leptons) families indices,  $i, j, k = [(e, \mu, \tau); (d, s, b); (u, c, t)]$ , subject to the antisymmetry properties,  $\lambda_{ijk} = -\lambda_{jik}$ ,  $\lambda''_{ijk} = -\lambda''_{ikj}$ . We use precedence conventions for operations on Dirac spinors such that charge conjugation acts first, chirality projection second and Dirac bar third, so that,  $\bar{\psi}_{L,R}^c = \overline{(\psi^c)_{L,R}}$ .

## 2.1 Charged lepton-antilepton pairs

### General formalism

The process  $l^-(k) + l^+(k') \rightarrow e_J^-(p) + e_{J'}^+(p')$ , for  $l = e, \mu; J \neq J'$ , can pick up a finite contribution at tree level from the R parity odd couplings,  $\lambda_{ijk}$ , only. For clarity, we treat in the following the case of electron colliders, noting that the case of muon colliders is easily deduced by replacing all occurrences in the RPV coupling constants of the index 1

by the index 2. There occur both t-channel and s-channel  $\tilde{\nu}_{iL}$  exchange contributions, of the type shown by the Feynman diagrams in (a) of Fig. 1. The scattering amplitude at tree level,  $M_t$ , reads :

$$\begin{aligned}
M_t^{JJ'} &= -\frac{1}{2(t - m_{\tilde{\nu}_{iL}}^2)} \left[ \lambda_{i1J} \lambda_{i1J'}^* \bar{u}_R(p) \gamma_\mu v_R(p') \bar{v}_L(k') \gamma_\mu u_L(k) \right. \\
&+ \left. \lambda_{iJ1}^* \lambda_{iJ'1} \bar{u}_L(p) \gamma_\mu v_L(p') \bar{v}_R(k') \gamma_\mu u_R(k) \right] \\
&- \frac{1}{s - m_{\tilde{\nu}_{iL}}^2} \left[ \lambda_{i11} \lambda_{iJJ'}^* \bar{v}_R(k') u_L(k) \bar{u}_L(p) v_R(p') + \lambda_{i11}^* \lambda_{iJJ'} \bar{v}_L(k') u_R(k) \bar{u}_R(p) v_L(p') \right],
\end{aligned} \tag{2.2}$$

where to obtain the saturation structure in the Dirac spinors indices for the t-channel terms, we have applied the Fierz rearrangement formula,  $\bar{u}_R(p) u_L(k) \bar{v}_L(k') v_R(p') = \frac{1}{2} \bar{u}_R(p) \gamma_\mu v_R(p') \bar{v}_L(k') \gamma_\mu u_L(k)$ . The t-channel (s-channel) exchange terms on the right hand side of eq.(2.2) include two terms each, called  $\mathcal{R}$ - and  $\mathcal{L}$ -type, respectively. These two terms differ by a chirality flip,  $L \leftrightarrow R$ , and correspond to the distinct diagrams where the exchanged sneutrino is emitted or absorbed at the upper (right-handed) vertex.

The Z-boson exchange amplitude (diagram (b) in Fig. 1) at loop level,  $M_l$ , reads :

$$M_l^{JJ'} = \left( \frac{g}{2 \cos \theta_W} \right)^2 \bar{v}(k') \gamma_\mu \left( a(e_L) P_L + a(e_R) P_R \right) u(k) \frac{1}{s - m_Z^2 + i m_Z \Gamma_Z} \Gamma_\mu^Z(p, p'), \tag{2.3}$$

where the Z-boson current amplitude vertex function,  $\Gamma_\mu^Z(p, p')$ , is defined through the effective Lagrangian density,

$$L = -\frac{g}{2 \cos \theta_W} Z^\mu \Gamma_\mu^Z(p, p').$$

For later convenience, we record for the processes,  $Z(P = p + p') \rightarrow f(p) + \bar{f}'(p')$  and  $Z(P) \rightarrow \tilde{f}_H(p) + \tilde{f}_H^*(p')$ , the familiar definitions of the Z-boson bare vertex functions,

$$\Gamma_\mu^Z(p, p') = \left[ \bar{f}(p) \gamma_\mu \left( a(f_L) P_L + a(f_R) P_R \right) f'(p') + (p - p')_\mu \tilde{f}_H^*(p') a(\tilde{f}_H) \tilde{f}_H(p) \right], \tag{2.4}$$

where the quantities denoted,  $a(f_H) \equiv a_H(f)$  and  $a(\tilde{f}_H)$ , taking equal values for both fermions and sfermions, are defined by,  $a(f_H) = a(\tilde{f}_H) = 2T_3^H(f) - 2Qx_W$ , where  $H = (L, R)$ ,  $x_W = \sin^2 \theta_W$ ,  $T_3^H$  are  $SU(2)_H$  Cartan subalgebra generators, and  $Q = T_3^L + Y$ ,  $Y$  are electric charge and weak hypercharge. These parameters satisfy the useful relations :  $a(\tilde{f}_H^*) = -a(\tilde{f}_H)$ ,  $a_L(f^c) = -a_R(f)$ ,  $a_R(f^c) = -a_L(f)$ . Throughout this paper we shall use the conventions in Haber-Kane review [59] (metric signature  $(+ - - -)$ ,  $P_{(R)} = (1 \mp \gamma_5)/2$ , etc...) and adopt the familiar summation convention on dummy indices.

The Lorentz covariant structure of the dressed Z-boson current amplitude in the process,  $Z(P) \rightarrow f_J(p) + \bar{f}_{J'}(p')$ , for a generic value of the Z-boson invariant mass  $s = P^2$ , involves three pairs of vectorial and tensorial vertex functions, which are defined in terms of the general decomposition :

$$\begin{aligned}
\Gamma_\mu^Z(p, p') &= \bar{u}(p) \left[ \gamma_\mu \left( \tilde{A}_L^{JJ'}(f) P_L + \tilde{A}_R^{JJ'}(f) P_R \right) \right. \\
&+ \left. \frac{1}{m_J + m_{J'}} \sigma_{\mu\nu} \left( (p + p')^\nu [i a^{JJ'} + \gamma_5 d^{JJ'}] + (p - p')^\nu [i b^{JJ'} + \gamma_5 e^{JJ'}] \right) \right] v(p'),
\end{aligned}$$

where,  $\sigma_{\mu\nu} = \frac{i}{2}[\gamma_\mu, \gamma_\nu]$ . The vector vertex functions separate additively into the classical (bare) and loop contributions,  $\tilde{A}_H^{JJ'}(f) = a_H(f)\delta_{JJ'} + A_H^{JJ'}(f)$ ,  $[H = L, R]$ . The tensor vertex functions, associated with  $\sigma^{\mu\nu}(p+p')_\nu$ , include the familiar magnetic and electric  $Z f \bar{f}$  couplings, such that the flavor diagonal vertex functions,  $-\frac{g}{2\cos\theta_W}\frac{1}{2m_J}[a^{JJ}, d^{JJ}]$ , identify, in the small momentum transfer limit, with the fermions  $Z$ -boson current magnetic and (P and CP-odd) electric dipole moments, respectively. In working with the spinors matrix elements, it is helpful to recall the mass shell relations,  $\bar{u}(p)\not{p} = m_J\bar{u}(p)$ ,  $\not{p}'v(p') = -m_{J'}v(p')$ , and the Gordon type identities, appropriate to the saturation of the Dirac spinor indices,  $\bar{u}(p)\cdots v(p')$ ,

$$\begin{aligned} \left[ (p \pm p')_\mu \begin{pmatrix} \gamma_5 \\ 1 \end{pmatrix} + i\sigma_{\mu\nu}(p \mp p')^\nu \begin{pmatrix} \gamma_5 \\ 1 \end{pmatrix} \right] &= (m_J + m_{J'})\gamma_\mu \begin{pmatrix} \gamma_5 \\ 1 \end{pmatrix}, \\ \left[ (p \mp p')_\mu \begin{pmatrix} \gamma_5 \\ 1 \end{pmatrix} + i\sigma_{\mu\nu}(p \pm p')^\nu \begin{pmatrix} \gamma_5 \\ 1 \end{pmatrix} \right] &= (m_J - m_{J'})\gamma_\mu \begin{pmatrix} \gamma_5 \\ 1 \end{pmatrix}. \end{aligned}$$

Based on these identities, one also checks that the additional vertex functions,  $[b^{JJ'}, e^{JJ'}]$ , associated with the Lorentz covariants,  $\sigma^{\mu\nu}(p-p')_\nu[1, \gamma_5]$ , can be expressed as linear combinations of the vector or axial covariants,  $\gamma_\mu[1, \gamma_5]$ , and the total momentum covariants,  $(p+p')_\mu[1, \gamma_5]$ . The latter will yield, upon contraction with the initial state  $Zl^-l^+$  vertex function, to negligible mass terms in the initial leptons.

Let us now perform the summation over the initial and final states polarizations for the summed tree and loop amplitudes,  $M^{JJ'} = M_t^{JJ'} + M_l^{JJ'}$ , where the lower suffices  $t, l$  stand for tree and loop, respectively. (We shall not be interested in this work in spin observables.) A straightforward calculation, carried out for the squared sum of the tree and loop amplitudes, yields the result (a useful textbook to consult here is ref. [60]) :

$$\begin{aligned} \sum_{pol} |M_t^{JJ'} + M_l^{JJ'}|^2 &= \left| -\frac{\lambda_{i1J}\lambda_{i1J'}^*}{2(t - m_{\tilde{\nu}_{iL}}^2)} + \left( \frac{g}{2\cos\theta_W} \right)^2 \frac{a(e_L)A_R^{JJ'}(e, s + i\epsilon)}{s - m_Z^2 + im_Z\Gamma_Z} \right|^2 16(k \cdot p)(k' \cdot p') \\ &+ 8m_J m_{J'}(k \cdot k')\varphi_{LL}(\mathcal{R}) + 8m_e^2(p \cdot p')\varphi_{RR}(\mathcal{R}) + \\ &+ \left| -\frac{\lambda_{iJ1}\lambda_{iJ1}^*}{2(t - m_{\tilde{\nu}_{iL}}^2)} + \left( \frac{g}{2\cos\theta_W} \right)^2 \frac{a(e_R)A_L^{JJ'}(e, s + i\epsilon)}{s - m_Z^2 + im_Z\Gamma_Z} \right|^2 16(k \cdot p)(k' \cdot p') \\ &+ 8m_J m_{J'}(k \cdot k')\varphi_{RR}(\mathcal{L}) + 8m_e^2(p \cdot p')\varphi_{LL}(\mathcal{L}) + 8 \left| \frac{\lambda_{i11}\lambda_{iJJ'}^*}{s - m_{\tilde{\nu}_{iL}}^2} \right|^2 (k \cdot k')(p \cdot p'), \end{aligned} \quad (2.6)$$

where we have introduced the following functions, associated with the  $\mathcal{R}$ - and  $\mathcal{L}$ -type contributions :

$$\begin{aligned} \varphi_{HH'}(\mathcal{R}) &= -\left( \frac{g}{2\cos\theta_W} \right)^2 \left( \frac{a(e_H)A_{H'}^{JJ'}(e, s + i\epsilon)}{s - m_Z^2 + im_Z\Gamma_Z} \right)^* \left( \frac{\lambda_{i1J}\lambda_{i1J'}^*}{2(t - m_{\tilde{\nu}_{iL}}^2)} \right) + c. c, \\ \varphi_{HH'}(\mathcal{L}) &= -\left( \frac{g}{2\cos\theta_W} \right)^2 \left( \frac{a(e_H)A_{H'}^{JJ'}(e, s + i\epsilon)}{s - m_Z^2 + im_Z\Gamma_Z} \right)^* \left( \frac{\lambda_{iJ1}\lambda_{iJ1}^*}{2(t - m_{\tilde{\nu}_{iL}}^2)} \right) + c. c. \end{aligned} \quad (2.7)$$

The two sets of terms in eqs.(2.7) and (2.6), labelled by the letters,  $\mathcal{R}, \mathcal{L}$ , are associated with the two t-channel exchange contributions in the tree amplitude, eq.(2.2), which differ by the spinors chirality structure and the substitutions,  $\lambda_{i1J}\lambda_{i1J'}^* \rightarrow \lambda_{iJ1}\lambda_{iJ1}^*$ . The

terminology,  $\mathcal{L}$ ,  $\mathcal{R}$ , is motivated by the fact that these contributions are controlled by the Z-boson left and right chirality vertex functions,  $A_L$  and  $A_R$ , respectively, in the massless limit.

The imaginary shift in the argument,  $s + i\epsilon$  (representing the upper lip of the cut real axis in the complex  $s$ -plane) of the vertex functions,  $A_H^{JJ'}(f, s + i\epsilon)$ , has been appended to remind us that the one-loop vertex functions are complex functions in the complex plane of the virtual Z-boson mass squared,  $s = (p + p')^2$ , with branch cuts starting at the physical thresholds where the production processes, such as,  $Z \rightarrow f + \bar{f}$  or  $Z \rightarrow \tilde{f} + \tilde{f}^*$ , are raised on-shell. For notational simplicity, we have omitted writing several terms proportional to the initial leptons masses and also some of the small subleading terms arising from the loop amplitude squared. At the energies of interest, whose scale is set by the initial center of mass energy or by the Z-boson mass, the terms involving factors of the initial leptons masses  $m_e$ , are entirely negligible, of course. Thus, the contributions associated with  $\varphi_{RR}(\mathcal{R})$ ,  $\varphi_{LL}(\mathcal{L})$  can safely be dropped. Also, the contribution from  $\varphi_{LL}(\mathcal{R})$  and  $\varphi_{RR}(\mathcal{L})$  which are proportional to the final state leptons masses,  $m_J$ , and  $m_{J'}$ , can to a good approximation be neglected for leptons production. Always in the same approximation, we find also that interference terms are absent between the s-channel exchange and the t-channel amplitudes and between the s-channel tree and Z-boson exchange loop amplitudes. Similarly, because of the opposite chirality structure of the first two terms in  $M_t^{JJ'}$ , their cross-product contributions give negligibly small mass terms.

## CP asymmetries

Our main concern in this work bears on the comparison of the pair of CP conjugate reactions,  $l^-(k) + l^+(k') \rightarrow e_J^-(p) + e_{J'}^+(p')$  and  $l^-(k) + l^+(k') \rightarrow e_{J'}^-(p) + e_J^+(p')$ . Denoting the summed tree and one-loop probability amplitudes for these reactions as,  $M^{JJ'} = M_t^{JJ'} + M_l^{JJ'}$ ,  $\bar{M}^{JJ'} = M_t^{JJ'} + M_l^{JJ'} = M^{JJ'}$ , we observe that these amplitudes are simply related to one another by means of a specific complex conjugation operation. The general structure of this relationship can be expressed schematically as :

$$M^{JJ'} = a_0^{JJ'} + \sum_{\alpha} a_{\alpha}^{JJ'} F_{\alpha}^{JJ'}(s + i\epsilon), \quad \bar{M}^{JJ'} = a_0^{JJ'\star} + \sum_{\alpha} a_{\alpha}^{JJ'\star} F_{\alpha}^{JJ'}(s + i\epsilon), \quad (2.8)$$

where for each of the equations above, referring to amplitudes for pairs of CP conjugate processes, the first and second terms correspond to the tree and loop level contributions, with  $a_0^{JJ'}$ ,  $a_0^{JJ'} = a_0^{JJ'\star}$ , representing the tree amplitudes and  $a_{\alpha}^{JJ'}$ ,  $a_{\alpha}^{JJ'} = a_{\alpha}^{JJ'\star}$  and  $F_{\alpha}^{JJ'}$ ,  $F_{\alpha}^{JJ'} = F_{\alpha}^{JJ'}$  representing the complex valued coupling constants products and momentum integrals in the loop amplitudes. The functions  $F^{JJ'}$  must be symmetric under the interchange,  $J \leftrightarrow J'$ . The summation index  $\alpha$  labels the family configurations for the intermediate fermions-sfermions which can run inside the loops. Defining the CP asymmetries by the normalized differences,

$$\mathcal{A}_{JJ'} = \frac{|M^{JJ'}|^2 - |\bar{M}^{JJ'}|^2}{|M^{JJ'}|^2 + |\bar{M}^{JJ'}|^2},$$

and inserting the decompositions in eq.(2.8), the result separates additively into two types of terms :

$$\mathcal{A}_{JJ'} = \frac{2}{|a_0|^2} \left[ \sum_{\alpha} \text{Im}(a_0 a_{\alpha}^{\star}) \text{Im}(F_{\alpha}(s + i\epsilon)) \right]$$

$$- \sum_{\alpha < \alpha'} \text{Im}(a_\alpha a_{\alpha'}^*) \text{Im}(F_\alpha(s+i\epsilon) F_{\alpha'}^*(s+i\epsilon)) \Big], \quad (2.9)$$

where, for notational simplicity, we have suppressed the fixed external family indices on  $a_0^{JJ'}$ ,  $a_\alpha^{JJ'}$  and  $F_\alpha^{JJ'}$ , and replaced the full denominator by the tree level amplitude, since this is expected to dominate over the loop amplitude. The first term in (2.9) is associated with an interference between tree and loop amplitudes and the second with an interference between terms arising from different family contributions in the loop amplitude. In the second term of eq.(2.9), the two imaginary parts factors are antisymmetric under the interchange of indices,  $\alpha$  and  $\alpha'$ , so that their product is symmetric and allows one to write,  $\sum_{\alpha < \alpha'} = \frac{1}{2} \sum_{\alpha \neq \alpha'}$ . To obtain a more explicit formula, let us specialize to the specific case where the Z-boson vertex functions decompose as,  $A_H^{JJ'}(f, s+i\epsilon) = \sum_\alpha b_{JJ'}^{H\alpha} I_{H\alpha}^{JJ'}(s+i\epsilon)$ . The first factors,  $b_{JJ'}^{H\alpha} = \lambda_{ijJ} \lambda_{ijJ'}^*$  (using  $\alpha = (ij)$  and notations for the one-loop contributions to be described in the next subsection), include the CP-odd phase from the R parity odd coupling constants. The second factors,  $I_{H\alpha}^{JJ'}$ , include the CP-even phase from the unitarity cuts associated to the physical on-shell intermediate states. In the notations of eq.(2.8),

$$a_\alpha^{JJ'} = \left(\frac{g}{2 \cos \theta_W}\right)^2 a(e_{H'}) b_{JJ'}^{H\alpha}, \quad F_\alpha^{JJ'} = I_{H\alpha}^{JJ'}(s+i\epsilon)/(s - m_Z^2 + im_Z \Gamma_Z),$$

where the right hand sides incorporate appropriate sums over the chirality indices,  $H'$ ,  $H$  of the initial and final fermions, respectively.

Applying eq.(2.8) to the asymmetry integrated with respect to the scattering angle, one derives for the corresponding integrated tree-loop interference contribution,

$$\begin{aligned} \mathcal{A}_{JJ'} &= -4 \left(\frac{g}{2 \cos \theta_W}\right)^2 a(e_L) \text{Im}(\lambda_{i1J} \lambda_{i1J'}^* a_{JJ'}^{\alpha\star}(f_R)) \text{Im}\left(\frac{I_\alpha^R(s+i\epsilon)}{s - m_Z^2 + im_Z \Gamma_Z}\right) \\ &\times \int_{-1}^1 dx \frac{(1-x)^2}{(2(t - m_{\nu_{iL}}^2))} \left[ \sum_i |\lambda_{i1J} \lambda_{i1J'}^*|^2 \int_{-1}^1 dx \frac{(1-x)^2}{4(t - m_{\nu_{iL}}^2)^2} \right]^{-1}, \end{aligned} \quad (2.10)$$

where,  $\theta$ ,  $[x = \cos \theta]$  denotes the scattering angle variable in the center of mass frame and the Mandelstam variables in the case of massless final state fermions take the simplified expressions,  $s \equiv (k + k')^2$ ,  $t \equiv (k - p)^2 = -\frac{1}{2}s(1-x)$ ,  $u \equiv (k - p')^2 = -\frac{1}{2}s(1+x)$ . Useful kinematical relations in the general case with final fermions masses,  $m_J$ ,  $m_{J'}$ , are :  $\sqrt{s} = 2k = E_p + E_{p'}$ ,  $t = m_J^2 - sE_p(1 - \beta x)$ ,  $u = m_{J'}^2 - sE_{p'}(1 + \beta' x)$ , where,  $E_p = (s + m_J^2 - m_{J'}^2)/(2\sqrt{s})$ ,  $E_{p'} = (s + m_{J'}^2 - m_J^2)/(2\sqrt{s})$ ,  $\beta = p/E_p$ ,  $\beta' = p/E_{p'}$ , with  $k$ ,  $p$  denoting the center of mass momenta of the two-body initial and final states, respectively. The unpolarized differential cross section reads then,  $d\sigma/dx = \frac{|p|}{128\pi s|k|} \sum_{pol} |M|^2$ .

For the Z-boson pole observables, the flavor non-diagonal branching ratios and CP asymmetries (where one sets,  $s = m_Z^2$ ) are defined in terms of the notations specified in the preceeding paragraph by the equations,

$$\begin{aligned} B_{JJ'} &\equiv \frac{\Gamma(Z \rightarrow f_J + \bar{f}_{J'}) + \Gamma(Z \rightarrow f_{J'} + \bar{f}_J)}{\Gamma(Z \rightarrow \text{all})} = 2 \frac{|A_L^{JJ'}(f)|^2 + |A_R^{JJ'}(f)|^2}{\sum_f |a_L(f)|^2 + |a_R(f)|^2}, \\ \mathcal{A}_{JJ'} &\equiv \frac{\Gamma(Z \rightarrow f_J + \bar{f}_{J'}) - \Gamma(Z \rightarrow f_{J'} + \bar{f}_J)}{\Gamma(Z \rightarrow f_J + \bar{f}_{J'}) + \Gamma(Z \rightarrow f_{J'} + \bar{f}_J)} \\ &= -2 \frac{\sum_{H=L,R} \sum_{\alpha < \alpha'} \text{Im}(b_{JJ'}^{H\alpha} b_{JJ'}^{H\alpha'\star}) \text{Im}(I_{H\alpha}^{JJ'}(s+i\epsilon) I_{H\alpha'}^{JJ'\star}(s+i\epsilon))}{\sum_{H=L,R} |\sum_\alpha b_{JJ'}^{H\alpha}(f) F_H^\alpha(s+i\epsilon)|^2}. \end{aligned} \quad (2.11)$$

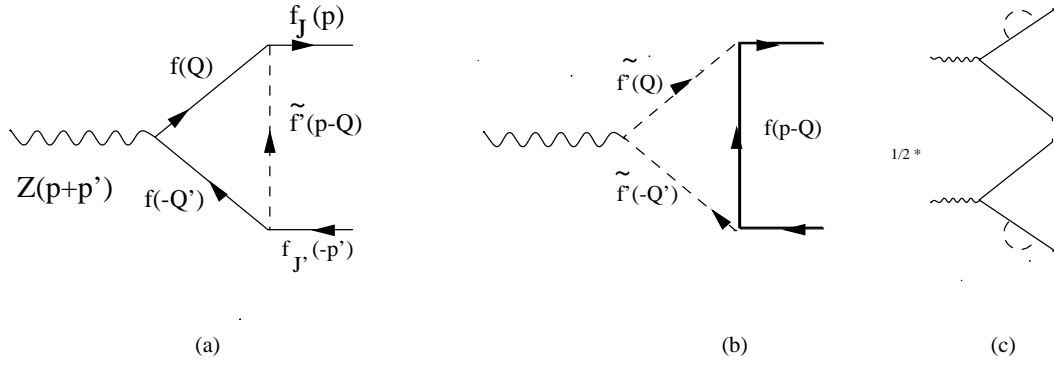


FIG. 2: One-loop diagrams for the dressed  $Z(P) f(p) \bar{f}(p')$  vertex. The flow of four-momenta for the intermediate fermions in (a) is denoted as,  $Z(P) \rightarrow f(Q) + \bar{f}(Q') \rightarrow f_J(p) + \bar{f}_{J'}(p')$ . Similar notations are used for the sfermions diagram in (b) where,  $Z(P) \rightarrow \tilde{f}'(Q) + \tilde{f}'^*(Q')$ , and for the self-energy diagrams in (c).

For completeness, we recall the formula for the Z-boson decay width in fermion pairs (massless limit),

$$\Gamma(Z \rightarrow f_J + \bar{f}_{J'}) = \frac{G_F m_Z^3 c_f}{12\sqrt{2}\pi} (|A_L^{JJ'}(f)|^2 + |A_R^{JJ'}(f)|^2),$$

where,  $c_f = [1, N_c]$ , for  $[f = l, q]$  ( $N_c = 3$  is the number of colors in the  $SU(3)_c$  color group) and the experimental value for the total width,  $\Gamma(Z \rightarrow all)_{exp} = 2.497$  GeV.

The expressions in eqs.(2.10) and (2.11) for the CP asymmetries explicitly incorporate the property of these observables of depending on combinations of the RPV coupling constants, such as,  $Arg(\lambda_{i1J} \lambda_{i1J'}^* \lambda_{i'jJ} \lambda_{i'jJ'}^*)$ , or  $Arg(\lambda_{ijJ} \lambda_{ijJ'}^* \lambda_{i'j'J} \lambda_{i'j'J'}^*)$ , which are invariant under complex phase redefinitions of the fields. This freedom under rephasings of the quarks and leptons superfields actually removes 21 complex phases from the complete general set of 45 complex RPV coupling constants.

## One-loop amplitudes

The relevant triangle Feynman diagrams, which contribute to the dressed Z-boson leptonic vertex,  $Z(P) l^-(p) l^+(p')$ , appear in three types, fermionic, scalar and self-energy, as shown in Fig. 2. We consider first the contributions induced by the R parity odd couplings,  $\lambda'_{ijk}$ . The intermediate lines can assume two distinct configurations which contribute both, in the limit of vanishing external fermions masses, to the left-chirality vertex functions only. We shall refer to such contributions by the name  $\mathcal{L}$ -type contributions, reserving the name  $\mathcal{R}$ -type to contributions to the right-chirality vector couplings. The two allowed configurations for the internal fermions and sfermions are :  $f = \begin{pmatrix} d_k \\ u_j^c \end{pmatrix}$ ;  $\tilde{f}' = \begin{pmatrix} \bar{u}_{jL}^* \\ \bar{d}_{kR} \end{pmatrix}$ . Our calculations of the triangle diagrams employ the kinematical conventions for the flow of electric charge and momenta indicated in Fig.2, where  $P = p + p' = Q + Q' = k + k'$ . The summed fermion and scalar Z-boson current contributions are given by :

$$\Gamma_\mu^Z(\mathcal{L}) = +iN_c \lambda'^*_{Jjk} \lambda'_{J'jk} \left[ \int_Q \frac{\bar{u}(p) [P_R(Q + m_f) \gamma_\mu (a(f_L) P_L + a(f_R) P_R) (-Q' + m_f) P_L] v(p')}{(Q^2 - m_f^2)((Q - p - p')^2 - m_f^2)((Q - p)^2 - m_{\tilde{f}'}^2)} \right]$$

$$+ \int_Q \frac{a(\tilde{f}_L')(Q - Q')_\mu \bar{u}(p) [P_R(\not{p} - \not{Q} + m_f) P_L] v(p')}{(Q^2 - m_{\tilde{f}'}^2)((Q - p - p')^2 - m_{\tilde{f}'}^2)((Q - p)^2 - m_f^2)} \Big]. \quad (2.12)$$

The integration measure is defined as,  $\int_Q = \frac{1}{(2\pi)^4} \int d^4Q$ . For a convenient derivation of the self-energy diagrams, one may invoke the on shell renormalization condition which relates these to the fields renormalization constants. Defining schematically the self-energy vertex functions for a Dirac fermion field  $\psi$  by the Lagrangian density,  $L = i\bar{\psi}(\not{p} - m + \Sigma(p))\psi$ ,  $\Sigma(p) = m\sigma_0 + \not{p}(\sigma^L P_L + \sigma^R P_R)$ , the transition from bare to renormalized fields and mass terms may be effected by the replacements,

$$\psi_H \rightarrow \frac{\psi_H}{(1 + \sigma_H)^{\frac{1}{2}}} = \psi_H Z_H^{\frac{1}{2}}, \quad m \rightarrow m \frac{(1 + \sigma^L)^{\frac{1}{2}}(1 + \sigma^R)^{\frac{1}{2}}}{(1 - \sigma_0)}. \quad [H = L, R]$$

By a straightforward generalization to the case of several fields, labelled by a family index  $J$ , the fields renormalization constants become matrices,  $Z_{JJ'}^H = (1 + \sigma^H)_{JJ'}^{-1}$ . The self-energy contributions to the dressed Z-boson vertex function is then described as,

$$\begin{aligned} \Gamma_\mu^Z(p, p')_{SE} &= \sum_{H=L,R} \left( (Z_{JJ'}^H Z_{JJ'}^{H*})^{\frac{1}{2}} - 1 \right) \bar{u}(p) \gamma_\mu a(f_H) P_H v(p') \\ &= - \sum_{H=L,R} \frac{1}{2} (\sigma_{JJ'}^H(p) + \sigma_{JJ'}^{H*}(p')) \bar{u}(p) \gamma_\mu a(f_H) P_H v(p'), \end{aligned} \quad (2.13)$$

where for the case at hand,

$$\Sigma_{JJ'}(p) = -iN_c \lambda_{Jjk}'^* \lambda_{J'jk}' \int_Q \frac{P_R(\not{Q} + m_f) P_L}{(-Q^2 + m_f^2)((Q - p)^2 + m_{\tilde{f}'}^2)}, \quad (2.14)$$

so that  $\sigma_{JJ'}^R = 0$  and  $\sigma_0 = 0$ . Similar Feynman graphs to those of Fig. 2, and similar formulas to those of eqs.(2.12) and (2.13), obtain for the dressed photon current case,  $\gamma(P)l^-(p)l^+(p')$ .

We organize our one-loop calculations in line with the approach developed by 't Hooft and Veltman [55] and Passarino and Veltman[56], keeping in mind that our spacetime metric has an opposite signature to theirs,  $(-+++)$ . For definiteness, we recall the conventional notations for the two-point and three-point integrals,

$$\frac{i\pi^2}{(2\pi)^4} [B_0, -p_\mu B_1] = \int_Q \frac{[1, Q_\mu]}{(-Q^2 + m_1^2)((Q - p)^2 + m_2^2)}, \quad (2.15)$$

$$\begin{aligned} \frac{i\pi^2}{(2\pi)^4} [C_0, -p_\mu C_{11} - p'_\mu C_{12}, p_\mu p_\nu C_{21} + p'_\nu p'_\mu C_{22} + (p_\mu p'_\nu + p_\nu p'_\mu) C_{23} - g_{\mu\nu} C_{24}] \\ = \int_Q \frac{[1, Q_\mu, Q_\mu Q_\nu]}{(-Q^2 + m_1^2)((Q - p)^2 + m_2^2)((Q - p - p')^2 + m_3^2)}, \end{aligned} \quad (2.16)$$

where the arguments for the  $B$ - and  $C$ - functions are defined as :  $B_A(-p, m_1, m_2)$ ,  $[A = 0, 1]$  and  $C_B(-p, -p', m_1, m_2, m_3)$ ,  $[B = 0, 11, 12, 21, 22, 23, 24]$ . In the algebraic derivation of the one-loop amplitudes, we find it convenient to introduce the definitions :  $p_\mu = \frac{1}{2}P_\mu + \rho_\mu$ ,  $p'_\mu = \frac{1}{2}P_\mu - \rho_\mu$ , where  $P = p + p'$ ,  $\rho = \frac{1}{2}(p - p')$ . The terms proportional to the Lorentz covariant  $P^\mu = (p + p')^\mu$  will then reduce, for the full Z-boson exchange amplitude in eq. (2.3), to negligible mass terms in the initial leptons.



Dropping mass terms for all external fermions, the tensorial couplings cancel out and we need keep track of the vector couplings only, with the result :

$$\begin{aligned} A_L^{JJ'}(\mathcal{L}) &= N_c \frac{\lambda_{jk}^* \lambda_{j'jk}}{(4\pi)^2} \left[ a(f_L) m_f^2 C_0 + a(f_R) \left( B_0^{(1)} - 2C_{24} - m_{\tilde{f}'}^2 C_0 \right) + 2a(\tilde{f}'_L) \tilde{C}_{24} + a(f_L) B_1^{(2)} \right], \\ A_R^{JJ'}(\mathcal{L}) &= 0. \end{aligned} \quad (2.17)$$

The cancellation of the right chirality vertex function in this case is the reason behind our naming these contributions as  $\mathcal{L}$ -type. The two-point and three-point integrals functions without a tilde symbol arise through the fermion current triangle contribution and the self-energy contribution (represented by the term proportional to  $B_1^{(2)}$ ). These involve the argument variables according to the following conventions,

$B_A^{(1)} = B_A(-p - p', m_f, m_f)$ ,  $B_A^{(2)} = B_A(-p, m_f, m_{\tilde{f}'})$ ,  $B_A^{(3)} = B_A(-p', m_{\tilde{f}'}, m_f)$ , and  $C_B = C_A(-p, -p', m_f, m_{\tilde{f}'}, m_f)$ . The integral functions with a tilde arise in the sfermion current diagram and are described by the argument variables,  $\tilde{C}_A = C_A(-p, -p', m_{\tilde{f}'}, m_f, m_{\tilde{f}'})$ .

A very useful check on the above results concerns the cancellation of ultraviolet divergencies. This is indeed expected on the basis of the general rule that those interaction terms which are absent from the classical action, as is the case for the flavor changing currents, cannot undergo renormalization. A detailed discussion of this property is developed in [61]. The logarithmically divergent terms in eq.(2.17), proportional to the quantity,  $\Delta = -\frac{2}{D-4} + \gamma - \ln \pi$ , as defined in [56], arise from the two- and three-point integrals as,  $B_0 \rightarrow \Delta$ ,  $B_1 \rightarrow -\frac{1}{2}\Delta$ ,  $C_{24} \rightarrow \frac{1}{4}\Delta$ , all other integrals being finite. Performing these substitutions, we indeed find that  $\Delta$  comes accompanied by the overall factors,  $[-a(e_L) + a(\tilde{u}_L^*) + a(d_R)]$ , or  $[-a(e_L) + a(\tilde{d}_R) + a_R(u^c)]$ , which both do vanish in the relevant configurations for  $f, f'$ .

Let us now consider the R parity odd Yukawa interactions involving the  $\lambda_{ijk}$ . These contribute through the same triangle diagrams as in Fig. 2. There arise contributions of  $\mathcal{L}$ -type, in the single configuration,  $f = e_k, \tilde{f}' = \tilde{\nu}_{iL}^*$  and of  $\mathcal{R}$ -type in the two configurations,  $f = \begin{pmatrix} e_j \\ \nu_i \end{pmatrix}, \tilde{f}' = \begin{pmatrix} \tilde{\nu}_{iL} \\ \tilde{e}_{jL} \end{pmatrix}$ . Following the same derivation as above, and neglecting all of the external mass terms, we obtain the following results for the one-loop vector coupling vertex functions :

$$\begin{aligned} A_L^{JJ'}(\mathcal{L}) &= \frac{\lambda_{ijk}^* \lambda_{ij'k}}{(4\pi)^2} [a(f_L) m_f^2 C_0 + a(f_R) (B_0^{(1)} - 2C_{24} - m_{\tilde{f}'}^2 C_0) + 2a(\tilde{f}'_L) \tilde{C}_{24} + a(f_L) B_1^{(2)}], \\ A_R^{JJ'}(\mathcal{R}) &= \frac{\lambda_{ijJ} \lambda_{ij'J'}^*}{(4\pi)^2} [a(f_R) m_f^2 C_0 + a(f_L) (B_0^{(1)} - 2C_{24} - m_{\tilde{f}'}^2 C_0) + 2a(\tilde{f}'_L) \tilde{C}_{24} + a(f_R) B_1^{(2)}], \end{aligned} \quad (2.18)$$

with  $A_R^{JJ'}(\mathcal{L}) = 0$ ,  $A_L^{JJ'}(\mathcal{R}) = 0$ . We note that the  $\mathcal{L}$ ,  $\mathcal{R}$  contributions are related by a mere chirality flip transformation and that the color factor,  $N_c$ , is absent in the present case.

## 2.2 Down-quark-antiquark pairs

The processes involving flavor non-diagonal final down-quark-antiquark pairs,  $l^-(k) + l^+(k') \rightarrow d_J(p) + \bar{d}_{J'}(p')$ , pick up non vanishing contributions only from the  $\lambda'_{ijk}$  interactions. Our discussion here will be brief since this case is formally similar to the leptonic

case treated in subsection 2.1. In particular, the external fermions masses, for all three families, can be neglected to a good approximation at the energy scales of interest. The tree level amplitude comprises an  $\mathcal{R}$ -type single t-channel  $\tilde{u}$ -squark exchange diagram and two s-channel diagrams involving  $\tilde{\nu}$  and  $\tilde{\bar{\nu}}$  sneutrinos of the type shown in (a) of Fig. 1,

$$M_t^{JJ'} = -\frac{\lambda'_{1jJ}\lambda_{1jJ'}^*}{2(t-m_{\tilde{u}_{jL}}^2)}\bar{u}_R(p)\gamma_\mu v_R(p')\bar{v}_L(k')\gamma_\mu u_L(k) \\ - \frac{1}{s-m_{\tilde{\nu}_{iL}}^2}\left[\lambda_{i11}\lambda_{iJJ'}^*\bar{v}_R(k')u_L(k)\bar{u}_L(p)v_R(p') + \lambda_{i11}^*\lambda'_{iJJ'}\bar{v}_L(k')u_R(k)\bar{u}_R(p)v_L(p')\right], \quad (2.19)$$

where a Kronecker symbol factor,  $\delta_{ab}$ , expressing the dependence on the final state quarks color indices,  $d^a\bar{d}_b$ , has been suppressed. This dependence will induce in the analog of the formula in eq.(2.6) expressing the rates, an extra color factor,  $N_c$ .

At one-loop level, the dressed  $Z d_J \bar{d}_{J'}$  vertex functions in the Z-boson s-channel exchange amplitude can be described by the same type of triangle diagrams as in Fig. 2. The fields configurations circulating in the loop correspond now to quarks-sleptons of  $\mathcal{L}$ -type,  $f = d_k; \tilde{l}' = \tilde{\nu}_{iL}^*$ , and of  $\mathcal{R}$ -type,  $f = \begin{pmatrix} d_j \\ u_j \end{pmatrix}; \tilde{l}' = \begin{pmatrix} \tilde{\nu}_{iL} \\ \tilde{e}_{iL} \end{pmatrix}$ . There also occurs corresponding leptons-squarks fields configurations of  $\mathcal{L}$ -type,  $l = \nu_i^c; \tilde{f}' = \tilde{d}_{kR}$ , and  $\mathcal{R}$ -type,  $l = \begin{pmatrix} \nu_i \\ e_i \end{pmatrix}; \tilde{f}' = \begin{pmatrix} \tilde{d}_{jL} \\ \tilde{u}_{jL} \end{pmatrix}$ . The  $\mathcal{L}$ - and  $\mathcal{R}$ - type contributions differ by a chirality flip, the first contributing to  $A_L^{JJ'}$  and the second to  $A_R^{JJ'}$ . The calculations are formally similar to those in subsection 2.1 and the final results have a nearly identical structure to those given in (2.17). For clarity, we quote the final formulas for the one-loop vector coupling vertex functions,

$$A_L^{JJ'}(\mathcal{L}) = \frac{\lambda_{iJk}^*\lambda_{1jJ'}^*}{(4\pi)^2}[a(f_L)m_f^2C_0 + a(f_R)(B_0^{(1)} - 2C_{24} - m_{\tilde{f}'}^2C_0) + 2a(\tilde{f}'_L)\tilde{C}_{24} + a(d_L)B_1^{(2)}], \\ A_R^{JJ'}(\mathcal{R}) = \frac{\lambda_{ijJ'}^*\lambda_{iJJ}'}{(4\pi)^2}[a(f_R)m_f^2C_0 + a(f_L)(B_0^{(1)} - 2C_{24} - m_{\tilde{f}'}^2C_0) + 2a(\tilde{f}'_L)\tilde{C}_{24} + a(d_R)B_1^{(2)}], \quad (2.20)$$

where the intermediate fermion-sfermion fields are labelled by the indices  $f, \tilde{f}'$ . There are implicit sums in eq.(2.20) over the above quoted leptons-squarks and quarks-sleptons configurations. The attendant ultraviolet divergencies are accompanied again with vanishing factors,  $a(\tilde{d}_R) - a(d_L) + a(\nu_R^c) = 0, \quad a(\tilde{d}_L) - a(d_R) + a(\nu_L) = 0$ .

## 2.3 Up-quark-antiquark pairs

The production processes of up-quark-antiquark pairs of different families,  $l^-(k) + l^+(k') \rightarrow u_J(p) + \bar{u}_{J'}(p')$ , may be controlled by the  $\lambda'_{ijk}$  interactions only. The tree amplitude is associated with an u-channel  $\tilde{d}$ -squark exchange, of type similar to that shown by (a) in Fig. 1, and can be expressed as,

$$M_t^{JJ'} = -\frac{\lambda_{1Jk}^*\lambda'_{1J'k}}{2(u-m_{\tilde{d}_{kR}}^2)}\bar{v}_L(k')\gamma^\mu u_L(k)\bar{u}_L(p)\gamma_\mu v_L(p'), \quad (2.21)$$

after using the Fierz reordering identity, appropriate to commuting Dirac (rather than anticommuting field) spinors,  $\bar{u}^c(k)P_L v(p')\bar{u}(p)P_R v^c(k') = +\frac{1}{2}\bar{v}_L(k')\gamma^\mu u_L(k)\bar{u}_L(p)\gamma_\mu v_L(p')$ .

We have omitted the Kronecker symbol  $\delta_{ab}$  on the  $u^a \bar{u}_b$  color indices, which will result in an extra color factor  $N_c = 3$  for the rates, as shown explicitly in eq.(2.22) below. The present case is formally similar to the leptonic case treated in subsection 2.1, except for a chirality flip in the final fermions. We are especially interested here in final states containing a top-quark, such as  $t\bar{c}$  or  $t\bar{u}$ , for which external particles mass terms cannot obviously be ignored. The equation, analogous to (2.6), which expresses the summations over the initial and final polarizations in the total (tree and loop) amplitude, takes now the form,

$$\sum_{pol} |M_t^{JJ'} + M_l^{JJ'}|^2 = N_c \left[ \left| -\frac{\lambda'_{1J'k} \lambda'^*_{1Jk}}{2(u - m_{d_{kR}}^2)} + \left( \frac{g}{2 \cos \theta_W} \right)^2 \frac{a(e_L) A_L^{JJ'}(u, s + i\epsilon)}{s - m_Z^2 + im_Z \Gamma_Z} \right|^2 \right. \\ \left. \times 16(k \cdot p')(k' \cdot p) + 8m_J m_{J'}(k \cdot k') \varphi_{LR}(\mathcal{L}) \right], \quad (2.22)$$

where  $O(m_e^2)$  terms were ignored and we have denoted,

$$\varphi_{LR}(\mathcal{L}) = + \left( \frac{g}{2 \cos \theta_W} \right)^2 \left( \frac{a(e_L) A_R^{JJ'}(i\epsilon)}{s - m_Z^2 + im_Z \Gamma_Z} \right)^* \left( \frac{\lambda'_{1J'k} \lambda'^*_{1Jk}}{2(u - m_{d_{kR}}^2)} \right) + c. c. \quad (2.23)$$

The modified structure for the kinematical factors in the above up-quarks case, eq.(2.22), in comparison with the leptons and d-quarks case, eq.(2.6), reflects the difference in chiral structure for the RPV tree level amplitude.

In the massless limit for both the initial and final fermions (where helicity,  $h = (-1, +1)$ , and chirality,  $H = (L, R)$ , coincide) the RPV interactions contribute to the helicity amplitudes for the process,  $l^- + l^+ \rightarrow f_J + \bar{f}_{J'}$ , in the mixed type helicity configurations,  $h_{l^-} = -h_{l^+}$ ,  $h_{f_J} = -h_{\bar{f}_{J'}}$ , (same as for the RPC gauge interactions) which are further restricted by the conditions,  $h_{l^-} = -h_{f_J}$ , for leptons and d-quarks production, and  $h_{l^-} = h_{f_J}$ , for up-quarks production. The dependence of the RPV scattering amplitudes on scattering angle has a kinematical factor in the numerator of the form,  $[1 + h_{l^-} h_{f_J} \cos \theta]^2$ . [The parts in our formulas in eqs. (2.22) and (2.6), containing the interference terms between RPV and RPC contributions, partially agree with the published results [40, 41]. We disagree with [40, 41] on the relative signs of RPV and RPC contributions and with [41] on the helicity structure for the up-quarks case. Concerning the latter up-quarks case, our results concur with those reported in a recent study [43].]

The states in the internal loops of the triangle diagrams occur in two distinct  $\mathcal{L}$ -type configurations,  $f = \begin{pmatrix} d_k \\ e_i^c \end{pmatrix}$ ;  $\tilde{f}' = \begin{pmatrix} \tilde{e}_{iL}^* \\ \tilde{d}_{kR} \end{pmatrix}$ . The calculations involved in keeping track of the mass terms are rather tedious. They were performed by means of the mathematica software package, “Tracer” [62] whose results were checked against those obtained by means of “FeynCalc” [63]. The relevant formulas for the vertex functions read :

$$A_L^{JJ'}(\mathcal{L}) = \frac{\lambda'_{iJ'k} \lambda'^*_{iJk}}{(4\pi)^2} \left[ a_L(u) B_1^{(2)} + a(f_L) m_f^2 C_0 + a(\tilde{f}') \left( 2\tilde{C}_{24} + 2m_J^2 (\tilde{C}_{12} - \tilde{C}_{21} + \tilde{C}_{23} - \tilde{C}_{11}) \right) \right. \\ \left. + a(f_R) \left( B_0^{(1)} - 2C_{24} - m_{\tilde{f}'}^2 C_0 + m_J^2 \left( C_0 + 3C_{11} - 2C_{12} + 2C_{21} - 2C_{23} \right) - m_{J'}^2 C_{12} \right) \right], \\ A_R^{JJ'}(\mathcal{L}) = \frac{\lambda'_{iJ'k} \lambda'^*_{iJk}}{(4\pi)^2} m_J m_{J'} \left[ 2a(\tilde{f}') \left( -\tilde{C}_{23} + \tilde{C}_{22} \right) + a(f_R) \left( -C_{11} + C_{12} - 2C_{23} + 2C_{22} \right) \right]. \quad (2.24)$$

The above formulas include an implicit sum over the two allowed configurations for the internal fermion-sfermions, namely,  $a(d_{kH})$ ,  $a(\tilde{e}_{iL}^*)$  and  $a(e_{iH}^c)$ ,  $a(\tilde{d}_{kR})$ . For completeness, we also display the formula expressing the tensorial covariants,

$$\begin{aligned} \Gamma_\mu^Z(p, p')_{\text{tensorial}} &= \frac{\lambda'_{iJ'k} \lambda_{iJk}^*}{(4\pi)^2} i\sigma_{\mu\nu} p^\nu \left[ m_J P_L \left( a(f_R)(C_{11} - C_{12} + C_{21} - C_{23}) \right. \right. \\ &- \left. \left. a(\tilde{f}')(\tilde{C}_{11} + \tilde{C}_{21} - \tilde{C}_{12} - \tilde{C}_{23}) \right) + m_{J'} P_R \left( + a(f_R)(C_{22} - C_{23}) + a(\tilde{f}')(\tilde{C}_{23} - \tilde{C}_{22}) \right) \right]. \end{aligned} \quad (2.25)$$

The complete  $Z f_J \bar{f}_{J'}$  vertex function,  $\Gamma^\mu = \Gamma_{\text{vectorial}}^\mu + \Gamma_{\text{tensorial}}^\mu$ , should (after extracting the external Dirac spinors and the RPV coupling constant factors) be symmetrical under the interchange,  $J \leftrightarrow J'$ , or more specifically, under the interchange,  $m_J \leftrightarrow m_{J'}$ . This property is not explicit on the expressions in eqs. (2.24) and (2.25), but can be established by reexpressing the Lorentz covariants by means of the Gordon identity. The naive use of eq.(2.11) to compute CP-odd asymmetries would seem to yield finite contributions (even in the absence of a CP-odd phase) from the mass terms in the vectorial vertex functions,  $A_L^{JJ'}$ , owing to their lack of symmetry under,  $m_J \leftrightarrow m_{J'}$ . Clearly, this cannot hold true and is an artefact of restricting to the vectorial couplings. Including the tensorial couplings is necessary for a consistent treatment of the contributions depending on the external fermions masses. Nevertheless, we emphasize that the tensorial vertex contributions will not included in our numerical results.

Finally, we add a general comment concerning the photon vertex functions,  $A_{L,R}^{\gamma JJ'}$ , and the way to incorporate the  $\gamma$ -exchange contributions in the total amplitudes, eqs.(2.6) and (2.22). One needs to add terms obtained by substituting,  $\frac{g}{2 \cos \theta_W} \rightarrow \frac{e}{2} = \frac{g \sin \theta_W}{2}$ ,  $a_{L,R}(f) \rightarrow 2Q(f)$ ,  $(s - m_Z^2 + im_Z \Gamma_Z)^{-1} \rightarrow s^{-1}$ , along with the substitution of Z-boson by photon vertex functions,  $A_{L,R}^{JJ'}(\tilde{e}, s + i\epsilon) \rightarrow A_{L,R}^{\gamma JJ'}(\tilde{e}, s + i\epsilon)$ . The substitution which adds in both Z-boson and photon exchange contributions reads explicitly :

$$[a_{R,L}(e) A_{L,R}^{JJ'}] \rightarrow \left[ a_{R,L}(e) \sum_f a(f) C_f + 2Q(e) \sin^2 \theta_W \cos^2 \theta_W [(s - m_Z^2 + im_Z \Gamma_Z)/s] \sum_f 2Q(f) C_f \right],$$

where we have used the schematic representation,  $A_{L,R}^{JJ'} = \sum_f a(f) C_f$ .

## 3 Basic assumptions and results

### 3.1 General context of flavor changing physics

To place the discussion of the RPV effects in perspective, we briefly review the current situation of flavor changing physics. In the standard model, non-diagonal effects with respect to the quarks flavor arise through loop diagrams. The typical structure of one-loop contributions to, say, the  $Z f \bar{f}$  vertex function,  $\sum_i V_{iJ}^* V_{iJ'} I(m_i^{f2}/m_Z^2)$ , involves a summation over quark families of CKM matrices factors times a loop integral. This schematic formula shows explicitly how the CKM matrix unitarity, along with the near quarks masses degeneracies relative to the Z-boson mass scale (valid for all quarks with the exception of the top-quark) strongly suppresses flavor changing effects. Indeed, for the down-quark-antiquark case, the Z-boson decays branching fractions,  $B_{JJ'}$ , were estimated at the values,  $10^{-7}$  for  $(\bar{b}s + \bar{s}b)$ ,  $10^{-9}$  for  $(\bar{b}d + \bar{d}b)$ ,  $10^{-11}$  for  $(\bar{s}d + \bar{d}s)$ , and the

corresponding CP asymmetries,  $\mathcal{A}_{JJ'}$ , at the values,  $[10^{-5}, 10^{-3}, 10^{-1}] \sin \delta_{CKM}$  [48, 49], respectively.

By contrast, flavor changing effects are expected to attain observable levels in several extensions of the standard model. Thus, one to three order of magnitudes can be gained on rates  $B_{JJ'}$  in models accommodating a fourth quark family [48, 49]. For the two Higgs doublets extended standard model, a recent comprehensive study of fermion-antifermion pair production at leptonic colliders [51] quotes for the flavor changing rates,  $B_{JJ'} \approx 10^{-6} - 10^{-8}$  for  $Z \rightarrow (\bar{b} + s) + (\bar{s} + b)$  and  $\sigma_{JJ'} \approx 10^{-5} - 10^{-6} R$ , where,  $R = \sigma(e^+ + e^- \rightarrow \mu^+ + \mu^-) = 4\pi\alpha^2/(3s) = 86.8/(\sqrt{s})^2 \text{fbarns} (TeV)^{-2}$ . Large CP violation signals are also found in the reaction,  $p\bar{p} \rightarrow t\bar{b}X$ , in the two Higgs doublets and supersymmetric models[52].

For the minimal supersymmetric standard model, due to the expected nearness of superpartners masses to  $m_Z$ , flavor changing loop corrections can become threateningly large, unless their contributions are bounded by postulating either a degeneracy of the soft supersymmetry breaking scalars masses parameters or an alignment of the fermion and scalar superpartners current-mass bases transformation matrices. An early calculation of the contribution to Z-boson decay flavor changing rates,  $Z \rightarrow qJ\bar{q}J'$ , induced by radiative corrections from gluino-squark triangle diagrams of squarks flavor mixing, found [53] :  $B_{JJ'} \approx 10^{-5}$ . This result is suspect since a more complete calculation of the effect performed subsequently [54] obtained considerably smaller contributions. Both calculations rely on unrealistic inputs, including a wrong mass for the top-quark and too low values for the superpartners mass parameters. It is hoped that a complete updated study could be soon performed. In fact, during the last few years, the study of loop corrections in extended versions of the standard model has evolved into a streamlined activity. For instance, calculations of loop contributions to the magnetic moment of the  $\tau$ -lepton or of the heavy quarks, such as those reported in [64] (two-Higgs doublets model) or in [65] (minimal supersymmetric standard model) could be usefully transposed to the case of fermion pair production observables.

The information from experimental searches on flavor changing physics at high energy colliders is rather meager [66]. Upper bounds for the leptonic Z-boson branching ratios,  $B_{JJ'}$ , are reported [67] at,  $1.7 \cdot 10^{-6}$  for  $(\bar{e}\mu + \bar{\mu}e)$ ,  $9.8 \cdot 10^{-6}$  for  $(\bar{e}\tau + \bar{\tau}e)$  and  $1.7 \cdot 10^{-5}$  for  $(\bar{\mu}\tau + \bar{\tau}\mu)$ . No results have been quoted so far for  $d$ - or  $u$ - quark pairs production, reflecting the hard experimental problems faced in identifying quarks flavors at high energies. The prospect for experimental measurements at the future leptonic colliders is brightest for cases involving one top-quark owing to the easier kinematical identification offered by the large mass disparity in the final state jets. For leptonic colliders at energies above those of LEP, the reactions involving the production of Higgs or heavy  $Z'$ -gauge bosons which subsequently decay to fermion pairs could be effective sources of flavor non-diagonal effects, especially when a top-quark is produced. At still higher energies, in the TeV regime, the production subprocesses involving collisions of gauge bosons pairs radiated by the incident leptons, as in  $l^- + l^+ \rightarrow W^- + W^+ + \nu + \bar{\nu}$ , could lead to flavor non-diagonal final states, such as,  $\nu + \bar{\nu} + t + \bar{c}$  with rates of order a few fbarns [68].

### 3.2 Choices of parameters and models

Our main assumption in this work is that no other sources besides the R parity odd interactions contribute significantly to the flavor changing rates and CP asymmetries. However, to infer useful information from possible future experimental results, we must deal with two main types of uncertainties. The first concerns the family structure of the coupling constants. On this issue, one can only postulate specific hypotheses or make model-dependent statements. At this point, we may note that the experimental indirect upper bounds on single coupling constants are typically,  $\lambda < 0.05$  or  $\lambda' < 0.05$  times  $\frac{\tilde{m}}{100\text{GeV}}$ , except for three special cases where strong bounds exist :  $\lambda'_{111} < 3.9 \cdot 10^{-4} (\frac{\tilde{m}_g}{100\text{GeV}})^2 (\frac{\tilde{m}_g}{100\text{GeV}})^{\frac{1}{2}}$ , ( $0\nu\beta\beta$ - decay [22])  $\lambda'_{133} < 2 \cdot 10^{-3}$  ( $\nu_e$  mass [21]) and  $\lambda'_{imk} < 2 \cdot 10^{-2} (\frac{m_{\tilde{d}_{kR}}}{100\text{GeV}})$ , [ $i, k = 1, 2, 3; m = 1, 2$ ], ( $K \rightarrow \pi\nu\bar{\nu}$  [17]). Strong bounds have been derived for products of coupling constants pairs in specific family configurations. For instance, a valuable source for the  $\lambda_{ijk}$  coupling constants is provided by the rare decays,  $e_l^- \rightarrow e_m^- + e_n^- + e_p^+$  [19], which probe the combinations of coupling constants,  $F_{abcd} = \sum_i (\frac{100\text{GeV}}{m_{\tilde{\nu}_{iL}}})^2 \lambda_{iab} \lambda_{icd}^*$ . Except for the strong bound,  $F_{1112}^2 + F_{2111}^2 < 4.3 \cdot 10^{-13}$ , [ $\mu \rightarrow 3e$ ] the other combinations of coupling constants involving the third generation are less strongly bound, as for instance,  $F_{1113}^2 + F_{3111}^2 < 3.1 \cdot 10^{-5}$  [ $\tau \rightarrow 3e$ ] [19]. Another useful source is provided by the neutrinoless double beta decay process [23, 22, 24]. The strongest bounds occur for the following configurations of flavour indices (using the reference value  $\tilde{m} = 100\text{GeV}$ ) :  $\lambda'_{113} \lambda'_{131} < 7.9 \times 10^{-8}$ ,  $\lambda'_{112} \lambda'_{121} < 2.3 \times 10^{-6}$ ,  $\lambda'_{111} < 4.6 \times 10^{-5}$ , quoting from [24] where the initial analysis of [23] was updated. Finally, the strongest bounds deduced from neutral mesons ( $B\bar{B}$ ,  $K\bar{K}$ ) mixing parameters are :  $F'_{1311} < 2 \cdot 10^{-5}$ ,  $F'_{1331} < 3.3 \cdot 10^{-8}$ ,  $F'_{1221} < 4.5 \cdot 10^{-9}$ , [19], where  $F'_{abcd} = \sum_i (\frac{100\text{GeV}}{m_{\tilde{\nu}_{iL}}})^2 \lambda'_{iab} \lambda'_{icd}^*$ .

The second type of uncertainties concerns the spectrum of scalar superpartners. At one extreme, are the experimental lower bounds, which reach for sleptons, 40 – 65 GeV, and for squarks, 90 – 200 GeV, and at the other extreme, the theoretical naturalness requirement which sets an upper bound at 1 TeV.

In order to estimate the uncertainties on predictions emanating from the above two sources, it is necessary to delineate the dependence of amplitudes on sfermion masses. Examining the structure of the relevant contributions to flavor changing rates for, say, the lepton case, we note that the t-channel exchange tree amplitudes are given by a onefold summation over sfermions families,  $\sum_i |t_{JJ'}^i|/\tilde{m}_i^2$ , involving the combination of coupling constants,  $t_{JJ'}^i = \lambda_{i1J} \lambda_{i1J'}^*$ . The typical structure for the leptonic loop amplitudes is a twofold summation over fermions and sfermions families,  $\sum_{ij} l_{JJ'}^{ij} F_{JJ'}^{ij}(s + i\epsilon)$ , where  $l_{JJ'}^{ij} = \lambda_{ijJ} \lambda_{ijJ'}^*$ , and the loop integrals,  $F_{JJ'}^{ij}$ , have a non-trivial dependence on the fermions and sfermions masses, as exhibited on the formulas derived in subsections 2.1, 2.2 and 2.3 [see, e.g., eq.(2.20)].

The effective dependence on the superparticle masses involves ratios,  $m_f^2/\tilde{m}^2$  or  $s/\tilde{m}^2$ , in such a way that the dependence is suppressed for large  $\tilde{m}$ . (Obviously,  $s = m_Z^2$  for Z-boson pole observables.) In applications such as ours where,  $s \geq m_Z^2$ , all the fermions, with the exception of the top-quark, can be regarded as being massless. In particular, the first two light families (for either  $l$ ,  $d$ ,  $u$ ) should have comparable contributions, the third family behaving most distinctly in the top-quark case. A quick analysis, taking the explicit mass factors into account, indicates that loop amplitudes should scale with sfermions masses as,  $(s/\tilde{m}^2)^n$ , with a variable exponent ranging in the interval,  $1 < n < 2$ .

Any possible enhancement effect from the explicit sfermions mass factors in eq.(2.20) is moderated in the full result by the fact that the accompanying loop integral factor has itself a power decrease with increasing  $\tilde{m}^2$ . Thus, the Z-boson pole rates should depend on the masses  $\tilde{m}$  roughly as  $(1/\tilde{m}^2)^{2n}$ , while the off Z-boson pole rates, being determined by the tree amplitudes, should behave more nearly as  $(1/\tilde{m}^2)^2$ . As for the asymmetries, since these are given by ratios of squared amplitudes, one expects them to have a weak sensitivity on the sfermion masses.

To infer the physical implications on the RPV coupling constants, we avoid making too detailed model-dependent assumptions on the scalar superpartners spectrum. Thus, we shall neglect mass splittings between all the sfermions and set uniformly all sleptons, sneutrinos and squarks masses at a unique family (species) independent value,  $\tilde{m}$ , chosen to vary in the wide variation interval,  $100 < \tilde{m} < 1000$  GeV. This prescription should suffice for the kind of semi-realistic predictions at which we are aiming. This approximation makes more transparent the dependence on the RPV coupling constants, which then involves the quadratic products designated by  $t_{JJ'}^i$  (tree) and  $l_{JJ'}^{ij}$  (loop), where the dummy family indices refer to sfermions (tree) and fermion-sfermions (loop). For off Z-boson-pole observables, flavor non diagonal rates are controlled by products of two different couplings,  $|t_{JJ'}^i|^2$ , and asymmetries by normalized products of four different couplings,  $Im(t_{JJ'}^{i'\star} l_{JJ'}^{ij})/|t_{JJ'}^{i''}|^2$ . For Z-boson pole observables, rates and asymmetries are again controlled by products of two and four different coupling constants,  $|l_{JJ'}^{ij}|^2$  and  $Im(l_{JJ'}^{i'j'\star} l_{JJ'}^{ij})/|l_{JJ'}^{i''j''}|^2$ , respectively. Let us note that if the off-diagonal rates were dominated by some alternative mechanism, the asymmetries would then involve products of four different coupling constants rather than the above ratio.

It is useful here to set up a catalog of the species and families configurations for the sfermions (tree) or fermion-sfermions (loop) involved in the various cases. In the tree level amplitudes, these configurations are for leptons :  $t_{JJ'}^i = \lambda_{iJ1} \lambda_{iJ'1}^*$ ,  $\tilde{\nu}_{iL}$  ( $\mathcal{L}$ -type),  $t_{JJ'}^i = \lambda_{i1J} \lambda_{i1J'}^*$ ,  $\tilde{\nu}_{iL}$  ( $\mathcal{R}$ -type); for d-quarks,  $t_{JJ'}^j = \lambda'_{1jJ} \lambda'_{1jJ'}^*$ ,  $\tilde{u}_{jL}$  ( $\mathcal{R}$ -type); for u-quarks,  $t_{JJ'}^k = \lambda'_{1Jk} \lambda'_{1J'k}$ ,  $\tilde{d}_{kR}$  ( $\mathcal{L}$ -type). In the loop level amplitudes, the coupling constants and internal fermion-sfermion configurations are for leptons :

$$l_{JJ'}^{jk} = \lambda'_{Jjk}^* \lambda'_{J'jk}, \left[ \begin{pmatrix} d_k \\ \tilde{u}_{jL}^* \end{pmatrix}, \begin{pmatrix} u_j^c \\ \tilde{d}_{kR} \end{pmatrix} \right]; \quad l_{JJ'}^{ik} = \lambda_{iJk}^* \lambda_{iJ'k}, \begin{pmatrix} e_k \\ \tilde{\nu}_{iL}^* \end{pmatrix} \text{ (}\mathcal{L}\text{-type)};$$

$$l_{JJ'}^{ij} = \lambda_{iJj} \lambda_{iJ'j}^*, \left[ \begin{pmatrix} e_j \\ \tilde{\nu}_{iL} \end{pmatrix}, \begin{pmatrix} \nu_i \\ \tilde{e}_{jL} \end{pmatrix} \right] \text{ (}\mathcal{R}\text{-type)};$$

for d-quarks :

$$l_{JJ'}^{ik} = \lambda'_{iJk} \lambda'_{iJ'k}, \left[ \begin{pmatrix} d_k \\ \tilde{\nu}_{iL}^* \end{pmatrix}, \begin{pmatrix} \nu_i^c \\ \tilde{d}_{kR} \end{pmatrix} \right] \text{ (}\mathcal{L}\text{-type)};$$

$$l_{JJ'}^{ij} = \lambda'_{iJj} \lambda'_{iJ'j}, \left[ \begin{pmatrix} d_j \\ \tilde{\nu}_{iL} \end{pmatrix}, \begin{pmatrix} u_j \\ \tilde{e}_{iL} \end{pmatrix}; \quad \begin{pmatrix} \nu_i \\ \tilde{d}_{jL} \end{pmatrix}, \begin{pmatrix} e_i \\ \tilde{u}_{jL} \end{pmatrix} \right] \text{ (}\mathcal{R}\text{-type)};$$

for u-quarks,

$$l_{JJ'}^{ik} = \lambda'_{iJk} \lambda'_{iJ'k}, \left[ \begin{pmatrix} d_k \\ \tilde{e}_{iL}^* \end{pmatrix}, \begin{pmatrix} e_i^c \\ \tilde{d}_{kR} \end{pmatrix} \right] \text{ (}\mathcal{L}\text{-type)}.$$

We shall present numerical results for a subset of the above list of cases. For leptons and d-quarks, we shall restrict consideration to the  $\mathcal{R}$ -type terms which contribute to the Z-boson vertex function,  $A_R$ . We also retain the sleptons-quarks internal states for d-quark production (involving  $\lambda'_{iJj} \lambda'_{iJ'j}$ ) and the sleptons-leptons for lepton production (involving  $\lambda'_{iJj} \lambda'_{iJ'j}$ ). For the up-quark production, we consider the  $\mathcal{L}$ -type terms (involving  $\lambda'_{iJk} \lambda'_{iJ'k}$ ) and, for the off Z-boson pole case, omit the term  $\varphi_{LR}$  in eq.(2.22) in the numerical results.

Since the running family index in the parameters relevant to tree level amplitudes refers to sfermions, consistently with the approximation of a uniform family independent mass spectrum, we may as well consider that index as being fixed. Accordingly, we shall

set these parameters at the reference value,  $t_{JJ'}^i = 10^{-2}$ . In contrast to the off Z-boson pole rates, the asymmetries depend non trivially on the fermion mass spectrum through one of the two family indices in  $l_{JJ'}^{ij}$  ( $i$  or  $j$ ) associated to fermions. To discuss our predictions, rather than going through the list of four distinct coupling constants, we shall make certain general hypotheses regarding the generation dependence of the RPV interactions for the fermionic index. At one extreme is the case where all three generations are treated alike, the other extreme being the case where only one generation dominates. We shall consider three different cases which are distinguished by the interval over which the fermions family indices are allowed to range in the quantities,  $l_{JJ'}^{ij}$ . We define Case **A** by the prescription of equal values for all three families of fermions ( $i = 1, 2, 3$ ); Case **B**, for the second and third families ( $i = 2, 3$ ); and Case **C**, for the third family only ( $i = 3$ ). For all three cases, we set the relevant parameters uniformly at the reference values,  $l_{JJ'}^{ij} = 10^{-2}$ . While the results in Case **C** reflect directly on the situation associated with the hypothesis of dominant third family configurations, the corresponding results in situations where the first or second family are assumed dominant, can be deduced by taking the differences between the results in Cases **A** and **B** and Cases **B** and **C**, respectively.

In order to obtain non-vanishing CP asymmetries, we still need to specify a prescription for introducing a relative CP-odd complex phase, denoted  $\psi$ , between the various RPV coupling constants. We shall set this at the reference value,  $\psi = \pi/2$ . Since the CP asymmetries are proportional to the imaginary part of the phase factor, the requisite dependence is simply reinstated by inserting the overall factor,  $\sin \psi$ . Different prescriptions must be implemented depending on whether one considers observables at or off the Z-boson pole. The Z-boson pole asymmetries are controlled by a relative complex phase between the combinations of coupling constants denoted,  $l_{JJ'}^{ij}$  only. For definiteness, we choose here to assign a non-vanishing complex phase only to the third fermion family, namely,  $\arg(l_{JJ'}^{ij}) = [0, 0, \pi/2]$ , for [ $i$  or  $j = 1, 2, 3$ ]. In fact, a relative phase between light families only would contribute insignificantly to the Z-boson pole asymmetries, because of the antisymmetry in  $\alpha \rightarrow \alpha'$  in eq.(2.9) and the fact that  $F_\alpha^{JJ'}(m_Z^2)$  are approximately equal when the fermion index in  $\alpha = (i, j)$  belongs to the two first families. The off Z-boson pole asymmetries are controlled by a relative complex phase between the tree and loop level amplitudes. For definiteness, we choose here to assign a vanishing argument to the coupling constants combination,  $t_{JJ'}^i$  appearing at tree level and non-vanishing arguments to the full set of loop amplitude combinations, namely,  $\arg(l_{JJ'}^{ij}) = \pi/2$ , where the fermion index ( $i$  or  $j$  as the case may be) varies over the ranges relevant to each of the three cases **A**, **B**, **C**.

### 3.3 Numerical results and discussion

#### Z-boson decays observables

We start by presenting the numerical results for the integrated rates associated with Z-boson decays into fermion pairs. These are given for the d-quarks, leptons and u-quarks cases in Table 3. We observe a fast decrease of rates with increasing values of the mass parameter,  $\tilde{m}$ . Our results can be approximately fitted by a power law dependence which is intermediate between  $\tilde{m}^{-2}$  and  $\tilde{m}^{-3}$ . Explicitly, the Z-boson flavor non diagonal decay rates to d-quarks, leptons and u-quarks, are found to scale approximately as,  $B_{JJ'} \approx (\frac{\lambda_{ijJ}\lambda_{ijJ'}}{0.01})^2 (\frac{100GeV}{\tilde{m}})^{2.5} \times 10^{-9} [5., 1., 2.]$ , respectively. When a top-quark intermediate state



is allowed in the loop amplitude, this dominates over the contributions from the light families. This is clearly seen on the d-quarks results which are somewhat larger than those for up-quarks and significantly larger than those for leptons, the more so for larger  $\tilde{m}$ . This result is explained partly by the color factor, partly by the presence of the top-quark contribution only for the down-quarks case. For contributions involving other intermediate states than up-quarks, whether the internal fermion generation index in the RPV coupling constants,  $\lambda_{ijk}$ , runs over all three generations (Case **A**), the second and third generations (Case **B**) or the third generation only (Case **C**), we find that rates get reduced by factors roughly less than 2 in each of these stages. Therefore, this comparison indicates a certain degree of family independence for the Z-boson branching fractions for the cases where either leptons or d-quarks propagate inside the loops.

Proceeding next to the CP-odd asymmetries, since these are proportional to ratios of the RPV coupling constants, it follows in our prescription of using uniform values for these, that asymmetries must be independent of the specific reference value chosen. As for their dependence on  $\tilde{m}$ , we see on Table 3 that this is rather strong and that the sense of variation with increasing  $\tilde{m}$  corresponds (for absolute values of  $\mathcal{A}_{JJ'}$ ) to a decrease for d-quarks and an increase for u-quarks and leptons. The comparison of different production cases shows that the CP asymmetries are largest,  $O(10^{-1})$ , for d-quarks at small  $\tilde{m} \simeq 100 GeV$ , and for u-quarks at large  $\tilde{m} \simeq 1000 GeV$ . For leptons, the asymmetries are systematically small,  $O(10^{-3} - 10^{-4})$ . The above features are explained by the occurrence for d-quarks production of an intermediate top-quark contribution and also by the larger values of the rates at large  $\tilde{m}$  in this case. The comparison of results in Cases **A** and **B** indicates that the first two light families give roughly equal contributions in all cases.

For Case **C**, the CP-odd asymmetries are vanishingly small, as expected from our prescription of assigning the CP-odd phase, since Case **C** corresponds then to a situation where only single pairs of coupling constants dominate. Recall that for the specific cases considered in the numerical applications, namely,  $\mathcal{R}$ -type for d-quarks and leptons and  $\mathcal{L}$ -type for u-quarks, the relevant products of RPV coupling constants are,  $\lambda_{ijJ'}^* \lambda'_{ijJ}$ ,  $\lambda_{ijJ'}^* \lambda_{ijJ}$ ,  $\lambda_{iJk}^* \lambda'_{iJ'k}$ , respectively, where the fermions generation index amongst the dummy indices pairs,  $(ij)$ ,  $(ik)$ , refers to the third family. Non vanishing contributions to  $\mathcal{A}_{JJ'}$  could arise in Case **C** if one assumed that two pairs of the above coupling constants products with different sfermions indices dominate, and further requiring that these sfermions are not mass degenerate. Another interesting possibility is by assuming that the hypothesis of single pair of RPV coupling constants dominance applies for the fields current basis. Applying then to the quark superfields the transformation matrices relating these to mass basis fields, say, in the distinguished choice [17] where the flavor changing effects bear on u-quarks, amounts to perform the substitution,  $\lambda'_{ijk} \rightarrow \lambda'^B_{ink} V_{nj}^\dagger$ , where  $V$  is the CKM matrix. The CP-odd factor, for the d-quark case, say, acquires then the form,  $Im(l_{JJ'}^{ij*} l_{JJ'}^{ij'}) \rightarrow |\lambda'^B_{inJ'} \lambda'^{B*}_{imJ}|^2 Im((V^\dagger)_{nj} (V^\dagger)_{mj}^* (V^\dagger)_{nj'}^* (V^\dagger)_{mj'})$ , where the second factor on the right-hand side is recognized as the familiar plaquette term, proportional to the products of sines of all the CKM rotation angles times that of the CP-odd phase.

It may be useful to examine the bounds on the RPV coupling constants implied by the current experimental limits on the flavor non diagonal leptonic widths [67],  $B_{JJ'}^{exp} < [1.7, 9.8, 17.] 10^{-6}$  for the family couples,  $[JJ' = 12, 23, 13]$ . The contributions associated with the  $\lambda$  interactions can be directly deduced from the results in Table 3. Choosing the

value,  $\tilde{m} = 100$  GeV, and writing our numerical result as,  $B_{JJ'} \approx (\frac{\lambda_{ijJ}\lambda_{ijJ'}^*}{0.01})^2 4 \cdot 10^{-9}$ , then under the hypothesis of a pair of dominant coupling constants, one deduces,  $\lambda_{ijJ}\lambda_{ijJ'}^* < [0.46, 1.1, 1.4]$ , for all fixed choices of the family couples,  $i, j$ . (An extra factor 2 in  $B_{JJ'}$  has been included to account for the antisymmetry property of  $\lambda_{ijk}$ .) For the  $\lambda'$  interactions, stronger bounds obtain because of the extra color factor and of the internal top-quark contributions. A numerical calculation (not reported in Table 3) performed with the choice,  $\tilde{m} = 100\text{GeV}$  for Case **C**, gives us :  $B_{JJ'} \approx (\frac{\lambda_{Jjk}^*\lambda'_{J'jk}}{0.01})^2 1.17 \cdot 10^{-7}$ , which, by comparison with the experimental limits, yields the bounds :  $\lambda_{Jjk}^*\lambda'_{J'jk} < [0.38, 0.91, 1.2]10^{-1}$ , for the same family configurations,  $[J J' = 12, 23, 13]$ , as above. These results agree in size to within a factor of 2 with results reported in a recently published work [69].

## Fermion anti-fermion pair production rates

Let us now proceed to the off Z-boson pole observables. The numerical results for the flavor non-diagonal integrated cross sections and CP asymmetries are shown in Table 3 for two selected values of the center of mass energy,  $\sqrt{s} = 200$  and  $500$  GeV. The numerical results displaying the variation of these observables with the center of mass of energy (fixed  $\tilde{m}$ ) and with the superpartners mass parameter (fixed  $\sqrt{s}$ ) are given in Fig.4 and Fig.5, respectively. All the results presented in this work include both photon and Z-boson exchange contributions. We observe here that the predictions for asymmetries are sensitive to the interference effects between photon and Z-boson exchange contributions.

We discuss first the predictions for flavor non diagonal rates. We observe a strong decrease with increasing values of  $\tilde{m}$  and a slow decrease with increasing values of  $\sqrt{s}$ . Following a rapid initial rise at threshold, the rates settle at values ranging between  $(10 - 10^{-1})$  fbarns for a wide interval of  $\tilde{m}$  values. The dependence on  $\tilde{m}$  can be approximately represented as,  $\sigma_{JJ'}/[|\frac{t_{JJ'}}{0.01}|^2(\frac{100}{\tilde{m}})^2 - 3] \approx (1 - 10) \text{ fbarns} \approx R(\frac{\sqrt{s}}{(1 \text{ TeV})})^2(10^{-1} - 1)$ . The rate of decrease of  $\sigma_{JJ'}$  with  $\tilde{m}$  slows down with increasing  $s$ . It is interesting to note that if we had considered here constant values of the product  $\lambda (\tilde{m}/100\text{GeV})$ , rather than constant values of  $\lambda$ , the power dependence of rates on  $\tilde{m}$  would be such as to lead to interestingly enhanced rates at large  $\tilde{m}$ .

The marked differences exhibited by the results for lepton pair production, apparent on windows (c) and (d) in Figures 4 and 5 are due to our deliberate choice of adding the s-channel  $\tilde{\nu}$  pole term for the lepton case while omitting it for the d-quark case. The larger rates found for leptons as compared to d-quarks, in spite of the extra color factor present for d-quarks (recall that the  $l^+l^- \rightarrow f_J\bar{f}_{J'}$  reactions rates for down-quarks and up-quarks pick up an extra color factor  $N_c$  with respect to those for leptons) is thus explained by the strong enhancement induced by adding in the sneutrino exchange contribution. This choice was made here for illustrative purposes, setting for orientation the relevant coupling constant at the value,  $\lambda_{1JJ'} = 0.1$ . The  $\tilde{\nu}$  propagator pole was smoothed out by employing the familiar shifted propagator prescription,  $(s - m_{\tilde{\nu}}^2 + im_{\tilde{\nu}}\Gamma_{\tilde{\nu}})^{-1}$ , while describing approximately the sneutrinos decay width in terms of the RPV contributions alone, namely,  $\Gamma(\tilde{\nu}_i \rightarrow l_k^- + l_j^+) = \frac{\lambda_{ijk}^2\tilde{m}_i}{16\pi}$  and  $\Gamma(\tilde{\nu}_i \rightarrow d_k + \bar{d}_j) = N_c \frac{\lambda_{ijk}^2\tilde{m}_i}{16\pi}$ .

Proceeding next to the CP-odd asymmetries, we note that since these scale as a function of the RPV coupling constants as,  $Im(t_{JJ'}^{ij}t_{JJ'}^{i'j'\star})/|t_{JJ'}^{i''}|^2$ , our present predictions are independent of the uniform reference value assigned to these coupling constants. If the

generational dependence of the RPV coupling constants were to exhibit strong hierarchies, this peculiar rational dependence could induce strong suppression or enhancement factors.

The cusps in the dependence of  $\mathcal{A}_{JJ'}$  on  $\sqrt{s}$  (Fig. 4) occur at values of the center of mass energy where one crosses thresholds for fermion-antifermion (for the energies under consideration,  $t\bar{t}$ ) pair production,  $\sqrt{s} = 2m_f$ , and scalar superpartners pair production,  $\sqrt{s} = 2\tilde{m}$ . These are the thresholds for the processes,  $l^- + l^+ \rightarrow f\bar{f}$  or  $l^- + l^+ \rightarrow \tilde{f}'\tilde{f}'^*$ , at which the associated loop amplitudes acquire finite imaginary parts. Correspondingly, in the dependence of  $\mathcal{A}_{JJ'}$  on  $\tilde{m}$  (Fig. 5) the cusps appear at  $\tilde{m} = \sqrt{s}/2$ . We note on the results that the  $t\bar{t}$  contributions act to suppress the asymmetries whereas the  $\tilde{f}'\tilde{f}'^*$  contributions rather act to enhance them. Sufficiently beyond these two-particle thresholds, the asymmetries vary weakly with  $\tilde{m}$ . A more rapid variation as a function of energy occurs in the leptons production case due to the addition there of the sneutrino pole contribution.

The comparison of results for asymmetries in Cases **A**, **B**, **C** reflects on the dependence of loop integrals with respect to the internal fermions masses. An examination of Table 3 reveals that for leptons and up-quarks, where intermediate states involve leptons or d-quarks, all three families have nearly equal contributions. The results for down-quarks production are enhanced because of the intermediate top-quark contribution, which dominates over that of lighter families. However, this effect is depleted when the finite imaginary part from  $t\bar{t}$  sets in. The asymmetries for up-quarks production assume values in the range,  $10^{-2} - 10^{-3}$ , irrespective of the fact that the final fermions belong to light or heavy families.

## 4 Conclusions

The two-body production at high energy leptonic colliders of fermion pairs of different families could provide valuable information on the flavor structure of the R parity odd Yukawa interactions. One can only wish that an experimental identification of lepton and quark flavors at high energies becomes accessible in the future. Although the supersymmetric loop corrections to these processes may not be as strongly suppressed as their standard model counterparts, one expects that the degeneracy or alignment constraints on the scalar superpartners masses and flavor mixing should severely bound their contributions. Systematic studies of the supersymmetry corrections to the flavor changing rates and CP asymmetries in fermion pair production should be strongly encouraged.

An important characteristic of the R parity odd interactions is that they can contribute to integrated rates at tree level and to CP asymmetries through interference terms between the tree and loop amplitudes. While we have restricted ourselves to the subset of loop contributions associated with Z-boson exchange, a large number of contributions, involving quark-sleptons or lepton-squarks intermediate states in various families configurations, could still occur. The contributions to rates and asymmetries depend strongly on the values of the R parity odd coupling constants. Only the rates are directly sensitive to the supersymmetry breaking scale. To circumvent the uncertainties from the particles spectrum, we have resorted to the simplifying assumption that the scalar superpartners mass differences and mixings can be neglected. We have set the RPV coupling constants at a uniform value while sampling a set of cases from which one might reconstruct the family dependence of the RPV coupling constants. We have also embedded a CP complex phase in the RPV coupling constants in a specific way, meant to serve mainly as an

illustrative example. Although the representative cases that we have considered represent a small fraction of the host of possible variations, they give a fair idea of the sizes to expect. Since these processes cover a wide range of family configurations, one optimistic possibility could be that one specific entry for the family configurations would enter with a sizeable RPV coupling constant.

The contributions to the flavor changing rates have a strong sensitivity on the RPV coupling constants and the superpartners mass, involving high powers of these parameters. We find a generic dependence for the flavor changing Z-boson decay branching ratios of form,  $(\frac{\lambda\lambda}{0.01})^2 (\frac{100}{\tilde{m}})^{2.5} 10^{-9}$ . For the typical bounds on the RPV coupling constants, it appears that these branchings are three order of magnitudes below the current experimental sensitivity. At higher energies, the flavor changing rates are in order of magnitude,  $(\frac{\lambda\lambda}{0.01})^2 (\frac{100}{\tilde{m}})^{2-3} (1-10)$  fbarns. Given the size for the typical integrated luminosity,  $\mathcal{L} = 50 fb^{-1}/\text{year}$ , anticipated at the future leptonic machines, one can be moderately optimistic on the observation of clear signals.

The Z-boson pole CP-odd asymmetries are of order,  $(10^{-1} - 10^{-3}) \sin \psi$ . For the off Z-boson pole reactions, a CP-odd phase,  $\psi$ , embedded in the RPV coupling constants shows up in asymmetries with reduced strength,  $(10^{-2} - 10^{-3}) \sin \psi$  for leptons, d-quarks and u-quarks. The largely unknown structure of the RPV coupling constants in flavor space leaves room for good or bad surprises, since the peculiar rational dependence on the coupling constants,  $Im(\lambda\lambda^*\lambda\lambda^*)/\lambda^4$ , and similarly with  $\lambda \rightarrow \lambda'$ , may lead to strong enhancement or suppression factors.

	Z-pole				Off Z-pole			
	$\tilde{m} = 100$		$\tilde{m} = 1000$		$\tilde{m} = 100$		$\tilde{m} = 1000$	
	$B_{JJ'}$	$\mathcal{A}_{JJ'}$	$B_{JJ'}$	$\mathcal{A}_{JJ'}$	$\sigma_{JJ'}$	$\mathcal{A}_{JJ'}$	$\sigma_{JJ'}$	$\mathcal{A}_{JJ'}$
<b>d<sub>J</sub>d<sub>J'</sub></b>								
<b>A</b>	$5.6d - 9$	0.38	$4.2d - 11$	0.068	11.5 3.62	$-5.50d - 3$ $-2.90d - 3$	$1.46d - 2$ $6.90d - 2$	$-5.72d - 3$ $+3.17d - 3$
<b>B</b>	$4.68d - 9$	0.20	$4.12d - 11$	0.034	11.5 3.62	$-6.80d - 3$ $-3.47d - 4$	$1.46d - 2$ $6.90d - 2$	$-7.14d - 3$ $+1.32d - 3$
<b>C</b>	$3.8d - 9$	0.0	$3.98d - 11$	0.0	11.5 3.62	$-8.11d - 3$ $+2.20d - 3$	$1.46d - 2$ $6.90d - 2$	$-8.55d - 3$ $-5.18d - 4$
<b>l<sub>J</sub>l<sub>J'</sub><sup>+</sup></b>								
<b>A</b>	$3.2d - 9$	$-0.44d - 3$	$3.6d - 12$	0.049	38.2 4.57	$-1.18d - 3$ $-6.90d - 3$	$3.84d - 2$ $3.67d - 1$	$-1.61d - 3$ $-1.04d - 3$
<b>B</b>	$1.3d - 9$	$-0.55d - 3$	$1.5d - 12$	$-0.54d - 3$	38.2 4.57	$-7.90d - 4$ $-4.60d - 3$	$3.84d - 2$ $3.67d - 1$	$-1.08d - 3$ $-6.93d - 3$
<b>C</b>	$6.53d - 10$	0.0	$7.5d - 13$	0.0	38.2 4.57	$-3.95d - 4$ $-2.30d - 3$	$3.84d - 2$ $3.67d - 1$	$-5.38d - 4$ $-3.46d - 4$
<b>u<math>\bar{c}</math></b>								
<b>A</b>	$6.5d - 9$	$-0.69d - 3$	$8.9d - 12$	$-0.12$	11.5 3.62	$2.63d - 3$ $1.04d - 2$	$1.46d - 2$ $6.90d - 2$	$2.96d - 3$ $6.62d - 3$
<b>B</b>	$2.56d - 9$	$-0.89d - 3$	$3.8d - 12$	$-0.11$	11.5 3.62	$1.76d - 3$ $6.93d - 3$	$1.46d - 2$ $6.90d - 2$	$1.98d - 3$ $4.42d - 3$
<b>C</b>	$1.26d - 9$	0.0	$1.95d - 12$	0.0	11.5 3.62	$8.90d - 4$ $3.47d - 3$	$1.46d - 2$ $6.90d - 2$	$1.00d - 3$ $2.21d - 3$
<b>t<math>\bar{c}</math></b>								
<b>A</b>					5.66 4.29	$2.15d - 3$ $7.02d - 3$	$1.60d - 3$ $5.95d - 2$	$3.31d - 3$ $6.56d - 3$
<b>B</b>					5.66 4.29	$1.43d - 3$ $4.68d - 3$	$1.60d - 3$ $5.95d - 2$	$2.22d - 3$ $4.38d - 3$
<b>C</b>					5.66 4.29	$7.22d - 4$ $2.34d - 3$	$1.60d - 3$ $5.95d - 2$	$1.13d - 3$ $2.19d - 3$

FIG. 3: Flavor changing rates and CP asymmetries for d-quarks, leptons and u-quarks pair production in the three cases, appearing in line entries as Cases **A**, **B** and **C**, which correspond to internal lines belonging to all three families, the second and third families and the third family, respectively. The results for d-quarks and leptons, unlike those for up-quarks, are obtained in the approximation where one neglects the final fermions masses. The first four column fields (Z-pole column entry) show results for the Z-boson pole branching fractions  $B_{JJ'}$  and asymmetries,  $\mathcal{A}_{JJ'}$ . The last four column fields (off Z-pole column entry) show results for the flavor non-diagonal cross sections,  $\sigma_{JJ'}$ , in fbarns and for the asymmetries,  $\mathcal{A}_{JJ'}$ , with photon and Z-boson exchanges added in. The results in the two lines for the off Z-boson pole are associated to the two values for the center of mass energy,  $s^{1/2} = 200, 500$  GeV. The columns subentries indicated by  $\tilde{m}$  correspond to the sfermions mass parameter,  $\tilde{m} = 100, 1000$  GeV. The notation  $d - n$  stands for  $10^{-n}$ .

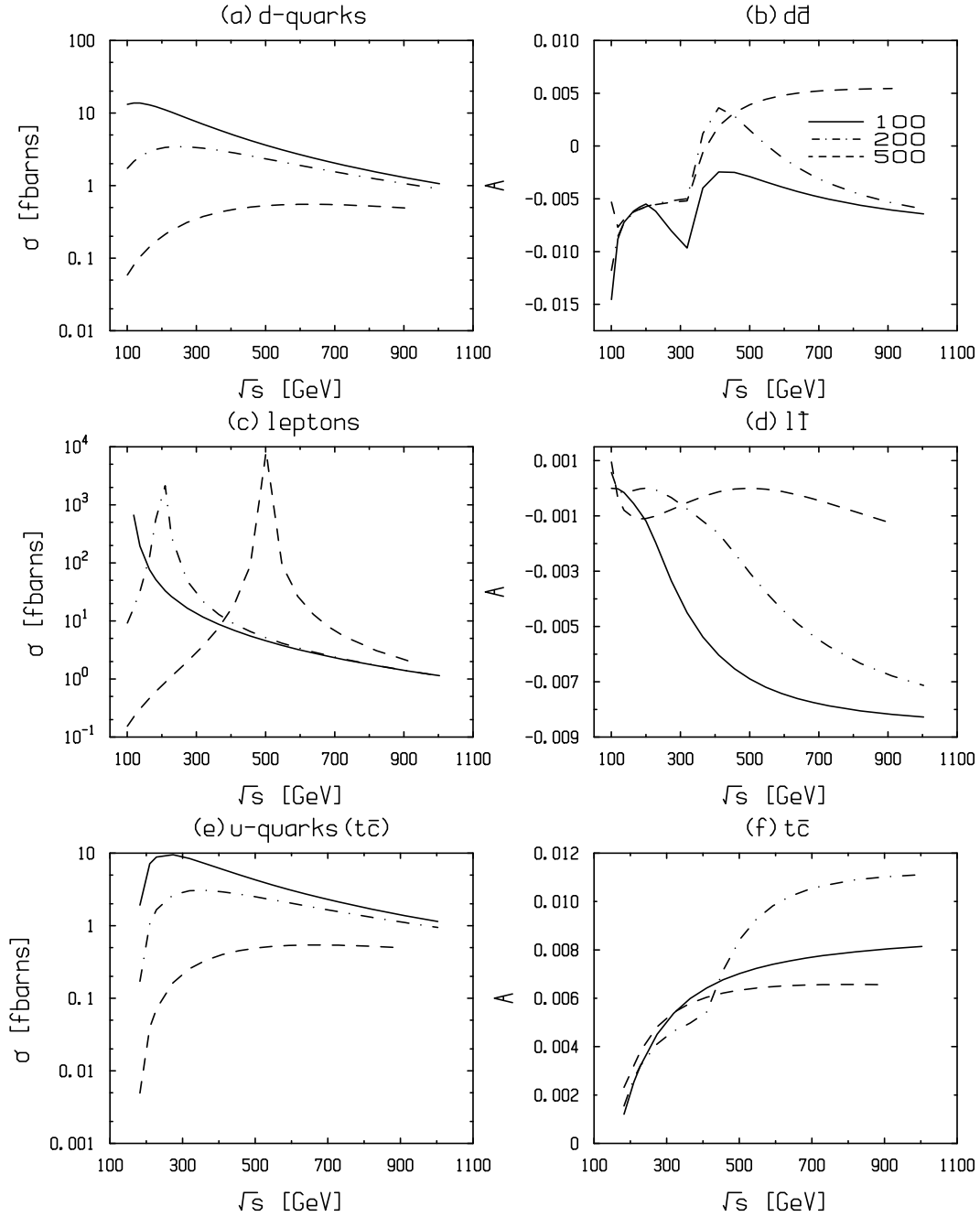


FIG. 4: Integrated flavor non-diagonal cross sections (left hand side windows) and asymmetries (right hand side windows) as functions of the center of mass energy in the production of down-quark-antiquark pairs (two upper figures (a) and (b)), lepton-antilepton pairs (two intermediate figures (c) and (d)) and up-quark-antiquark pairs of type  $\bar{t}c + c\bar{t}$  (two lower figures (e) and (f)). The tree level amplitude includes only the t-channel contribution for the d-quark case, both t- and s-channel exchange contributions for the lepton case, and the u-channel exchange for the up-quark case. The one-loop amplitudes, with both Z-boson and photon exchange contributions, include all three internal fermion generations, corresponding to Case A. Three choices for the superpartners uniform mass parameter,  $\tilde{m}$ , are considered :  $100\text{GeV}$  (continuous lines),  $200\text{GeV}$  (dashed-dotted lines),  $500\text{GeV}$  (dashed lines).

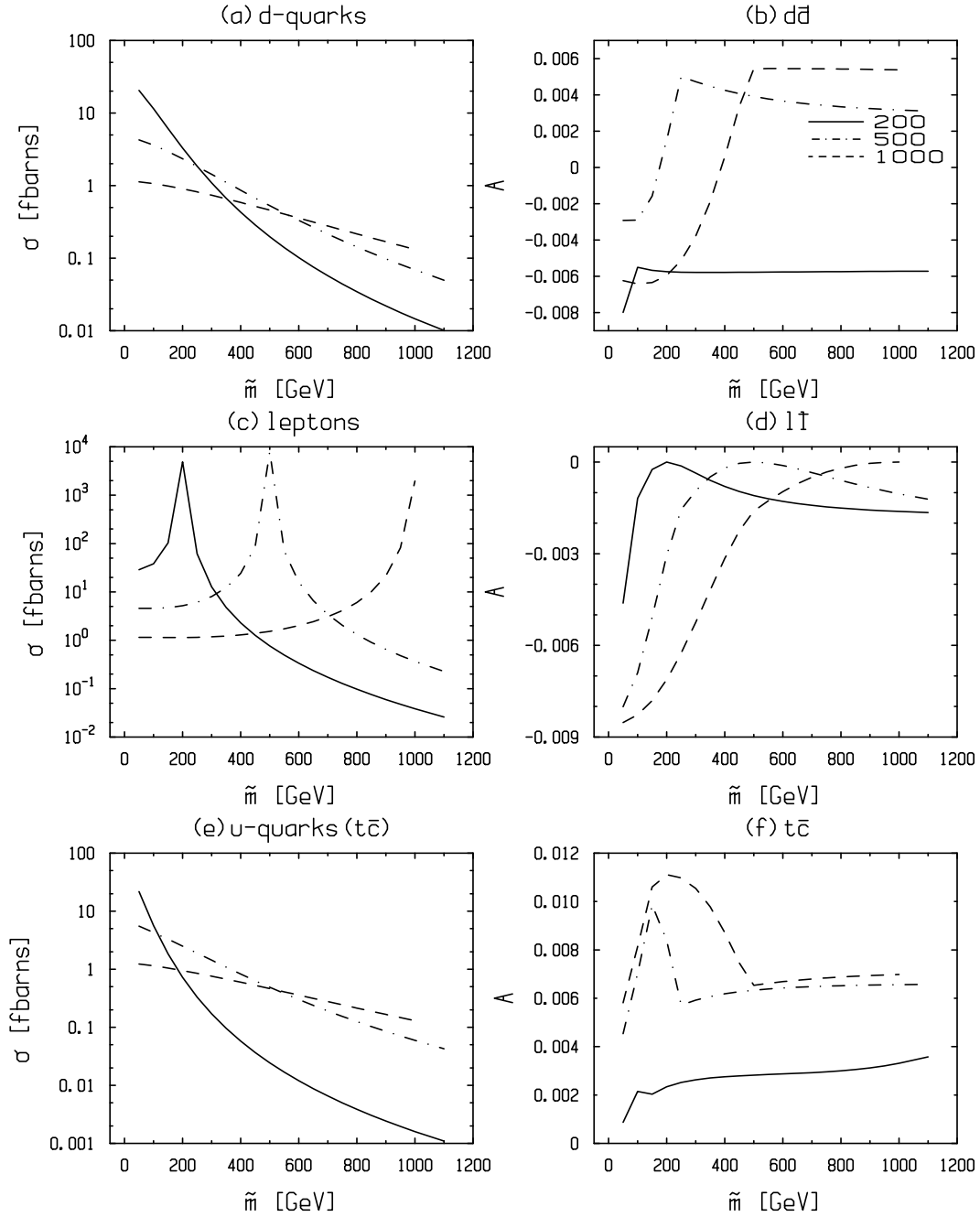


FIG. 5: Integrated flavor non-diagonal cross sections (left hand side windows) and CP-odd asymmetries (right hand side windows) as functions of the scalar superpartners mass parameter,  $\tilde{m}$ , in the production of down-quark-antiquark pairs (two upper figures (a) and (b)), lepton-antilepton pairs (two intermediate figures (c) and (d)) and up-quark-antiquark pairs of type  $\bar{t}c$  or  $\bar{c}t$  (two lower figures (e) and (f)). The tree level amplitude includes only the t-channel contribution for the d-quark case, both t- and s-channel exchange contributions for the lepton case, and the u-channel exchange for the up-quark case. The one-loop amplitudes, with both photon and Z-boson exchange contributions, include all three internal fermions generations, corresponding to Case **A**, with three families running inside loops. Three choices for the center of mass energy,  $s^{1/2}$ , are considered : 200 GeV (continuous lines), 500 GeV (dashed-dotted lines), 1000 GeV (dashed lines).

# References

- [1] C. Aulakh and R. Mohapatra, Phys. Lett. **B119**, 136 (1983)
- [2] F. Zwirner, Phys. Lett. **B132**, 103 (1983)
- [3] L. Hall and M. Suzuki, Nucl. Phys. **B231**, 419 (1984)
- [4] I.H. Lee, Nucl. Phys. **B246**, 120 (1984)
- [5] J. Ellis, G. Gelmini, C. Jarlskog, G. G. Ross and J. W. F. Valle, Phys. Lett. **B150**, 142 (1985)
- [6] G. G. Ross and J. W. F. Valle, Phys. Lett. **B151**, 375 (1985)
- [7] S. Dawson, Nucl. Phys. **B261**, 297 (1985)
- [8] R. Barbieri and A. Masiero, Nucl. Phys. **B267**, 679 (1986)
- [9] S. Dimopoulos and L. J. Hall, Phys. Lett. **B207**, 210 (1988)
- [10] V. Barger, G.F. Giudice and T. Han, Phys. Rev. **D40**, 2987 (1989)
- [11] H. Dreiner and G. G. Ross, Nucl. Phys. **B365**, 591 (1991)
- [12] L. Ibáñez and G. G. Ross, Phys. Lett. **B260**, 291 (1991); Nucl. Phys. **B368**, 3 (1992)
- [13] I. Hinchliffe and T. Kaeding, Phys. Rev. **D47**, 279 (1993)
- [14] R. Mohapatra, Prog. Part. Nucl. Phys. **31**, 39 (1993)
- [15] G. Bhattacharyya, Susy '96, Nucl. Phys. B (Proc. Suppl.) **52A**, 83 (1997)
- [16] H. Dreiner, hep-ph/9707435
- [17] K. Agashe and M. Graesser, Phys. Rev. **D54**, 4445 (1996)
- [18] J. Ellis, S. Lola and G. G. Ross, CERN-TH/97-205, hep-ph/9803308
- [19] D. Choudhury and P. Roy, Phys. Lett. **B378**, 153 (1996)
- [20] J. E. Kim, P. Ko and D.-G. Lee, Phys. Rev. **D56**, 100 (1997)
- [21] R. M. Godbole, R. P. Roy and X. Tata, Nucl. Phys. **B401**, 67 (1993)
- [22] M. Hirsch, H. V. Klapdor-Kleingrothaus and S. G. Kovalenko, Phys. Rev. Lett. **75**, 17 (1995); ibidem, Phys. Rev. **D53**, 1329 (1996); ibidem, Susy '96 Nucl. Phys. B (Proc. Suppl.) **52A**, 257 (1997)
- [23] K. S. Babu and R. N. Mohapatra, Phys. Rev. Lett. **75**, 2276 (1995)
- [24] M. Hirsch and H. V. Klapdor-Kleingrothaus, Susy '97 Nucl. Phys. B (Proc. Suppl.) **62**, 224 (1998)
- [25] A. Yu. Smirnov and F. Vissani, Phys. Lett. **B380**, 317 (1996)
- [26] C. E. Carlson, P. Roy and M. Sher, Phys. Lett. **B357**, 95 (1995)



- [27] J. L. Goity and M. Sher, Phys. Lett. **B346**, 69 (1995)
- [28] Y. Grossman and M. P. Worah, Phys. Lett. **B395**, 241 (1997)
- [29] D. E. Kaplan, “Violating R parity at the B factory”, hep-ph/9703347
- [30] S. Abel, Phys. Lett. **B410**, 173 (1997)
- [31] D. Guetta, WIS-98/9/May-DPP, hep-ph/9805274
- [32] Ji-Ho Jang and Jae Sik Lee, KAIST-TH 98/12, hep-ph/9808406
- [33] C. H. Chen, C. Q. Geng and C. C. Lih, Phys. Rev. **D56**, 6856 (1997)
- [34] R. Adhikari and U. Sarkar, Phys. Lett. **B427**, 59 (1998)
- [35] S. Bar-Shalom, G. Eilam and A. Soni, Phys. Rev. Lett. **80**, 4629 (1998)
- [36] S. Bar-Shalom, G. Eilam and A. Soni, hep-ph/9804339
- [37] T. Handoko and J. Hashida, Phys. Rev. **D58**, 094008 (1998)
- [38] M. Frank and H. Hamidian, hep-ph/9706510
- [39] D. Choudhury, Phys. Lett. **B376**, 201 (1996)
- [40] J. Kalinowski, R. Rückl, H. Spiesberger and P.M. Zerwas, Phys. Lett. **B406**, 314 (1997)
- [41] J. Kalinowski, R. Rückl, H. Spiesberger and P.M. Zerwas, Phys. Lett. **B414**, 297 (1997)
- [42] J. Kalinowski, Acta. Phys. Polon. **B28**, 2423 (1997)
- [43] V. Mahanta and A. Ghosal, Phys. Rev. **D57**, 1735 (1998)
- [44] J. Bernabéu and M. B. Gavela, in “CP violation” ed. C. Jarlskog (World Scientific, Singapore, 1988); D. Chang, Workshop on physics at current accelerators and super-colliders, (June 2-5, 1993, Argonne Nat. Lab.); A. Soni, Nucl. Phys. B (Proc. Suppl.) **51A** (1996) 32
- [45] A. Axelrod, Nucl. Phys. **B209**, 349 (1982); E. Ma and A. Pramudita, Phys. Rev. **D22**, 214 (1980)
- [46] M. Clements, C. Footman, A. Kronfeld, S. Narasimhan and D. Fotiadis, Phys. Rev. **D27**, 570 (1983)
- [47] V. Ganapathi, T. Weiler, E. Laermann, I. S. Schmidt and P. M. Zerwas, Phys. Rev. **D27**, 579 (1983)
- [48] J. Bernabéu, A. Santamaria and M.B. Gavela, Phys. Rev. Lett. **57**, 1514 (1986)
- [49] W.-S. Hou, N.G. Deshpande, G. Eilam and A. Soni, Phys. Rev. Lett. **57**, 1406 (1986)
- [50] G. Eilam, J. L. Hewett and A. Soni, Phys. Rev. Lett. **67**, 1979 (1991); B. Grzadkowski, J. F. Gunion and P. Krawczyk, Phys. Lett. **B268**, 106 (1991)
- [51] D. Atwood, L. Reina and A. Soni, Phys. Rev. **D53**, 1199 (1996); ibidem **D55**, 3157 (1997)
- [52] D. Atwood, S. Bar-Shalom, G. Eilam and A. Soni, Phys. Rev. **D54**, 5412 (1996)
- [53] M. J. Duncan, Phys. Rev. **D31**, 1139 (1985)
- [54] B. Mukhopadhyaya and A. Raychaudhuri, Phys. Rev. **D39**, 280 (1989)
- [55] G. 't Hooft and M. Veltman, Nucl. Phys. **B153**, 365 (1979)

- [56] G. Passarino and M. Veltman, Nucl. Phys. **B160**, 151 (1979)
- [57] G. Bhattacharyya, J. Ellis and K. Sridhar, Mod. Phys. Letters, **A10**, 1583 (1995)
- [58] G. Bhattacharyya, D. Choudhury and K. Sridhar, Phys. Lett. **B355**, 193 (1995)
- [59] H.E. Haber and G.L. Kane, Phys. Rep. **117**, 175 (1985)
- [60] M. E. Peskin and D. V. Schroeder, An Introduction to Quantum Field Theory (Addison-Wesley Publishing Company, 1995)
- [61] J. M. Soares and A. Barroso, Phys. Rev. **D39**, 1973 (1989)
- [62] M. Jamin and M. E. Lauterbacher, Comput. Phys. Comm. **B74**, 265 (1993)
- [63] R. Mertig, M. Böhm and A. Denner, Comput. Phys. Comm. **B64**, 345 (1991)
- [64] J. Bernabéu, D. Comelli, L. Lavoura and J. P. Silva, Phys. Rev. **D53**, 5222 (1996)
- [65] W. Hollik, J. I. Illana, S. Rigolin and D. Stöckinger, Phys. Lett. **B416**, 345 (1998)
- [66] M. Z. Akrawy et al., (OPAL Collaboration) **B254**, 293 (1991) ; M. Davier, Joint Intl. Lepton-Photon Symposium and Europhysics Conf. on High Energy Physics, Geneva, Switzerland (1991), eds. S. Hegarty, K. Potter and E. Quercigh, (World Scientific, 1992, Singapore)
- [67] Particle Data Group, *Tests of Conservation Laws*, Phys. Rev. **D54**, 60 (1996)
- [68] S. Bar-Shalom, G. Eilam, A. Soni and J. Wudka, Phys. Rev. Lett. **79**, 1217 (1997) ; W.-S. Hou, G.-L. Lin and C.-Y. Ma, Phys. Rev. **D56**, 7434 (1997)
- [69] M. Anwar Mughal, M. Sadiq and K. Ahmed, Phys. Lett. **B417**, 87 (1998)





# Publication VIII



# Polarized single top production at leptonic colliders from broken R parity interactions incorporating CP violation

M. Chemtob, G. Moreau

*Service de Physique Théorique  
CE-Saclay F-91191 Gif-sur-Yvette, Cedex France*

Phys. Rev. **D61** (2000) 116004, hep-ph/9910543

## Abstract

*The contribution from the R parity violating interaction,  $\lambda'_{ijk} L_i Q_j D_k^c$ , in the associated production of a top quark (antiquark) with a charm antiquark (quark) is examined for high energy leptonic colliders. We concentrate on the reaction,  $l^- + l^+ \rightarrow (t\bar{c}) + (c\bar{t}) \rightarrow (b\bar{l}\nu\bar{c}) + (\bar{b}l\nu c)$ , associated with the semileptonic top decay. A set of characteristic dynamical distributions for the signal events is evaluated and the results contrasted against those from the standard model W-boson pair production background. The sensitivity to parameters (R parity violating coupling constants and down-squark mass) is studied at the energies of the CERN LEP-II collider and the future linear colliders. Next, we turn to a study of a CP-odd observable, associated with the top spin, which leads to an asymmetry in the energy distribution of the emitted charged leptons for the pair of CP-conjugate final states,  $b\bar{l}\nu\bar{c}$  and  $\bar{b}l\nu c$ . A non vanishing asymmetry arises from a CP-odd phase, embedded in the R parity violating coupling constants, through interference terms between the R parity violating amplitudes at both the tree and loop levels. The one-loop amplitude is restricted to the contributions from vertex corrections to the photon and Z-boson exchange diagram. We predict unpolarized and polarized rate asymmetries of order  $O(10^{-3}) - O(10^{-2})$ . An order of magnitude enhancement may be possible, should the R parity violating coupling constants  $\lambda'_{ijk}$  exhibit a hierarchical structure in the quarks and leptons generation spaces.*

# 1 Introduction

The flavor non diagonal fermion-antifermion pair production,  $l^-l^+ \rightarrow f_J\bar{f}_{J'}$ , where  $J \neq J'$  are flavor labels, represents a class of reactions where the high energy colliders could contribute their own share in probing new physics incorporating flavor changing and/or CP violation effects. As is known, the standard model contributions here are known to be exceedingly small, whereas promising contributions are generally expected in the standard model extensions. (Consult ref. [1] for a survey of the literature.) Of special interest is the case where a top quark (antiquark) is produced in association with a lighter (charm or up) antiquark (quark). The large top mass entails a top lifetime,  $\tau_{top} = [1.56 \text{ GeV}(\frac{m_t}{180 \text{ GeV}})^3]^{-1}$ , significantly shorter than the QCD hadronization time,  $1/\Lambda_{QCD}$ , which simplifies the task of jet reconstruction. [2] The top polarization effects also constitute a major attraction. [3, 4, 5, 6, 7] The large top mass entails a spin depolarization time of the top which is longer than its lifetime,  $\tau_{depol} = [1.7 \text{ MeV}(\frac{180}{m_t})]^{-1} > \tau_{top}$ , thus providing an easy access to top polarization observables. Polarization studies for the top-antitop pair production reaction, in both production and decay, have been actively pursued in recent years. [8, 9, 10] (An extensive literature can be consulted from these references.)

It appears worthwhile applying similar ideas to the flavor non diagonal fermion pair production process involving a single top production. This reaction has motivated several theoretical studies aimed at both leptonic ( $l^-l^+$ ,  $e\gamma$  and  $\gamma\gamma$ ) and hadronic ( $p\bar{p}$ ,  $pp$ ) colliders. Exploratory theoretical studies have been pursued at an implicit level, via the consideration of higher dimension contact interactions [11, 12, 13], and at an explicit level, via the consideration of mechanisms involving leptoquarks, [14] an extended Higgs doublet sector, [15, 16] supersymmetry based on the minimal supersymmetric standard model with an approximately broken R parity, [1, 17, 18, 19, 20] quark flavor mixing, [21] standard model loops and four matter generations, [22, 23] or higher order standard model processes with multiparticle final states,  $l^-l^+ \rightarrow t\bar{c}\nu\bar{\nu}$ . [24] A survey of the current studies is provided in ref.[12].

In this work, pursuing an effort started in our previous paper, [1] we consider a test of the R parity violating (RPV) interactions aimed at the top-charm associated production. Our study will focus on the contributions to the process,  $l^-l^+ \rightarrow (t\bar{c}) + (\bar{t}c)$ , arising at the tree level from the trilinear RPV interactions,  $\lambda'_{ijk}L_iQ_jD_k^c$ , via a  $\bar{d}_{kR}$  squark exchange. We examine the signal associated with the (electron and muon) charged semileptonic decay channel of the top,  $t \rightarrow bW^+ \rightarrow bl^+\nu$ . The final states,  $(bl^+\nu\bar{c}) + (\bar{b}l^-\bar{\nu}c)$ , [ $l = e, \mu$ ] consist of an isolated energetic charged lepton, accompanied by a pair of  $b$  and  $c$  quark hadronic jets and missing energy. The standard model background may arise from the W-boson pair production reaction,  $l^+l^- \rightarrow W^+W^-$ , and possibly, in the case of an imperfect  $b$  quark tagging, from the  $b - \bar{b}$  quark pair production reaction,  $l^+l^- \rightarrow b\bar{b}$ , followed by a semileptonic decay of one of the  $b$  quarks,  $b \rightarrow cl^-\bar{\nu}$ .

The present work consists of two main parts. In the first part, we discuss the signal associated with the top semileptonic decay channel. We evaluate a set of characteristic dynamical distributions for the signal and for the standard model background and obtain predictions for the effective rates based on a judicious choice of selection cuts on the final state kinematical variables. Our discussion will develop along similar lines as in a recent work of Han and Hewett, [12] which was focused on the contributions initiated by the dimension,  $\mathcal{D} = 6$ , four fields couplings of the Z-boson with fermion pairs and the



neutral Higgs boson. In the second part of the paper, we examine a specific CP-odd top polarization observable which corresponds to an asymmetry in the energy distribution of the final state charged lepton with respect to the sign of its electric charge.

The contents of the paper are organised into 3 sections. In Section 2, we focus on the total and partial semileptonic decay rates for both the signal and standard model background, allowing for the case of an imperfect  $b$  quark tagging. We discuss the constraints from the indirect bounds on the RPV coupling constants, study the dependence of rates on the down-squark mass parameter and evaluate a set relevant dynamical distributions that are of use in devising an appropriate set of selection cuts. In Section 3, we discuss a test of CP violation involving top polarization effects. The CP violating observable arises through interference terms between the tree and one-loop contributions to the amplitude and a CP-odd phase which is embodied in the RPV coupling constants. Following an approach similar to one used in earlier proposals, [6, 7] we describe the top production and decay by means of a factorization approximation and examine the induced charge asymmetry in the energy distribution of the final state charged leptons. The production amplitudes are evaluated in the helicity basis. Our main conclusions are summarized in Section 4.

## 2 Top-charm associated production

### 2.1 Integrated rates

In a  $l^-l^+$  collision, the tree level transition amplitude for single top production, as initiated by the RPV interactions,  $\lambda'_{ijk} L_i Q_j D_k^c$ , proceeds via the  $u$ -channel exchange of a right-handed down-squark,  $\tilde{d}_{kR}$ , as represented in Fig.1. By use of a Fierz ordering identity, the transition amplitude for the flavor non diagonal production of an up quark-antiquark pair,  $l^-(k) + l^+(k') \rightarrow u_J(p) + \bar{u}_{J'}(p')$ , can be written in the form of a Lorentz covariant vectorial coupling,

$$M_t^{JJ'} = -\frac{\lambda'_{lJk} \lambda'^*_{lJ'k}}{2(u - m_{\tilde{d}_{kR}}^2)} \bar{v}_L(k') \gamma^\mu u_L(k) \bar{u}_L(p) \gamma_\mu v_L(p'). \quad (2.1)$$

We shall specialize henceforth to the case of electron-positron colliders, corresponding to the choice  $l = 1$  for the generation index. The squared amplitude, summed over the initial and final fermion spins, reads : [1]

$$\sum_{pol} |M_t^{JJ'}|^2 = N_c \left| -\frac{\lambda'_{1J'k} \lambda'^*_{1Jk}}{2(u - m_{\tilde{d}_{kR}}^2)} \right|^2 16(k \cdot p')(k' \cdot p). \quad (2.2)$$

The production rate for unpolarized initial leptons, integrated over the scattering angle in the interval,  $0 \leq |\cos \theta| \leq x_c$ , is given by the analytic formula,

$$\begin{aligned} \sigma &= \frac{N_c |\lambda'_{1J'k} \lambda'^*_{1Jk}|^2}{64\pi s^2} [(u_- - u_+) + (2\tilde{m}^2 - m_J^2 - m_{J'}^2) \ln \left| \frac{u_- - \tilde{m}^2}{u_+ - \tilde{m}^2} \right| \\ &- (\tilde{m}^2 - m_J^2)(\tilde{m}^2 - m_{J'}^2) \left( \frac{1}{u_- - \tilde{m}^2} - \frac{1}{u_+ - \tilde{m}^2} \right)], \end{aligned} \quad (2.3)$$

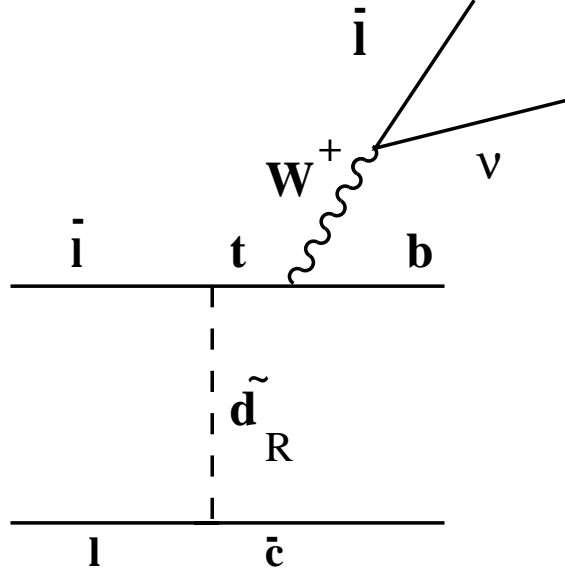


FIG. 1: Feynman diagram for the tree level amplitude of the process,  $l^+l^- \rightarrow \bar{c}t \rightarrow \bar{c}l^+\nu$ .

where,  $u_{\pm} = m_J^2 - \sqrt{s}(E_p \pm px_c)$ . For the top-charm associated production case, in the limit,  $m_J = m_t \gg m_{J'} = m_c$ , one has,  $u_+ \simeq m_t^2 - s$ ,  $u_- \simeq 0$ . For fully polarized initial beams, since the RPV amplitude selects a single helicity configuration for the initial state leptons,  $l_L^- l_R^+$ , (left handed  $l^-$  and right handed  $l^+$ ) the corresponding polarized rate would be still described by the same formula as above, only with an extra enhancement factor of 4. The predicted rates for  $t\bar{c}$  production are controlled by quadratic products of the RPV coupling constants,  $\lambda'_{13k} \lambda'^*_{12k}$ ,  $[k = 1, 2, 3]$  and the squark mass,  $m_{\tilde{d}_{kR}}$ , denoted for short as,  $\tilde{m}$ . Allowing for the existence in the RPV interactions of an up-quark flavor mixing, such as would be induced by the transformation from flavor to mass basis, one may express the amplitude in terms of a single RPV coupling constant and the CKM matrix,  $V$ , by rewriting the coupling constant dependence as,  $\lambda'_{12k} \lambda'^*_{13k} \rightarrow \lambda'_{1Mk} \lambda'_{1M'k} (V^\dagger)_{M'2} (V^\dagger)_{M3}^*$ , and selecting the maximal contribution associated with the configurations,  $M = M' = 2$  or 3. This yields the order of magnitude estimate,  $\lambda'_{13k} \lambda'^*_{12k} \rightarrow |\lambda'_{12k}|^2 (V^\dagger)_{22} (V^\dagger)_{23}^* \approx 2|\lambda'_{12k}|^2 \lambda^2$  or  $2|\lambda'_{13k}|^2 \lambda^2$ , respectively, where,  $\lambda \approx \sin \theta_c \approx 0.22$ , denotes the Cabibbo angle parameter.

We pause briefly to recall the current bounds on the RPV coupling constants of interest in the present study. [25] The relevant single coupling constant bounds are,  $\lambda'_{12k} < 4. \times 10^{-2}$ ,  $\lambda'_{13k} < 0.37$  (charged current universality);  $\lambda'_{1j1} < 3 \times 10^{-2}$  (atomic physics parity violation);  $\lambda'_{12k} < 0.3-0.4$ ,  $\lambda'_{13k} < 0.3 - 0.6$  (neutral current universality); and  $\lambda'_{122} < 7. \times 10^{-2}$ ,  $\lambda'_{133} < 3.5 \times 10^{-3}$  (neutrino Majorana mass). [26] The superpartners scalar particles masses are set at  $100 \text{ GeV}$ . Unless otherwise stated, all the dummy flavor indices for quarks and leptons are understood to run over the three generations. Using the above results for individual coupling constants bounds, we may deduce for the following upper bounds on the relevant quadratic products, [27]  $\lambda'_{13k} \lambda'_{12k} < [O(10^{-3}), O(10^{-2}), O(10^{-4})]$ ,  $[k = 1, 2, 3]$ . The indirect quadratic products bounds,  $\lambda'_{ijk} \lambda'_{i'j3} < 1.1 \times 10^{-3}$ ,  $\lambda'_{ijk} \lambda'_{i'j3} < 1.1 \times 10^{-3}$ ,  $[i' = 1, 2]$  ( $B \rightarrow X_q \nu \bar{\nu}$ ) are roughly comparable to these single coupling constants bounds. We also note that using the CKM flavor mixing along with a single dominant coupling constant in the current basis, as described at the end of the previous paragraph, may not

be especially beneficial in avoiding the above stronger pair product bound. The bound on the corresponding coupling constant factor,  $2|\lambda'_{13k}|^2\lambda^2 < O(10^{-2})$ , is competitive for the generation indices,  $k = 1, 3$ .

Numerical results for the integrated rates have already been reported in previous works [19, 1]. Setting the relevant RPV coupling constants at the reference value,  $\lambda' = 0.1$ , one predicts rates of order  $1 - 10 \text{ fb}$ , for  $\tilde{m} = O(100) \text{ GeV}$ . As the center of mass energy varies in the interval,  $\sqrt{s} = 192 - 1000 \text{ GeV}$ , the rates rise sharply from threshold, reaching smoothly a plateau around  $\sqrt{s} \simeq 400 \text{ GeV}$ . This contrasts with the predictions from gauge boson mediated higher dimension interactions [12] where the rise of the rates with incident energy is a more gradual one. The rates are also found to have a strong dependence on  $\tilde{m}$ , which weakens for increasing center of mass energies. One may roughly parametrize the dependence on  $s$  and  $\tilde{m}$  by the approximate scaling law,  $\sigma \approx (\frac{\lambda'\lambda'}{0.01})^2 (\frac{100 \text{ GeV}}{\tilde{m}})^{x(s)}$ , where the power exponent is a fastly decreasing function of energy, taking the approximate values,  $x(s) \approx [3.65, 1.86, 0.94]$ , at,  $\sqrt{s} = [0.192, 0.5, 1.] \text{ TeV}$ .

Although the predicted rates seem to be severely constrained by the above indirect bounds, one could envisage an optimistic scenario where the supersymmetry decoupling limit,  $\tilde{m} \rightarrow \infty$ , is realized with fixed values for the products,  $\lambda'_{ijk}(\frac{100 \text{ GeV}}{\tilde{m}}) \approx 0.1$ , consistently with the current indirect bounds. The results obtained with this prescription are displayed in Figure 2. The integrated rates now depend on  $\tilde{m}$  as,  $\sigma \propto (\frac{100 \text{ GeV}}{\tilde{m}})^{-4+x(s)}$ , which leads at high energies to an enhancement by up to three orders of magnitudes, compared to the case where the RPV coupling constants are taken independent of  $\tilde{m}$ . The initial energy of LEP-II falls right in the regime where the cross section is sharply rising with increasing initial energy. The decrease with increasing  $\tilde{m}$  is stronger at LEP-II energies than at the future linear colliders energies. Note that at the largest values of the superpartner mass,  $\tilde{m} \simeq 1. \text{ TeV}$ , the RPV coupling constants in our prescription enter a strong coupling regime ( $\lambda' = O(1)$ ) and it is not clear then whether the tree level prediction makes sense.

Next, we consider the process incorporating the top semileptonic decay, as pictured by the Feynman diagram shown in Fig.1. We assume that the top decay is dominated by the electroweak semileptonic decay channel, with branching fraction,  $B(t \rightarrow b + W^+) \approx 1$ . We also include the pair of CP-conjugate final states,  $t\bar{c}$  and  $c\bar{t}$  production, which multiplies the rate by a factor of 2. Note, however, that we restrict ourselves to the  $u_{J'} = c$  charm quark mode only. The numerical results for rates, including a branching fraction factor of  $\frac{2}{9}$  (experimental value, 21.1%) to account for the  $W \rightarrow l\nu$ , [ $l = e, \mu$ ] decay channels, are displayed in Table 15. We also show the standard model background rate from the  $W$ -boson pair production,  $l^-l^+ \rightarrow (W^+W^-) \rightarrow (l^+\nu\bar{u}_i d_j) + (l^-\bar{\nu} d_j u_i)$ , with one  $W$ -boson decay leptonically and the other hadronically, where  $i, j$  are generation indices. The irreducible background from,  $W^- \rightarrow \bar{c}b$  or  $W^+ \rightarrow \bar{b}c$ , is strongly suppressed, due to the small branching factor, given approximately by,  $0.32|V_{cb}|^2 \approx 5 \cdot 10^{-4}$ . It is safer, however, to allow for the possibility where the light quark hadronic jets could be misidentified as  $b$  quark hadronic jets. Accounting for the leptonic decay for one of the  $W$ -boson and the hadronic decay for the other  $W$ -boson, introduces for the total rate, which includes all the subprocesses, the branching fraction factor,  $2 \times (21.1 \pm 0.64)\% \times (67.8 \pm 1.0)\% = 0.286 \pm 0.024$ . Our numerical results in Table 15 for the standard model background rates are in qualitative agreement with those quoted ( $\sigma = [2252, 864] \text{ fb}$  at  $s^{\frac{1}{2}} = [0.5, 1.] \text{ TeV}$ ) by Han and Hewett. [12] One should be aware of the existence of

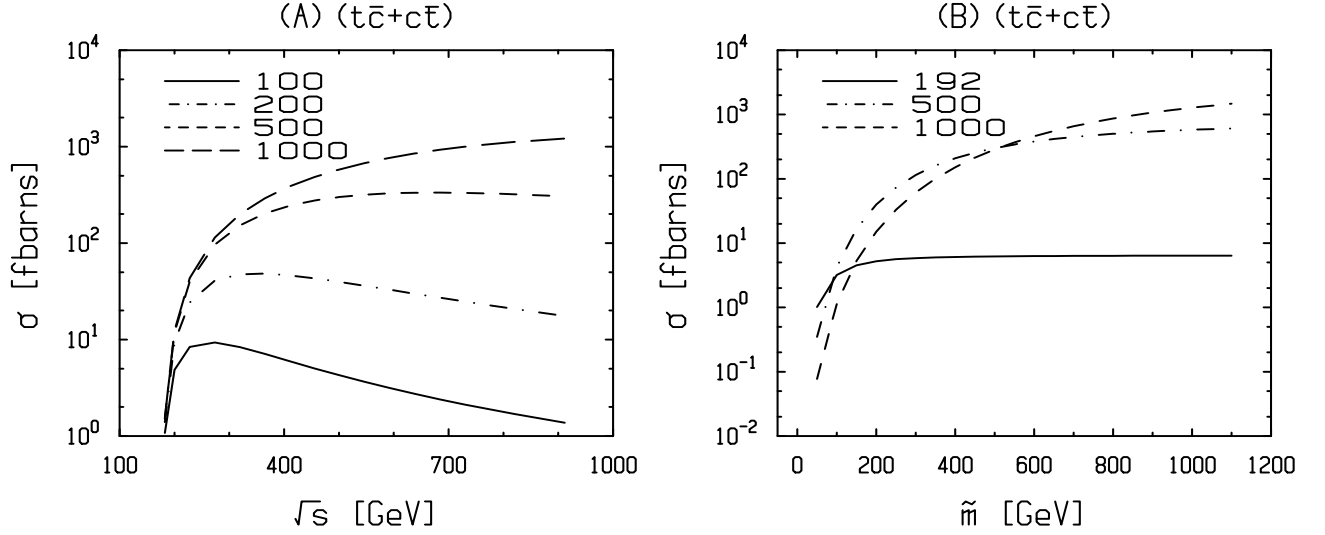


FIG. 2: The total integrated rate for the RPV induced reaction,  $l^+l^- \rightarrow (t\bar{c}) + (\bar{t}c)$ , setting the values of the relevant coupling constants as,  $\lambda'_{12k} = \lambda'_{13k} = 0.1 (\tilde{m}/100 \text{ GeV})$ , is plotted in window (A) as a function of center of mass energy,  $s^{1/2}$  for fixed down squark mass,  $\tilde{m} = [100, 200, 500, 1000] \text{ GeV}$  and in window (B) as a function of  $\tilde{m}$  for fixed  $s^{1/2} = [192, 500, 1000] \text{ GeV}$ . We integrate over an interval of the scattering angle,  $0 \leq |\cos \theta| \leq 0.9848$ , corresponding to an opening angle with respect to the beams axis larger than  $10^\circ$ .

<i>Energy(TeV)</i>	0.192	0.5	1.0
Total rate $\sigma(fb)$	4.099	4.291	1.148
Signal (fb)	0.68	0.91	0.24
$W^+W^-$ Background (fb)	5076	2080	876
Cut Signal (fb)	0.54	0.74	0.21
$W^+W^-$ Cut Background (fb)	17.	5.0	2.6

TAB. 15: Production rates for the top-charm production signal and the W-boson pair production background. The line entries give successively the total integrated rate for the reaction,  $l^+l^- \rightarrow (t\bar{c}) + (c\bar{t})$ , using,  $\lambda' = 0.1$ ,  $\tilde{m} = 100 \text{ GeV}$ , the rate for signal events,  $(b\bar{l}\nu\bar{c}) + (\bar{b}l\bar{\nu}c)$ , associated with the top semileptonic decay, the W-boson pair production background rate,  $l^-l^+ \rightarrow W^+W^- \rightarrow (l^+\nu\bar{u}_id_j) + (l^-\bar{\nu}d_ju_i)$ , and the corresponding cut signal and background rates, as obtained by applying the selection cuts quoted in the text. The results include the first two generations of charged leptons,  $l = e, \mu$ .

large loop corrections to the  $W^+W^-$  production rate, especially at high energies. The predictions including the electroweak and QCD standard model one-loop contributions read, [28]  $\sigma = [4624, 1647, 596] \text{ fb}$  at  $s^{1/2} = [0.192, 0.5, 1.] \text{ TeV}$ . We conclude therefore that our use of the tree level predictions for the  $W^+W^-$  background overestimates the true cross sections by [9%, 20%, 32%] at the three indicated energies.

Let us discuss briefly other possible sources of background. The next important contribution is that arising from the non resonant  $W$ -boson virtual propagation in the amplitude with the intermediate  $W^+W^-$  bosons branching into four fermions ( $l\nu q\bar{q}'$ ). This could be possibly estimated by subtracting the resonant contribution from the total background cross sections, weighted by the suitable branching factors, as independently evaluated by numerical methods in the literature. The results for the integrated total cross sections,  $l^-l^+ \rightarrow (4f) + (4f + \gamma)$ , [29] including the initial state radiation and Coulomb corrections, indicate that the off-shell contributions amount to a small relative correction lower than  $O(10\%)$ . Alternatively, one may consider, after reconstructing the neutrino momentum from the missing energy, a procedure to impose suitable cuts on the  $bW$  invariant mass, aimed at suppressing the non resonant production background.

One other potentially important background is that arising from the  $b - \bar{b}$  quark pair production reaction,  $l^+l^- \rightarrow \gamma^*/Z \rightarrow b\bar{b} \rightarrow \bar{b}(cl^-\bar{\nu}) + b(\bar{c}l^+\nu)$ . [19] The numerically derived predictions for the rates, as obtained by means of the PYTHIA generator, are :  $\sigma = [1.631 \cdot 10^4, 2.12 \cdot 10^3, 5.35 \cdot 10^2] fb$ , at  $s^{\frac{1}{2}} = [0.192, 0.5, 1.]TeV$ . It would appear desirable, in view of these large predicted rates, to eliminate this background by performing a double  $b$  quark tagging analysis on the events sample. This can be performed at a reasonably low cost, given that the detection efficiency of  $b$  quark jets is currently set at 50%. If one performs a single  $b$  quark tagging, the rates for the corresponding events,  $l^+l^- \rightarrow \gamma^*/Z \rightarrow b\bar{b} \rightarrow (cl^-\bar{\nu})\bar{b}$ , are reduced by a branching fraction,  $B(b \rightarrow cl\nu) \approx 10\%$ , but this is compensated by the probability of misidentifying a light quark jet as a  $b$  quark jet, which lies at the small value of 0.4% with the current silicon vertex techniques. If no  $b$  quark tagging is performed at all, then the above large rates may make it necessary to resort to an analysis of isolation cuts of the type to be discussed in the next subsection.

## 2.2 Distributions for the semileptonic top decay events

In order to separate the signal from background, we consider the same set of characteristic final state kinematical variables as proposed in the study by Han and Hewett. [12] These are the maximum and minimum energy of the two jets,  $E_j^{high}$ ,  $E_j^{low}$ , the dijet invariant mass,  $M_{jj}$ , the charged lepton energy,  $E_l$ , and rapidity,  $y_l = \frac{1}{2} \log \frac{E_l + p_{l\parallel}}{E_l - p_{l\parallel}}$ . The distributions in these 6 variables for the signal and background, at a center of mass energy,  $\sqrt{s} = 0.5TeV$ , are plotted in Fig.3. These numerical results were obtained by means of the PYTHIA [30] event generator. One notices marked differences between signal and background. The maximum jet energy distribution is uniformly distributed for the background but sharply peaked for the signal, where the peak position is determined by the top mass and the incident energy as,  $m_t^2 = (m_c^2 - s + 2\sqrt{s}E_p)$ . The minimum jet energy is uniformly distributed for both signal and background, but happily the corresponding intervals are very partially overlapping. The signal events rapidity distributions for the maximum energy jet are more central for signal than background. A similar trend holds for the lepton rapidity distributions. The dijet invariant mass is a most significant variable in discriminating against the background due to its pronounced peak at the  $W$  mass. For the signal, the dijet invariant mass is uniformly spread out. Although we do not show here the distributions for the top mass reconstruction, this also features a strong contrast between a strongly peaked signal and a uniform background. The lepton energy distributions for the signal and background are peaked at the opposite low and high energy ends of

the physical interval, respectively. This is a familiar effect associated with the correlation between the W-boson spin polarization, which is predominantly longitudinal in the top decay and transverse in the direct W-boson decay, and the velocity of the emitted charged lepton. In the signal decay amplitude,  $t \rightarrow b\bar{l}\nu$ , the fact that the left handed b-quark must carry the top polarization, forces the lepton to travel with opposite velocity to that of top. In the background decay amplitude,  $W^- \rightarrow l\bar{\nu}$ , the charged lepton is emitted with a velocity pointing in the same direction as that of the W-boson. Thus, the Lorentz boost effects on the emitted charged leptons act in opposite ways for the signal and background events.

While the above distinctive features between signal and background events get further pronounced with increasing center of mass energy, opposite trends occur as the initial energy is lowered. The distributions at the LEP-II center of mass energy,  $\sqrt{s} = 0.192 \text{ TeV}$ , are plotted in Fig.4. At this energy, the monovalued distribution for the signal jet, which is now the softer lower energy jet, is still well separated from the corresponding background jet distribution. So, this variable, along with the dijet invariant mass stand up as useful discrimination tests for the signal. By contrast, the energy and rapidity distributions for the maximum signal jet may not be easily distinguished from the background. Similarly, the lepton energy distributions in the signal and background are overlapping due to the small Lorentz boost effect.

The distributions obtained with the RPV interactions are rather similar to those found with the higher dimension operator mechanism. [12] This is due to the formal structure of the RPV amplitude, involving an effective  $u$ -channel vector particle exchange. In fact, the selection cuts proposed by Han and Hewett [12] appear to be quite appropriate also in the RPV case, and, for convenience, we recapitulate below the cut conditions used to characterize the selected events.

$$\begin{aligned} E_j^{low} < 20, E_j^{high} > 60, E_l > 0, \delta_{jj} > 10, \delta_t < 5, \quad [\sqrt{s} = 192] \\ E_j^{low} > 20, E_j^{high} > 200, E_l < 150, \delta_{jj} > 10, \delta_t < 40, \quad [\sqrt{s} = 500] \\ E_j^{low} > 20, E_j^{high} > 460, E_l < 350, \delta_{jj} > 10, \delta_t < 100. \quad [\sqrt{s} = 1000] \end{aligned}$$

The above listed variables correspond to the minimum and maximum energy of the two jets,  $E_j^{low}$ ,  $E_j^{high}$ , the charged lepton energy,  $E_l$ , the distance between the dijet invariant mass and W-boson mass,  $\delta_{jj} = |M_{jj} - m_W|$ , the distance of the reconstructed top mass to the true mass,  $\delta_t = |m_t^{reconst} - m_t|$ . The assigned numerical values are all expressed in GeV units. Besides the above cuts, we also impose the usual detection cuts on energies and rapidities,  $E_{j,l} > 10 \text{ GeV}$ ,  $|\eta_{j,l}| < 2$ , aimed at removing the particles travelling too close to the beam pipe. We allow for the detection efficiency of the particle energies only in an approximate way, namely, by accounting for the following approximate uncertainties,  $\Delta E/E = 40\%$ ,  $10\%$ , on the jets and lepton energies, respectively, at the level of imposing the above selection cuts, rather than by the usual procedure of performing a Gaussian smearing of the particle energies.

The numerically evaluated efficiencies on the signal and background events are,  $\epsilon_S \simeq 0.8$ ,  $\epsilon_B \simeq 3.10^{-3}$ , with a very weak dependence on the center of mass energy and, for the signal, a weak dependence on the mass parameter  $\tilde{m}$ , which was set at  $\tilde{m} = 100 \text{ GeV}$  in the numerical simulations. After applying the cuts, the background rates are,  $\sigma_B \epsilon_B = [17., 5., 2.] \text{ fb}$ , and the signal rates,  $\sigma_S \epsilon_S = [0.68, 0.74, 0.21] \text{ fb}$ , for  $\sqrt{s} = [192., 500., 1000] \text{ GeV}$ . The results for the cut signal and background rates, as given in Table 15, show that the background is very significantly reduced by the cuts.

The situation is clearly far more favorable for the future linear colliders than for LEP-II. Nevertheless, the number of surviving signal events is still one order of magnitude below that of the surviving background, so that the option of cutting down the background by means of a  $b$  quark tagging procedure is to be preferred since the ensuing reduction would be much more drastic. An integrated luminosity of  $\mathcal{L} = 100 \text{ fb}^{-1}$  would lead to a number of signal events,  $(\lambda'_{12k}\lambda'_{13k}/10^{-2}) \times O(30)$ .

We have also performed an indicative event generator study of the background,  $l^+l^- \rightarrow b\bar{b} \rightarrow l^\pm + \text{hadrons}$ , restricting consideration to the emitted charged leptons only. A jet reconstruction of the partonic level distributions is a task beyond the scope of the present work. We focus on the first charged lepton emitted during the semileptonic decays of the produced  $B$ ,  $\bar{B}$  mesons, since this carries the largest velocity. As seen on Fig.3, the distribution for the first emitted charged lepton energy is peaked at low energies. One expects that the most energetic lepton is that produced in the semileptonic decays of the  $B$  mesons. The rapidity distribution is less central than for the signal and nearly overlaps with that of the  $W^+W^-$  background. Therefore, imposing the additional lower bound cut on the lepton energy, say, at  $E_l > 20 \text{ GeV}$ , for  $s^{\frac{1}{2}} = 500 \text{ GeV}$ , should be sufficient to appreciably suppress the  $b - \bar{b}$  background without much affecting the signal.

We may infer the reach with respect to the free parameters by evaluating the statistical significance ratio for a discovery, as defined by,  $\hat{\sigma} = \frac{S}{\sqrt{S+B}}$ ,  $S = \sigma_S \mathcal{L}$ ,  $B = \sigma_B \mathcal{L}$ , where  $\mathcal{L}$  denotes the integrated luminosity. Setting this at the value,  $\hat{\sigma} = 3$ , corresponding to a 95% confidence level, one deduces a dependence of the RPV coupling constant as a function of the superpartner mass parameters for a fixed initial energy and integrated luminosity. The sensitivity reach contour plot for the relevant parameters,  $\lambda'\lambda' = \lambda'_{12k}\lambda'_{13k}$  and  $\tilde{m} = m_{\tilde{d}_{kR}}$ , is shown in Fig.5. We note that the sensitivity limit on the product of coupling constants,  $\lambda'\lambda'$ , scales with the luminosity approximately as,  $1/\sqrt{\mathcal{L}}$ . While the reach on the RPV coupling constants products,  $\lambda'_{12k}\lambda'_{13k} < O(10^{-1})$ , lies well above the current indirect bounds, this covers a wide interval of the down squark mass which extends out to  $1 \text{ TeV}$ . To compare with analogous collider physics processes, we note that while the flavor diagonal fermion pair production reactions,  $e^-e^+ \rightarrow f_J \bar{f}_J$ , may have a higher sensitivity reach, these are limited to information on the single coupling constants,  $\lambda'_{1jk}$  [31]. The special reaction,  $e^-e^+ \rightarrow b\bar{b}$ , proceeding via a sneutrino  $s$ -channel resonance, may probe quadratic products such as,  $\lambda_{131}\lambda'_{333}$ , [32] or  $\lambda_{131}\lambda'_{311}$  [33] at levels of  $O(10^{-3})$ , but this is subject to the existence of a wide sneutrino resonance. The  $t\bar{b}$  associated production at the hadronic Fermilab Tevatron [17, 18] and the Cern LHC [18] colliders can be initiated via a charged slepton  $\tilde{e}_{iL}$   $s$ -channel exchange. The sensitivity reach on the linear combination of quadratic coupling constants products,  $\lambda'_{i11}\lambda'_{i33}$ , is of order  $10^{-2} - 10^{-1}$ . This information should prove complementary to that supplied by our study aimed at the leptonic colliders. To conclude this brief comparison, we observe that the information provided by the single top production reaction appears to be rather unique in view of the very characteristic signature of the associated events.

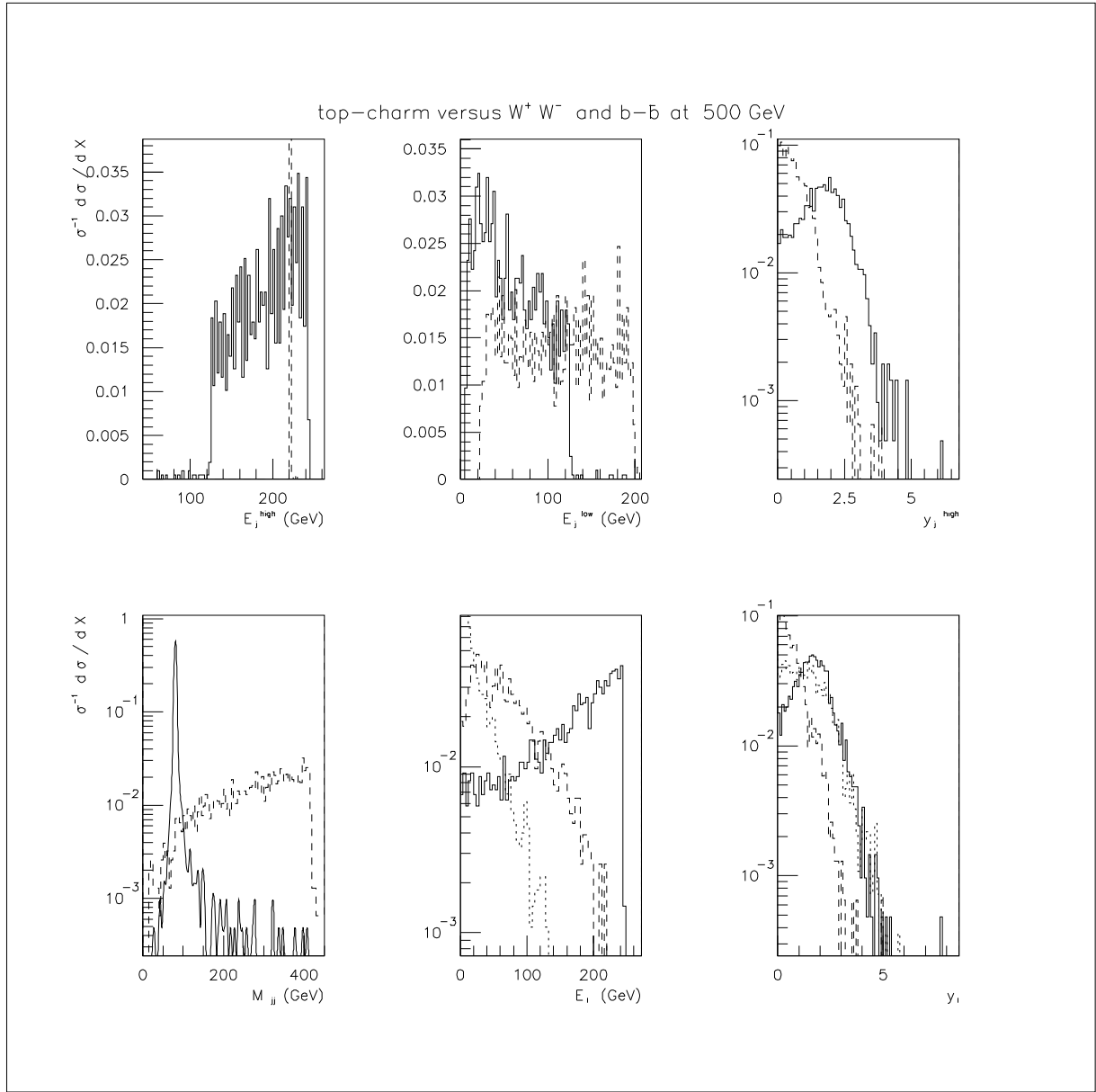


FIG. 3: Normalized dynamical distributions associated with the signal events,  $l^+l^- \rightarrow (t\bar{c}) + (\bar{t}c) \rightarrow (bl^+\nu\bar{c}) + (\bar{b}l^-\bar{\nu}c)$ , (dashed line) at  $\tilde{m} = 100 \text{ GeV}$ , and the background events,  $l^+l^- \rightarrow W^+W^- \rightarrow (l^+\nu\bar{q}q') + (l^-\bar{\nu}q\bar{q}')$ , (continuous line) at a center of mass energy,  $s^{\frac{1}{2}} = 500 \text{ GeV}$ . The kinematical variables in the histograms, from left to right and up to down, are the jets maximum energy, the jets minimum energy, the rapidity for the highest energy jet, the di-jet invariant mass, the charged lepton energy and the charged lepton rapidity. The charged lepton energy and rapidity distributions are also plotted for the  $b - \bar{b}$  background production events,  $l^+l^- \rightarrow b\bar{b} \rightarrow l^\pm + \text{hadrons}$  (dotted line).

### 3 Top polarization observables and a test of CP violation

Should single top production become experimentally observable in the future, an important next step to take is in examining top polarization observables. In this section, we



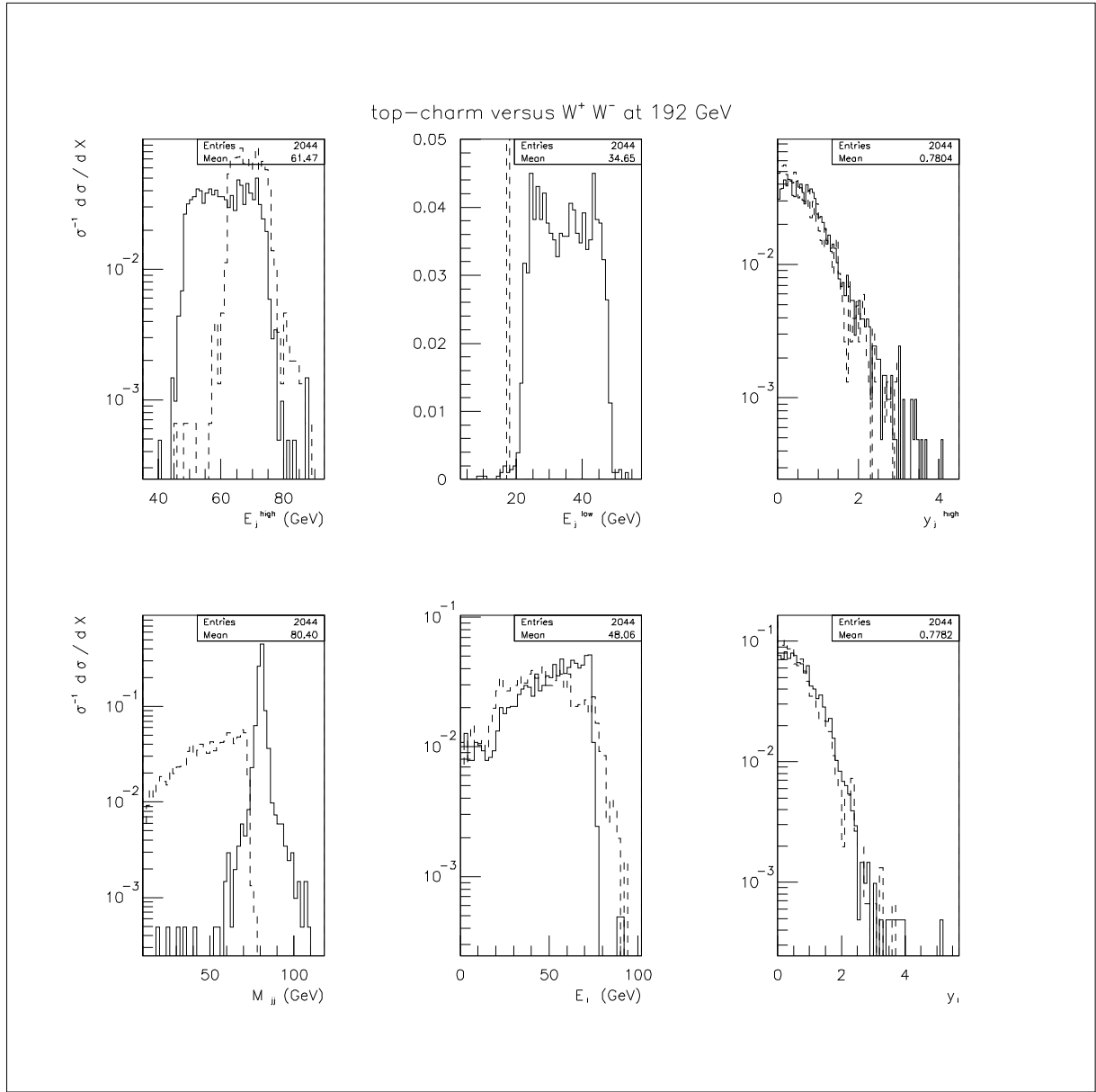


FIG. 4: Same distributions as in Fig.3, at a center of mass energy  $s^{\frac{1}{2}} = 192 \text{ GeV}$ .

present an approximate study for the top semileptonic decay signal in top-charm associated production aiming at a test of CP violation. We exploit an idea which was developed in early studies of  $t - \bar{t}$  production. [5, 6] Interesting extensions are currently pursued [8, 9, 10]. The basic observation is that any CP-odd quantity depending on the top polarization, such as the difference of rates between the pair of CP conjugate reactions,  $\sigma(l^- l^+ \rightarrow t_L \bar{c}) - \sigma(l^- l^+ \rightarrow \bar{t}_R c)$ , can become observable by analyzing the top polarization through the kinematical distributions of its emitted decay ( $b$  quark or charged lepton) products. An especially interesting observable is the charged lepton energy distribution for a polarized top. Any finite contribution to the CP-odd observables must arise through an interference term involving imaginary parts of loop and tree amplitudes factors, the

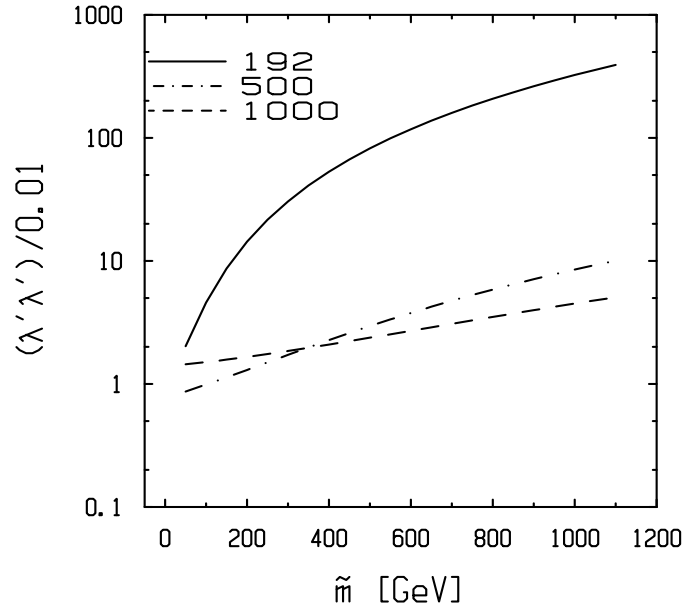


FIG. 5: Sensitivity reach plot for the RPV coupling constants product,  $\lambda'_{12k}\lambda'_{13k}/0.01$ , as a function of the down squark mass,  $\tilde{m}$ , for fixed center of mass energy,  $s^{\frac{1}{2}} = [192., 500, 1000]$  GeV, and corresponding fixed integrated luminosity,  $\mathcal{L} = [2., 100., 100.]$  fb $^{-1}$ , using an acceptance for the background,  $\epsilon_B = 3 \cdot 10^{-3}$ , and an acceptance for the signal,  $\epsilon_S = 0.8$ , assumed to be independent of  $\tilde{m}$ .

loop amplitude factor bringing a CP-even final state interaction complex phase with the CP-odd relative complex phase arising from the coupling constants in the product of loop and tree amplitudes.

### 3.1 Helicity basis amplitudes

Building on our previous work, [1] we shall combine the tree level RPV induced amplitude discussed in Section 2 with the one-loop RPV induced amplitude associated to the photon and Z-boson exchange diagrams, restricting ourselves to the vertex corrections in the electroweak neutral current vertices,  $\gamma \bar{f}_J(p) f_{J'}(p')$  and  $Z \bar{f}_J(p) f_{J'}(p')$ . The Z-boson vertex admits the general Lorentz covariant decomposition,

$$\begin{aligned}
 J_\mu^Z &= -\frac{g}{2 \cos \theta_W} \Gamma_\mu^{JJ'}(Z), \\
 \Gamma_\mu^{JJ'}(Z) &= \gamma_\mu (A_L^{JJ'}(f) P_L + A_R^{JJ'}(f) P_R) + \frac{1}{m_J + m_{J'}} \sigma_{\mu\nu} (p + p')^\nu (i a^{JJ'} + \gamma_5 d^{JJ'}),
 \end{aligned}
 \tag{3.1}$$

where the vectorial vertex functions,  $A_{L,R}^{JJ'} = A_{L,R}^{JJ'}|_{tree} + A_{L,R}^{JJ'}|_{loop}$ , have a tree level contribution given by,  $A_{L,R}^{JJ'}|_{tree} = \delta_{JJ'} a_{L,R}(f)$ ,  $a_{L,R}(f) = 2T_3^{L,R} - 2Q(f) \sin^2 \theta_W$ , and the tensorial vertex functions,  $a^{JJ'}$ ,  $d^{JJ'}$ , are associated with the anomalous transition magnetic moment and the CP-odd, P-odd electric transition dipole moment, respectively. An analogous

decomposition applies for the photon,  $J_\mu^\gamma = -\frac{g \sin \theta_W}{2} \Gamma_\mu^{JJ'}(\gamma)$ , with  $a_{L,R}(f) = 2Q(f)$ , determined by the electric charge  $Q(f)$ . It is convenient to work with the  $Z f_J \bar{f}_{J'}$  vertex in the alternate Lorentz covariant decomposition,  $\Gamma_\mu^{JJ'}(Z) = \gamma_\mu(\mathcal{A} - \mathcal{B}\gamma_5) + \frac{1}{2}(p - p')_\mu(\mathcal{C} - \mathcal{D}\gamma_5)$ , where the vertex functions,  $\mathcal{A}$ ,  $\mathcal{B}$ ,  $\mathcal{C}$ ,  $\mathcal{D}$ , (omitting the up quarks generation indices  $J$ ,  $J'$  for convenience) are related to the previously defined vectorial and tensorial ones, eq. (3.1), as,

$$\begin{aligned}\mathcal{A} &= \frac{1}{2}(A_L^{JJ'}(f) + A_R^{JJ'}(f)) + a^{JJ'}, \quad \mathcal{B} = \frac{1}{2}(A_L^{JJ'}(f) - A_R^{JJ'}(f)) + \frac{m_J - m_{J'}}{m_J + m_{J'}} id^{JJ'}, \\ \mathcal{C} &= -\frac{2}{m_J + m_{J'}} a^{JJ'}, \quad \mathcal{D} = -\frac{2}{m_J + m_{J'}} id^{JJ'}.\end{aligned}\quad (3.2)$$

The one-loop Z-boson exchange amplitude may then be written in the form,

$$\begin{aligned}M_l^{JJ'}(Z) &= \left(\frac{g}{2 \cos \theta_W}\right)^2 \bar{v}(\vec{k}', \mu') \gamma_\sigma \left(a(e_L) P_L + a(e_R) P_R\right) u(\vec{k}, \mu) \frac{1}{s - m_Z^2 + im_Z \Gamma_Z} \\ &\times \bar{u}(\vec{p}, \lambda) [\gamma^\sigma (\mathcal{A} - \mathcal{B}\gamma_5) + \frac{1}{2}(p - p')^\sigma (\mathcal{C} - \mathcal{D}\gamma_5)] v(\vec{p}', \lambda').\end{aligned}\quad (3.3)$$

Combining the above loop amplitude with the RPV tree amplitude, eq. (2.1), which we rewrite as,

$$M_t^{JJ'} = \mathcal{R} \bar{v} \gamma_\mu (1 - \gamma_5) u \bar{u} \gamma^\mu (1 - \gamma_5) v, \quad \mathcal{R} = -\frac{\lambda_{1Jk}^* \lambda'_{1J'k}}{8(u - m_{\tilde{d}_{kR}}^2)}, \quad (3.4)$$

one obtains,

$$\begin{aligned}M^{JJ'} &= M_t^{JJ'} + M_l^{JJ'}(Z) = [(Ga^+ \mathcal{A} + \mathcal{R})(\gamma_\mu)(\gamma^\mu) - (Ga^+ \mathcal{B} + \mathcal{R})(\gamma_\mu)(\gamma^\mu \gamma_5) \\ &- (Ga^- \mathcal{A} + \mathcal{R})(\gamma_\mu \gamma_5)(\gamma^\mu) + (Ga^- \mathcal{B} + \mathcal{R})(\gamma_\mu \gamma_5)(\gamma^\mu \gamma_5) \\ &+ \frac{1}{2}(p - p')^\mu [Ga^+ \mathcal{C}(\gamma_\mu)(1) - Ga^+ \mathcal{D}(\gamma_\mu)(\gamma_5) - Ga^- \mathcal{C}(\gamma_\mu \gamma_5)(1) + Ga^- \mathcal{D}(\gamma_\mu \gamma_5)(\gamma_5)],\end{aligned}\quad (3.5)$$

where,  $a^\pm = \frac{1}{2}(a_L(e) \pm a_R(e))$ , and we have omitted writing the contractions of the Dirac spinors indices for the initial and final fermions, respectively. The photon exchange contribution can be incorporated by treating the parameters  $a^\pm$  as operators acting on the vertex functions,  $\mathcal{A}$ ,  $\mathcal{B}$ ,  $\mathcal{C}$ ,  $\mathcal{D}$ , by means of the formal substitutions,

$$\begin{aligned}Ga^\pm \mathcal{A} &= G_Z \frac{a_L(e) \pm a_R(e)}{2} \left( \frac{A_L^{JJ'}(f) \pm A_R^{JJ'}(f)}{2} + a^{JJ'} \right) \\ &+ G_\gamma \begin{pmatrix} 2Q(f) \\ 0 \end{pmatrix} \left( \frac{A_L^{\gamma JJ'}(f) \pm A_R^{\gamma JJ'}(f)}{2} + a^{JJ'} \right), \\ G_Z &= \left(\frac{g}{2 \cos \theta_W}\right)^2 \frac{1}{s - m_Z^2 + im_Z \Gamma_Z}, \quad G_\gamma = \left(\frac{g \sin \theta_W}{2}\right)^2 \frac{1}{s}.\end{aligned}\quad (3.6)$$

Analogous formulas to the above ones hold for the other products,  $Ga^\pm \mathcal{B}$ ,  $Ga^\pm \mathcal{C}$ ,  $Ga^\pm \mathcal{D}$ . We have labelled the vertex functions for the photon current by the suffix  $\gamma$ . The formulas expressing the RPV one-loop contributions to the vertex functions are provided in Appendix 1, quoting the results derived in our previous work. [1] The amplitude  $M^{JJ'}$  in eq.(3.5) may be viewed as a  $4 \times 4$  matrix in the fermions polarization space,

$(f(p, \lambda) \bar{f}_{\lambda'}(p', \lambda') |M| l^+(k', \mu') l^-(k, \mu))$ . The various products in eq. (3.5) for the matrix elements with respect to the two pairs of Dirac spinors separate into 8 distinct terms. The calculation of the helicity amplitudes is most conveniently performed with the help of the ‘Mathematica’ package. Of the 16 configurations only the 8 helicity off diagonal configurations in the initial fermions are non vanishing. The explicit formulas for the helicity amplitudes are provided in Appendix 1.

### 3.2 Charged lepton energy distribution

The differential cross section for top production and decay is described in the factorization approximation. Ignoring the spin correlations, which corresponds to dropping the spin non diagonal contributions between the production and decay stages, yields :

$$\begin{aligned} d\sigma &= \frac{|p|}{128\pi s|k|} \frac{m_t}{\pi} \int d(\cos \theta) \sum_{\lambda} |M_{prod}(l^- l^+ \rightarrow t_{\lambda} \bar{c})|^2 \int dp^2 \frac{1}{|p^2 - m_t^2 + im_t \Gamma_t|^2} d\Gamma_t, \\ d\Gamma_t &= \frac{1}{(2\pi)^3 8m_t} \sum_{\lambda'} |M_{dec}(t_{\lambda'} \rightarrow b l^+ \nu)|^2 dE_l^* dE_b^*. \end{aligned} \quad (3.7)$$

The production amplitude is denoted,  $M_{prod}$ , the top decay amplitude,  $M_{dec}$ , and  $\lambda, \lambda' = \pm 1$ , are polarization labels, which will also be written for short as,  $\pm$ . We shall assume a narrow resonance approximation for the top propagator,  $|p^2 - m_t^2 + im_t \Gamma_t|^{-2} \rightarrow \frac{\pi}{m_t \Gamma_t} \delta(p^2 - m_t^2)$ . For the energies of interest, all the leptons and quarks, with the exception of the top, may be treated as massless. Two frames of interest are the laboratory ( $l^- l^+$ ) rest frame and the top rest frame. The letters denoting momentum variables in the  $l^- l^+$  center of mass (laboratory) frame are distinguished from those in the top rest frame by the addition of a star. Standard kinematical methods [34] can be used to transform variables between these frames. Exploiting the rotational invariance, one may conveniently choose to work in the spatial frame where the top momentum lies in the  $xOz$  plane ( $\theta, \phi = 0$ ) and the charged lepton points in an arbitrary direction described by the spherical angles,  $\theta_l, \phi_l$ . The relations between angles may be obtained by use of the spherical triangle identities, for example, the angle between lepton and top reads,  $\cos \theta_{lt} = \cos \theta_l \cos \theta + \sin \theta_l \sin \theta \cos \phi_l$ . The Lorentz boost from the top rest frame to the laboratory frame, involves a velocity parameter,  $\vec{v} = \vec{p}/E_p$ ,  $\beta = p/E_p$ ,  $\gamma = (1 - \beta^2)^{-1/2} = E_p/m_t$ , and yields for the charged lepton momentum four vector and polar angle relative to the top momentum,  $E_l^* = \gamma(E_l - \vec{v} \cdot \vec{k}_l)$ ,  $\vec{k}_l^* = \vec{k}_l + \gamma \vec{v} (\frac{\gamma \vec{v} \cdot \vec{k}_l}{\gamma + 1} - E_l)$ ,  $\cos \theta_{lt}^* = \frac{\cos \theta_{lt} - \beta}{1 - \beta \cos \theta_{lt}}$ .

The top differential semileptonic decay rate has been thoroughly studied in the literature. [35] One representation convenient for our purposes is the double differential rate with respect to the final charged lepton energy,  $E_l^*$ , and the final lepton and neutrino invariant mass squared,  $W^2 = (k_l + k_{\nu})^2$ . The result for the unpolarized rate carries no dependence on the scattering angles and reads, quoting from ref.[35],

$$\begin{aligned} d\Gamma_t &= \frac{N_l G_F^2 m_t^5}{16\pi^3} dx_l \int dy \frac{x_l(x_M - x_l)}{(1 - y\xi)^2 + \gamma^2}, \\ &= \frac{N_l G_F^2 m_t^5}{16\pi^3} \frac{2}{m_t} \frac{x_l(x_M - x_l)}{\gamma\xi} \tan^{-1} \frac{\gamma\xi x_l(x_M - x_l)}{(1 + \gamma^2)(1 - x_l) - \xi x_l(x_M - x_l)} dE_l^*. \end{aligned} \quad (3.8)$$

The kinematical variables for the emitted charged lepton and neutrino are defined as,  $x_l = 2E_l^*/m_t$ ,  $y = W^2/m_t^2$ ,  $[W = k_l + k_{\nu}]$  with the bounds,  $0 < x_l < x_M$ ,  $0 < y <$

$\frac{x_l(x_M - x_l)}{1 - x_l}$  and we employ the following notations,  $N_l$  for the number of light lepton flavors,  $\gamma = \Gamma_W/m_W$ ,  $\xi = m_t^2/m_W^2$ ,  $x_M = 1 - \epsilon^2$ ,  $\epsilon = m_b/m_t$ ,  $\tan^{-1} A = \text{Artan}|A| + \pi\theta(-A)$ . Recall that the number of light lepton flavors,  $N_l$ , is set to  $N_l = 2$  in our analysis. A useful trick to obtain the distribution with respect to the laboratory frame lepton energy,  $E_l$ , is to choose the top momentum along the  $Oz$  axis fixed frame and introduce the top rest frame electron energy by means of the change of variable,  $(E_l, \cos\theta_l^*) \rightarrow (E_l, E_l^*)$ , associated with the Lorentz boost between the top rest frame and the laboratory frame,  $E_l = \gamma E_l^*(1 + \beta \cos\theta_l^*)$ . The result reads,

$$\frac{d\Gamma_t}{dE_l} = \int_{-1}^{+1} d\cos\theta_l^* \frac{d^2\Gamma_t}{dE_l d\cos\theta_l^*} = \frac{2}{m_t\gamma\beta} \int_{x_l^-}^{x_l^+} \frac{dx_l}{x_l} \frac{d^2\Gamma_t}{dx_l d\cos\theta_l^*}, \quad (3.9)$$

where the integration interval over  $x_l$  is bounded at,  $x_l^\pm = \frac{2E_l}{m_t\gamma(1\pm\beta)}$ .

### 3.3 Top polarization observables

An essential use will be made of the factorization property of the double differential distribution for the top decay semileptonic rate with respect to the emitted lepton energy and angle relative to the top spin polarization vector. This distribution is described at the tree level as,  $\frac{d^2\Gamma_t}{dE_l^* d\cos\psi_l} = \frac{d\Gamma_t}{dE_l^*} \frac{1+\cos\psi_l}{2}$ , where,  $\cos\psi_l = -s(p) \cdot k_l$ , is the angle between the lepton momentum and the top spin polarization vector,  $s_\mu(p)$ , in the top rest frame. Equivalently,  $\frac{d^2\Gamma_t}{dx_l d\cos\theta_l^*} = \frac{d\Gamma_t}{dx_l} \frac{1+\cos\psi_l}{2} \frac{d\cos\psi_l}{d\cos\theta_l^*}$ . [35] As it turns out, this representation remains valid to a good approximation when one-loop QCD corrections are included. [36] We choose to describe the top polarization in the spin helicity formalism, using techniques familiar from previous works. [5, 37] The definition for the helicity basis Dirac spinors is provided in Appendix 1. Since the polarization axis coincides then with the top momentum, the dependence on  $\psi_l$  can also be simply rewritten as,  $(1 + \cos\psi_l)/2 = (1 + \lambda \cos\theta_l^*)/2$ , such that,  $\lambda = [-1, +1]$ , correspond to  $[L, R]$  helicity, respectively.

The helicity amplitudes associated to the pair of CP-conjugate processes are related by the action of  $CP$  as,  $\langle f_\lambda \bar{f}_{\lambda'} | M | l_{\mu'}^+ l_{\mu}^- \rangle \rightarrow \langle f_{-\lambda'}^* \bar{f}_{-\lambda} | M | l_{-\mu}^+ l_{-\mu'}^- \rangle$ . Unlike the process,  $l^+ l^- \rightarrow t\bar{t}$ , where both the initial and final states are self-conjugate under CP, here only the initial state is self-conjugate, while the action of CP relates the different final states,  $t\bar{c}$  and  $c\bar{t}$ . Let us express the amplitudes for the pair of CP-conjugate processes as sums of tree and loop terms,  $M^{JJ'} = a_0 + \sum_\alpha b_\alpha f_\alpha(s + i\epsilon)$ ,  $\bar{M}^{JJ'} = a_0^* + \sum_\alpha b_\alpha^* f_\alpha(s + i\epsilon)$ , where the loop terms,  $b_\alpha f_\alpha(s + i\epsilon)$ , are linear combinations with real coefficients of the vertex functions,  $A_L^{JJ'}$ ,  $A_R^{JJ'}$ ,  $a^{JJ'}$ ,  $id^{JJ'}$ , with the energy dependent complex functions,  $f_\alpha(s + i\epsilon)$ , representing the factors in loop amplitudes which include the absorptive parts. In terms of these notations, a CP asymmetry associated with the difference of rates for the pair of CP-conjugate processes in some given CP-conjugate configurations of the particles polarizations, can be written schematically as,

$$\begin{aligned} | \langle \lambda \lambda' | M | \mu' \mu \rangle |^2 &- | \langle -\lambda' - \lambda | M | -\mu - \mu' \rangle |^2 \propto \sum_\alpha \text{Im}(a_0 b_\alpha^*) \text{Im}(f_\alpha(s + i\epsilon)) \\ &- \sum_{\alpha < \alpha'} \text{Im}(b_\alpha b_{\alpha'}^*) \text{Im}(f_\alpha(s + i\epsilon) f_{\alpha'}^*(s + i\epsilon)). \end{aligned} \quad (3.10)$$

Thus, the necessary conditions for a non vanishing polarized asymmetry to arise from the tree-loop interference term are a relative complex CP-odd phase between the tree and

loop coupling constants and an absorptive part from the loop terms. The angle integrated production rates for the CP-conjugate reactions,  $l^+l^- \rightarrow t\bar{c}$  and  $l^+l^- \rightarrow c\bar{t}$ , for the case of polarized top and antitop, respectively, are obtained by summing over the polarization of the  $c$ ,  $\bar{c}$  quarks as,

$$\begin{aligned}\sigma(t_L) &= \sigma(t_L\bar{c}_R) + \sigma(t_L\bar{c}_L), \quad \sigma(t_R) = \sigma(t_R\bar{c}_L) + \sigma(t_R\bar{c}_R), \\ \sigma(\bar{t}_L) &= \sigma(\bar{t}_L c_R) + \sigma(\bar{t}_L c_L), \quad \sigma(\bar{t}_R) = \sigma(\bar{t}_R c_L) + \sigma(\bar{t}_R c_R).\end{aligned}\quad (3.11)$$

Forming the half differences and sums of rates,  $\delta\sigma = \frac{1}{2}(\sigma(t_L) - \sigma(t_R))$ ,  $\delta\bar{\sigma} = \frac{1}{2}(\sigma(\bar{t}_R) - \sigma(\bar{t}_L))$ ,  $\sigma_{av} = \frac{1}{2}(\sigma(t_L) + \sigma(t_R))$ ,  $\bar{\sigma}_{av} = \frac{1}{2}(\sigma(\bar{t}_R) + \sigma(\bar{t}_L))$ , such that,  $\sigma(t_{L,R}) = \sigma_{av} \pm \delta\sigma$ ,  $\bar{\sigma}(t_{R,L}) = \bar{\sigma}_{av} \pm \delta\bar{\sigma}$ , one can define the following two CP-odd combinations,

$$\mathcal{A} = \frac{\sigma_{av} - \bar{\sigma}_{av}}{\sigma_{av} + \bar{\sigma}_{av}} = \frac{\sigma_{t\bar{c}} - \sigma_{\bar{t}c}}{\sigma_{t\bar{c}} + \sigma_{\bar{t}c}}, \quad \mathcal{A}^{pol} = \frac{\delta\sigma - \delta\bar{\sigma}}{\sigma_{av} + \bar{\sigma}_{av}}, \quad (3.12)$$

which will be designated as unpolarized and polarized integrated rate asymmetries. The above definition for the unpolarized asymmetry,  $\mathcal{A}$ , is identical to the one studied in our previous work. [1] The asymmetries depend on the RPV coupling constants through the ratio of loop to tree amplitudes as,  $Im(\frac{\lambda'_{ijk}\lambda'_{i'j'k'}}{\lambda'_{1jk'}\lambda'_{1j'k'}}) \propto \sin\psi$ , where the dependence on the CP violation angle parameter,  $\psi$ , reflects the particular prescription adopted in this study to include the CP-odd phase. The index  $k'$  refers to the d-squark generation in the tree amplitude and the indices  $i, k$  to the fermion-sfermion generations for the internal fermion-sfermion pairs,  $(\begin{smallmatrix} d_k \\ \tilde{e}_{iL}^* \end{smallmatrix})$ ,  $(\begin{smallmatrix} e_i^c \\ \tilde{d}_{kR} \end{smallmatrix})$ , in the loop amplitude.

It is important not to confuse the above analysis with that of the top-antitop pair production,  $l^-l^+ \rightarrow t\bar{t}$ , where a CP-odd asymmetry observable for a single final state may be defined in terms of the difference of helicity configurations,  $\sigma(t_L\bar{t}_L) - \sigma(t_R\bar{t}_R)$ . A non vanishing value for the corresponding difference of polarized rates can only arise via tree-loop interference terms involving the absorptive part of the top quark electric dipole moment,  $Im(d_t^{JJ})$ . [6, 7] One should note here that the one-loop contribution of the RPV  $\lambda'$  interactions to  $Im(d_t^{JJ})$  vanishes. Two closely related processes, which are amenable to an analogous treatment, are the  $b\bar{b}$  quark pair [38] and  $\tau^+\tau^-$  lepton pair production. Double spin correlation observables for the latter reaction,  $l^-l^+ \rightarrow \tau^-\tau^+$ , have been examined in a recent work. [39] We note that the RPV  $\lambda$  interactions can give a non vanishing contribution to  $Im(d_\tau^{JJ})$ .

The results for the rate asymmetries are displayed in Fig.6. The numerical results for the unpolarized case (window (A) in Fig.6) update the results presented in ref. [1] since the present calculation includes the contributions from the Lorentz covariant tensorial ( $\sigma_{\mu\nu}$ ) coupling which were ignored in our previous work. [1] The asymmetry for the polarized case (window (B) in Fig.6) involves the difference of the spin helicity asymmetry in the total production cross sections for the CP mirror conjugate top and antitop mirror reactions. While this CP-odd polarized asymmetry is not directly observable, it enters as an important intermediate quantity in evaluating the measurable kinematic distributions of the top decay products dependent on the top spin. We have assumed all the relevant RPV coupling constants to be equal and set the CP-odd phase at  $\sin\psi = 1$ . The rapid change in slope for the  $\tilde{m} = 200 \text{ GeV}$  case are due to the threshold effect from the imaginary part in the superpartner one-loop contributions, which set at  $\sqrt{s} = 400 \text{ GeV}$ . Aside from this large discontinuous contribution, one sees that both asymmetries comprise

another contribution which is nearly independent of  $\tilde{m}$  and increases smoothly with the initial energy. Both asymmetries,  $\mathcal{A}$  and  $\mathcal{A}^{pol}$ , take values of order a few  $10^{-3}$ , reaching  $O(10^{-2})$  at the highest incident energies.

The statistical uncertainties on the asymmetry may be evaluated in terms of the signal cross sections and the integrated luminosity by considering the approximate definition,  $\delta\mathcal{A} = 1/[\mathcal{L}(\sigma_{t\bar{c}} + \sigma_{\bar{t}c})]^{1/2}$ . Using the same input value for the luminosity  $\mathcal{L} = 100. fb^{-1}$  at the three cm energies,  $\sqrt{s} = [0.192, 0.5, 1.] TeV$ , along with the cut signal rates in Table 15, we obtain statistical errors on the asymmetries of order  $O(10^{-1})$ . These values lie nearly two order of magnitudes above the value obtained for the signal. At this point, it is important to observe that in getting the above estimates for the rates we have been using somewhat conservative assignments for the RPV coupling constants. As already noted, the single top production cross sections could possibly be two order of magnitudes larger if we were to use coupling constants values of order,  $\lambda'_{12k}\lambda'_{13k} \simeq 10^{-1}$ . Such values are compatible with the indirect bounds only for the extreme down squark mass  $\tilde{m} = O(1 TeV)$  range. In the hypothetical case where the production rates would be enhanced by two order of magnitudes, the statistical errors on the asymmetries would correspondingly get reduced by a factor  $O(10^{-1})$ , thereby reaching the same order of magnitude as the signal asymmetries. Nevertheless, as plotted in window (A) of Fig.6, the corresponding errors would still be somewhat larger than the signals. We should note here that the contribution to the one-loop amplitude from internal sfermion and fermion lines belonging to the third generation is controlled by the coupling constants quadratic product,  $\lambda'_{323}\lambda'_{333}$ , which is subject to weak constraints. Should the RPV coupling constants exhibit a hierarchical structure with respect to the quarks and leptons generations, one cannot exclude the possibility of a factor 10 enhancement from the ratio,  $Im(\lambda'_{323}\lambda'_{333}/\lambda'_{123}\lambda'_{133})$ . Such an order of magnitude gain on this ratio would raise the asymmetries up to  $O(10^{-1})$  bringing them well above the experimental uncertainties. Lastly, we observe that a more complete formula for the uncertainties on the asymmetries reads,  $(\delta\mathcal{A})^2 = 2(\delta\sigma_{t\bar{c}})^2[1 - C + (1 + C)\mathcal{A}^2]/(\sigma_{t\bar{c}} + \sigma_{\bar{t}c})^2$ , where we used equal standard deviations for the CP conjugate reactions rates,  $\delta\sigma_{t\bar{c}} = \delta\sigma_{\bar{t}c}$ , and denoted the correlated error on these two rates as,  $C = \langle \delta\sigma_{t\bar{c}}\delta\sigma_{\bar{t}c} \rangle / \delta\sigma_{t\bar{c}}^2$ . Clearly, an improvement on the statistical treatment of the  $t\bar{c} + \bar{t}c$  events sample, allowing for a positive non vanishing value of the error correlation associated with the identification of isolated single negatively and positively charged lepton events, should greatly help in reducing the experimental uncertainties caused by the small event rates.

The energy distribution for the negatively and positively charged leptons in the pair of CP-conjugate reactions may be defined as,

$$\begin{aligned} \langle \sigma^+ \rangle &\equiv \langle \frac{d\sigma^+}{dE_l} \rangle = \langle \sigma(t_L)f_L + \sigma(t_R)f_R \rangle, \\ \langle \sigma^- \rangle &\equiv \langle \frac{d\sigma^-}{dE_l} \rangle = \langle \sigma(\bar{t}_R)f_L + \sigma(\bar{t}_L)f_R \rangle, \end{aligned} \quad (3.13)$$

where the correlations between the top spin lepton momentum are described by the factors,  $f_{L,R} = \frac{1}{2}(1 \mp \cos\theta_l^*)$ , and the brackets stand for the angular integration. The occurrence of angular correlation factors of opposite signs in the  $\bar{t}$  production case accounts for the kinematical fact that the antitop is oriented in space with a momentum  $-\vec{p}$ . A CP-odd charge asymmetry observable with respect to the charged lepton energy distribution may

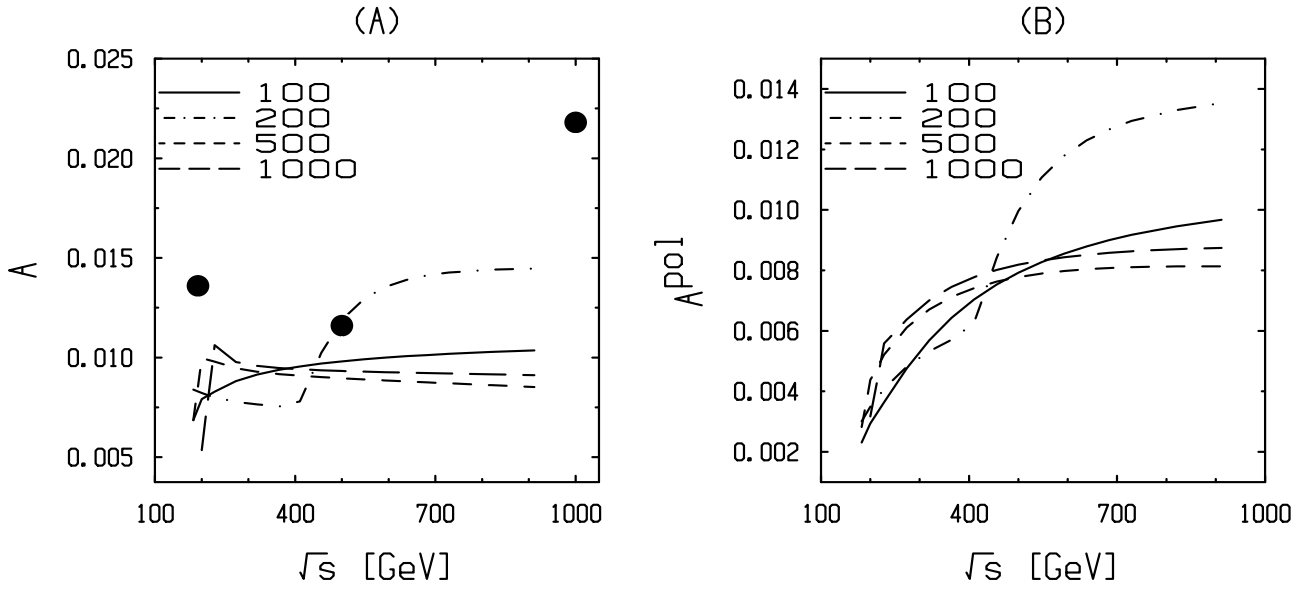


FIG. 6: The CP-odd production rate asymmetries as a function of the center of mass energy,  $s^{\frac{1}{2}}$ , for fixed values of the down squark mass,  $\tilde{m} = [100, 200, 500, 1000] \text{ GeV}$ . The left hand plot (A) gives the unpolarized asymmetry,  $\mathcal{A} = (\sigma_{av} - \bar{\sigma}_{av})/(\sigma_{av} + \bar{\sigma}_{av})$ . The upper bounds for the absolute values of the statistical errors on the asymmetries, as evaluated with  $\lambda'_{12k}\lambda'_{13k} = 0.1$ ,  $\tilde{m} = 100 \text{ GeV}$  and integrated luminosities  $\mathcal{L} = 100. \text{ fb}^{-1}$  are shown as full circles. The right hand plot (B) gives the spin polarization dependent asymmetry,  $\mathcal{A}^{pol} = (\delta\sigma - \delta\bar{\sigma})/(\sigma_{av} + \bar{\sigma}_{av})$ .

be defined by considering the following normalized difference of distributions,

$$\Delta\mathcal{A}^{pol} = \frac{\langle \sigma^+ \rangle - \langle \sigma^- \rangle}{\langle \sigma^+ \rangle + \langle \sigma^- \rangle} = \frac{(\sigma_{av} - \bar{\sigma}_{av}) + \langle (\delta\sigma - \delta\bar{\sigma})(f_L - f_R) \rangle}{(\sigma_{av} + \bar{\sigma}_{av}) + \langle (\delta\sigma + \delta\bar{\sigma})(f_L - f_R) \rangle}. \quad (3.14)$$

The numerical results for the charged lepton energy distributions and for the above defined charge asymmetry in the lepton energy distributions are displayed in Fig.7. (Note that the transverse energy distribution, in the plane orthogonal with respect to the top momentum, may be simply obtained as,  $\frac{d\Gamma}{dE_{lT}} = \frac{d\Gamma}{dE_l} \frac{1}{\sin\theta_{lt}^*}$ . The distribution in the plane orthogonal to the collision axis is less trivial to evaluate since this requires an additional integration over the lepton azimuthal angle.) The energy distributions for the unpolarized cross section essentially reproduce the results found in our above quoted event generator predictions, Fig.3. The energy distributions for the polarized asymmetry lie at values of order of magnitude,  $O(10^{-3})$ , always retaining the same positive sign as the lepton energy varies. For a fixed energy of the emitted lepton, the asymmetry increases with the initial energy, reaching values of order  $O(10^{-2})$ . In window (B) of Fig.7 we have plotted the experimental uncertainties using the same inputs for the luminosities and the rates as in the discussion of the unpolarized asymmetries given above. To ease the comparison with experiment, we divide the charged leptons energy interval into three bins of width  $100 \text{ GeV}$  each, centered at the three lepton energies,  $E_l = (50, 150, 250) \text{ GeV}$ . The statistical errors on the asymmetries in the energy distributions lie at the same level as those associated to the



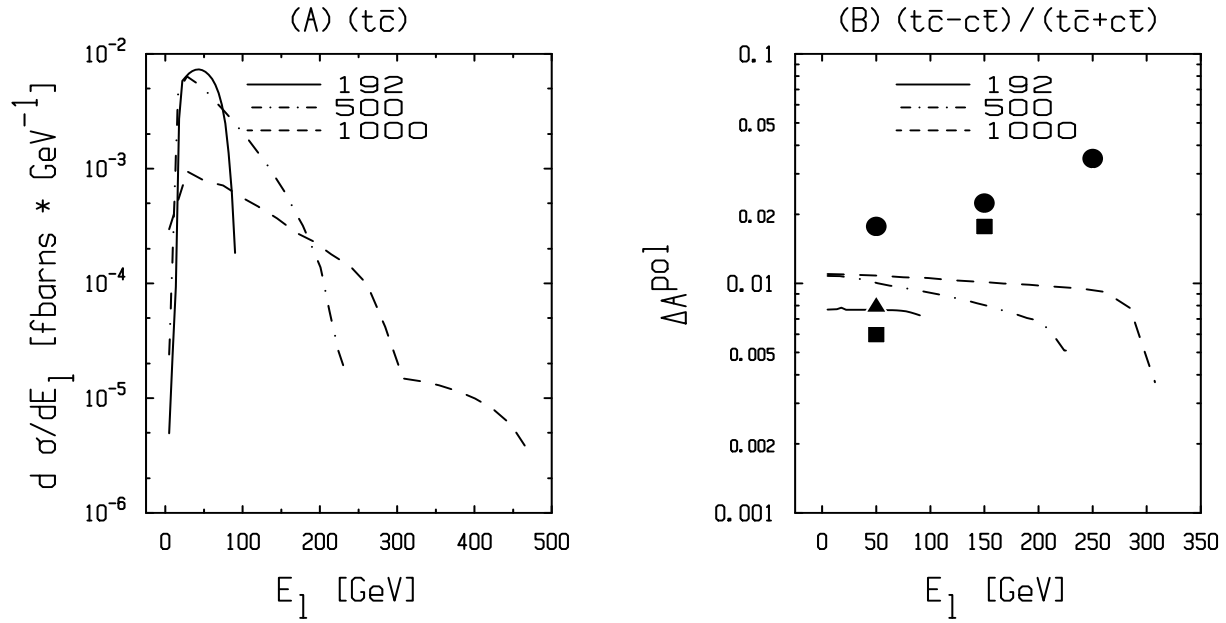


FIG. 7: Energy distribution for the charged lepton as a function of the laboratory frame lepton energy, for a set of center of mass energy,  $s^{\frac{1}{2}} = [192, 500, 1000] \text{ GeV}$ . The parameters are set at,  $\lambda' = 0.1$ ,  $\tilde{m} = 100 \text{ GeV}$ . The left hand plot (A) gives the differential lepton energy distribution,  $\frac{d\sigma}{dE_l}$ . The right hand plot (B) gives the asymmetry in the energy distribution for leptons of opposite charges in the CP-conjugate final state channels,  $(t\bar{c})$  and  $(c\bar{t})$ :  $\Delta\mathcal{A}^{pol} = [\frac{d\sigma^+}{dE_l} - \frac{d\sigma^-}{dE_l}] / [\frac{d\sigma^+}{dE_l} + \frac{d\sigma^-}{dE_l}]$ . The upper bounds for the absolute values of the statistical errors on the asymmetries, as evaluated with  $\lambda'_{12k}\lambda'_{13k} = 0.1$  and with integrated luminosities,  $\mathcal{L} = 100. \text{ fb}^{-1}$ , are shown for three energy bins of width  $100 \text{ GeV}$  each, centered at the charged lepton energies,  $E_l = (50, 150, 250) \text{ GeV}$ . The results for three values of the center of mass energy,  $s^{\frac{1}{2}} = [192, 500, 1000] \text{ GeV}$  are displayed by full triangles, squares and circles.

total asymmetries, so that similar conclusions should apply. Setting ourselves within the same optimistic scenario by using  $\lambda'_{12k}\lambda'_{13k} = 10^{-1}$  and  $\mathcal{L} = 100 \text{ fb}^{-1}$ , we obtain expected errors of order  $O(10^{-2})$ . These values are insufficient for a comfortable identification of a signal asymmetry. However, we reiterate, as in the above discussion, that an enhancement of the signal asymmetries to an observable level of  $O(10^{-1})$ , due to a hierarchical structure in the generation dependence of the  $\lambda'_{ijk}$ , is a real possibility.

## 4 Conclusions

We have demonstrated that single top production through the RPV interactions could be observed at the future linear colliders or else be used to set bounds on the RPV coupling constants,  $\lambda'_{12k}\lambda'_{13k} < O(10^{-2})$ , over a wide interval for the down squark mass,  $m_{\tilde{d}_{kR}} < 1. \text{ TeV}$ . The  $b$  quark tagging would help greatly to overcome the background. Even with an imperfect  $b$  quark tagging, it is still possible to drastically reduce the background,

from  $WW$  and  $b\bar{b}$ , without much harming the signal. The analysis of top polarization observables via the semileptonic decay channel of the top allows to test for the presence of a CP violating complex phase, embedded in quadratic products of the RPV coupling constants. We have focused on the asymmetry in the energy distributions of the charged leptons in the CP-conjugate pair of final states,  $bl^+\nu\bar{c}$  and  $\bar{b}l^-\bar{\nu}c$ , obtaining asymmetries of order  $10^{-3} - 10^{-2}$  for the incident energies expected at the future leptonic colliders. These values lie somewhat below the anticipated limits of observability. However, it may be possible to obtain enhanced values of order  $10^{-1}$ , should the RPV coupling constants  $\lambda'_{ijk}$  exhibit large hierarchies with respect to the quarks or leptons generations. Future promising extensions might include analogous reactions accessible with lepton-photon or photon-photon colliding beams,  $l\gamma \rightarrow t\bar{c}$ ,  $\gamma\gamma \rightarrow t\bar{c}$ , where the expected production rates are substantially larger than those for the  $l^-l^+$  colliders.

# 1 Helicity amplitudes and one-loop $\mathcal{R}_p$ vector boson vertex functions

## Helicity amplitudes.

The helicity spin basis Dirac spinors for a fermion or an antifermion, of mass  $m$  and four momentum,  $k_\mu = (E_k = (k^2 + m^2)^{\frac{1}{2}}, \vec{k})$ , and polar coordinates,  $\vec{k} = (\theta, \phi)$ , can be written in the form of direct products of the Dirac spinor two-component space with the two-component space of Pauli helicity basis spinors,  $\phi_\lambda(\vec{k})$ , satisfying,  $\vec{\sigma} \cdot \hat{k} \phi_\lambda(\vec{k}) = \lambda \phi_\lambda(\vec{k})$ . In the Dirac representation for the Dirac matrices,  $\gamma_0 = \beta$ ,  $\vec{\gamma} = \beta \vec{\alpha}$ ,  $\gamma_5 = \begin{pmatrix} 0 & 1 \\ -1 & 0 \end{pmatrix}$ , the spinors read,

$$\begin{aligned} u(\vec{k}, \lambda) &= \sqrt{\epsilon_k} \begin{pmatrix} 1 \\ \tilde{k}_\lambda \end{pmatrix} \times \phi_\lambda(\vec{k}), \quad v(\vec{k}, \lambda) = \sqrt{\epsilon_k} \begin{pmatrix} -\tilde{k}_\lambda \\ 1 \end{pmatrix} \times \phi_{-\lambda}(\vec{k}), \\ \phi_{-1}(\vec{k}) &= \begin{pmatrix} -\sin(\theta/2)e^{-i\phi} \\ \cos(\theta/2) \end{pmatrix}, \quad \phi_{+1}(\vec{k}) = \begin{pmatrix} \cos(\theta/2) \\ \sin(\theta/2)e^{+i\phi} \end{pmatrix}, \end{aligned} \quad (1.1)$$

where,  $\epsilon_k = E_k + m$ ,  $\tilde{k} = |\vec{k}|/(E_k + m)$ , and  $\chi_\lambda$ ,  $[\lambda = \pm 1]$ , are the Pauli spinors in the basis with a fixed quantization axis identified with the spatial three-axis,  $Oz$ . The helicity basis spin eigenstates with a space parity reversed three momentum are defined as,  $\phi_\lambda(-\vec{k}) = e^{-i(\phi+\pi)(\lambda'-\lambda)/2} (e^{-i\frac{(\pi-\theta)}{2}\sigma_y})_{\lambda'\lambda} \chi_{\lambda'} = \phi_\lambda(\vec{k})|_{[\theta \rightarrow \pi-\theta, \phi \rightarrow \phi+\pi]}$ .

The 8 non vanishing helicity amplitudes for the process,  $l^+(k', \mu') + l^-(k, \mu) \rightarrow u_J(p, \lambda) + \bar{u}_{J'}(p', \lambda')$ , are listed in the formulas below :

$$\begin{aligned} M_1 = M(+ - + -) &= 4\mathcal{F} [-(1 + \tilde{p}\tilde{p}') (X_1 + X_2) + (\tilde{p} + \tilde{p}') (X_3 + X_4)] \sin^2(\theta/2), \\ M_2 = M(+ - + +) &= 2\mathcal{F} [(-1 + \tilde{p}\tilde{p}') (X_1 + X_2) + (\tilde{p} - \tilde{p}') X_3 + (\tilde{p} - \tilde{p}') X_4 \\ &\quad + 2p(\tilde{p} + \tilde{p}') (X_5 + X_6) + 2p(1 + \tilde{p}\tilde{p}') (X_7 + X_8)] \sin(\theta), \\ M_3 = M(- + + -) &= -4\mathcal{F} [-(1 + \tilde{p}\tilde{p}') (-X_1 + X_2) - (\tilde{p} + \tilde{p}') (X_3 - X_4)] \cos^2(\theta/2), \\ M_4 = M(- + + +) &= 2\mathcal{F} [(-1 + \tilde{p}\tilde{p}') (-X_1 + X_2) + (-\tilde{p} + \tilde{p}') (X_3 - X_4) \\ &\quad - 2p(\tilde{p} + \tilde{p}') (X_5 - X_6) - 2p(1 + \tilde{p}\tilde{p}') (X_7 - X_8)] \sin(\theta), \\ M_5 = M(+ - - -) &= 2\mathcal{F} [(-1 + \tilde{p}\tilde{p}') (X_1 + X_2) + (-\tilde{p} + \tilde{p}') X_3 + (-\tilde{p} + \tilde{p}') X_4 \\ &\quad + 2p(\tilde{p} + \tilde{p}') (X_5 + X_6) - 2p(1 + \tilde{p}\tilde{p}') (X_7 - X_8)] \sin(\theta), \\ M_6 = M(+ - - +) &= -4\mathcal{F} [(1 + \tilde{p}\tilde{p}') (X_1 + X_2) + (\tilde{p} + \tilde{p}') (X_3 + X_4)] \cos^2(\theta/2), \\ M_7 = M(- + - -) &= 2\mathcal{F} [(-1 + \tilde{p}\tilde{p}') (-X_1 + X_2) + (\tilde{p} - \tilde{p}') (X_3 - X_4) \\ &\quad - 2p(\tilde{p} + \tilde{p}') (X_5 - X_6) + 2p(1 + \tilde{p}\tilde{p}') (X_7 - X_8)] \sin(\theta), \\ M_8 = M(- + - +) &= 4\mathcal{F} [-(1 + \tilde{p}\tilde{p}') (X_1 - X_2) - (\tilde{p} + \tilde{p}') (X_3 - X_4)] \sin^2(\theta/2). \end{aligned} \quad (1.2)$$

The arguments refer to the fermions helicity in the following order,  $M_i((h_{e^+}, h_{e^-}, h_f, h_{\bar{f}}))$ . The remaining helicity amplitudes, omitted from the above list, are understood to vanish identically. We denote by  $\theta$  the top scattering angle,  $\cos \theta = \vec{k} \cdot \vec{p}$ , by  $[E_p, E'_p] = (s \pm m_J^2 \mp m_{J'}^2)/2\sqrt{s}$ , the top and charm quarks energies, and use the following abbreviated notations,  $\tilde{p} = \frac{p}{E_p + m_J}$ ,  $\tilde{p}' = \frac{p}{E'_p + m_{J'}}$ ,  $\mathcal{F} = \frac{1}{2}[s(E_p + m_J)(E'_p + m_{J'})]^{\frac{1}{2}}$ , along with the useful compact notations,

$$\begin{aligned} X_1 &= Ga^+ \mathcal{A} + \mathcal{R}, \quad X_2 = Ga^- \mathcal{A} + \mathcal{R}, \quad X_3 = Ga^+ \mathcal{B} + \mathcal{R}, \quad X_4 = Ga^- \mathcal{B} + \mathcal{R}, \\ X_5 &= \frac{1}{2}Ga^+ \mathcal{C}, \quad X_6 = \frac{1}{2}Ga^- \mathcal{C}, \quad X_7 = \frac{1}{2}Ga^+ \mathcal{D}, \quad X_8 = \frac{1}{2}Ga^- \mathcal{D}, \end{aligned} \quad (1.3)$$

where  $Ga^\pm \mathcal{A}, \dots$  are defined in eq. (3.6),  $\mathcal{R}$  in eq. (3.4), and  $\mathcal{A}, \dots, \mathcal{D}$ , in eq. (3.2).

### One-loop RPV vector boson vertex functions.

The one-loop vertex functions, as derived in [1], are given by the formulas,

$$\begin{aligned}
A_L^{JJ'} &= \frac{\lambda'_{iJ'k} \lambda'^{\star}_{iJk}}{(4\pi)^2} [a_L(u) B_1^{(2)} + a(f_L) m_f^2 C_0 + a(\tilde{f}') (2\tilde{C}_{24} + 2 m_J^2 (\tilde{C}_{12} - \tilde{C}_{21} + \tilde{C}_{23} - \tilde{C}_{11})) \\
&+ a(f_R) (B_0^{(1)} - 2 C_{24} - m_{\tilde{f}'}^2 C_0 + m_J^2 (C_0 + 3C_{11} - 2C_{12} + 2C_{21} - 2C_{23}) - m_{J'}^2 C_{12})], \\
A_R^{JJ'} &= \frac{\lambda'_{iJ'k} \lambda'^{\star}_{iJk}}{(4\pi)^2} m_J m_{J'} [2a(\tilde{f}') (-\tilde{C}_{23} + \tilde{C}_{22}) + a(f_R) (-C_{11} + C_{12} - 2C_{23} + 2C_{22})] \\
\begin{pmatrix} a^{JJ'} \\ -i d^{JJ'} \end{pmatrix} &= \frac{\lambda'_{iJ'k} \lambda'^{\star}_{iJk}}{(4\pi)^2} \frac{m_J + m_{J'}}{4} \left[ \pm m_J [a(f_R) (C_{11} - C_{12} + C_{21} - C_{23}) \right. \\
&- a(\tilde{f}') (\tilde{C}_{11} + \tilde{C}_{21} - \tilde{C}_{12} - \tilde{C}_{23})] + m_{J'} [a(f_R) (C_{22} - C_{23}) + a(\tilde{f}') (\tilde{C}_{23} - \tilde{C}_{22})] \Big]. \tag{1.4}
\end{aligned}$$

The relevant configurations for the internal fermion and sfermion propagating in the loop are :  $\begin{pmatrix} f \\ \tilde{f}' \end{pmatrix} = \begin{pmatrix} d_k \\ \tilde{e}_{iL}^* \end{pmatrix}, \begin{pmatrix} e_i^c \\ \tilde{d}_{kR} \end{pmatrix}$ . The notations for the Passarino-Veltman two-point and three-point integrals, as specified in our work, [1] are defined according to the following conventions,  $B_A^{(1)} = B_A(-p - p', m_f, m_f)$ ,  $B_A^{(2)} = B_A(-p, m_f, m_{\tilde{f}'})$ ,  $[A = 0, 1]$  and  $C_A = C_A(-p, -p', m_f, m_{\tilde{f}'}, m_f)$ ,  $\tilde{C}_A = C_A(-p, -p', m_{\tilde{f}'}, m_f, m_{\tilde{f}'})$ .  $[A = 0, 11, 12, 21, 22, 23]$  The integral functions with a tilde are associated with the one-loop diagram for the sfermion current.

# References

- [1] M. Chemtob and G. Moreau, Phys. Rev. **D59**, 116012 (1999)
- [2] C. Quigg, hep-ph/9802320; S. Willenbrock, hep-ph/9709355
- [3] J. Donoghue and G. Valencia, Phys. Rev. Lett. **58**, 451 (1987); ibidem, **60**, 243 (1988) (E); C.A. Nelson, Phys. Rev. **D41**, 2805 (1990)
- [4] D. Atwood and A. Soni, Phys. Rev. **D45**, 2405 (1992); W. Bernreuther, T. Schröder, and T.N. Pham, Phys. Lett. **B279**, 389 (1992); W. Bernreuther, O. Nachtmann, P. Overmann, and T. Schröder, Nucl. Phys. **B388**, 53 (1992); B. Grzadkowski and J. Gunion, Phys. Lett. **B287**, 237 (1992)
- [5] G.L. Kane, G.A. Ladinsky, and C.P. Yuan, Phys. Rev. **D45**, 124 (1992)
- [6] C. R. Schmidt and M.E. Peskin, Phys. Rev. Lett. **69**, 410 (1992); C.R. Schmidt, Phys. Lett. **B293**, 111 (1992)
- [7] D. Chang and W.-Y. Keung, Phys. Lett. **B305** (1993) 261; D. Chang, W.-Y. Keung, and I. Phillips, Nucl. Phys. **B408** (1993) 286; ibidem, **B429**, 255 (1994) (E)
- [8] W. Bernreuther and A. Brandenburg, Phys. Rev. **D49**, 4481 (1994); T. Arens and L.M. Seghal, Phys. Rev. **D50**, 4372 (1994); P. Poulose and S. Rindani, Phys. Lett. **B349**, 379 (1995); B. Grzadkowski and Z. Hioki, Nucl. Phys. **B484**, 17 (1997); H.-Y. Zhou, Phys. Rev. **D58**, 114002 (1998)
- [9] A. Bartl, E. Christova, T. Gajdosik, and W. Majerotto, Phys. Rev. **D58**, 074007 (1998); ibidem, Phys. Rev. **D59**, 077503 (1999)
- [10] W. Hollik, J.I. Illana, S. Rigolin, C. Schappacher, and D. Stöckinger, Nucl. Phys. **B551**, 3 (1999); ibidem, **B557**, 407 (1999)
- [11] K.-I. Hikasa Phys. Lett. **B149**, 221 (1984)
- [12] T. Han and J.L. Hewett, hep-ph/9811237
- [13] K.J. Abraham, K. Whisnant, and B.-L. Young, Phys. Lett. **B419**, 381 (1998)
- [14] V. Barger and H. Hagiwara, Phys. Rev. **D37**, 3320 (1988)
- [15] D. Atwood, L. Reina, and A. Soni, Phys. Rev. **D53**, 1199 (1996); ibidem **D55**, 3157 (1997); Phys. Rev. Lett. **75**, 3800 (1995)
- [16] D. Atwood, S. Bar-Shalom, G. Eilam, and A. Soni, Phys. Rev. **D54**, 5412 (1996)
- [17] A. Datta, J.M. Yang, B.-L. Young, and X. Zhang, Phys. Rev. **D56**, 3107 (1997)
- [18] R.J. Oakes, K. Whisnant, J.M. Yang, B.-L. Young, and X. Zhang, Phys. Rev. **D57**, 534 (1998)
- [19] V. Mahanta and A. Ghosal, Phys. Rev. **D57**, 1735 (1998)

- [20] Z.-H. Yu, H. Pietschmann, W.-G. Ma, L. Han, and J. Yi, hep-ph/9903471 ; ibidem, hep-ph/9910323
- [21] Y. Koide, hep-ph/9701261
- [22] C.H. Chang, X.-Q. Li, J.-X. Wang, and M.-Z. Yang, Phys. Lett. **B313**, 389 (1993)
- [23] C.S. Huang, X.-H. Wu, and S.H. Zhu, Phys. Lett. **B452**, 143 (1999)
- [24] S. Bar-Shalom, G. Eilam, A. Soni, and J. Wudka, Phys. Rev. Lett. **79**, 1217 (1997) ; ibidem, Phys. Rev. **D57**, 2957 (1998) ; W.-S. Hou, G.-L. Lin and C.-Y. Ma, Phys. Rev. **D56**, 7434 (1997) ; D. Atwood and M. Sher, Phys. Lett. **B411**, 306 (1997)
- [25] G. Bhattacharyya, Susy '96, Nucl. Phys. B (Proc. Suppl.) **52A** (1997) 83
- [26] R.M. Godbole, R.P. Roy, and X. Tata, Nucl. Phys. **B401**, 67 (1993)
- [27] Y. Grossman, Z. Ligeti, and E. Nardi, Nucl. Phys. **B465**, 369 (1996)
- [28] W. Beenakker and A. Denner, Int. J. Mod. Phys. **A9**, 4837 (1994)
- [29] D. Bardin, M. Bilenky, A. Olachevsky, and T. Riemann, Phys. Lett. **B308**, 403 (1993)
- [30] T. Sjöstrand, Comput. Phys. Comm. **82**, 74 (1994)
- [31] D. Choudhury, Phys. Lett. **B376**, 201 (1996)
- [32] J. Erler, J. Feng, and N. Polonsky, Phys. Rev. Lett. **78**, 3012 (1997)
- [33] J. Kalinowski, R. Rückl, H. Spiesberger, and P.M. Zerwas, Phys. Lett. **B414**, 297 (1997)
- [34] E. Byckling and K. Kajantie, “Particle Kinematics”, John Wiley and Sons, London, 1973
- [35] M. Jezabek and J.H. Kühn, Nucl. Phys. **320**, 20 (1989)
- [36] A. Czarnecki, M. Jezabek, and J.H. Kühn, Nucl. Phys. **351**, 70 (1991) ; M. Jezabek and J.H. Kühn, Phys. Lett. **B329**, 317 (1994)
- [37] G.R. Farrar and F. Neri, Phys. Lett. **B130**, 109 (1980) ; G.A. Ladinsky, Phys. Rev. **D39**, 2515 (1989)
- [38] G. Valencia and A. Soni, Phys. Lett. **B263**, 517 (1991)
- [39] S. Bar-Shalom, G. Eilam, and A. Soni, Phys. Rev. Lett. **80**, 4629 (1998)







# Publication IX



# CP violation flavor asymmetries in slepton pair production at leptonic colliders from broken R-parity

M. Chemtob, G. Moreau

*Service de Physique Théorique  
CE-Saclay F-91191 Gif-sur-Yvette, Cedex France*

Phys. Lett. **B448** (1999) 57, hep-ph/9808428

## Abstract

*We examine the effect of the R parity odd, lepton number violating, renormalizable interactions on flavor non-diagonal rates and CP asymmetries in the production of slepton pairs,  $e^- + e^+ \rightarrow \tilde{e}_{HJ} + \tilde{e}_{H'J'}^*$ ,  $[J \neq J']$ ,  $[H, H' = (L, R)]$  at leptonic colliders. The R parity odd coupling constants are assumed to incorporate CP odd complex phases. The flavor changing rates are controlled by tree level amplitudes and quadratic products of different R parity violating coupling constants and the CP violating asymmetries by interference terms between tree and loop level amplitudes and quartic products. The consideration of loop amplitudes is restricted to the photon and Z-boson vertex corrections. We present numerical results using a family and (quarks and leptons) species independent mass parameter,  $\tilde{m}$ , for all the scalar superpartners and making simple assumptions for the family dependence of the R parity odd coupling constants. The flavor non-diagonal rates,  $\sigma_{JJ'}$ , vary in the range,  $(\frac{\lambda}{0.1})^4 2 - 20$  fbarns, for sleptons masses  $\tilde{m} < 400$  GeV, as one spans the interval of center of mass energies from the Z-boson pole up to 1000 GeV. For sleptons masses,  $\tilde{m} > 150$  GeV, these observables could be of use at NLC energies to set useful bounds on the R parity odd coupling constants. The predicted asymmetries are in order of magnitude,  $\mathcal{A}_{JJ'} = \frac{\sigma_{JJ'} - \sigma_{J'J}}{\sigma_{JJ'} + \sigma_{J'J}} \simeq 10^{-2} - 10^{-3}$ .*

# 1 Introduction

On side of the familiar low energy tests of CP symmetry non-conservation, a large number of tests have been developed over the years for high energy colliders [1, 2, 3]. The existing proposals have dealt with different types of CP odd observables (quark and leptons flavor asymmetries [4], spin polarization asymmetries [5, 6, 7], heavy quarks or leptons electric dipole moments [8], ...) and covered a wide variety of physical processes, ranging from decay reactions ( $Z$ ,  $W^\pm$  gauge bosons [4, 9], Higgs bosons [10, 11] or top-quarks [12]) to production reactions (leptons-antileptons and light quarks-antiquarks pairs [4], single top-quarks [13], top-antitop-quark pairs [14, 15, 16], or superpartners pairs,  $\tilde{\chi}^+\tilde{\chi}^-$ , [17]  $\tilde{q}\tilde{q}$ , [18] and  $\tilde{l}^+\tilde{l}^-$  [19, 20]). For lack of space, we have referred to those works from which one could hopefully trace the extensive published literature.

One of the primary motivations for these high energy tests is the search for physics beyond the standard model. The supersymmetry option is especially attractive in this respect since any slight generalization of the minimal model, allowing, say, for some generational non universality in the soft supersymmetry breaking parameters or for an approximate R parity symmetry, would introduce several new parameters, with a non trivial structure on quarks and leptons flavors which could accommodate extra CP violating phases. As is known, high energy supercolliders are expected to provide for precision determinations of these supersymmetry parameters. Regarding the much studied sleptons pair production reaction [21, 22, 23], one can define a simple spin-independent CP asymmetry observable in terms of the difference of integrated rates,  $(\sigma_{JJ'} - \sigma_{J'J})$ , with  $\sigma_{JJ'} = \sigma(e^- + e^+ \rightarrow \tilde{e}_J^- + \tilde{e}_{J'}^+)$ , for the case of sleptons pairs of different flavors,  $J \neq J'$ . Recent works, based on the mechanism of sleptons flavor oscillations, have examined for correlated slepton pairs production, the flavor non-diagonal rates [24, 25] and the CP-odd flavor asymmetries, defined as,  $\mathcal{A}_{JJ'} = \frac{\sigma_{JJ'} - \sigma_{J'J}}{\sigma_{JJ'} + \sigma_{J'J}}$  [19, 20]. Encouraging values of order,  $\mathcal{A}_{JJ'} \approx 10^{-3}$  were predicted at the next linear colliders (NLC) energies [19, 20]. While the rates,  $\sigma_{JJ'}$ , depend on pairwise non-degeneracies in the sleptons mass spectra, the asymmetries,  $\mathcal{A}_{JJ'}$ , entail the much stricter conditions that both non-degeneracies and mixing angles between all slepton flavors, as well as the CP odd phase, must not vanish.

Our main observation in this work is that the R parity odd interactions could provide an alternative mechanism for explaining flavor non-diagonal CP asymmetries through possible complex CP odd phases incorporated in the relevant dimensionless coupling constants. While these interactions can contribute to flavor changing processes already at tree level, their contributions to CP asymmetries involve interference terms between tree and loop amplitudes. Two important questions then are, first, whether the contributions from the RPV (R parity violating) interactions, given the known bounds on the R parity odd coupling constants, could lead to observable production rates; second, whether the CP asymmetries could reach observable levels. We shall present in this work a study of the contributions to the CP asymmetries, in the reactions,  $e^- + e^+ \rightarrow \tilde{e}_{HJ} + \tilde{e}_{HJ'}^*$ , [ $H = L, R$ ,  $J \neq J'$ ], at the high energy leptonic colliders, for center of mass energies from the Z-pole up to 1000 GeV. The RPV lepton number violating interactions are defined by the familiar superpotential,  $W_{R-odd} = \sum_{ijk} [\frac{1}{2} \lambda_{ijk} L_i L_j E_k^c + \lambda'_{ijk} Q_i L_j D_k^c]$ . A comparison with the oscillations mechanism should enhance the impact of future experimental measurements of these observables at the future high energy colliders.

The contents are organized into 3 sections. In Section 2, we develop the basic formalism

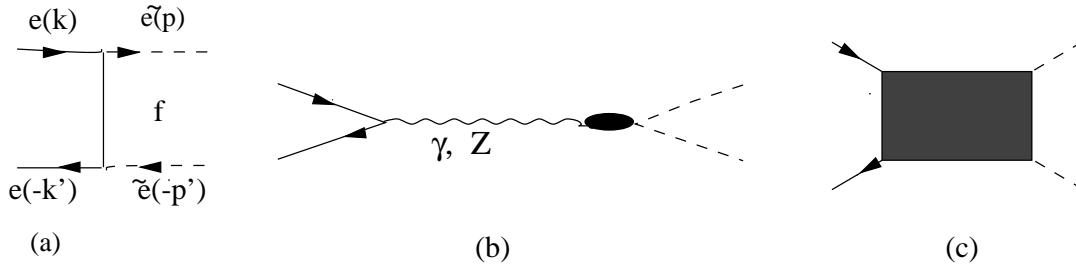


FIG. 1: Flavor non-diagonal process of  $e^-e^+$  production of a sfermion-antisfermion pairs,  $e^-(k) + e^+(k') \rightarrow \tilde{e}_J^-(p) + \tilde{e}_{J'}^+(p')$ . The tree level diagram in (a) represents a neutrino,  $f = \nu$ ,  $t$ -channel exchange amplitude. The loop level diagram in (b) represents  $\gamma$ - and  $Z$ - boson exchange amplitudes with dressed vertices and that in (c) box amplitudes.

for describing the scattering amplitudes at tree and one-loop levels for the production of slepton pairs,  $\tilde{e}_L^-\tilde{e}_L^+$  and  $\tilde{e}_R^-\tilde{e}_R^+$ . In Section 3, we present and discuss our numerical results for the integrated cross sections and the CP asymmetries.

## 2 Production of charged sleptons pairs

### 2.1 General formalism

The evaluation of spin-independent CP asymmetries in the production of a pair of sleptons,  $e^-(k) + e^+(k') \rightarrow \tilde{e}_{HJ}^-(p) + \tilde{e}_{H'J'}^+(p')$ , of different flavors,  $J \neq J'$ , with chiralities,  $H = (L, R)$ ,  $H' = (L, R)$ , involves both tree and loop amplitudes. Let us start with the case of two left-chirality sleptons,  $H = H' = L$ . At tree level, the R parity odd couplings,  $\lambda_{ijk}$ , give a non-vanishing contribution which is described by a neutrino,  $\nu_i$ ,  $t$ -channel exchange Feynman diagram, as displayed in (a) of Fig. 1. The associated flavor non-diagonal amplitude reads :

$$M_{tree}^{JJ'}(\tilde{e}_L) = -\frac{\lambda_{iJ1}^* \lambda_{iJ'1}}{t - m_{\nu_i}^2} \bar{v}(k') P_L (\not{k} - \not{p}) P_R u(k). \quad (2.1)$$

Under our working assumption that flavor changing effects are absent from the supersymmetry breaking interactions, no other tree level contributions arise, since the gauge interactions can contribute, through the familiar neutralinos  $t$ -channel and gauge bosons  $s$ -channel exchanges, to flavor diagonal amplitudes,  $J = J'$ , only.

At one-loop level, there occurs  $\gamma$ - and  $Z$ -boson exchange amplitudes with dressed  $\gamma\tilde{f}\tilde{f}'$  and  $Z\tilde{f}\tilde{f}'$  vertices involving three-point vertex correction loop diagrams, as well as box diagrams, of the type depicted schematically in (b) and (c) of Fig.1. We shall restrict consideration to the one-loop triangle diagrams contributions in the gauge bosons exchange amplitude only. Defining the dressed vertex functions for the  $Z$ -boson coupling to sleptons of chirality  $Z_\mu(P) \rightarrow \tilde{f}_H^J(p) + \tilde{f}_H^{J'*}(p')$ , [ $H = L, R$ ], by the effective Lagrangian,

$$L = -\frac{g}{2 \cos \theta_W} Z^\mu \Gamma_\mu^Z(p, p'), \quad \Gamma_\mu^Z(p, p') = (p - p')_\mu [a_H(\tilde{f}_H) \delta_{JJ'} + A_H^{JJ'}(\tilde{f}, s + i\epsilon)], \quad (2.2)$$

where,  $a(\tilde{f}_H) = a(f_H) = a_H(f) = 2T_3^H(f) - 2Q(f)x_W$ , [ $x_W = \sin^2 \theta_W$ ] such that,  $a(e_L) =$

$-1 + 2x_W$ ,  $a(e_R) = 2x_W$ , we can express the one-loop Z-boson exchange amplitude as :

$$M_{loop}^{JJ'}(\tilde{e}_H) = \left( \frac{g}{2 \cos \theta_W} \right)^2 \bar{v}(k') \gamma^\mu \left( a(e_L) P_L + a(e_R) P_R \right) u(k) \frac{1}{s - m_Z^2 + im_Z \Gamma_Z} \times (p - p')_\mu [a(\tilde{e}_H) \delta_{JJ'} + A_H^{JJ'}(\tilde{e}, s + i\epsilon)], \quad (2.3)$$

where the shifted complex argument,  $s + i\epsilon$ , is incorporated to remind us that the vertex functions are complex functions in the complex plane of the Z-boson virtual mass squared,  $s = (k + k')^2 = (p + p')^2$ , to be evaluated at the upper lip of the cut along the positive real axis. In the dressed vertex function describing the coupling,  $Z \tilde{f} \tilde{f}^*$ , eq.(2.2), we have omitted the Lorentz covariant proportional to,  $P_\mu = (p + p')_\mu = (k + k')_\mu$ , since this will give negligibly small lepton mass terms upon contraction in the total Z-boson exchange amplitude, eq.(2.3), with the initial state leptons vertex covariant. It is most convenient to describe the initial leptons polarizations in the helicity eigenvalue basis. In the limit of vanishing initial leptons masses, only the two helicity flip configurations,  $e_R^- e_L^+$ ,  $e_L^- e_R^+$ , are non vanishing. While the gauge bosons  $s$ -channel exchange contributes to both of these configurations, the R parity violating neutrino  $s$ -channel exchange contributes only to the first. The summed tree and loop amplitude,  $M^{JJ'}(\tilde{e}_L) = M_{tree}^{JJ'}(\tilde{e}_L) + M_{loop}^{JJ'}(\tilde{e}_L)$ , in the relevant configuration, namely,  $e_R^- + e_L^+ = e^-(h = -\frac{1}{2}) + e^+(\bar{h} = \frac{1}{2})$ , reads :

$$M^{JJ'}(\tilde{e}_L) = M(e_R^- + e_L^+ \rightarrow \tilde{e}_{LJ}^- + \tilde{e}_{LJ'}^+) = -\frac{1}{2} \beta s \sin \theta \left[ \frac{\lambda_{iJ1}^* \lambda_{iJ'1}}{t - m_{\nu_i}^2} + 2 \left( \frac{g}{2 \cos \theta_W} \right)^2 \frac{a(e_R) A_L^{JJ'}(\tilde{e}, s + i\epsilon)}{s - m_Z^2 + im_Z \Gamma_Z} \right]. \quad (2.4)$$

The Z-boson exchange contribution to the other helicity flip configuration,  $e_L^- e_R^+$ , is simply obtained by the substitution,  $a(e_R) \rightarrow a(e_L)$ . We also note that the  $\gamma$  exchange contribution has the same formal structure as that of the Z-boson exchange, and can be easily incorporated by adding to the above amplitudes the terms obtained by the replacements,  $\frac{g}{2 \cos \theta_W} \rightarrow \frac{g \sin \theta_W}{2}$ ,  $a_{L,R}(f) \rightarrow 2Q(f)$ ,  $(s - m_Z^2 + im_Z \Gamma_Z)^{-1} \rightarrow s^{-1}$ , along with the substitution of Z-boson by photon vertex functions,  $A_{L,R}^{JJ'}(\tilde{e}, s + i\epsilon) \rightarrow A_{L,R}^{\gamma JJ'}(\tilde{e}, s + i\epsilon)$ . The kinematical notations here refer to the center of mass system, where  $\beta = \frac{p}{k} = \frac{2p}{\sqrt{s}}$ ,  $\theta$  is the scattering angle and the differential cross section for unpolarized initial leptons reads :  $d\sigma/d\cos\theta = \frac{p}{128\pi sk} \sum_{pol} |M^{JJ'}|^2$ . (For unpolarized beams, one must remove the polarization sums and multiply by a factor of 4. Our results agree with those quoted in [22].) Denoting the amplitude for the charge conjugate process,  $e^- + e^+ \rightarrow \tilde{e}_{HJ}^- + \tilde{e}_{HJ'}^+$ , [ $H = L, R$ ], by  $\bar{M}^{JJ'}(\tilde{e}_H)$  and using the simple relationship,  $\bar{M}^{JJ'}(\tilde{e}_H) = M^{JJ'}(\tilde{e}_H)$ , one can describe the decomposition into tree and loop components for the pair of CP conjugate processes as,

$$M^{JJ'}(\tilde{e}_H) = a_0^{JJ'} + \sum_\alpha a_\alpha^{JJ'} F_\alpha^{JJ'}(s + i\epsilon), \quad \bar{M}^{JJ'}(\tilde{e}_H) = a_0^{JJ'\star} + \sum_\alpha a_\alpha^{JJ'\star} F_\alpha^{JJ'}(s + i\epsilon). \quad (2.5)$$

A spin-independent CP asymmetry can be defined in the familiar way as the normalized difference of rates,

$$\mathcal{A}_{JJ'}(\tilde{e}_H) = \frac{|M^{JJ'}(\tilde{e}_H)|^2 - |\bar{M}^{JJ'}(\tilde{e}_H)|^2}{|M^{JJ'}(\tilde{e}_H)|^2 + |\bar{M}^{JJ'}(\tilde{e}_H)|^2} \simeq \frac{2}{|a_0|^2} \sum_\alpha \text{Im}(a_0 a_\alpha^*) \text{Im}(F_\alpha(s + i\epsilon)), \quad (2.6)$$

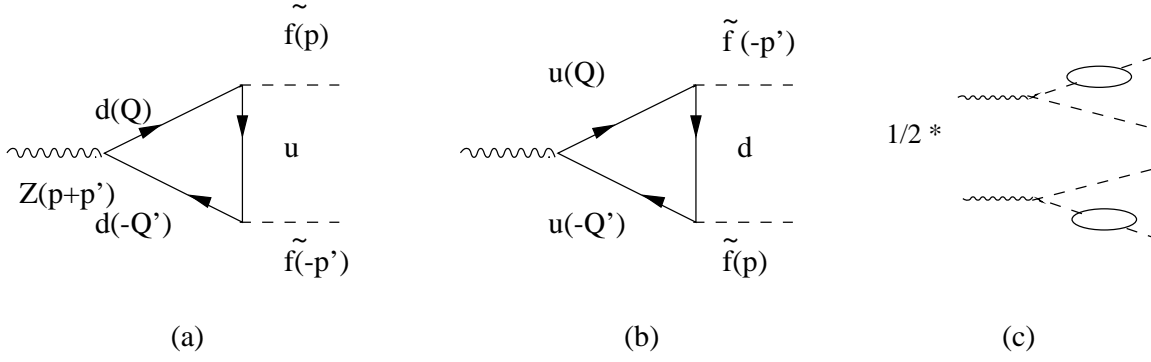


FIG. 2: One-loop diagrams for the dressed  $Z \tilde{f} \tilde{f}^*$  vertex. The flow of four-momenta for the intermediate fermions is denoted as,  $Z(P = k + k') \rightarrow f(Q) + \bar{f}(Q') \rightarrow \tilde{f}_J(p) + \tilde{f}_{J'}^*(p')$ .

where we have assumed in the second step that the tree level flavor non-diagonal amplitude,  $a_0$ , dominates over the loop level amplitude,  $a_\alpha F_\alpha$ , and used the index  $\alpha$  to label the internal states running inside the loop.

## 2.2 Loop amplitudes

The one-loop triangle diagrams, describing the dressed vertex functions,  $Z \tilde{f}_L \tilde{f}_L^*$ , arise in two distinct charge configurations, shown in Fig. 2 by the diagrams (a) and (b), which involve the d- and u-quark Z-boson currents, respectively. The associated vertex functions read :

$$\begin{aligned}
 \Gamma_\mu^Z(p, p')|_a &= -iN_c \lambda_{Jjk}^* \lambda'_{J'jk} \\
 &\times \int_Q \frac{\text{Tr}[P_R(\not{Q} + m_{d_k}) \gamma_\mu (a(d_L)P_L + a(d_R)P_R) (-\not{P} + \not{Q} + m_{d_k}) P_L (\not{Q} - \not{p} + m_{u_j})]}{(-Q^2 + m_{d_k}^2)(-(Q - p - p')^2 + m_{d_k}^2)(-(Q - p)^2 + m_{u_j}^2)}, \\
 \Gamma_\mu^Z(p, p')|_b &= -iN_c \lambda_{Jjk}^* \lambda'_{J'jk} \\
 &\times \int_Q \frac{\text{Tr}[P_R(\not{Q} + \not{p} + m_{d_k}) P_L (\not{Q} + \not{p} + \not{p}' + m_{u_j}) \gamma_\mu (a(u_L)P_L + a(u_R)P_R) (\not{Q} + m_{u_j})]}{(-Q^2 + m_{u_j}^2)(-(Q + p + p')^2 + m_{u_j}^2)(-(Q + p)^2 + m_{d_k}^2)}.
 \end{aligned} \tag{2.7}$$

Applying the formalism of Passarino-Veltman [26], the vertex function from diagram (a) can be expressed in the form :

$$\begin{aligned}
 A_L^{JJ'}|_a &= \frac{\lambda_{Jjk}^* \lambda'_{J'jk}}{2(4\pi)^2} N_c \left[ 2a(d_L)m_d^2(C_0 + C_{11} - C_{12}) + a(d_R) \left( B_0^{(2)} + B_0^{(3)} + 2P \cdot p(C_{11} - C_{12}) \right. \right. \\
 &\quad \left. \left. + P^2 C_0 + 2m_{e_j}^2(-C_{11} + C_{12}) - 2m_d^2 C_0 + 2m_u^2(C_{11} - C_{12}) \right) \right].
 \end{aligned} \tag{2.8}$$

The conventions of ref.[26] are used for the two-point and three-point integral functions,  $B_X$  [ $X = 0, 1$ ] and  $C_X$  [ $X = 0, 11, 12, 21, 22, 23, 24$ ]. For notational convenience, we have introduced the following abbreviations for the dependence on argument variables :  $B_X^{(1)} = B_X(-p - p', m_d, m_d)$ ,  $B_X^{(2)} = B_X(-p, m_d, m_u)$ ,  $B_X^{(3)} = B_X(-p', m_u, m_d)$  and  $C_X(-p, -p', m_d, m_u, m_d)$ . The amplitude from diagram (b) can be obtained from that

of diagram (a) by performing the following substitutions :  $m_{d_k} \rightarrow m_{u_j}$ ,  $p \rightarrow p'$ ,  $P_L \rightarrow P_R$ ,  $a(d_H)P_H \rightarrow a(u_H)P_H$ ,  $[H = L, R]$ . The self-energy contributions, which are represented by the diagrams (c) in Fig. 2, with a single configuration only for the d- and u-quarks which propagate inside the loop, are most conveniently calculated through a consideration of the scalar fields renormalization factors  $Z_{JJ'}$ . Starting from the schematic equations for the scalar field  $\phi$  bare Lagrangian density,  $L = \phi^*(p^2 - m^2 + \Pi(p))\phi$ , where,  $\Pi(p) = \Pi_1 p^2 - m^2 \Pi_0 + \dots$ , one transfers from bare to renormalized quantities by applying the substitutions,  $\phi \rightarrow \phi/(1 + \Pi_1)^{\frac{1}{2}}$ ,  $m^2 \rightarrow m^2(1 + \Pi_1)/(1 + \Pi_0)$ , such that the renormalization equations for the fields and mass parameters read,  $\phi_J = Z_{JJ'}\phi_{J'}^{ren}$ ,  $m_{JJ'}^2 = Z_{JK}^m m_{KK'}^{ren2}$ , with  $Z = (1 + \Pi_1)^{-1}$ ,  $Z^m = (1 + \Pi_0)(1 + \Pi_1)^{-1}$ , using a matrix notation for the flavor dependence. The self-energy contribution in the vertex function becomes then,

$$A_L^{JJ'}|_{SE} = [(Z_{JJ'}Z_{JJ'}^*)^{\frac{1}{2}} - 1]\Gamma_\mu^Z = 2N_c \frac{\lambda_{Jjk}^* \lambda'_{J'jk}}{(4\pi)^2} a_L(\tilde{e}) B_1^{(2)}. \quad (2.9)$$

Grouping together the self-energy and the fermionic triangle diagram contributions, such that the total amplitudes read as,  $A_L^{JJ'}(\tilde{e}) = A_L^{JJ'}(\tilde{e})_a + A_L^{JJ'}(\tilde{e})_b$ , yields the final formulas :

$$\begin{aligned} A_L^{JJ'}(\tilde{e})_a &= \frac{N_c}{2} \frac{\lambda_{Jjk}^* \lambda'_{J'jk}}{(4\pi)^2} \left[ 2a(d_L)m_d^2(C_0 + C_{11} - C_{12}) + a(d_R) \left( B_0^{(2)} + B_0^{(3)} + 2P \cdot p(C_{11} - C_{12}) \right. \right. \\ &\quad \left. \left. + P^2 C_0 + 2m_J^2(-C_{11} + C_{12}) - 2m_d^2 C_0 + 2m_u^2(C_{11} - C_{12}) \right) + 2a(\tilde{e}_L)B_1^{(2)} \right], \\ A_L^{JJ'}(\tilde{e})_b &= -\frac{N_c}{2} \frac{\lambda_{Jjk}^* \lambda'_{J'jk}}{(4\pi)^2} \left[ 2a(u_R)m_u^2(C_0 + C_{11} - C_{12}) + a(u_L) \left( B_0^{(2)} + B_0^{(3)} + 2P \cdot p(C_{11} - C_{12}) \right. \right. \\ &\quad \left. \left. + P^2 C_0 + 2m_J^2(-C_{11} + C_{12}) - 2m_u^2 C_0 + 2m_d^2(C_{11} - C_{12}) \right) - 2a(\tilde{e}_L)B_1^{(2)} \right]. \end{aligned} \quad (2.10)$$

For notational convenience, we have split the self-energy contribution into two equal parts that we absorbed within the above two amplitudes, distinguished by the suffices  $a$  and  $b$ . Note that the arguments in the  $B$ - and  $C$ -integrals for the amplitude  $b$  are deduced from those of the amplitude  $a$  by replacing,  $d_k \rightarrow u_j$ . To obtain these results we have used the mathematica routine package “Tracer” [27] and, for a cross-check, “FeynCalc” [28]. A very useful check concerns the cancellation of the ultraviolet divergencies. We indeed find that the familiar [26] logarithmically divergent term,  $\Delta$ , enters with the factors,  $+a(\tilde{e}_L) - 2a(d_R)$  (amplitude  $a$ ) and  $a(\tilde{e}_L) + 2a(u_L)$  (amplitude  $b$ ), whose total sum vanishes identically.

The interactions associated with the coupling constants,  $\lambda_{ijk}$ , can also contribute at one-loop order. Exploiting the formal similarity between the  $\lambda$  and  $\lambda'$  interaction terms in the Lagrangian density, namely,  $L = -\lambda'_{ijk}\tilde{e}_{iL}\bar{d}_{kR}u_{jL} - \lambda_{ijk}\tilde{e}_{iL}\bar{e}_{kR}\nu_{jL} + \dots$ , dispenses us from performing a new calculation. The results can be derived from those in eq.(2.10) by substituting for the internal lines,  $d_k \rightarrow e_k$ ,  $u_j \rightarrow \nu_j$ , and for the parameters,  $a_H(u) \rightarrow a_H(\nu)$ ,  $a_H(d) \rightarrow a_H(e)$ ,  $\lambda_{Jjk}^* \lambda'_{J'jk} \rightarrow \lambda_{Jjk}^* \lambda_{J'jk}$ .

Let us now turn to the production of right-chirality sleptons where analogous results can be derived. The tree level amplitude is related to that in eq.(2.1) by a simple chirality change,

$$M_{tree}^{JJ'}(\tilde{e}_R) = -\frac{\lambda_{i1J'}^* \lambda_{i1J}}{t - m_{\nu_i}^2} \bar{v}(k') P_R (\not{k} - \not{p}) P_L u(k). \quad (2.11)$$

There occurs only one non-vanishing helicity flip configuration for the initial leptons, namely,  $e_L^- e_R^+$ , in which the neutrinos  $t$ -channel and the gauge bosons  $s$ -channel contributions



interfere. The amplitude is given by a formula similar to eq.(2.4), except for the substitution in the second term,  $a_R(e)A_L^{JJ'}(\tilde{e}, s + i\epsilon) \rightarrow a_L(e)A_R^{JJ'}(\tilde{e}, s + i\epsilon)$ . Concerning the one-loop contribution to the vertex function  $A_R^{JJ'}(\tilde{f})$ , we find that the RPV interactions with the coupling constants  $\lambda_{ijk}$  can only contribute, while those with  $\lambda'_{ijk}$  vanish identically. Diagram (a) in Fig. 2 refers to an  $e_j$  current and diagram (b) to a  $\nu_i^c$  current. The results can be derived by inspection from eq.(2.10) by substituting,  $\lambda'_{j'jk}\lambda_{ijk}^* \rightarrow \lambda_{ijj}\lambda_{ijj'}^*$ ,  $d_{jR} \rightarrow e_{jL}$ ,  $u_{jL} \rightarrow \nu_{iR}^c$ ,  $\tilde{e}_L \rightarrow \tilde{e}_R$  and, accordingly,  $a(d_H) \rightarrow a(e_H)$ ,  $a(u_H) \rightarrow a(\nu_H^c)$ ,  $[H = L, R]$ ,  $a(\tilde{e}_L) \rightarrow a(\tilde{e}_R)$ . For definiteness, we quote the explicit formulas :

$$\begin{aligned}
A_R^{JJ'}(\tilde{e})_a &= \frac{N_c}{2} \frac{\lambda_{ijj}\lambda_{ijj'}^*}{(4\pi)^2} \left[ 2a(e_R)m_e^2(C_0 + C_{11} - C_{12}) + a(e_L) \left( B_0^{(2)} + B_0^{(3)} + 2P \cdot p(C_{11} - C_{12}) \right. \right. \\
&\quad \left. \left. + P^2C_0 + 2m_j^2(-C_{11} + C_{12}) - 2m_e^2C_0 + 2m_\nu^2(C_{11} - C_{12}) \right) + 2a(\tilde{e}_R)B_1^{(2)} \right], \\
A_R^{JJ'}(\tilde{e})_b &= -\frac{N_c}{2} \frac{\lambda_{ijj}\lambda_{ijj'}^*}{(4\pi)^2} \left[ 2a(\nu_L^c)m_\nu^2(C_0 + C_{11} - C_{12}) + a(\nu_R^c) \left( B_0^{(2)} + B_0^{(3)} + 2P \cdot p(C_{11} - C_{12}) \right. \right. \\
&\quad \left. \left. + P^2C_0 + 2m_j^2(-C_{11} + C_{12}) - 2m_\nu^2C_0 + 2m_e^2(C_{11} - C_{12}) \right) - 2a(\tilde{e}_R)B_1^{(2)} \right]. \quad (2.12)
\end{aligned}$$

The discussion of the mixed chiralities cases,  $\tilde{e}_{LJ}^-\tilde{e}_{RJ'}^+$ ,  $\tilde{e}_{RJ}^-\tilde{e}_{LJ'}^+$ ,  $[J \neq J']$  turns out to be quite brief. The tree level RPV contributions, which can only come from the  $\lambda_{ijk}$  interactions, vanish identically for massless neutrinos. As for the one-loop contributions to the vertex,  $Z\tilde{f}_L\tilde{f}_R^*$ , this also vanishes up to mass terms in the internal fermions. Since flavor non-diagonal rates arise then from loop contributions only and CP asymmetries from interference of distinct loop contributions, one concludes that both observables should be very small.

Finally, let us add here a general comment concerning the photon vertex functions,  $A_{L,R}^{\gamma JJ'}$ , which are given by formulas similar to those in eqs.(2.10) or (2.12) with the appropriate replacements,  $a_{L,R}(f) \rightarrow 2Q(f)$ . Therefore, to incorporate the  $\gamma$ -exchange contributions in the total amplitudes (eq.(2.4) and related equations) one needs to substitute,

$$a_{R,L}(e)A_{L,R}^{JJ'} \rightarrow a_{R,L}(e) \sum_f a(f)C_f + 2Q(e) \sin^2 \theta_W \cos^2 \theta_W [(s - m_Z^2 + im_Z \Gamma_Z)/s] \sum_f 2Q(f)C_f,$$

where we have used the schematic representation,  $A_{L,R}^{JJ'} = \sum_f a(f)C_f$ .

### 3 Results and discussion

Let us first comment briefly on the experimental observability of flavor non-diagonal sleptons pair production. One convenient non degraded signal here is that which corresponds to lepton pair final states,  $e_j^- e_{j'}^+$ , which are produced through the two-body decay channels for sleptons,  $\tilde{e}_{[J,J']}^\pm \rightarrow e_{[J,J']}^\pm + \tilde{\chi}_1^0$ . Of course, in the broken R parity case, the produced lightest neutralinos are unstable and could conceivably be reconstructed through their dominant decay channels which involve two leptons, or two jets, together with missing energy. We shall not elaborate further on this issue, except to note that the efficiency factors at NLC energies for the flavor diagonal rates, assuming a stable  $\tilde{\chi}_1^0$ , and including rough detection cuts, such that the physical rates for the fermion pairs channels is,  $\sigma_{JJ'}\epsilon$ , are typically set at  $\epsilon \approx 30\%$  [25].

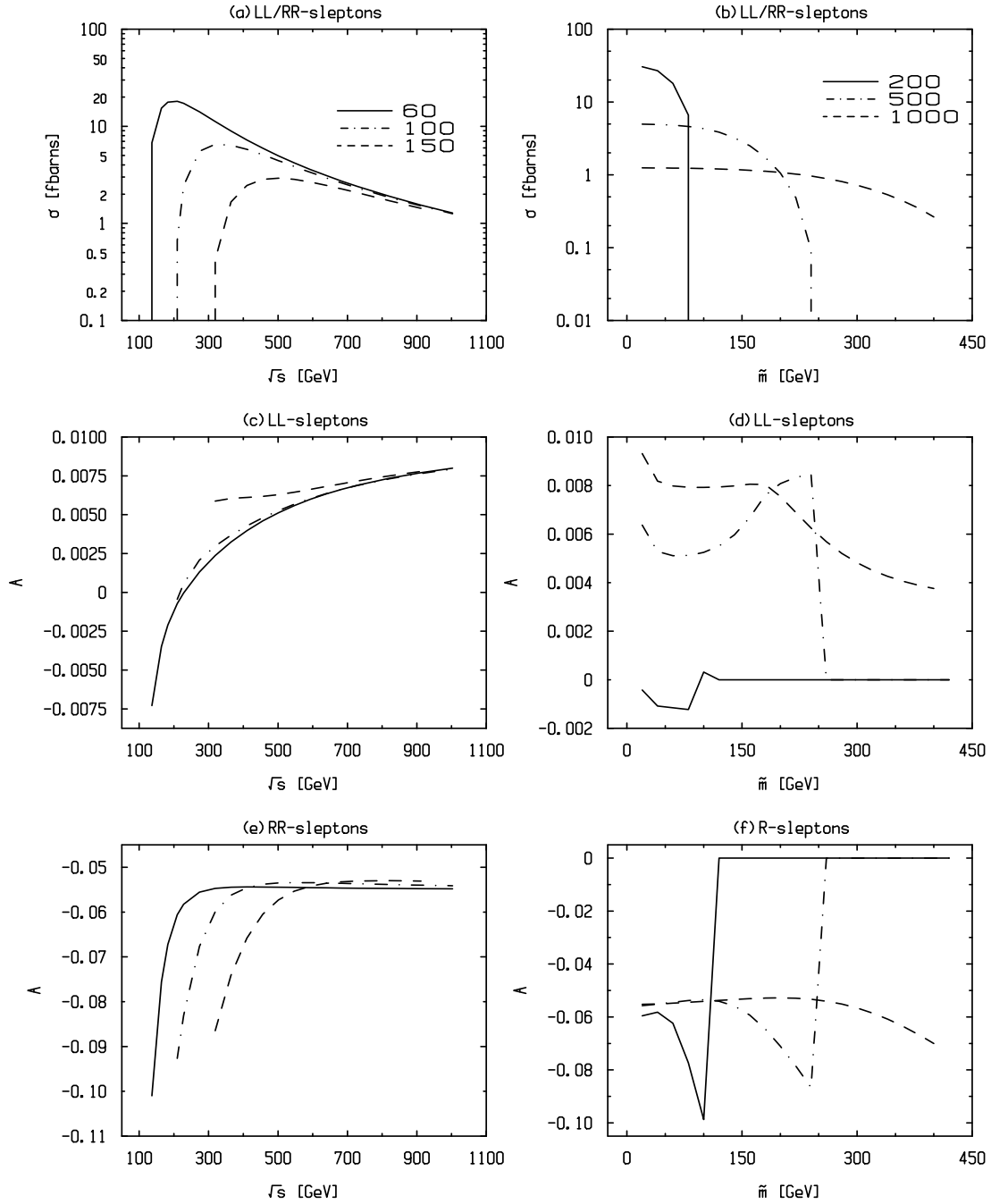


FIG. 3: Integrated flavor non-diagonal cross sections and CP asymmetries in the production of slepton-antislepton pairs of left-chirality (L) (interactions  $\lambda'_{ijk}$  only) and of right-chirality (R) (interactions  $\lambda_{ijk}$ ). The three windows on the left-hand side ((a), (c), (e)) show the variation with center of mass energy,  $s^{1/2}$ , for three choices of the scalar superpartners mass parameter,  $\tilde{m}$  :  $60\text{GeV}$  (continuous lines),  $100\text{GeV}$  (dashed-dotted lines),  $150\text{GeV}$  (dashed lines). The three windows on the right-hand side ((b), (d), (f)) show the variation with scalar superpartner mass,  $\tilde{m}$ , for three choices of the center of mass energy  $s^{1/2} = 200\text{GeV}$  (continuous lines),  $500\text{GeV}$  (dashed-dotted lines),  $1000\text{GeV}$  (dashed lines). The tree level amplitude includes the t-channel exchange contribution. The one-loop amplitudes (with both photon and Z-boson exchanges) correspond to Case **IV** which includes the contributions from all three internal fermions generations.

Proceeding to the predictions, we observe that the main source of uncertainties concerns the RPV coupling constants. The sfermion mass eigenvalues are not known, but these parameters appear explicitly through the kinematics. We shall neglect mass splittings and mixings between L- and R-sleptons. A unique sleptons mass parameter,  $\tilde{m}$ , will be used and varied in the interval,  $60 < \tilde{m} < 400$  GeV. Regarding the RPV coupling constants, it is useful here to catalog the family configurations and intermediate states entering the calculations. Examining the structure of the flavor non-diagonal tree amplitudes, we note that these involve a onefold summation over leptons families weighted by the factors,  $t_{JJ'}^i = \lambda_{iJ1}^* \lambda_{iJ'1}$ , for L-sleptons and  $t_{JJ'}^i = \lambda_{i1J}^* \lambda_{i1J'}$ , for R-sleptons. The loop amplitudes involve a twofold summation over leptons families of form,  $\sum_{jk} l_{JJ'}^{jk} F^{jk}(m_j, m_k, s + i\epsilon)$ , where  $l_{JJ'}^{jk}$  depend quadratically on the RPV coupling constants while the loop integrals,  $F^{jk}$ , have a non-trivial dependence on the fermions masses, as exhibited on the formulas derived in Section 2 [see, e.g., eq. (2.10)]. The relevant coupling constants, the species and family configurations for the internal fermions are for L-sleptons,  $l_{JJ'}^{jk} = \lambda_{Jjk}^* \lambda'_{J'jk}, [d_k, u_j]$ ;  $l_{JJ'}^{jk} = \lambda_{Jjk}^* \lambda_{J'jk}, [e_k, \nu_j]$ ; and for R-sleptons,  $l_{JJ'}^{ij} = \lambda_{ijJ} \lambda_{ijJ'}^*, [e_j, \nu_i^c]$ . The dependence of rates on the RPV coupling constants has the schematic structure,  $\sigma_{JJ'} \simeq \sum_i |t_{JJ'}^i|^2$ , and that of CP asymmetries,  $\mathcal{A}_{JJ'} \simeq \sum_{ijk} \text{Im}(l_{JJ'}^{jk} t_{JJ'}^{i*}) / \sum_l |t_{JJ'}^l|^2$  for L-sleptons and  $\mathcal{A}_{JJ'} \simeq \sum_{ijk} \text{Im}(l_{JJ'}^{ij} t_{JJ'}^{k*}) / \sum_l |t_{JJ'}^l|^2$  for R-sleptons. Therefore, rates (asymmetries) are controlled by two (four) RPV coupling constants in different family configurations. Note the expected invariance of asymmetries under phase redefinitions of the fields.

While the dependence on the mass of the exchanged neutrino family index in  $t_{JJ'}^i$  can be clearly ignored, that on the pair of indices  $(i, j)$  in  $l_{JJ'}^{ij}$ , which involves the ratios of the masses of the appropriate internal fermions,  $m_{i,j}$ , to the external scale associated with the center of mass energy,  $\sqrt{s}$ , can be ignored as long as,  $\sqrt{s} \gg m_{i,j}$ . Therefore, at the energies of interest, the only relevant fermion mass parameter is that of the top-quark. Instead of listing the various distinct family configurations for the quadratic (tree) or quartic (loop) products of the RPV coupling constants, we shall consider a set of specific assumptions concerning the family dependence. First, for the cases involving  $[e_j, \nu_i^c]$  or  $[e_k, \nu_j]$  internal states, neglecting neutrino masses, we need only account for the masses of charged leptons. For the case with  $[d_k, u_j]$  internal states, we restrict consideration to the diagonal family configuration, namely,  $k = j$ . Second, we include a CP odd phase,  $\psi$ , between  $t_{JJ'}^i$  and all of the  $l_{JJ'}^{jk}$  or  $l_{JJ'}^{ij}$ , as the case may be. Finally, we consider the following four discrete choices for the variation intervals on which run the internal fermion indices indices,  $j = k$  or  $i, j$ . Case **I** :  $\{1\}$ ; Case **II**  $\{2\}$ ; Case **III**  $\{3\}$ ; Case **IV**  $\{1, 2, 3\}$ . In all these four cases, we set the relevant coupling constants at the reference values,  $l_{JJ'}^{ij} = l_{JJ'}^{jk} = 10^{-2}$ ,  $t_{JJ'}^i = 10^{-2}$  and use a maximal CP odd phase,  $\arg(l_{JJ'}^{[ij,jk]} t_{JJ'}^l) \equiv \psi = \pi/2$ . Because of the proportionality of asymmetries to the imaginary part of the phase factor, the requisite dependence may be simply reinstated by inserting a factor,  $\sin \psi$ . To illustrate the dependence of asymmetries on the internal fermions families and on the  $\lambda'$  or  $\lambda$  interaction types, we display in Table 3 a set of representative results obtained for selected subsets of Cases **I**, **II**, **III**, **IV**. The reason is that the results for Cases **I**, **II** (light families) are identical in all cases, while those for Case **III** (heavy families) differ only for cases involving up-quarks. As one sees on Table 3, the interference between photon and Z-boson exchange contributions has a significant effect on the results. The strongly reduced values for the L-sleptons asymmetries found in Cases **I** for the  $\lambda' \lambda^*$

		$s^{1/2} = 200 \text{ GeV}$	$s^{1/2} = 500 \text{ GeV}$		
		$\tilde{m} = 60$	$\tilde{m} = 60$	$\tilde{m} = 100$	$\tilde{m} = 200$
<hr/>					
$\tilde{e}_L \tilde{e}_L$					
$\lambda' \lambda'^*$					
<b>I</b>	$Z$	$-2.1d - 5$	$-3.3d - 6$	$-2.6d - 6$	$-2.4d - 6$
	$\gamma + Z$	$-7.7d - 5$	$-1.39d - 5$	$-1.09d - 5$	$-1.03d - 5$
$\lambda \lambda^*$					
<b>III</b>	$Z$	$+2.6d - 4$	$-1.6d - 3$	$-1.8d - 3$	$-2.3d - 3$
	$\gamma + Z$	$-1.01d - 3$	$+5.1d - 3$	$+5.3d - 3$	$+8.1d - 3$
<hr/>					
$\tilde{e}_R \tilde{e}_R$					
$\lambda \lambda^*$					
<b>I</b>	$Z$	$-7.2d - 3$	$-5.5d - 3$	$-5.4d - 3$	$-7.2d - 3$
	$\gamma + Z$	$-2.1d - 2$	$-1.83d - 2$	$-1.80d - 2$	$-2.40d - 2$
<hr/>					

TAB. 16: CP asymmetries,  $\mathcal{A}_{JJ'}$ , in sleptons pair production at two values of the center of mass energy,  $s^{1/2} = 200, 500 \text{ GeV}$  and for values of the sleptons mass parameter,  $\tilde{m} = 60, 100, 200 \text{ GeV}$ , appearing in the column fields. For each case, the first line ( $Z$ ) is associated with the gauge Z-boson exchange contribution and the second line ( $\gamma + Z$ ) with both photon and Z-boson exchanges added in together. The contributions to left-chirality ( $\tilde{e}_L \tilde{e}_L$ ) and right-chirality ( $\tilde{e}_R \tilde{e}_R$ ) sleptons, induced by the  $\lambda'_{ijk}$  and  $\lambda_{ijk}$  interactions, are distinguished by the labels,  $\lambda' \lambda'^*$ ,  $\lambda \lambda^*$ , respectively. Cases **I**, **III** correspond to internal fermions belonging to the first and third families, respectively. The notation  $nd - x$  stands for  $n \cdot 10^{-x}$ .

interactions and in all Cases for the  $\lambda \lambda^*$  interactions, arise from the existence of a strong cancellation between the amplitudes termed (a) and (b) for nearly massless internal quarks or leptons. Case **III** with the  $\lambda' \lambda'^*$  interactions is relatively enhanced thanks to the top-quark contribution (configuration  $\bar{t} b$ ). That the above cancellation is not generic to the RPV contributions is verified on the results for R-sleptons production, where all three families of leptons give nearly equal, unsuppressed contributions to loop amplitudes.

In the currently favored situation where the RPV coupling constants are assumed to exhibit a strong hierarchical structure, the peculiar rational dependence of CP asymmetries on ratios of quartic products of the coupling constants, might lead to strong

enhancement factors. We recall the schematical structure of this dependence,  $\mathcal{A}_{JJ'} \propto [\sum_{ijk} \text{Im}(\lambda'_{Jjk} \lambda'_{J'jk} \lambda'_{iJ1} \lambda'_{iJ'1}) / \sum_l |\lambda_{lJ1} \lambda'_{lJ'1}|^2]$ , and note that the coupling constants involving third family indices are amongst those that are the least strongly constrained. Therefore, assuming that the coupling constants take the values given by the current bounds from low energy constraints [29], one would obtain,

$$\mathcal{A}_{J=3, J'=2} \simeq [\text{Im}(\lambda'_{333} \lambda'_{323} \lambda'_{331} \lambda'_{321}) / |\lambda_{131} \lambda'_{121}|^2] \approx 90 \sin \psi.$$

The dependence of rates and asymmetries on center of mass energy and sleptons masses are displayed for Case **IV** in Figure 3. Regarding the variation with energy (figure (a)), after a rapid rise at threshold (with the expected  $\beta^3$   $p$ -wave like behavior) the rates settle, roughly as  $\tilde{m}^2/s$ , to constant values with growing energy, and vary inside the range,  $(\frac{\lambda^* \lambda}{0.01})^2 20 - 2$  fbarns, as one sweeps through the interval,  $\tilde{m} \in [60, 400]$  GeV. The variation with  $\tilde{m}$  (figure (b)) is rather smooth. For the envisaged integrated luminosities,  $\mathcal{L} \simeq 50 - 100 \text{ fbarns}^{-1}/\text{yr}$ , these results indicate that reasonably sized samples of order 100 events could be collected at NLC. Noting that the dependence of rates on energy rapidly saturates for  $\sqrt{s} > \tilde{m}$ , we conclude that the relevant bounds that could be inferred on quadratic products of different the RPV coupling constants, should, for increasing sleptons masses, become competitive with those deduced from low energy constraints, which scale typically as,  $[\lambda\lambda, \lambda'\lambda'] < 0.1(100\text{GeV}/\tilde{m})^2$ . The results in Fig.3 (c,d,e,f) for the CP asymmetries,  $\mathcal{A}_{JJ'}$ , indicate the existence of a wide, nearly one order of magnitude, gap between L-sleptons with  $\lambda'^* \lambda'$  interactions and R-sleptons with  $\lambda^* \lambda$  interactions, with values that lie at a few times  $10^{-3}$  and  $10^{-2}$ , respectively.

In our prescription of using equal numerical values for the RPV coupling constants ( $t_{JJ'}^i$  and  $l_{JJ'}^{ij}$ ) which control tree and loop contributions, the asymmetries are independent of the specific reference values chosen. In the event that the rates would be dominated by some alternative mechanism, say, lepton flavor oscillations, whereas RPV effects would remain significant in asymmetries, these would then scale as,  $\text{Im}(t_{JJ'}^{ik} l_{JJ'}^{jk})$ . It is instructive in view of such a possibility to compare with predictions found in the flavors oscillation approach. Scanning over wide intervals of values for the relevant parameters,  $[\cos 2\theta_R, x = \Delta\tilde{m}/\Gamma]$ , associated with the common values for all three mixing angles and ratios of families mass differences to the total sleptons decay widths, respectively, the authors of [25] found flavor non-diagonal rates which ranged between 250 and 0.1 fbarns for  $\sqrt{s} = 190$  GeV and 100 and 0.01 fbarns for  $\sqrt{s} = 500$  GeV. Our predictions,  $\sigma_{JJ'} \simeq (\frac{\lambda}{0.1})^4 2 - 20$  fbarns, which hold approximately for energies,  $\sqrt{s} > \tilde{m}$ , lie roughly in between these extreme values. On the other hand, the authors of [19] found CP asymmetry rates,  $S_{JJ'} = \sigma_{JJ'} - \sigma_{J'J} \approx 3 - 16$  fbarns. For comparison, our predicted asymmetry rates for the same quantity, namely,  $S_{JJ'} = 2\sigma_{JJ'} \mathcal{A}_{JJ'} \approx 10^0 - 10^{-1}$  fbarns, lie around one order of magnitude below these values. It should be said, however, that the flavor oscillation contributions could have a stronger model dependence than the variation range exhibited by the above predictions, and that these predictions were obtained subject to assumptions that tend to maximize CP violation effects. The existing constraints, [30] which are mostly derived from low energy phenomenology, constrain only a small subset of the parameters describing the scalar superpartners mass spectra and generational mixings.

To summarize, we have shown that moderately small contributions to flavor non-diagonal rates and CP violating spin-independent asymmetries in sleptons pair production could arise from the RPV interactions. These contributions seem to be of smaller size than

those currently associated with flavor oscillations, although the model dependence of predictions in the flavor oscillation approach is far from being under control. An experimental observation of the non-diagonal slepton production rates would give information on quadratic products of different coupling constants,  $\lambda\lambda^*$ . Owing to the smooth dependence of rates on the slepton masses, already for masses,  $\tilde{m} > 100$  GeV, it should be possible here to deduce stronger bounds than the current ones inferred from low energy constraints. The observation of CP violating asymmetries requires the presence of non vanishing CP odd phases in quartic products of the coupling constants,  $Im(\lambda_{Jjk}^*\lambda_{J'jk}\lambda_{iJ1}\lambda_{iJ'1}^*)$ , (and similarly with  $\lambda \rightarrow \lambda'$ ) which remain largely unconstrained so far. The peculiar rational dependence,  $Im(\lambda\lambda^*\lambda\lambda^*)/\lambda^4$ , leaves room for possible strong enhancement factors.

# References

- [1] J. Bernabéu and M. B. Gavela, in “CP violation” ed. C. Jarlskog (World Scientific, Singapore, 1988)
- [2] D. Chang, Workshop on physics at current accelerators and supercolliders, (June 2-5, 1993, Argonne Nat. Lab.)
- [3] A. Soni, Nucl. Phys. B (Proc. Suppl.) **51A** (1996) 32
- [4] J. Bernabéu, A. Santamaria and M.B. Gavela, Phys. Rev. Lett. **57** (1986) 1514; W.-S. Hou, N.G. Deshpande, G. Eilam and A. Soni, Phys. Rev. Lett. **57** (1986) 1406
- [5] J. F. Donoghue and G. Valencia, Phys. Rev. Lett. **58** (1997) 451
- [6] G. L. Kane, G. A. Ladinsky and C. P. Yuan, Phys. Rev. **D45** (1992) 124
- [7] A. Bilal, E. Masso and A. de Rujula, Nucl. Phys. **B355** (1991) 549
- [8] N. Worme, Nucl. Phys. (Proc. Suppl.) **55C** (1997) 313
- [9] W. Bernreuther and O. Nachtmann, Z. Phys. **C73** (1997) 647
- [10] D. Chang and W.-Y. Keung, Phys. Lett. **B305** (1993) 261
- [11] B. Grzadkowski, Phys. Lett. **B338** (1994) 71
- [12] B. Grzadkowski and Z. Hioki, Nucl. Phys. **B484** (1997) 17
- [13] D. Atwood, S. Bar-Shalom, G. Eilam and A. Soni, Phys. Rev. **D 54** (1996) 5412
- [14] C. R. Schmidt and M. Peskin, Phys. Rev. Lett. **69** (1992) 410
- [15] A. Bartl, E. Christova and W. Majoretto, Nucl. Phys. **B 460** (1996) 235; Erratum, Nucl. Phys. **B 465** (1996) 365
- [16] M. S. Baek, S. Y. Choi and C. S. Kim, Phys. Rev. **D 56** (1997) 6835
- [17] Y. Kizukuri, Phys. Lett. **B193** (1987) 337
- [18] A. Pilaftsis and M. Nowakowsky, Phys. Lett. **B245** (1990) 185
- [19] N. Arkani-Hamed, J.L. Feng, L.J. Hall, Nucl. Phys. **B505** (1997) 3
- [20] D. Bowser-Chao and W.-Y. Keung, Phys. Rev. **D56**(1997) 2924
- [21] M. M. Nojiri, K. Fujii and T. Tsukamoto, Phys. Rev. **D54** (1996) 6756
- [22] M. E. Peskin, Int. J. Mod. Phys. **A13** (1998) 2299, SLAC-PUB-7759, hep-ph/9803279
- [23] S. Thomas, SU-ITP 98-17, hep-ph/9803420
- [24] N.V. Krasnikov, Phys. Lett. **B388**(1996) 783
- [25] N. Arkani-Hamed, H. C. Cheng, J.L. Feng, L.J. Hall, Phys. Rev. Lett. **77**(1996) 1937
- [26] G. 't Hooft and M. Veltman, Nucl. Phys. **B153**(1979) 365; G. Passarino and M. Veltman, Nucl. Phys. **B160**(1979) 151

- [27] M. Jamin and M. E. Lauterbacher, Comput. Phys. Comm. **B74**(1993) 265
- [28] R. Mertig, M. Böhm and A. Denner, Comput. Phys. Comm. **B64**(1991) 345
- [29] G. Bhattacharyya, Susy '96, Nucl. Phys. B (Proc. Suppl.) **52A**(1997) 83
- [30] F. Gabbiani, E. Gabrielli, A. Masiero and L. Silvestrini, Nucl. Phys. **B477**(1996) 321







# Annexe A

## Dimensions

Notons  $M$ ,  $L$  et  $T$  les dimensions de masse, de longueur et de temps. L'action  $\mathcal{S}$  a la dimension de la constante de Planck réduite  $\bar{h} = h/2\pi$ , à savoir une dimension d'énergie ( $ML^2T^{-2}$ ) fois une dimension de temps :

$$[\mathcal{S}] = [\bar{h}] = ML^2T^{-1}. \quad (\text{A.1})$$

Le lagrangien  $\mathcal{L}$  étant relié à l'action par,

$$\mathcal{S} = \int \mathcal{L} d^4x, \quad (\text{A.2})$$

il a la dimension suivante,

$$[\mathcal{L}] = ML^{-1}T^{-2}, \quad (\text{A.3})$$

puisque,

$$[d^4x] = L^3T. \quad (\text{A.4})$$

Tout au long de cette thèse, nous adoptons les 2 hypothèses simplificatrices  $c = 1$ ,  $c$  étant la célérité de la lumière, et  $\bar{h} = 1$  qui ont respectivement pour conséquence que  $L = T$  et  $M = L^{-2}T$ , d'après Eq.(A.1). Dans le cadre de ces 2 hypothèses, nous avons donc,

$$M = L^{-1} = T^{-1}. \quad (\text{A.5})$$

Prenant l'unité de masse comme unité de référence, les dimensions de l'action, de  $d^4x$  et du lagrangien sont, selon Eq.(A.5),

$$[\mathcal{S}] = 0, \quad [d^4x] = -4 \text{ et } [\mathcal{L}] = 4. \quad (\text{A.6})$$

Les termes de masse d'un champ de spin  $1/2$   $\psi$  (à 4 composantes) et d'un champ scalaire  $z$  s'écrivant  $\mathcal{L} = m\psi\bar{\psi}$  et  $\mathcal{L} = m^2 z^* z$ , nous déduisons de Eq.(A.6) les dimensions suivantes,

$$[\psi] = \frac{3}{2}, \quad [z] = 1 \text{ et } [\partial_\mu] = \left[\frac{\partial}{\partial x^\mu}\right] = 1. \quad (\text{A.7})$$





## Résumé :

L'extension supersymétrique du Modèle Standard peut contenir des interactions violant la symétrie dite de R-parité. La présence de tels couplages engendrerait une violation des nombres leptonique et/ou baryonique et modifierait en profondeur la phénoménologie de la supersymétrie auprès des futurs collisionneurs de particules. Nous avons développé des tests des interactions violant la R-parité. D'une part, nous avons étudié des signaux clairs de la production d'un seul partenaire supersymétrique de particule du Modèle Standard, qui implique les couplages violant la R-parité, dans le cadre de la physique aux prochains collisionneurs leptoniques et hadroniques. Les résultats montrent que de fortes sensibilités pourront être obtenues sur les paramètres de brisure douce de la supersymétrie et indiquent la possibilité d'une amélioration d'un à deux ordres de grandeur des limites indirectes actuelles sur les valeurs de plusieurs constantes de couplage violant la R-parité. De plus, il a été vérifié que l'analyse de la production d'un seul superpartenaire offre l'opportunité de reconstruire de façon indépendante du modèle théorique diverse masses de superpartenaires avec une grande précision. D'autre part, nous avons étudié des effets de violation de la symétrie CP aux futurs collisionneurs leptoniques dans la production de paire de fermions de saveurs différentes, ou de leur superpartenaire, permettant de mettre en évidence d'éventuelles phases complexes des constantes de couplage violant la R-parité. Nous avons vu notamment que la production d'un quark top accompagné d'un quark charmé permet de tester la violation de CP dans le secteur hadronique. La conclusion de ces travaux est que les phases complexes de certaines constantes de couplage violant la R-parité pourraient être observées, et plus particulièrement dans un scénario où ces couplages exhiberaient une grande hiérarchie dans l'espace des saveurs.